MINERALOGY, PETROLOGY AND GEOCHEMISTRY OF THE LOWER AND LOWER CRITICAL ZONES, NORTHWESTERN BUSHVELD COMPLEX

THESIS
Submitted in fulfilment of the
Requirements for the Degree of
DOCTOR OF PHILOSOPHY
in the Department of Geology,
Rhodes University

by

BERND TEIGLER
(Hauptdiplom, Justus - Liebig - University, Giessen, Germany)

December 1990

ABSTRACT

This study of the lower part of the Rustenburg Layered Suite in the Western Bushveld Complex is based mainly on drill core samples from three localities, which are approximately 130 km apart. The NG-sequence, situated in the northwestern sector of the complex (Union Section, R.P.M.) extends from the floor of the complex to the base of the upper Critical Zone. The sequence is ca. 1800 m thick and it comprises mainly ultramafic cumulates, namely pyroxenites, olivine pyroxenites, harzburgites and dunites. Norites and anorthosites are present only in minor proportion. Within the upper half of the NG-sequence ten prominent chromitite layers are correlated with the LG1 - MG4-interval. Correlation is also established between published sequences and the two other sequences studied, located 8 km and 55 km, respectively, east of Rustenburg.

Whole-rock chemical data (major and trace elements), microprobe, and Sr isotope data are presented. Petrographic studies provide modal analyses and measurements of grain size.

All petrographic, mineralogical and other geochemical data point to an origin of the cumulates of the NG-sequence by crystallization from liquids of the U-type lineage and derivatives thereof. No evidence is found for the involvement of parental liquids with a distinctly different composition or crystallization order (A-liquids). However, subtle compositional variations of the parental liquids are evident in slight changes of the Cr content in orthopyroxene or in variations of Sr isotope ratio. The NG-sequence is characterized by intervals with reversed fractionation trends caused by repeated influxes of pristine magma (during periods of high magmatic activity) resulting in a high degree of rejuvenation. These intervals are overlain by others with a normal fractionation trend, interpreted as cumulates formed in periods with low or no magmatic activity, in which fractional crystallization controlled bulk composition of the evolving liquid.

The Lower Zone in the NG-sequence is dominated by a progressive shift towards more primitive compositions, while in the Critical Zone fractionation was the major operating process in the magma chamber. However, during deposition of the pyroxenitic lower Critical Zone several replenishment events occurred, during which fresh Cr-rich magma was emplaced. Massive chromitite layers were deposited after mixing between the newly emplaced magma and the resident residual liquid shifted bulk compositions into the primary field of chrome-spinel. Cumulus plagioclase crystallized after bulk composition of the residual liquid was driven to the orthopyroxene - plagioclase cotectic by continued fractional crystallization; this occurred once in the Lower Zone, yielding a single, thin norite layer, and again in the upper Critical Zone of the NG-sequence.

A facies model is proposed based on the stratigraphic and compositional variations along strike in the Western Bushveld Complex. This model explains the variations by means of the position of the sequence with regard to a feeder system. The olivine- and orthopyroxene-rich, but plagioclase-poor NG-sequence represents the proximal facies, while the SF-sequence (poor in ferromagnesian phases, but plagioclase-rich) is developed as a distal facies, close to the Brits graben.

ACKNOWLEDGEMENTS

I would like to express my sincere gratitude to Prof. H.V. Eales. He not only initiated the NG-drilling programme, but also supervised me through the 4 years of this study. His guidance, assistance, criticism and encouragement is gratefully acknowledged. I also wish to thank him for all his efforts in improving my English in drafts, papers as well as in conversation.

I wish to thank all academic staff of the Department of Geology, Rhodes University, who assisted me in various ways (R. Jacob and A. Butcher - petrography; C. Mallinson and R. Harris - computing; N. Hiller - library; I. Reynolds - microprobe sample preparation); special thanks to J.S. Marsh for his help and support with the XRF-technique. I also extend my gratitude to the technical staff, specifically R. Skae for his assistance during my microprobe studies and J. Hepple, B. Bongwana and W. Hashe for their contribution to organize and prepare thin and microprobe sections.

I particularly would like to thank my fellow research students, specifically S. Haikney, B. de Klerk, W. Maier and H. Smithies for their numerous contributions during discussions in the last 4 years. S. Haikney is also thanked for permission to use her data in this thesis.

I am indebted to R. Scoon, who was my supervisor for 10 months in 1987, during which he shared his knowledge and many ideas. After joining a mining company in 1987 his cooperation and support continued by way of provision of samples, data and discussions, which led to joint papers. My thanks are extended to F.J. Kruger for his Sr isotope analyses and cooperation.

I would like to express my gratitude to the CSIR (National Geoscience Programme, Sub-programme: Bushveld Complex) for the financial support over three years as NGP-research officer and for the FRD-doctoral bursary during 1990. The financial contribution by Genmin for the PGE analyses is gratefully acknowledged.

Grateful acknowledgement is made to the Geological Survey of South Africa for drilling the NG-boreholes; to Golden Dumps Expl. Ltd., to Rand Mines, specifically to D.M. Bristow, and to Genmin for their co-operation and support during this study. I wish to thank the geological staff of all the mines visited during the duration of this work.

Finally, I would like to thank Ms. Penny Scott for her constant encouragement and her contribution to the improvement of my English.

DECLARATION

All work in this thesis is the original work of the author except where specific acknowledgement is made to the work of others.

No portion of this thesis, or the analytical data presented herein, may be reproduced or published without written permission of the author.

Date: 22.11.1990.

Signed: Teigler

B. Teigler

CONTENTS

CHAPTER 3: Petrography

CHAPTER 4: Mineralogy

CHAPTER 5: Whole-rock Geochemistry

CHAPTER 6: Platinum Group Element Distribution in the NG-sequence

LIST OF FIGURES

LIST OF TABLES

LIST OF PLATES

PART A: THE NG-SEQUENCE

CHAPTER 1: INTRODUCTION

1.1. Introduction

The Bushveld Igneous Complex (BIC, Fig. 1) is the largest layered mafic complex on Earth and a major source for Cr, V and Pt. Its size and the well developed igneous layering have important implications for modelling petrogenetic processes involved in the formation of ultramafic and mafic cumulates and associated stratiform mineralization.

The complex underlies an area of approximately 65000 km^2 (Tankard et al., 1982) and the persistence and regularity of some units or layers is a unique feature. After Hall (1932) and Willemse (1964, 1969) five magmatic stages in the Bushveld Magmatic Province (Irvine, 1982), which occurred before and during the emplacement of the complex, are recognisable: a) an initial phase, which forms volcanic rocks and is contemporaneous with the sediments of the Pretoria Group of the Transvaal Supergroup. Age determination on rocks from the Hekpoort Andesite Formation using the Rb/Sr-technique yielded an age of 2224 ± 21 My (Burger and Coertze, 1973); b) a sill phase comprising sheets of diorite, norite and diabase intruding into the Transvaal Supergroup; c) an epicrustal phase, which is represented by the Rooiberg Felsite Group; d) a main plutonic phase, namely the Rustenburg Layered Suite (hereafter **RLS**), consisting of layered ultramafic and mafic rocks. Several geochronological studies were done on rocks from different zones and an average Rb/Sr-age for the layered rocks of 2050 ± 22 My is generally accepted (unpublished data from Sharpe, published in von Gruenewaldt et al., 1985; Hamilton, 1977); and e) a late plutonic phase, which is represented by the Bushveld Granites (Lebowa Granite Suite). The age of the granites is between 2010 ± 20 My (Nebo granite, U/Pb-method, Retief, (unpublished data from von Gruenewaldt et al., op.cit.) and 1670 ± 30 My (Makhutso granite, U/Pb-method, Coertze et al., 1978).

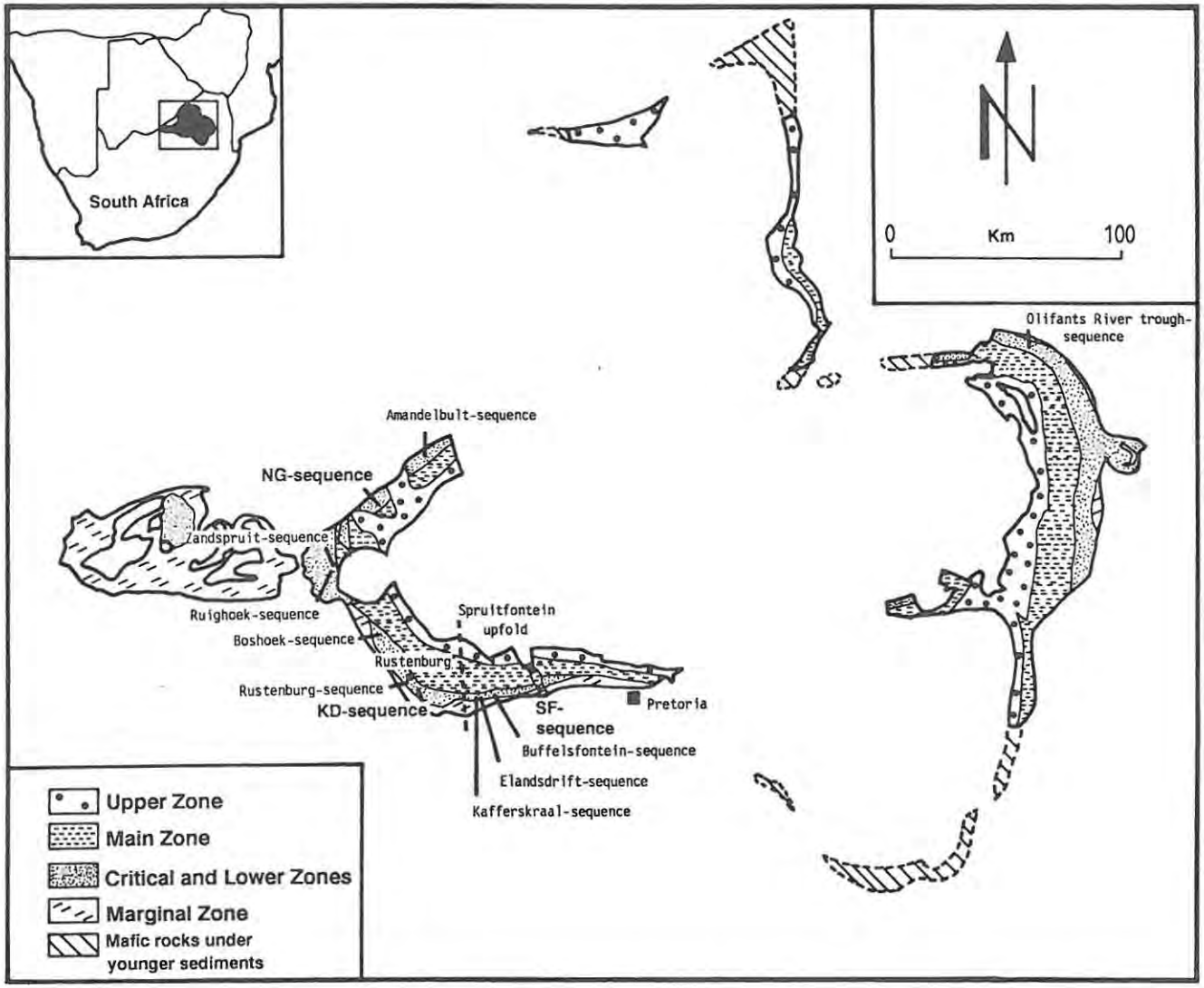

Fig. 1 Geological map of the Bushveld Complex (Rustenburg Layered Suite) with the locations of the sequences studied and mentioned in the Text.

Economically important deposits of metalliferous ores as well as industrial minerals are associated with the complex. In the metamorphic aureole, Al-rich sediments contain high-quality andalusite, which is exploited by mining operations. Magnesite deposits, formed by alteration of ultramafic rocks, are exploited in the eastern part of the complex. Tin and fluorite deposits are hosted within the granites or in sequences located close to them, e.g., Zaaiplaats (Sn), Rooiberg (Sn) and Warmbaths (CaF_2). In addition to these significant resources the economically most important are stratiform platinum-group element (hereafter PGE, platinum-group elements PGEs), chromium and vanadiferous iron oxide deposits within the RLS. PGE- and chromite-hosting layers are developed in the lower part of the complex, while the magnetite layers occur in the upper portion. Some of the mineralized units or individual layers are persistent over remarkable strike-lengths of ca. 150 km.

This thesis describes in the first part the lower units of the RLS in the northern sector of the western BIC. Correlation with sequences in other parts of the complex is done by comparison of the lithostratigraphy, the petrography and the geochemistry in the second part. Note that in all maps in this thesis true North is depicted.

1.2. Terminology for Cumulus Rocks

Wager, Brown and Wadsworth (1960) introduced the term "cumulate". They called a rock, which was formed by crystal accumulation, a cumulate. Differences in textures were explained by crystallization processes, which took place after settling of the crystal precipitate, yielding ad-, meso- and orthocumulates. Since this early work many additional names were proposed by several authors, e.g. Wager and Brown (1968) and Jackson (1967). A critical review of the terminology for layered intrusions is given by Irvine (1982, 1987a, b). In this thesis the author generally follows Irvine's definitions and proposals. A cumulate, sensu Irvine (op.cit.), is an igneous rock characterized by a framework of touching mineral crystals, which were evidently formed and concentrated through fractional crystallization; hence, this term is strictly descriptive. Typical cumulate rocks are defined by their amount of postcumulus material: a) orthocumulates 25-50 vol.%, b) mesocumulates 7-25 vol.%., and c) adcumulates <7 vol.%.

1.3. The Rustenburg Layered Suite of the Bushveld Complex

Numerous general documentations have been published since that of Hall (1932) and it is not the author's intention to give here a complete list of these. The following broad discussion of the stratigraphy and tectonic setting of the entire Bushveld Complex is based on the work of Wager and Brown (1968), Willemse (1969) and reviews and compilations of previous studies presented by Tankard et al. (1982), von Gruenewaldt et al. (1985) and Hatton and von Gruenewaldt (1987). The stratigraphic subdivision of the complex as proposed by the South African Committee for Stratigraphy (SACS, 1980) is also used though it has never found much support in the literature.

The RLS was emplaced into the 12 km-thick succession of clastic and chemical sediments, which were deposited in the Transvaal basin. Due to the transgressive character of the intrusion different formations of the Transvaal Sequence constitute the floor rocks. The layered sequence comprises a 7000-9000 m-thick pile of mafic and ultramafic rocks, which is subdivided into zones (see below). Criteria which are commonly used to distinguish between individual zones include the mineral assemblage, i.e. appearance or disappearance of cumulus phases, and/or positions of prominent marker layers, i.e. conspicuous layers which can easily be recognised in the field or in drill cores. The generally used and accepted informal subdivision of the RLS is based on these parameters.

The general description below refers to the entire complex. Because of significant differences in thickness of some zones and units between the eastern and western BIC the thicknesses quoted might not be valid for individual sequences or parts of the complex.

The Marginal Zone (basal or chill zone of Hall, 1932), hereafter abbreviated to MZ, comprises fine-grained noritic rocks, pyroxenites and olivine-rich cumulates. Xenoliths of metamorphosed sediments are abundant. The MZ is generally 100-250 m thick. This extraordinary thickness, and the presence of cumulus textures and igneous layering contradict early interpretations that norites represent the parental magma of the complex, or that this is a true marginal chill. In the floor rocks of the layered

sequence, especially in the eastern compartment, numerous sill-like intrusions are found. The field relations and the geochemistry of these sills and other marginal rocks were investigated in detail by Harmer and Sharpe (1985); Davies and Tredoux (1985) studied the noble metal contents of these rocks.

The Lower Zone (LZ), comprising pyroxenite, harzburgite, dunite and minor norite, is up to 1600 m thick. Prominent chromitite layers are normally not developed. The occurrence of two thin layers of noritic rocks is an interesting feature in the otherwise uniformly ultramafic assemblage of this zone.

The overlying Critical Zone (CZ), 930-1500 m thick, is subdivided into a lower Critical (pyroxenite subzone, lCZ) and an upper Critical Zone (anorthosite subzone, uCZ). The lCZ contains the massive chromitites, which are subject to intensive mining operations. The most prominent and consistent layer is the LG6-chromitite (Main or Steelpoort chromitite). This subzone is dominated by almost monomineralic pyroxenites with two conspicuous olivine-rich units (the C_1- and C_3-units of Cameron, 1980). The uCZ hosts the world's largest Pt-deposits; ca. 69.6% of the known resources of PGEs are concentrated in the Merensky Reef and the UG2-chromitite (Naldrett and Duke, 1980). The boundary between these two subzones is defined by the reappearance of cumulus plagioclase, which is normally positioned between two chromitite layers (the Middle Group 2 and 3 chromitites). In the eastern limb of the complex this contact is exposed in spectacular outcrops. The prominent and massive chromitite layers within the CZ are traditionally divided into three groups (Cousins and Feringa, 1964): the Lower Group- (LG), Middle Group- (MG) and Upper Group-(UG) chromitites. This nomenclature is arbitrary and somewhat unfortunate in regard to the subdivison of the CZ described above, i.e. the MG-chromitites are split between the lCZ and uCZ.

Above the CZ the Main Zone (up to 4400 m thick) is represented by anorthosites, norites, gabbronorites, gabbros and minor pyroxenites. Plagioclase, orthopyroxene and clinopyroxene are the dominant phases and chromite and olivine are absent throughout. Three subzones can be distinguished (von Gruenewaldt, 1973). Subzone A, between the top of the

CZ and the appearance of pigeonite, is overlain by subzone B, the sequence between "pigeonite-in" and the Pyroxenite Marker. Subzone C constitutes the interval between the Pyroxenite Marker and the first appearance of cumulus magnetite, which straddles the boundary between Main Zone and Upper Zone (UZ).

The UZ, ca. 2000 m thick, comprises gabbros, gabbronorites, norites, anorthosites and ferrodiorites. It hosts the economically important magnetite layers, some vanadiferous. Four subzones were defined by Molyneux (1970) and von Gruenewaldt (1973): a) subzone A - appearance of cumulus magnetite; b) subzone B - olivine-free lithologies above the main magnetite layer; c) subzone C - reappearance of cumulus olivine (Fe-rich at this level); and d) subzone D - appearance of cumulus apatite.

Discordant pegmatites truncating the layered rocks are abundant within the RLS. Viljoen and Scoon (1985) classified such postcumulus rocks into three groups: a) iron-rich pegmatite, b) non-platiniferous magnesian dunite, c) platiniferous ultramafic pipes, with a fourth group for other occurrences that are not members of the groups above, e.g. anorthosite pegmatite, orthopyroxenite pegmatite etc.. Pegmatite bodies within group c), e.g., the Onverwacht pipe, contributed a considerable amount of platinum to the South African production during the first half of this century (Wagner, 1929).

A feature which shows layers transgressing those of the underlying sequence, i.e., the so-called potholes, is not well understood yet. Potholes are transgressive circular, ovoid or irregular depressions with more or less steeply inclined walls (Viljoen et al., 1986a, b; Ballhaus, 1988). Different theories have been proposed as mechanisms for pothole formation: a) local erosion of the layered sequence by magmatic currents (Schmidt, 1952; Ferguson and Botha, 1963), b) local resorption by fresh hot magma (e.g. Campbell et al., 1983; Campbell, 1986) or after a break-down of diffusive interfaces (Irvine et al., 1983), c) local concentration of volatiles (e.g. Stumpfl, 1974; Buntin et al. 1985), and d) sites of non-deposition (Ballhaus, 1988). This range of ideas is wide and further work is necessary to clarify the genesis of potholes.

Despite the very important role of the BIC in the development of the South African economy, information concerning the structure of the complex is surprisingly limited. Early interpretations (Hall, 1932) explained the shape as a simple lopolith, but subsequent geophysical investigations (Smit et al., 1962; Meyer and de Beer, 1987) demonstrated that the complex is a complicated structure built up by several compartments as proposed by Cousins, (1959),i.e. the rocks of the RLS were intruded as several separate bodies. The major compartments now recognised are: a) the far-western lobe, b) the western lobe, c) the eastern lobe, d) the northern lobe, and e) the Bethal lobe. In the areas adjacent to these main outcropping bodies numerous mafic satellite intrusions are regarded as related to the complex and indicate extensions to the major compartments. Broad similarity in the stratigraphic succession is ascribed to comparable magma compositions and physical conditions controlling crystallization in the separate chambers (von Gruenewaldt et al., 1985). A connection of all compartments to a master magma chamber at depth was proposed by Sharpe et al. (1981).

The tectonic setting of the complex is still obscure and proposed hypotheses can be grouped within three categories: a) a tectonic initiation (Hall, 1932), i.e. the complex intruded in an area of crustal weakness caused by the intersection of two major tectonic trends in Southern Africa. These are the Great Dyke trend and a trend striking ENE-WSW, indicated by the strike directions of some greenstone belts; b) an extraterrestrial initiation, i.e. the intrusion of the complex was caused by impact of a meteorite (Dietz, 1963); and c) a subsidence initiation, i.e. the magmatism was triggered by crustal loading (Sharpe et al., 1981).

Influence of early tectonic activity on the emplacement history of the complex is indicated by significant lithostratigraphic changes associated with fold structures of the floor rocks (Hatton and von Gruenewaldt, 1987). Late tectonic movements with possible initiation during the emplacement of the complex resulted in the formation of faults and graben structures, e.g. Brits graben, (Hatton and von Gruenewaldt, op.cit.).

1.4. Previous Work

Because of the vast amount of literature dealing with the Bushveld Complex this review will be constrained to work relevant to two aspects: a) the regional geology, and b) the objectives of this thesis.

The geology of the north-western part of the Bushveld Complex has been studied by various authors including Hall (1932), Kupferbuerger et al. (1937), Cousins (1959), Coertze and Schumann (1962) and Vermaak (1970). Wasserstein (1936) noted the breaks in the continuity of the Merensky Reef and the chromitite layers in the area north-east of the Pilanesberg and attributed these discontinuities to displacement due to faulting. However, Coertze (1958), after his investigation of platinum, chromite and magnetite deposits in the Western Transvaal, stated that the breaks or gaps are the results of transgressions of upper zone rocks. He also interpreted the entire CZ as a sequence of intrusions of diverse magmas.

The bulk of the investigations of rocks hosting the LG-chromitites was done before 1960. Up to this year an intensive exploration drilling and mapping programme in these areas provided the data-base for most of the work. The Zwartkop Chrome Mine had already commenced mining operations during 1935 (Von Gruenewaldt and Worst, 1986), and the Rustenburg Platinum Mines (R.P.M.) Union Section and Amandelbult Section during 1950 and 1974, respectively (Viljoen et al., 1986a, b). Due to the emphasis on platinum operations in the uCZ and the shut-down of Zwartkop Chrome Mine in 1980 (Vermaak, 1986) more recent work on rocks of the lCZ in both sections is scarce; studies from the north-western sector of the complex (de Klerk, 1982; Eales et al., 1986, 1988) were focused on the uCZ.

Von Gruenewaldt and Worst (1986) investigated the chromitite layers at Zwartkop, which is contiguous with the Amandelbult Section, and described the stratigraphical succession and mineral chemistry of chromite. Their findings of a reversal in the normal fractionation trend in the lower part of the lCZ was in agreement with the work of McDonald (1967), who studied the lCZ on the farm Ruighoek further to the south-west. Botha (1987) investigated the LG-chromitites and host rocks on the farm Zandspruit adjacent to McDonald's field area. He found a correlation between the

thickness of the chromitite layers and the thickness of the silicate pile embraced by the chromitite layers, from which he concluded that liquid mixing - a new hot melt with a cooler, upwardly streaming residual liquid- produces robust chromitite layers.

The elegant and widely accepted model of magma mixing to shift bulk magma composition into the phase field of chromite was proposed by Irvine (1975). His original model was subsequently broadened to include also mixing of liquids of distinctly different lineages (Irvine et al., 1983; Sharpe and Irvine, 1983; Sharpe, 1985, 1986). Other hypotheses for the origin of chromitite layers are: a) separation of chromium-rich immiscible liquid (Sampson, 1932; van Zyl, 1970), b) crystal settling (Campbell, 1978), and c) changes of the physico-chemical conditions in the magma chamber, e.g. total pressure, oxygen fugacity, and bulk composition (inter alia Ulmer, 1969; Cameron, 1980; von Gruenewaldt and Worst, 1986; McDonald, 1967; and Irvine, op.cit.). Hatton and von Gruenewaldt (1987) review the geological setting and genesis of all stratiform chromitite layers in the complex.

In the eastern limb of the BIC Cameron's work (1978, 1980, 1982) on the lower part of the layered sequence is a thorough petrographic and microprobe-analyser study of these rocks.

Several authors have given their attention to the PGE mineralization in the complex. A striking feature is the close association of mineralization and occurrence of massive chromite layers (Naldrett and von Gruenewaldt, 1988). The currently popular R-model (Campbell and Naldrett, 1979; Campbell et al., 1983) is also based on a mixing event of two compositionally distinct liquids, which causes sulphur saturation in the bulk silicate melt, so that immiscible sulphide droplets can scavenge the platinoids from a great volume of silicate liquid. General geochemical behaviour of the PGEs was studied and described by Barnes et al. (1985), who found that the PGEs fractionate in order of descending melting points.

More detailed reviews will be introduced in the relevant sections of later chapters.

1.5. The Nooitgedacht Sequence, and Motivation for this Study

In the western Bushveld Complex exposures of the layered mafic sequence are poor, and detailed studies are restricted to drill cores and underground exposures in mining operations. In the area in which the study boreholes were drilled, north-east of the Pilanesberg Alkaline Complex, the mined orebodies (the Merensky Reef and the UG2-chromitite) are hosted within the uCZ and hence the lCZ and LZ are not exposed in mine workings. A 1-5 m-thick black soil, the so-called 'black turf', covers most of the ground such that surface mapping and/or sampling are almost impossible.

To model the petrogenesis of the Bushveld Complex complete stratigraphic coverage is regarded as one of the most important conditions. The boreholes Nooitgedacht 1, 2 and 3 (hereafter NG1, NG2 and NG3), drilled by the Geological Survey of South Africa, provided samples of cumulates from the LZ and CZ and offer a unique opportunity to investigate these zones at Union Section, especially taking into account the research carried out earlier by Eales and co-workers (1986, 1988).

CHAPTER 2 : THE REGIONAL SETTING OF THE NG-BOREHOLES

2.1. Regional Geology

The following short summary of the regional geology is based on reviews by de Klerk (1982) and Viljoen et al. (1986a , b). The regional geology of Union Section, Rustenburg Platinum Mines, is shown in Fig. 2.

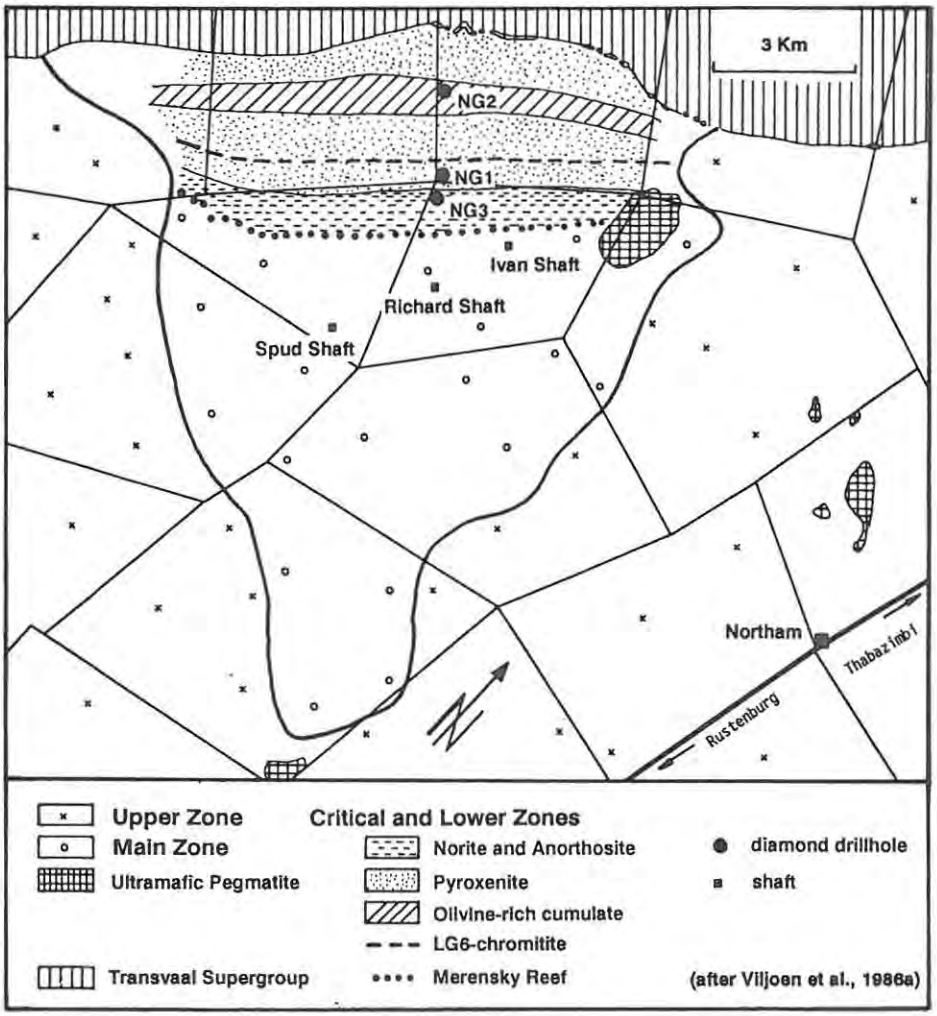

Fig. 2 Regional geology and locations of the NG-boreholes.

Union Section forms a triangular segment of LZ-, CZ- and Main Zone-lithologies truncated along strike by UZ-gabbroic rocks. The shape of the segment is ascribed to transgressions of UZ-assemblages (Coertze, 1958), but the origin of these 'gap' areas is still under discussion. The interpretation of the 'gap' areas is of some economic importance due to

the possibility of PGE-mineralized layers underneath the gabbroic UZ-rocks. Feringa (1959) proposed that faulting caused the displacement of the LZ, CZ and MZ followed by a transgression of the UZ-assemblage into the 'gap' areas. An intrusion of the UZ-rocks into the well-layered underlying rocks and subsequent obliteration of the latter is the explanation of Coertze (1974). Structural control due to folding of the floor rocks was proposed by Walraven and Darracott (1976).

The floor of the Bushveld Complex in the area is a resistant but narrow quartzite, which dips at 65° SE (Viljoen et al., 1986a). A marginal norite, which generally forms identifiable outcrops in the southern areas of the Western Bushveld Complex, seems to be absent or poorly developed at Union Section.

Pyroxenites and harzburgites of the MZ and LZ overlie the sedimentary rocks. The harzburgitic sequence is commonly capped at outcrop by secondary birbirite, a product of intensive surface weathering leading to an enrichment of opaline silica and lateritic material (Viljoen et al., op.cit.). The lCZ comprises mainly monomineralic, monotonous pyroxenites that host the LG-chromitites, which have never been mined at Union Section. The MG-chromitites straddle the boundary between lCZ and uCZ, the latter dominated by plagioclase-rich cumulates. Accordingly, norites of varying colour index represent the dominant rock type. Outcrop of norite and anorthosite is limited.

The general strike of the layered rocks is SW-NE with an average dip of 25° SE. The adjacent UZ-lithologies are also poorly exposed, but their distribution is indicated by the development of a dark red or brown soil due to their iron-enriched character. The vanadiferous magnetite layers hosted by the gabbroic lithologies display at outcrop dip directions almost concentrically outwards from the Union Section segment.

Post-emplacement features are diabase sills as well as 'Pilanesberg' dykes and faults, which displace parts of the CZ.

2.2. The Locations of the Nooitgedacht Boreholes

After representations by Prof. H.V. Eales to the Director of the Geological Survey,the decision to study the lower part of the RLS at Union Section as part of the National Geoscience Programme was made and the Geological Survey of South Africa drilled three stratigraphic boreholes for study purposes (Fig. 2). The primary idea for the layout of the drilling programme was to cover the layered sequence below the UG1-chromitite with a fence of two short holes to cut costs and to assure good core recovery. The expected thickness was approximately 1200 m and accordingly each hole would have been drilled to a depth of ca. 600 m. Events proved the thickness of the sequence to be close on 1.5 times greater than projections had indicated.

The drilling site for NG1 was determined by extrapolation using data of underground exposure of the MG-chromitites in the deepest mine workings (Spud shaft, ca. 2500 m downdip) and an average dip of the layers of 19°. A parallel shift towards NE was necessary in order to locate the boreholes within South African territory. NG1 is situated on the farm Nooitgedacht KQ 406 and it reached a final vertical depth of 831.06 m. The core provided samples for most of the lCZ and the upper part of the LZ. NG2, situated on the same farm, was commenced after finishing NG1, but was interrupted twice. It was stopped by the geologist of the Geological Survey after intersecting only one metre of a hornfels-type rock (interpreted as the Transvaal floor sequence) at a final depth of 774.70 m. NG3, (final depth below collar 260.41 m), was drilled on the farm Swartklip KQ 405, ca. 400 m downdip of NG1, because the latter did not intersect the MG-chromitites as planned. Accordingly, borehole NG3 provided samples of the MG-chromitites and the boundary between lCZ and uCZ.

The overlap between the individual holes was established by means of stratigraphic, textural and geochemical parameters: this overlap is ca. 10 m between NG3 and NG1 and ca. 40 m between NG1 and NG2.

Accordingly, in all diagrams which display the depths of samples, taken at their midpoints, the depth below the NG3-collar is used, and when the three boreholes are combined within a single column depths of samples are calculated using the following equations:

a) $depth_{NG}$ = drillhole $depth_{NG3}$ for NG3-samples

b) $depth_{NG}$ = drillhole $depth_{NG1}$ + 250 m for NG1-samples

c) $depth_{NG}$ = drillhole $depth_{NG2}$ +1040 m for NG2-samples.

The collar elevations of all three boreholes are approximately 1030 m above sea level. Additionally, NG1 was surveyed by Sperry Sun to determine its true dip and direction. The overall vertical thickness of the sequence is 1814.70 m uncorrected; the measured borehole deviation at a depth of 600 m was ca. 6° up-dip, which yields a true thickness of ca. 1706 m.

2.3. The Stratigraphic Succession of the NG-sequence

This section presents the lithostratigraphy encountered in the NG-boreholes (Fig. 3). Correlation with the formal as well as informal zonal subdivision is also established. All following descriptions are in stratigraphically ascending order, which is thought to be the genetic sequence for most of the rocks. Accordingly, the sequence in NG2 is described first, followed by NG1 and, finally, NG3. The detailed logs of the boreholes are attached in the Appendix.

2.3.1. Lithostratigraphy of NG2, NG1 and NG3

The floor rocks of the complex are represented by two lithologies. A recrystallized, contact-metamorphic hornfels constitutes the final 0.86 m of NG2. Whether this porphyroblastic hornfels is in fact the floor rock or a xenolith is impossible to state. However, petrographic and geochemical evidence from the rocks comprising the last 40 m indicate the close proximity of the floor rocks.

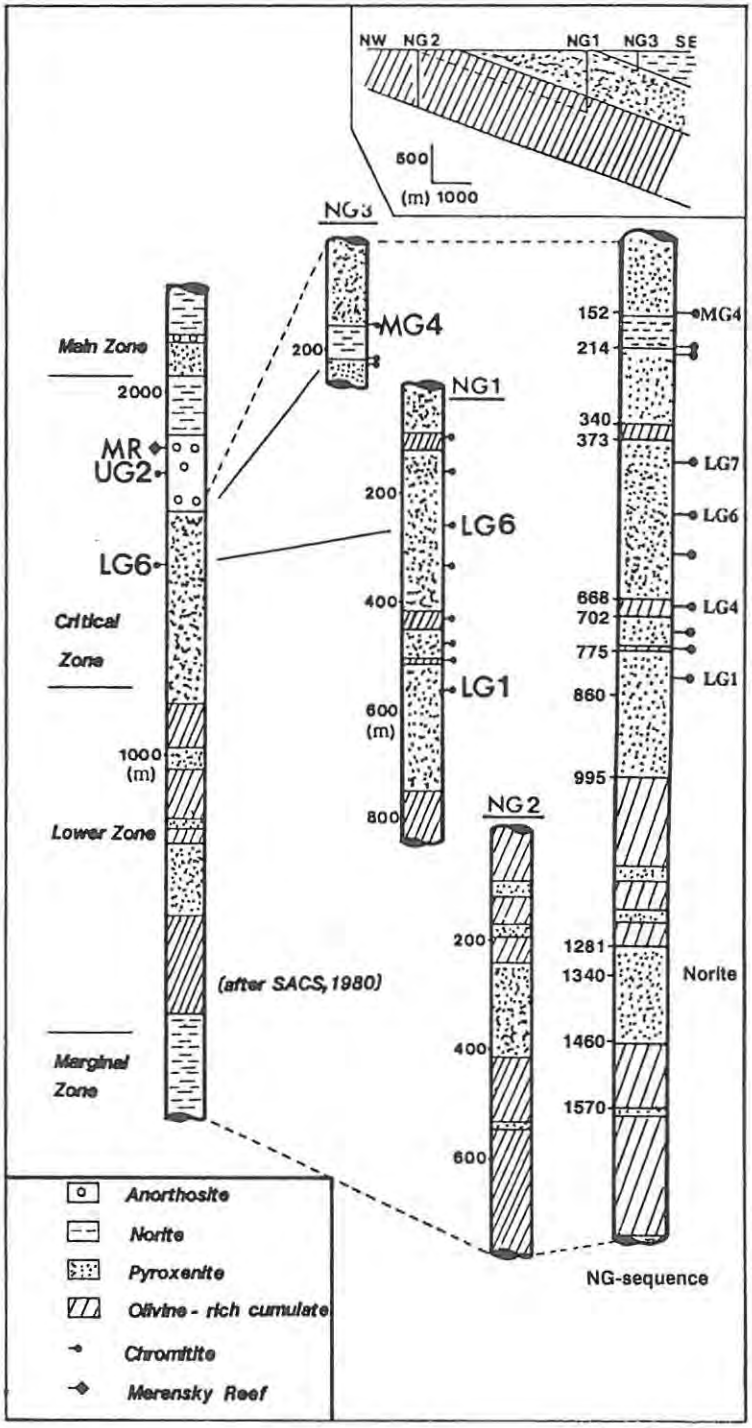

Fig. 3 The NG-boreholes and the combined NG-sequence in comparison with the type sequence of the western BIC.(Note the different scales).

A quartzitic xenolith was intersected at a depth of 1806.33 m. The thickness of this meta-sediment inclusion is 0.58 m. Upwards, to a depth of 1779.00 m, the dominant rocks in NG2 are conspicuously fine-grained, highly feldspathic pyroxenites with thin layers or laminae of harzburgite.

A thin (0.40 m) gabbroic norite forms the immediate contact with the hornfels. This sequence is equated with the MZ or the Kolobeng Norite (SACS, 1980), though this zone appears from outcrop to be atypical at Union Section, i.e. a well-developed marginal norite was not intersected by NG2. The absence of such thick norites can also be deduced from the geological maps of this area compiled by Viljoen et al. (1986a, b).

The LZ in NG2 and NG1 comprises four intervals: a) from ca. 1778.00-1458.95 m multiple interlayered units of pyroxenites and olivine-rich cumulates. The thickness of individual layers ranges from mm to dm. This subzone is correlated with the Eerlyk Bronzitite (SACS, 1980); b) from 1458.95-1281.09 m a package of pyroxenites, which is divided by a leuconorite (intersected at 1337.25 m) constitutes the Makgope Bronzitite (SACS, 1980). From ca. 1410.00 m downwards some minor olivine-bearing cumulates are present, heralding the change to the Eerlyk Bronzitite; c) the remainder of NG2 and the lowermost part of NG1 (up to 995.00 m) are dominated by almost monomineralic olivine cumulates totalling ca. 286 m in thickness. This interval is equated with the Groenfontein Harzburgite (SACS, 1980). d) from 995.00-860.00 m monotonous pyroxenites, divided by one olivine-rich unit at ca. 900.00 m constitute the Tweelaagte Bronzitite, which forms the uppermost subzone of the LZ (SACS, 1980).

The CZ covered by NG1 and NG3 is the economically important zone. In NG1 pyroxenites (Ruighoek Pyroxenite (SACS, 1980)) dominate the sequence. The pyroxenitic package is divided by three olivine-bearing units, which occur at depths of 755.64-773.98 m, 668.10-702.00 m and 340.30-372.98 m. The middle of these units is very consistent throughout the complex and is also found within the eastern compartment. It hosts the LG4-chromitite and makes therefore an excellent unit for correlation. NG3 is barren of olivine and below the boundary lCZ/uCZ at 213.95 m (sample NG3-214.05) below collar elevation the rocks are monotonous pyroxenites displaying variable amounts of chromite and intercumulus phases, as well as variations in grain size. Above the appearance of cumulus plagioclase, norites are the most common rock type upwards to a depth of 151.87 m. The remainder of NG3 comprises pyroxenites, which contain minor anorthosite lenses or schlieren. The textures of these rocks are complex. Eales et al. (1990a) described the textural features and compositional variations encountered at this stratigraphic level in detail.

TABLE 1 Chromitite Layers in the NG-sequence

Layer No	Borehole	Distance to LG6 in m	Thickness in cm	Characteristic features	Host rocks	Correlation with Cousins and Feringa, 1964
1	NG3	+354	98	m	p	MG4B
2	NG3	+351	148	m	p/a	MG4A
3	NG3	+294	75	m	a/n	MG3
4	NG3	+287	50	m	p	MG2
5	NG1	+166	13	d	p	MG1
6	NG1	+104	3	m	p	LG7
7	NG1	+ 14	18	m	p	LG6A
8	NG1	0	104	m	p	LG6
9	NG1	- 75	55	m	p	LG5
10	NG1	- 76	32	m	p	LG5
11	NG1	-173	27	m	d	LG4
12	NG1	-196	11	m	d	
13	NG1	-219	49	m	p	LG3
14	NG1	-225	7	m	p	
15	NG1	-240	8	m	p	
16	NG1	-250	20	d	d	LG2B
17	NG1	-268	20	m	p	LG2A
18	NG1	-291	2	m	p	
19	NG1	-304	36	m	p	LG1
20	NG1	-353	6	m	p	
21	NG1	-389	20	d	p	

Notes: 1) datum: LG6-chromitite

2) massive (m): chromite is the only cumulus phase

3) disseminated (d): chromite and silicate phases are cumulus minerals

4) host rocks denoted are hangingwall and footwall: p=pyroxenite, d=dunite, n=norite, a=anorthosite

NG1 and NG3 intersected numerous massive chromitite layers and chromite-rich layers. A summary of the most characteristic features of the chromitite layers is presented in Table 1. The top of the thickest chromitite layer in the pyroxenite subzone, i.e. the LG6-chromitite, is chosen as datum. Additional to these chromitite layers listed numerous horizons with modal chromite above 10 vol.% were intersected.

No ultramafic or other discordant bodies were intersected by the NG-boreholes. In general the degree of alteration is very low to moderate. However, layers close to the surface and some olivine-rich lithologies might be serpentinised. Post-Bushveld intrusives were not encountered, and no unequivocal evidence of fault-controlled displacement was seen.

2.3.2. The Distribution of the Different Lithologies in the NG-sequence

In this section the distribution of the different rock types in the NG-sequence is summarized. The cumulative thickness of different rock types is:

66.2 % pyroxenite
31.0 % olivine pyroxenite, granular and poikilitic harzburgite and dunite (hereafter: olivine-rich cumulates)
2.2 % norite
0.4 % chromitite
0.2 % anorthosite.

Split into the individual zones the distribution is as follows (note that thicknesses are vertical thicknesses):

Zone	Rock Type	Thickness (m)	%	
uCZ	pyroxenite	167.62	79.0	
	norite	37.16	17.5	
	anorthosite	4.11	1.9	
	chromitite	3.21	1.5	
	Total:	212.20		
lCZ	pyroxenite	695.17	88.6	(of which 2.1 % are chromitiferous with an average of 28.2 vol.% chromite)
	olivine-rich cumulates	85.44	10.9	
	chromitites	4.34	0.5	
	Total:	784.95		
LZ and MZ	pyroxenite	338.73	41.4	
	olivine-rich cumulates	476.60	58.2	
	norite	3.27	0.4	
	Total:	818.60		

It is evident from this compilation that the LZ is dominated by olivine-rich rocks in contrast to the lCZ, in which pyroxenite is by far the most abundant rock type. This relationship might indicate a major change of the processes involved in the formation of the cumulate pile.

2.3.3. Discussion and Conclusions on Correlation

Since Young (1978) mapped the RLS west of the Pilanesberg most of his proposed names and subdivisions of the mafic rocks were adopted by SACS (1980). The type sequence derived from the latter and the type sequence for the eastern BIC (Cameron, 1978, 1980, 1982) are shown in Fig. 4 together with the NG-sequence.

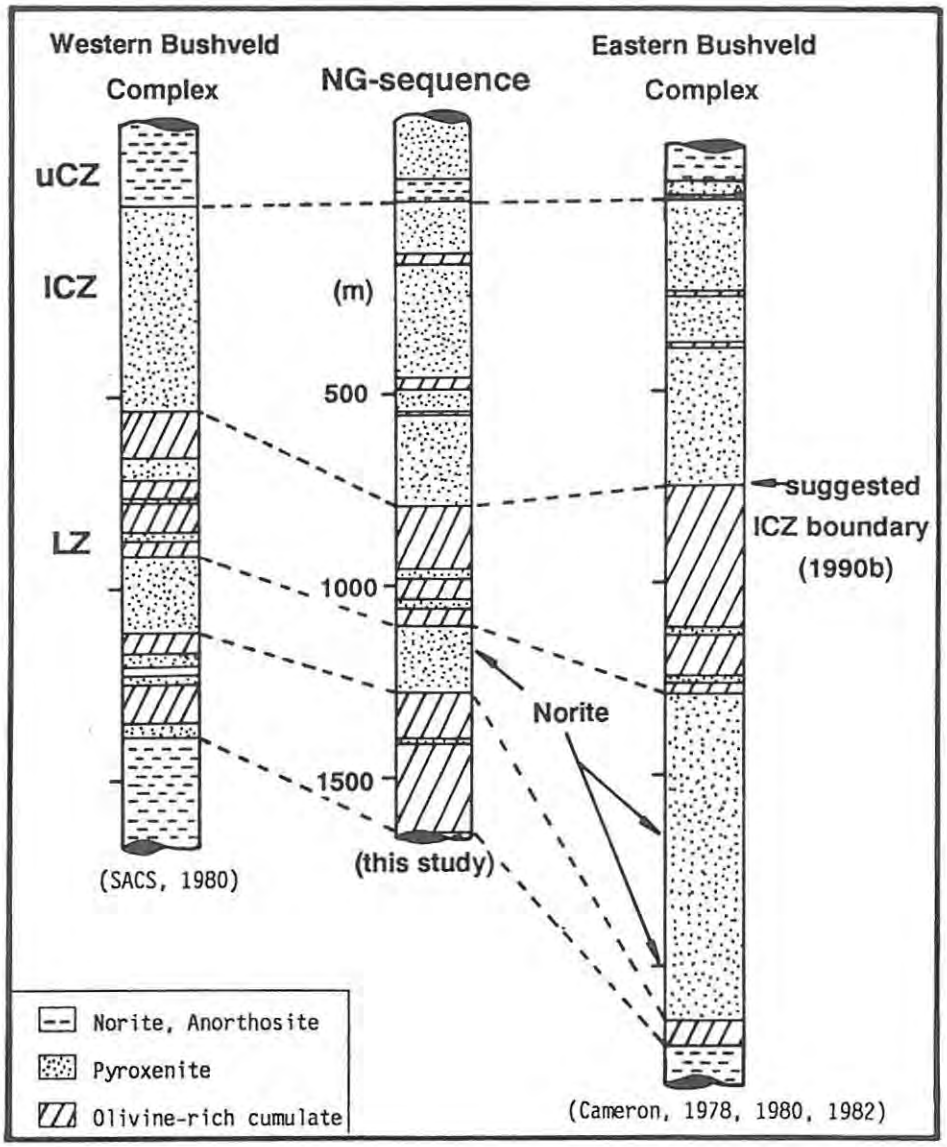

Fig. 4 Comparison of the lCZ, LZ and MZ through the Bushveld Complex.

The broad similarity of all sections is striking, especially when considering the distance between the NG-sequence and the sequence in the eastern BIC (ca. 300 km). However, thicknesses of individual zones and units vary significantly.

The following features are noteworthy:

a) a marginal gabbroic norite with significant thickness variations along strike forms the base of the complex;

b) a sequence dominated by olivine-rich lithologies overlies these marginal rocks;

c) a thick package of pyroxenite constitutes the next unit;

d) a further olivine-rich interval with subordinate pyroxenites overlies the latter and caps the LZ (as newly defined by Eales et al., 1990b);

e) pyroxenites with the majority of the conspicuous massive chromitite layers are the most prominent rocks in the lCZ;

f) the appearance of cumulus plagioclase marks the boundary between the lCZ/uCZ, and norites (sensu lato) are the most abundant rock type above this level.

Detailed comparisons along strike will be the subject of the second part of this thesis but there seems to be more agreement in details between the NG-sequence and the sequence from the Olifants River trough (Cameron's section) in the eastern limb than with the type section of the western limb. An unequivocal explanation is not readily found. Because of the poor outcrop in the western compartment, surface mapping in detail is scarcely feasible and this could result in different subdivisions and the apparent absence of some units. In contrast to the western part, the exposure in the eastern limb is adequate and therefore stratigraphic columns derived from surface mapping are possible to construct in great detail. A further possible explanation is that the NG-sequence and the Olifants River sequence are indeed more similar because of their locations in the northern half of the complex, which shows generally different lithostratigraphies to its southern counterparts (Hatton and von Gruenewaldt, 1987).

CHAPTER 3: PETROGRAPHY

The different lithologies and their distinctive textures are the subject of this chapter, which is biased towards a descriptive character. However, genetic implications of the observed features will be discussed briefly here and then in more detail in the discussion after presentation of the geochemistry.

3.1. Nomenclature of Cumulates

The table attached to the Streckeisen diagram (Fig. 5, Streckeisen, 1974) displays the cumulate terminology (after Irvine, 1982) as well as the conventional names for ultramafic and gabbroic rocks. In agreement with most published work and the terminology used by mine and field geologists, the conventional rock names (Fig. 5) will be used, but some additional remarks are necessary for complete understanding.

In cumulates the name of any particular rock is dependent upon the modal composition of the major cumulus phases, e.g., a rock consisting of plagioclase and orthopyroxene as the sole cumulus minerals is called a norite (further subdivisions are possible by means of the actual proportions of felsic and mafic phases), but in the case where only one major cumulus phase is present, this rock would be named anorthosite or orthopyroxenite (in the NG-sequence all cumulus pyroxenes are orthopyroxenes apart from some scarce cumulus clinopyroxenes in the MZ, therefore the name orthopyroxenite is abbreviated to pyroxenite). Cumulus minerals exhibit three main habits: a) as euhedral to subhedral grains defining the cumulate framework, b) as inclusions in later cumulus and postcumulus phases, and c) as discrete grains between cumulus minerals, but not enclosed in postcumulus material. The space between cumulus minerals is filled by postcumulus material, which occurs commonly in two habits: a) as filling of interstices between cumulus phases, or b) as large oikocrysts poikilitically enclosing cumulus and/or earlier crystallized postcumulus phases. Later subsolidus reactions, e.g., exsolution of clinopyroxene blebs and lamellae in orthopyroxene, yield additional habits not listed above.

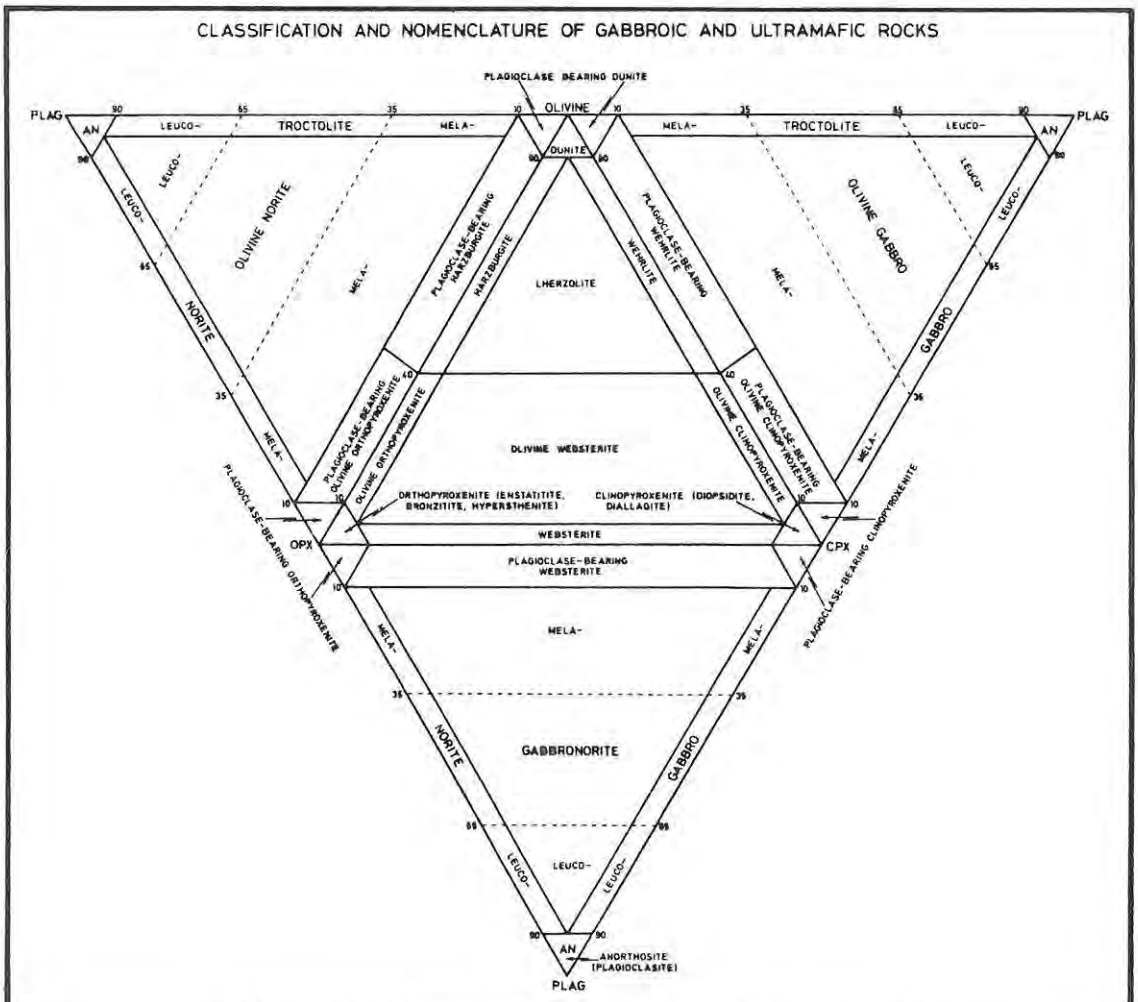

Conventional rock names for the more common types of ultramafic and gabbroic cumulates

Cumulate type	Conventional rock name
Peridotitic cumulates	
Olivine-(chromite)	Dunite, peridotite, picrite
Olivine-chromite	Chromite dunite, peridotite
Olivine-augitic clinopyroxene	Wehrlite
Olivine-orthopyroxene	Harzburgite
Olivine-clinopyroxene-orthopyroxene	Picritic websterite
Pyroxenitic cumulates	
Clinopyroxene	Clinopyroxenite
Clinopyroxene-olivine	Olivine clinopyroxenite
Clinopyroxene-orthopyroxene	Websterite
Clinopyroxene-orthopyroxene-olivine	Olivine websterite
Clinopyroxene-orthopyroxene-plagioclase	Gabbroic websterite
Clinopyroxene-magnetite	Magnetite clinopyroxenite
Orthopyroxene	Orthopyroxenite
Orthopyroxene-olivine	Olivine orthopyroxenite
Orthopyroxene-chromite	Chromite orthopyroxenite
Gabbroic cumulates	
Plagioclase	Anorthosite
Plagioclase-olivine	Troctolite
Plagioclase-augitic clinopyroxene	Gabbro
Plagioclase-clinopyroxene-olivine	Olivine gabbro
Plagioclase-orthopyroxene	Norite
Plagioclase-clinopyroxene-orthopyroxene	Two-pyroxene gabbro
Plagioclase-orthopyroxene-clinopyroxene	Noritic gabbro
Plagioclase-clinopyroxene-magnetite	Magnetite gabbro
Plagioclase-clinopyroxene-apatite	Apatite gabbro
Olivine-plagioclase	Picritic troctolite
Oxide cumulates	
Chromite	Chromitite
Chromite-olivine	Olivine chromitite
Magnetite	(Cumulate name preferred)
Ilmenite	(Cumulate name preferred)

The cumulus minerals are listed in order of decreasing abundance; accessory minerals are in parenthesis. A maximum of only three cumulus phases is considered; additional minerals would be varietal phases in the conventional rock names.

(after Irvine, 1982)

Fig. 5 Nomenclature and classification of ultramafic and gabbroic cumulates.

Late-stage magmatic processes (e.g., postcumulus metasomatism, hydrothermal alteration) may cause an overprint, which could result in complete transformation (Irvine, op.cit.). Throughout this thesis, abbreviations are used as follows: opx for orthopyroxene; cpx for clinopyroxene; ol for olivine; pla for plagioclase and chr for chromite.

3.1.1 Rocks of Sedimentary Origin

In the last few meters of NG2 one quartzitic sample, presumed to be a xenolith, surrounded by a mm-thin rind of a very fine-grained norite, was intersected. The xenolith is an impure quartzite with mica, amphibole and feldspar. The quartz grains do not show undulose extinction.
The last meter of NG2 yielded a darkish, hornfels-type rock, which is interpreted as a contact-metamorphic, fine-grained meta-sediment. The rock displays under the microscope porphyroblastic, needle-shaped orthopyroxene crystals (ca. 2 mm long) in a quartz-feldspar-mica matrix with some cpx grains.

3.1.2. Anorthosite

In anorthosite, pla is the only major cumulus phase, and other cumulus phases are present in proportions less than 10 vol.%; opx and cpx are interpreted, in terms of texture, as postcumulus phases. Alteration (saussuritization) is variable and depends often on the stratigraphic position.
Anorthosites in the NG-sequence are generally of allotriomorphic-granular texture and two types are present: a) chromitiferous anorthosite and b) anorthosite sensu stricto, i.e. without any further cumulus phases. The latter type occurs just below the MG3-chromitite and forms a layer 0.73 m thick. Immediately beneath the latter chromitite layer the anorthosite is altered and the petrographic description below is based on the fresh basal part in sample NG3-212.93 (at a depth of 212.93 m). Plagioclase crystals are sub- to anhedral, i.e. in some areas triple-point junctions and polygonal grain shapes are probably caused by annealing processes. The subhedral grains are lath-shaped and grain sizes range from 0.3 to 2 mm. Igneous foliation was not observed in this sample. The only other phase present is cpx, which forms rims or infillings around or between the pla-framework.

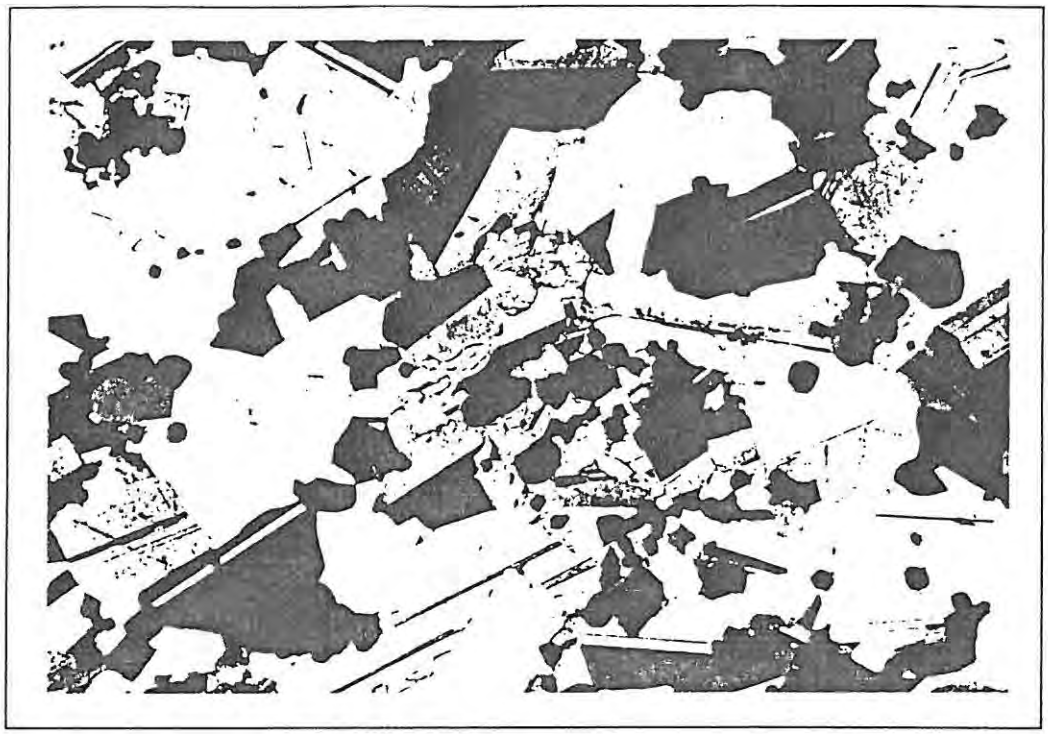

Plate 1. Chromitiferous anorthosite showing lamination subparallel to the macroscopic layering and a postcumulus orthopyroxene grain (in the centre). Sample NG3-158.10, upper Critical Zone, ca. 6 m below the MG4-chromitite. Field width 3.5 mm; crossed nicols.

Plate 2. Norite, upper Critical Zone, ca. 20 m above the lCZ - uCZ boundary. Note the eu- to subhedral prismatic shape of orthopyroxene and the partly developed clinopyroxene rim around the orthopyroxene grain in the centre of the photomicrograph. Sample NG3-194.74 . Field width 3.5 mm; crossed nicols.

Chromitiferous anorthosite is developed below the the MG4-chromitite. The layer, ca. 3.10 m thick, resembles the footwall of the UG1-chromitite at Dwars River in the eastern BIC; variable proportions of chr in disseminations, layers, blebs, schlieren and stringers are embedded in the anorthosite. Mottles formed by poikilitic opx are also present. The grain size of pla is also variable and a foliation parallel to the layering might be developed. The degree of annealing is greater compared with the second type, thus polygonal and anhedral crystal forms are more abundant. Zonal structures can be sporadically found under the microscope.

3.1.3. Norite

Opx (10-90 vol.%) and pla (90-10 vol.%) in variable ratios constitute norites. Chr can be an accessory, minor or major cumulus phase; ol was not encountered in noritic rocks. The most abundant postcumulus phase is cpx. Norites are, like anorthosites, only a minor rock type in the NG-sequence, and are generally panidiomorpic to hypidiomorphic-granular. Opx is of eu- to subhedral prismatic shape, whereas pla displays commonly a lath-like form. The grain sizes are variable depending on modal proportions and degree of annealing. Pla shows a bimodal distribution with a smaller grain size fraction revolving around 0.3 mm and the bigger around 2 mm. In some samples opx contains numerous small inclusions of pla, which show features of resorption and are commonly ovoid in shape. Zoning of pla is sometimes developed; foliation is scarce.

A gabbroic norite, only 0.40 m thick at the base of the complex, is thought to represent the marginal facies. It is characterised by cumulus cpx and postcumulus apatite, mica and quartz, none of which is commonly found in the CZ-norites. Mica occurs as flakes up to 2 mm long with abundant inclusions of opaque oxides. Apatite (0.2 mm) forms euhedral crystals associated with mica. Pla and opx are elongated to form needles up to 4 mm long without preferred orientation. The exsolution of cpx in opx is bleb-like but parallel to (100). Opx shows resorption pits and embayments. Quartz is an abundant postcumulus phase, filling interstices or poikilitically enclosing earlier phases. It is clear and displays no undulose extinction. Cpx, commonly 0.5 mm in grain size, forms stubby prisms with thin opx-exsolution lamellae. The overall character of this rock resembles more an ophitic texture with the framework of needle-shaped pla and opx and the remaining phases as mesostasis.

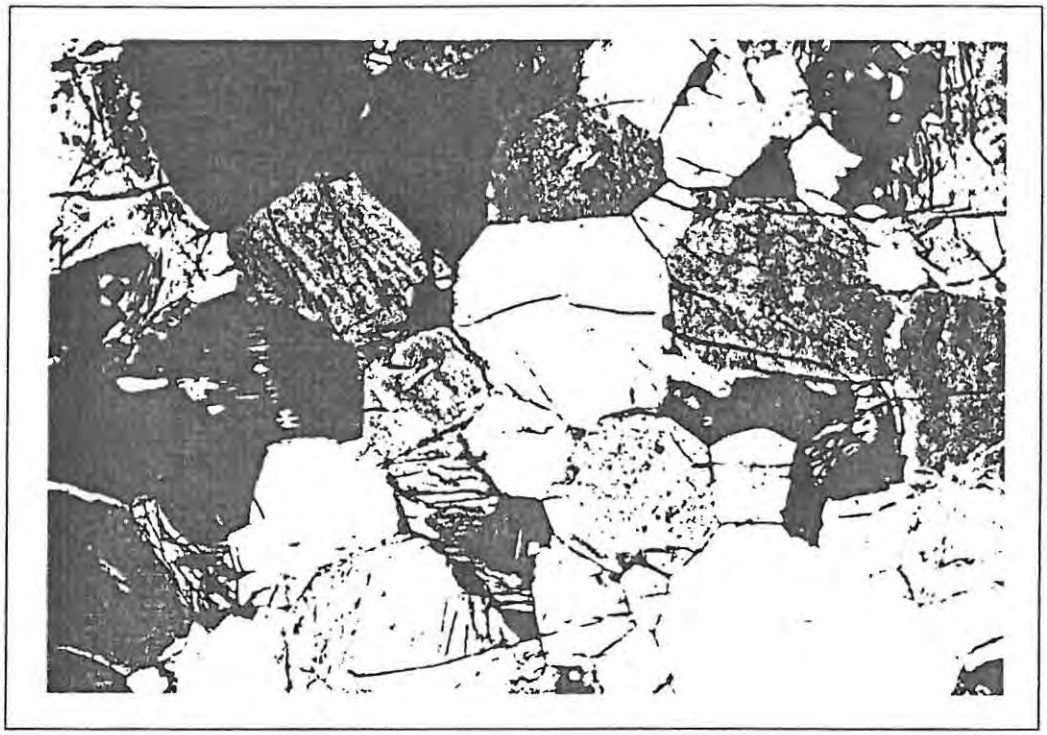

Plate 3. Adcumulate pyroxenite with well-developed triple-point junctions. Sample NG1-250.15, lower Critical Zone, ca. 5 m above the LG6-chromitite. Field width 3.5 mm; crossed nicols.

Plate 4. Orthocumulate pyroxenite showing abundant plagioclase. White quartz and dark brown phlogopite can also be observed (top right). Sample NG2-294.12, Lower Zone, ca. 3 m above the norite layer in the Lower Zone. Field width 3.5 mm; crossed nicols.

3.1.4. Pyroxenite

Pyroxenites are the most common rock type in the NG-sequence. Opx is the only major cumulus mineral; however, ol and chr are locally present in proportions less than 5 vol.%. As stated earlier, chromitiferous pyroxenites, (i.e. with more than 5 vol.% chr) are an abundant rock type in the lCZ. Postcumulus phases are in order of decreasing abundance: pla, cpx, mica, quartz and amphibole. Pyroxenites close to the base of NG2 show also rutile as an accessory phase, commonly enclosed in mica. Pla in proportions greater than 10 % by volume can de denoted by using the term "feldspathic" as prefix, but, by definition, such rocks are not norites.

The cumulus opx grains are generally equigranular with few exceptionally large grains, which might be xenocrysts; however, no significant compositional variations were found. The form varies from stumpy-prismatic to lath-like, when igneous foliation is developed. No systematic relationship between foliation and stratigraphic position is apparent. The grain size is variable from 1-2 mm as displayed by anhedral crystals in adcumulate pyroxenites, to 15 mm in the case of eu- to subhedral grains in coarse-grained pegmatoidal pyroxenites. Opx commonly shows cpx exsolution lamellae parallel to (100), which are ca. 1 μm thick and spaced ca. 5 μm apart, thus up to 10 vol.% of the opx grain might be cpx. These lamellae tend to disappear towards the margins of the crystal. A strained extinction of opx is sometimes caused by bent exsolution lamellae, which might point to post-depositional deformation. Closer towards the base of the cumulate column, i.e. the base of NG2, the exsolution becomes more and more blebby, but nevertheless remains parallel to (100). The accessory euhedral chr can be enclosed by all postcumulus phases, but most commonly by pla. Opx grains with chr inclusions are relatively scarce but occur at all stratigraphic levels. Chr is very often rimmed by a thin selvage of mica or pla thus preventing a direct contact with opx. Pla forms large oikocrysts up to 10 mm enclosing older phases. It also occurs as small triangular fillings of interstices in between the cumulus opx. As in the uCZ-norites, the uCZ-pyroxenites and uppermost pyroxenites of the lCZ (to a depth of ca. 240 m) contain opx grains with ovoid pla inclusions. These pla inclusions are corroded and partially resorbed and according to Eales et al. (1990a) remnants of cumulus pla. Some of these inclusions are

rimmed by cpx exsolution rinds. Cpx is present either as oikocrysts (up to 15 mm) or as interstitial fillings apart from its occurrence as exsolved lamellae. Cumulus cpx was not found. In more evolved pyroxenites some cpx displays rims or patches of amphibole, this being evidence for interaction of cpx with late-stage fluids. Amphibole might also fill interstices in those pyroxenites. Mica is an abundant accessory or minor phase. In high-mesostasis pyroxenites mica is associated with quartz, apparently the latest phase to crystallise, thus enclosing all other phases. The quartz is clear and commonly shows no strained extinction.

3.1.5. Olivine pyroxenite and Harzburgite

Olivine pyroxenites and harzburgites sensu stricto are composed of the two cumulus phases ol and opx as major constituents. Chr is an ubiquitous accessory mineral. Pla and mica are the most abundant postcumulus phases. Jackson (1961) introduced the terms "granular" and "poikilitic" harzburgite, which have a strong genetic implication. In this work the useful distinction is also made. In olivine pyroxenites and granular harzburgites ol and opx are both cumulus phases, while in poikilitic harzburgites ol, the sole major cumulus phase, is replaced by anhedral opx forming oikocrysts with ol-remnants as cores. Strictly speaking such rocks might be regarded as dunites in terms of the textural classification used. The overall texture is xenomorphic. In chr-rich cumulates chr forms chains, probably outlining the ol-crystals before replacement (e.g. NG1-90.33). In olivine pyroxenites and granular harzburgites ol is commonly equigranular with grain sizes up to 4 mm; however, extremely fine-grained variations (ca. 0.5 mm) were also encountered. Coexistent cumulus opx is equigranular subhedral, but generally smaller in size. Ol is sub- to anhedral, often with resorption embayments or more rounded shapes.

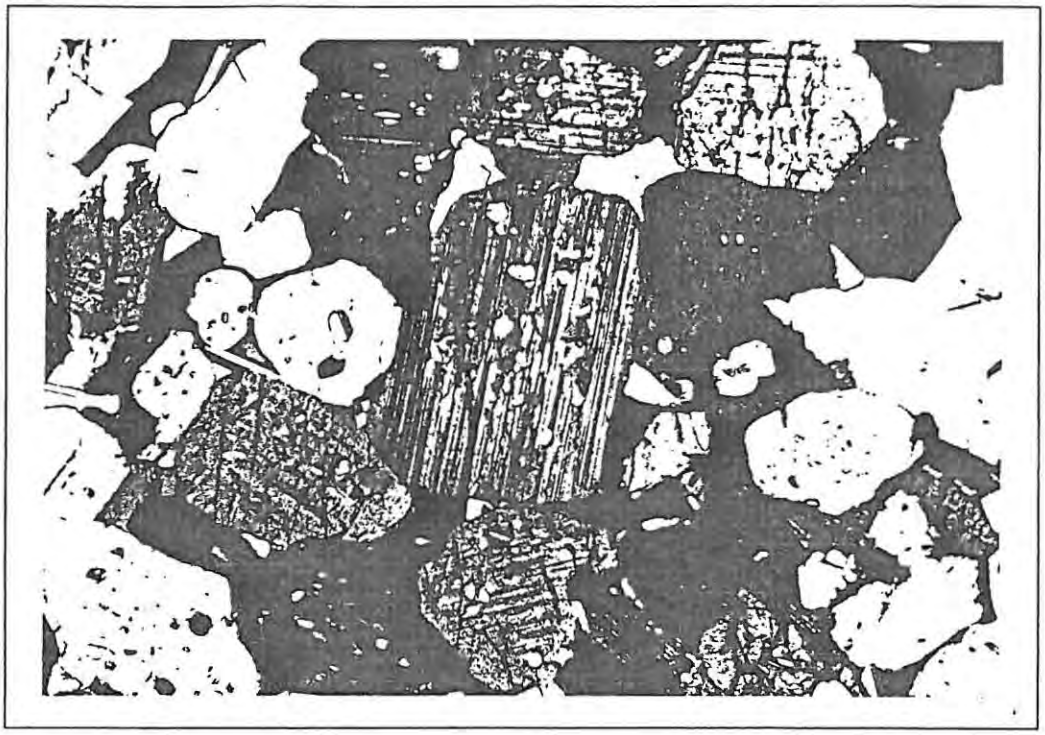

Plate 5. Pyroxenite with orthopyroxene showing numerous ovoid plagioclase inclusions, mainly concentrated in the core domains of the pyroxene grains. Sample NG3-16.20, upper Critical Zone, ca. 135 m above the MG4-chromitite. Field width 3.5 mm; crossed nicols.

Plate 6. Granular harzburgite with chromite and postcumulus plagioclase. Sample NG2-73.60, Lower Zone. Field width 3.5 mm; crossed nicols.

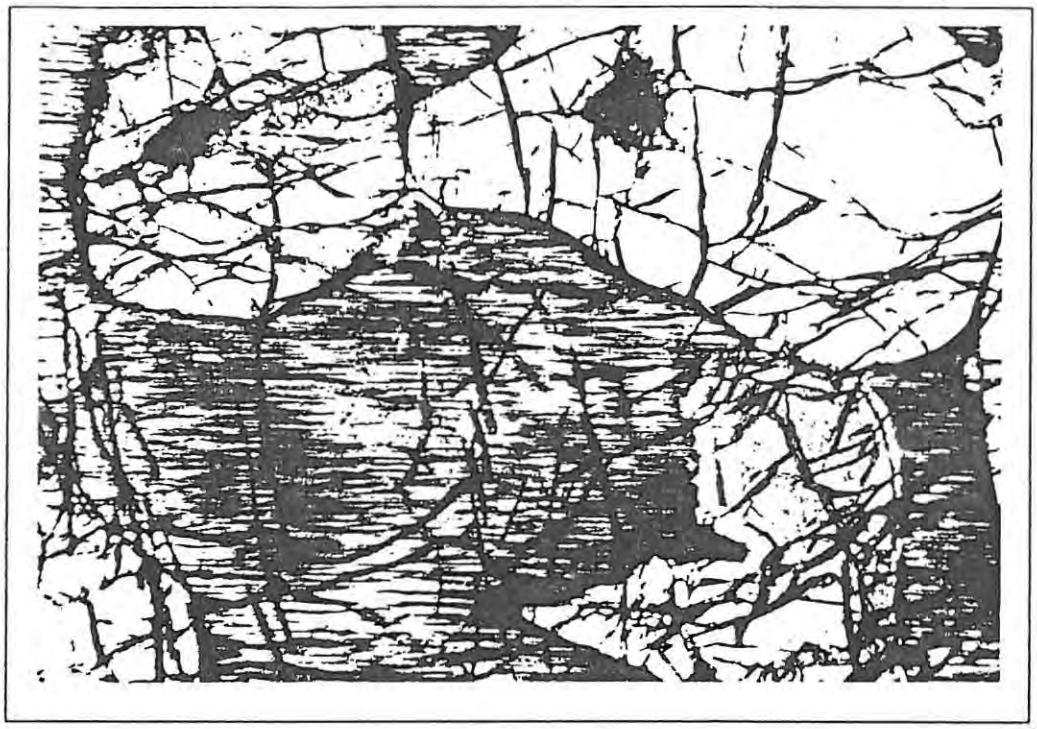

Plate 7. Poikilitic harzburgite showing embayed olivine grains enclosed in one optically continuous orthopyroxene oikocryst. Sample NG2-127.15, Lower Zone. Field width 3.5 mm; crossed nicols.

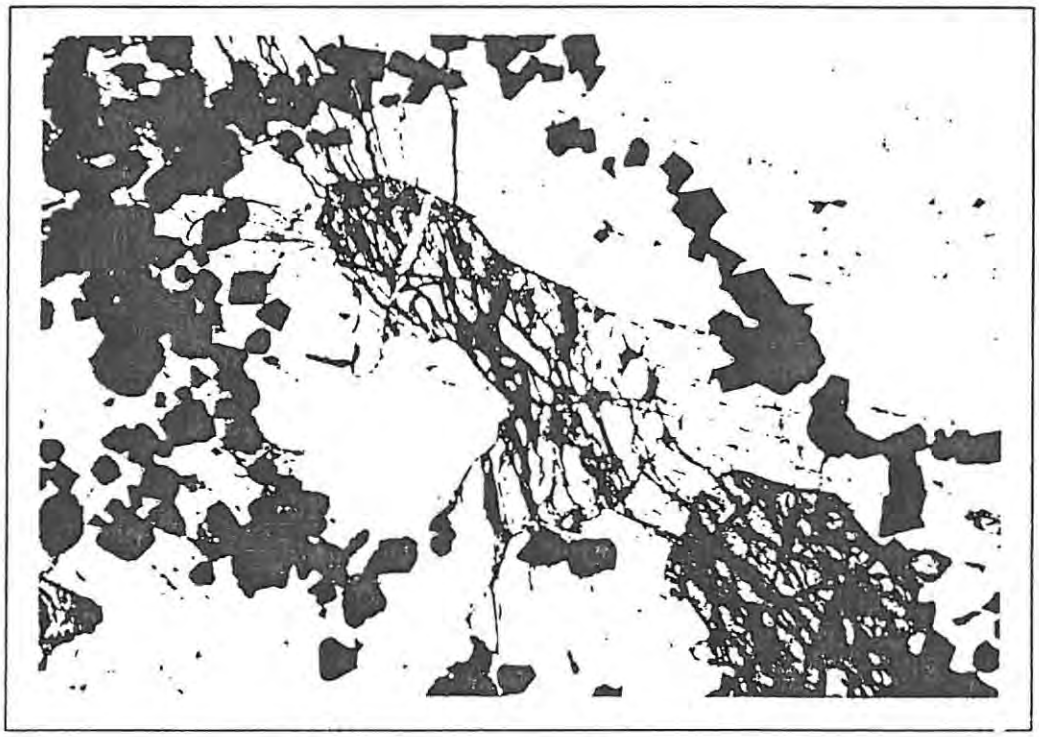

Plate 8. Chromitiferous poikilitic harzburgite showing chromite grains outlining the original shape and size of the olivine crystal. Sample NG2-241.72A, Lower Zone. Field width 3.5 mm, crossed nicols.

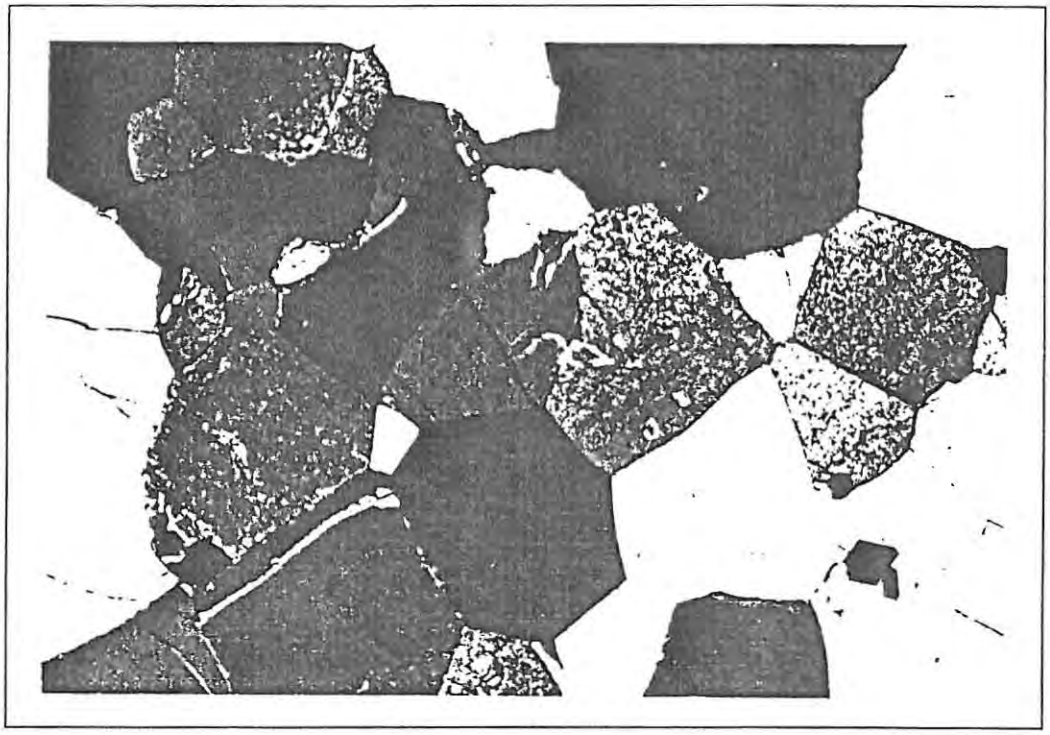

Plate 9. Adcumulate dunite with minor chromite (bottom right) showing perfectly developed triple-point junctions. Sample NG1-802.23, Lower Zone. Field width 3.5 mm, crossed nicols.

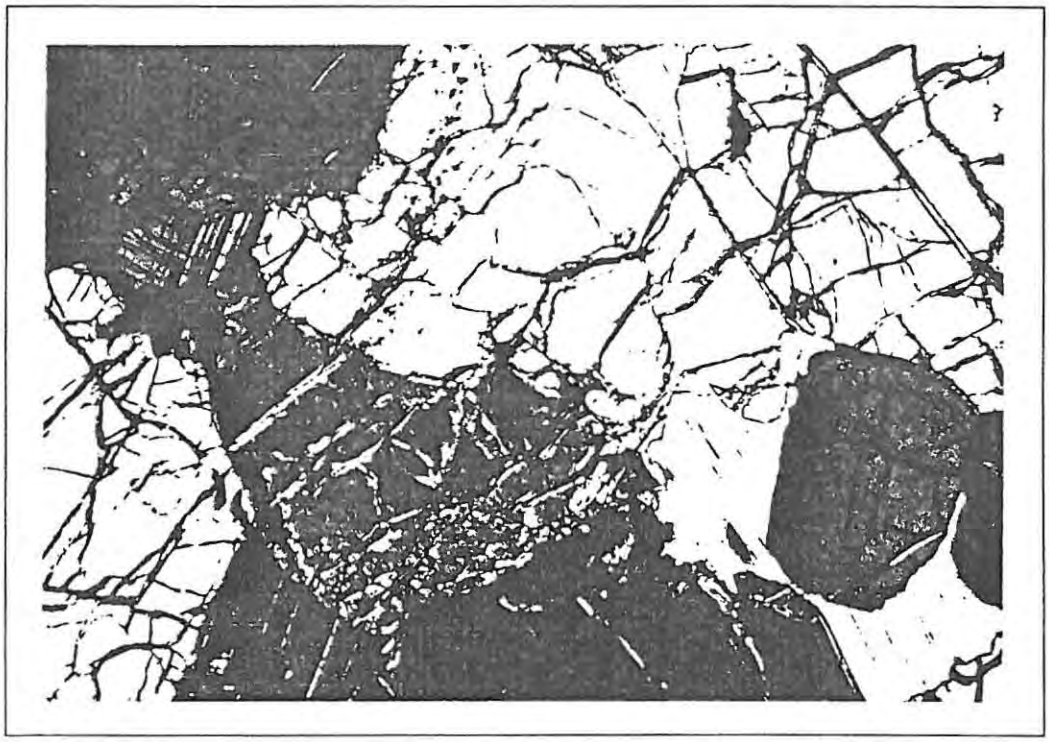

Plate 10. Dunite with postcumulus phlogopite and plagioclase. Sample NG1-818.10, Lower Zone. Field width 3.5 mm; crossed nicols.

3.1.6. Dunite

Ol is the only major cumulus phase (>90 vol.%); other cumulus phases (opx and chr) can be present in proportions totalling less than 10 % by volume. Opx, pla, cpx and mica are locally present as postcumulus minerals.

In the NG-sequence the equigranular dunites display a wide range of grain sizes (1-2 mm in adcumulate-textured and 4-5 mm in mesocumulate-textured dunites). In the latter ol is subhedral and when rounded anhedral; in adcumulates ol is polygonal, hence anhedral. The extinction is sometimes undulose indicating post-depositional deformation. Serpentinisation is the most common alteration, often limited to the immediate vicinity of an interface. Postcumulus phases occur as oikocrysts of variable size or fillings of interstices. Depending upon the proportion of poikilitic opx a gradation to poikilitic harzburgites is possible.

3.1.7. Chromitite

In chromitites chr is the dominant cumulus mineral, i.e., more than 50 vol.% of the rock is composed of chrome-spinels. The expression "massive chromitite" denotes chr as the only cumulus phase, whereas in disseminated chromitites another cumulus phase is present.

Rocks with chr as a major constituent less than 50 % by volume are labelled with the adjectival modifier "chromitiferous", or alternatively give rise to use of the prefix chr-, e.g., chr-pyroxenite.

The grain size of chr in chromitites depends greatly upon the degree of annealing. The generally small accessory grains in the silicate rocks display a size range between 0.002 and 0.4 mm, whereas in some massive layers grains can reach sizes up to 3 mm.

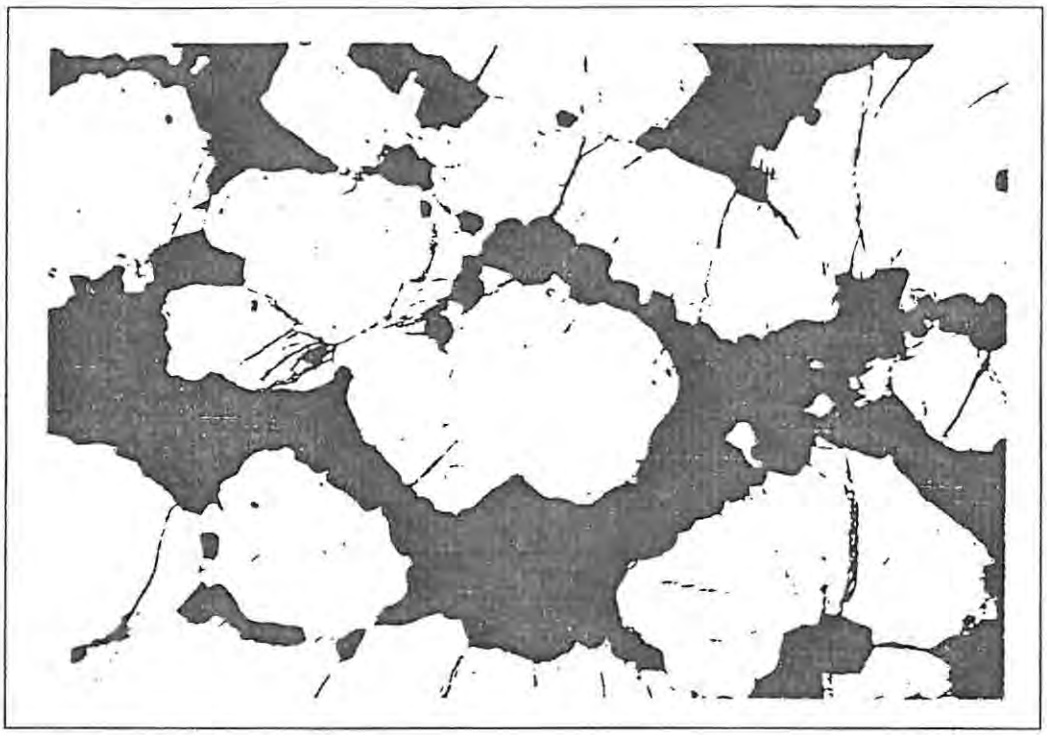

Plate 11. Chromitiferous pyroxenite with chromite grains filling the interstices. Sample NG1-597.62B, lower Critical Zone, ca. 40 below the LG1-chromitite. Field width 3.5 mm; plane polarized light.

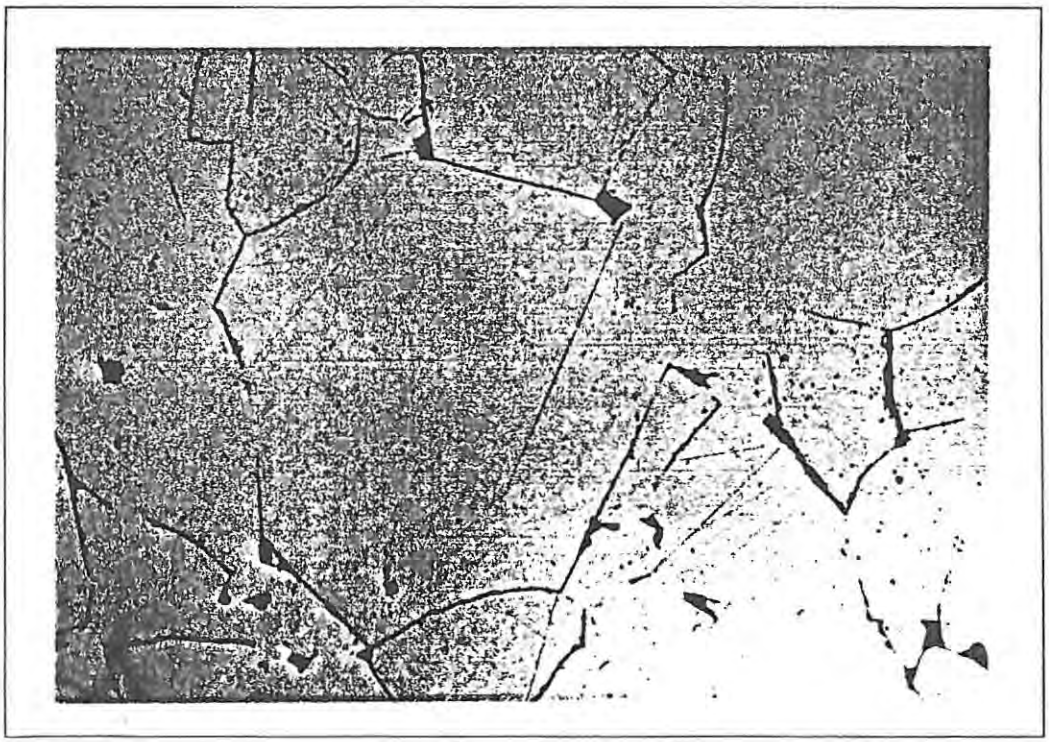

Plate 12. Massive chromitite layer with well-developed triple-point junctions. The dark grey silicate phase (top middle, bottom right) is orthopyroxene. Sample NG1-609.47C, lower Critical Zone, ca. 60 m below the LG1-chromitite. Field width 2.2 mm; plane polarized reflected light.

Chr enclosed in silicate phases in the massive layers is also smaller in size, which might be due to early encapsulation preventing annealing. In well annealed areas triple-point junctions and polygonal grain shapes are perfectly developed. Associated silicate phases in chromitite layers might be cumulus ol (mainly in the vicinity of the LG2- and LG4-chromitites), but mostly opx. In massive chromitites postcumulus silicates (opx, pla) may form large oikocrysts sometimes giving the layer a mottled appearance. The MG-chromitites contain higher proportions of postcumulus phases, and hence are generally not as well annealed as LG-chromitites. Mica might be present as a further postcumulus phase.

3.2. Modal Proportions

Approximately 400 thin sections (included are 126 analyses by Haikney) were analysed for modal compositions . The technique applied was a point-counting method with a traverse- and count-spacing of 1 mm; this spacing gave an average of 400 counts per thin section. The relative error for each constituent can be determined using the diagram (Fig. 6) after Van der Plas and Tobi (1965). This error greatly depends on the proportion in vol.% of the respective phase. For phases present in high proportions the possible error is relatively small and increases with decreasing abundance. The standard deviation calculated after this equation:

$$s = \left[\frac{(p*(100-p))}{n} \right]^{\frac{1}{2}}$$ where p = modal percentage and n = points counted

is also depicted in the diagram.

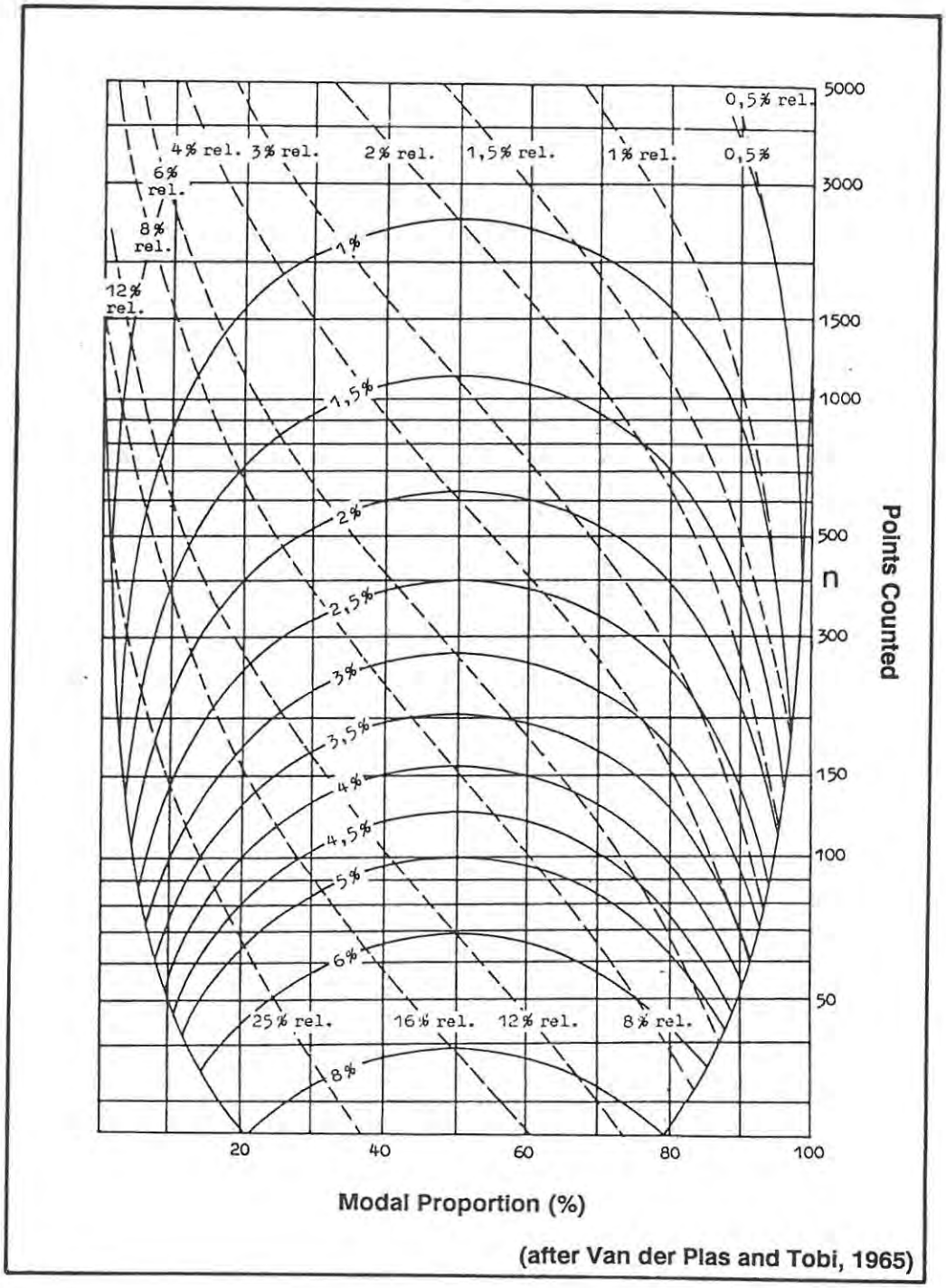

Fig. 6 Graphical error estimation of the point-counting technique applied (solid lines : standard deviation; broken lines : relative error).

Additional to the actual error of the applied technique, an error caused by the selection and cutting of the thin section has to be considered, as proportions of poikilitic phases are strongly controlled by these factors. The error is somewhat reduced by the close sample spacing, especially for NG1.

The results of the modal analyses give a first impression of variations through the sequence and compositional variations within the different rock types.

3.2.1. The Modal Compositions and Variations within the Different Rock Types

Anorthosites constitute only 1.5 m of the entire cumulate pile studied, therefore no modal analyses were performed. Chromitites were also omitted despite the occurrence of some chromitites of the uCZ associated with considerable amounts of interstitial pla.

3.2.2. Plagioclase Cumulates

Noritic rocks were intersected in three intervals. Their modal compositions were determined in seven samples. The ranges of the major constituents are, for pla 32.5 - 63.5 and for opx, 33.5 - 62.5 vol.%. Modal compositions of selected samples and the average modal composition of norite are tabulated below:

Sample:	NG3-181.70	NG3-194.74	average norite	NG2-773.60
Depth (m)	181.70	194.74		1818.60
mineral	mode in vol.%			
opx	62.5	33.5	51.6	46.7
pla	34.4	63.5	45.7	36.9
cpx	2.8	3.0	2.3	7.0
mica	0.0	0.0	0.0	6.0
quartz	0.0	0.0	0.0	2.4
chr	0.0	0.0	0.1	0.7
Total	99.7	100.0	99.7	99.7

(Note that the average modal composition was calculated omitting the gabbroic norite of the MZ (sample NG2-773.60)).

Chrome-spinel might be present as another cumulus phase but only in accessory proportions. No mica or quartz was counted in the uCZ-norites. Because of the restricted abundance of noritic rocks a further subdivision was avoided.

Sample NG2-773.60 is the only cumulus cpx-bearing norite (7.0 vol.%), which gives it a gabbronoritic character. This sample also shows apatite as accessory and minor proportions of mica and quartz (see tabulation above). Thus, its stratigraphic position at the base of the complex is also manifested by a somewhat special modal composition.

3.2.3. Pyroxenites

Pyroxenites are the most abundant ultramafic cumulates, comprising ca. 66% of the NG-sequence. 225 thin sections were point-counted to establish compositional variations through the sequence. The calculated average composition of pyroxenite is given below. Pyroxenites from the bottom of NG2 are included (but see last paragraph of this section), while chr-pyroxenites are omitted; other minerals like amphiboles, base metal sulphides (BMS) or alteration phases are also not listed:

mineral	mode in vol.%	1 standard deviation (sd)
opx	88.0	± 5.8
pla	7.2	4.6
cpx	2.2	2.1
mica	0.8	1.3
quartz	0.5	1.2
chr	0.4	1.1
ol	0.4	1.6
Total	99.5	

The average sum of all postcumulus phases is 10.7 vol.% ± 5.6. The proportions of opx are surprisingly uniform . Apart from four samples close to the base of the sequence and two other samples (NG3-28.62 and NG1-29.80) the sum of the postcumulus phases never exceeds 25.0 vol.%, thus orthocumulate-textured pyroxenites are very rare throughout the sequence. Adcumulate pyroxenites, with less than 7.0 vol.% postcumulus material, are also very rare. The majority of the pyroxenites show a sum of the modes of postcumulus phases in a range between 10 and 20 % by volume and are thus mesocumulates. Pla is by far the most abundant intercumulus phase, followed by cpx, mica and quartz. However, only a few samples can be prefixed with "feldspathic". Sample NG1-61.71 is characterised by an unusually high amount of quartz (9.9 vol.%). Ol and chr are minor to accessory cumulus phases. Mica ranges from 0.2 to 7.7 vol.%.

The pyroxenites close to the base of the complex, starting ca. 30 m above the bottom of NG2, differ significantly from the overlying opx cumulates. They are characterised by unusually high contents of pla, cpx, mica and quartz. Rutile is also present in these samples. Textural features and juxtaposition to xenoliths and possibly the floor sequence rocks suggest that these rocks were relatively quickly cooled compared to the cumulates in stratigraphically higher positions. This zone, which includes the ol-rich rocks and the gabbroic norite at the base, is therefore regarded as the **Marginal Zone** of the NG-sequence.

3.2.4. The Olivine Cumulates

Olivine-rich rocks can be subdivided into four groups: a) olivine pyroxenites, b) granular harzburgites, c) poikilitic harzburgites, and d) dunites. However, for simplicity and clarity these four lithologies will be treated as one group (ol-rich cumulates) in most of the diagrams.

The olivine pyroxenites (n=36) display a wide range of modal compositions. Ol is present in proportions between 39.5 and 10.9 vol.%. Modal opx varies from 40.4 to 81.8 % by volume. The amount of pla is very variable, but only three samples can be termed as feldspathic olivine pyroxenites (NG1-118.87, NG-241.55B and NG2-772.36). Cpx is present in proportions up to 12.6 vol.%. Mica and chr are mostly accessory or minor constituents. The average composition of olivine pyroxenite is:

mineral	mode in vol.%	sd
ol	28.3	± 13.2
opx	60.6	15.2
pla	3.9	3.9
cpx	2.8	3.5
chr	3.2	4.5
mica	0.6	1.5
Total	99.4	

Granular harzburgites are not very common. None of the point-counted samples (n=14) showed more than 7.6 vol.% pla. Only two samples did not display any mica. Cpx and chr are present in all thin sections examined apart from samples NG2-198.85, NG2-200.50 and NG2-398.65. The ol fraction varies from 40.2 to 65.8 vol.%, and opx ranges from 18.6 to 54.7 vol.%.

The average composition is:

mineral	mode in vol.%	sd
ol	52.9	± 8.7
opx	38.6	9.9
pla	3.9	2.1
cpx	2.3	1.8
chr	1.5	1.4
mica	0.4	0.3
Total	99.6	

Poikilitic harzburgites (n=44) are very similar in their general modal composition, but here opx appears, on textural grounds, to be a postcumulus phase. The average composition of this rock type is:

mineral	mode in vol.%	sd
ol	67.8	± 10.7
opx	23.5	12.0
pla	3.0	2.7
cpx	3.0	4.6
chr	1.8	2.7
mica	0.6	0.7
Total	99.7	

Finally, dunites should have modal ol proportions greater than 90 % by volume, i.e. no other cumulus phase exceeds 10 vol.%. Thirty four samples were analysed and yielded the following average composition:

mineral	mode in vol.%	sd
ol	86.5	± 9.2
opx	2.6	3.3
pla	4.1	3.7
cpx	2.2	2.9
chr	1.2	0.9
mica	1.0	1.5
Total	97.6	

(Note that the lower total is caused by a generally higher degree of alteration.)

The 86.5 vol.% of ol for all phases recalculates to 98.6 vol.% of the cumulus phases (ol and chr) and thus justifies the use of the rock name. Only three samples displayed more than 10 vol.% pla and are therefore feldspathic dunites (NG1-95.00, NG1-118.00 and NG1-787.00). An interesting feature is the slightly but consistently higher amount of mica in dunites compared with all other rock types.

3.2.5. The Modal Proportions versus the CIPW-norm

To verify the quality of the point-counting technique a comparison with normative compositions calculated by a CIPW-norm program based on the procedures of Kelsey (1965) was done (n=89). Fig. 7 shows the results of this comparison for the major phases opx and ol and the minor and trace minerals pla and chr. The correlation coefficients (ccs) are 0.944, 0.951, 0.912 and 0.742, respectively. The following equations were derived by linear regression:

$$opx_{PC} = 1.03\ opx_{CIPW} + 4.89 \quad \text{for opx}$$

$$ol_{PC} = 0.92\ ol_{CIPW} - 1.20 \quad \text{for ol}$$

$$pla_{PC} = 1.05\ pla_{CIPW} - 3.48 \quad \text{for pla}$$

$$chr_{PC} = 1.60\ chr_{CIPW} - 1.01 \quad \text{for chr,}$$

wherein the subscripts PC and CIPW denote the point-counted modes and CIPW-norms, respectively. It should be noted that the norm overestimates pla because the Al contained in opx and mica is calculated as feldspar, and underestimates opx because all Cr is assigned to chr and all Al to pla. Correlation after recalculation of vol.% to wt.% does not change the regression equations considerably.

The total amount of postcumulus material, excluding mica because of its non-normative character, yielded a correlation coefficient (cc) of 0.805 for the expression $post_{PC} = 0.94\ post_{CIPW} - 2.87$.

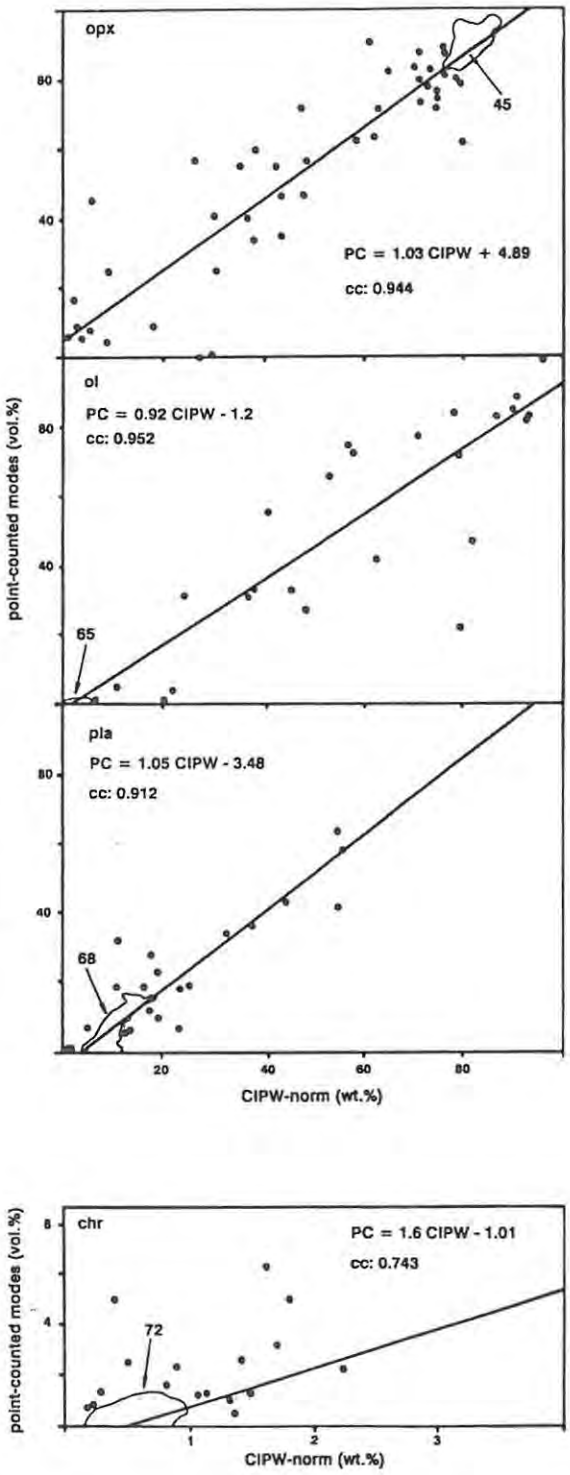

Fig. 7 Plot illustrating the correlation between modes (vol.%) and CIPW-norms (wt.%) with calculated least-squares regression lines.

Only cpx displays no relationship, which is probably due to the postcumulus exsolution in the opx. In the point-counting technique no distinction could be made between host mineral or exsolved lamellae because of the very small width of the latter, i.e., only clearly distinguishable exsolution blebs and poikilitic minerals were counted, but the CIPW-norm accounts also for the proportion of exsolved cpx lamellae. The correlation of chr was expected to be poor but is nevertheless surprisingly good despite there being no correction for the amount of Cr_2O_3 in the lattice of the pyroxenes in the CIPW-norm program.

The good correlations for the major cumulus constituents and pla allow estimates of major element compositions of samples to be made, even where only their modal compositions by point-counting and mineral compositions by electron microprobe analysis are available.

3.2.6. Variations of Modal Compositions with Stratigraphic Height

The compositional variations through the sequence are briefly described here. Fig. 8 illustrates the modal variations with stratigraphic height. The diagram clearly depicts the remarkably uniform modal composition of the pyroxenites. The proportions of opx and pla mirror each other, thus demonstrating the antipathetic behaviour of the two major components of the pyroxenites. Through the sequence two intervals can be distinguished:

a) **interval I** comprising the cumulates up to the level of the uppermost, thick, ol-rich unit below the LG1-chromitite, and b) **interval II** the remainding rocks of the NG-sequence above this level . Interval I is characterised by multiple deflections caused not only by variations in pla proportions but also by variable abundances of ol. An overall slight increase in opx proportions upwards with a consequent decrease in modal ol and pla might be also present. Interval II, however, shows a subtle general decline in modal opx, while the increasing proportions of pla are more prominent. Minor and accessory phases (not depicted in Fig. 8)show wide scatter of absolute values, but overall abundances of chr and quartz are greater in interval II, while mica seems to be present in greater proportions in interval I. Ol is conspicuously more concentrated in interval I, whereas only four thin sections of pyroxenites in NG1 were found to contain ol.

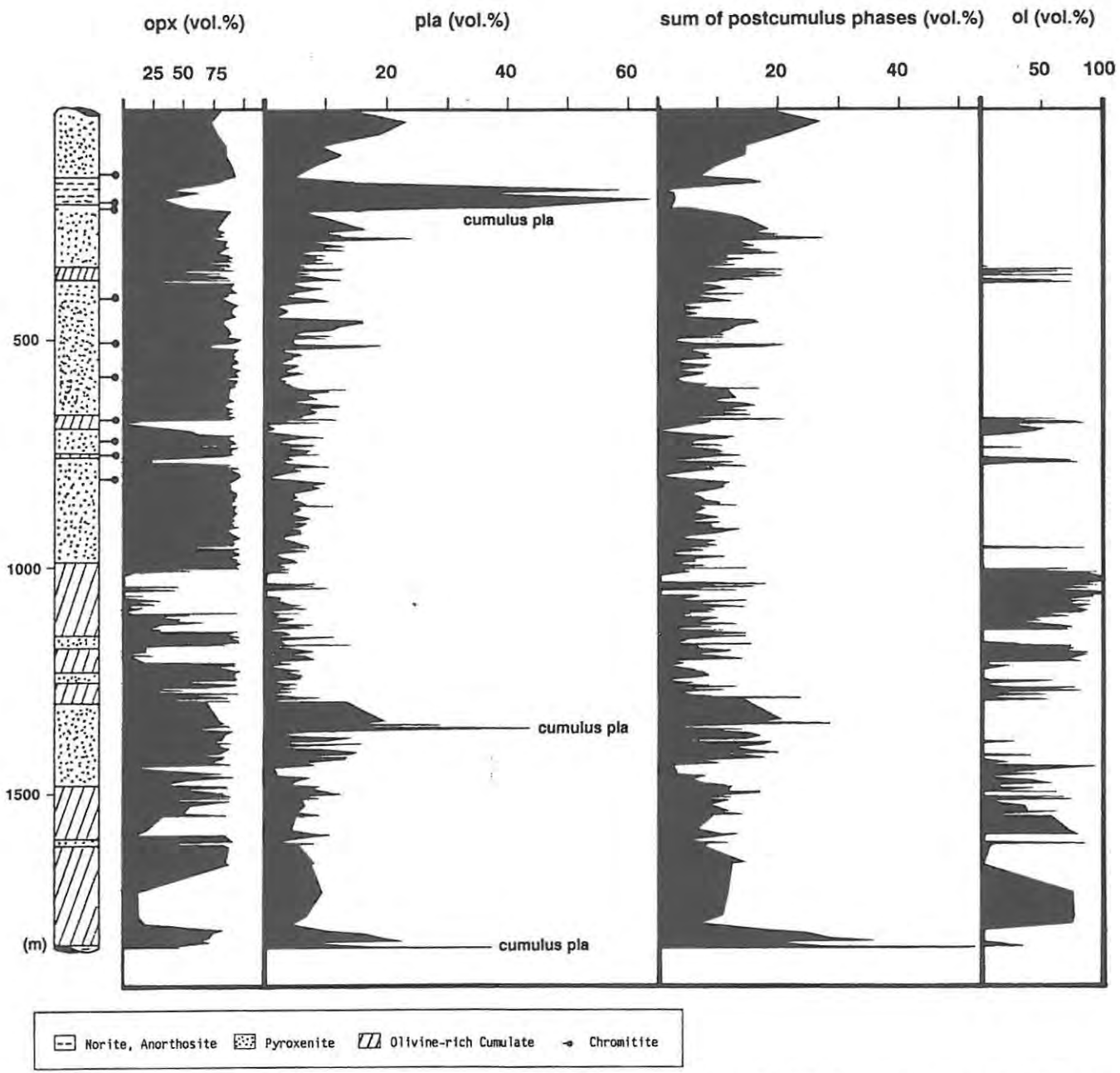

Fig. 8 Modal proportions of orthopyroxene, plagioclase and olivine through the NG-sequence.

Scrutiny of the modal pla and opx variations with height reveals major and minor deviations from the general trends described above . A major deflection can be observed in the middle part of interval I. This limited variation pattern reflects the development of a thick pyroxenite package with the anomalous leuconorite in an otherwise ol-dominated sequence and hence demonstrates superimposed, limited second order variations. A similar but less pronounced deviation occurs at the top of interval II up to the level of the MG4-chromitite.

3.2.7. Discussion and Conclusions Concerning the LZ - CZ Boundary

The variations of modal composition of pyroxenites in the NG-sequence give a first impression of cyclicity in the sequence. Although the point-counting technique applied spans theoretically a wide error range, the comparison with CIPW-norms shows the validity of the modes. Therefore the modal compositions can be used to demonstrate general developments in the magma chamber, now manifested in the rocks.

Cameron (1978, 1980) defined the base of the CZ in the eastern compartment of the BIC by a distinct increase in postcumulus pla in pyroxenites (or bronzitites) of his Upper Bronzitite unit. The first chromitite layer is positioned above this horizon. He describes the contact as a 30 m-wide zone, in which more feldspathic pyroxenites are interlayered with feldspar-poor pyroxenites in units of 1 m thickness. His critical parameter, the proportion of postcumulus pla, increases from a value of 2.6 vol.% in the Upper Bronzitite (LZ) to more than 6.0 vol.% in CZ-pyroxenites.

If the criteria of Cameron (op.cit.) are applied to the NG-sequence, a clear boundary cannot be detected. Moreover, pyroxenite packages fitting in both ranges as defined by him can be found throughout the entire sequence. Therefore, the boundary between LZ and CZ should be redefined. In the light of the findings in the present study, the CZ in the NG-sequence will be taken to commence with the monotonous pyroxenite package above the uppermost thick ol-rich unit as in Eales et al. (1990b). Thus, the above-mentioned interval I comprises the MZ and LZ and interval II the lower part of the Critical Zone. This interface should be easily located throughout the whole complex and is proposed here as the logical LZ-CZ boundary. In following chapters the new subdivision will be supported by geochemical reversals associated with this stratigraphic position.

TABLE 2 Average Modal Compositions in different Stratigraphic Intervals

Lithology:	pyroxenite				ol-pyroxenite		granular poikilitic harzburgite				dunite	
Stratigraphic Interval:	uCZ	lCZ	LZ	MZ	lCZ	LZ	lCZ	LZ	lCZ	LZ	lCZ	LZ
vol.%												
pla	12.9	6.3	8.1	15.2	3.4	3.5	2.7	4.4	1.8	3.0	9.1	3.3
cpx	2.8	2.2	1.8	6.0	4.1	2.1	1.8	2.4	1.7	3.2	1.9	2.4
opx	83.8	89.5	87.4	72.9	57.6	66.6	35.8	38.5	31.2	26.5	2.5	2.7
ol	0.0	0.0	1.2	0.6	29.0	26.2	57.8	52.8	63.2	65.0	84.3	89.4
chr	0.1	0.8	0.2	0.2	4.8	1.3	1.4	1.5	1.6	1.7	1.3	1.2
mica	0.3	0.6	0.9	3.8	1.1	0.3	0.5	0.4	0.5	0.6	0.9	1.0
quartz	0.1	0.5	0.3	1.3	0.0	0.0	0.0	0.0	0.0	0.0	0.0	0.0
Recalculation into wt.%												
pla	10.5	5.1	6.6	12.6	2.6	2.8	2.1	3.5	1.4	2.4	7.3	2.6
cpx	2.7	2.1	1.7	5.9	3.8	2.0	1.7	2.3	1.6	3.0	1.8	2.2
opx	86.3	90.7	89.4	76.2	56.9	66.7	35.8	38.6	31.2	26.5	2.5	2.7
ol	0.0	0.0	1.2	0.6	28.7	26.3	57.8	53.0	63.1	65.0	85.6	89.7
chr	0.2	1.2	0.3	0.3	7.1	2.0	2.1	2.3	2.4	2.6	1.9	1.9
mica	0.3	0.5	0.8	3.3	0.9	0.2	0.4	0.3	0.4	0.5	0.8	0.9
quartz	0.1	0.4	0.2	1.1	0.0	0.0	0.0	0.0	0.0	0.0	0.0	0.0
standard deviation:												
vol.%												
pla	5.6	3.7	5.3	5.2	2.9	2.5	1.7	2.2	1.8	2.7	4.0	3.2
cpx	1.4	2.0	1.8	1.7	4.5	2.2	0.8	1.8	3.9	4.8	1.8	3.0
opx	6.0	4.8	5.3	5.9	9.0	11.0	0.9	10.5	18.7	17.3	3.4	3.4
ol	0.0	0.2	2.5	1.4	5.1	10.6	1.9	9.0	18.3	16.9	9.9	9.5
chr	0.3	1.4	0.5	0.3	5.9	1.0	0.9	1.4	1.7	2.5	0.9	1.0
mica	0.7	1.1	1.3	1.7	2.2	0.4	0.5	0.3	0.7	0.6	1.3	1.7
quartz	0.3	1.2	1.0	1.1	0.0	0.0	0.0	0.0	0.0	0.0	0.0	0.0
n	8	160	65	6	11	17	2	13	9	40	6	28

Notes: 1) all modal proportions in vol.% are recalculated to 100 %

2) only one sample of pyroxenite in the uCZ (NG3-153.15) shows chr, mica and quartz

3) only one sample of pyroxenite in the MZ (NG2-763.45) shows ol

4) densities used to calculate wt.% modes are:

pla 2.7; cpx 3.2; opx 3.4; ol 3.4; chr 5.1; mica 2.8; quartz 2.7

(source: Deer, Howie and Zussmann, 1966)

5) n: number of samples

3.2.8. The Average Modal Compositions of the MZ, LZ and CZ

In Table 2 the average modal compositions of the different lithologies for the individual zones are summarised. Significant findings are:

a) apart from MZ-pyroxenites, all pyroxenites have similar modal compositions;

b) uCZ- and MZ-pyroxenites display higher amounts of modal pla;

c) cpx is present in all zones but is more common in the MZ-rocks;

d) LZ-lithologies have generally higher proportions of ol;

e) accessory chr is most abundant in the lCZ-lithologies.

3.3. Grain Size Measurements

Pyroxenites of the lCZ were analysed for grain size. Variations in grain size will be put into context with textural, geochemical and stratigraphic parameters.

The accuracy of grain size determinations in thin sections is always debatable and depends greatly not just on the actual grain size, but also on grain form, grain orientation and effects of orientation and position of the thin section cut. Therefore, the applied procedure does not try to determine absolute grain sizes, which is difficult for every hardrock type (some problems encountered are discussed in Textoris (1971) and Tucker (1988)) but the numbers resulting from the technique used reflect at least relative differences in grain sizes, and demonstrate distribution and variations through the sequence of NG1.

3.3.1. Technique

In each of the selected thin sections (n=71) 50 large, eu- to subhedral opx crystals were measured along regular traverse intervals. Minimum and maximum diameters of each selected grain were determined and averaged. These averages were grouped into ten classes and the median value (50 % line of the cumulative frequency curve) was read. For simplicity this value is called "grain size". A similar technique was used by McDonald (1967) in his study of the ICZ at Ruighoek.

Estimation of possible errors during the actual measurement is difficult because of factors such as the definition of grain boundaries, etc.. The final total error, however, depends upon the steepness of the cumulative frequency curve at the 50 % line and therefore the range of error can be gauged by the reader by referring to some selected cumulative frequency curves (Fig. 9).

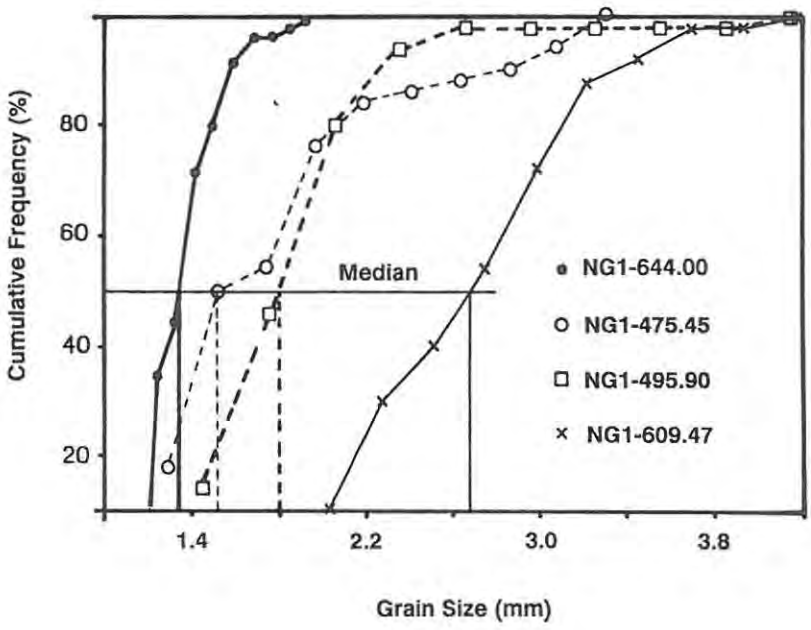

Fig. 9 Selected cumulative frequency curves of grain size determined by measurements under the microscope.

3.3.2. Grain Size Variations versus Stratigraphic Height

In Fig. 10 the size distribution relative to stratigraphic height is shown. The following features can be observed: a) the determined grain sizes vary considerably within limited intervals, b) larger grain sizes (above 2 mm) occur generally in two stratigraphic positions of which one is approximately in the central portion of intervals sandwiched between two chromitite layers (e.g. between the LG6- and LG7-chromitites and above the LG4-chromitite), while the other is associated with a lithological interface (e.g. in the pyroxenites just below the LG6- and LG7-chromitites), and c) a general trend through the sequence is not apparent.

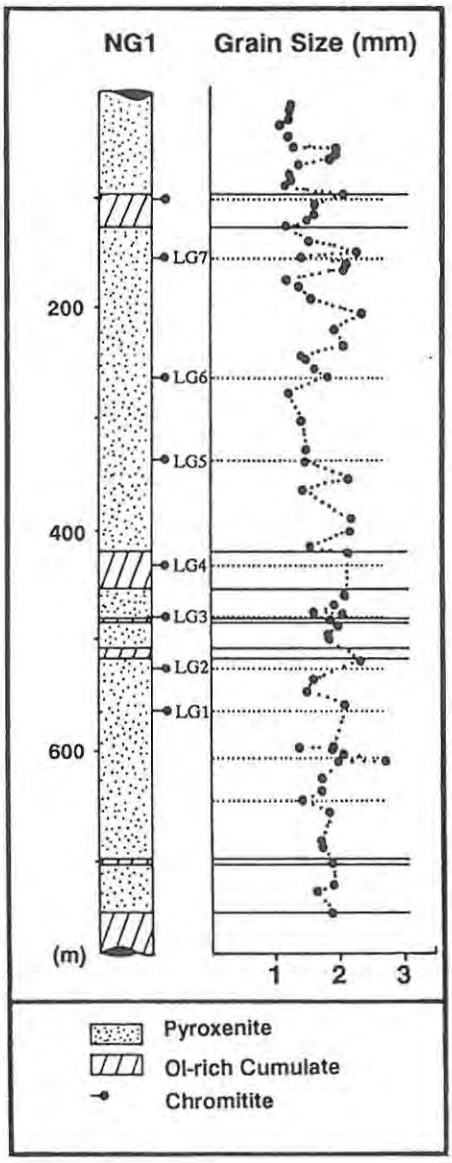

Fig. 10 Grain-size variations of orthopyroxene (for definition see text) through the lCZ of NG1.

The range of grain size extends from 1.04 to 2.68 mm, and significant size variations can occur over cm-ranges as illustrated below:

Sample	Grain size (mm)
NG1- 55.40	1.28
NG1- 56.00	1.92
NG1-597.62	1.36
NG1-597.77	1.86
NG1-609.47	2.68
NG1-609.68	1.97

3.3.3. The Grain Size in Relation to Textural and Geochemical Parameters

Fig. 11 shows the modal compositions and selected whole-rock data plotted against the grain size distribution.

The relationship of grain size and mineral geochemistry ($Mg\#_{opx}$) is shown below:

Sample	Grain size [mm]	$Mg\#_{opx}$
NG1- 55.40	1.28	0.832
NG1- 56.00	1.92	0.819
NG1-148.20	2.25	0.828
NG1-152.20	1.38	0.846
NG1-158.20	2.12	0.832
NG1-163.27	2.06	0.846
NG1-262.17	1.80	0.817
NG1-277.25	1.20	0.830
NG1-338.45	1.45	0.852
NG1-353.40	2.10	0.844
NG1-364.25	1.40	0.851
NG1-390.60	2.14	0.851
NG1-414.85	1.50	0.868
NG1-500.50	1.80	0.861
NG1-519.26	2.28	0.852

In each of the seven cases tested, higher $Mg\#_{opx}$ are associated with finer grain sizes.

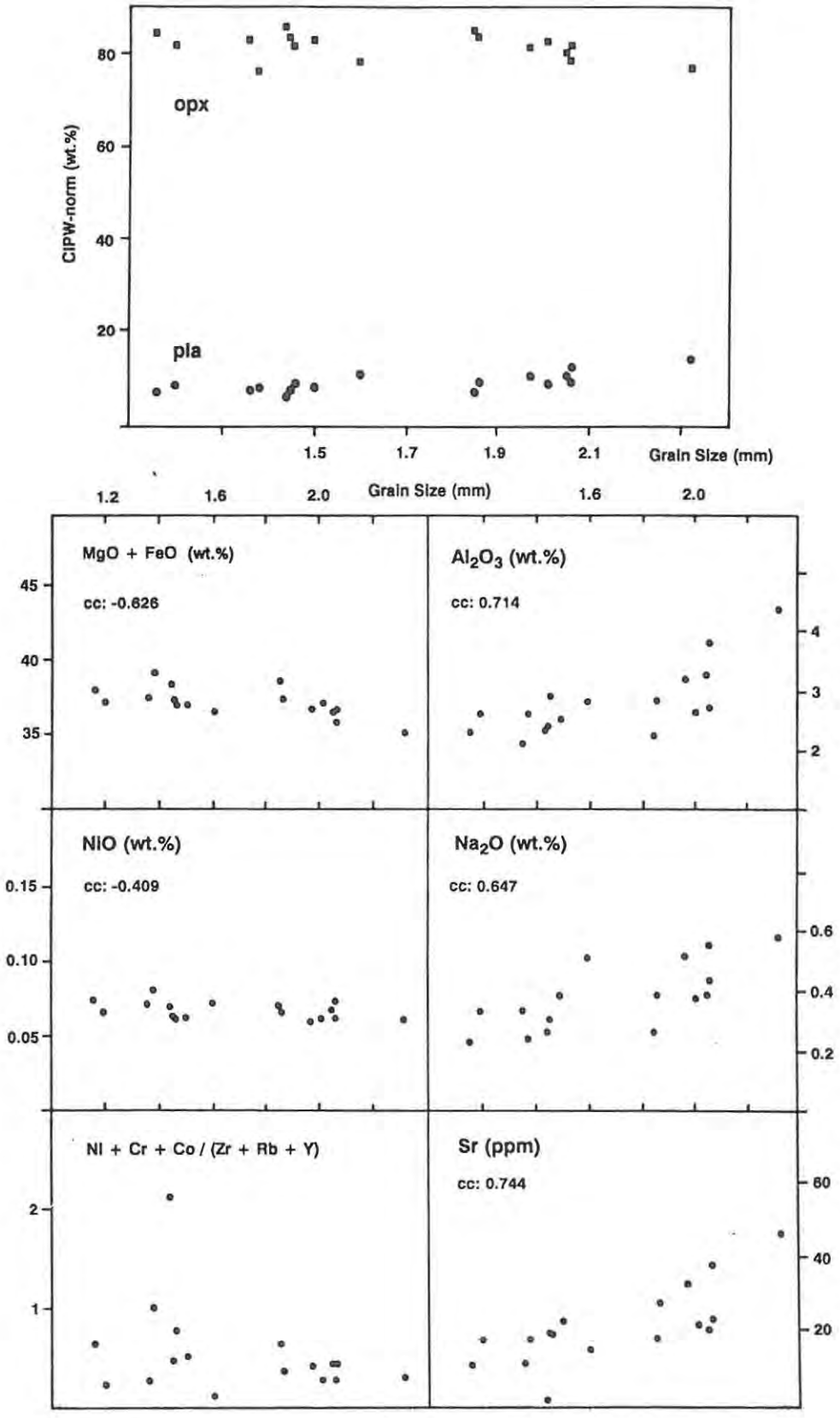

Fig. 11 Selected geochemical parameters plotted against grain size.

Though the correlations in direct variation diagrams of Fig. 11 are poor two conclusions can be drawn: a) the grain size has a slight negative relationship with MgO + FeO, NiO and the ratio of Ni+Cr+Co/Zr+Rb+Y, i.e., the ratio compatible/incompatible trace elements, and b) finer grained rocks show lower concentrations in Al_2O_3, Na_2O and Sr than coarse-grained cumulates. The very gentle slopes for the majority of the diagrams explain the absence of a detectable correlation of norm and grain size (Fig. 11). However, subtle covariant relationships between cumulus and postcumulus phases are indicated. No correlation was found in plots of grain size versus TiO_2, Zr and Rb. However, a clear relationship can be deduced from mineral composition data within limited intervals (see above). In fine-grained pyroxenites opx displays generally higher Mg#, whilst in coarser-grained variants the Mg# is lower.

In summary, fine-grained pyroxenites are characterised by high proportions of opx (± ol and chr), small modal amounts of postcumulus material and high $Mg\#_{opx}$. Coarse-grained pyroxenites display relatively more postcumulus material (mainly feldspar) than their fine-grained variants. This conclusion is supported by textural differences between fine- and coarse-grained pyroxenites. Well-developed triple-point junctions with 120° dihedral angles and polygonisation of grain boundaries, are a significant and distinctive feature for most of the fine-grained rocks. Their content of postcumulus material is, as demonstrated above, low. In contrast, coarse-grained pyroxenites often display euhedral opx crystals embedded in a matrix of postcumulus pla; contacts between the cumulus crystals are limited and much less common than in finer-grained versions.

3.3.4. Discussion and Conclusions

Despite the large number of publications dealing with cumulate theory and resulting textures, detailed studies of grain size variations and explanations thereof are scarce. Most of the recent work (Morse, 1986; Marsh, 1988, 1989) is focused on adcumulus growth and formation of adcumulates with little or no reference to associated grain sizes.

Any crystallization process follows three basic stages: a) supersaturation and/or supercooling of the liquid, b) formation of crystal nuclei, and c) growth of the crystals (Mullin, 1961). After nucleation and initial growth of the cumulus mineral - the primary or crystallization stage of Irvine (1982) - the primary crystal will undergo postcumulus modification, including resorption (size reduction) and overgrowth (size increase). These two opposed processes can occur separately or sequentially, which means that after a grain size increase this increase might be reversed at a later stage. Resorption or reaction of crystals with the liquid can lead to complete obliteration of a primary phase. This is very often the case in poikilitic harzburgites and in chromitiferous dunites.

Rocks formed by replacement are described from the Stillwater (Hess, 1960), Duke Island and Skaergaard (Irvine, 1974, 1980) complexes. Another example of resorption is the occurrence of rounded and embayed pla inclusions with distinct resorption features enclosed in opx, found by Cameron (1982) and by Eales et al. (1990a). These postcumulus modification mechanisms make it almost impossible to assess primary grain size. However, eu- to subhedral opx inclusions in poikilitic phases are up to five times smaller than unenclosed crystals and give an indication of crystal growth subsequent to accumulation.

Bowen (1915) described a series of experiments in which a melt with crystallized ol was quenched and thin sections were made from the resulting glass. In one of these runs the thin sections revealed clear differences in grain sizes: the bottom layer was fine-grained and an upward coarsening of the crystals could be noticed. He ascribed this grain size gradient to a difference of settling velocity. Although this explanation might be dubious the fact remains that different grain sizes were encountered. Irvine (1974) described the occurrence of grain-size graded layers in the Duke Island ultramafic complex. In these layers the grain size decreases upwards, but thicker layers are generally coarser overall. The bases of graded layers are defined by abrupt increases in grain size, i.e., the coarser-grained layer overlies a fine-grained one. Deposition from currents is given by Irvine (op.cit.) as an explanation for the grading. Cameron (1969) reported an enlargement factor of three or more for untrapped crystals and described a decline of the opx/pore minerals ratio upward in the sequence. Jackson (1961) described three types of sharp vertical size changes within the Ultramafic Zone of the Stillwater complex, of which one occurs within layers of pyroxenite or other silicate cumulates without change in mineral constitution. He also found gradual increases and decreases in grain size, which are related to cycles. His observation, that earliest opx crystals in each cyclic unit are relatively fine-grained and are followed by coarser-grained pyroxenites, which are again overlain by fine-grained cumulates, is comparable to the findings of the present writer. McDonald (1967) explained the grain size variations by differences in the settling distance of the cumulus crystals; a greater settling distance would produce coarser grains because more time was available for crystal growth. Botha (1987) concluded that expulsion of interstitial melt from opx cumulates at early stages of crystallization might produce fine-grained rocks - a feature that finds some support in the present study.

In summary, investigations of grain size distributions are rare and few workers have tried to establish patterns of grain size distribution through cyclic units. Interpretation of the data is ambiguous and difficult, because most rocks do not show their primary or initial grain sizes. However, some general conclusions might clarify the situation: a) significant grain size variations occur in many layered complexes and b) some pattern of cyclicity can be observed in relation to stratigraphic positions.

Before presenting a model, some important features resulting from this study may be emphasized: a) the majority of sharp grain-size changes occur in close association with lithological breaks, but in some cycles variations are also positioned in a middle region, b) coarse-grained pyroxenites are generally more evolved, i.e. whole-rock and mineral chemistry display a more fractionated signature than the fine-grained variants, and c) fine-grained pyroxenites have more than 90 vol.% opx and many of those show well-developed polygonisation textures. The latter might contradict Marsh's conclusion (1988, p.1729) that annealing destroys the smaller crystals at the expense of larger ones.

It is proposed here that the key parameter for grain size variation is the rate of nucleation. A high rate of nucleation in the case of bottom growth, or nucleation and settling where gravitative settling is important, controlled by the degree of supercooling and supersaturation, causes a low primary porosity. This allows, after continued growth, and subsequent to accumulation and compaction, the touching minerals to anneal, but without complete recrystallization of the individual crystals. In contrast, a low nucleation rate would yield a high primary porosity, which enables the cumulus crystals to grow into the liquid-filled pore spaces, thus expelling, and in part consuming, the interstitial liquid. However, this expulsion is limited by the growth of the cumulus phases and in the case of the pyroxenites the resulting final porosity, evident in the amount of postcumulus minerals, is still very high. The level of Sr in the rock (Fig. 11) is a useful index here. Additional to the differences in the nucleation rate, a progressive enrichment in volatiles, lowering the viscosity and thus enhancing the postcumulus growth, may have been superimposed. The influence of late magmatic fluids, enriched in volatiles below layers which impede the upstreaming of interstitial liquid, might possibly have caused the development of a pegmatitic texture in response to recrystallization of an orthocumulate layer, e.g. as described for the Merensky "pegmatoid" by Barnes and Campbell (1988).

CHAPTER 4: MINERALOGY

4.1. Technique and General Comments

All mineral analyses were performed on an automated Jeol CXA-733 electron probe microanalyser using a variety of international standards as well as pure synthetic crystals for calibration. Most work on the silicate phases was done with a defocused 10 μm beam, while for the spinel analyses the beam was mostly focused (1 μm). The analytical details of operation are listed in the Appendix. Long-term machine drift was monitored by using sample NG1-74.45 as a secondary standard. No significant deviations were detected over the 3-year study period. Whole-rock data, modified by calculations taking into account modal proportions, provided a further check of machine reproducibility and precision. For the most important phases opx, chr and pla, analytical precision was tested by 10 closely spaced analyses in the core domains of the respective phases. The results are tabulated below in Table 3A, 3B and 3C. For opx the data clearly show that for the majority of elements analysed the reproducibility of the microanalyser is extremely good. Coefficients of variation, calculated as (100 * sd)/ mean concentration are in the region of 0.25 % for major components (0.22 % for Si cations in opx; 0.27 % for Si cations in pla; 0.31 % for Cr cations in chr.) but increase as absolute concentration levels decline. Accordingly, coefficients are 0.5 % - 1 % for concentrations within the range 5 - 20 wt.% (1.09 % for Fe cations in opx; 0.89 % for Ca cations in pla; and 0.55 % for Mg cations in spinel) and rise above 1 % as absolute levels approach the 1 wt.% level (1.45 for Al cations in opx; 3.78 % for Na cations in pla). At absolute concentration levels of 0.1 - 0.2 wt.%, coefficients may rise to 5 % and more (5.29 % for Mn cations in opx; 5.24 % for Fe cations in pla; and 6.81 % for Mn cations in chr). The influence of clinopyroxene (cpx) exsolution on individual analyses cannot be avoided. However, the effect is virtually limited to the element Ca. Thus, because of the variable width of the cpx lamellae under the electron beam the absolute levels of Ca in opx might show wide scatter, which is not related to primary cryptic variations, but is proportional to the percentage of the beam irradiating cpx lamellae or blebs. Hence, a somewhat artificial limit of 2.0 wt.% CaO was set during selection of superior analyses, based on the compilation in Deer, Howie and Zussman (1978), who state that in most opx analyses CaO does not exceed 1.5 wt.%.

TABLE 3A Determination of Coefficients of Variation: Orthopyroxene

Sample: NG3-163.45

Analysis no.:

	198.5	198.6	199.1	199.2	199.3	199.4	199.5	199.6	199.7	199.8	mean	sd	c.v.
wt.%													
SiO_2	55.19	55.16	54.88	54.52	55.19	54.68	54.63	55.35	54.45	54.63	54.87	0.3121	0.57
TiO_2	0.15	0.16	0.14	0.14	0.13	0.13	0.13	0.11	0.13	0.14	0.14	0.0127	9.32
Al_2O_3	1.20	1.22	1.16	1.21	1.21	1.20	1.20	1.22	1.22	1.22	1.21	0.0165	1.36
Cr_2O_3	0.44	0.41	0.48	0.47	0.48	0.47	0.51	0.49	0.50	0.49	0.47	0.0292	6.17
FeO	12.52	12.66	12.71	12.22	12.75	12.64	12.41	12.82	12.73	12.69	12.62	0.1726	1.37
MnO	0.24	0.22	0.25	0.24	0.25	0.23	0.24	0.23	0.21	0.22	0.23	0.0125	5.37
NiO	0.07	0.13	0.07	0.09	0.10	0.05	0.09	0.11	0.06	0.09	0.09	0.0222	25.44
MgO	29.18	28.87	29.26	28.68	29.37	28.93	28.99	29.42	28.94	29.05	29.07	0.2231	0.77
CaO	1.11	1.47	1.38	1.71	1.41	1.54	1.54	1.39	1.66	1.44	1.46	0.1583	10.82
Na_2O	0.01	0.01	0.03	0.01	0.01	0.03	0.03	0.02	0.04	0.02	0.02	0.0094	45.38
Total	100.11	100.30	100.37	99.29	100.90	99.89	99.77	101.15	99.96	99.99	100.17		
cations (based on 6 oxygens):													
Si	1.9632	1.9620	1.9529	1.9584	1.9533	1.9550	1.9543	1.9541	1.9482	1.9518	1.9553	0.0044	0.22
Ti	0.0040	0.0042	0.0038	0.0038	0.0033	0.0035	0.0036	0.0029	0.0036	0.0038	0.0037	0.0003	9.50
Al	0.0505	0.0510	0.0488	0.0514	0.0504	0.0504	0.0507	0.0508	0.0516	0.0513	0.0507	0.0007	1.45
Cr	0.0122	0.0115	0.0136	0.0133	0.0134	0.0132	0.0144	0.0136	0.0142	0.0138	0.0133	0.0008	6.27
Fe^{2+}	0.3724	0.3766	0.3782	0.3672	0.3775	0.3779	0.3712	0.3784	0.3810	0.3792	0.3760	0.0041	1.08
Mn	0.0074	0.0065	0.0074	0.0072	0.0074	0.0071	0.0074	0.0069	0.0064	0.0067	0.0070	0.0004	5.29
Ni	0.0021	0.0038	0.0020	0.0026	0.0029	0.0016	0.0026	0.0031	0.0018	0.0025	0.0025	0.0006	25.21
Mg	1.5472	1.5307	1.5516	1.5354	1.5492	1.5414	1.5455	1.5481	1.5435	1.5468	1.5439	0.0062	0.40
Ca	0.0423	0.0558	0.0526	0.0657	0.0534	0.0588	0.0590	0.0524	0.0637	0.0550	0.0559	0.0062	11.16
Na	0.0004	0.0008	0.0024	0.0010	0.0008	0.0018	0.0018	0.0014	0.0025	0.0016	0.0014	0.0007	45.51
Total	4.0017	4.0030	4.0133	4.0060	4.0118	4.0106	4.0104	4.0115	4.0166	4.0126	4.0097		
cationic ratio:													
$Mg\#_{opx}$	0.8060	0.8025	0.8040	0.8070	0.8041	0.8031	0.8064	0.8036	0.8020	0.8031	0.8042	0.0016	0.20

Notes: 1) $Mg\#_{opx}$: cationic ratio of $Mg/(Mg + Fe^{2+})$

2) sd : standard variation

3) c.v.: coefficient of variation

TABLE 3B Determination of Coefficients of Variation: Chromite

Sample: NG3-159.20

Analysis no.:

	177.1	177.2	177.3	177.4	177.5	177.6	177.7	177.8	177.9	177.10	mean	sd	c.v. [%]
wt.%													
TiO_2	0.87	0.92	0.87	0.88	0.89	0.91	0.89	0.88	0.90	0.88	0.89	0.0158	1.78
Al_2O_3	16.35	16.54	16.61	16.71	16.60	16.56	16.66	16.54	16.62	16.66	16.58	0.0951	0.57
Cr_2O_3	41.85	42.04	41.97	42.13	41.83	41.93	42.11	42.00	41.86	42.07	41.98	0.1022	0.24
FeO	20.98	21.19	21.09	21.45	21.12	21.09	21.24	21.16	21.24	21.33	21.19	0.1270	0.60
Fe_2O_3	9.57	9.69	9.72	9.87	10.07	9.81	9.73	9.95	9.95	9.69	9.81	0.1457	1.49
MnO	0.28	0.28	0.32	0.28	0.27	0.26	0.26	0.29	0.32	0.29	0.29	0.0193	6.77
NiO	0.14	0.15	0.14	0.11	0.16	0.14	0.16	0.15	0.16	0.16	0.15	0.0164	11.11
MgO	8.85	8.93	8.94	8.91	9.01	9.00	8.96	8.96	8.91	8.85	8.93	0.0522	0.58
Total	98.89	99.73	99.66	100.33	99.95	99.71	100.01	99.93	99.94	99.93	99.81		
cations (based on 32 oxygens):													
Ti	0.1720	0.1798	0.1701	0.1712	0.1736	0.1781	0.1737	0.1724	0.1759	0.1712	0.1738	0.0030	1.74
Al	5.0651	5.0795	5.1028	5.1029	5.0858	5.0841	5.1009	5.0702	5.0933	5.1084	5.0893	0.0140	0.28
Cr	8.6985	8.6609	8.6501	8.6299	8.5972	8.6367	8.6487	8.6370	8.6078	8.6523	8.6419	0.0267	0.31
Fe^{2+}	4.6128	4.6173	4.5971	4.6475	4.5905	4.5954	4.6151	4.6029	4.6191	4.6410	4.6139	0.0179	0.39
Fe^{3+}	1.8925	1.9000	1.9069	1.9248	1.9698	1.9228	1.9030	1.9480	1.9470	1.8970	1.9212	0.0248	1.29
Mn	0.0631	0.0615	0.0700	0.0619	0.0591	0.0580	0.0567	0.0643	0.0699	0.0643	0.0629	0.0043	6.81
Ni	0.0297	0.0318	0.0292	0.0220	0.0336	0.0294	0.0340	0.0320	0.0328	0.0340	0.0308	0.0034	11.10
Mg	3.4664	3.4692	3.4738	3.4398	3.4904	3.4954	3.4679	3.4732	3.4542	3.4318	3.4662		
cationic ratios:													
Cr/Al	1.7173	1.7051	1.6952	1.6912	1.6904	1.6988	1.6955	1.7035	1.6900	1.6938	1.6981	0.0081	0.48
$Mg\#_{chr}$	0.4291	0.4290	0.4304	0.4253	0.4319	0.4320	0.4290	0.4301	0.4279	0.4251	0.4290	0.0023	0.53
FFE	0.2909	0.2915	0.2932	0.2929	0.3003	0.2950	0.2920	0.2974	0.2965	0.2901	0.2940	0.0031	1.05
Cr/(Cr + Al)	0.6320	0.6303	0.6290	0.6284	0.6283	0.6295	0.6290	0.6301	0.6283	0.6288	0.6294	0.0011	0.18
weight ratio of metals:													
Cr/Fe	1.2450	1.2374	1.2384	1.2226	1.2202	1.2337	1.2355	1.2276	1.2206	1.2322	1.2313	0.0079	0.64

Notes: 1) sd : standard variation
2) c.v. : coefficient of variation
2) $Mg\#_{chr}$: cationic ratio of $Mg/(Mg + Fe^{2+})$
3) FFE : cationic ratio of $Fe^{3+}/(Fe^{3+} + Fe^{2+})$
4) Cr/Fe : weight ratio of Cr metal to Fe metal

TABLE 3C Determination of Coefficients of Variation: Plagioclase

Sample: NG3-208.15

Analysis no.:

	222.1	222.2	222.3	222.4	222.5	222.6	222.7	222.8	222.9	222.10	mean	sd	c.v. [%]
wt.%													
SiO_2	47.76	47.56	47.21	47.06	47.66	47.33	47.64	47.38	47.10	47.28	47.40	0.2326	0.49
Al_2O_3	33.66	33.07	33.11	32.98	33.24	33.06	32.89	32.68	33.20	33.12	33.10	0.2408	0.73
FeO	0.26	0.26	0.27	0.27	0.25	0.27	0.26	0.29	0.27	0.24	0.26	0.0133	5.02
CaO	17.41	17.05	17.23	16.79	17.07	17.18	16.84	17.23	17.03	17.25	17.11	0.1820	1.06
Na_2O	2.24	2.31	2.29	2.27	2.35	2.22	2.52	2.30	2.22	2.21	2.29	0.0869	3.79
K_2O	0.11	0.10	0.10	0.17	0.10	0.11	0.11	0.12	0.16	0.11	0.12	0.0244	20.64
Total	101.45	100.36	100.21	99.54	100.66	100.17	100.26	100.00	99.98	100.22	100.29		
cations (based on 32 oxygens):													
Si	8.6765	8.7282	8.6867	8.7076	8.7198	8.7062	8.7511	8.7369	8.6814	8.6943	8.7089	0.0236	0.27
Al	7.2071	7.1522	7.1790	7.1918	7.1659	7.1669	7.1211	7.1022	7.2116	7.1789	7.1677	0.0332	0.46
Fe^{2+}	0.0393	0.0405	0.0421	0.0421	0.0384	0.0419	0.0404	0.0441	0.0412	0.0361	0.0406	0.0021	5.24
Ca	3.3894	3.3525	3.3959	3.3289	3.3449	3.3862	3.3143	3.4046	3.3635	3.3990	3.3679	0.0301	0.89
Na	0.7904	0.8218	0.8177	0.8127	0.8338	0.7926	0.8973	0.8206	0.7916	0.7891	0.8168	0.0308	3.78
K	0.0247	0.0231	0.0225	0.0393	0.0227	0.0258	0.0259	0.0278	0.0383	0.0268	0.0277	0.0058	20.98
Total	20.1275	20.1182	20.1439	20.1225	20.1255	20.1196	20.1500	20.1362	20.1277	20.1242	20.1295		
cationic ratio:													
An	0.8061	0.7987	0.8017	0.7962	0.7961	0.8053	0.7821	0.8005	0.8021	0.8064	0.7995	0.0068	0.85

Notes: 1) sd : standard variation
2) c.v.: coefficient of variation
3) An : cationic ratio of Ca/(Ca + Na + K)

In summary, these tests defined the precision of the electron microprobe used. Hence, intra- and intersample variations greater than the determined standard deviations can be attributed to genuine compositional changes. For most of the diagrams presented later in this chapter an average composition for each mineral was calculated using 4-6 analyses of core domains only, but in fact only minor zoning patterns were detected in the ferromagnesian phases and chr (see below). This average composition is regarded as representative of the sample. However, great intrasample variability, easily detectable because of the greater sd, especially for postcumulus phases (pla), might warrant special treatment. This will be dealt with in the relevant section.

4.2. Orthopyroxene

Opx, by far the most common phase, occurs in three habits: a) as a cumulus phase in norites, pyroxenites, olivine pyroxenites and granular harzburgites, b) as a replacement or postcumulus poikilitic phase in poikilitic harzburgites and dunites, and c) as a postcumulus phase in chromitites and anorthosites.

A total of 261 samples (1653 analyses) including 26 samples (121 analyses) by Haikney (1990) was used to compile the average compositions, which are listed in the Appendix.

Zonation was constantly monitored by means of traverses from core to rim as well as by couplets of core-rim analyses of the same grain, which were selected randomly but roughly equidistantly. Selected core-rim couplets are presented in Table 4, and in Fig. 12 some of the step-by-step traverses are schematically depicted to illustrate the findings.

TABLE 4 Selected Microprobe Analyses of Core and Rim Domains of Orthopyroxene

Sample	Domain	$Mg\#_{opx}$	Cr_2O_3	Al_2O_3	TiO_2	adjacent phases
NG1-105.45	Core	0.8260	0.51	1.43	0.10	
	Rim	0.8253	0.33	0.69	0.13	opx
	Core	0.8237	0.47	1.27	0.13	
	Rim	0.8272	0.30	0.72	0.21	pla
NG1-225.90	Core	0.8275	0.47	1.07	0.10	
	Rim	0.8334	0.46	0.93	0.10	pla
	Core	0.8321	0.51	1.02	0.12	
	Rim	0.8279	0.44	0.93	0.12	opx
NG1-292.30	Core	0.8414	0.55	1.13	0.08	
	Rim	0.8426	0.55	1.13	0.10	pla
	Core	0.8409	0.51	1.07	0.07	
	Rim	0.8436	0.46	0.88	0.08	opx
NG1-469.40	Core	0.8530	0.48	0.91	0.09	
	Rim	0.8572	0.34	0.70	0.12	pla, chr
	Core	0.8565	0.51	1.09	0.02	
	Rim	0.8546	0.47	0.91	0.17	pla
	Rim	0.8584	0.47	1.00	0.15	opx
NG1-655.10	Core	0.8510	0.48	1.11	0.08	
	Rim	0.8475	0.28	0.77	0.09	mica
NG1-706.90	Core	0.8478	0.47	1.23	0.05	
	Rim	0.8485	0.46	1.06	0.11	pla
	Rim	0.8548	0.47	1.07	0.12	chr
NG2-530.95	Core	0.8695	0.46	1.22	0.10	
	Rim	0.8676	0.48	1.23	0.11	ol

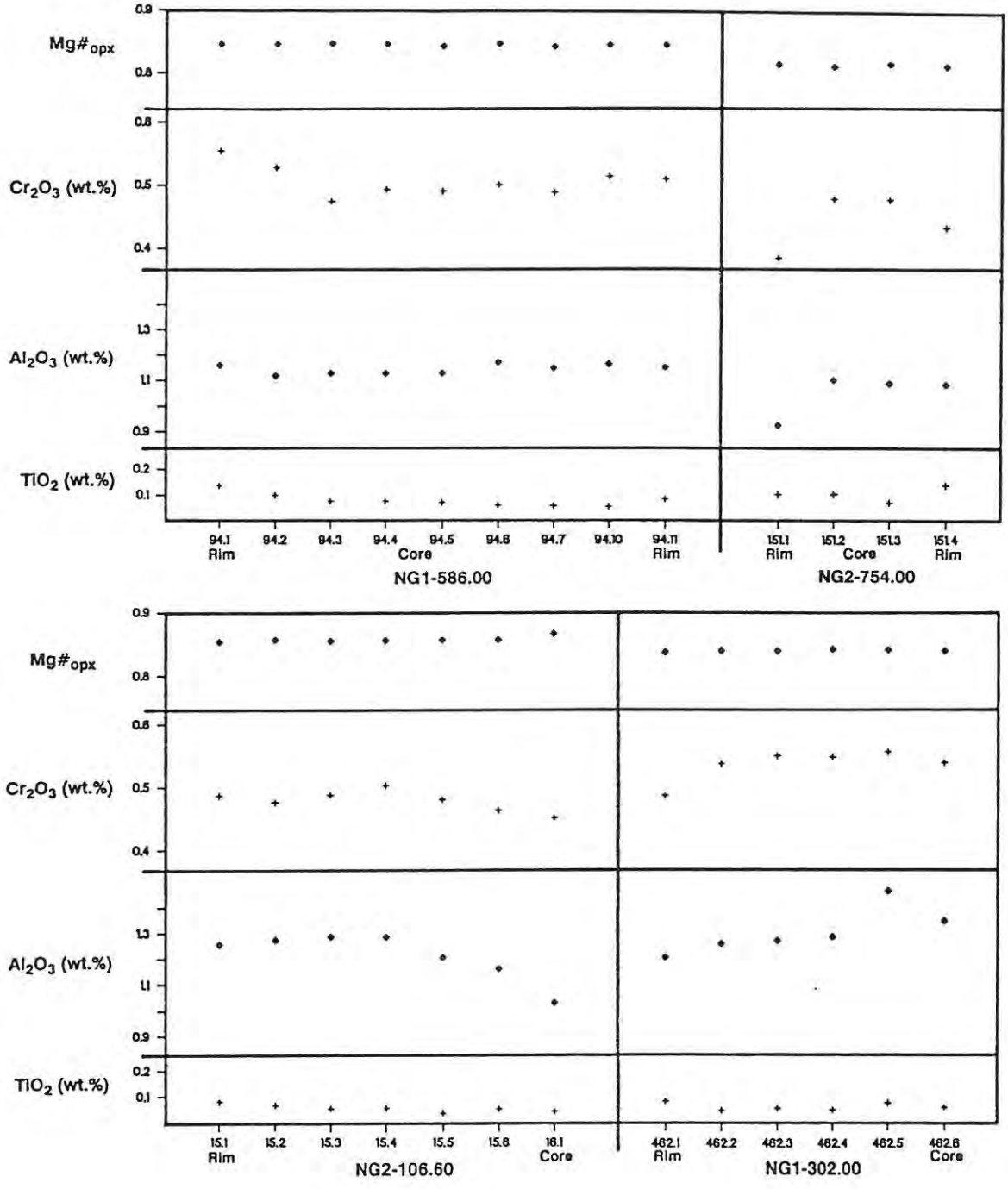

Fig. 12 Zonation in orthopyroxene

No significant zoning structures were detected with respect to $Mg\#_{opx}$, but concentrations of minor elements (TiO_2, Cr_2O_3 and Al_2O_3) might show variations due to zonation. The levels of Al_2O_3 decrease sharply in some opx grains when the margin of the mineral is approached. This effect seems to be more pronounced if the adjacent grain is a feldspar. These relationships might be attributed to three possible processes, which are able to cause such kinds of geochemical gradients: a) sudden changes in temperature or pressure (Deer, Howie and Zussman, 1978), b) subsolidus re-equilibration and c) the onset of the nucleation of other phases, thus rapidly changing the liquid composition. It is also evident from Table 4 that for the majority of the grains investigated Cr concentrations are lower in the rim domains (e.g. NG1-105.45), while Ti values show contemporaneous enrichment towards the margins. However, reversed gradients can be also found (e.g. see Cr_2O_3 in sample NG1-586.00; Fig. 12). In some MZ-cumulates (e.g. NG2-754.00) zoning structures seem to be developed. But as seen above, the Mg# remains steady, whereas the rim domains display lower values of Al_2O_3 and Cr_2O_3. Whether this zoning is due to the different cooling history of these MZ-lithologies close to the floor of the intrusion, (suggested by the more bleb-like exsolution of cpx instead of well-defined lamellae), or to one or more of the above processes cannot be decided conclusively.

Subsolidus re-equilibration or competition within late-crystallizing domains between opx and chr, pla and phlogopite is indicated in the data presented. Significant changes of opx compositions occur only in the immediate vicinity (cm-range, normally only detectable in the sample covering the interface) of the massive chromitite layers, where a substantial shift of MgO and FeO occurs (see also Table 9). Their rather exceptional compositions (Fig. 15A), expressed by their very high Mg#, pinpoint a cation exchange, which was described by McDonald (1967), Cameron (1969) and Eales and Reynolds (1986). In a later section this cation interchange will be further dealt with.

In the conventional triangle for pyroxenes (Fig. 13) the opx under study plot in a well-defined field regardless of their textural habit or stratigraphic position.

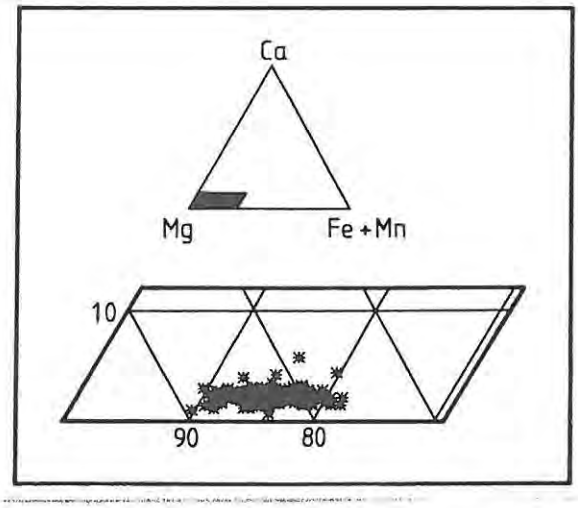

Fig. 13 Compositional range (cations) of orthopyroxene in the NG-sequence.

All samples cluster in a small area . Marginal Zone- and uCZ-opx plot towards higher FeO concentrations, whilst poikilitic and re-equilibrated opx are more MgO-rich. The ranges of the cation % are:

	Mg	Fe+Mn	Ca
cumulus opx	72.4-89.2	26.3- 9.6	0.77-3.60
poikilitic opx	80.8-87.7	10.6-14.9	1.20-4.40

Thus all opx are enstatites in terms of the new nomenclature (Subcommittee on pyroxenes, 1989). Because of the abundance of Cr (> 0.01 cations) the majority can be further classified as chromian-enstatites. The ranges of oxide concentrations are as follows:

	opx	
	poikilitic	cumulus
wt.%		
SiO_2	55.42 - 57.55	54.34 - 57.54
TiO_2	0.05 - 0.28	0.04 - 0.21
Al_2O_3	0.87 - 1.59	0.88 - 1.71
Cr_2O_3	0.16 - 0.51	0.23 - 0.60
FeO	6.95 - 9.58	6.24 - 16.72
MnO	0.16 - 0.24	0.14 - 0.32
NiO	0.02 - 0.10	0.02 - 0.14
MgO	29.68 - 33.42	26.25 - 33.40
CaO	0.63 - 2.23	0.40 - 1.85
Na_2O	0.00 - 0.11	0.00 - 0.11

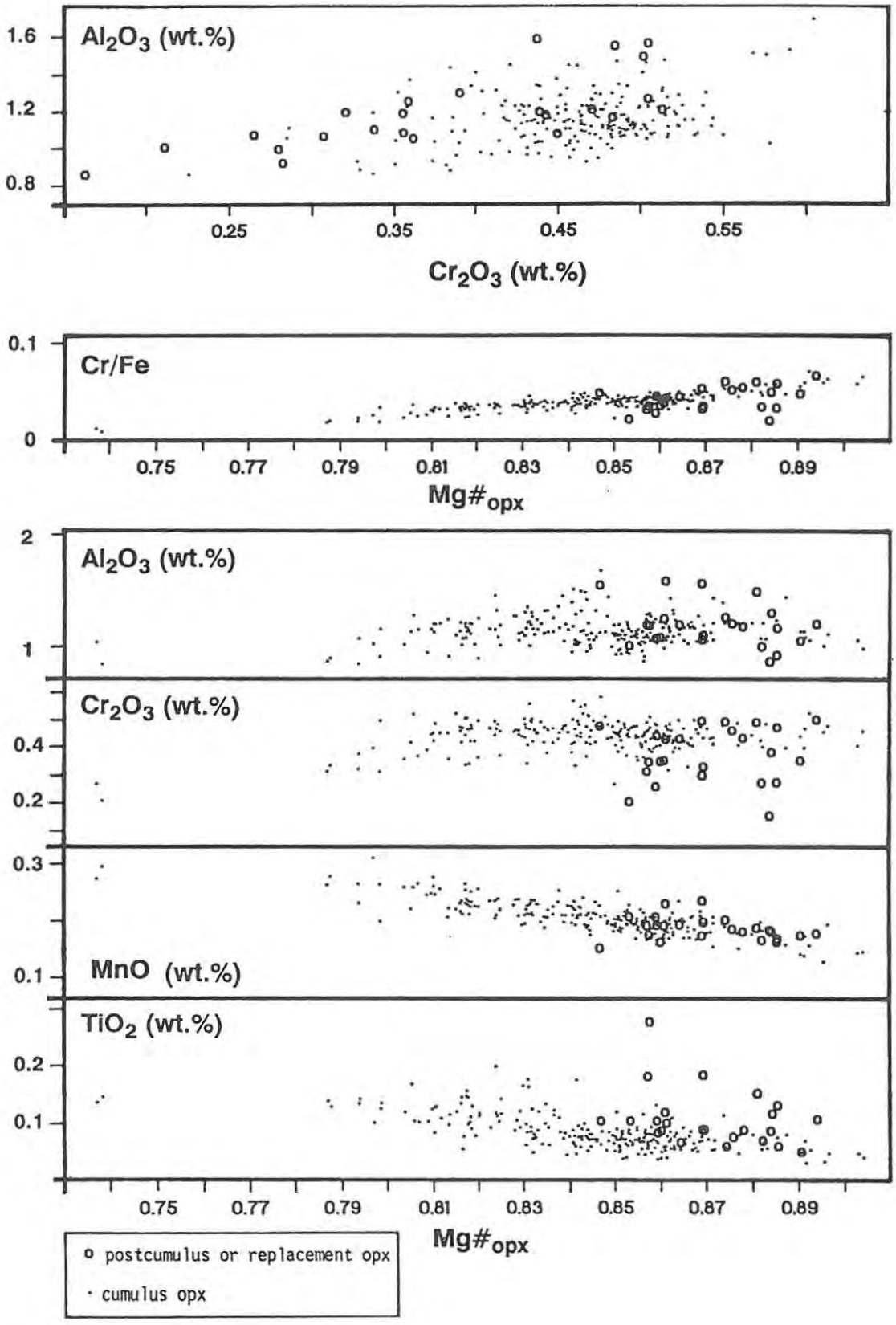

Fig. 14 Orthopyroxene mineralogy - variation diagrams (note the scale breaks).

Figure 14 shows some element concentrations and ratios plotted against the Mg# and Cr_2O_3. Levels of TiO_2 and MnO display overall trends which follow the expected fractional crystallization path. Titanium and Mn correlate positively with Fe, hence negatively with the Mg# (cc: -0.655 and -0.797, respectively). No link can be observed between Cr, Al, Ni and Na (both latter not depicted) and Mg#. However, for poikilitic opx a cc of 0.724 was obtained for the expression

$$Al_2O_3 \text{ (wt.\%)} = 1.4 * Cr_2O_3 \text{ (wt.\%)} + 0.65 .$$

In general, the interelement relationships are not very well defined for the entire opx population in the NG-sequence. The influence of other phases could be a possible explanation, but no evidence was found in diagrams plotting opx compositions versus modal plagioclase which is for the majority of the pyroxenites the most abundant postcumulus phase. Possible reasons for the observed poor correlations might be: a) cryptic variations through limited stratigraphic intervals are overshadowed by variations through the entire sequence and b) elements sensitive to fractional crystallization (Ni or Cr) might be present always at or close to saturation levels, thus no trend can be detected. However, the variations in the Mg# indicate depletion of elements during the crystallization and therefore mechanism a) seems most likely to cause the poor correlations displayed for the total population. If this is true better correlation should be yielded in limited intervals of the sequence.

Several intervals were tested and two selected ones are listed in Table 5 together with the linear regression equations with ccs. Although the ccs are still below 0.9 (apart from TiO_2 in interval A) a clearer relationship is evident. This points to linear relationships within limited intervals, which are concealed when the entire opx population is used.

TABLE 5 Correlation of some Selected Parameters of Orthopyroxene Mineralogy in Limited Stratigraphic Intervals

	Interval A	Interval B
Depth [m]:	0 to 152.00	603.40 to 705.65
Number of Samples:	7	9
	Al_2O_3 = 11.91 $Mg\#_{opx}$ - 8.49 cc: 0.829	Al_2O_3 = 6.82 $Mg\#_{opx}$ - 4.79 cc: 0.761
	Cr_2O_3 = 2.28 $Mg\#_{opx}$ - 1.45 cc: 0.525	Cr_2O_3 = 2.27 $Mg\#_{opx}$ - 1.48 cc: 0.643
	TiO_2 = -1.47 $Mg\#_{opx}$ + 1.30 cc:-0.722	TiO_2 = -0.63 $Mg\#_{opx}$ + 0.62 cc:-0.310
	Cr/Al = -1.25 $Mg\#_{opx}$ + 1.24 cc:-0.613	
	Cr/Fe = 0.28 $Mg\#_{opx}$ - 0.20 cc: 0.704	Cr/Al = 0.54 $Mg\#_{opx}$ - 0.42 cc: 0.875
	TiO_2 = -0.43 Cr_2O_3 + 0.28 cc:-0.912	TiO_2 = -0.33 Cr_2O_3 + 0.24 cc:-0.576
	Al_2O_3 = 2.57 Cr_2O_3 + 0.07 cc: 0.777	Al_2O_3 = 1.06 Cr_2O_3 + 0.57 cc: 0.419

Notes: 1) equations derived after linear regressions

2) all ratios are cationic ratios, where $Mg\#_{opx} = Mg/(Mg + Fe^{2+})$

3) oxides in wt.%

4) cc: correlation coefficient

The cryptic variations of opx through the sequence are illustrated in Fig. 15A. The most important parameter, the Mg#, ranges from 0.847 to 0.894 for poikilitic opx and from 0.737 to 0.904 for cumulus opx (including the re-equilibrated samples). By means of this ratio the sequence can be broken into 10 segments. Segments 10 - 4 of this subdivision directly correspond to segments 8 - 2 of Eales et al. (1990b), while segment 1 of the latter is now broken into segments 1, 2 and 3. In these segments the trend line exhibits a saw-tooth pattern.

Scrutiny of the turnover points shows that most segments are not defined by lithological breaks, i.e. the geochemical reversal is decoupled from the lithology, normally beneath the actual change in rock type (Teigler, 1990). Highest Mg# of non-equilibrated opx occur at the top of the LZ, and above this level a general but irregular decline is evident. The relatively high Mg# obtained from the leucocratic cumulates sandwiched between the MG3- and MG4-chromitites is noteworthy. The above-described enrichment of poikilitic opx in MgO (high Mg#) is clearly demonstrated. However, any trend initiated within thick sequences of cumulus opx is invariably extended into overlying olivine-rich cumulates.

The Cr_2O_3 levels do not show much variation throughout the sequence, but the opx in the lCZ contain slightly more Cr than opx in other zones and less variation to low levels. In the LZ the values scatter considerably. Poikilitic or replacement opx display generally lower Cr concentrations. A possible reason for this might be the crystallization sequence ol ± chr followed by opx. Due to the incompatibility of Cr within the ol lattice chr nucleation might be enhanced (as indicated by slightly higher proportions of accessory chr in the ol-rich cumulates) thus depleting the liquid more rapidly in Cr so that late crystallizing opx will have lower Cr concentrations. The highest levels of Cr were encountered in cumulus opx in the leuconorite of the LZ despite relatively low Mg#s. This enrichment might point to a modally controlled relationship, i.e. the partition coefficient of Cr increases with decreasing modal proportion of cumulus opx. However, this conclusion is tentative and the subject is beyond the scope of this study.

Average compositions in successive stratigraphic zones (Table 6) support the differences derived from Fig. 15A. The average cumulus LZ-opx contains 0.45 wt.% Cr_2O_3 (n = 68, sd: ±0.053), while the lCZ-opx averages 0.48 wt.% (n = 130, sd: ±0.034). The Cr_2O_3 of the uCZ-opx is 0.45 wt.% (n = 29, sd: ±0.07). In the uCZ (above 214.05 m) the first indication of Cr depletion becomes apparent. Poikilitic opx can have Cr concentrations similar to the cumulus opx, but tends to lower values in the LZ. For the elements Mn and Al (see Fig. 15A) similar trends are observable. Up to depth of ca. 700 m the levels scatter around average values of 0.21 and 1.18 wt.% oxides, respectively.

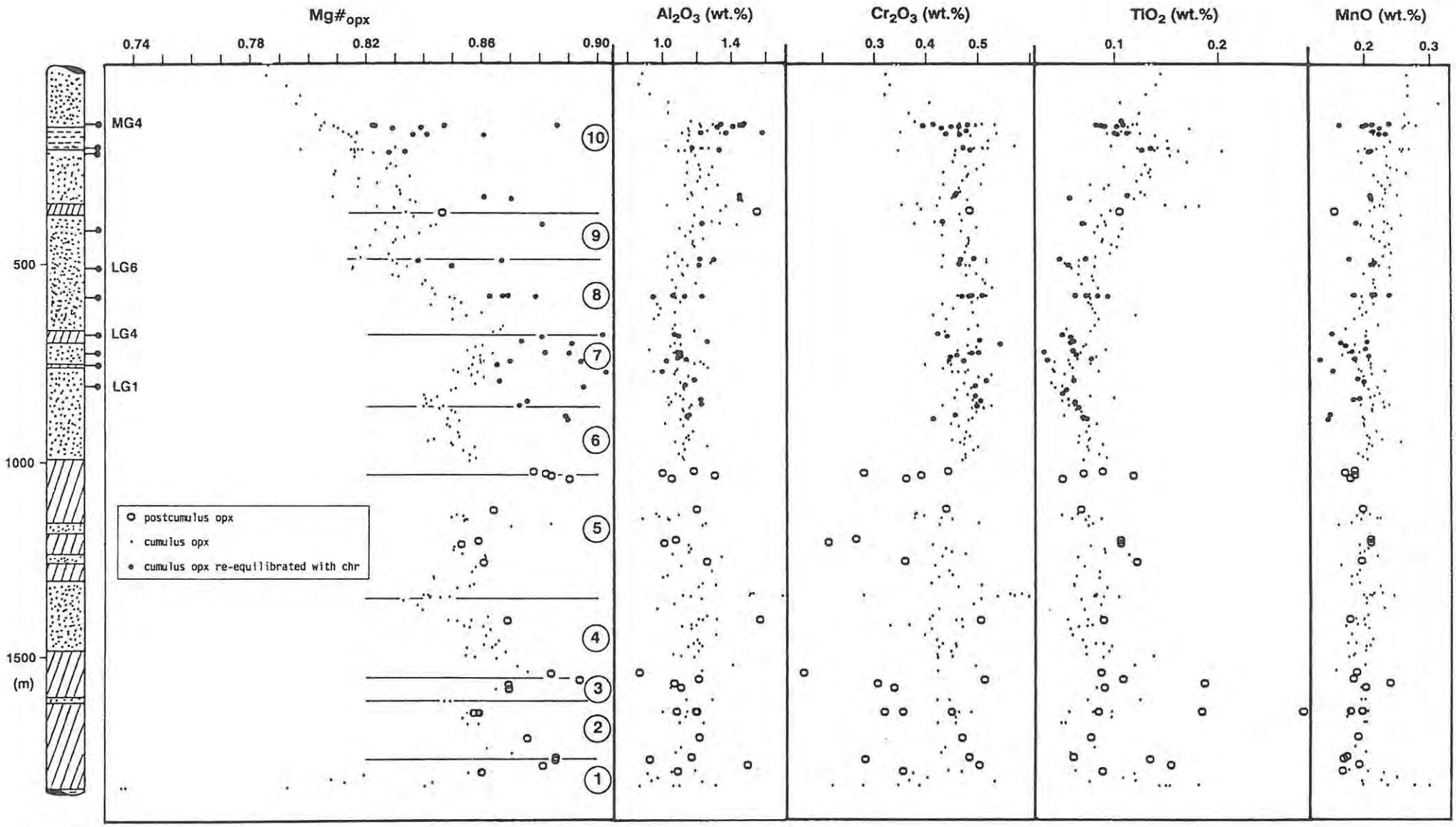

Fig. 15A Cryptic variations of orthopyroxene through the NG-sequence (note number in circle denotes segment, see text for explanations).

TABLE 6 Orthopyroxene Compositions in different Stratigraphic Intervals

Stratigraphic Interval:	All	uCZ	lCZ	LZ	uCZ	lCZ	LZ	MZ
Textural Habit:	samples		postcumulus			cumulus		
wt.%								
SiO_2	55.98	56.10	55.85	56.59	55.30	56.06	55.99	55.24
TiO_2	0.09	0.10	0.08	0.11	0.12	0.09	0.08	0.13
Al_2O_3	1.18	1.59	1.41	1.15	1.21	1.17	1.20	1.06
Cr_2O_3	0.45	0.44	0.50	0.37	0.45	0.48	0.45	0.37
FeO	9.82	9.18	8.80	8.36	11.75	9.74	9.30	12.86
MnO	0.21	0.23	0.18	0.19	0.24	0.21	0.21	0.24
NiO	0.07	0.07	0.06	0.07	0.08	0.07	0.09	0.07
MgO	30.84	31.98	30.49	32.01	29.55	30.70	31.49	28.87
CaO	1.20	0.74	2.18	1.11	1.13	1.27	1.19	0.77
Na_2O	0.02	0.00	0.04	0.03	0.01	0.02	0.03	0.02
Total	99.88	100.43	99.59	100.00	99.85	99.81	100.00	99.63
cations (based on 6 oxygens):								
Si	1.9706	1.9562	1.9674	1.9742	1.9653	1.9743	1.9645	1.9743
Ti	0.0025	0.0027	0.0022	0.0029	0.0033	0.0023	0.0023	0.0036
Al	0.0489	0.0653	0.0585	0.0475	0.0508	0.0484	0.0484	0.0448
Cr	0.0127	0.0121	0.0146	0.0105	0.0127	0.0133	0.0126	0.0104
Fe^{2+}	0.2894	0.2678	0.2593	0.2441	0.3495	0.2869	0.2730	0.3852
Mn	0.0063	0.0069	0.0054	0.0056	0.0074	0.0064	0.0059	0.0074
Ni	0.0021	0.0020	0.0016	0.0018	0.0022	0.0019	0.0025	0.0021
Mg	1.6175	1.6619	1.6009	1.6646	1.5650	1.6109	1.6466	1.5369
Ca	0.0454	0.0278	0.0825	0.0415	0.0431	0.0475	0.0446	0.0293
Na	0.0017	0.0000	0.0029	0.0026	0.0008	0.0016	0.0018	0.0011
cationic ratio:								
$Mg\#_{opx}$	0.8483	0.8612	0.8605	0.8721	0.8175	0.8488	0.8578	0.7997
n	261	1	2	22	30	130	68	8
a	1657	5	4	107	133	948	388	72
standard deviation:								
wt.%								
SiO_2	0.6117		0.2575	0.5350	0.5431	0.5116	0.5235	0.5923
TiO_2	0.0335		0.0225	0.0512	0.0216	0.0317	0.0181	0.0300
Al_2O_3	0.1342		0.1425	0.1569	0.1678	0.1011	0.1393	0.1467
Cr_2O_3	0.0621		0.0100	0.0955	0.0695	0.0337	0.0534	0.0859
FeO	1.5175		0.7750	0.7481	1.2885	1.2761	0.6673	2.3928
MnO	0.0283		0.0250	0.0160	0.0318	0.0239	0.0179	0.0334
NiO	0.0210		0.0075	0.0184	0.0242	0.0162	0.0224	0.0174
MgO	1.1564		0.8125	0.7176	0.9409	0.9812	0.5591	1.6299
CaO	0.2665		0.0475	0.2829	0.3411	0.1931	0.2376	0.1732
Na_2O	0.0119		0.0075	0.0191	0.0062	0.0096	0.0095	0.0069

Notes: 1) $Mg\#_{opx}$: cationic ratio of $Mg/(Mg + Fe^{2+})$

2) n : number of samples

3) a : number of analyses

Above this position an irregular increase in both elements is apparent. The appearance of cumulus pla at 214.05 m appears to trigger a decrease in Al_2O_3 concentrations, whereas MnO levels continue to increase. A comparable trend with more marked steps and deviations is displayed by the TiO_2 contents.

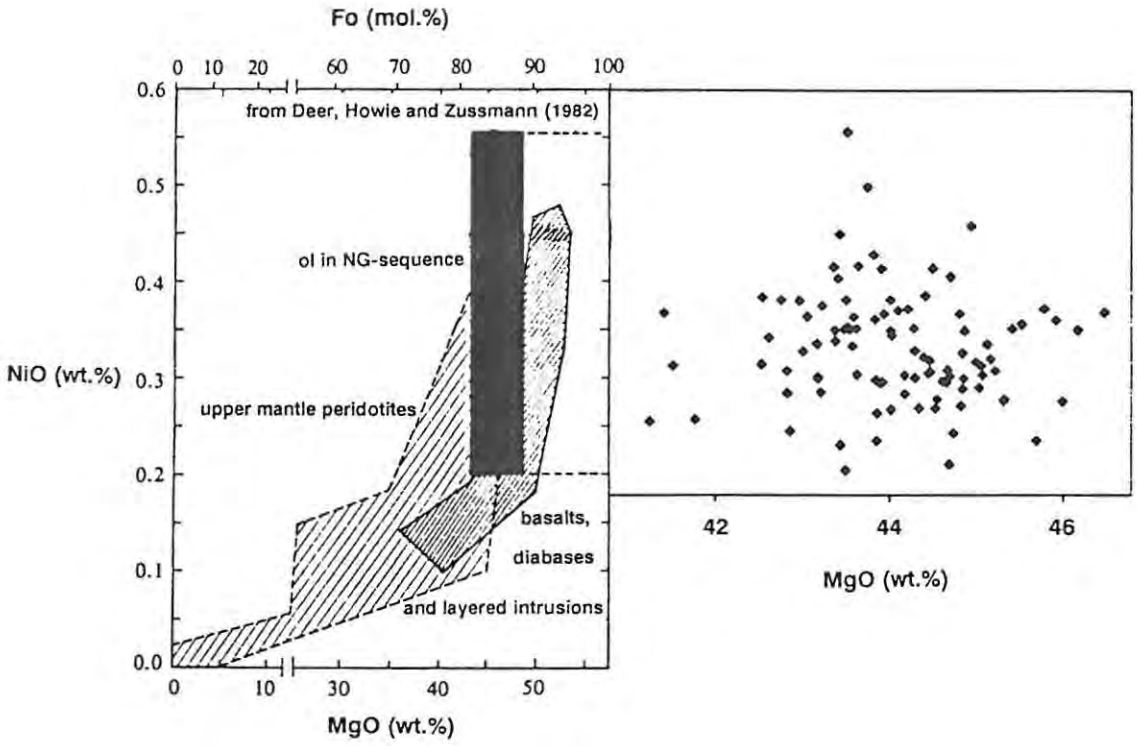

Fig. 16 Variation of NiO and MgO in olivines of the NG-sequence.

4.3. Olivine

Ol was investigated to determine cryptic variations in MgO, FeO and NiO. Haikney (1990) analysed the bulk of the samples (63 samples, 464 analyses), whereas the remainder (36 samples, 166 analyses) were analysed by the author. Because of the emphasis of Haikney's M.Sc.-study (geochemistry and mineralogy of the olivine-rich rocks in NG1 and upper part of NG2) only major features of olivine compositions will be presented here, so as not to pre-empt her work.

As in the case of opx, zoning was constantly monitored throughout the sequence but no significant gradients due to zonation were detected. The cumulus ol displays a very limited range of composition. The levels of SiO_2 range between 38.3 and 41.3 wt.%, whilst CaO does not exceed 0.03 wt.%. MnO values vary between 0 and 0.2 wt.%. The concentrations of FeO and MgO are 10.2 - 18.2 and 43.2 - 48.5 wt.%, respectively, thus yielding Fo levels 80.9 - 89.4. The NiO levels (0.2 - 0.6 wt.%) show no correlation with the Fo content, if the entire ol population is plotted (Fig. 16).

However, through limited intervals the following relationships can be observed. The uppermost olivine-rich unit above the LG7-chromitite yields the equation:

$$NiO = 0.04\ Fo - 3.36\ (n=3);$$

and the ol-rich cumulates associated with the LG4- and LG2-chromitites:

$$NiO = 0.02\ Fo - 1.80\ \ (cc:0.863;\ n=10).$$

Scoon and de Klerk (1987) established a comparable regression equation ($NiO = 0.0633\ Fo - 4.7932$; cc: 0.97; n=37) for ol in the uCZ and showed a close approximation with theoretical fractionation curves assuming initial liquids with 15 and 10 wt.% MgO. In the olivine-dominated LZ no interval displays any significant correlation.

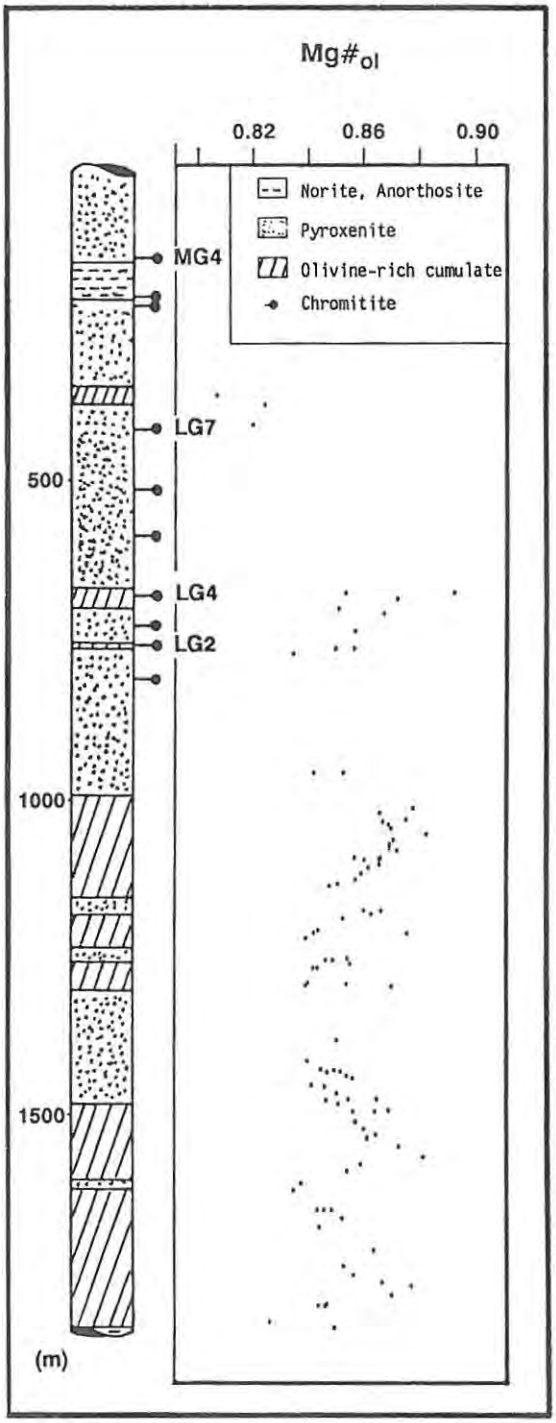

Fig. 17 Variations in Fo content of olivine through the NG-sequence.

In Fig. 17 the Fo content is plotted against stratigraphic height. The variations in Fo content mimic the trends set by the $Mg\#_{opx}$ and gaps in the trend line caused by the absence of cumulus opx (see Fig. 15B) might be closed. A further detailed discussion of this follows in the section dealing with equilibration between coexistent phases.

TABLE 7 Olivine Compositions in different Stratigraphic Intervals

Stratigraphic Interval:	All samples	ICZ	LZ	Range of Composition
wt.%				
SiO_2	39.75	39.71	39.75	38.3 - 41.3
FeO	13.73	14.26	13.63	10.2 - 18.2
MnO	0.15	0.11	0.15	0.0 - 0.2
NiO	0.33	0.29	0.34	0.2 - 0.6
MgO	46.09	45.63	46.17	43.2 - 48.5
CaO	0.01	0.01	0.01	0.0 - 0.03
Total	100.05	100.01	100.05	
cations (based on 4 oxygens):				
Si	0.9932	0.9946	0.9930	
Fe^{2+}	0.2870	0.2992	0.2849	
Mn	0.0031	0.0024	0.0032	
Ni	0.0067	0.0058	0.0069	
Mg	1.7164	1.7032	1.7188	
Ca	0.0003	0.0003	0.0003	
Total	3.0068	3.0054	3.0070	
n	99	15	84	
a	634	72	562	
Fo	0.8567	0.8507	0.8578	0.8092 - 0.8943
standard deviation:				
wt.%				
SiO_2	0.4015	0.6309	0.3444	
FeO	1.2559	1.8822	1.0799	
MnO	0.0324	0.0451	0.0256	
NiO	0.0576	0.0453	0.0552	
MgO	1.0061	1.4101	0.8910	
CaO	0.0068	0.0075	0.0065	

Notes: 1) n: number of samples

a: number of analyses

Average compositions were also calculated and are tabulated in Table 7. The more primitive traits of the LZ-ol are expressed in a higher Fo content and NiO value. The scatter in Ni levels is reflected in a relatively higher sd.

4.4. Chromite

Chr is the most common accessory cumulus phase throughout the entire sequence. Chr-free lithologies are in fact very rare and are limited to intervals in the uCZ (above the MG4-chromitite) and LZ (in the vicinity of the leuconorite). Apart from this accessory occurrence some of the most interesting rock types are the chromitiferous cumulates, i.e. rocks which comprise either chr as major or sole cumulus phase. Because of the great economic as well as petrological importance of massive chromitites some aspects of their mineralogy will be discussed separately.

Though the focus of this study is not a detailed investigation of chr chemistry and its dependence upon the lithological microenvironment, it seems necessary to summarize some results of earlier workers and put these into context with the new data. The importance of chromian-spinel as a petrogenetic indicator was described by Irvine (1965, 1967). He concluded that chr has generally formed simultaneously with ol and that chr crystallization has been terminated in many occurrences by a reaction relation forming pyroxene. Eales et al. (1980) described the evolution of spinels in Karoo dolerites and gabbros in four stages: a) an early stage, in which Cr-rich spinels are crystallizing with a tendency to more Al-rich compositions due to the coprecipitation of ol, b) a middle stage, which is characterized by the onset of pla crystallization, thus depleting the liquid in Al_2O_3, c) a late stage marked by a sharp decrease in Cr in the liquid by virtue of clinopyroxene nucleation, which is an effective Cr scavenger, and d) a final stage characterized by the crystallization of Ti-magnetite. Between stage c and d a hiatus in spinel crystallization might occur, the so-called "spinel gap". The primary composition of the crystallizing spinel is thus dependent on: a) the composition of the liquid, b) coprecipitating phases, c) temperature and pressure (inter alia Hill and Roeder, 1974) and d) oxygen fugacity (Ulmer, 1969). A further complication arises due to modification of cumulus compositions, by processes of subsolidus re-equilibration, described inter alia in McDonald (1967), Cameron (1975) and Eales and Reynolds (1986). Roeder and Campbell (1985) found that chr compositions can be related to the cumulate type and to the nature of the surrounding silicate mineral.

Their data suggested that in ad- and mesocumulates chr displays a restricted compositional range (high in Mg, Al and Cr). In orthocumulates chr compositions shift to an enrichment in Fe and Ti and depend upon the host silicate chemistry: chr included in opx was protected from reaction whereas interstitial chr could react longer with the liquid and shows higher Fe and Ti levels. They also described the ability of chr to equilibrate with the interstitial liquid, even if the chr grains were enclosed in ol. No obvious correlation between grain size and composition was found by the latter authors for grains within a particular silicate phase. Botha (1987) reported a similar TiO_2 enrichment in grains interstitial to opx or included in postcumulus pla.

In the light of the factors noted above, the following parameters for all grains analysed were recorded:

a) position of the beam (rim or core domains);

b) the adjacent phase for rim domain analyses;

c) the status of the grain, i.e. inclusion or interstitial grain;

d) including phase or surrounding minerals;

e) the size of the grain;

f) the host rock.

Thus the microenvironment of each chr grain can be recalled, when necessary. A detailed study of zonation was not attempted, but sporadic core - rim pair analyses were made to detect significant geochemical gradients. In each of the samples NG1-569.20 and NG3-219.42 one spinel was analysed in more detail (Table 8; Fig. 18 grains B and C).

TABLE 8 Selected Microprobe Analyses of Core and Rim Domains of Chromite

Sample:	NG1-74.45		NG1-197.50		NG1-327.45		NG1-644.20		NG1-65-5		NG1-433.608		NG1-569.20						NG3-219.42			
Habit:	int pla		inc opx		inc opx		int opx		poly		poly		int pla		inc opx				polygonal grain in massive layer			
Domain:	core	rim	core	rim	core	rim	core	rim	core	rim	core	rim	core	rim	rim	core	core	rim	core	towards		rim
Size (in μm):	250		90		130		170		>300		250		50			50			300			
Analysis no.:	827.1	827.2	841.1	841.2	858.1	858.2	880.3	880.4	922.1	922.2	910.1	910.2	874.1	874.2	875.1	875.2	875.3	875.4	153.1	153.2	153.3	153.4
wt.%																						
TiO_2	1.22	0.98	0.23	0.21	0.65	0.53	0.58	0.53	0.58	0.62	0.57	0.56	0.71	0.41	0.14	0.13	0.14	0.13	0.72	0.73	0.74	0.71
Al_2O_3	10.35	10.63	12.80	12.24	10.25	10.31	14.17	13.63	13.01	12.89	15.73	15.88	7.75	7.71	7.60	7.69	7.71	7.66	17.72	17.76	17.77	17.77
Cr_2O_3	43.18	44.08	45.71	47.34	47.50	48.16	48.73	48.64	47.84	47.62	46.78	46.69	50.79	49.51	49.23	51.14	50.73	50.55	41.60	41.61	41.62	41.40
FeO	25.24	25.36	26.01	26.17	25.23	25.32	18.06	17.78	18.88	18.98	18.67	18.66	25.50	25.06	25.02	25.62	25.48	25.39	18.91	18.64	18.84	18.82
Fe_2O_3	12.62	12.61	9.31	8.72	10.17	9.94	6.80	6.97	8.84	9.04	7.10	7.10	8.45	9.06	10.16	9.38	9.31	9.30	10.06	10.09	9.92	10.11
MnO	0.39	0.39	0.26	0.30	0.38	0.36	0.28	0.27	0.24	0.28	0.30	0.31	0.43	0.35	0.36	0.38	0.33	0.34	0.27	0.29	0.28	0.29
NiO	0.18	0.15	0.10	0.10	0.12	0.14	0.10	0.08	0.16	0.12	0.06	0.09	0.17	0.06	0.08	0.09	0.08	0.06	0.14	0.16	0.15	0.11
MgO	5.49	5.54	4.97	4.90	5.44	5.41	10.48	10.41	9.84	9.76	10.32	10.33	4.75	4.59	4.49	4.46	4.46	4.44	10.47	10.63	10.51	10.50
Total	98.68	99.73	99.40	99.99	99.75	100.16	99.21	98.32	99.39	99.31	99.52	99.62	98.55	96.74	97.08	98.90	98.24	97.86	99.90	99.89	99.83	99.71
cations (based on 32 oxygens):																						
Ti	0.2548	0.2028	0.0482	0.0430	0.1348	0.1095	0.1141	0.1053	0.1156	0.1222	0.1111	0.1094	0.1516	0.0882	0.0305	0.0279	0.0300	0.0276	0.1388	0.1399	0.1433	0.1377
Al	3.3849	3.4358	4.1205	3.9299	3.3171	3.3225	4.3637	4.2435	4.0440	4.0130	4.8069	4.8443	2.5759	2.6127	2.5708	2.5556	2.5760	2.5703	5.3530	5.3568	5.3673	5.3727
Cr	9.4705	9.5574	9.8699	10.1963	10.3114	10.4138	10.0698	10.1599	9.9714	9.9455	9.5868	9.5537	11.3266	11.2506	11.1726	11.3985	11.3767	11.3819	8.4292	8.4204	8.4333	8.3991
Fe^{2+}	5.8556	5.8150	5.9413	5.9626	5.7935	5.7898	3.9482	3.9293	4.1618	4.1935	4.0465	4.0389	6.0157	6.0230	6.0052	6.0406	6.0458	6.0471	4.0532	3.9890	4.0374	4.0380
Fe^{3+}	2.6350	2.6012	1.9131	1.7877	2.1020	2.0446	1.3382	1.3859	1.7534	1.7971	1.3842	1.3832	1.7944	1.9603	2.1955	1.9901	1.9874	1.9926	1.9402	1.9429	1.9128	1.9527
Mn	0.0913	0.0896	0.0607	0.0697	0.0877	0.0836	0.0629	0.0613	0.0540	0.0618	0.0661	0.0676	0.1019	0.0840	0.0870	0.0898	0.0792	0.0811	0.0591	0.0619	0.0599	0.0620
Ni	0.0391	0.0333	0.0215	0.0227	0.0267	0.0304	0.0204	0.0163	0.0332	0.0256	0.0123	0.0184	0.0381	0.0135	0.0186	0.0214	0.0185	0.0137	0.0281	0.0322	0.0314	0.0217
Mg	1.4326	2.2649	2.0248	1.9881	2.2270	2.2058	4.0826	4.0984	3.8666	3.8413	3.9862	3.9846	1.9959	1.9677	1.9197	1.8760	1.8865	1.8857	3.9984	4.0568	4.0145	4.0160
cationic ratios:																						
Cr/Al	2.7979	2.7817	2.3953	2.5945	3.1086	3.1343	2.3076	2.3942	2.4658	2.4783	1.9944	1.9721	4.3971	4.3062	4.3459	4.4602	4.4165	4.4282	1.5746	1.5719	1.5712	1.5633
$Mg\#_{chr}$	0.1966	0.2803	0.2542	0.2501	0.2777	0.2759	0.5084	0.5105	0.4816	0.4781	0.4962	0.4966	0.2491	0.2463	0.2422	0.2370	0.2378	0.2377	0.4966	0.5042	0.4986	0.4986
FFE	0.3103	0.3091	0.2436	0.2307	0.2662	0.2610	0.2531	0.2607	0.2964	0.3000	0.2549	0.2551	0.2298	0.2456	0.2677	0.2478	0.2474	0.2478	0.3237	0.3275	0.3215	0.3260
Cr/(Cr + Al)	0.7367	0.7356	0.7055	0.7218	0.7566	0.7581	0.6977	0.7054	0.7115	0.7125	0.6660	0.6635	0.8147	0.8115	0.8129	0.8169	0.8154	0.8158	0.6116	0.6112	0.6111	0.6099
weight ratio of metals:																						
Cr/Fe	1.04	1.06	1.17	1.22	1.22	1.24	1.77	1.78	1.57	1.55	1.64	1.64	1.35	1.31	1.27	1.32	1.32	1.32	1.31	1.32	1.32	1.31

Notes: 1) int pla: interstitial with plagioclase as adjacent phase
int opx: interstitial with orthopyroxene as adjacent phase
int chr: interstitial with chromite as adjacent phase
inc opx: inclusion in orthopyroxene
poly: polygonal grain in chromitite layer

2) $Mg\#_{chr}$: cationic ratio of $Mg/(Mg + Fe^{2+})$

3) FFE : cationic ratio of $Fe^{3+}/(Fe^{3+} + Fe^{2+})$

4) Cr/Fe : weight ratio of Cr metal to Fe metal

TABLE 9 Selected Microprobe Analyses of Core Domains of Chromite in Different Host Minerals

Sample:	NG1-29.80		NG1-55.40		NG1-191.00			NG1-414.85			NG1-609.47	
Host:	opx	pla	opx	pla	pla	opx	pla	opx	opx	opx	pla	opx
Size (in μm) :	50	200	60	200	100	50	300	100	120	50	100	250
Analysis no. :	37.1	37.4	50.1	50.5	49.1	49.4	55.1	55.3	55.6	55.7	230.3	231.1
wt.%												
TiO_2	0.48	0.91	0.58	1.17	0.24	0.37	0.70	0.55	0.63	0.35	0.90	0.43
Al_2O_3	11.49	8.32	10.59	9.17	9.23	10.16	8.65	9.79	8.19	9.00	8.32	12.95
Cr_2O_3	45.23	46.00	43.53	42.20	47.03	47.52	51.13	49.89	51.83	51.29	49.13	45.49
Fe_0	25.60	26.27	26.03	26.17	25.88	25.83	25.45	23.22	24.18	24.06	25.90	24.90
Fe_2O_3	10.97	13.30	13.88	16.42	11.85	10.08	8.22	7.95	7.95	8.12	10.18	9.50
MnO	0.38	0.33	0.42	0.35	0.36	0.34	0.41	0.41	0.34	0.37	0.43	0.35
NiO	0.10	0.13	0.18	0.26	0.10	0.08	0.05	0.10	0.15	0.12	0.09	0.11
MgO	5.16	4.77	4.89	5.12	4.58	4.80	5.22	6.34	5.79	5.79	4.97	5.79
Total	99.40	100.03	100.10	100.87	99.27	99.18	99.83	98.25	99.06	99.11	99.90	99.52
cations (based on 32 oxygens):												
Ti	0.0983	0.1903	0.1208	0.2418	0.0508	0.0773	0.1453	0.1139	0.1324	0.0737	0.1871	0.0884
Al	3.7189	2.7255	3.4296	2.9658	3.0348	3.3202	2.8183	3.1949	2.6824	2.9353	2.7204	4.1381
Cr	9.8186	10.1113	9.4590	9.1587	10.3750	10.4220	11.1810	10.9219	11.3891	11.2253	10.7801	9.7479
Fe^{2+}	5.8777	6.1064	5.9814	6.0077	6.0381	5.9917	5.8857	5.3779	5.6209	5.5709	6.0122	5.6444
Fe^{3+}	2.2658	2.7825	2.8699	3.3920	2.4886	2.1032	1.7101	1.6555	1.6636	1.6920	2.1253	1.9372
Mn	0.0872	0.0781	0.0970	0.0812	0.0852	0.0809	0.0957	0.0962	0.0800	0.0868	0.1004	0.0807
Ni	0.0224	0.0292	0.0405	0.0583	0.0224	0.0187	0.0115	0.0234	0.0325	0.0261	0.0200	0.0233
Mg	2.1111	1.9765	2.0018	2.0946	1.9051	1.9859	2.1524	2.6165	2.3991	2.3900	2.0545	2.3400
cationic ratios:												
Cr/Al	2.6402	3.7099	2.7580	3.0881	3.4187	3.1390	3.9673	3.4185	4.2458	3.8243	3.9627	2.3556
$Mg\#_{chr}$	0.2643	0.2445	0.2508	0.2585	0.2398	0.2489	0.2678	0.3273	0.2991	0.3002	0.2547	0.2931
FFE	0.2782	0.3130	0.3242	0.3609	0.2919	0.2598	0.2251	0.2354	0.2284	0.2330	0.2612	0.2555
Cr/Cr+Al	0.7253	0.7877	0.7339	0.7554	0.7737	0.7584	0.7987	0.7737	0.8094	0.7927	0.7985	0.7020
weight ratio of metals:												
Cr/Fe	1.12	1.06	1.00	0.91	1.13	1.20	1.37	1.45	1.46	1.44	1.23	1.20

Notes: 1) $Mg\#_{chr}$: cationic ratio of $Mg/(Mg + Fe^{2+})$
2) FFE : cationic ratio of $Fe^{3+}/(Fe^{3+} + Fe^{2+})$
3) Cr/Fe : weight ratio of Cr metal to Fe metal

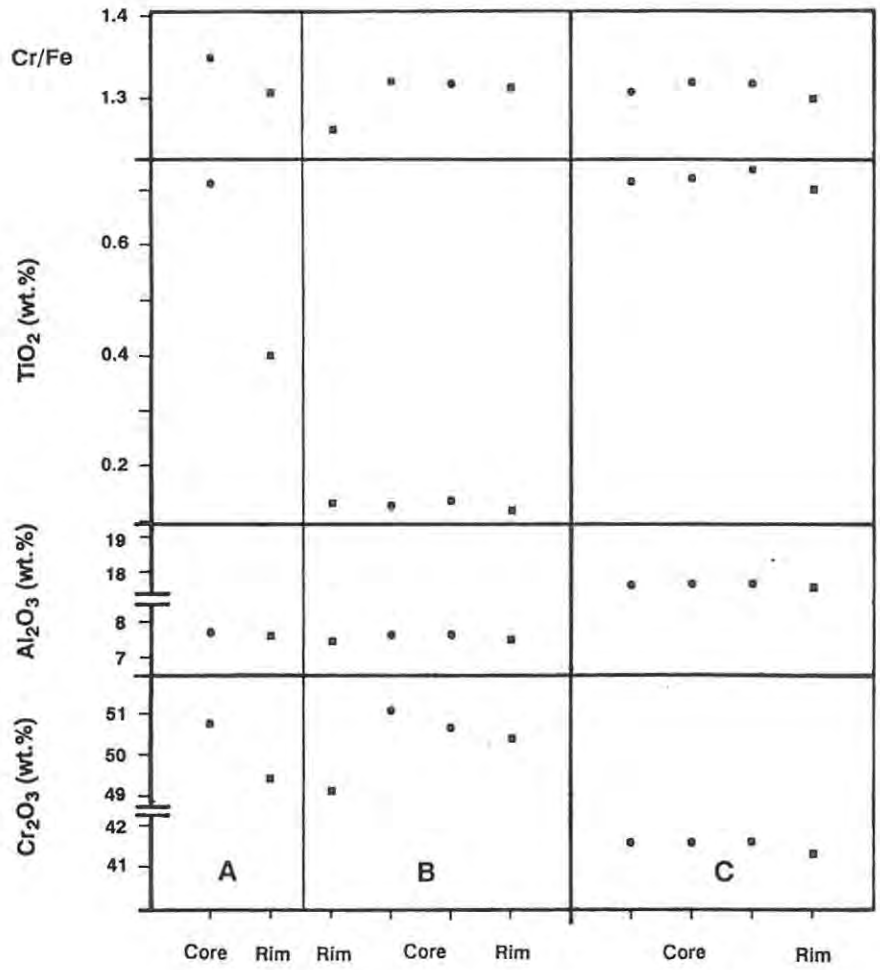

Fig. 18 Selected parameters of chromite mineralogy of different microdomains (see also Table 9).

The majority of the grains do not show significant and systematic zoning structures. More significant intra-sample variations are evident, when grains included in opx are compared with interstitial ones (Table 9). The latter are generally enriched in Ti and Fe, but depleted in Al; other major elements are in similar concentrations. These findings are in agreement with the results of Botha (op.cit.) and Roeder and Campbell (1985). However, not all grains analysed follow such general trends and the influence of coprecipitating phases such as Ti-rich mica might shift chr compositions in the interstices to very low Ti values (Fig. 18; grain A). In summation, each chr analysis represents a subsolidus equilibrium composition, which is a combination of magma composition, temperature, pressure, oxygen fugacity and subsolidus re-equilibration.

It is obvious that, in the case of re-equilibration, the ratio of phase : liquid is of major importance, i.e. the modal proportions of the co-crystallizing phases have to be considered. Because of this complexity it is very difficult to assess which composition of chr represents the least modified, near-liquidus composition.

Because the thrust of this study is on geochemical trends through the ca. 1800 m cumulate pile, and the fact that the majority of accessory chr is interstitial to opx, which means it was able to react with the surrounding liquid, all chr analyses of each sample were averaged to obtain a chr composition "representative" of each sample. High intra-sample variations are revealed by high sd. A total of 213 samples (1142 analyses; 38 samples with 153 analyses by Haikney included) were used to compile the following diagrams and tables. The Fe_2O_3 concentrations were calculated on the stoichiometrical distribution of the cations after the equations:

$$16 = ((Fe^{2+})_{usp} + Ti) + Fe^{3+} + Al + Cr$$

where $(Fe^{2+})_{usp}$ = Ti in ulvöspinel molecule

$$8 = Fe^{2+} + Mg + Mn + Ni.$$

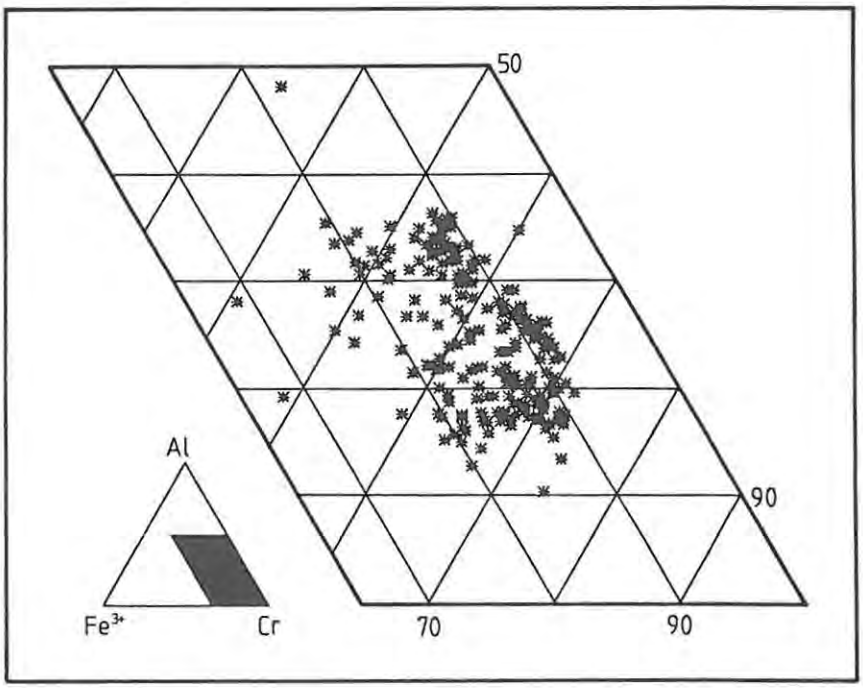

Fig. 19 Triangular diagram of the trivalent cations Cr, Fe^{3+} and Al (in cation %) of chromite in the NG-sequence.

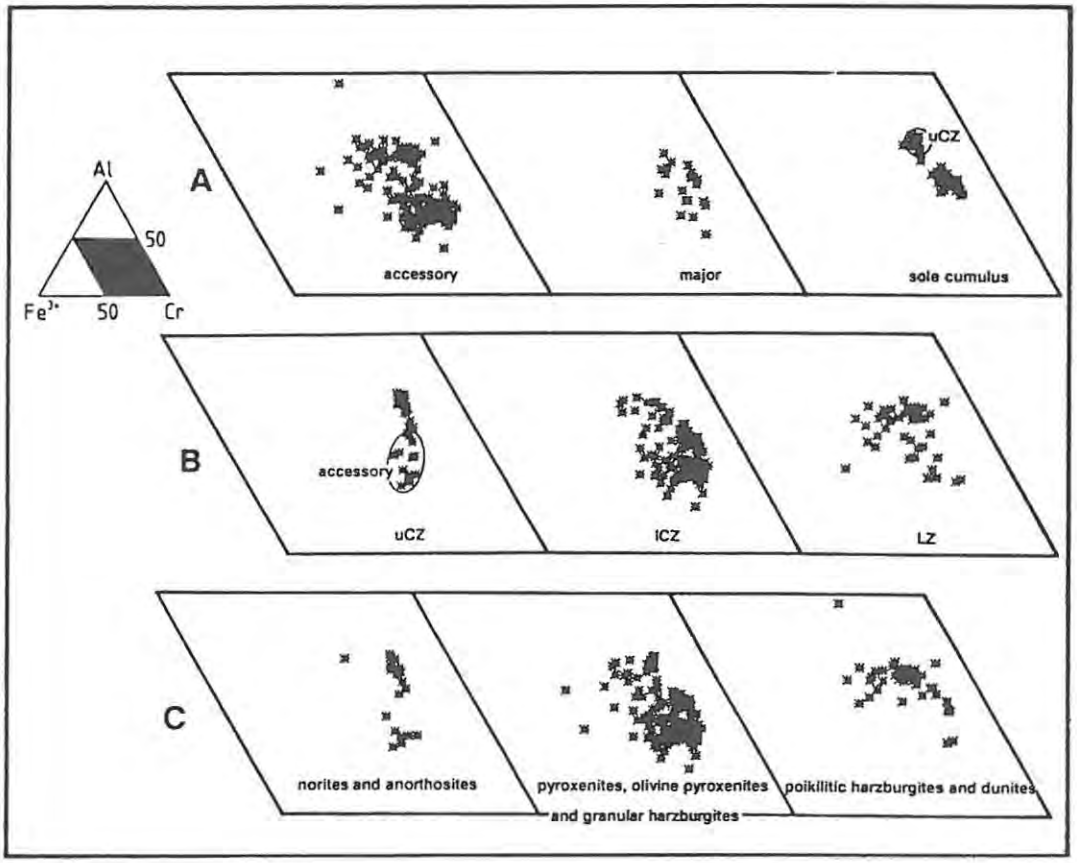

Fig. 20 Triangular diagram of the trivalent cations of chromite in the NG-sequence showing compositional variations with: A) modal proportion, B) stratigraphic height, and C) host rock.

In the conventional triangular diagram (Fig. 19 and Fig. 20) depicting the trivalent cations in % the compositional variations of chr in the NG-sequence are illustrated. General observations are:

a) chr from massive layers (ML) is Fe^{3+}-poorer than chr present in accessory or major proportions (Fig. 20A). Cameron (1977) reports a similar decrease in ML-chr of the eastern BIC;

b) the ML-chr in the uCZ have distinctly higher Al concentrations than ML-chr of the lCZ despite the nucleation of cumulus pla in the under- and overlying cumulates (Fig. 20A, 20B);

c) chr hosted in olivine-dominated rocks shows elevated Al concentrations (Fig. 20C) as predicted by Eales et al. (1980) and described by Botha (1987) and Wilson (1982) for the Great Dyke. Using Al cations and splitting the chr-population into those above and those below the lCZ/uCZ boundary the resulting diagram (Fig. 21B) is in agreement with that published by Eales (1987; inset in Fig. 21B);

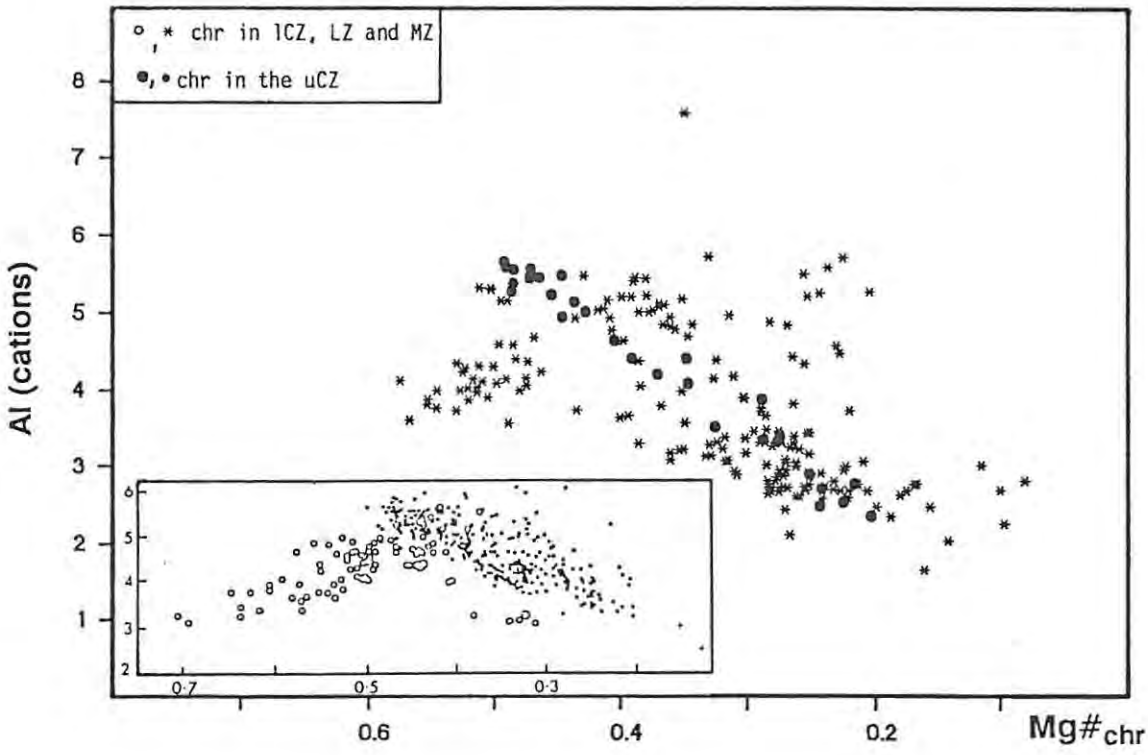

Fig. 21B Plot of Al (cations) versus $Mg\#_{chr}$.

d) compositional differences between chr as a major phase and accessory chr (Fig. 20A) are subdued;

e) accessory chr hosted in norites and anorthosites in the uCZ is conspicuously depleted in Al, indicating the influence of pla crystallization (Fig. 20B).

TABLE 10A Range of Composition: Chromite

Stratigraphic Interval:	uCZ		lCZ, LZ and MZ		CZ
Modal proportion:	acc	maj	acc	maj	ML
wt.%					
TiO_2	0.55 - 1.16	0.82 - 1.06	0.08 - 1.64	0.42 - 0.99	0.37 - 0.88
Al_2O_3	7.12 - 15.11	11.05 - 16.19	4.89 - 25.39	6.42 - 15.48	11.51 - 18.63
Cr_2O_3	41.62 - 46.20	42.84 - 43.21	27.38 - 53.04	42.61 - 52.67	40.47 - 53.43
FeO	21.81 - 27.00	20.51 - 23.93	19.19 - 30.37	17.67 - 25.64	15.76 - 21.61
Fe_2O_3	9.43 - 15.37	9.61 - 13.34	4.45 - 23.36	6.65 - 11.44	6.13 - 11.39
MnO	0.31 - 0.41	0.29 - 0.32	0.25 - 0.46	0.27 - 0.40	0.24 - 0.33
NiO	0.10 - 0.21	0.12 - 0.20	0.03 - 0.43	0.03 - 0.16	0.05 - 0.18
MgO	3.86 - 8.32	6.48 - 9.27	1.52 - 10.53	4.88 - 10.47	8.10 - 11.97
cationic ratios:					
Cr/Al	1.9539 - 4.2107	1.7762 - 2.6254	0.7244 - 7.0949	1.9801 - 5.5078	1.4574 - 3.0476
$Mg\#_{chr}$	0.2033 - 0.4047	0.3254 - 0.4460	0.0813 - 0.4944	0.2521 - 0.5124	0.4005 - 0.5751
FFE	0.2736 - 0.3388	0.2747 - 0.3340	0.1597 - 0.4440	0.2204 - 0.3107	0.2383 - 0.3573
Cr/(Cr + Al)	0.6615 - 0.8081	0.6398 - 0.7242	0.4201 - 0.8765	0.6644 - 0.8463	0.5931 - 0.7529
weight ratio of metals:					
Cr/Fe	0.96 - 1.27	1.06 - 1.29	0.54 - 1.64	1.14 - 1.83	1.25 - 2.16

Notes: 1) acc : accessory or minor phase

maj : major phase

ML : sole cumulus phase

2) $Mg\#_{chr}$: cationic ratio of $Mg/(Mg + Fe^{2+})$

3) FFE : cationic ratio of $Fe^{3+}/(Fe^{3+} + Fe^{2+})$

4) Cr/Fe: weight ratio of Cr metal to Fe metal

TABLE 10B Chromite Compositions in different Stratigraphic Intervals

Stratigraphic Interval:	uCZ			lCZ			LZ	MZ
Modal proportion:	all	acc + maj	ML	all	acc + maj	ML	acc[7)]	acc
wt.%								
TiO_2	0.86	0.93	0.77	0.64	0.68	0.53	0.63	0.69
Al_2O_3	17.83	11.08	17.83	11.12	10.17	13.46	14.16	13.31
Cr_2O_3	41.78	44.22	41.78	47.56	47.01	48.92	41.61	37.98
FeO	19.88	24.53	19.88	23.05	24.88	18.54	23.63	27.18
Fe_2O_3	9.05	12.00	9.05	9.80	10.60	7.82	12.06	15.27
MnO	0.28	0.35	0.28	0.34	0.36	0.29	0.36	0.37
NiO	0.13	0.16	0.13	0.11	0.12	0.11	0.15	0.17
MgO	9.80	6.02	9.80	6.97	5.67	10.18	6.77	4.34
Total	99.77	99.47	99.68	99.72	99.62	99.98	99.50	99.45
cations (based on 32 oxygens):								
Ti	0.1492	0.1908	0.1492	0.1300	0.1400	0.1050	0.1285	0.1437
Al	5.4204	3.5531	5.4204	3.5267	3.2783	4.1412	4.5079	4.2135
Cr	8.5242	9.5823	8.5242	10.2045	10.2426	10.1103	8.9265	8.3443
Fe^{2+}	4.2916	5.6315	4.2916	5.2553	5.7395	4.0573	5.2899	6.2756
Fe^{3+}	1.7570	2.4830	1.7570	2.0089	2.1991	1.5385	2.5249	3.1549
Mn	0.0622	0.0809	0.0622	0.0784	0.0841	0.0641	0.0837	0.0854
Ni	0.0276	0.0348	0.0276	0.0258	0.0269	0.0231	0.0368	0.0374
Mg	3.7678	2.4436	3.7678	2.7720	2.2917	3.9602	2.5108	1.7453
n	29	17	12	132	94	38	46	6
a		78	70		539	227	206	22
cationic ratios:								
Cr/Al	1.5754	2.8694	1.5754	3.0970	3.3408	2.4941	2.1127	2.5778
$Mg\#_{chr}$	0.4675	0.3025	0.4675	0.3454	0.2853	0.4940	0.3198	0.2177
FFE	0.2905	0.3041	0.2905	0.2745	0.2745	0.2744	0.3171	0.3327
Cr/(Cr + Al)	0.6113	0.7311	0.6113	0.7432	0.7570	0.7089	0.6648	0.6618
weight ratio of metals:								
Cr/Fe	1.31	1.11	1.31	1.36	1.22	1.70	1.09	0.83
standard deviation:								
wt.%								
TiO_2	0.1584	0.1720	0.0649	0.2378	0.2600	0.1210	0.3085	0.2800
Al_2O_3	0.7129	2.7731	0.7129	2.9157	2.7501	1.7652	2.9474	6.5690
Cr_2O_3	0.5875	1.1717	0.5875	3.9175	4.0461	3.1934	4.1370	8.1889
FeO	0.6911	1.8602	0.6911	3.4561	2.0270	1.6617	1.9570	1.7868
Fe_2O_3	0.5214	1.8884	0.5214	2.5037	2.4496	1.1933	3.3574	3.9597
MnO	0.0119	0.0367	0.0119	0.0461	0.0343	0.0284	0.0335	0.0386
NiO	0.0190	0.0361	0.0190	0.0382	0.0413	0.0286	0.0642	0.0799
MgO	0.4916	1.5503	0.4916	2.4942	1.5182	1.1737	1.6141	1.8291

Notes: 1) acc : accessory or minor phase
maj : major phase
ML : sole cumulus phase
2) $Mg\#_{chr}$: cationic ratio of $Mg/(Mg + Fe^{2+})$
3) FFE : cationic ratio of $Fe^{3+}/(Fe^{3+} + Fe^{2+})$
4) Cr/Fe : weight ratio of Cr metal to Fe metal
5) n : number of samples
6) a : number of analyses
7) sample NG2-158.60 (LZML) included

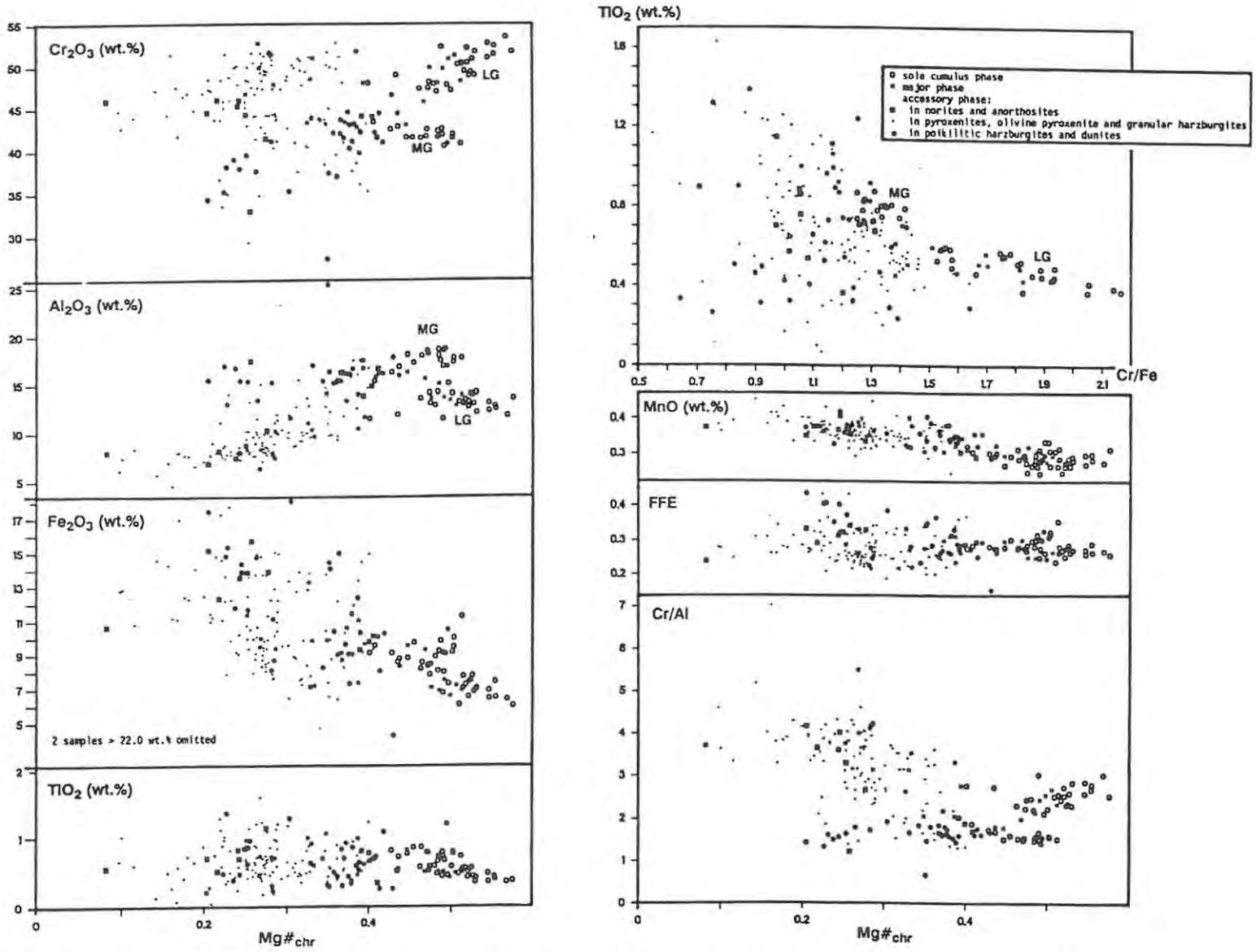

Fig. 21A Chromite mineralogy - variation diagrams ($Mg\#_{chr}$, FFE and Cr/Al cationic ratios, Cr/Fe weight ratio of metals).

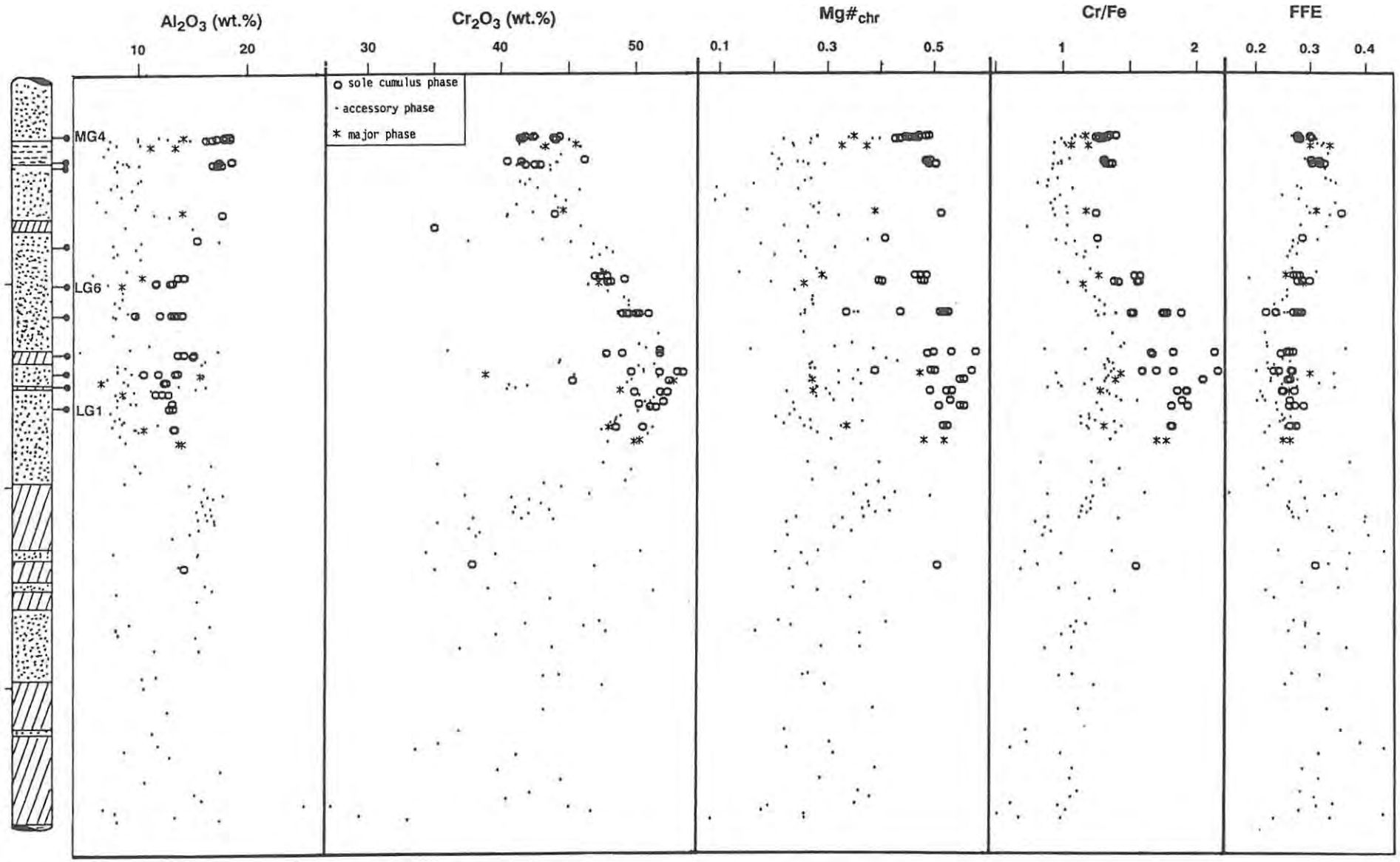

Fig. 22 Cryptic variations of chromite through the NG-sequence.

The ranges of compositions and average compositions in different stratigraphic intervals are tabulated in Tables 10A and 10B. In Fig. 21A Mg_{chr} and Cr/Fe ratio (atomic ratio using total Fe) were selected as parameters for the abscissa and from those diagrams and Fig. 22 further observations are derived:

f) the influence of the host rock described above is evident in some diagrams (Al_2O_3, Cr_2O_3 and ratios thereof), i.e. contrasting trends for different rock types can be detected;

g) the highest $Mg\#_{chr}$ (range: 0.40 - 0.58) are found in ML-chr, and chromitites in the lCZ have generally higher ratios than uCZ-chromitites;

h) with decreasing $Mg\#_{chr}$ the Al levels increase or remain steady in ol-rich cumulates, while in pyroxenites, granular harzburgites and norites Al concentrations decline;

i) scrutiny of the Cr concentrations reveals two general trends. In ultramafic cumulates a positive relationship with the $Mg\#_{chr}$ is indicated. However, chr in pyroxenites and granular harzburgites is shifted to Cr-richer compositions despite the compatibility of Cr in the opx-lattice. It is suggested here that this shift is caused by the higher Cr_2O_3 concentrations in chr of the lCZ (see Fig. 22). In pla cumulates of the uCZ a weak negative correlation of $Mg\#_{chr}$ and Cr_2O_3 might point to a relative enrichment of Cr in the liquid probably due to the scarcity of Cr-bearing phases;

j) the Cr/Fe ratio is generally positively linked with the $Mg\#_{chr}$ (not depicted in Fig. 21, but see Fig. 22);

k) no significant dependence on the silicate host rock was detected for the elements Fe, Mn and Ti. For Fe and Mn a negative relationship might be developed, while for the latter element no general trend can be detected.

The cryptic variations of chr through the sequence are illustrated in Fig. 22. In all diagrams the distinctly different compositions of the ML-chr are apparent; their concentrations in all elements fall invariably outside the trend outlined by the accessory chr grains. The Cr_2O_3 contents show a conspicuous enrichment in the lCZ apart from a limited deflection in the vicinity of the LG2-chromitite.

ML-chr of the uCZ appear to contain less Cr than accessory chr in this zone, whilst in the lCZ this relationship seems to be reversed. The concentrations of Al in accessory chr reflect clearly the host lithology (see above). They remain more or less steady with low values when hosted in pyroxenites and granular harzburgites, while those hosted in dunites and poikilitic harzburgites display higher concentrations. The FFE ratio ($Fe^{3+}/Fe^{3+} + Fe^{2+}$) shows wide scatter in the LZ, while in the CZ a more limited range is displayed with a general increase upwards. Finally, the $Mg\#_{chr}$ shows no general trends through the sequence, although feature (g) above is clearly illustrated.

4.4.1. The Mineralogy of the Massive Chromitite Layers

In the NG-sequence all LG- and MG-chromitites as well as numerous chromite-rich layers were intersected. As mentioned earlier the MG1-chromitite seems to be absent at Union Section, but a chromitiferous layer (sample: NG1-90.33) at a depth of 340.33 m might be equivalent to the MG1-chromitite. In Table 11 the average compositions of each chromitite layer are listed (included are data from the Merensky Reef chromitite stringers, the UG2-and UG1-chromitites from Eales and Reynolds (1986) as well as minor chromitite layers). These compositions were calculated from microprobe data of chr and hence represent the average compositions of the ML-chr and not the whole-rock composition of the chromitite layer. The number of samples used for the calculation is denoted as n.

The fields of the individual ML-chr analyses were presented in the triangular diagram (Fig. 20) and no further comment is necessary. Figure 23 depicts the compositional variations (in cations) of the chromitites through the sequence.

TABLE 11A Composition of Chromite in the Massive Chromitite Layers

Layer:	MRB[1)]	MRA[1)]	UG2[1)]	UG1[1)]	MG4B	MG4A	MG3	MG2	NG1-90	LG7	LG6A
wt.%											
TiO_2	1.16	0.92	0.91	0.67	0.76	0.83	0.69	0.79	0.74	0.71	0.54
Al_2O_3	16.81	17.83	17.00	18.36	18.18	17.92	18.21	17.27	17.69	15.39	13.99
Cr_2O_3	41.34	38.98	43.75	43.23	42.15	41.51	41.23	41.91	40.72	43.32	47.20
FeO	21.05	21.84	20.11	19.87	19.45	20.23	19.17	18.74	18.43	21.61	19.19
Fe_2O_3	9.86	11.22	8.33	7.64	8.66	8.99	9.49	9.64	11.39	9.69	8.16
MnO	0.52	0.55	0.49	0.48	0.29	0.28	0.28	0.27	0.26	0.30	0.28
NiO	0.19	0.18	0.19	0.15	0.13	0.12	0.14	0.14	0.14	0.14	0.11
MgO	9.07	8.48	9.22	9.60	10.17	9.63	10.24	10.44	10.85	8.36	9.66
Total	100.00	100.00	100.00	100.01	99.81	99.51	99.44	99.21	100.22	99.53	99.13
cations (based on 32 oxygens):											
Ti	0.2270	0.1800	0.1750	0.1293	0.1464	0.1615	0.1333	0.1544	0.1415	0.1401	0.1062
Al	5.1410	5.4530	5.1510	5.5310	5.4938	5.4540	5.5164	5.2569	5.3184	4.7781	4.3410
Cr	8.4780	7.9970	8.8890	8.7407	8.5425	8.4758	8.3802	8.5603	8.2130	9.0218	9.8290
Fe^{2+}	4.5680	4.7410	4.4970	4.3380	4.1696	4.3687	4.1214	4.0473	3.9317	4.7623	4.2270
Fe^{3+}	1.9250	2.1910	1.6120	1.4707	1.6709	1.7472	1.8367	1.8739	2.1856	1.9199	1.6176
Mn	0.1140	0.1240	0.1070	0.1037	0.0621	0.0619	0.0599	0.0592	0.0567	0.0677	0.0633
Ni	0.0390	0.0380	0.0390	0.0313	0.0277	0.0249	0.0279	0.0290	0.0284	0.0291	0.0232
Mg	3.5050	3.2780	3.5310	3.6563	3.8869	3.7060	3.9241	4.0189	4.1247	3.2674	3.7928
n	1	1	16	3	3	4	3	3	1	1	3
a	8	7	135	19	21	22	18	21	6	37	17
cationic ratios:											
Cr/Al	1.6491	1.4665	1.7257	1.5803	1.5554	1.5549	1.5209	1.6290	1.5443	1.8882	2.2650
$Mg\#_{chr}$	0.4342	0.4088	0.4398	0.4574	0.4825	0.4590	0.4877	0.4982	0.5120	0.4069	0.4729
FFE	0.2965	0.3161	0.2639	0.2532	0.2860	0.2855	0.3082	0.3165	0.3573	0.2873	0.2768
Cr/(Cr+Al)	0.6225	0.5946	0.6331	0.6124	0.6086	0.6085	0.6031	0.6195	0.6070	0.6538	0.6937
weight ratio of metals:											
Cr/Fe	1.22	1.07	1.40	1.42	1.36	1.29	1.31	1.35	1.25	1.26	1.57
standard deviation:											
wt.%											
TiO_2				0.0189	0.0242	0.0428	0.0234	0.0122			0.0370
Al_2O_3				0.9622	0.2139	0.4414	0.5465	0.3307			0.2546
Cr_2O_3				0.6188	0.2676	0.0753	0.5411	0.4425			0.1810
FeO				1.0195	0.3590	0.3421	0.2200	0.2293			0.2993
Fe_2O_3				0.3774	0.4913	0.5258	0.3296	0.3633			0.1466
MnO				0.0735	0.0065	0.0114	0.0095	0.0267			0.0194
NiO				0.0205	0.0003	0.0093	0.0211	0.0138			0.0124
MgO				0.8874	0.1378	0.2002	0.0282	0.1771			0.1796

Notes: 1) data from Eales and Reynolds (1986)
2) notation after Cousins and Feringa (1964)
3) FWC : massive layer below LG1-chromitite
LZML : massive chromitite lens in LZ
4) $Mg\#_{chr}$: cationic ratio of $Mg/(Mg + Fe^{2+})$
5) FFE : cationic ratio of $Fe^{3+}/(Fe^{3+} + Fe^{2+})$
6) Cr/Fe : weight ratio of Cr metal to Fe metal
7) n : number of samples
a : number of analyses
8) standard deviation calculated only where sample populations exceed one; see Appendix for intra-sample standard deviations

TABLE 11B Composition of Chromite in the Massive Chromitite Layers (cont.)

Layer:	LG6	LG5	LG4	LG3	LG2B	LG2A	LG1	FWC	LZML
wt.%									
TiO_2	0.64	0.55	0.43	0.44	0.39	0.44	0.47	0.52	0.59
Al_2O_3	12.30	12.77	14.43	12.28	12.40	12.12	12.89	13.22	14.06
Cr_2O_3	47.96	49.69	49.06	51.36	52.53	52.04	51.17	50.39	47.06
FeO	20.35	18.93	17.63	18.74	16.61	17.83	17.22	17.84	18.40
Fe_2O_3	9.14	7.56	6.90	7.05	6.59	6.92	7.28	7.36	9.27
MnO	0.29	0.29	0.31	0.29	0.27	0.29	0.29	0.29	0.33
NiO	0.12	0.11	0.09	0.09	0.09	0.11	0.10	0.12	0.18
MgO	8.89	9.84	10.78	9.97	11.37	10.56	11.10	10.73	10.36
Total	99.70	99.74	99.63	100.23	100.26	100.29	100.53	100.45	
cations (based on 32 oxygens):									
Ti	0.1286	0.1083	0.0840	0.0864	0.0760	0.0861	0.0917	0.1006	0.1148
Al	3.8455	3.9488	4.4147	3.7896	3.7911	3.7266	3.9320	4.0373	4.3090
Cr	10.0693	10.3383	10.0684	10.6465	10.7702	10.7424	10.4667	10.3270	9.6672
Fe^{2+}	4.5227	4.1739	3.8271	4.1153	3.6015	3.8936	3.7266	3.8670	3.9999
Fe^{3+}	1.8281	1.4962	1.3489	1.3911	1.2867	1.3589	1.4178	1.4346	1.8132
Mn	0.0659	0.0658	0.0677	0.0652	0.0601	0.0633	0.0642	0.0629	0.0731
Ni	0.0262	0.0239	0.0185	0.0195	0.0190	0.0222	0.0201	0.0243	0.0374
Mg	3.5138	3.8447	4.1707	3.8864	4.3953	4.1069	4.2808	4.1463	4.0134
n	4	7	3	5	2	3	3	2	1
a	26	29	18	17	10	12	18	7	5
cationic ratios:									
Cr/Al	2.6260	2.6534	2.2881	2.8426	2.8411	2.8866	2.6625	2.5579	2.2435
$Mg\#_{chr}$	0.4372	0.4794	0.5215	0.4857	0.5496	0.5133	0.5346	0.5174	0.5008
FFE	0.2881	0.2651	0.2607	0.2539	0.2632	0.2588	0.2759	0.2706	0.3119
Cr/(Cr+Al)	0.7237	0.7237	0.6951	0.7375	0.7396	0.7425	0.7269	0.7189	0.6917
weight ratio of metals:									
Cr/Fe	1.48	1.71	1.82	1.82	2.05	1.91	1.90	1.81	1.55
standard deviation:									
wt.%									
TiO_2	0.0839	0.0315	0.0546	0.0475	0.0228	0.0103	0.0205	0.0048	
Al_2O_3	0.7068	1.4202	0.6032	1.2824	0.0979	0.4823	0.1551	0.0334	
Cr_2O_3	0.1078	0.7062	1.5852	1.4072	0.1445	0.2243	0.1746	0.0053	
FeO	1.2804	1.9384	1.2646	2.1021	0.1145	0.5539	0.7444	0.0897	
Fe_2O_3	0.4199	0.7126	0.4783	0.4753	0.0318	0.2105	0.2078	0.1789	
MnO	0.0394	0.0381	0.0162	0.0245	0.0057	0.0172	0.0029	0.0261	
NiO	0.0130	0.0312	0.0154	0.0351	0.0158	0.0367	0.0238	0.0221	
MgO	0.8796	1.5339	0.7511	1.4495	0.1010	0.4172	0.4507	0.1054	

Notes: 1) data from Eales and Reynolds (1986)
2) notation after Cousins and Feringa (1964)
3) FWC : massive layer below LG1-chromitite
LZML : massive chromitite lens in LZ
4) $Mg\#_{chr}$: cationic ratio of $Mg/(Mg + Fe^{2+})$
5) FFE : cationic ratio of $Fe^{3+}/(Fe^{3+} + Fe^{2+})$
6) Cr/Fe : weigth ratio of Cr metal to Fe metal
7) n : number of samples
a : number of analyses
8) standard deviation calculated only where sample populations exceed one; see Appendix for intra-sample standard deviations

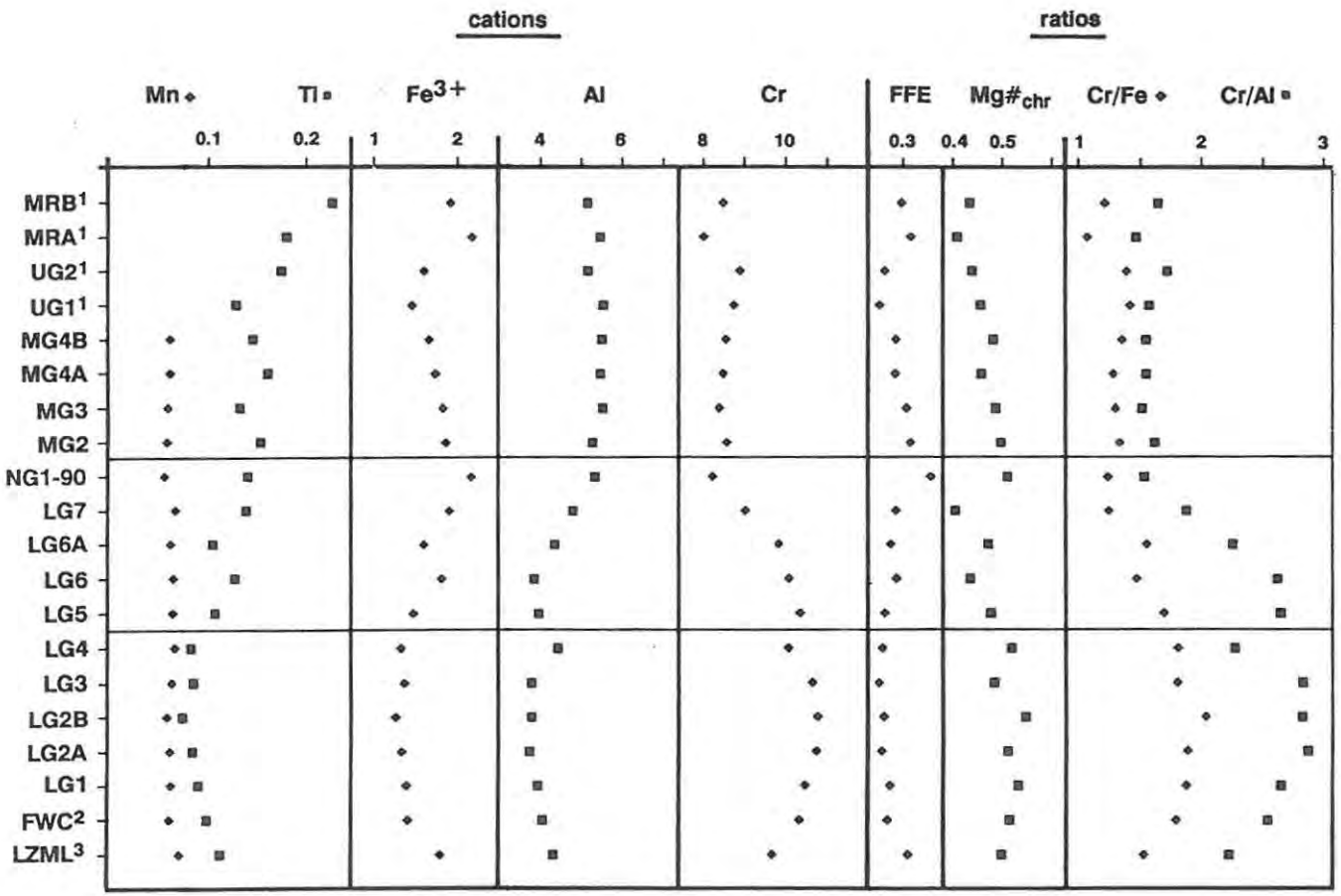

Fig. 23 Compositions of chrome-spinel from chromitite layers at Union Section (solid lines depict group boundaries, see text).

The level of Ti as an indicator element for fractionation increases upwards. This enrichment trend commences at a level above the LG4-chromitite; Fe^{3+} follows a similar distribution pattern. There is no significant variation in Mn values or the FFE number, which implies that the ratio of ferric to ferrous iron remains more or less steady. The most common cations Cr and Al display an antipathetic relationship in support of the described cation exchange. At the level of the sample NG1-90.33 the Al_2O_3 concentrations are in excess of 17.0 wt.% (>5.0 cations) and this continues throughout the remainder of the ML-chr. At the same level the Cr cations drop below 9.0 and though a slight increase towards the UG2-chromitite is apparent this value is not reached again. The Cr levels are highest within the layers associated with or between the olivine-rich intervals, but the LG4-chromitite, the sole chromitite layer with a dunite as immediate foot- and hangingwall, does not show the highest values. The Cr/Fe and Cr/Al ratios duplicate the trend set by Cr.

In summary, the following conclusions can be drawn:

a) the variations displayed by the massive chromitite layers appear to reflect the evolution of the silicate rocks in which they are hosted;

b) no simple general distribution pattern is evident;

c) the appearance of cumulus pla can not be detected in the mineralogy of the ML-chr; the shift to significantly higher Al values occurs at a stratigraphic level ca. 125 m below the actual lCZ - uCZ boundary. However, the remnants of cumulus pla as rounded and absorbed inclusions in opx below this boundary points to the possibility of cumulus pla having been present in the liquid at much lower levels (Eales et al., 1990a,b).

d) the massive chromitite layers can be geochemically subdivided into three groups (Teigler, 1990):

Group 1	LG1- to LG4-chromitites	Cr/Fe >1.75	Fe^{3+}<1.45	Ti<0.1
Group 2	LG5- to LG7-chromitites	Cr/Fe <1.72	Fe^{3+}>1.48	Ti>0.1
Group 3	all MG-and UG-chromitites	Cr/Al <1.70	Ti> 0.128	

4.5. Plagioclase Feldspar

Feldspar occurs as a cumulus phase in three intervals of the sequence and as the most abundant postcumulus phase in the remainder. A total of 250 samples (1216 analyses; 36 samples by Haikney are included) were investigated. Apart from two K-feldspar grains in sample NG1-496.43C at a depth of 746.53 m all remaining analysed feldspars are plagioclase feldspars. The unusual K-feldspar has the composition $An_{4.3}Ab_{41.4}Or_{54.3}$. For all further calculations and in most diagrams this sample was omitted. A plot of average compositions in the triangular diagram (Fig. 24) demonstrates the range of pla compositions.

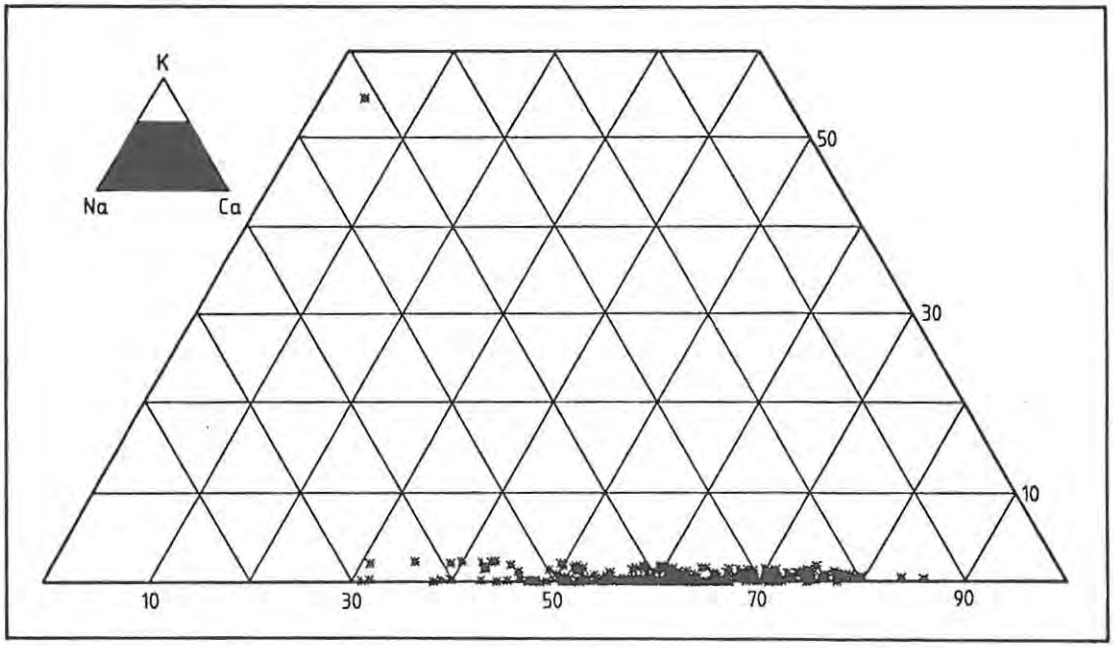

Fig. 24 Compositional range of plagioclase in the NG-sequence.

Cumulus pla ranges from $An_{51.4}$ to $An_{85.7}$, whereas postcumulus species display An values between 30.8 and 77.4 mol.%. This means that postcumulus pla has generally 10 - 20% less An molecule. Postcumulus pla displays not only a high intersample but also intrasample variability (easily detectable by a high sd), which can cover a range of more than 39 % in An molecule (e.g. sample NG2-120.45: $An_{min}26.4$ - $An_{max}66.1$, core domains).

Therefore for most of the samples the An_{min} and An_{max} are also depicted in Fig. 26. This high intrasample variability may conceal any trend in diagrams depicting variations with height.

TABLE 12 Selected Microprobe Analyses of Core and Rim Domains of Cumulus Plagioclase

Sample:	NG3-170.34			NG3-174.44			NG3-194.74		NG3-213.18	
Analysis no.:	120.3	120.4	121.3	121.6	121.4	121.5	122.3	122.4	123.3	123.4
Domain:	Core	Rim	Core	Rim	Core	Rim	Core	Rim	Core	Rim
wt.%										
SiO_2	49.03	48.03	48.78	48.21	48.79	46.74	48.26	47.85	47.93	46.86
Al_2O_3	31.69	32.89	32.54	32.88	32.52	34.05	32.55	32.46	32.37	32.96
FeO	0.20	0.22	0.23	0.32	0.21	0.23	0.23	0.20	0.25	0.33
CaO	15.57	16.64	15.59	15.92	15.54	17.14	16.02	15.82	16.45	16.94
Na_2O	2.85	2.36	2.64	2.52	2.76	1.79	2.51	2.59	2.45	2.17
K_2O	0.14	0.09	0.14	0.14	0.17	0.07	0.13	0.10	0.14	0.10
Total	99.48	100.23	99.93	99.98	99.99	100.03	99.69	99.02	99.59	99.36
cations (based on 32 oxygens):										
Si	9.0282	8.8051	8.9377	8.8461	8.9377	8.5952	8.8786	8.8631	8.8462	8.6895
Al	6.8776	7.1060	7.0276	7.1097	7.0218	7.3789	7.0586	7.0844	7.0413	7.2032
Fe^{2+}	0.0314	0.0335	0.0355	0.0486	0.0316	0.0356	0.0352	0.0314	0.0388	0.0504
Ca	3.0712	3.2680	3.0617	3.1306	3.0498	3.3777	3.1573	3.1395	3.2531	3.3643
Na	1.0161	0.8369	0.9385	0.8960	0.9808	0.6393	0.8942	0.9280	0.8758	0.7804
K	0.0329	0.0220	0.0333	0.0319	0.0403	0.0166	0.0306	0.0248	0.0320	0.0227
Total	20.0575	20.0714	20.0344	20.0630	20.0619	20.0433	20.0544	20.0712	20.0871	20.1105
cationic ratio:										
An	0.7454	0.7919	0.7591	0.7714	0.7492	0.8374	0.7734	0.7672	0.7818	0.8073

Notes: 1) An : cationic ratio of Ca/(Ca + Na + K)

Although no detailed study of zonation of feldspar was done, mainly because of the focus of this study, some findings derived mainly from core - rim couplets are outlined below. Cumulus pla appears to be reversely zoned, i.e. in 4 out of 5 samples (Table 12) the rim analyses are higher in An component. The FeO concentrations are correspondingly higher. Similar reversed zoning patterns were described by Field (1987). A sharp decline in K levels (Table 13) was also observed by Field (op.cit.). Postcumulus pla was investigated in a similar way, despite the problems of an equivocal determination of domains in interstitial phases. The results are listed in Table 14.

TABLE 13 Selected Microprobe Analyses of Core and Rim Domains of Postcumulus Plagioclase

Sample:	NG1-91.40		NG1-29.80		NG1-35.00		NG1-685.40		NG1-475.10		NG2-754.00	
Analysis no.:	6.1	6.2	27.2	27.1	346.3	346.4	795.1	795.2	916.1	916.2	266.1	266.2
Domain:	Core	Rim	Core	Rim	Core	Rim	Core	Rim	Core	Rim	Core	Rim
wt.%												
SiO_2	59.02	58.92	55.52	55.64	49.99	51.24	52.49	53.87	55.59	55.22	57.22	52.50
Al_2O_3	25.67	26.18	28.25	28.17	31.48	30.70	30.34	29.99	29.32	28.84	27.21	29.64
FeO	0.12	0.17	0.26	0.23	0.22	0.25	0.12	0.24	0.14	0.12	0.21	0.14
CaO	8.27	8.36	10.53	10.50	14.79	13.83	12.40	11.85	11.60	11.05	9.80	12.49
Na_2O	6.89	6.84	5.33	5.44	3.05	3.42	4.46	4.90	4.55	5.17	6.16	4.43
K_2O	0.50	0.47	0.06	0.08	0.00	0.01	0.02	0.03	0.11	0.14	0.27	0.23
Total	100.47	100.93	99.95	100.05	99.52	99.43	99.82	100.89	101.32	100.54	100.87	99.43
cations (based on 32 oxygens):												
Si	10.5296	10.4662	9.9991	10.0114	9.1610	9.3648	9.5258	9.6617	9.8801	9.9018	10.2089	9.5812
Al	5.3964	5.4808	5.9954	5.9738	6.7993	6.6123	6.4891	6.3386	6.1420	6.0945	5.7212	6.3755
Fe^{2+}	0.0174	0.0247	0.0394	0.0351	0.0338	0.0381	0.0185	0.0358	0.0211	0.0185	0.0315	0.0207
Ca	1.5814	1.5920	2.0316	2.0246	2.9037	2.7073	2.4103	2.2769	2.2083	2.1220	1.8734	2.4428
Na	2.3814	2.3535	1.8605	1.8964	1.0828	1.2114	1.5676	1.7050	1.5690	1.7959	2.1301	1.5687
K	0.1135	0.1059	0.0147	0.0175	0.0004	0.0017	0.0041	0.0070	0.0256	0.0324	0.0612	0.0530
Total	20.0197	20.0231	19.9407	19.9587	19.9810	19.9356	20.0155	20.0250	19.8462	19.9652	20.0262	20.0419
cationic ratio:												
An	0.3879	0.3930	0.5200	0.5141	0.7283	0.6906	0.6053	0.5708	0.5807	0.5372	0.4609	0.6010

Notes: 1) An : cationic ratio of Ca/(Ca + Na + K)

In contrast to the cumulus species the core domains are usually Ca-richer than the rim domains apart from sample NG2-754.00. A possible decoupling of FeO and An contents in postcumulus pla , i.e. FeO-enriched rims in spite of lower An contents, might point to an enrichment of Fe in the interstitial liquid. In the cumulus variety a positive relationship of Fe and An content can be attributed to a number of processes: a) contemporaneous enrichment of FeO and CaO in the liquid, b) increase in temperature and/or pressure, c) introduction of H_2O, volatiles, or any element which changes the activity of Ca and/or Fe in the liquid.

Morse and Nolan (1984) suggested that the origin of An-rich rims in plagioclase in the Kiglapait intrusion stems from intercumulus liquid, which is increasingly enriched in augite component. A subsolidus genesis is ruled out by these authors. This theory would explain the observed geochemical gradients of the cumulus pla and is therefore favoured. The An-rich core domains of postcumulus, interstitial pla might indicate that these grains did not nucleate at the interface between cumulus crystal and liquid, but somewhere in the central part of the pore space. This is difficult to explain because homogeneous nucleation demands a far higher degree of supercooling or supersaturation than heterogeneous crystallization. However, release of crystallization heat in the immediate vicinity of the cumulus phase might prevent nucleation at the interface. Because no detailed and systematic study was done the conclusions are tentative.

Another interesting pla population occurs in the limited interval from the top of the NG-sequence to a depth of ca. 240 m. Here, many of the cumulus opx grains contain small pla inclusions, which are commonly well rounded and/or display features of resorption. The upper part of this sequence, the hangingwall of the MG4-chromitite (or deep footwall of the UG1-chromitite) was the objective of a detailed study by Eales et al. (1990a). They interpreted these inclusions as earlier-generation feldspar, which was subsequently exposed to liquids which had only opx on the liquidus, thus resorption and subsequent inclusion could take place.

A limited number of these inclusions were analysed by the present writer and compared with not-included grains. The results are summarized in Table 14. In pyroxenites above and below the MG4-chromitite the included grains do not differ systematically and significantly from the interstitial pla. However, in norites below the MG4-chromitite (below the depth of ca. 152 m; last three samples in Table 14) the inclusions contain invariably more An molecule than the free pla grains. This is in agreement with the findings of Eales et al. (1990a).

TABLE 14 Selected Microprobe Analyses of Core Domains of Plagioclase Inclusions and Cumulus or Postcumulus Grains

Sample:	NG3-3.98					NG3-28.62		NG3-55.00		NG3-79.60		
Analysis no.:	104.1	104.2	104.3	104.4	104.5	111.2	111.4	112.3	112.5	107.1	107.4	107.5
Habit:	disp	inc	disp	inc	disp	disp	inc	disp	inc	disp	inc	inc
wt.%												
SiO_2	51.38	50.38	50.16	51.42	49.43	48.82	50.51	50.26	50.09	51.44	50.10	51.77
Al_2O_3	30.59	31.59	31.01	30.18	31.42	31.77	30.74	30.58	30.60	30.53	31.59	30.40
FeO	0.21	0.41	0.25	0.35	0.37	0.16	0.45	0.25	0.36	0.33	0.51	0.34
CaO	13.53	14.56	14.34	13.16	14.80	15.36	14.01	14.81	14.79	13.37	14.53	13.28
Na_2O	3.81	3.41	3.32	3.85	3.11	2.80	3.58	3.28	3.15	3.72	3.24	3.94
K_2O	0.27	0.20	0.24	0.34	0.16	0.18	0.19	0.20	0.19	0.26	0.19	0.23
Total	99.79	100.54	99.32	99.28	99.29	99.09	99.49	99.38	99.17	99.65	100.16	99.96
cations (based on 32 oxygens):												
Si	9.3750	9.1618	9.2203	9.4286	9.1066	9.0191	9.2707	9.2451	9.2341	9.3938	9.1458	9.4251
Al	6.5785	6.7699	6.7186	6.5211	6.8223	6.9174	6.6503	6.6298	6.6476	6.5710	6.7962	6.5225
Fe^{2+}	0.0322	0.0621	0.0382	0.0538	0.0574	0.0247	0.0694	0.0384	0.0551	0.0510	0.0777	0.0521
Ca	2.6445	2.8360	2.8244	2.5845	2.9208	3.0394	2.7545	2.9189	2.9206	2.6166	2.8410	2.5914
Na	1.3490	1.2010	1.1821	1.3671	1.1123	1.0021	1.2733	1.1698	1.1238	1.3152	1.1455	1.3917
K	0.0622	0.0459	0.0562	0.0784	0.0379	0.0414	0.0454	0.0458	0.0455	0.0613	0.0451	0.0535
Total	20.0414	20.0767	20.0396	20.0336	20.0573	20.0440	20.0636	20.0478	20.0268	20.0089	20.0513	20.0363
cationic ratio:												
An	0.6520	0.6946	0.6952	0.6413	0.7175	0.7444	0.6762	0.7060	0.7141	0.6553	0.7047	0.6420

Sample:	NG3-99.60			NG3-126.05			NG3-175.05		NG3-208.15		NG3-212.93	
Analysis no.:	109.2	109.4	109.5	113.1	113.3	113.4	218.2	218.5	221.3	221.2	209.6	209.2
Habit:	disp	inc	inc	disp	disp	inc	inc	disc	inc	disc	inc	disc
wt.%												
SiO_2	49.70	49.82	48.30	49.51	51.35	50.30	48.29	48.50	47.61	48.00	46.55	47.22
Al_2O_3	32.00	32.02	32.48	31.53	30.37	31.10	32.62	32.54	33.31	33.30	33.49	33.43
FeO	0.24	0.28	0.60	0.28	0.20	0.39	0.20	0.15	0.26	0.25	0.41	0.27
CaO	15.26	14.80	15.70	14.90	13.75	14.54	16.62	16.21	17.07	16.78	17.63	17.05
Na_2O	2.97	3.14	2.71	3.06	3.72	3.34	2.68	2.84	2.38	2.52	2.04	2.27
K_2O	0.17	0.16	0.14	0.18	0.24	0.21	0.11	0.12	0.12	0.13	0.09	0.12
Total	100.33	100.21	99.94	99.45	99.64	99.89	100.53	100.37	100.74	100.97	100.21	100.36
cations (based on 32 oxygens):												
Si	9.0617	9.0851	8.8801	9.1035	9.3876	9.2053	8.8353	8.8764	8.7064	8.7483	8.5819	8.6689
Al	6.8766	6.8821	7.0377	6.8332	6.5424	6.7076	7.0349	7.0183	7.1786	7.1530	7.2765	7.2335
Fe^{2+}	0.0359	0.0421	0.0929	0.0435	0.0307	0.0603	0.0313	0.0235	0.0391	0.0378	0.0626	0.0414
Ca	2.9807	2.8915	3.0918	2.9347	2.6934	2.8506	3.2577	3.1787	3.3446	3.2770	3.4833	3.3538
Na	1.0498	1.1084	0.9641	1.0888	1.3187	1.1846	0.9499	1.0060	0.8428	0.8887	0.7299	0.8066
K	0.0405	0.0375	0.0333	0.0414	0.0559	0.0496	0.0263	0.0290	0.0285	0.0293	0.0212	0.0269
Total	20.0451	20.0468	20.0998	20.0451	20.0285	20.0580	20.1353	20.1320	20.1400	20.1342	20.1554	20.1311
cationic ratio:												
An	0.7322	0.7162	0.7561	0.7220	0.6621	0.6978	0.7694	0.7544	0.7933	0.7812	0.8226	0.8009

Notes: 1) incl: plagioclase inclusion in orthopyroxene
disc: discrete cumulus grain
disp: discrete postcumulus grain
2) An : cationic ratio of Ca/(Ca + Na + K)

In the diagrams of Fig. 25 the elements Ca, Na and Fe are plotted against Al (all in wt.% oxides).

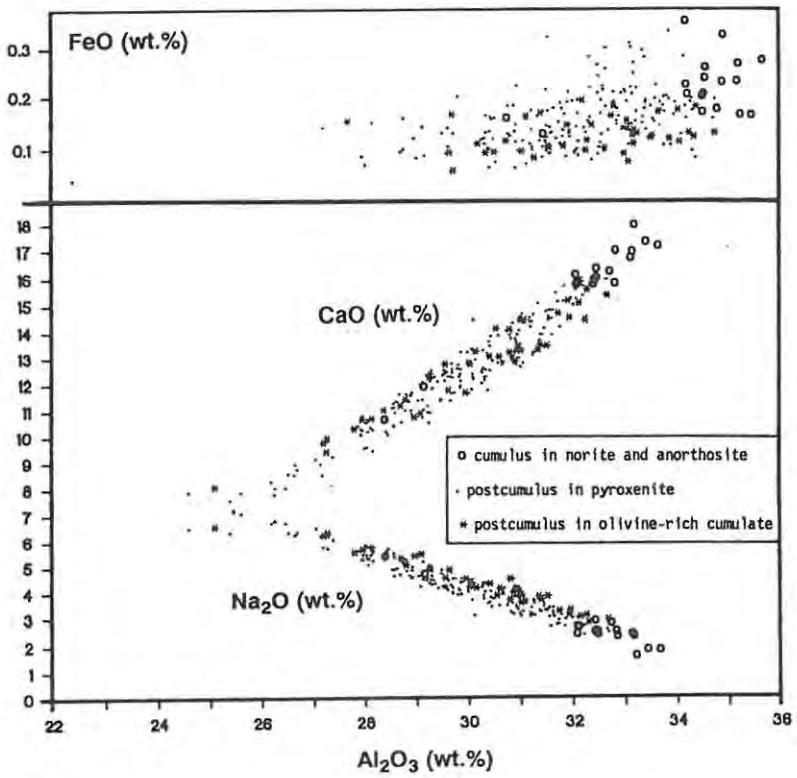

Fig. 25 Plagioclase mineralogy - variation diagrams (note scale breaks).

The positive and negative relationship of Ca and Na in both textural species requires no further explanation. The FeO concentrations indicate a weak positive relationship but show a wide scatter of the datum points on the An-rich side.

Finally, the variations of pla in An content with height (depicted are average, maximum and minimum values, Fig. 26) show the wide spread discussed. However, an increase with height is initiated at a depth of ca. 1000 m (Eales et al., 1990b). This irregular increase is accompanied by a general increase of Fe concentrations as well as the modal proportion of pla in the cumulate pile. This might suggest that a gradual enrichment in pla components in the supernatant liquid (ca. 1000 - 215 m depth) led eventually to the nucleation of cumulus pla in the uCZ.

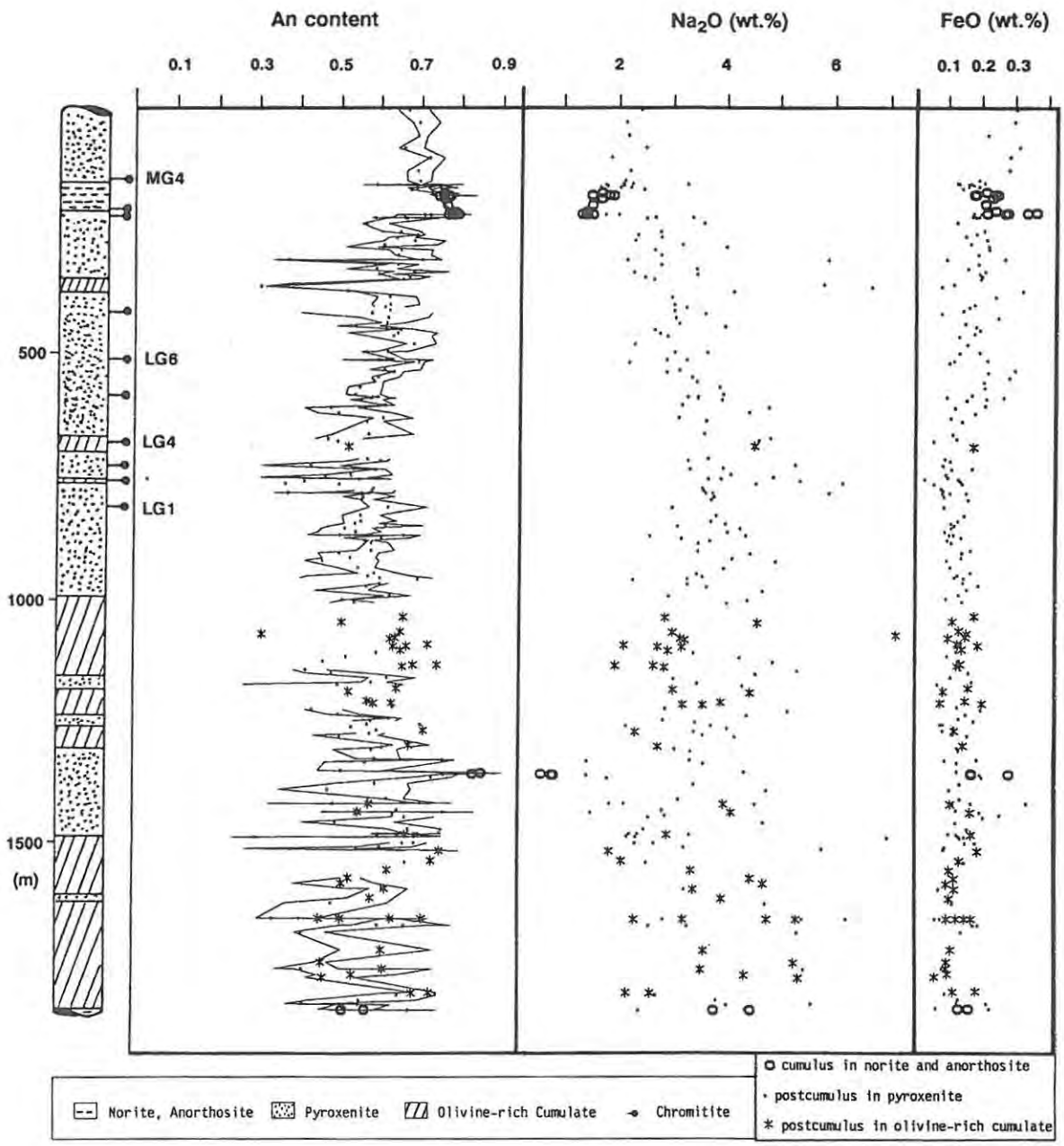

Fig. 26 Cryptic variations of plagioclase throught the NG-sequence, solid lines show maximum and minimum An values.

4.6. Other postcumulus phases

In this section the mineralogy of cpx, amphibole and phlogopite will be briefly described. No detailed and systematic study was done. However, the data obtained permit a classification of these phases and allow an assessment of their possible impact on whole-rock geochemistry.

4.6.1. Amphibole

Amphibole is an accessory late postcumulus phase and occurs in some coarse-grained, mesocumulate pyroxenites in the form of fillings of interstices, as selvages around cpx or as blebs in opx (probably altered cpx blebs). The association of the majority of the amp with cpx may point to an origin as a late-stage alteration product of cpx and minor opx (uralitisation). A total of 26 analyses of core domains (12 samples in the lCZ) were analysed and selected amp analyses are presented in Table 15. The cations were calculated on the basis of 23 oxygens following the recommendation by the Subcommittee on the Amphibole Group (1978). After this classification all analysed amphibole grains are calcic amphiboles, and hence plot in the fields of tremolite, tremolitic hornblende, actinolitic hornblende and one grain in the field of magnesio-hornblende, depending upon their Si concentrations (Fig. 27).

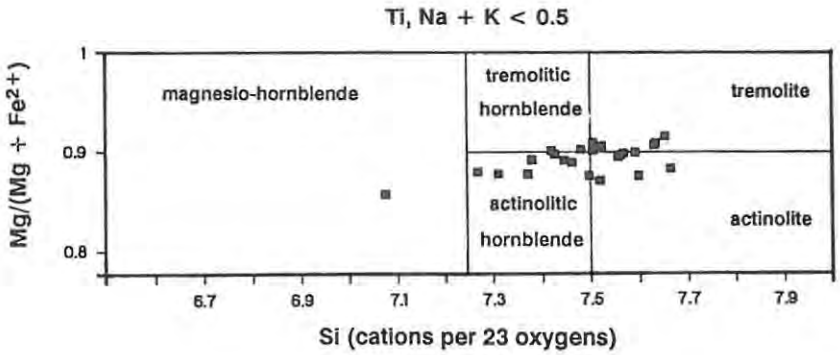

Fig. 27 Classification of amphiboles in the NG-sequence (after Subcommittee on the Amphibole Group, 1978).

For the purpose of this study the $Mg\#_{amp}$ was calculated using total Fe as determined by the microprobe. The variations in Cr_2O_3 values (0.11-1.24 wt.%) might indicate two possible stages of amphibole formation: a) a late-stage magmatic origin with low Cr and b) a postmagmatic formation by alteration of pyroxenes, which led to amphibole with higher Cr levels.

Because of the wide sample spacing an in-depth interpretation of variations with height is not possible, but the trend displayed by the $Mg\#_{amp}$ in the investigated interval (Fig. 28) appears to be roughly parallel to the pattern set by the $Mg\#_{opx}$.

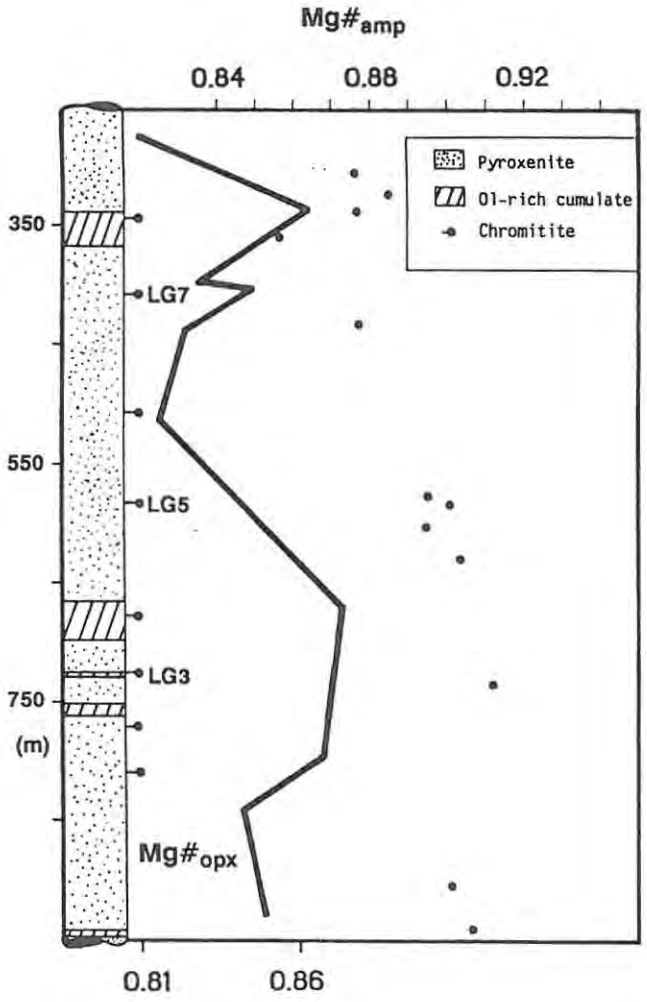

Fig. 28 Cryptic variations of the $Mg\#_{amp}$ with height in NG1.

TABLE 15 Selected Microprobe Analyses: Amphibole

Sample: NG1-	56.60	74.45	89.55	110.52	183.70	327.45	353.40	380.35	486.55	655.10	690.90
Analysis no.:	584.1	590.3	588.1	596.1	602.1	624.1	628.3	633.1	641.1	669.3	688.1
wt.%											
SiO_2	55.24	52.03	52.38	50.54	51.68	55.06	54.55	53.38	55.52	54.52	55.23
TiO_2	0.08	0.23	0.45	0.43	0.55	0.08	0.30	0.26	0.08	0.23	0.04
Al_2O_3	3.05	5.47	5.06	7.03	5.11	3.64	3.70	4.18	3.18	3.80	2.60
Cr_2O_3	0.13	1.24	0.57	1.21	1.24	0.26	0.47	0.79	0.39	0.29	0.11
FeO	5.11	5.07	5.11	6.03	5.12	4.33	4.38	4.03	3.88	4.27	4.11
MnO	0.10	0.06	0.09	0.10	0.07	0.11	0.10	0.03	0.07	0.09	0.09
NiO	0.04	0.11	0.07	0.10	0.12	0.06	0.09	0.05	0.08	0.03	0.01
MgO	21.82	20.81	20.56	20.30	20.68	21.89	21.54	21.01	21.91	22.06	22.62
CaO	11.34	12.00	11.66	10.91	11.11	12.15	11.85	12.39	12.64	12.58	12.68
Na_2O	0.58	0.85	0.84	1.59	0.74	0.43	0.67	0.64	0.47	0.62	0.40
Total	97.48	97.87	96.79	98.23	96.40	98.00	97.66	96.76	98.23	98.50	97.91
cations (based on 23 oxygens):											
Si	7.6646	7.2692	7.3725	7.0757	7.3119	7.5920	7.5609	7.4800	7.6335	7.5044	7.6305
Ti	0.0085	0.0246	0.0477	0.0449	0.0585	0.0088	0.0317	0.0277	0.0087	0.0242	0.0043
Al	0.4994	0.9013	0.8389	1.1604	0.8521	0.5917	0.6045	0.6908	0.5157	0.6173	0.4241
Cr	0.0144	0.1369	0.0630	0.1337	0.1384	0.0279	0.0516	0.0875	0.0420	0.0321	0.0120
Fe^{2+}	0.5930	0.5921	0.6011	0.7058	0.6059	0.4991	0.5075	0.4718	0.4465	0.4912	0.4744
Mn	0.0115	0.0074	0.0109	0.0121	0.0083	0.0127	0.0117	0.0037	0.0080	0.0103	0.0105
Ni	0.0040	0.0123	0.0082	0.0117	0.0136	0.0065	0.0103	0.0051	0.0084	0.0039	0.0016
Mg	4.5117	4.3327	4.3130	4.2366	4.3610	4.4983	4.4510	4.3893	4.4907	4.5261	4.6586
Ca	1.6854	1.7958	1.7585	1.6358	1.6838	1.7948	1.7595	1.8602	1.8626	1.8550	1.8768
Na	0.1555	0.2297	0.2297	0.4312	0.2019	0.1155	0.1810	0.1742	0.1262	0.1647	0.1084
Total	15.1478	15.3019	15.2436	15.4480	15.2353	15.1472	15.1698	15.1903	15.1421	15.2291	15.2013
cationic ratio:											
$Mg\#_{amp}$	0.8838	0.8798	0.8777	0.8572	0.8780	0.9001	0.8977	0.9029	0.9096	0.9021	0.9076

Notes: 1) $Mg\#_{amp}$: cationic ratio of $Mg/(Mg + Fe^{2+})$

4.6.2. Phlogopite

The analytical results are tabulated in Table 16. Because K_2O concentrations were not determined Table 16 also gives three analyses from other parts of the complex. It is evident from the analyses that the mica encountered is a phlogopite with a Mg : Fe ratio of > 3:1 (based on wt.%). The Ti contents range from 2.2 to 5.1 wt.% with Cr_2O_3 levels of 0.84 - 1.88 wt.%.

TABLE 16 Selected Microprobe Analyses: Phlogopite

Sample: NG1-	380.35	500.50	532.14	655.10	660.90	690.90	695.50	720.15	ZS	R	CS
Analysis no.:	634.1	648.4	266.3	669.4	674.1	688.2	108.6	690.4	280	M4	
wt.%											
SiO_2	39.16	36.73	39.76	40.58	40.24	39.92	39.58	39.65	39.26	39.35	39.14
TiO_2	3.04	5.09	2.51	2.90	2.81	3.81	2.71	3.62	3.78	5.32	4.96
Al_2O_3	13.93	13.23	13.57	13.91	13.98	13.77	13.23	13.87	13.81	13.79	15.36
Cr_2O_3	1.62	1.75	1.88	1.31	1.11	0.84	1.22	1.25	1.87	1.33	1.66
FeO	5.33	5.69	4.88	5.51	5.85	6.17	5.82	5.43	5.23	8.60	2.67
MnO	0.01	0.03	0.01	0.05	0.05	0.01	0.00	0.00	0.03		0.04
NiO	0.16	0.16	0.24	0.13	0.11	0.16	0.15	0.14	0.20		
MgO	20.24	20.10	22.54	21.89	21.81	20.73	21.00	20.67	21.21	17.71	22.42
CaO	0.08	0.00	0.04	0.00	0.00	0.01	0.00	0.03			
Na_2O	0.23	0.17	0.19	0.18	0.15	0.16	0.19	0.17	0.47		1.24
K_2O	NA	NA	NA	NA	NA	NA	NA	NA	9.03	9.17	8.14
Total	83.79	82.95	85.62	86.46	86.11	85.59	83.90	84.82	94.89		
cations (based on 23 oxygens):											
Si	6.2333	5.9661	6.1950	6.2550	6.2362	6.2339	6.2978	6.2294			
Ti	0.3633	0.6221	0.2945	0.3364	0.3271	0.4471	0.3246	0.4272			
Al	2.6139	2.5321	2.4923	2.5259	2.5539	2.5338	2.4805	2.5687			
Cr	0.2044	0.2246	0.2310	0.1601	0.1361	0.1040	0.1531	0.1555			
Fe^{2+}	0.7096	0.7729	0.6357	0.7105	0.7578	0.8062	0.7751	0.7129			
Mn	0.0010	0.0038	0.0007	0.0067	0.0063	0.0019	0.0000	0.0000			
Ni	0.0199	0.0208	0.0304	0.0158	0.0141	0.0200	0.0192	0.0176			
Mg	4.8010	4.8645	5.2349	5.0290	5.0367	4.8267	4.9804	4.8394			
Ca	0.0129	0.0000	0.0065	0.0000	0.0002	0.0014	0.0003	0.0043			
Na	0.0702	0.0533	0.0559	0.0524	0.0463	0.0499	0.0593	0.0523			
Total	15.0294	15.0601	15.1768	15.0918	15.1148	15.0249	15.0903	15.0074			
cationic ratio:											
$Mg\#_{phl}$	0.8712	0.8629	0.8917	0.8762	0.8692	0.8569	0.8653	0.8716			

Notes: 1) ZS-280 : analysis from Botha (1987); in pyroxenite below the lower ol-rich unit the 1CZ (B-unit), Zandspruit
R-M4 : analysis from Kruger (1983); sample from Merensky cyclic unit, Rustenburg area
CS : analysis from Cameron (1980); in pyroxenite above the LG6-chromitite (E-unit), Eastern Bushveld Complex
2) NA : not analysed; because K_2O levels in whole-rock analyses are generally < 0.3 wt.%
3) $Mg\#_{phl}$: cationic ratio of $Mg/(Mg + Fe^{2+})$

4.6.3. Clinopyroxene

Cpx, after pla the most abundant postcumulus phase, was investigated throughout the entire sequence. A total of 433 analyses were used to compile average compositions for 95 samples. Clinopyroxene is present in three habits : a) as a filling of interstices, b) as oikocrysts, or c) as exsolution lamellae or blebs in opx. The data of cpx in different microdomains (selected analyses are presented in Table 17 and Fig. 29) show no systematic and significant differences. Hence, all cpx species in each sample were formed under similar physico-chemical conditions, which implies that the exsolution within the opx and the formation of interstitial or poikilitic cpx happened more or less contemporaneously. Though it is difficult to determine crystal domains in postcumulus anhedral phases some cpx grains were probed along traverses to detect zoning structures. However, as demonstrated in Fig. 29 and Table 18 no general pattern was found. Hence, all analyses regardless of beam position were used to calculate average compositions.

In the new classification scheme of pyroxenes (Subcommittee on pyroxenes, 1989) the datum points of the average compositions occupy a field which straddles the diopside - augite boundary (Fig. 30).

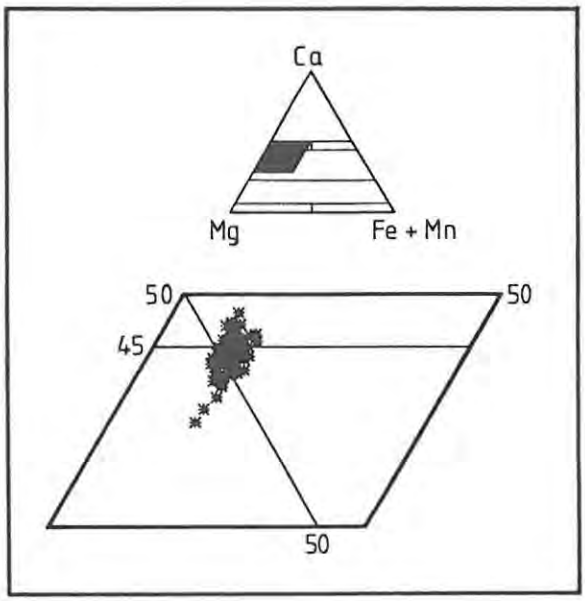

Fig. 30 Compositional range of clinopyroxene in the NG-sequence.

TABLE 17 Selected Microprobe Analyses of Core Domains of Clinopyroxene with Different Textural Habits

Sample:	NG1-29.80		NG1-79.75		NG1-589.60			NG1-603.10			NG1-695.5	
Analysis no.:	22.2	23.2	16.2	17.1	210.1	210.3	210.5	239.2	239.4	239.6	108.1	108.2
Habit:	poik	int	int	poik	int	poik	exs	poik	exs	int	exs	int
wt.%												
SiO_2	53.14	53.86	54.25	53.39	53.99	54.01	53.54	53.64	53.43	53.37	54.02	53.70
TiO_2	0.29	0.26	0.29	0.34	0.20	0.26	0.18	0.34	0.38	0.30	0.15	0.34
Al_2O_3	1.99	1.61	1.60	1.70	1.31	1.24	1.88	1.89	1.43	1.55	1.80	1.76
Cr_2O_3	0.85	0.82	0.83	0.73	0.74	0.75	1.02	0.92	0.97	0.87	0.79	0.94
FeO	4.12	3.79	4.06	4.28	3.03	3.22	3.31	3.77	3.59	3.75	3.25	3.71
MnO	0.12	0.08	0.14	0.12	0.07	0.09	0.09	0.12	0.12	0.12	0.05	0.07
NiO	0.02	0.02	0.06	0.02	0.05	0.04	0.05	0.09	0.09	0.09	0.04	0.03
MgO	17.18	16.83	15.85	17.04	17.39	17.57	17.02	17.16	17.06	17.54	17.08	17.17
CaO	21.76	22.18	22.41	21.87	22.78	22.48	22.56	21.66	22.36	21.86	22.73	21.73
Na_2O	0.40	0.40	0.33	0.35	0.37	0.41	0.46	0.44	0.42	0.43	0.47	0.44
Total	99.85	99.85	99.82	99.84	99.92	100.06	100.10	100.04	99.85	99.88	100.36	99.90
cations (based on 6 oxygens):												
Si	1.9429	1.9655	1.9816	1.9529	1.9658	1.9646	1.9501	1.9532	1.9539	1.9496	1.9593	1.9573
Ti	0.0078	0.0070	0.0081	0.0094	0.0055	0.0072	0.0048	0.0093	0.0104	0.0083	0.0040	0.0093
Al	0.0857	0.0694	0.0689	0.0733	0.0561	0.0531	0.0807	0.0812	0.0614	0.0667	0.0771	0.0754
Cr	0.0246	0.0237	0.0240	0.0211	0.0212	0.0215	0.0293	0.0264	0.0282	0.0251	0.0225	0.0271
Fe^{2+}	0.1261	0.1157	0.1239	0.1308	0.0924	0.0978	0.1007	0.1149	0.1097	0.1144	0.0984	0.1131
Mn	0.0038	0.0024	0.0044	0.0036	0.0023	0.0027	0.0027	0.0038	0.0036	0.0036	0.0014	0.0021
Ni	0.0006	0.0005	0.0017	0.0007	0.0014	0.0011	0.0014	0.0027	0.0027	0.0026	0.0011	0.0010
Mg	0.9362	0.9154	0.8628	0.9292	0.9439	0.9524	0.9238	0.9313	0.9300	0.9550	0.9232	0.9325
Ca	0.8523	0.8671	0.8769	0.8572	0.8888	0.8761	0.8803	0.8451	0.8760	0.8554	0.8834	0.8486
Na	0.0281	0.0286	0.0237	0.0249	0.0258	0.0290	0.0323	0.0311	0.0299	0.0308	0.0329	0.0313
Total	4.0081	3.9953	3.9758	4.0030	4.0030	4.0055	4.0062	3.9992	4.0059	4.0115	4.0033	3.9978
cationic ratio:												
$Mg\#_{cpx}$	0.8813	0.8878	0.8744	0.8766	0.9108	0.9069	0.9017	0.8902	0.8944	0.8930	0.9036	0.8918

Notes: 1) poik : poikilitic

int : interstitial

exs : exsolution bleb or lamina in orthopyroxene

2) $Mg\#_{cpx}$: cationic ratio of $Mg/(Mg + Fe^{2+})$

TABLE 18 Selected Microprobe Analysis of Core and Rim Domains of Clinopyroxene

Sample:	NG1-29.80			NG1-79.75			NG1-476.40			NG1-589.60	
Analysis no.:	21.2	21.1	21.3	18.3	18.1	209.6	209.7	209.5	209.8	210.7	210.8
Domain:	Core	Rim	Rim	Core	Rim	Core	Core	Rim	Rim	Core	Rim
Adjacent Phase:		opx	opx		opx			opx	opx		opx
Habit:		poik			int			int			poik
wt.%											
SiO_2	53.26	53.24	53.71	53.94	54.08	54.26	53.67	53.97	53.79	53.88	53.72
TiO_2	0.30	0.31	0.33	0.23	0.20	0.23	0.24	0.22	0.24	0.30	0.29
Al_2O_3	2.02	1.98	2.00	1.69	1.60	1.49	1.53	1.42	1.51	1.65	1.59
Cr_2O_3	0.93	0.94	0.93	0.96	0.89	0.88	0.87	0.79	0.84	0.87	0.93
FeO	4.20	3.90	3.96	3.79	4.32	3.44	3.26	3.08	3.45	3.74	3.21
MnO	0.15	0.14	0.16	0.14	0.16	0.08	0.11	0.09	0.08	0.13	0.11
NiO	0.06	0.09	0.07	0.02	0.05	0.05	0.04	0.04	0.04	0.03	0.03
MgO	17.12	16.65	16.66	16.35	16.23	18.43	17.83	17.36	18.48	17.76	17.09
CaO	21.90	22.55	22.07	22.57	22.29	21.21	21.52	22.67	21.10	21.43	22.17
Na_2O	0.39	0.39	0.39	0.34	0.34	0.42	0.43	0.45	0.41	0.42	0.45
Total	100.34	100.18	100.27	100.03	100.17	100.49	99.49	100.09	99.95	100.21	99.58
cations (based on 6 oxygens):											
Si	1.9401	1.9436	1.9541	1.9669	1.9721	1.9596	1.9596	1.9625	1.9543	1.9561	1.9623
Ti	0.0082	0.0085	0.0091	0.0062	0.0055	0.0062	0.0066	0.0060	0.0065	0.0083	0.0080
Al	0.0867	0.0850	0.0858	0.0728	0.0687	0.0633	0.0658	0.0610	0.0649	0.0705	0.0683
Cr	0.0269	0.0270	0.0267	0.0277	0.0257	0.0253	0.0252	0.0226	0.0240	0.0251	0.0269
Fe^{2+}	0.1280	0.1190	0.1204	0.1155	0.1318	0.1038	0.0994	0.0936	0.1047	0.1134	0.0980
Mn	0.0048	0.0044	0.0051	0.0043	0.0049	0.0024	0.0035	0.0027	0.0024	0.0040	0.0034
Ni	0.0018	0.0026	0.0020	0.0007	0.0014	0.0015	0.0011	0.0013	0.0012	0.0009	0.0007
Mg	0.9298	0.9060	0.9034	0.8889	0.8820	0.9924	0.9704	0.9407	1.0007	0.9612	0.9306
Ca	0.8550	0.8818	0.8602	0.8819	0.8710	0.8209	0.8418	0.8832	0.8213	0.8335	0.8676
Na	0.0276	0.0274	0.0277	0.0238	0.0242	0.0292	0.0303	0.0314	0.0292	0.0298	0.0321
Total	4.0087	4.0055	3.9944	3.9886	3.9873	4.0045	4.0035	4.0053	4.0093	4.0028	3.9980
cationic ratio:											
$Mg\#_{cpx}$	0.8790	0.8839	0.8824	0.8850	0.8700	0.9053	0.9071	0.9095	0.9053	0.8944	0.9047

Notes: 1) opx : orthopyroxene

2) poik : poikilitic

int : interstitial

3) $Mg\#_{cpx}$: cationic ratio of $Mg/(Mg + Fe^{2+})$

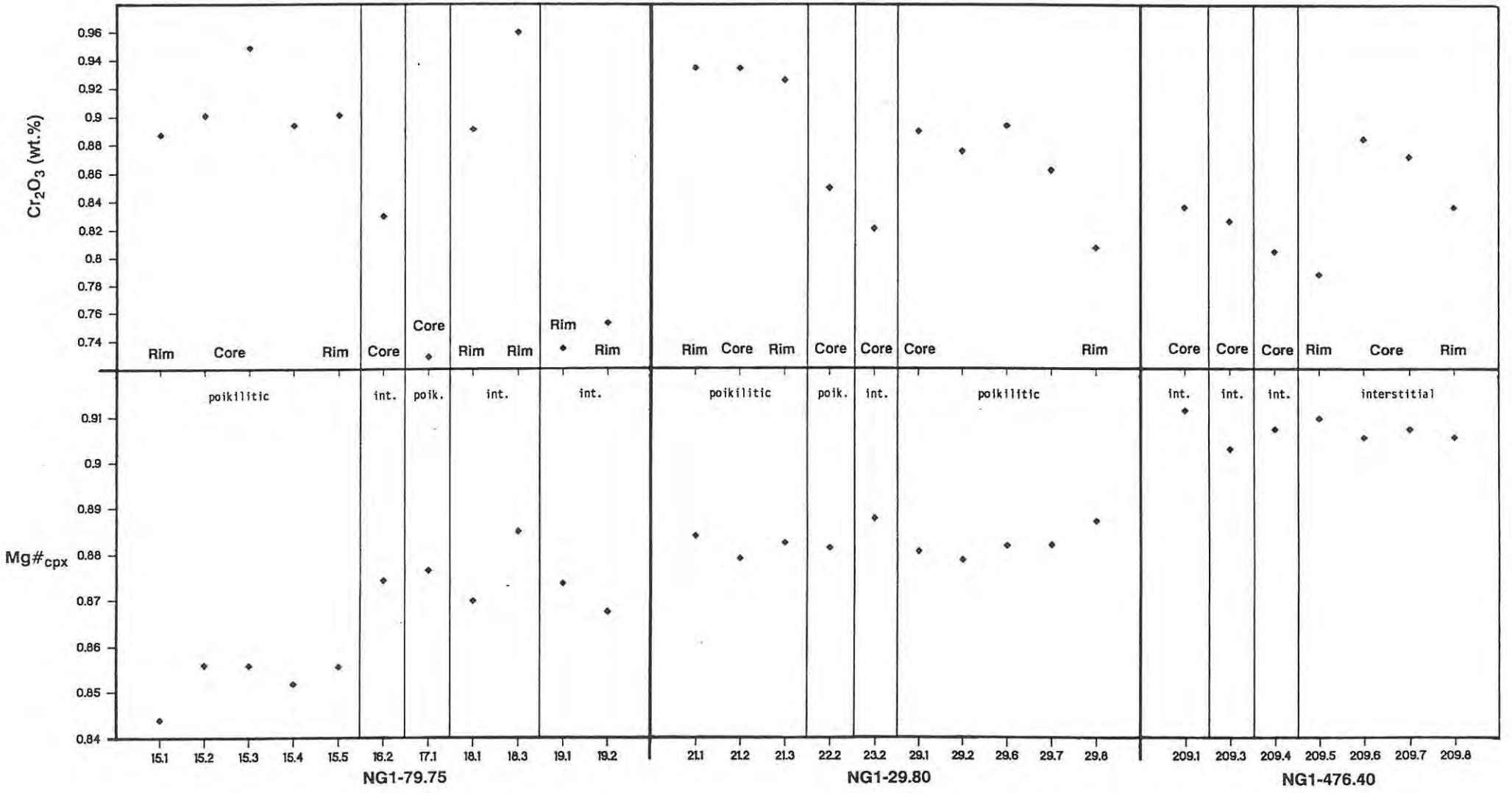

Fig. 29 Clinopyroxene mineralogy - zonation and composition in different textural habits (int.: interstitial, poik. : poikilitic; see also Table 18).

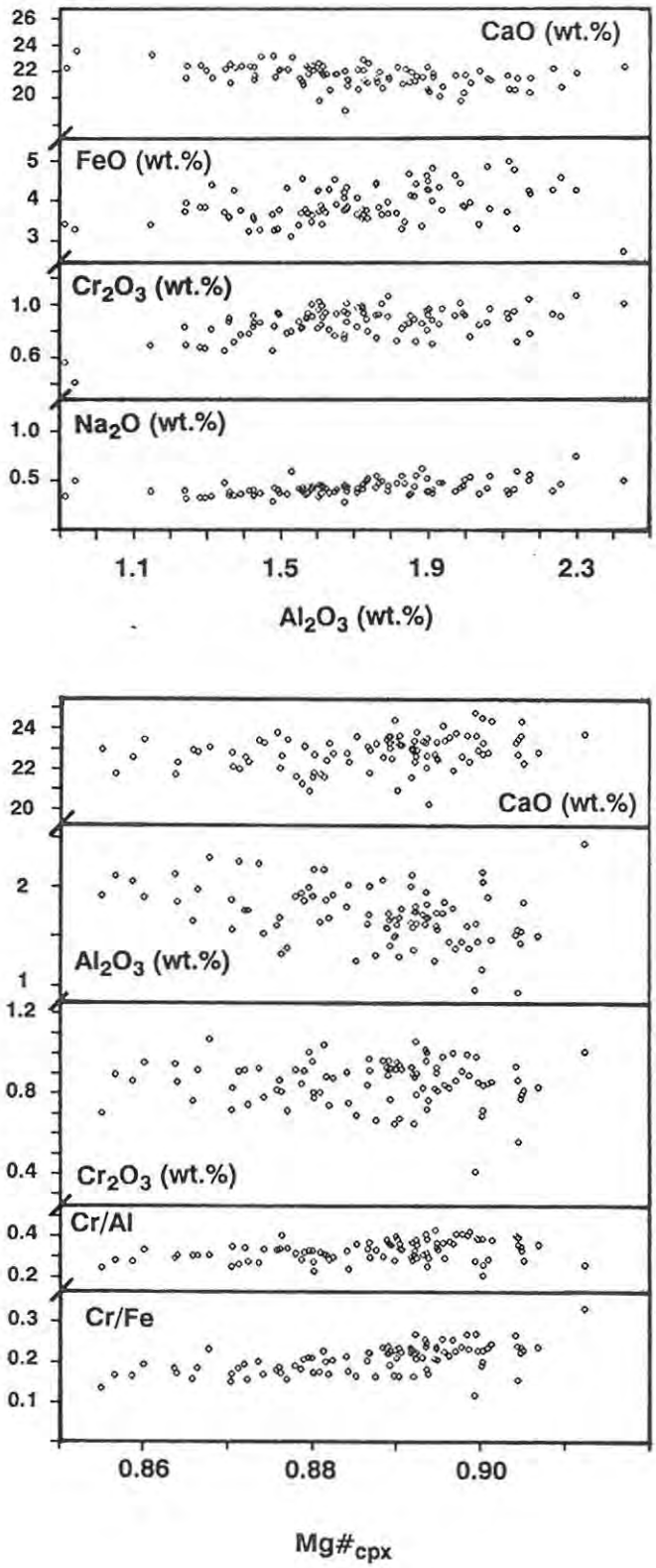

Fig. 31 Clinopyroxene mineralogy - variation diagrams (note scale breaks).

The ratio of augite to diopside for cpx in the NG-sequence is 62 : 32. The field is well-constrained with limited ranges in Fe+Mn (4.8-8.3 cationic % or 3.0-5.3 wt.% oxide) and Mg ranges from 46.6-51.4 cationic % (20.0-16.1 wt.% oxide). Apart from three samples (NG1-348.20; NG1-486.55 and NG2-115.20) all analyses cluster in this small area. The amount of Cr_2O_3 (0.4-1.1 wt.%) in the cpx lattice (≥0.02 cations), allows the use of the prefix chromian-; thus all cpx analysed are either chromian-diopsides or chromian-augites. Levels of NiO do not exceed 0.1 wt.%, whereas TiO_2 contents vary from 0.1 to 0.5 wt.%. Values of Al_2O_3 range from 0.9 to 2.4 wt.%. The range of composition is listed in Table 19 together with average compositions for different stratigraphic intervals.

In simple variation diagrams (Fig. 31) no statistically significant correlations can be detected (cc: 0.411-0.604) between Ca, Fe, Cr or Na, and Al_2O_3 or $Mg\#_{cpx}$, respectively. However, the following trends can be deduced from the diagrams:

a) Al-richer cpx are also enriched in Na, but display lower CaO values. Botha (1987) suggested that such a relationship might be a function of competition between co-nucleating cpx and pla. However, in a plot of Al and Na concentrations in cpx versus modal pla no distribution pattern is apparent;

b) Cr_2O_3 and FeO values appear to be positively linked with Al_2O_3 levels;

c) there is no relationship between $Mg\#_{cpx}$ and Cr content, but the Cr/Al and the Cr/Fe ratios show a weak positive relationship with the $Mg\#_{cpx}$.

Cryptic variations with height are depicted in Fig. 32. In general, the distribution patterns of cpx are sympathetic with those displayed by opx (Fig. 15A), but probably because of its postcumulus habit the trends are less sharply defined.

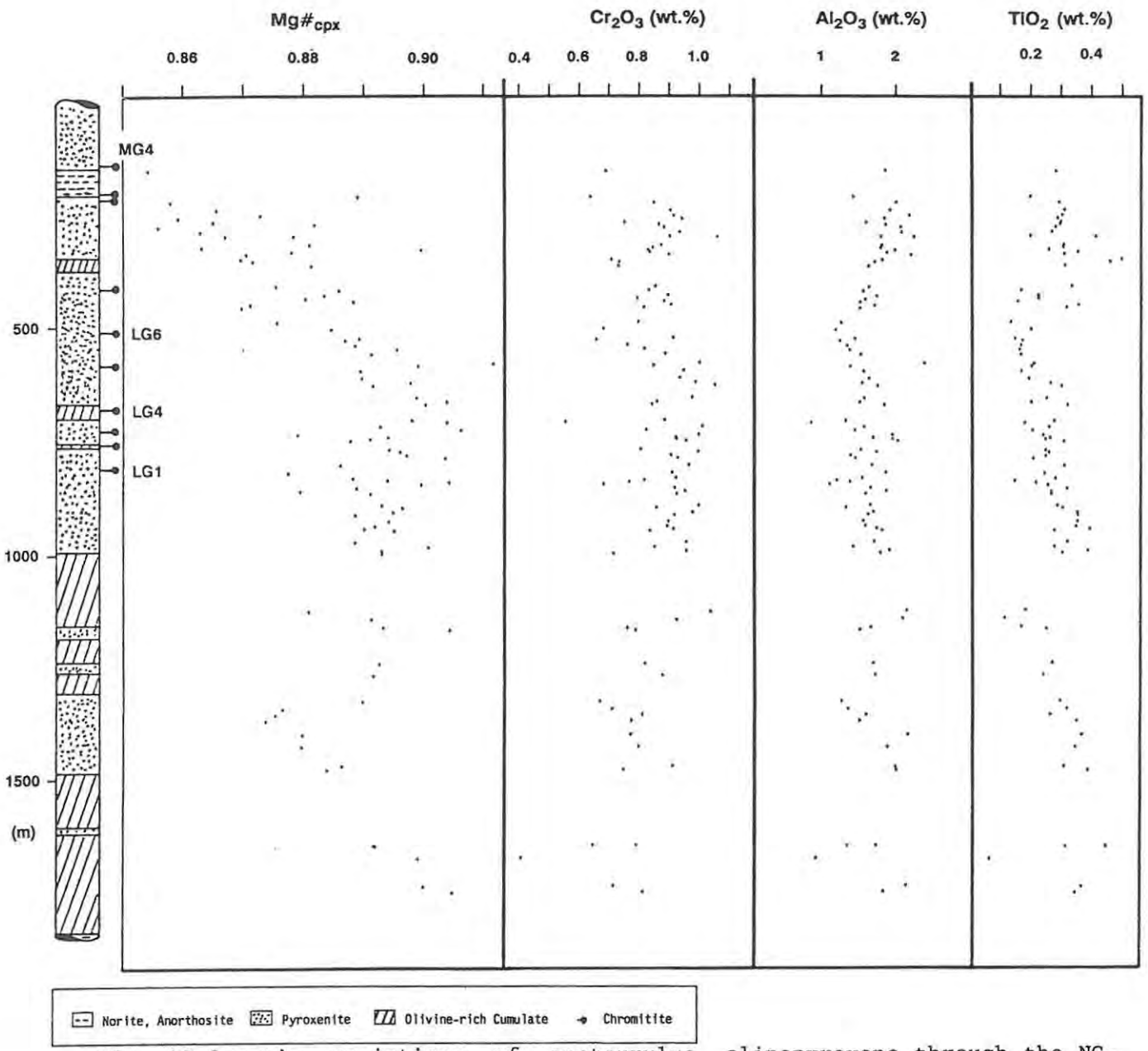

Fig. 32 Cryptic variations of postcumulus clinopyroxene through the NG-sequence.

TABLE 19 Clinopyroxene Compositions in different Stratigraphic Intervals

Stratigraphic Interval:	All	uCZ	lCZ	LZ	Range of composition
Textural Habit:	samples		postcumulus		
wt.%					
SiO_2	53.39	52.47	53.39	53.45	52.4 - 54.6
TiO_2	0.29	0.26	0.29	0.30	0.1 - 0.5
Al_2O_3	1.71	1.69	1.70	1.73	0.9 - 2.4
Cr_2O_3	0.86	0.68	0.88	0.78	0.4 - 1.1
FeO	3.95	4.29	3.96	3.88	2.9 - 5.1
MnO	0.12	0.12	0.12	0.10	0.1 - 0.2
NiO	0.04	0.03	0.04	0.06	0.0 - 0.1
MgO	17.44	16.44	17.45	17.45	16.1 - 20.0
CaO	21.75	22.60	21.73	21.82	19.1 - 23.6
Na_2O	0.43	0.33	0.42	0.47	0.3 - 0.7
Total	99.97	98.92	99.97	100.03	
cations (based on 6 oxygens):					
Si	1.9492	1.9448	1.9493	1.9489	
Ti	0.0079	0.0072	0.0078	0.0082	
Al	0.0734	0.0741	0.0731	0.0741	
Cr	0.0249	0.0199	0.0255	0.0226	
Fe^{2+}	0.1205	0.1329	0.1206	0.1182	
Mn	0.0036	0.0039	0.0037	0.0032	
Ni	0.0013	0.0009	0.0011	0.0017	
Mg	0.9479	0.9081	0.9485	0.9484	
Ca	0.8501	0.8974	0.8491	0.8527	
Na	0.0312	0.0240	0.0308	0.0330	
cationic ratio:					
$Mg\#_{cpx}$	0.8873	0.8724	0.8872	0.8892	0.8550 - 0.9123
n	95	1	72	19	
a	433	7	371	55	
standard deviation:					
wt.%					
SiO_2	0.4632		0.4414	0.5082	
TiO_2	0.0776		0.0729	0.0947	
Al_2O_3	0.2865		0.2745	0.3320	
Cr_2O_3	0.1115		0.0973	0.1253	
FeO	0.4524		0.4566	0.3867	
MnO	0.0203		0.0195	0.0184	
NiO	0.0199		0.0173	0.0223	
MgO	0.5947		0.5384	0.7326	
CaO	0.7973		0.7393	1.0065	
Na_2O	0.0750		0.0679	0.0897	

Notes: 1) $Mg\#_{cpx}$: cationic ratio of $Mg/(Mg + Fe^{2+})$

2) n : number of samples

3) a : number of analyses

Al_2O_3 levels show an irregular increase initiated at the level of the ol-rich interval hosting the LG4-chromitite. The levels of TiO_2 show a three-step saw-tooth pattern. Reversals to higher Ti levels are associated with the ol-rich cumulates. This cyclicity is probably a function of two processes: a) the compatibility of Ti within opx, which led to a depletion of the resident liquid, which probably caused the upwards decline of Ti concentrations in postcumulus cpx hosted in the pyroxenite packages and b) the rejuvenation by influxes of undepleted magma initiating a new cycle. The levels of Cr_2O_3 do not show great variations through the entire sequence, although cpx in the lCZ appears to contain slightly higher values (see also Table 19). The variations of the $Mg\#_{cpx}$ resemble the trend set by $Mg\#_{opx}$.

4.7. Coexisting Phases

In this section the Mg-Fe relationships of opx, ol, chr and cpx will be described as well as other interelement variations. Temperature estimations are also presented.

4.7.1 The Mg-Fe Relationship of the Ferromagnesian Phases and Chromite

The Mg-Fe relationship between coexisting silicates and spinels has been investigated by numerous workers and the reader might be referred to a comprehensive review in Deer et al. (1978, 1982). Morse (1979) found that the relationship in opx and ol in basaltic rocks can be expressed with the following equation:

$$Mg\#_{opx} = 0.85 * Mg\#_{ol} + 0.15$$

The data of the coexisting opx and ol in the NG-sequence yield the following equations after linear regression:

all samples (n=50) $Mg\#_{opx} = 0.87 * Mg\#_{ol} + 0.125$ cc:0.919

lCZ (n= 5) $Mg\#_{opx} = 0.86 * Mg\#_{ol} + 0.138$ cc:0.947

LZ (n=45) $Mg\#_{opx} = 0.88 * Mg\#_{ol} + 0.115$ cc:0.915

All equations obtained are very close to that found by Morse (op.cit.). For the coexisting pyroxenes the expressions listed below were found (see also Fig. 34):

all samples (n=93) $Mg\#_{cpx} = 0.58 * Mg\#_{opx} + 0.397$ cc:0.784

lCZ (n=74) $Mg\#_{cpx} = 0.65 * Mg\#_{opx} + 0.340$ cc:0.820

LZ (n=18) $Mg\#_{cpx} = 0.53 * Mg\#_{opx} + 0.435$ cc:0.666

Other silicate phases (phlogopite and amphibole) are not further discussed, but it appears (see Tables 15 and 16) that the relationships are as below:

$$Mg\#_{opx} < Mg\#_{phl} < Mg\#_{amp} .$$

Accordingly, the Mg-Fe relationships of the silicate phases might be summarized thus:

$$Mg\#_{cpx} > Mg\#_{amp} > Mg\#_{phl} > Mg\#_{opx} > Mg\#_{ol} .$$

The same sequence was found by Scoon (1985) in his study of the uCZ in the northwestern part of the BIC.

The distribution of Mg and Fe in ol and spinel was studied by Irvine (1965, 1967). Since his work it is now well established that the liquidus contents of Mg and Fe in chr change with falling temperature above the solidus of basaltic rocks with a resulting decline of the $Mg\#_{chr}$ (Hill and Roeder, 1974; Fisk and Bence, 1980). Below solidus temperatures this trend continues by means of re-equilibration with ferromagnesian phases by shifting the compositions of the silicates to higher and those of the spinels to lower values of Mg#. This cation-exchange is the base of the olivine-chromite geothermometer (Jackson, 1969; Roeder et al., 1979).

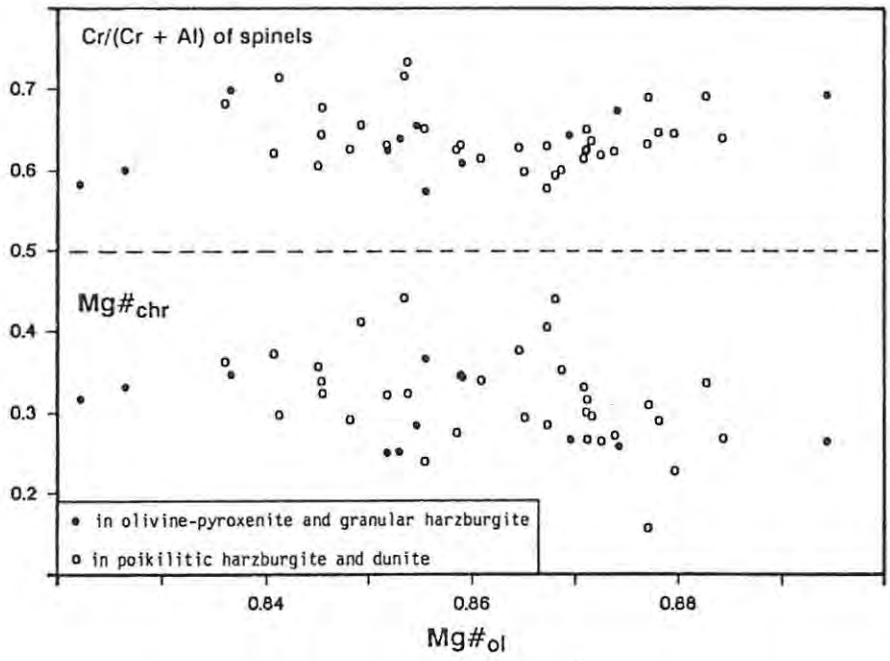

Fig. 33 Coexisting chromite and olivine compositions.

Figure 33 summarizes the interelement variations of ol and chr. The Cr/(Cr+Al) ratio of chr and $Mg\#_{chr}$ plotted against the Fo content of ol show no relationships. Eales and Reynolds (1986, Fig. 7) calculated a re-equilibration temperature extending down to 650°C for samples at Union Section. The ol - chr pairs in the NG-sequence yield an average equilibration temperature of 600°C (range: 369 - 840°C).

The effect of subsolidus re-equilibration is demonstrated by the change of compositions of chr in samples, wherein intimate contact of grains is assured by existence of an interface pyroxenite-chromitite. Table 20 lists some analyses. They are arranged such that the first analysis of each pair represents a composition of chr abundant in accessory or minor proportion and the second within a massive chromitite layer, where the effects of re-equilibration are more subdued.

TABLE 20 Selected Microprobe Analysis of Core Domains of Chromite showing the Effect of Subsolidus Re-equilibration (all samples straddle contacts between chromitite layers and silicate cumulates)

Sample:	NG3-154.72		NG3-159.20		NG3-219.22B		NG1-152.20		NG1-331.35BB		NG1-331.65B	
Analysis no.:	169.1	168.6	178.5	176.5	167.4	166.1	823.1	823.3	941.6	941.5	950.2	950.3
Mode:	acc	maj	acc	maj	acc	maj	acc	maj	acc	maj	acc	maj
wt.%												
TiO_2	0.90	0.78	1.11	0.85	1.21	0.80	0.98	0.73	0.73	0.63	0.68	0.56
Al_2O_3	15.16	17.95	8.95	15.84	10.92	16.06	12.74	15.00	10.00	13.82	10.16	12.85
Cr_2O_3	42.76	41.15	44.70	42.44	40.90	43.70	40.15	42.88	49.96	49.37	50.57	50.50
FeO	22.06	20.47	26.22	21.14	26.61	19.02	26.60	22.70	22.69	17.68	23.03	18.02
Fe_2O_3	10.00	8.49	12.24	9.20	14.32	8.67	12.62	9.13	9.18	7.96	8.89	8.04
MnO	0.29	0.27	0.39	0.30	0.38	0.25	0.31	0.34	0.39	0.29	0.36	0.31
NiO	0.16	0.12	0.15	0.12	0.15	0.13	0.16	0.12	0.21	0.16	0.14	0.13
MgO	8.14	9.24	4.59	8.59	4.78	10.05	4.67	7.35	7.20	11.03	7.16	10.71
Total	99.46	98.47	98.34	98.48	99.26	98.68	98.21	98.25	100.36	100.95	101.00	101.13
cations (based on 32 oxygens):												
Ti	0.1794	0.1529	0.2348	0.1688	0.2516	0.1573	0.2036	0.1477	0.1487	0.1211	0.1379	0.1096
Al	4.7210	5.5267	2.9730	4.9428	3.5635	4.9489	4.1617	4.7494	3.1809	4.1865	3.2115	3.9101
Cr	8.9328	8.4991	9.9603	8.8868	8.9500	9.0316	8.7992	9.1088	10.6580	10.0314	10.7185	10.3086
Fe^{2+}	4.8754	4.4718	6.1803	4.6831	6.1601	4.1585	6.1665	5.1017	5.1198	3.7988	5.1643	3.8907
Fe^{3+}	1.9875	1.6684	2.5970	1.8327	2.9833	1.7049	2.6320	1.8464	1.8638	1.5399	1.7943	1.5622
Mn	0.0639	0.0598	0.0922	0.0673	0.0880	0.0562	0.0728	0.0777	0.0896	0.0637	0.0828	0.0679
Ni	0.0335	0.0251	0.0339	0.0260	0.0328	0.0263	0.0351	0.0258	0.0448	0.0334	0.0301	0.0278
Mg	3.2066	3.5963	1.9285	3.3925	1.9707	3.9162	1.9291	2.9425	2.8945	4.2252	2.8606	4.1231
cationic ratios:												
$Mg\#_{chr}$	0.3968	0.4457	0.2378	0.4201	0.2424	0.4850	0.2383	0.3658	0.3612	0.5266	0.3565	0.5145
Cr/(Cr + Al)	0.6542	0.6060	0.7701	0.6426	0.7152	0.6460	0.6789	0.6573	0.7702	0.7055	0.7695	0.7250

Notes: 1) acc : accessory or minor phase
maj : major or sole cumulus phase
2) $Mg\#_{chr}$: cationic ratio of $Mg/(Mg + Fe^{2+})$

4.7.2. Coexisting Ortho- and Clinopyroxene

Coexisting pyroxenes were analysed in 182 samples, two of which have both pyroxenes as postcumulus phases. In the remainder opx is invariably cumulus and cpx postcumulus.

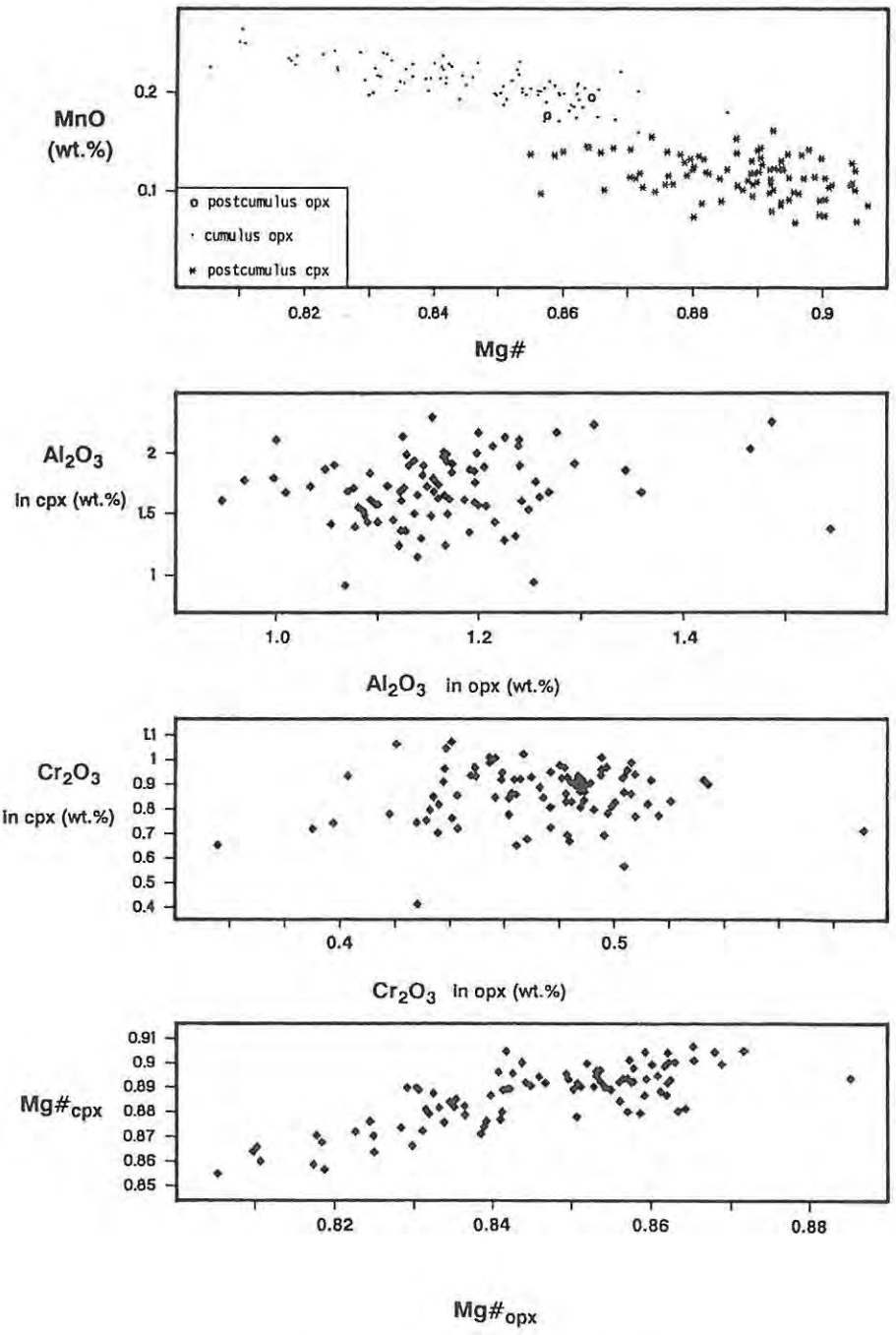

Fig.34 Mineralogy of coexisting pyroxenes.

The Mg-Fe relationship was discussed above, therefore no further comment is necessary here. In Fig. 34 Al_2O_3 and Cr_2O_3 concentrations of opx are plotted against the same element in cpx. No overall trends are displayed. A relationship between Mg# of pyroxene and MnO concentration (wt.%) is indicated in the top diagram. This relationship might be an expression of the higher compatibility of Mn with opx due to its geochemical behaviour being similar to that of Fe^{2+}. Two features emerging from Fig. 34 can be explained by this similarity:

a) the generally lower Mn concentrations in postcumulus cpx;

b) the higher MnO levels in opx with lower Mg# due to the overall enrichment in Mn in the liquid during fractional crystallization parallel to a Fe-enrichment trend.

In the triangular diagram (Fig. 35) all coexisting pyroxenes are depicted as well as some individual tielines; these tielines are not significantly different from those published in Atkins (1969) or in Deer et al. (1978).

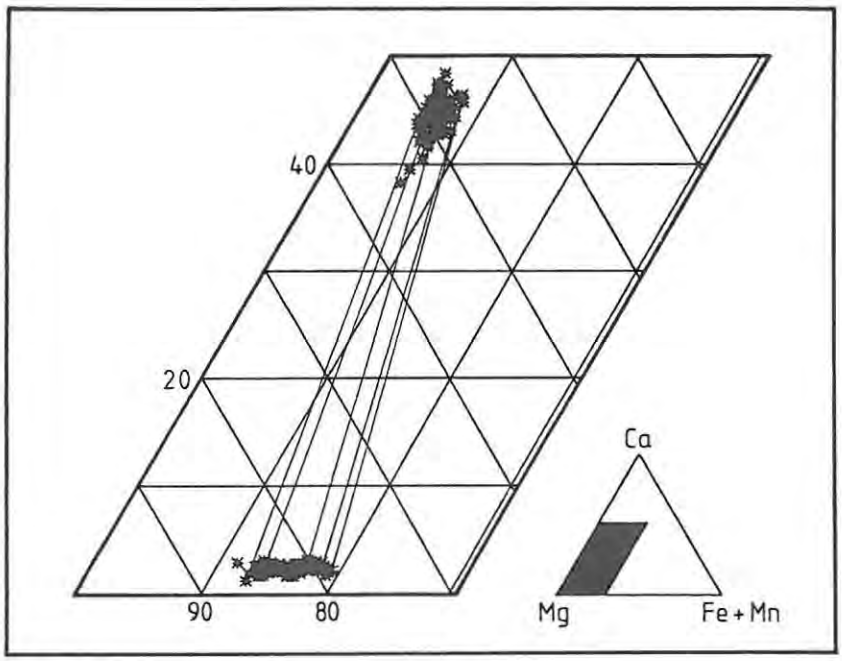

Fig. 35 Coexisting pyroxenes in the NG-sequence.

The pairs of pyroxenes were also used to determine equilibration temperatures using the formulations of Wells (1977), Wood and Banno (1973) and Mori and Green (1978). Although Mori and Green (op.cit.) stated that the ranges of application of their expression should be 950 - 1100°C and 30 - 40 kbar all three temperature sets obtained are within 120°C of each other (Fig. 36).

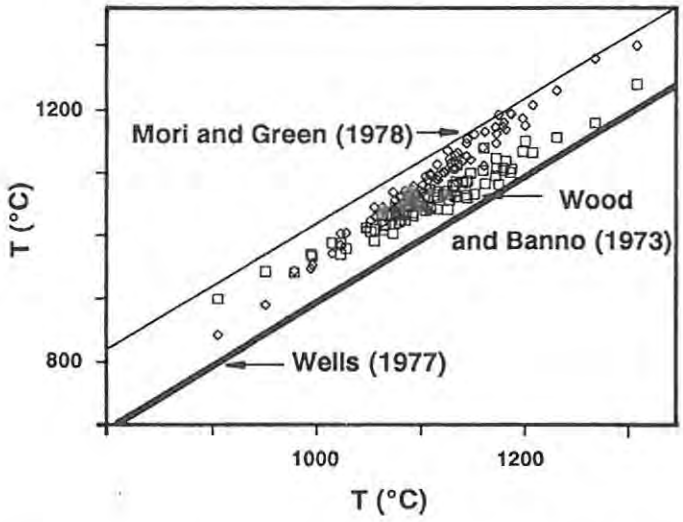

Fig. 36 Comparison of temperatures derived from different ortho-clinopyroxene thermometers. (Window between solid lines shows the maximum difference between the three thermometers, where the lower (bolder) one represents the temperature estimates using the formulation of Wells (1977); diamonds show temperatures using the equation of Mori and Green (1978) and squares those calculated after Wood and Banno (1973).

The data sets are tabulated in Table 21. Figure 37 presents the temperatures calculated after Wells (op.cit.) plotted against stratigraphic height. Throughout the sequence variations are in the range of 400°C (total range: 805 - 1208°C, average 1008°C). The highest temperature occurs at the lower contact of the olivine-rich interval (sample NG2-115.25 at a depth of 1155.25 m) at the top of the LZ. It is not considered that the indicated values offer information which may be applied with any degree of confidence. For example Lindsley (1983) refers to the thermometers of Wood and Banno (op.cit.) and Wells (1977) as "anachronisms".

TABLE 21 Temperature Determinations using Coexisting Pyroxenes and Olivine - Chromite Pairs

Depth: (m)	Sample:	A	B	C	D
			Temperature in °C		
163.45	NG3-163.45		955	993	1047
219.20	NG3-219.20		878	942	945
232.00	NG3-232.00		1008	1045	1101
248.25	NG3-248.25		1004	1041	1096
260.05	NG3-260.05		975	1020	1059
267.00	NG1- 17.00		928	981	1005
275.00	NG1- 25.00		973	1004	1071
279.80	NG1- 29.80		1008	1048	1098
285.00	NG1- 35.00		1050	1068	1162
296.25	NG1- 46.25		1061	1084	1167
305.40	NG1- 55.40		992	1033	1080
306.00	NG1- 56.00		923	971	1005
324.45	NG1- 74.45		1032	1064	1129
329.75	NG1- 79.75		1025	1043	1136
334.90	NG1- 84.90		1006	1064	1077
339.55	NG1- 89.55		1087	1107	1195
344.60	NG1- 94.60		1071	1097	1174
355.45	NG1-105.45		984	1025	1073
360.52	NG1-110.52		1027	1058	1124
369.90	NG1-119.90		981	1026	1065
372.80	NG1-122.80	557			
413.27	NG1-163.27		1043	1066	1148
423.37	NG1-173.37		991	1037	1074
433.70	NG1-183.70		1009	1047	1099
441.00	NG1-191.00		1085	1102	1196
447.50	NG1-197.50		964	1010	1047
454.50	NG1-204.50		1015	1044	1115
460.30	NG1-210.30		1044	1062	1154
492.70	NG1-242.70		1034	1064	1134
507.70	NG1-257.70		1074	1084	1193
527.25	NG1-277.25		980	1026	1063
532.25	NG1-282.25		978	1023	1064
542.30	NG1-292.30		956	1011	1031
552.00	NG1-302.00		986	1033	1067
562.20	NG1-312.20		1006	1052	1089
588.45	NG1-338.45		1030	1081	1108
598.20	NG1-348.20		1167	1181	1281
614.25	NG1-364.25		985	1040	1060
624.35	NG1-374.35		968	1034	1033
630.35	NG1-380.35		1014	1067	1092
656.40	NG1-406.40		962	1034	1022
664.85	NG1-414.85		1047	1101	1122
670.80	NG1-420.80	672			
671.00	NG1-421.00		1008	1075	1071
679.90	NG1-429.90	808			
695.45	NG1-445.45	739			
702.75	NG1-452.75	722			
705.65	NG1-455.65		1059	1105	1142
709.70	NG1-459.70		1002	1063	1072
719.40	NG1-469.40		999	1055	1073
726.40	NG1-476.40		1033	1088	1108
730.60	NG1-480.60	667			
736.55	NG1-486.55		1130	1157	1231
742.15	NG1-492.15		1031	1083	1108
746.43	NG1-496.43		1097	1135	1188
750.50	NG1-500.50		1016	1071	1091
765.15	NG1-515.15	607			
769.26	NG1-519.26		1043	1086	1128
773.90	NG1-523.90		1072	1109	1164
782.14	NG1-532.14		1039	1087	1120
786.95	NG1-536.95		996	1057	1066
803.33	NG1-553.33		1081	1120	1170
819.20	NG1-569.20		1107	1133	1209
831.00	NG1-581.00		952	1007	1026
836.00	NG1-586.00		1032	1073	1120
839.60	NG1-589.60		966	1019	1043
845.05	NG1-595.05		896	968	954
853.10	NG1-603.10		1028	1067	1117
859.47	NG1-609.47		1079	1105	1181
864.76	NG1-614.76		1002	1050	1083
889.95	NG1-639.95		1044	1089	1127
895.17	NG1-645.17		973	1032	1044
905.10	NG1-655.10		923	990	987
910.40	NG1-660.40		1015	1063	1097
925.25	NG1-675.25		995	1049	1070
935.40	NG1-685.40		1024	1073	1106
940.90	NG1-690.90		1001	1048	1083
945.50	NG1-695.50		964	1018	1039
947.80	NG1-697.80	736			
970.15	NG1-720.15		979	1039	1048
980.38	NG1-730.38		894	971	948
989.80	NG1-739.80		1072	1124	1149
994.70	NG1-744.70	720	979	1040	1049
1003.00	NG1-753.00	591			
1020.00	NG1-770.00	666			
1023.74	NG1-773.74	575			
1029.00	NG1-779.00	819			
1034.64	NG1-784.64	666			
1043.50	NG1-793.50	578			
1053.00	NG1-803.00	608			
1059.10	NG1-809.10	609			
1066.10	NG1-816.10	678			
1068.80	NG1-818.80	625			
1080.15	NG1-830.15	641			
1082.55	NG2- 42.55	558			
1090.20	NG2- 50.20	396			
1105.25	NG2- 65.25	548			
1113.60	NG2- 73.60	612			
1120.35	NG2- 80.35		1100	1152	1177
1123.75	NG2- 83.75	463			
1138.00	NG2- 98.00		1021	1068	1103
1155.25	NG2-115.25		1208	1241	1301
1160.40	NG2-120.40		850	944	890
1163.40	NG2-123.40	369			
1167.55	NG2-127.55	458			
1193.35	NG2-153.35	523			
1198.60	NG2-158.60	840			
1205.62	NG2-165.62	470			
1234.20	NG2-194.20		988	1063	1045
1240.50	NG2-200.50	675			
1253.30	NG2-213.30	468			
1317.15	NG2-277.15		975	1047	1035
1333.60	NG2-293.60		976	1033	1048
1347.10	NG2-307.10		947	1014	1012
1360.15	NG2-320.15		975	1037	1044
1366.86	NG2-326.86	654			
1390.50	NG2-350.50		1034	1114	1087
1398.66	NG2-358.66	602			
1416.10	NG2-376.10		1078	1109	1175
1460.05	NG2-420.05		997	1058	1067
1468.15	NG2-428.15		1022	1073	1101
1549.05	NG2-509.05	620			
1601.35	NG2-561.35	487			
1630.97	NG2-590.97		915	989	973
1631.03	NG2-591.03		976	1038	1045
1631.05	NG2-591.05	593			
1644.30	NG2-604.30	461			
1658.25	NG2-618.25	612	805	899	843
1694.56	NG2-654.56	637			
1718.64	NG2-678.64	573	989	1052	1057
1731.95	NG2-691.95		1060	1141	1113
1749.10	NG2-709.10	573			
1763.22	NG2-723.22	617			
1778.90	NG2-738.90	553			
1803.45	NG2-763.45	532			
1812.36	NG2-772.36	463			

Notes: 1) A : chromite - olivine thermometer after Jackson, 1969

B : ortho- clinopyroxene thermometer after Wells, 1977

C : ortho- clinopyroxene thermometer after Wood and Banno, 1973

D : ortho- clinopyroxene thermometer after Mori and Green, 1978

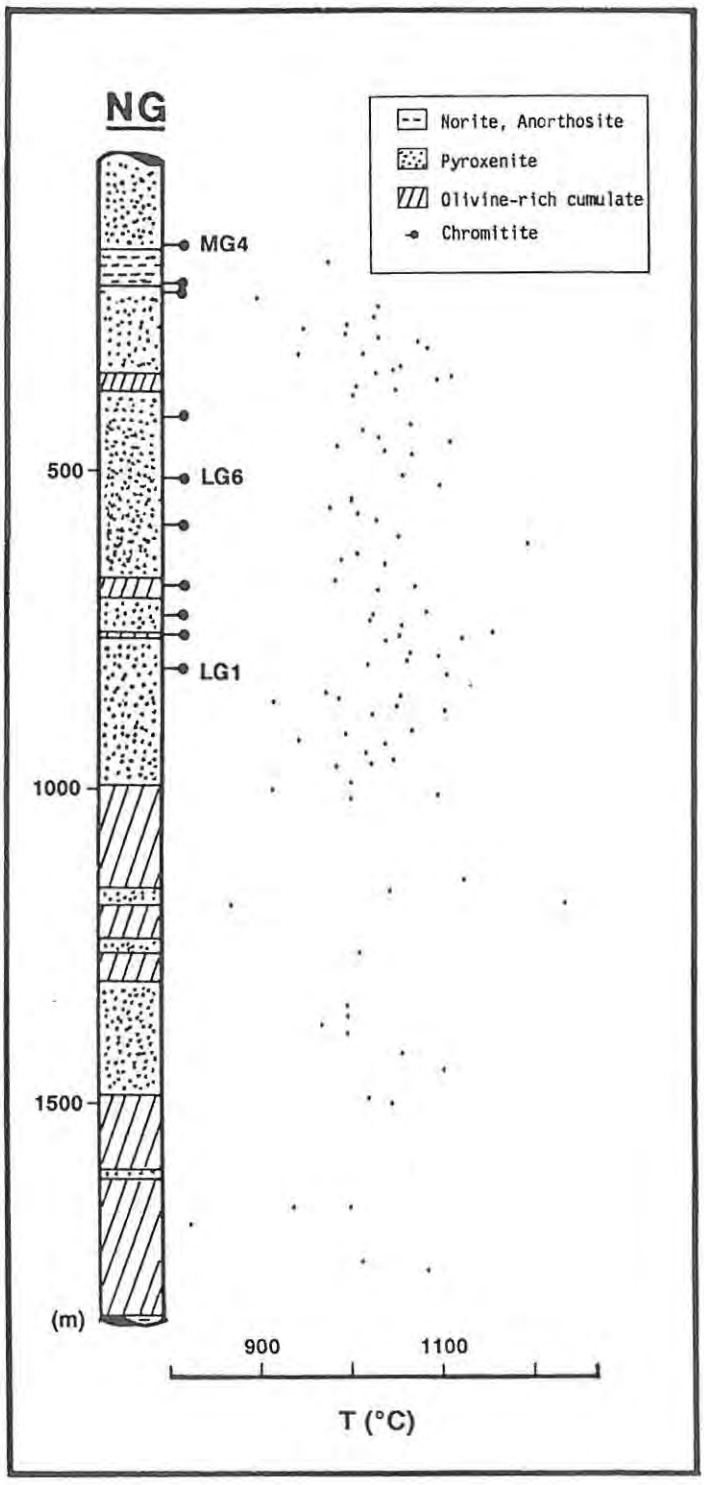

Fig. 37 Variations in temperature estimates through the NG-sequence using the ortho-clinopyroxene thermometer after Wells (1977).

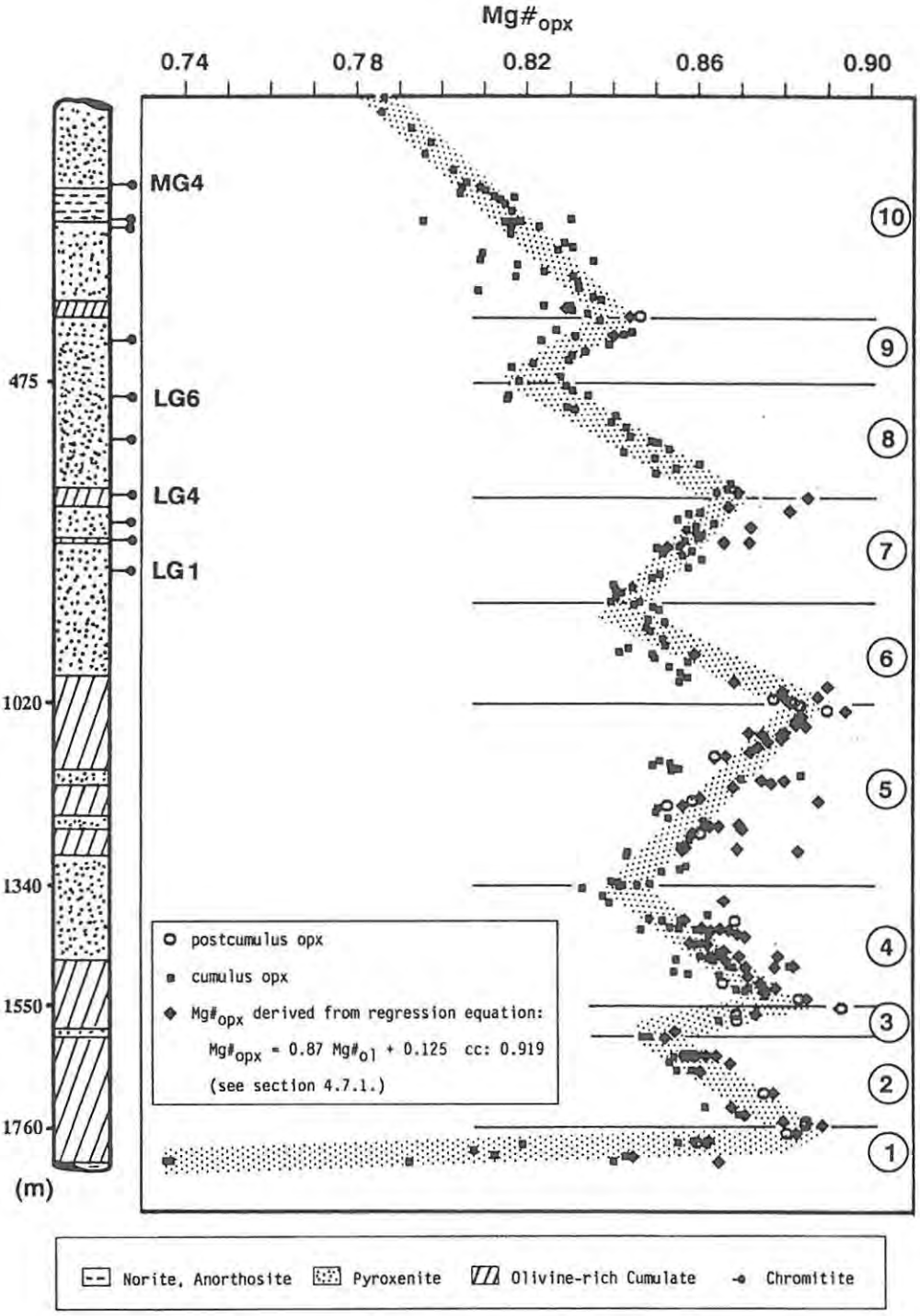

Fig.15B Variations of $Mg\#_{opx}$ through the NG-sequence (squares and open circles derived from microprobe analyses of orthopyroxene; diamonds show $Mg\#_{opx}$ derived after application of the regression equation of coexisting olivine and orthopyroxene in section 4.7.1.).

4.8. Summary of the most important findings

Significant cryptic variations with height recognisable in all major phases were described in the previous section. The salient features are summarized below:

a) all ferromagnesian phases vary sympathetically in composition and give thus important clues to the petrogenetic evolution of the cumulate pile;

b) by means of the ratio $Mg/(Mg+Fe^{2+})$ or Mg# of the silicates the sequence can be divided into a lower and an upper portion, which can be further subdivided into 10 segments (Fig. 15B). The lower portion, with an overall increase of the Mg#, can be equated with the MZ and LZ, while the upper portion, characterized by a general decrease, is part of the CZ;

c) in the upper portion the decrease of the Mg# is accompanied by an irregular and slight increase of An content in pla, an increase of the modal proportion of pla and slight increases of the Al_2O_3 content of opx and cpx. This combination may manifest the continuous enrichment of the liquid in feldspar components, which culminates eventually in the appearance of cumulus pla at a depth of 214.05 m between the MG2- and MG3-chromitites. However, the occurrence of pla inclusions in opx ca. 20 m beneath the actual appearance of the first norites points to the possibility of earlier crystallization of cumulus pla, which was subsequently resorbed (Eales et al., 1990a, 1990b);

d) all Cr-bearing phases of the lCZ are enriched in Cr relative to their equivalents in the uCZ, LZ and MZ, despite the occurrence of the massive chromitite layers and the higher modal proportions of accessory chr therein. This is interpreted as evidence for a distinctly higher amount of Cr in the liquid parental to the cumulates of the lCZ;

e) the mineralogy of the massive chromitite layers is not decoupled from the petrogenetic evolution of the silicate cumulate pile (Teigler, 1990). Cryptic variations of successive chromitite layers follow the trends set by the silicate phases.

CHAPTER 5: WHOLE-ROCK GEOCHEMISTRY

In this section the geochemical data derived by whole-rock XRF-analysis will be presented and discussed.

5.1. Technique

All samples were analysed by the XRF-method of Norrish and Hutton (1969) as modified for use in the Department of Geology, Rhodes University by Marsh (1979). Samples were taken more or less equidistantly in monotonous packages or adjacent to lithological interfaces. Chromite-rich cumulates were, if possible, avoided due to problems during the fusion procedure and uncertainty with regard to appropriate mass absorption coefficients (Botha, 1987). Analytical details are attached in the Appendix. Incorporated into the whole-rock data base are 35 samples analysed by Haikney. The total number of analyses available is 128.

5.2. Major and minor elements

All XRF-data are recalculated to 100 % L.O.I.-free (inclusive of Cr_2O_3 and NiO). Fe_2O_3 has been stated assuming a constant ratio of $FeO/Fe_2O_3 = 10$. The analyses are presented in the Appendix.

Plots (Fig. 38) of major, minor and trace elements against MgO show a clustering into three distinct fields: a) the ol-rich cumulates (MgO 32.5 - 46.5 wt.%), b) the pyroxenites (21.0 - 32.5 wt.% MgO), and c) the noritic rocks (MgO < 21.0 wt.%). The ol-rich lithologies can be further subdivided: granular harzburgites and olivine pyroxenites lie within the range of 32.5 - 36.7 wt.% MgO, while poikilitic harzburgites and dunites have more than 36.7 wt.% MgO apart from three samples, of which two are heavily altered and the third is anomalously high in Al_2O_3 and CaO. The latter is interpreted as the uppermost part of the MZ at a depth of 1778.90 m.

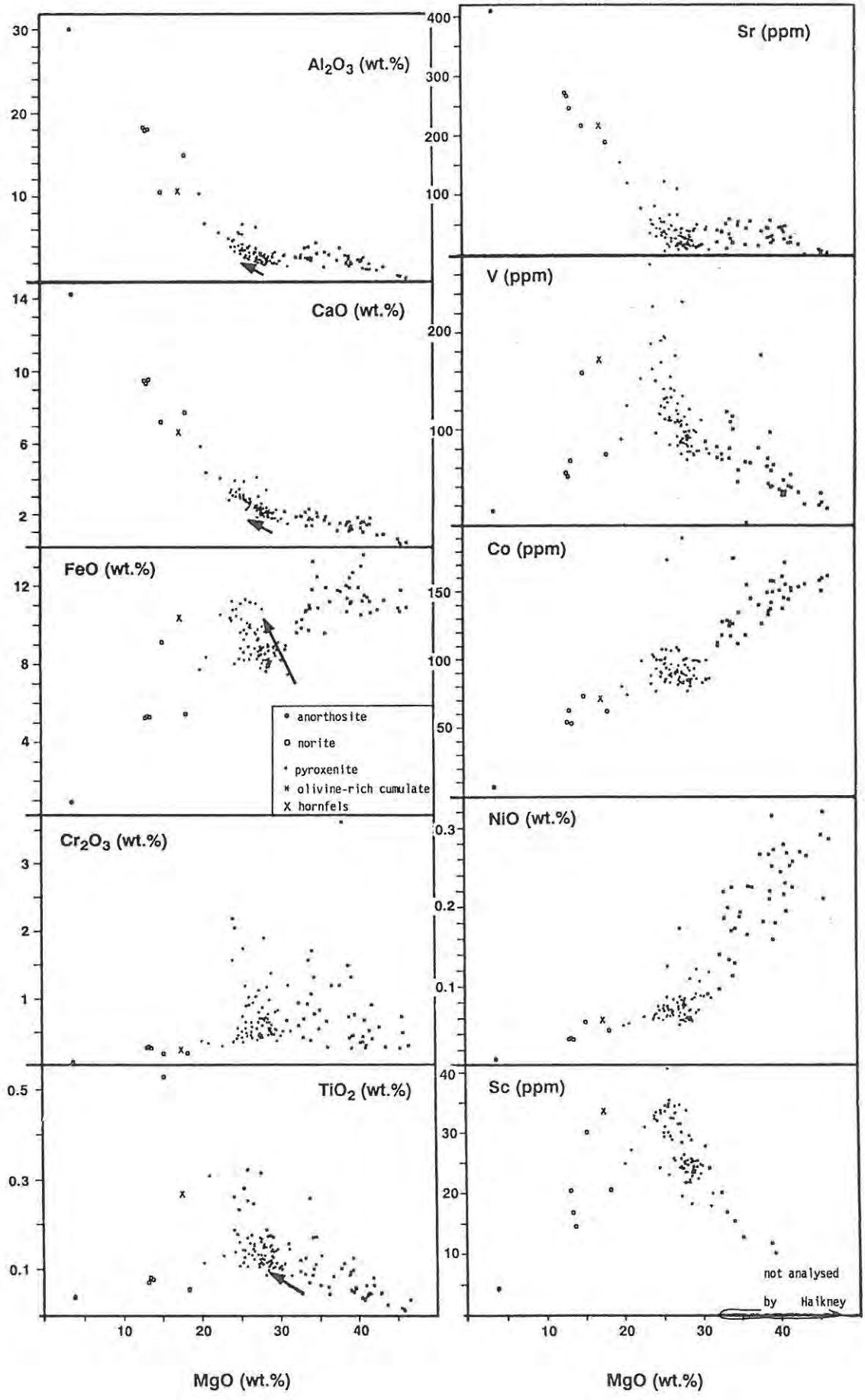

Fig. 38 Whole-rock data - interelement relationships between major, minor and trace elements (arrows depict orthopyroxene fractionation).

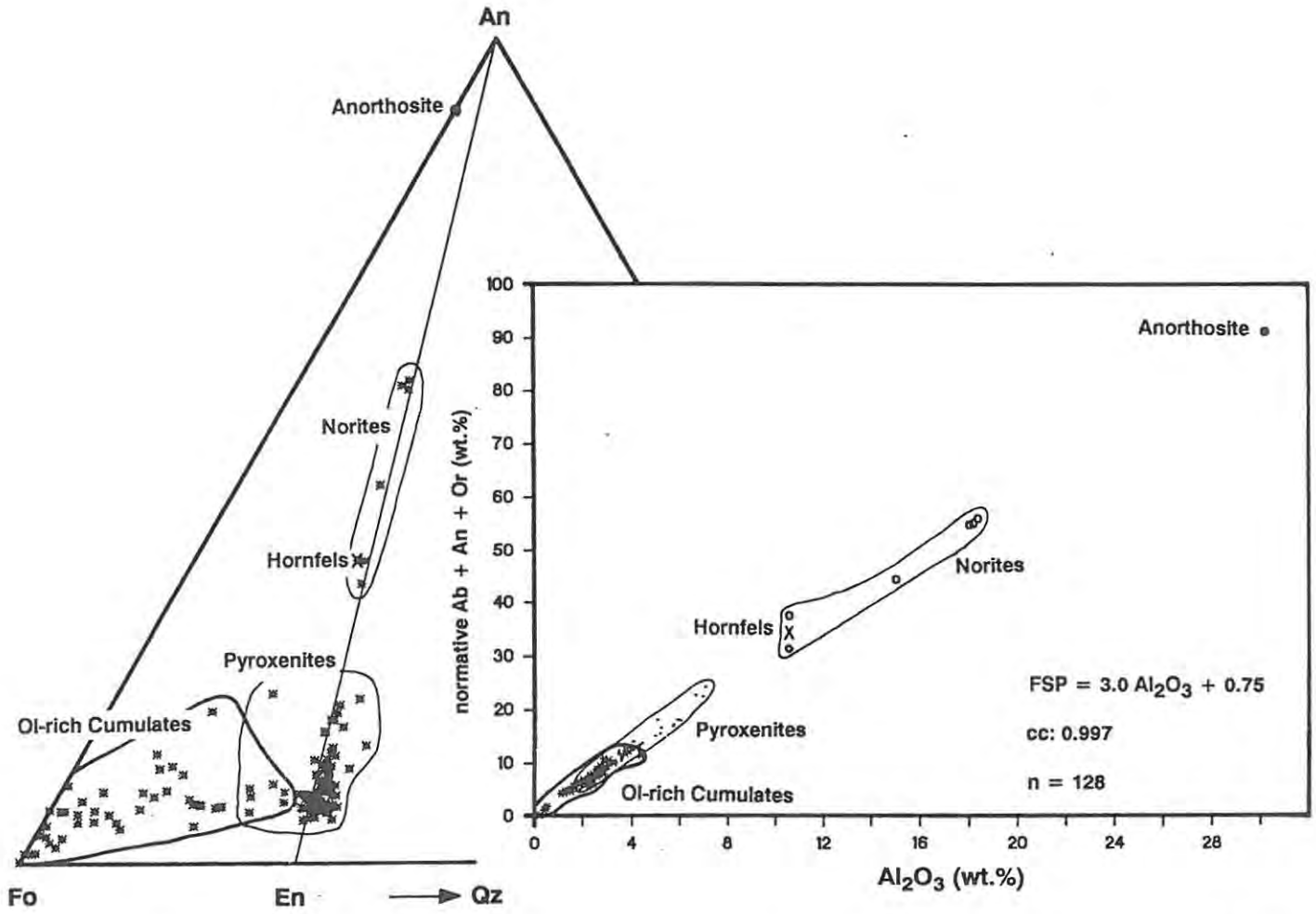

Fig. 39 Normative compositions of whole-rock samples (NG-sequence) in the system An - Fo - Q, and plot of normative feldspar against whole-rock Al_2O_3.

Concentrations of CaO and Al_2O_3 show good negative correlations with MgO. The wide range depends greatly on lithology and modal composition. The only anorthosite within the sequence (sample NG3-212.20) has a concentration of 30.2 wt.% Al_2O_3 and 14.3 wt.% CaO, while the remainder of the pla cumulates show Al_2O_3 values between 10.6 and 18.0 wt.%. The CaO ranges from 6.0 to 9.5 wt.%. All variations can probably be attributed to a variable ratio pla : opx in the rock. This relationship is better illustrated in a plot of normative feldspar (anorthite + albite + orthoclase) vs. Al_2O_3 (Fig. 39), which was successfully used by Eales et al. (1986) to subdivide the leucocratic cumulates of the uCZ. The linear regression of all NG data yields the following equation:

FSP (wt.%) = 3.0 * Al_2O_3 (wt.%) + 0.75 cc: 0.997, which proves to be

close to that of Eales et al. (1990a) whereby

FSP (wt.%) = 3.03 * Al_2O_3 (wt.%) + 0.73.

Due to the very limited range of Al and Ca concentrations, i.e. small amounts of pla, the ultramafic lithologies cluster in the left corner of the diagram. Ol-rich cumulates show limited variations of Al_2O_3 (0 - 4.0 wt.%) apart from the above-mentioned altered dunite (sample NG1-95.50), whilst in pyroxenites the concentrations are slightly higher (1.9 - 7.1 wt.%).

Positive correlations against MgO are displayed by the oxides FeO and NiO, both of which can be explained by variations in modal composition (ratio of pla to ferromagnesian phases). Contents of NiO show a sharp decrease in the sequence dunite (ca. 0.3 wt.%) - pyroxenite (ca. 0.1 wt.%) - norite (< 0.1 wt.%). FeO contents show an overall decrease from the ultramafic to the leucocratic cumulates, but within the ultramafic rock types the FeO concentrations plot in more or less elongated fields perpendicular to the general trend, thus displaying a negative relationship. This deviation seems to be related to cryptic variations of the ferromagnesian phases, of which opx is schematically depicted in the diagram (arrows). The whole-rock trend parallel to the fractionation path of opx is shifted towards the MgO-poorer side because of a dilution effect caused by pla contents. Cryptic variations of opx with respect to Al_2O_3 and CaO (arrows)

follow the whole rock trend, but minor proportions of pla shift the pyroxenite field to higher Ca and Al levels. In the plot of TiO_2 against MgO the pattern is more complicated. While the ultramafic cumulates define a trend with a negative slope, the noritic rocks and anorthosites indicate a positive correlation, again illustrating the dependence of element concentrations on modal compositions. However, as demonstrated by the fractionation path of opx (arrow), the whole-rock TiO_2 values seem in some samples to be anomalously shifted towards higher values, which can be explained by small amounts of Ti rich phases as phlogopite, cpx and chr.

No clear trends (indeed only wide scatter) are displayed by plotting K_2O and P_2O_5 against MgO. The relationship of MnO to MgO is similar to that of FeO. As expected, the Na_2O values show a negative trend as do Al and Ca, indicating the strong association of Na with feldspar (all latter elements not depicted in Fig. 38).

The major element contents can be summarized in the triangular diagram (Fig. 39) using the CIPW-norm minerals anorthite ($CaAl_2Si_2O_8$), forsterite (Mg_2SiO_4) and quartz, with enstatite ($Mg_2Si_2O_6$) lies between the latter. The four main lithologies plot according to their most abundant CIPW-cumulus phase in different fields. Dunites and poikilitic harzburgites generally plot close to the forsterite corner. Granular harzburgites and olivine pyroxenites lead over to the pyroxenite field, thus covering an intermediate area. Most of the pyroxenites plot in a limited field stretched along the tieline opx - an (apart from samples which are either ol-bearing or pyroxenites of the MZ).

5.3. Trace Elements

All whole-rock samples were analysed for the following trace elements: Zn, Cu, Co, V, Rb, Sr, Nb, Y, Zr and Sc. For Haikney's samples no Sc values are available. Ni and Cr were also determined, but recalculated to oxides and included as minor elements in the earlier section. The elements Rb and Sr of selected samples were also analysed by isotope dilution mass spectrometry (ID-MS) by F.J. Kruger to determine Sr isotopes (see also chapter 7).

A comparison of some of the data reveals the generally good agreement even for concentrations close to the lower level of detection by the XRF-technique:

Sample	Sr (ppm)		Rb (ppm)	
	XRF	ID-MS	XRF	ID-MS
NG1- 25.00	32.9	34.8	2.6	2.4
NG1-292.30	14.4	14.0	0.6	1.4
NG1-500.50	34.3	34.7	0.8	1.2
NG2-180.55	38.9	41.2	2.6	2.7
NG2-447.90	42.7	43.5	1.2	1.4
NG2-536.10	41.5	39.9	3.9	3.9

In general, levels of incompatible trace elements in cumulate rocks are unreliable guides to fractionation, as they are controlled by the amount of trapped intercumulus liquid within the sequence adcumulate - mesocumulate - orthocumulate (Henderson, 1975; Cawthorn and McCarthy, 1985). However, as described earlier (see on section grain size) fine-grained pyroxenites, which are generally adcumulate-textured, are characterized by more primitive geochemical traits in opx as well as whole-rock compositions, while the coarser variants, meso- to orthocumulates, display more evolved parameters. Hence, a complete decoupling of whole-rock trace element geochemistry and mineralogy is not expected.

Most of the trace elements follow regular trends when plotted against MgO (Fig. 38). A negative relationship is evident for Sr, while V and Sc show patterns comparable to the TiO_2 trend. In the Mg-rich, ultramafic lithologies a strong negative correlation is apparent, expressing the high partition coefficients of Sc and V for opx and chr. Concentrations of Co depend also on the modal proportion of ol and opx. Therefore, an overall positive correlation with MgO is displayed. Levels of Zn (not in Fig. 38) revolve around ca. 70 ppm in the ultramafic cumulates, but drop sharply in the leucocratic, noritic rocks. However, opx-rich norites show similar concentrations. The compositional field of pyroxenite shows a conspicuous elongated shape similar to FeO, which suggests a Zn-enrichment with opx fractionation. The element Cu, useful as an indicator of S when present in anomalously high concentrations, ranges from 6 to 66 ppm. These relatively low values show the paucity of BMS throughout the sequence. Levels of Zr are widely scattered (0 - 42 ppm).

Various element concentrations of the hornfelsic floor-rock are also depicted in the figures to demonstrate its geochemical features. Al_2O_3 and CaO values indicate a feldspar-rich matrix and some element levels (e.g. Cr, Sr and Co) do not differ significantly from those of the noritic cumulates. However, its extraordinary character is evident in anomalously high concentrations in TiO_2 (0.3 wt.%), FeO (10.3 wt.%), Sc (33 ppm) and V (171 ppm).

5.4. Other Interelement Relationships

In the variation diagram (Fig. 40C) Sr displays a very good correlation with Al_2O_3 (cc: 0.964); linear regression yields the following equations, of the form y = mx + c, where y = Sr (ppm), and x = Al_2O_3 (wt.%).

Rock Type	Number of Samples	m	c	cc
all	128	14.8	- 9.0	0.946
all norites	7	11.6	51.0	0.950
uCZ-norites	5	12.8	27.6	0.994
all pyroxenites	80	17.5	-22.6	0.872
uCZ-pyroxenites	9	15.9	-18.4	0.973
lCZ-pyroxenites	36	12.3	-11.3	0.845
LZ-pyroxenites	31	12.9	- 2.5	0.798
MZ-pyroxenites	3	28.7	-76.4	
all ol-rich rocks	40	13.2	- 1.3	0.766
lCZ-ol-cumulates	11	9.7	- 1.2	0.730
LZ-ol-cumulates	29	16.9	- 2.8	0.867

Note that sample NG3-220.17 was omitted for the calculation of the equation of the lCZ-pyroxenites.

From the above-listed equations and their coefficients it is evident that even in the ultramafic cumulates with low Al_2O_3 (<5 wt.%) a correlation is still possible. Although the slopes vary slightly, the regression lines for the major rock types are comparable. However, scrutiny after a division into different stratigraphic intervals reveals the distinctly different x-coefficients for the same rock type. This is especially evident for the pyroxenites and ol-rich cumulates.

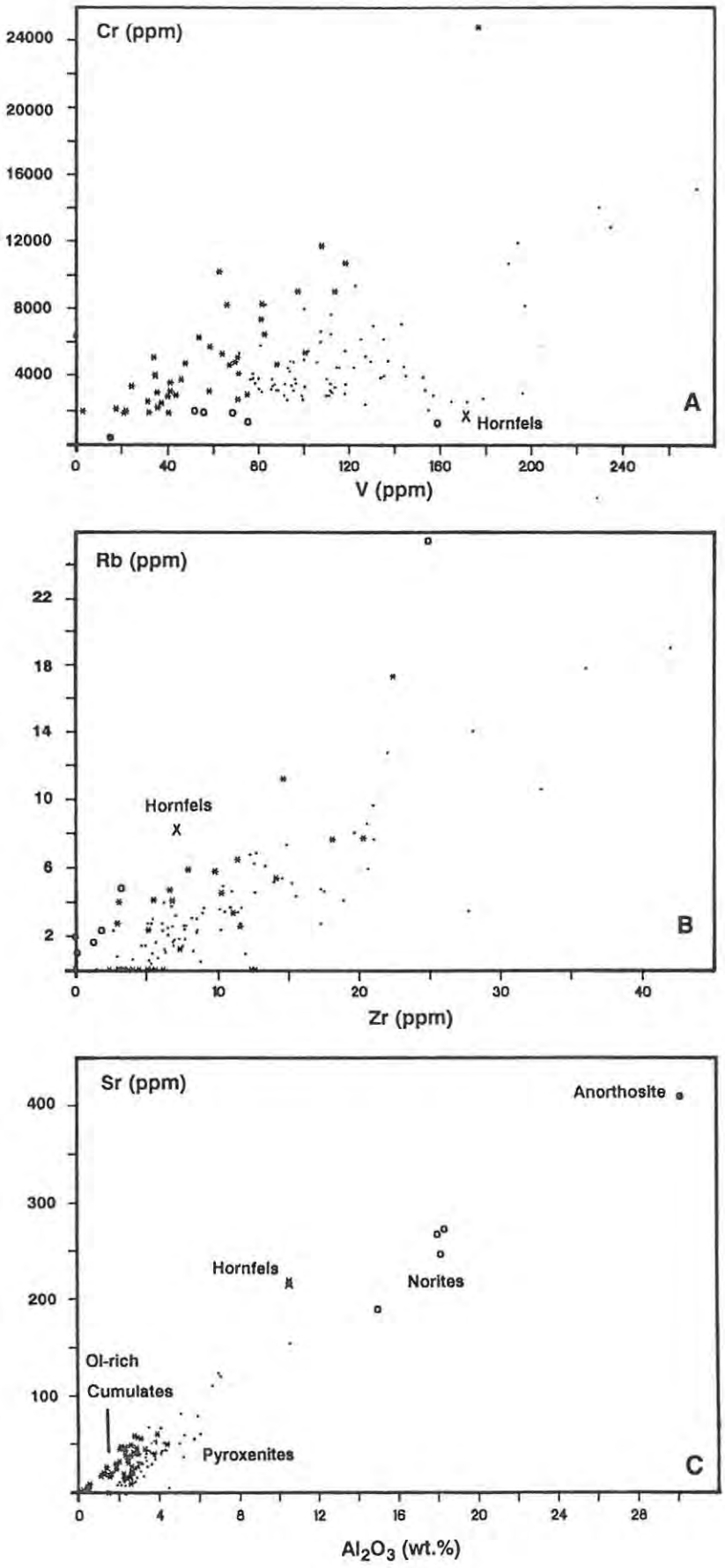

Fig. 40 Interelement relationships of A) Cr vs. V; B) Rb vs. Zr, and C) Sr vs. Al_2O_3 (all whole-rock data).

Another useful inter-element relationship is portrayed by Cr against V (Fig. 40A). The following values for constants m and c in the equation y = mx + c are obtained after linear regression, where y = Cr_2O_3 (wt.%), and x = V (ppm):

Rock Type	Number of Samples	m	c	cc
all	128	0.005	0.27	0.479
all norites	7	0.004	0.04	0.825
all pyroxenites	80	0.006	0.08	0.572
uCZ-pyroxenites	9	0.021	-2.95	0.812
lCZ-pyroxenites	36	0.008	-0.11	0.787
LZ-pyroxenites	31	0.002	0.42	0.197
all ol-rich rocks	40	0.016	-0.15	0.862
lCZ-ol-cumulates	11	0.018	-0.36	0.901
LZ-ol-cumulates	28	0.011	0.07	0.686

Note that sample NG3-220.17 was omitted for the calculation of the equation of the lCZ-pyroxenites and sample NG2-236.86 was excluded from the ol-rich cumulates of the LZ.

Although the correlation coefficients are in some cases in the statistically non-significant range and no relationship is evident for the LZ-pyroxenites, these equations can be applied to assess the concentrations of V and Sr in theoretically pure mineral phases.

The relationship Rb versus Zr was chosen to demonstrate the behaviour of incompatible trace elements. As illustrated in the variation diagram (Fig. 40B) the positive correlation indicates their sympathetic enrichment, and hence similar, low, distribution coefficients.

5.5. Chemical Variations with Stratigraphic Height

Figure 41 summarizes the chemical variations with stratigraphic height. Non-systematic variations of modal proportions will greatly affect some of the graphs, but selection of element ratios such as $Mg\#_{WR}$ should compensate for most of the modal effects.

By means of the TiO_2 and Sr concentrations the sequence can be subdivided into two major portions: a) the MZ and LZ with an general upward decrease and b) the CZ with an overall upward increase of levels of these oxides or elements. CaO and Al_2O_3 levels (not depicted) tend to

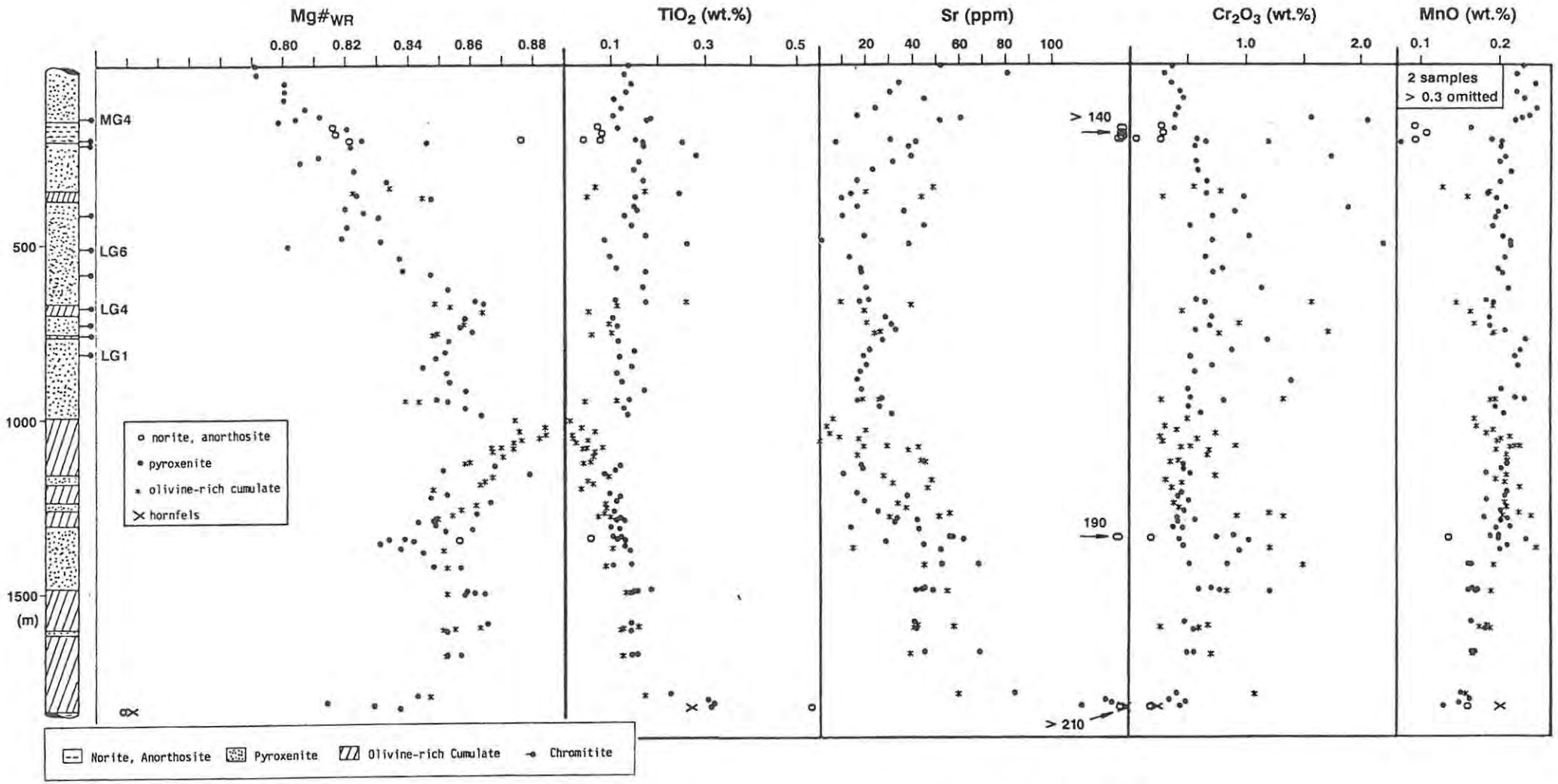

Fig. 41 Selected whole-rock data plotted against stratigraphic height (NG-sequence).

parallel this trend reflecting the amount of pla in the rocks. The occurrence of cumulus pla is manifested in major deflections of absolute values of these elements. The boundary between lCZ and uCZ is thus marked by a sharp deflection.

The subdivision into 10 segments as proposed earlier in this work based on the $Mg\#_{opx}$ (see Fig. 15A and B) is now strongly supported by the very good correlation of $Mg\#_{WR}$ and $Mg\#_{opx}$. Linear regression of $Mg\#_{WR}$ and $Mg\#_{opx}$ yields a cc of 0.966 for the equation:

$$Mg\#_{WR} = 0.9 * Mg\#_{opx} + 0.084 \quad (n=66),$$

which means that the $Mg\#_{WR}$ reflects the fractionation stage of the cumulus ferromagnesian phases despite minor disturbances caused by chr (low Mg#), cpx, phlogopite and amphibole. In the NG-sequence these phases are normally present in proportions less than 2 vol.% and therefore their influence is slight. The range of the $Mg\#_{WR}$ is from 0.749 (MZ-gabbroic norite) to 0.884. For the hornfelsic floor-rock a $Mg\#_{WR}$ of 0.751 was obtained. Ultramafic cumulates show a steady increase of MnO with minor deflections caused by ol-rich cumulates. This enrichment might point to the overall fractionation trend within the resident liquid. Cr_2O_3 levels in whole-rock data might greatly depend upon the amount of accessory chr, which is for values above ca. 0.6 wt.% Cr_2O_3 certainly true (see chapter on mineralogy). However, it appears that the minimum values of Cr_2O_3 in the uCZ-, LZ- and MZ-lithologies are lower than in the lCZ-rocks, which can be attributed to the Cr-enriched character of the lCZ as demonstrated in the previous chapter.

5.6. Comparison of the Four Major Rock Types

Average compositions of dunites, harzburgites, pyroxenites and norites in different stratigraphic intervals were calculated and compared. This was done by averaging all samples of the same lithology within a particular zone. It has to be noted here that whole-rock samples of chromitiferous rocks and chromitites were not analysed and their contribution to the average rock geochemistry is not considered here in section 5.6.

In Fig. 42 the average compositions of the lithologies are compared.

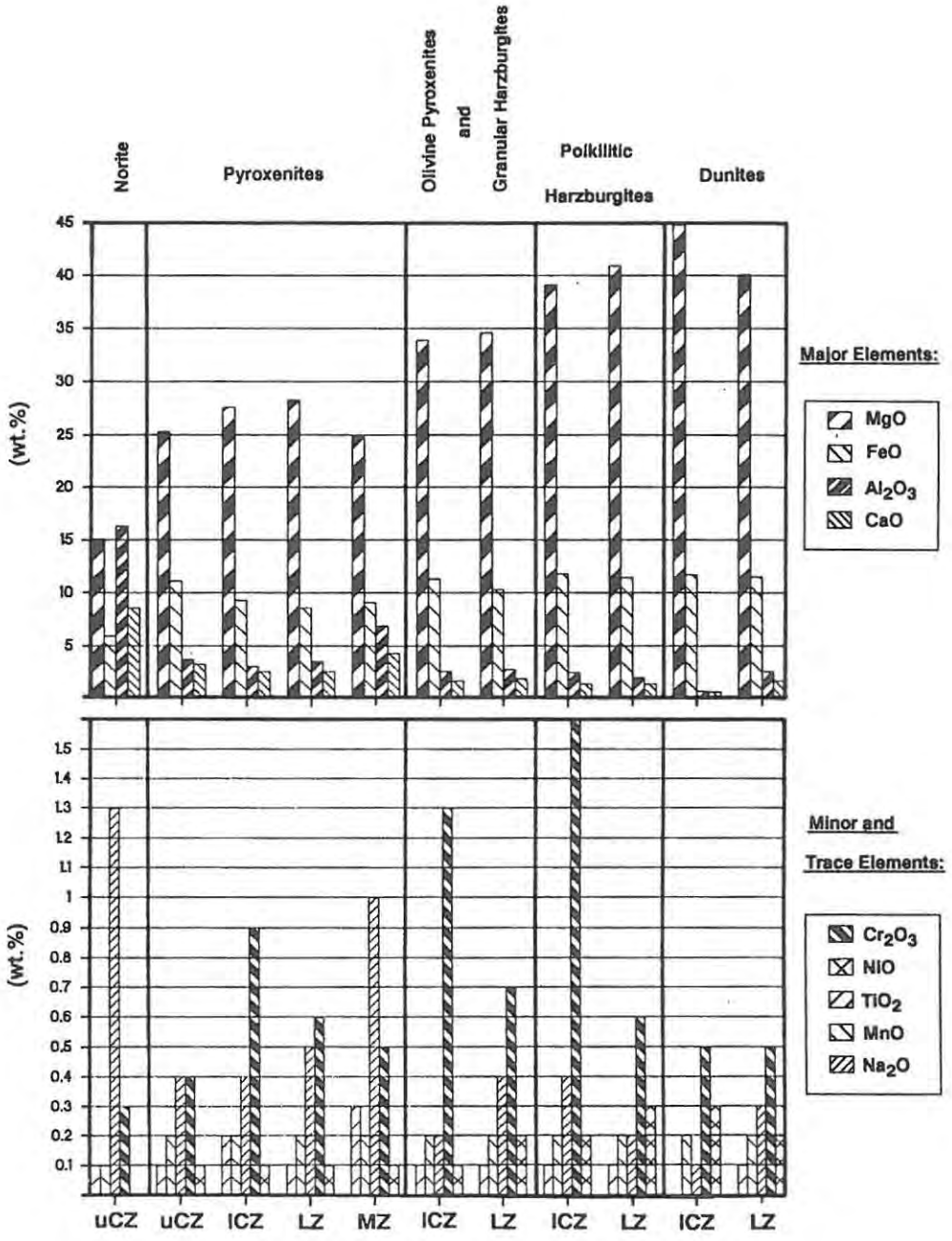

Fig. 42 Average compositions of the major lithologies in different stratigraphic intervals.

Norites comprise only 2.23 % of the NG-sequence and only 6 samples were analysed (4 located in the uCZ, 1 sample from the LZ and 1 sample of the gabbroic norite in the MZ). The average composition of norite in the uCZ does not differ considerably from that of the LZ-norite. The occurrence of cumulus cpx in the marginal gabbronorite together with the different whole-rock geochemistry supports its special stratigraphic position at the base of the entire complex.

Pyroxenite, which is by far the most abundant rock type is significantly different in its average composition in different stratigraphic intervals. Despite limited concentrations in Al_2O_3 and CaO (3.0 - 3.7 and 2.5 - 3.2 wt.%, respectively), apart from pyroxenite in the MZ (6.9 wt.% Al_2O_3 and 4.3 wt.% CaO; n=3) absolute MgO and FeO levels are distinctly different. This can not be explained by modal variations because of the limited ranges in pla components described above. It is clear here that pyroxenite changes its composition in response to the fractionation stage of the crystallizing liquid. The $Mg\#_{WR}$ derived from the average composition illustrates this behaviour:

Stratigraphic interval	$Mg\#_{WR}$	n
uCZ	0.803	10
lCZ	0.841	36
LZ	0.853	31
MZ	0.829	3

The NiO value of pyroxenite in the CZ (0.1 wt.%) is also significantly lower than in pyroxenite in the LZ (0.2 wt.%). No considerable variation was found in the TiO_2 contents. The higher Cr background value in the lCZ previously described finds confirmation in a higher concentration in the average rock composition. All lithologies in the lCZ are enriched in Cr_2O_3 (>0.9 wt.%), which means that almost every whole-rock sample in the lCZ has additional accessory chr. Selected trace elements Sr and Zn show also differences in their concentrations. Pyroxenite in the lCZ (25 ppm Sr) contains only ca. 60 % of the level of this element hosted by pyroxenite of the uCZ and LZ (42 ppm). The MZ-pyroxenite displays a very much higher concentration of Sr (122 ppm) together with a higher Al content.

Levels of Zn show the following distribution:

Stratigraphic interval	Zn (ppm)
uCZ	67
lCZ	62
LZ	70
MZ	87

5.7.The Bulk Composition of the lCZ and LZ

Cameron (1978, 1980) presented bulk compositions for the LZ and lCZ of the Eastern Bushveld Complex based on modal and mineral compositions of different stratigraphic intervals. A comparison with Cameron's data is presented in the second part of this thesis and therefore a similar calculation is given here.

The bulk compositions of the lCZ and LZ (including analyses of samples of the MZ with the latter, but excluding its marginal gabbroic norite) of the NG-sequence are derived from a) whole-rock data and b) mineral compositions together with modal data. In both methods the cumulative thickness of each rock type, weighted for each stratigraphic interval (section 2.3.2), was used. However, because 2.1 % of the lCZ comprises chromitiferous pyroxenite (average of 28.2 wt.% chr), incorporation of the average composition of such rocks (for which whole-rock analyses are not available) into method a) was necessary. Therefore its composition was calculated using the average composition of ML-chr and opx of the lCZ with a ratio chr : opx of 28.2 to 72.8. Massive chromitite layers were treated in both methods as 100 wt.% modal chr with the average ML-chr composition of the lCZ, a simplification that will yield negligible error.

The results of both methods are shown below:

	1CZ		LZ + MZ	
	a	b	a	b
SiO_2	53.0	54.7	48.4	49.2
TiO_2	0.2	0.1	0.1	0.1
Al_2O_3	3.0	2.8	2.9	2.7
Cr_2O_3	1.5	1.4	0.6	0.8
FeO	9.6	9.2	10.9	11.6
MnO	0.2	0.2	0.2	0.2
NiO	0.1	0.1	0.2	0.2
MgO	28.7	27.6	34.2	33.6
CaO	2.3	3.6	2.0	1.6
Na_2O	0.4	0.3	0.4	0.3
K_2O	0.1	0.0	0.1	0.0

The results are for most elements in good agreement. As expected from the findings of the earlier sections the bulk compositions for the LZ and 1CZ are seen to be significantly different. The most significant difference between both zones, apart from the major elements Mg, Fe and Si (which reflects the modal proportions of the ferromagnesian phases opx and ol) is the variation of Cr_2O_3. The bulk composition of the 1CZ shows a clear enrichment in Cr.

5.8. Discussion and Conclusions

Because of the effects of non-systematic variations in modal compositions on whole-rock geochemistry, this discussion highlights only some of the findings in respect of their relevance to pinpointing liquid compositions.

All rocks at the base of the complex (up to a depth of 1778.90 m; sample NG2-738.90) are distinctly different to those above (high in TiO_2, CaO and Al_2O_3) in their chemical composition, in support of the petrographical evidence. The pyroxenites in the MZ show also unusually high concentrations of Sr, as does the gabbroic norite at the basal contact. The enrichment in Sr of the latter sample is especially evident after application of the regression equation for Sr vs. Al_2O_3 for all noritic rocks: sample NG2-773.60 (at a depth of 1813.60 m) with 10.6 wt.% Al_2O_3 should contain 174 ppm Sr, but the actual value is 218 ppm by XRF (214 ppm by ID-MS). Average compositions show also significant variations in MgO, Cr_2O_3, and Sr.

These compositional variations might be due to three principal factors:

a) variations in parental magma compositions, and/or

b) different degrees of assimilation, and/or

c) secondary processes, e.g. hydrothermal alteration or metasomatism.

The data presented, especially the systematic changes with stratigraphic height, suggest rather subtle changes in parental liquid compositions. Recognising that the rocks of the column are cumulates, the information yielded by whole-rock analysis is of limited value in establishing the compositions of original liquids. That is, cumulates do not represent samples of the original liquids, but only derivative fractions thereof. However, these putative liquids from which the cumulates have been derived did not differ significantly, i.e. no compelling evidence was found that the parental magmas were of contrasting composition with different phases on the liquidus.

CHAPTER 6 : PLATINUM-GROUP ELEMENT DISTRIBUTION IN THE NG-SEQUENCE

The distribution of platinum-group elements (abbreviated here to PGEs) was investigated through the entire NG-sequence with emphasis on concentrations in the chromitite layers. Most of the results are published in Teigler (1990). However, some analytical work was completed later and is incorporated here. The data presented here together with published data for the UG2-chromitite and the Merensky Reef document for the first time the general distribution of PGEs through the lower part of the RLS.

Published data of the PGE distribution in silicate rocks or massive chromitites apart from the UG2-chromitite and the Merensky Reef are scarce. Lee and Tredoux (1986) studied the PGE contents of the silicate cumulates in the eastern limb of the BIC, while Sharpe's (1982) data are concentrated on marginal rocks. The PGE distribution of some massive chromitites is described in von Gruenewaldt et al. (1986) and Lee and Parry (1988).

6.1. PGE distribution in the Silicate Rocks

Eighteen samples (9 pyroxenites, 7 ol-rich cumulates, 2 cumulus pla-bearing rocks) were analysed for PGEs and Au by Sheen Analytical Services Ltd., Australia, using ICP-mass spectrometry after a Ni-sulphide collection technique. The sample positions are depicted in Fig. 43, while Fig. 44 presents the PGE contents of the samples and schematically exhibits their distribution relative to height.

Because of the sample spacing, the variation relative to height cannot be assessed quantitatively. In each sample the total sum of PGE+Au (ΣPGE) is very low compared with the abundance of PGEs in C1-chondrites (Naldrett and Duke, 1980). The average ΣPGE is 75 ppb and average values of Ru, Pt and Pd are 28, 15 and 17 ppb, respectively. The sums of Ru+Os+Ir (ΣRu, Ru-group) and Pt+Pd+Rh (ΣPt, Pt-group) are 34.7 and 35.5 ppb.

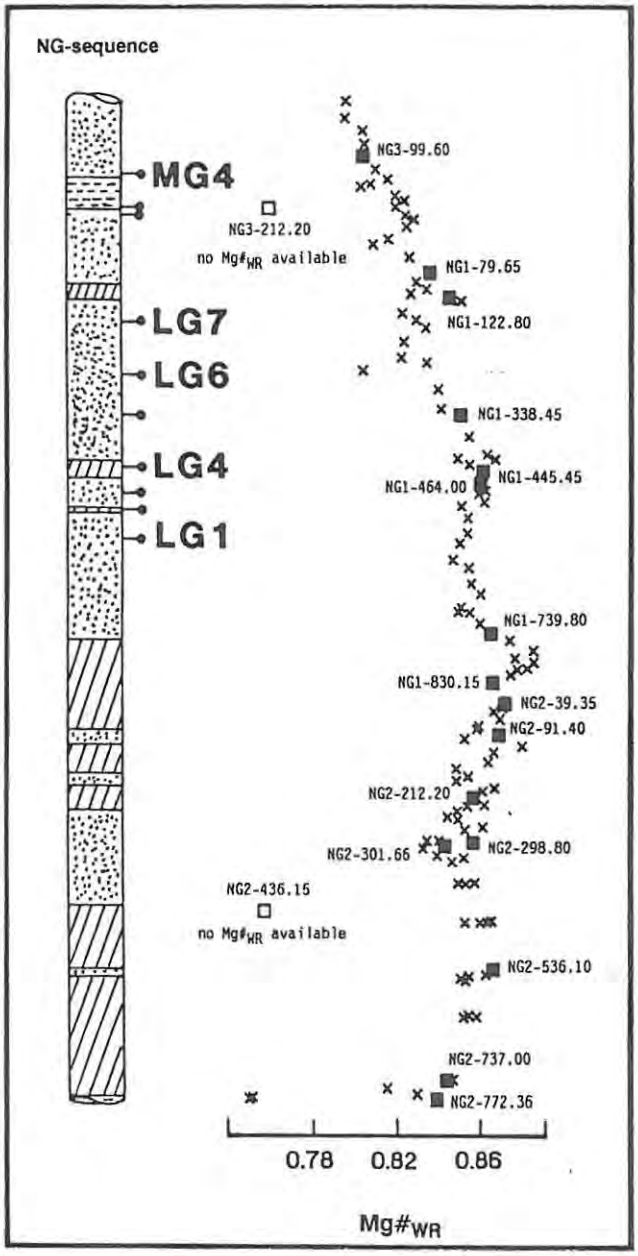

Fig. 43 Sample positions of silicate cumulates selected for PGE analysis.

Figure 45 shows some selected whole-rock data plotted against PGE data. The top diagram depicts the variation of the two PGE groups with the whole-rock Cr_2O_3 content. The Pt-group, associated with BMS (Scoates et al., 1988), displays a weak negative correlation (cc.: - 0.59). The Ru-group, chr associated (Scoates et al., op.cit.) shows a very poor positive correlation. This unexpected correlation can not be explained by redistributing the Cr_2O_3 to occurring mineral phases.

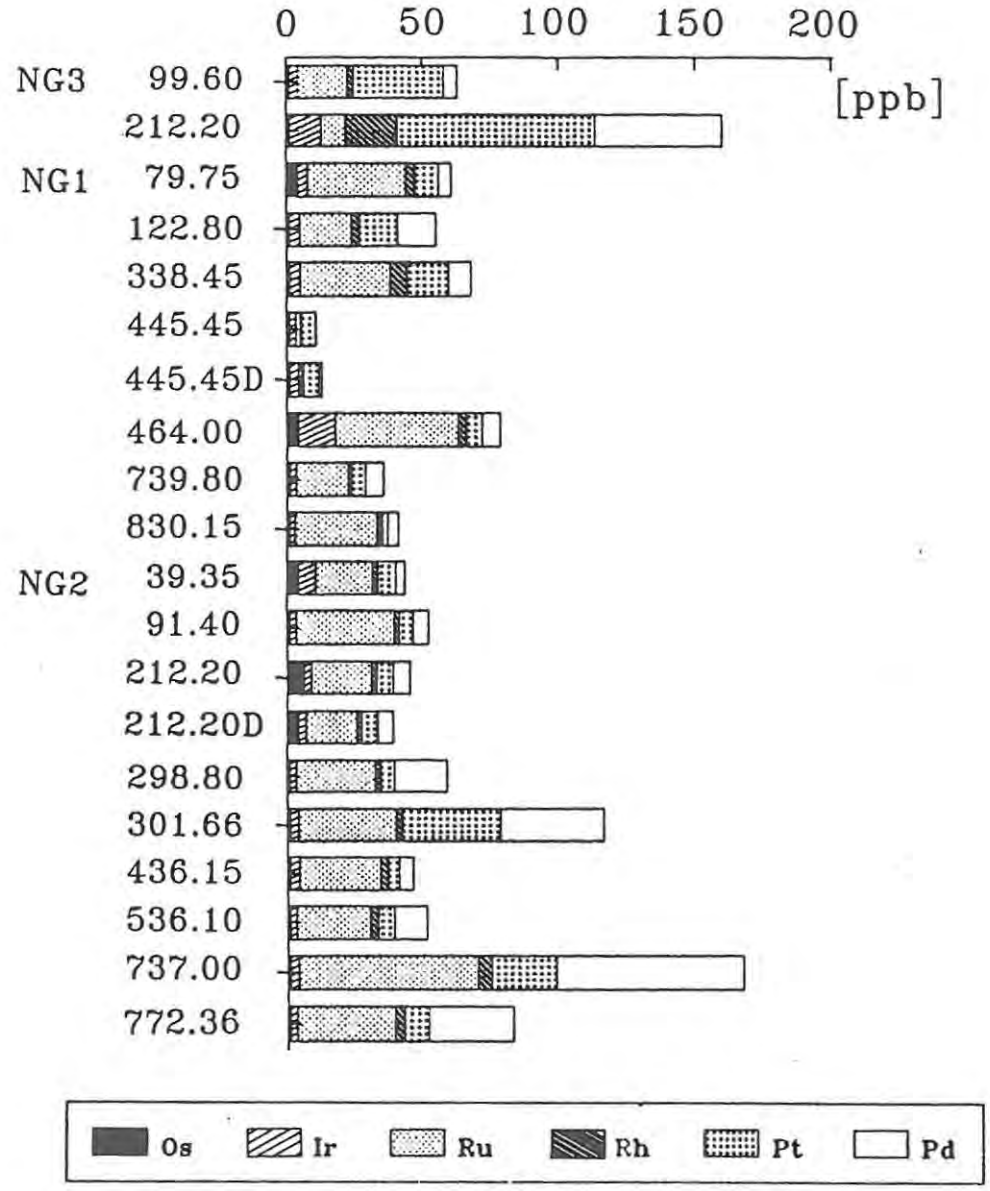

Fig. 44 The PGE contents of the silicate cumulates (see text for details).

The average Cr_2O_3 content in cumulus opx is 0.48 wt.% (868 analyses in NG1), which means only whole-rock values above 0.5 wt.% are generally attributable to chr in the sample because of the virtually negligible proportion of other Cr-bearing phases such as cpx or mica. After such a correction, with due regard to modal compositions, especially the ratio opx : ol, no correlation is apparent. It is evident from this described relationship, that chr as an accessory phase can not account for higher PGE values in these rocks.

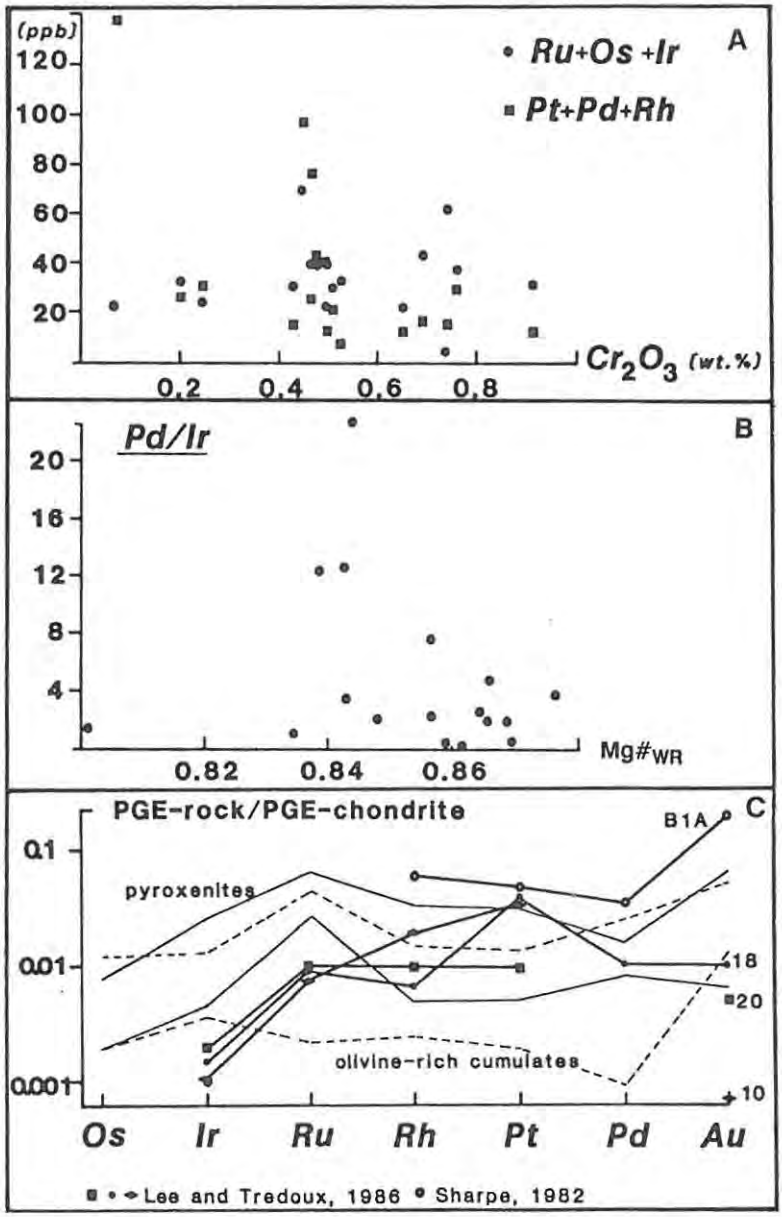

Fig. 45 Selected PGE data plotted against whole-rock data (A and B); C) chondrite normalized PGE data of the NG-cumulates in comparison with published data of Lee and Tredoux (1986) and Sharpe (1982); field between solid lines shows PGE distribution in pyroxenites and that between dashed lines in olivine-rich cumulates.

Naldrett and Barnes (1986) found an increasing Pd/Ir ratio with increasing fractionation of the host magma, accordingly a negative correlation between Pd/Ir and $Mg\#_{WR}$ might be expected. Figure 45B, it might be argued, exhibits such a trend.

If the PGE data are normalized to C1-chondrite concentrations, (Fig. 45C) the various lithologies display similar patterns, i.e. enrichment in Ru and relative depletion in the more chalcophile elements Pt and Pd. In such a diagram the pyroxenites are also characterized by their higher concentrations in Pt and Pd than ol-rich cumulates. Comparison with other published data (Sharpe, 1982; Lee and Tredoux, 1986) from the Eastern Bushveld Complex reveals similar PGE concentrations in silicate rocks.

6.2. PGE distribution in the Massive Chromitite Layers

Figure 46 presents the results of the chromitite samples selected for PGE analysis. Plots of the ΣRu and ΣPt against the metallic Cr/Fe_{total} ratio of chr show a wide scatter, but nevertheless some general conclusions can be drawn (Fig. 47). A very weak positive correlation between the ratio and the Ru-group is perhaps indicated (regression yields a cc of 0.36). For the Pt-group a general trend is not exhibited, but scrutiny of the diagram reveals a clustering into three fields:

a) samples of the section below and from the LG4- chromitite cluster in the right bottom corner of the diagram;

b) samples above the LG4 through to the LG7 form a intermediate field;

c) samples above the LG7-chromitite plot in the left field.

The Pd/Ir ratio plotted against the Cr/Fe ratio shows a weak negative relationship (cc: -0.471), which means that the more primitive chromitites (high Cr/Fe ratios) display low Pd/Ir ratios in contrast with evolved chromitites (low Cr/Fe ratio) with high Pd/Ir ratios.

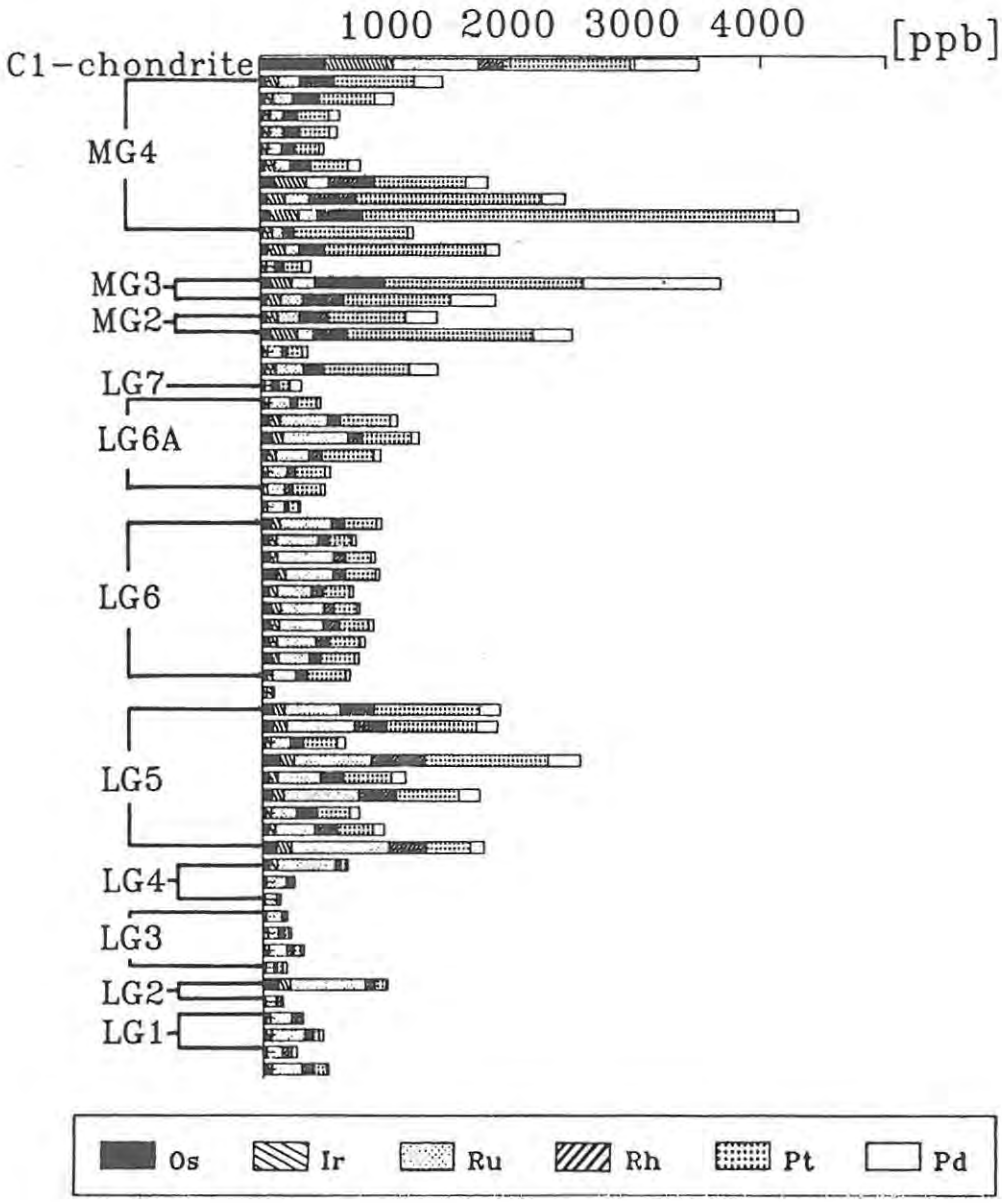

Fig. 46 The PGE contents in the chromitite layers of the NG-sequence.

In summary, the mineralogy of the chromitite layers as described earlier is reflected by the distribution pattern of the PGEs, especially when those are divided into the Ru- and Pt-group. The Cr/Fe ratio segregates the chromitite layers into distinct groups ,which also show significantly different PGE distributions. Hence, an estimation of the range of the PGE concentrations and their relative distribution can be made from the Cr/Fe ratio of a massive chromitite layer.

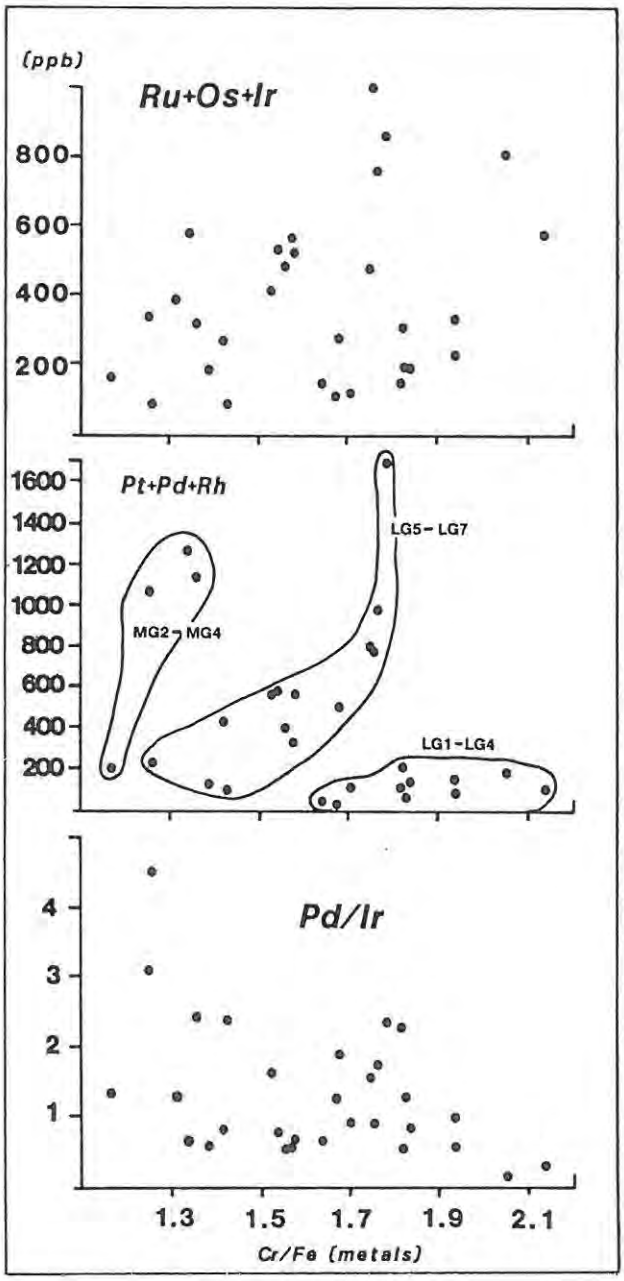

Fig. 47 PGE data versus the Cr/Fe ratio of chromite.

Figure 48 shows selected interelement relationships of the PGEs. The two PGE groups show generally good within-group correlations apart from the high Ir concentrations of some MG-chromitite samples , which will be discussed below. The cc are for Ru vs.Os 0.78, Ru vs.Ir 0.93 excluding the high Ir-samples (0.28, when included), Pt vs Pd 0.57 and Pt vs. Rh 0.75. There is no correlation between elements from different groups as

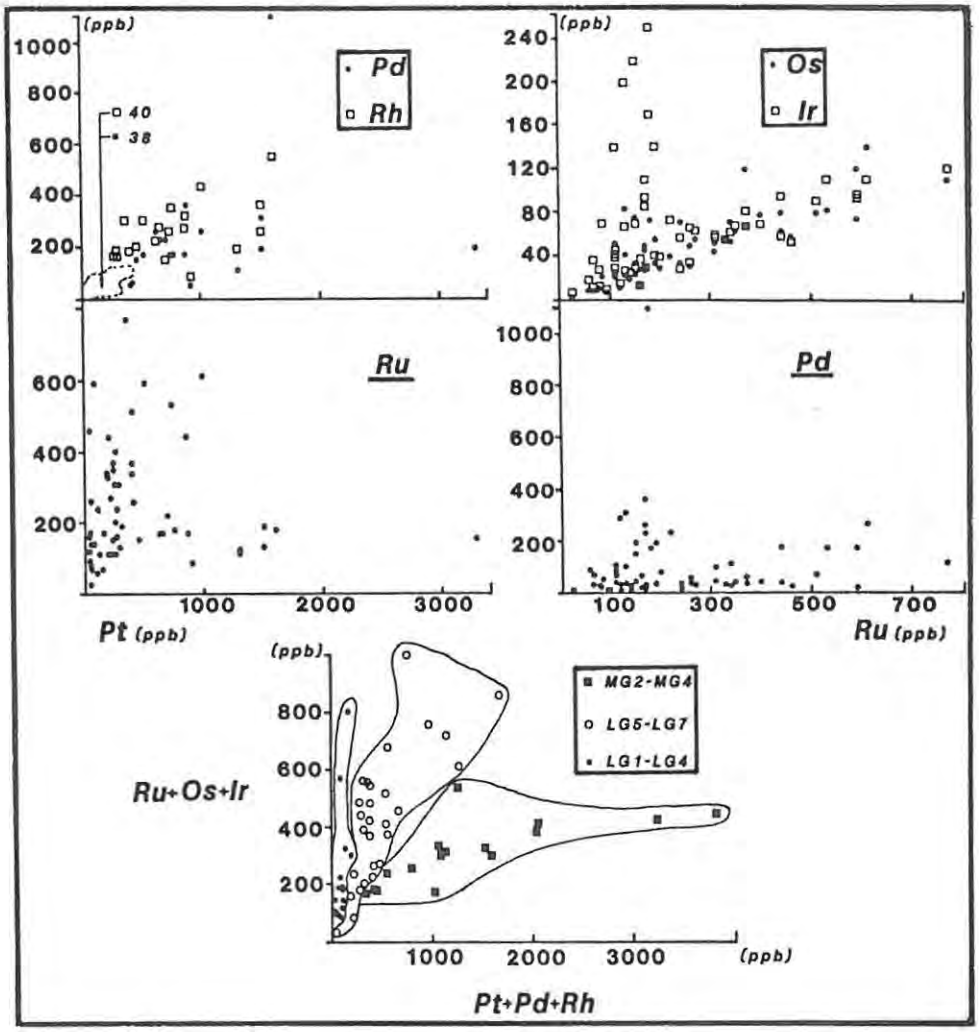

Fig. 48 Interelement relationships of the PGEs.

demonstrated in the plots Pt vs. Ru and Ru vs. Pd. These relationships clearly support the division of the PGEs into two groups, which is based on their mode of occurrence. The most likely phase for the Ru-group is laurite ($(Ru,Os,Ir)S_2$), which is closely associated with chr (Scoates et al., 1988). The anomalously high Ir concentrations in some MG-chromitites suggest that a second Ir-rich phase is present in those samples. The Pt-group is associated with interstitial BMS and only in minor degree with chr (Scoates et al., op.cit.). The current data support that these elements are mainly concentrated together.

The plotting of the two PGE groups against each other (Fig. 48, bottom) summarizes the interelement relationships and repeats a three-field distribution pattern, which was already discussed above. Samples below and from the LG4-chromitite fall into the left field, samples from the LG5, LG6 and LG7 are in the intermediate field and samples above the LG7-chromitite extends towards the right.

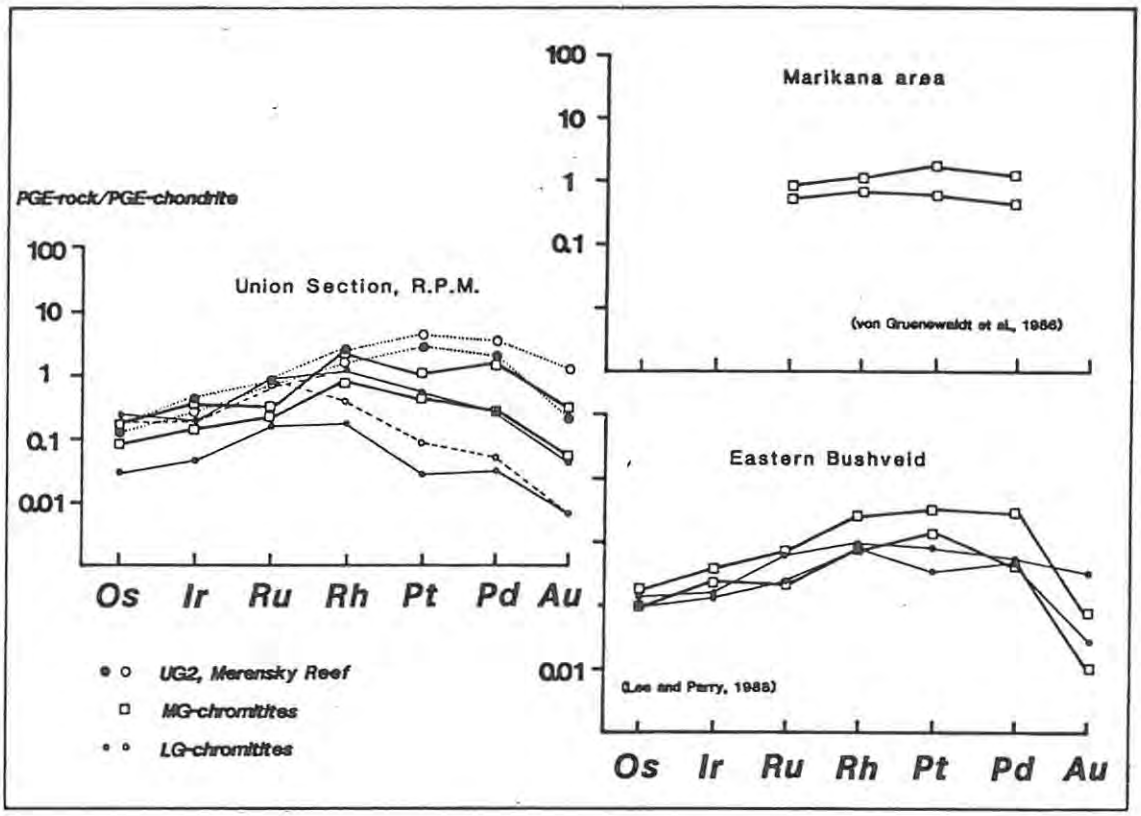

Fig. 49 Comparison of the PGE distribution at Union Section with that depicted in other published data.

Figure 49 and Fig. 50 are based on average PGE concentrations of the chromitites. These data were computed by weighting analytical results relative to sample thickness. In Fig. 49 a comparison of data of the current study with other published data (von Gruenewaldt et al., 1986; Lee and Parry, 1988) using chondrite normalized data sets reveal generally similar concentrations. However, the MG-chromitites at Union Section show relatively lower values in Ru and Pt than their equivalent layers in the Marikana area east of Rustenburg.

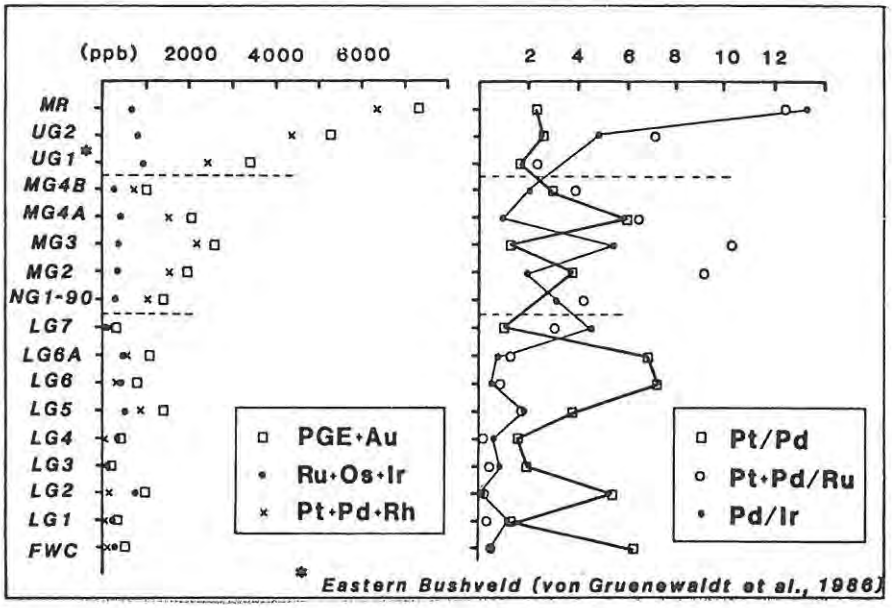

Fig. 50 PGE distribution through the chromitites at Union Section (R.P.M.).

The MG-chromitites from the Eastern Bushveld Complex do not differ significantly from their counterparts in the west. The diagram depicts also the differences in the chromitites at Union Section. The first three PGEs (Os, Ir, Ru) show similar ranges of concentration for all chromitites, although the UG2-chromitite and the Merensky Reef display generally higher values; the significant change occurs in the concentrations of Pt and Pd. The UG-, MG-and LG-chromitites are partially separated due to their different enrichment in these elements.

Figure 50 summarizes the distribution of PGEs in the chromitite layers analysed in this study, relative to stratigraphic height, together with published data for the Merensky Reef, the UG2-chromitite (both Union Section) and the UG1-chromitite (Eastern Bushveld; data from von Gruenewaldt et al., 1986).

Several conclusions can be drawn from the diagram:

a) an irregular general increase of ΣPGE upwards through the sequence is apparent;

b) within each group of chromitites and/or mineralized layers, LG-, MG-, and UG-chromitites and Merensky Reef, the highest concentrations occur in the upper part of the group, but not in the uppermost mineralized layer. (note: no data are available for the Bastard Reef). Hence, general trends may be concealed, when mineralized layers are investigated separately.

c) the LG1- to LG4-chromitites are strongly biased towards the Ru-group, suggesting that the PGE-bearing phase is laurite as proposed by Stockman and Hlava (1984) and Lee and Parry (1988). Accordingly, ΣRu is for the majority of the LG-layers greater than ΣPt.

d) the Pd/Ir and (Pt+Pd)/Ru ratio (fractionation indices) both display upwards-increasing trends, suggesting the more and more evolved character of the PGE mineralization. In contrast to these relationships, the Pt/Pd ratio is lower in stratigraphically higher chromitites, indicating a relative enrichment of Pd with fractionation.

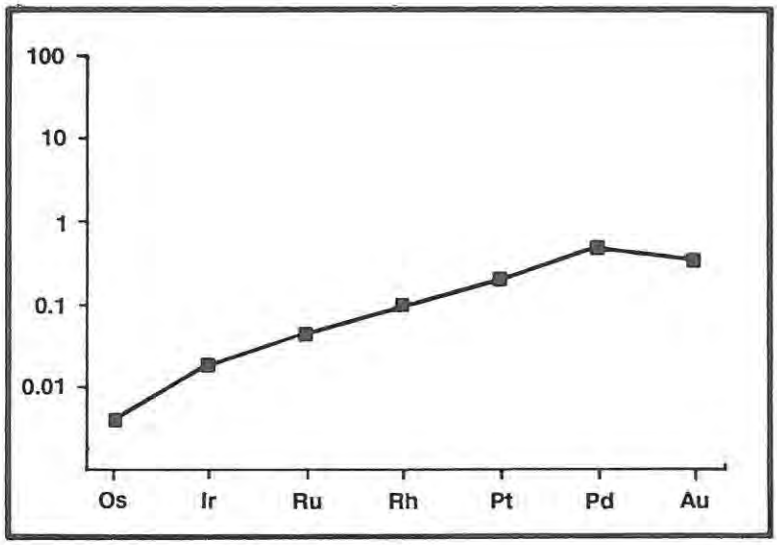

Fig. 51 PGE distribution in the sulphide-rich sample NG2-736.66 (chondrite normalized).

6.3. PGE distribution in the Sulphide-rich Sample NG2-736.66

Only one sample within the entire NG-sequence (NG2-736.66) at a depth of 1776.66 m was found to be enriched in BMS. The sample contains less than 5 vol.% interstitial sulphide, which is disseminated over 0.20 m close to the contact of MZ and LZ. The host rock is a granular harzburgite, which directly overlies the top of the MZ, a feldspathic pyroxenite (NG2-737.00). The results of the PGE analyses in ppb of the BMS-rich sample are listed below (length of sample 7.5 cm):

	Os	Ir	Ru	Rh	Pt	Pd	Au	ΣPGE	ΣRu	ΣPt	Pt/Pd	Pd/Ir
NG2-736.66	2	10	31	18	200	250	50	561	43	468	0.8	25.0
NG2-736.66 (duplicate)	<2	9	35	14	190	240	40	529	45	444	0.8	26.7

Because of the almost identical results of the analyses only the first data set was used for all diagrams and calculations. In Fig. 51 the PGE content in the sample is displayed using chondrite normalized data. In comparison with Fig. 45C and 49 the distribution pattern of the BMS-rich sample is distinctly different. A smooth increase from element to element is displayed. No other sample in the NG-sequence showed a similar trend. The PGE-enrichment factor of the sample is 7.5, compared with average PGE concentrations in the silicate rocks. The displayed trend has a tenor typical of sulphide-hosted PGE mineralization as described by Naldrett and Duke (1980) and Barnes et al. (1985).

6.4. Discussion and Conclusions

The data presented demonstrate the close association of chromitite and PGE mineralization in sulphide-free parageneses, which was also described by von Gruenewaldt et al.(1986) and Naldrett and von Gruenewaldt (1988). However, their comments on the association chromitite - PGE mineralization were restricted to their close spatial relationship. The current data reveal, further, a geochemical relationship between chr mineralogy and PGE distribution.

Chromitite layers in this study, which were mineralogically subdivided earlier into three principal groups, are now seen to vary also significantly in their PGE contents and distribution patterns. Group 1 chromitites (LG1 through LG4) are characterized by the domination of the PGEs by the Ru-group elements; Ru is by far the most abundant PGE. This distribution can probably be attributed to variable amounts of laurite, with only minor Pt-, Pd- and Rh-bearing phases. Group 2 chromitites can be distinguished by their generally higher contents of ΣPGE. The dominance of the Ru-group is here not apparent and the ΣRu and ΣPt are either very close or the latter is marginally greater. These chromitites exhibit PGE characteristics that are intermediate between group 1 and group 3 chromitites. Group 3 chromitites display a complete separation of the two PGE groups, i.e. ΣPt >> ΣRu, the former comprising more than 73% of ΣPGE (compared to between 74 and 44% in the group 2 chromitites and less than 40% in the group 1 chromitites).

This evolution of the PGE distribution might be attributed to the fractionation order of the PGEs as defined by Barnes et al. (1985), which is Os < Ir < Ru < Rh < Pt < Pd. Hence, the observed enrichment in the more chalcophile elements Pt and Pd in stratigraphically higher chromitite layers might be explained by a progressive concentration of those elements in the more fractionated residual liquid in the chamber. Despite probably continuous crystallization of laurite in all chromitites, as indicated by the bulk PGE distribution, a depletion of the liquid in Ru, Os and Ir is not apparent. Multiple replenishment by influxes of primitive magma is the most likely mechanism to explain this feature. This explanation gains further support from the geochemical data presented on the silicate cumulates. All chromitite layers are enriched in PGEs over their host rocks. The PGEs in the LG3-chromitite are enriched to more than three times the content of the average silicate rock; and for the Merensky Reef this concentration factor increases to 98. In summary, PGE distribution and geochemistry of chromitite layers are so closely related, that the petrogenesis of massive chromitites must be regarded as a key to interpreting PGE mineralization within the Critical Zone of the BIC.

CHAPTER 7 : Sr ISOTOPE VARIATIONS

Since the early work by Hamilton (1977) and Kruger and Marsh (1982), who established the significance of the ratio $^{87}Sr/^{86}Sr$ (Sr_i) for magma mixing models, numerous studies have followed (Kruger and Mitchell, 1985; Kruger et al., 1987; Sharpe, 1985; Harmer and Sharpe, 1985; Lee and Butcher, 1990) and established that multiple injections of magma occurred during the evolution of the RLS. However, emphasis of these studies was placed upon isotopic data of mineralized layers or marginal rocks. Only for the cumulate sequence at Union Section are Sr isotope data available covering systematically the Main, Critical and Lower Zones. These data are reported in Eales et al. (1986, 1988, 1990a, b) and Mitchell (1986). The samples provided by the NG-boreholes made a continuation of the systematic study of the Sr_i of rocks below the lCZ possible.

All analytical work on the NG samples was done by F.J. Kruger (Bernard Price Institute, Johannesburg) following the procedures outlined in Eales et al. (1990a). So far 28 samples were analysed; results are listed in Table 22. Most data are derived from whole-rock powders; mineral separates (phases denoted in brackets) have been analysed in samples NG1-237.50 (pla, cpx), NG2-754.60 (pla) and NG2-773.60 (pla). The Sr_i values calculated for an age of the BIC of 2050 ± 25 My are plotted against stratigraphic height in Fig. 52.

Apart from the samples (NG2-134.40, NG2-180.55 and NG2-212.20) forming a horizon, ca. 80 m thick, with unusually high Sr_i levels, the remaining samples fall in a window ranging from 0.7047 to 0.7060. As discussed in Eales et al. (1990b) no unique lithological assemblage typifies these high Sr_i numbers. The highest Sr_i (0.7072) obtained from sample NG2-180.55 at a depth of 1220.55 m is in the range of ratios normally associated with Upper Zone lithologies (0.7073 ± 1, Kruger et al. 1987; see insert in Fig. 52). Further work is therefore necessary to verify the significance and cause of this inflection. The remaining Sr_i values revolve around an average of 0.7053 and an overall increase is displayed from the LZ to a value of 0.7090 in the Main Zone (Eales et al., 1990b).

TABLE 22 Whole-rock and Mineral Separate Rb-Sr isotopic Data

Sample:	Depth: (m)	Lithology:	Rb (ppm)	Sr (ppm)	$^{87}Rb/^{86}Sr$	$^{87}Sr/^{86}Sr_p$	Sr_i
NG1- 25.00	275.00	p	2.38	34.8	0.1979	0.71142 ± 15	0.7056 ± 1
NG1- 49.75	299.75	p	1.76	31.9	0.1597	0.71024 ± 8	0.7055 ± 1
NG1-152.20	402.20	p	1.97	18.4	0.3100	0.71404 ± 7	0.7049 ± 2
NG1-163.27	413.27	p	2.71	39.6	0.1981	0.71110 ± 9	0.7052 ± 1
NG1-204.50	454.50	p	2.80	46.5	0.1743	0.71041 ± 5	0.7053 ± 1
NG1-237.50	487.50	p (pla)	15.70	501.0	0.0907	0.70790 ± 6	0.7052 ± 1
NG1-237.50		p (cpx)	0.73	14.0	0.1499	0.70958 ± 7	0.7052 ± 1
NG1-292.30	542.30	p	1.35	14.0	0.2791	0.71343 ± 21	0.7052 ± 2
NG1-327.45	577.45	p	1.71	20.9	0.2368	0.71187 ± 6	0.7049 ± 2
NG1-327.45D		duplicate	1.69	20.8	0.2352	0.71190 ± 6	0.7050 ± 2
NG1-414.85	664.85	p	1.18	23.2	0.1472	0.70912 ± 5	0.7048 ± 1
NG1-464.00	714.00	p	1.93	31.9	0.1751	0.71008 ± 7	0.7049 ± 1
NG1-486.55	736.55	p	2.15	35.1	0.1773	0.71014 ± 7	0.7049 ± 1
NG1-500.50	750.50	p	1.15	34.7	0.0834	0.70801 ± 6	0.7055 ± 1
NG1-528.50	778.50	p	2.37	29.4	0.2333	0.71171 ± 5	0.7048 ± 2
NG1-528.50D		duplicate	2.36	30.1	0.2269	0.71175 ± 6	0.7050 ± 2
NG1-619.85	869.85	p	3.71	20.2	0.4546	0.72102 ± 10	0.7054 ± 3
NG1-695.50	945.50	p	4.31	29.4	0.4246	0.71781 ± 5	0.7053 ± 3
NG1-701.75	951.75	p	4.31	18.0	0.2943	0.71405 ± 5	0.7054 ± 2
NG1-739.80	989.80	p	1.83	34.4	0.2247	0.71210 ± 12	0.7055 ± 2
NG2- 83.75	1123.75	poik hzb	1.98	46.3	0.1238	0.70956 ± 6	0.7060 ± 1
NG2-134.40	1174.40	poik hzb	1.67	45.5	0.1062	0.71005 ± 6	0.7069 ± 1
NG2-180.55	1220.35	p	2.65	41.2	0.1862	0.71258 ± 8	0.7071 ± 1
NG2-212.20	1252.20	ol p	1.17	37.6	0.0900	0.70886 ± 8	0.7062 ± 1
NG2-298.80	1338.80	no	4.20	201.6	0.0603	0.70698 ± 12	0.7052 ± 1
NG2-320.15	1360.15	p	4.46	48.4	0.2668	0.71358 ± 5	0.7057 ± 2
NG2-447.90	1487.90	p	1.41	43.5	0.0938	0.70757 ± 11	0.7048 ± 1
NG2-536.10	1576.10	p	3.85	39.9	0.2793	0.71368 ± 8	0.7054 ± 2
NG2-622.70	1662.70	p	4.77	51.0	0.2708	0.71330 ± 12	0.7053 ± 2
NG2-754.60	1794.00	p (pla)	2.78	522.0	0.0154	0.70518 ± 4	0.7047 ± 1
NG2-773.60	1813.60	no	24.20	213.9	0.3276	0.71530 ± 9	0.7056 ± 2
NG2-773.60		no (pla)	28.60	631.4	0.1311	0.70872 ± 10	0.7049 ± 1

Notes: 1) analytical work was done by F.J. Kruger at the Bernard Price Institute

2) rock types: p = pyroxenite, poik hzb = poikilitic harzburgite
ol p = olivine-pyroxenite, no = norite

3) (pla) or (cpx) : data are derived from mineral separates;
pla = plagioclase, cpx = clinopyroxene

4) $^{87}Sr/^{86}Sr_p$: present day ratio; uncertainty is 2 standard error of the mean

5) Sr_i : initial ratio calculated for an age of 2050 My

6) errors are given at the 68%-certainty level

7) calculations made using the GEO-date program, CSIR

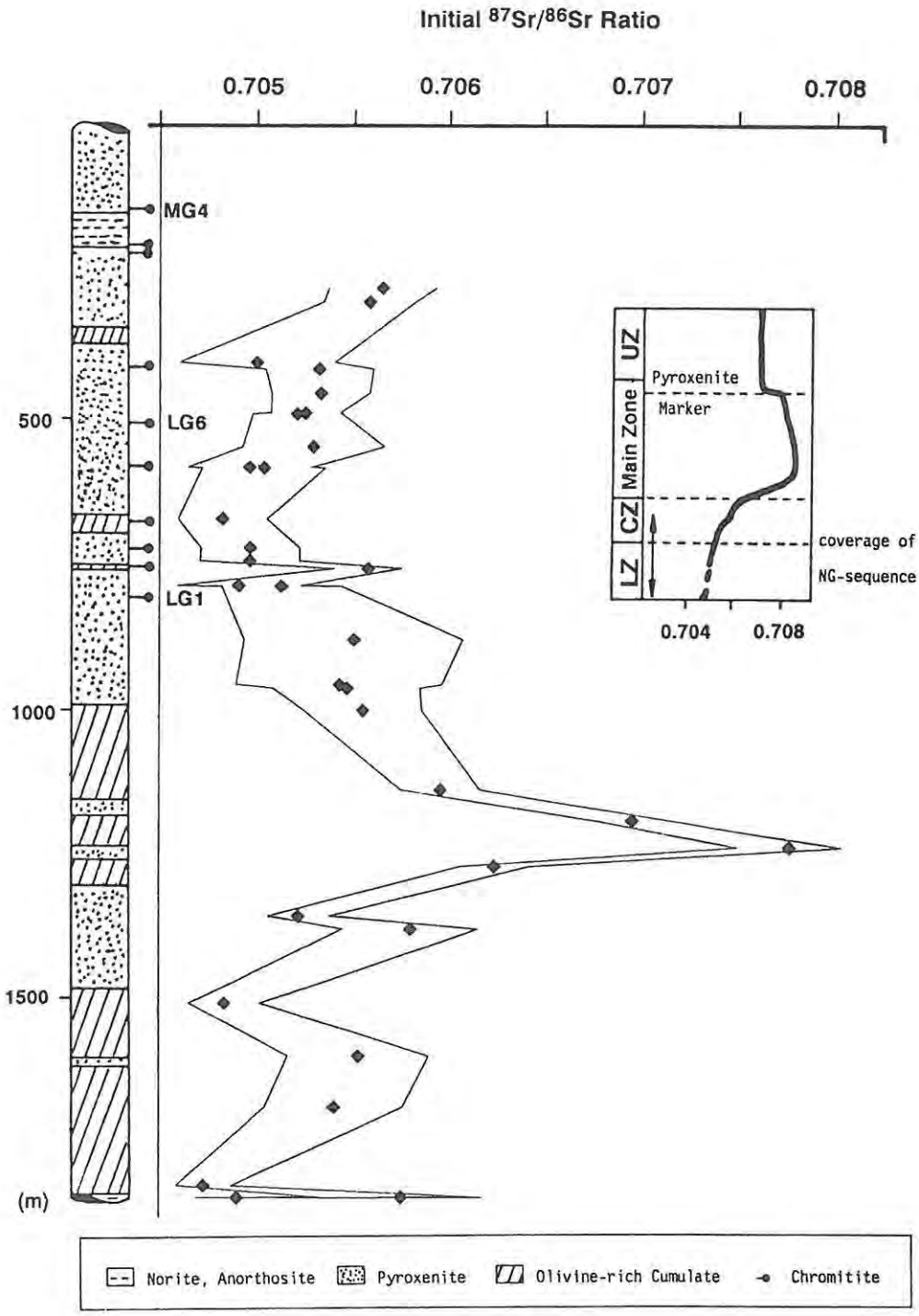

Fig. 52 Variations of Sr_i ratio in the NG-sequence (envelope depicts one standard deviation) - inset diagram shows generalized trend through the entire RLS of the Eastern Bushveld Complex (after Sharpe, 1986).

Two features are worthy of mention:

a) the anomalous norite in the LZ (at a depth of ca. 1340 m) has a Sr_i of 0.7052, which is typical for the majority of the LZ- and lCZ-samples but too low for rocks of uCZ-lineage (0.7060; Eales et al. 1990 a, b). This might point to an in-situ origin of the norite. However, the origin as a sill-like intrusion of a noritic magma with a coincidentally identical Sr_i signature is still feasible (see chapter 8).

b) in the lCZ the lowest Sr_i values (0.7049 ± 1) are displayed by rocks associated with ol-rich cumulates, which might indicate a relationship between Sr_i and petrogenetic evolution. A similar trend was described by Eales et al. (1990a), who found a subtle correlation between Sr_i and $Mg\#_{opx}$.

CHAPTER 8 : DETAILED DESCRIPTIONS OF LIMITED INTERVALS IN THE NG-SEQUENCE

In this chapter description of some selected intervals regarded as important to the interpretation of the petrogenesis of the cumulate pile will be presented. The possible constraints they impose on the compositions of the putative parental liquids will be also addressed.

8.1. The Occurrence of Cumulus Plagioclase in the Lower and Marginal Zones of the NG-sequence

Cumulus pla occurs twice in stratigraphic positions lower than the uCZ: a) a gabbroic norite at the base of the RLS in the MZ and b) the anomalous norite ca. 340 m below the boundary of the lCZ and LZ.

The MZ (Fig. 53) at Union Section, as intersected by NG2, is some 30 m thick with a medium- to coarse grained (>2 mm) gabbroic norite, 0.50 m thick, at the basal contact. However, because of the uncertainty of the status of the hornfelsic floor-rock a greater thickness might be possible. No chilled margin was encountered, but recent work by Huppert and Sparks (1989) showed that chilled margins might disappear due to an excessive heat flux from the magma. In the NG-sequence the gabbroic norite is directly overlain by granular harzburgite. Sedimentary xenoliths within the ultramafic cumulates in the MZ are rimmed by mm-thick rinds of very fine-grained norite. Lithologies of the MZ are also characterized by unusually high amounts of modal pla causing high Al and Ca concentrations. The $Mg\#_{opx}$ shows a sharp but gradational increase from 0.738 to 0.861 (the greatest variation in the sequence) together with an increase in An content of pla. It is the only occurrence within the NG-sequence of cumulus pla with less An molecule than the postcumulus species in the overlying ultramafic rocks. The cumulus pla in the gabbroic norite displays An values of 54%, which is conspicuously low. After Wager and Brown (1968) such values are associated with Main and Upper Zone gabbroic cumulates. However, it is not clear yet what the causes for such low An values are.

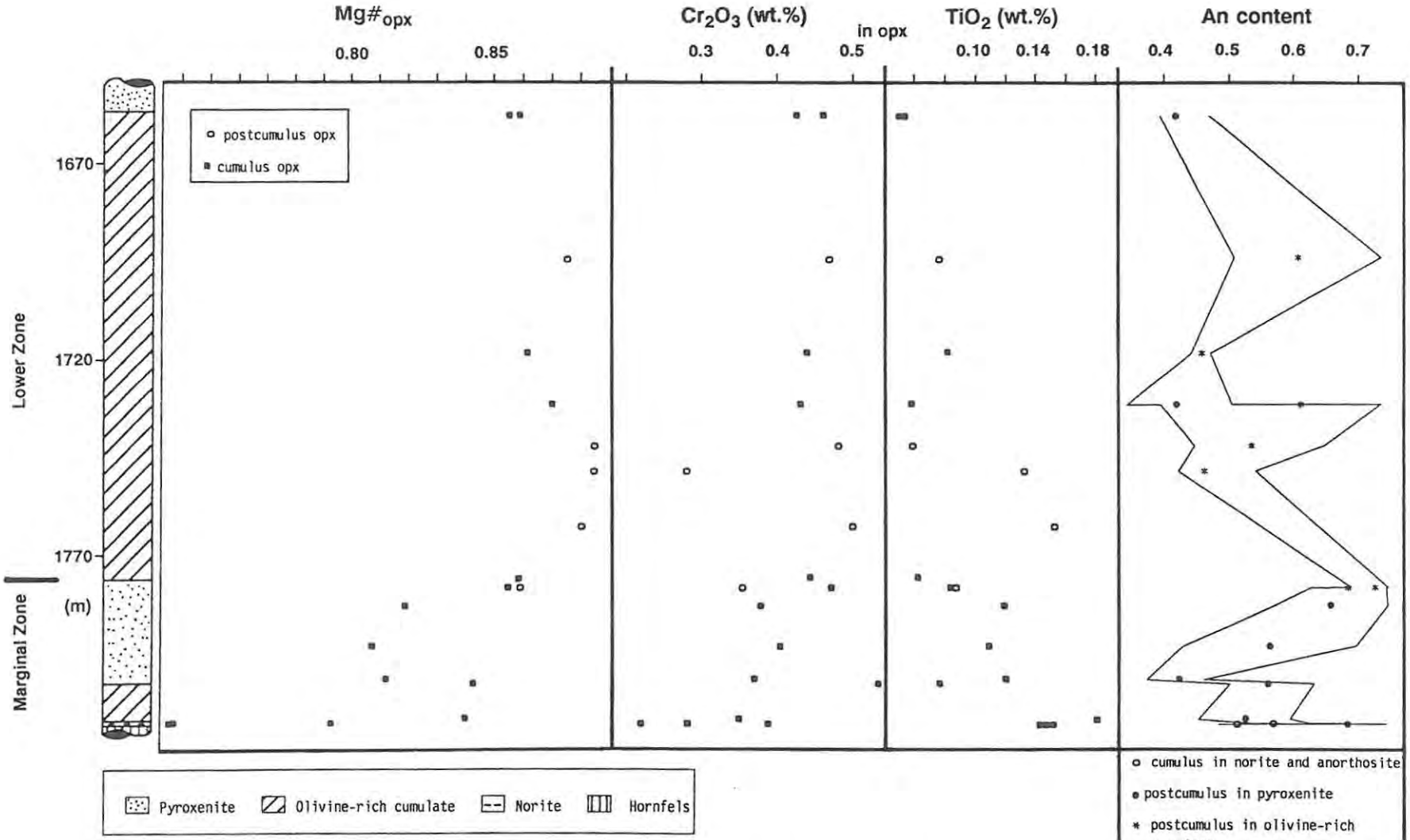

Fig. 53 Selected geochemical parameters covering the MZ - LZ contact in the NG-sequence, solid lines show maximum and minimum An values.

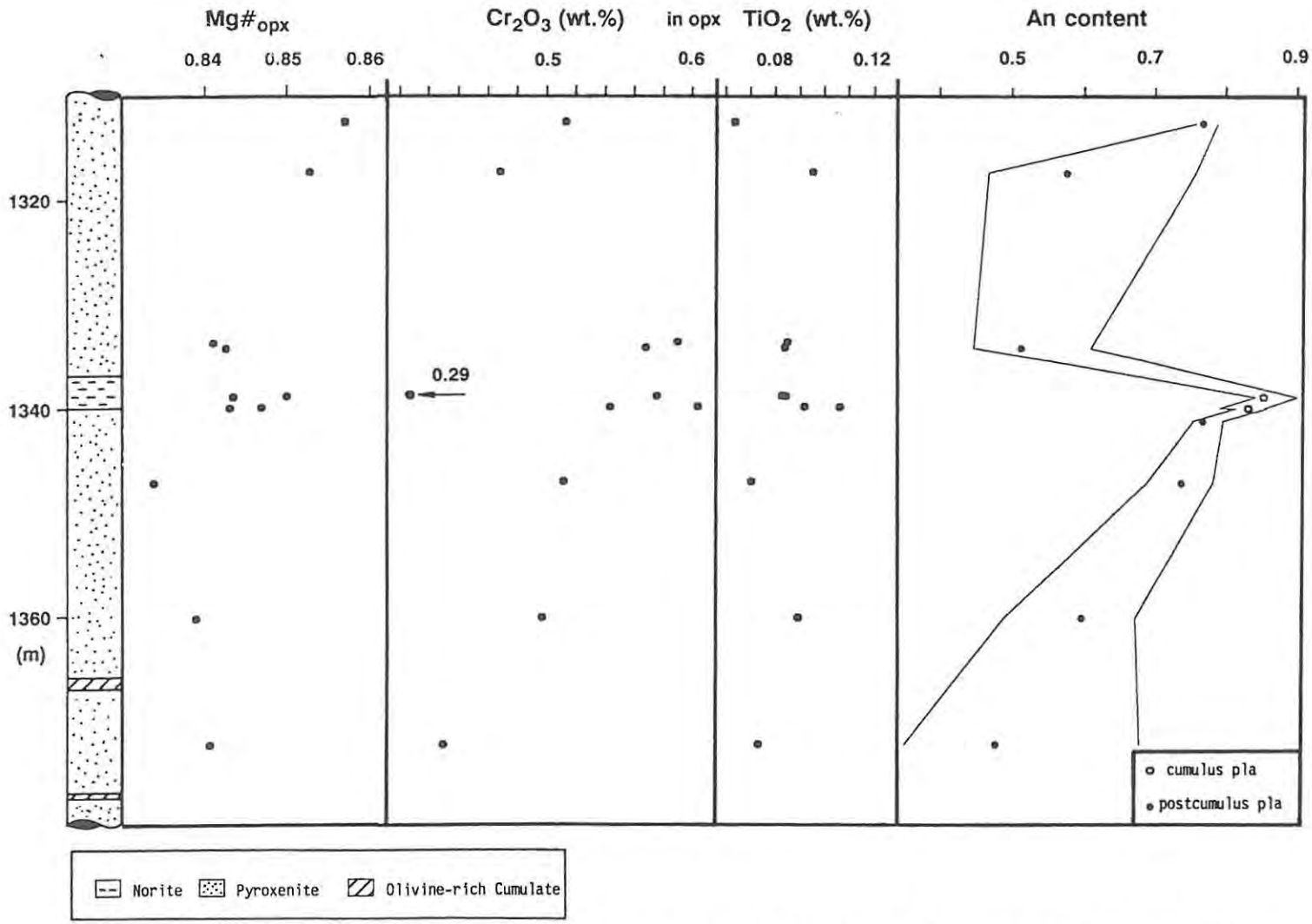

Fig. 54 Selected geochemical parameters covering the interval hosting the norite in the LZ of the NG-sequence at a depth of ca. 1340 m, solid lines show maximum and minimum An values.

Contamination with floor-rocks rich in feldspar components as indicated by the whole-rock composition of the hornfels might be the most probable explanation. Further explanations might be : a) a very high degree of supercooling, or b) an intrusive origin postdating the ultramafic cumulates. However, the Sr_i (0.7049 for a pla separate) is very similar to those obtained from samples above. In summary, the MZ (including its gabbroic norite) is interpreted as part of the cumulate sequence. All described geochemical variations can be attributed to the juxtaposition to the floor sediments. The gradational transition from the gabbroic norite to the ultramafic cumulates as evident in the mineral data of Fig. 53 points to a rapid establishment of the physico-chemical conditions conducive to the genesis of the ultramafic cumulates of the LZ.

The second appearance of cumulus pla beneath the lCZ - uCZ-boundary is associated with the leucocratic norite (2.87 m thick) at a depth of ca. 1340 m. Its Sr_i signature was discussed earlier and more geochemical and petrographic features are summarized in Fig. 54. The leuconorite is over- and underlain by pyroxenite. The upper contact is sheared, while the lower one is sharp and outlined by a discontinuous one grain-thick lamina of chr. The lowermost cm of the norite shows a conspicuously lower opx proportion than the remainder. The $Mg\#_{opx}$ does not differ significantly but appears to be slightly higher in the norite. Within the norite the $Mg\#_{opx}$ remains steady (range: 0.844 - 0.850), while the Cr content of opx decreases sharply (0.60 wt.% to 0.29 wt.%). The An content of pla increases steadily from ca. 30 m below the norite (sample NG2-332.35: An_{49}) to An_{77} just below the contact. Within the norite An values of 84% and 86% are obtained. These values are the highest in the NG-sequence (see Fig. 26); they are also in the range predicted by Wager and Brown (1968). The An levels of postcumulus pla drop sharply in the overlying pyroxenite (An_{52}). An increase in modal pla in pyroxenite is also apparent at this stratigraphic level. The chr composition of the thin boundary layer is distinctly different from the accessory variety below and above. It shows a compositional signature of a ML-chr with high Al and Mg ($Mg\#_{chr}$ 0.410) and low Fe and Mn. However, the Cr content is conspicuously low (41.9 wt.%) in comparison with accessory chr (>46.0 wt.%) in the over- and underlying pyroxenite. Lee et al. (1983) ascribed the origin of minor chromitite layers, which occur at the interface between pla-rich and ultramafic cumulates, to a reaction of pla and high-Cr chr with interstitial liquid. The formation of the very thin and discontinuous Al-rich chromitite lamina is probably the result of a related, similar process.

In summary, no significant geochemical variations outside the general trends set by the ultramafic cumulates are detectable at this stratigraphic level; the appearance of the norite layer is heralded in the pyroxenite below by simultaneous increases in An content and modal pla. The Sr_i ratio is in the range of those obtained from over- and underlying pyroxenite. Therefore, an in-situ origin of the leucocratic norite by fractionation is preferred to an intrusive model. The presence of two noritic layers in a similar stratigraphic position in the eastern limb of the BIC (see Fig. 4) was reported by Cameron (1978) and supports this conclusion. Cameron (op.cit.) also stated that the sequence (his basal subzone) is possibly a conformable sequence. It is therefore most probable that the norite crystallized from an evolved liquid, which was a fractionated derivative of the parental magma. In other words, the putative resident magma could have had pla on its liquidus in an early stage of the development of the RLS, if fractional crystallization had not been reset by repeated influxes of a more primitive parental magma.

8.2. Cyclic Units in the NG-sequence

Cyclic units are defined by Irvine (1987a) as repeated successions of layers, in which the rock sequence depends upon the fractional crystallization of the parental magma. Cyclicity can be expressed in the order of the appearance of cumulus phases, their modal proportions and/or their cryptic variations. Eales et al. (1986) defined cyclic units as a succession of cumulates, in which geochemical parameters either remain constant, or evolve progressively from some primitive value within each cycle and display a saw-tooth pattern through the succession.

In the LZ and CZ of the BIC an ideally complete cyclic unit should consist of the following cumulate sequence: ol-rich cumulates - chromitite - pyroxenite (with or without ol) - norite - anorthosite. Scoon and de Klerk (1987) listed a similar sequence for an uCZ-cyclic unit. However, it appears that either ol or chr (or both) can be the first liquidus phase(s), thus giving rise to different basal layers of units. In the lCZ of the NG-sequence the massive chromitite layers and chromitiferous cumulates associated with ol-rich lithologies (Fig. 3) are situated towards the top of such units, suggesting that ol crystallized earlier than chr. In the Great Dyke chromitites occur at the bases of macro-units (Wilson, 1982), whereas in the ultramafic zone of the Stillwater complex the base of cycles are ol-rich rocks followed by chromitites (Jackson, 1961).

In the LZ, cyclicity is evident by multiple repetitions of the sequence: dunite - poikilitic harzburgite - granular harzburgite - olivine pyroxenite - pyroxenite. In the ol-rich cumulates chr is an abundant accessory phase, while pyroxenite is often barren (Eales et al., 1990b). The interlayering is in the range of mm, cm or dm; complete cycles are scarce and units might be truncated and restarted at any stage. This complexity and the lack of uniformity of thickness of the layers forming cycles (see log of NG2, Appendix) impede an in-depth investigation. Whole-rock geochemical as well as mineralogical data do generally not differ significantly in a cm-range.

In the lCZ an ideal cyclic unit should be: ol-rich cumulate - chromitite - pyroxenite. However, only two massive chromitite layers (LG2- and LG4-chromitites) are directly underlain by ol-rich rocks. Geochemical and petrographic data of the interval from 475.90 to 664.85 m are shown in Fig. 55.

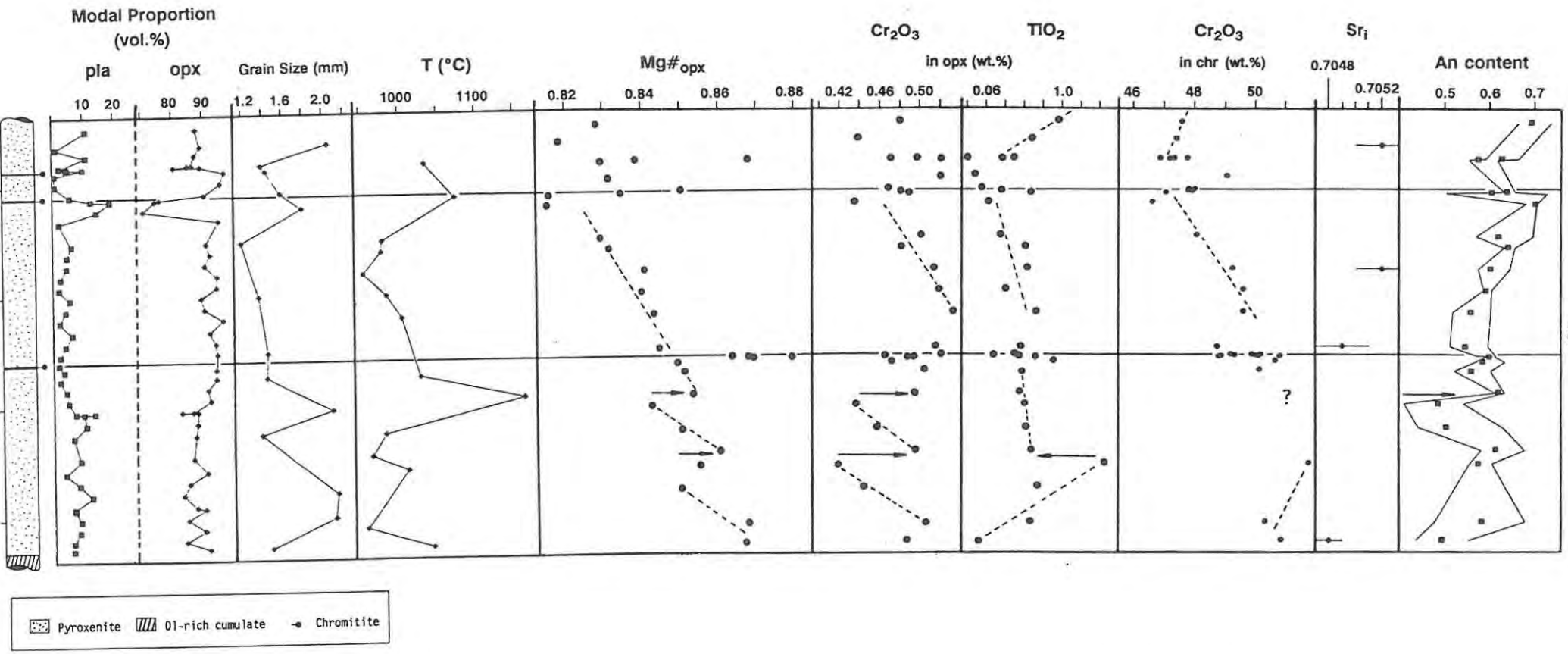

Fig. 55 Selected petrographic and geochemical parameters in the interval starting above the LG4-chromitite and ending ca. 30 m above the LG6-chromitite. (Envelope in diagram showing the An content depicts maximum and minimum An values; arrows mark positions of pronounced reversals).

This interval was chosen because of the following reasons:

a) it contains two chromitite layers (LG5 and LG6) and hence should display some cyclicity;

b) the overall fractionation path within the cumulate pile is well defined (Fig. 15B);

c) a generous set of geochemical and petrographic data is available;

d) no ol is found in the interval and cryptic variations of opx are therefore not influenced by another cumulus ferromagnesian silicate;

e) no minor chromitite layers or chromitiferous pyroxenites were intersected (apart from those in the vicinity of the LG5-, LG6- and LG6A-chromitites);

f) the selected interval commences just above the LG4-hosting ol-rich interval and thus straddles the stratigraphic level at which, according to Hatton and von Gruenewaldt (1987) a new magma type (A-magma) entered the Bushveld chamber.

From Fig. 55 the following observations can be made:

a) the overall geochemical trends show both major and minor deflections;

b) reversals (shifts to more primitive values) are initiated either some metres beneath or at the level of the massive chromitite layers. The former case can be seen ca. 16 m below the LG5-chromitite, where the $Mg\#_{opx}$ increases sharply. Beneath the LG6-chromitite no increase is evident (sample NG1-257.10 just below displays a higher $Mg\#_{opx}$, but this value is more logically attributed to postcumulus re-equilibration). Other reversals (Cr_2O_3 in opx, modes of pla and opx, grain size and estimated temperature) occur at the same position;

c) despite great intrasample variation in An content the levels of the reversals are indicated by shifts to An-richer feldspars (≥10 % An molecule), which is substantially greater than the inter-sample differences elsewhere in this interval. Smaller intrasample variations are also connected with the stratigraphic positions of the reversals;

d) the Sr_i variations are small and within the limits of analytical error. There is no difference of the ratio below and above the chromitites;

e) at the depth of ca. 630 m a reversal can be traced in the majority of the parameters displayed. No chromitite layer is developed, but sample NG1-380.35 at a depth of 630.35 m has a distinctly higher amount of accessory chr than over- and underlying pyroxenite;

f) opx grains > 1.6 mm occur only immediately below the reversals apart from the uppermost sample, while grains in the central parts of the units are < 1.6 mm. A subtle decline is displayed between the LG5- and LG6-chromitites;

h) the temperature profile runs parallel to the trend displayed by the grain size distribution apart from one deviation at the bottom of the interval. This suggests a strong dependence of grain size on temperature.

In the uCZ of the NG-sequence the cyclic units should be ideally topped by felsic cumulates. However, because of the stratigraphic coverage of the NG3-borehole only the unit between the MG2- and MG3-chromitites comprises leucocratic rocks. Consequently, this interval was also selected for scrutiny and Fig. 56 presents the geochemical details through the interval (194.70 - 248.25 m). The unit also straddles the boundary lCZ - uCZ. The entire unit (bottom contact MG2 chromitite to bottom contact MG3-chromitite) is 7.75 m thick, of which 5.45 m is pyroxenite, overlain by 1.02 m norite and 0.73 m anorthosite. The MG2-chromitite is 0.55 m thick; the lowermost 5 cm appear to be sheared and heavily altered as is the underlying 0.22 m of pyroxenitic footwall (sample NG3-220.17 is therefore omitted). The MG3-chromitite, 0.75 m thick, is under- and overlain by felsic cumulates, a further variation of host lithologies.

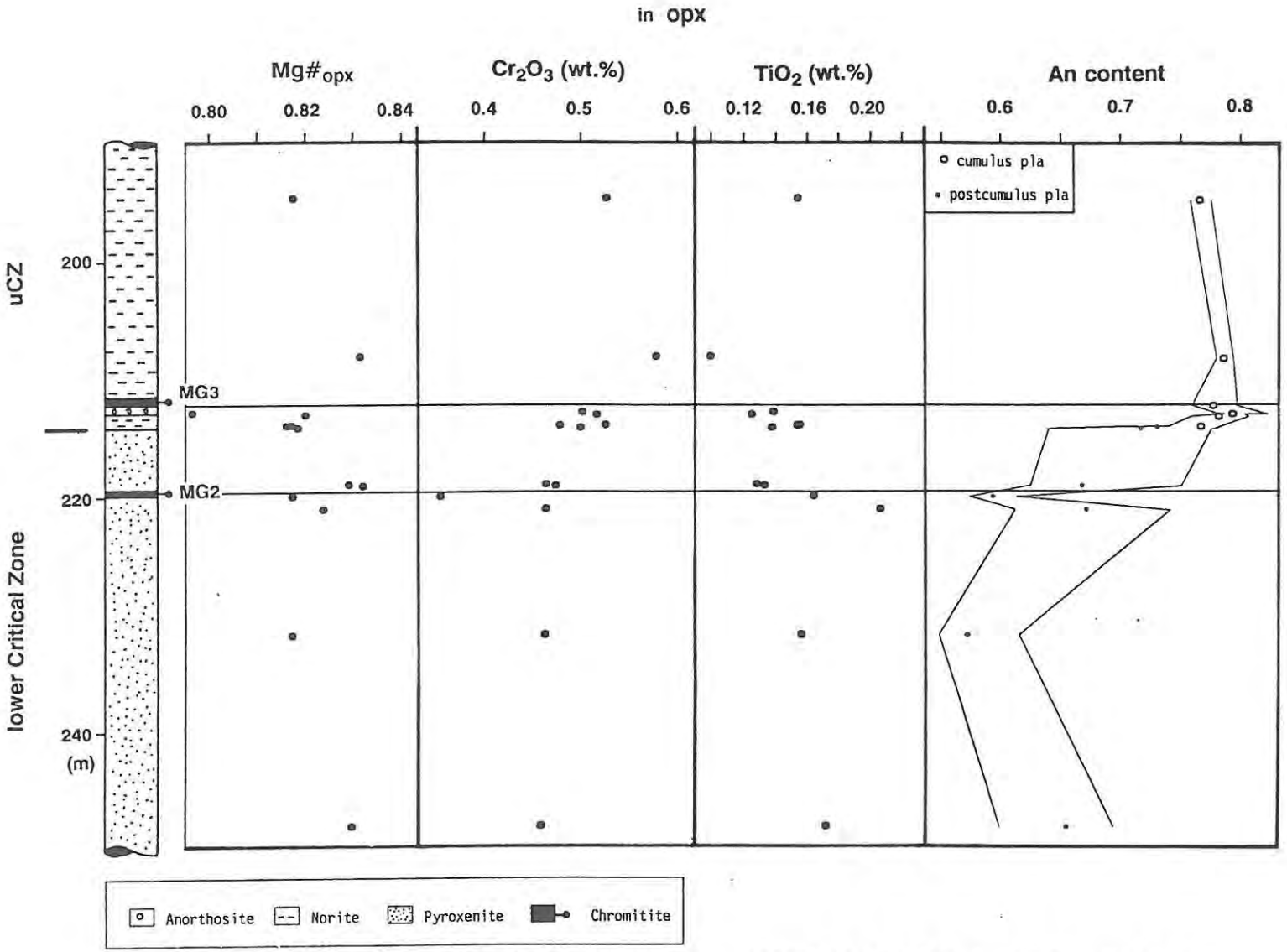

Fig. 56 Selected geochemical parameters covering the lCZ - uCZ boundary in the NG-sequence. (Envelope in diagram showing the An content depicts maximum and minimum An values).

The $Mg\#_{opx}$ shows a restricted variation with a sharp decline in the anorthosite below the MG3-chromitite, above which the reversal to a high ratio similar to those from samples ca. 20 m below the MG2-chromitite is evident. The Cr_2O_3 concentrations in opx displays a similar trend in the pyroxenites below the MG2-chromitite and in the norites above the MG3-chromitite. However, in the interval between the two chromitite layers an antipathetic trend is apparent. Here the feature of an increasing partition coefficient with decreasing modal proportion mentioned earlier (see section 4.2.) might be superimposed. In contrast to these trends Ti levels in opx decrease with the minimum value above the MG3-chromitite. These variations can be interpreted as the result of a replenishment event shifting the composition to relatively higher Mg and Cr values, but lower Ti concentrations (see Fig. 15A). The appearance of pla on the liquidus is heralded by the steady increase in An content of postcumulus feldspar and the occurrence of pla inclusions in opx below the actual contact lCZ - uCZ. The decoupling of the $Mg\#_{opx}$ and the An content between the MG2- and MG3-chromitites is evident (see also Fig. 15A and Fig. 26, which show large scale decoupling of these two parameters in the upper part of the NG-sequence).

In summary, all data presented in this section show definite trends of cyclicity caused by reversals in geochemical and petrographic parameters. However, all reversals can be explained by the repeated emplacement of primitive liquids (U-type liquids of Irvine et al., 1983) into the magma chamber. No evidence was found in support of models which postulate additions of liquids with a different crystallization order (i.e. pla as the first phase to crystallize; A-type liquids of Irvine et al., op.cit.) in the CZ of the BIC. $Mg\#_{opx}$ and Cr_2O_3 levels in opx are repeatedly set back to values typical of the lCZ, while the continuous increase in An molecule in postcumulus pla initiated at the base of the CZ heralds the appearance of cumulus pla. This conclusion finds further support in the occurrence of partially resorbed pla inclusions 10 - 15 m below the lCZ/uCZ boundary (Eales et al., 1990b).

8.3. The Formation of Cyclic Units and the Evolution of the Cumulate Pile of the NG-sequence

Every hypothesis for the formation of cyclic units in the NG-sequence is constrained by the criteria listed below:

a) the variability of foot- and/or hangingwall cumulates of the massive chromitite layers;

b) the geochemical reversals occurring in the basal part of cyclic units;

c) the nucleation of copious amounts of chr leading to the formation of massive chromitite layers;

d) the limited variations of the Sr_i ratio;

e) the occurrence of ol-rich cumulates throughout the study section;

f) the coupling of chromitite- and silicate chemistry with progressive evolution of both throughout the sequence.

The genesis of chromitite layers is a long-debated subject and it is therefore necessary to describe various models and their applicability to explain the features presented. Early theories favouring the formation of chromitite layers from immiscible chromium-rich liquids (Sampson, 1932; McDonald, 1965) are nowadays regarded as not feasible processes in natural systems (Hatton and von Gruenewaldt, 1987). Ulmer (1969) and Cameron and Desborough (1969) ascribed the origin of chromitite layers to sudden changes in oxygen fugacity (fO_2). The suggested increase in fO_2 triggering chr precipitation should, however, result in higher ferric iron levels in the ML-chr. But, as presented earlier, ML-chr is characterized by distinctly lower Fe^{3+} levels than accessory grains in the silicate cumulates. Changes in pressure (de Villiers, 1970; Cameron, 1978) based on experimental studies (inter alia Osborn, 1978) offer a further possibility to precipitate chr alone. No data are available in support of pressure fluctuations. Compositional variations in the silicate phases (e.g. Al in opx) juxtaposed to the chromitite layers do not indicate any considerable pressure differences during, before or after formation of massive chromitite layers.

In 1975 Irvine developed a new model based on his work on the Muskox intrusion. He concluded that by mixing of a primitive magma with magma contaminated with Si-rich crustal components the resulting hybrid might be placed in the stability field of chr, thus precipitating only chr. The original hypothesis was subsequently expanded to include mixing of a primitive magma with fractionated derivatives of it (Irvine, 1977) and mixing of magmas of different lineages (U- and A-magma model of Sharpe and Irvine, 1983). Most of these models imply also a temperature difference between the mixing liquids, and thus use the decreasing solubility of Cr with falling temperatures (Murck and Campbell, 1986) to enhance chr precipitation.

The data presented here exclude Irvine's (op.cit.) original hypothesis of contamination with Si-rich material because of the repeated nucleation of ol throughout the sequence and the relatively small variations of the Sr_i ratio in the lCZ. Hence, if mixing is the trigger mechanism (as generally accepted) the liquids involved would have to be either of one lineage or of two distinctively different lineages.

For the BIC the primitive liquids or U-magmas (U for ultramafic affinity) have the crystallization sequence ol - opx - pla - cpx, whereas liquids of the second lineage (A-magmas; A for anorthositic affinity) crystallize in the order pla - ol - cpx - opx (Irvine et al., 1983). After Hatton and von Gruenewaldt (1987) the LG1- to LG4-chromitites, which are generally thinner than the massive chromitite layers higher up in the sequence, originate from a mixing of U-magma with a fractionated derivative of it, while for the thicker layers (LG5- through UG2-chromitite) the U-A-mixing model is favoured. This model implies the input of A-magmas in the lCZ at a level above the LG4-chromitite. Characteristic chemical attributes of A-type liquids are, after Sharpe (1986), a low Mg# (65), Sr concentrations between 400 - 600 ppm and a very high Sr_i of ± 0.709.

In the NG-sequence ca. 116 m of ultramafic cumulates with repeated reversals to $Mg\#_{opx}$ >0.83 are developed between the LG5-chromitite and the lCZ - uCZ-boundary. The ol-rich unit at a depth of ca. 340 m (ca. 30 m thick; see Fig. 3) and the abundance of ol-rich cumulates in the interval

between the UG2-chromitite and the Merensky Reef (Eales et al., 1986) suggest strongly a continued influx of U-magma. Unequivocal isotopic evidence for the emplacement of batches of A-magma with an high Sr_i is rare below the Merensky cyclic unit. However, the overall increase within the CZ (Eales et al., 1990b) points to a progressive blending-in of liquids with a higher Sr_i or a change in the mantle source. The unexpectedly high levels of the Sr_i ratio in the LZ might ,however, warrant a reassessment of models mainly based on Sr isotope data. All data presented fail to show a major geochemical break in the lCZ, but do so at the boundary LZ - lCZ. Furthermore, cumulates and their major phases display generally the same geochemical characteristics throughout the entire lCZ and lower part of the uCZ (e.g. Cr concentrations in opx or whole-rock Sr levels) The PGE distribution in the silicate rocks is in the same range for all cumulates throughout the sequence. In summation, all cumulates in the NG-sequence appear to be derived from liquids of one lineage (U-magma, P-magma of Eales et al., 1990b) and residual liquids thereof.

8.3.1. A Model for the Formation of the Cumulate Pile of the NG-sequence

Before a model is presented some thoughts should be given to earlier ideas and the question of the mechanism of the replenishment process. The data presented by the writer refute Cameron's suggestion (1978) that the LZ was formed from a single heave of magma, with pressure changes in the magma chamber causing the variations of the crystallization order. Other ideas on the origin of cyclic units (Vermaak, 1976; Irvine et al., 1983; Campbell et al.,1983) are based on work on the uCZ, or more precisely, on the interval between the UG2-chromitite and the Bastard unit, where the assemblage harzburgite - anorthosite or chromitite - anorthosite in juxtaposition is the striking feature. Hence, these models are not applicable for the genesis of cyclic units in the NG-sequence, in which pla cumulates are subordinate rocks.

Campbell and Turner (1986b) suggested formation of the chromitite layers below the LG6-chromitite in the lCZ by repeated mixing events of U-type magma with the residual liquid, a derivative of previous influxes. For the chromitite layers above and including the LG6-chromitite they favoured a mixing of newly emplaced A-liquids with the residual liquid. However, in section 8.3. the conclusion was derived by the present author that all cumulates of the NG-sequence crystallized from U-type liquids and derivatives thereof and no evidence was found indicating the emplacement of A-type liquids into the LZ, lCZ and lower part of the uCZ. The origin of the silicate cumulates of the NG-sequence from U-type liquids and derivatives of it constrains considerably any ideas on the dynamics of the replenishment. Three general possibilities exist. The new liquid might enter the magma chamber as a plume (Turner and Gustafson, 1978; Barnes and Naldrett, 1986), as a fountain (Campbell and Turner, 1989) or as a basal layer at the interface of the supernatant liquid (S-liquid) and underlying crystal mush (Huppert and Sparks, 1980; Huppert and Turner, 1981). The restriction to one form or the other is dependent upon densities of the replenishing and residual liquid, viscosity (Campbell and Turner, 1986a) and the momentum of the new pulse (Campbell and Turner, 1989). The density of the resident liquid depends greatly on the stage of fractionation and hence on which phase has crystallized in major proportions. For U-type liquids this implies that the new heave of magma is denser and hotter as well as more primitive in composition than the derivative due to prior crystallization of ol, opx and chr. Hence, a plume model based on influxes of liquids being less dense than the fractionated derivatives of U-type liquids is rejected. The remaining two styles of replenishment (fountain or basal flow) are very difficult to distinguish by their final products, because any fountain will eventually spread out as a basal layer after losing its momentum. It is, therefore, scarcely possible to establish at which stratigraphic position a fountain evolved into a basal flow. However, it seems unlikely that the filling of a magma chamber, especially one as large as the BIC, was wholly achieved by the rather passive style of basal flows. Hence, for the model outlined below a replenishment by fountains with subsequent development of basal flows is favoured. It is obvious that in such a model the supply of fresh magma would be greatest near the feeder zone, i.e. with distance from the feeder the volume of the primitive liquid would decrease.

With this postulate, a model for the formation of cyclic units and the entire cumulate pile of the NG-sequence can be developed as follows (see Fig. 3 and Fig. 15B). After establishment of stable physico-chemical conditions (i.e. after the development of the MZ with its marginal gabbroic norite) repeated influxes of U-type liquids into the chamber gave rise to the formation of the ol-dominated cumulates of segments 1, 2 and 3 (1760 - 1550 m) with cyclic units comprising successive, thin packages of dunite, poikilitic and granular harzburgite, olivine pyroxenite and minor pyroxenite. Bulk composition of the liquid in the chamber became progressively more and more primitive in segment 1, possibly caused by progressive melting of the mantle source. During a short period, in which replenishment decreased and crystal fractionation dominated (segment 2), Mg# of the cumulates declined and the episode terminated with the deposition of the pyroxenite package (ca. 15 m thick) at a depth of ca. 1570 m. Consequently, the reversed fractionation trend is seen to have ceased in the ol-rich cumulates some 200 m beneath this pyroxenite layer and a normal trend is evident here. However, this period was shortlived and new pulses shifted the bulk composition again towards more primitive traits (segment 3). Cyclic units similar to those exposed below developed.

The rejuvenation reached its culmination at a depth of ca. 1550 m, above which fractionation became once more the dominant process operating in the chamber. Hence, a normal fractionation trend was again initiated, as shown in Fig. 15B. As continued fractionation shifted bulk composition into the primary field of opx the dominant rock type became pyroxenite (segment 4). During this period of continued fractional crystallization of opx (with $Mg\#_{opx}$ declining to the lowest levels within the LZ) the residual liquid (S-liquid) became more and more enriched in pla components, which eventually led to the formation of the leuconorite at a depth of ca. 1340 m. Here the crystallizing liquid precipitated pla and opx cotectically. It is noteworthy that this cumulus-feldspar package overlies the thickest sequence of pyroxenites in the LZ, and disappearance of cumulus feldspar at the top of the layer coincides with a reversal of fractionation trends.

After the accumulation of the thin layer of leucocratic rock, magmatic activity commenced again and a gradual increase in the proportion of primitive to S-liquid caused the reversed fractionation trend within the pyroxenites of segment 5 (third major reversal). Initially, this reversal did not yield enrichment in ol, until the 1280 m level was reached. This period then culminated in the development of the most primitive silicate cumulates of the NG-sequence; i.e. the dunites just below the top of the LZ, at a depth of ca. 1020 m. Within segment 5 two pyroxenite packages with associated normal fractionation trends are the result of short episodes with reduced magmatic activity. During the accumulation and formation of segment 5 the replenishing liquid itself changed slightly in composition. It was still a U-type liquid, but relatively richer in Cr, which gave rise to the formation of a minor chromitite layer at ca. 1200 m and the higher proportions of modal chr in these ol-rich lithologies, as well as the higher Cr_2O_3 concentrations in opx of the lCZ.

After waning of the magmatic activity opx was soon back on the liquidus, forming the monotonous pyroxenites of segment 6. Fractional crystallization became once more the dominant process, shifting $Mg\#_{opx}$ to more evolved values. Protracted opx separation enriched the S-liquid consequently in pla components. A general transformation in the evolution of the cumulate pile took place at the LZ/CZ boundary. In the LZ rejuvenation by virtue of a high frequency of influxes was the major operating process. This led to a generally reversed fractionation trend and fractional crystallization was only of importance in periods of limited duration, with less or no magmatic activity. By contrast the CZ was dominated by fractionation with only two episodes (segments 7 and 9) of rejuvenation. Hence, the CZ is characterized by an overall decrease in $Mg\#_{opx}$ with a decoupled, systematic increase in modal proportion and An-content of postcumulus pla indicating the evolution of the S-liquid. The progressive enrichment of postcumulus pla in Ca is not clearly understood at present, but must be related to a damping of the processes of accumulation which cause intercumulus pla to be Na-enriched in lower parts of the sequence.

At the top of segment 6 (just below the LG1-chromitite) new pulses entered the magma chamber and produced the fourth major reversal, which culminated in the formation of the ol-rich rocks in segment 7. The pyroxenites of segment 8 developed soon after the decrease in the replenishment process. Because of the limited degree of rejuvenation, fractional crystallization soon shifted the composition of the crystallizing liquid to a composition matching that prior to the reversal event (i.e. $Mg\#_{opx}$ reaches values equal or lower than those in segment 6). Finally, at a depth of 475 m the last major reversal (segment 9) was caused by voluminous influxes of U-type liquids. Again, during the onset of the magmatic activity the formation of pyroxenites prevailed (with progressively more primitive traits) until bulk composition of the crystallizing liquid fell into the primary field of ol. Accordingly, ol-rich cumulates cap segment 9. However, as for segment 7 the period of rejuvenation was short and fractional crystallization took over. Pyroxenites were laid down (lower part of segment 10) until the crystallizing liquid reached the opx - pla cotectic, where rocks with cumulus pla were produced at the lCZ/uCZ boundary.

Within this framework of major reversals in the lCZ (or megacyclic units) minor reversals occurred. These second order influxes controlled nevertheless the genesis of most of the massive chromitite layers apart from those in segment 7, which consequently show the most primitive compositions (LG2-, LG3- and LG4-chromitites). Smaller pulses were not voluminous enough to shift bulk composition, especially after the mixing event, into the liquidus field of ol. Further evidence of the existence of minor influxes are the partially resorbed pla inclusions in opx, which were interpreted by Eales et al.(1990a, b) as remnants of cumulus pla crystals trapped in opx after the bulk composition of the liquid was shifted back into the primary field of opx by new pulses of primitive liquid. Hence, all massive chromitite layers in the NG-sequence were formed by mixing of pulses of U-type liquids with the residual S-liquid. In Fig. 57 the two principal mixing possibilities are outlined using phase boundaries of Irvine (1977) and Irvine et al. (1983).

It is evident from the diagram that the phase(s) on the liquidus after the mixing event would greatly depend upon the ratio U-liquid to S-liquid and their compositions, which eventually determined the composition of the hybrid liquid. Stratification within the S-liquid might have been present, but this is not absolutely necessary. However, if the S-liquid was not stratified huge volumes of P-magma would have been required in the upper parts of the sequence to shift the hybrid magma into the primary field of ol, if mixing occurred before its precipitation. It is therefore more likely that the S-liquid was stratified and only limited volumes, i.e. discrete layers, took part in the mixing event. The incorporation of expelled interstitial liquid during the mixing process might also have occurred, probably causing the formation of chromitite layers in the footwall of some massive chromitites. It is obvious that the degree of fractionation within the S-liquid (controlling its composition) would have been an important factor.

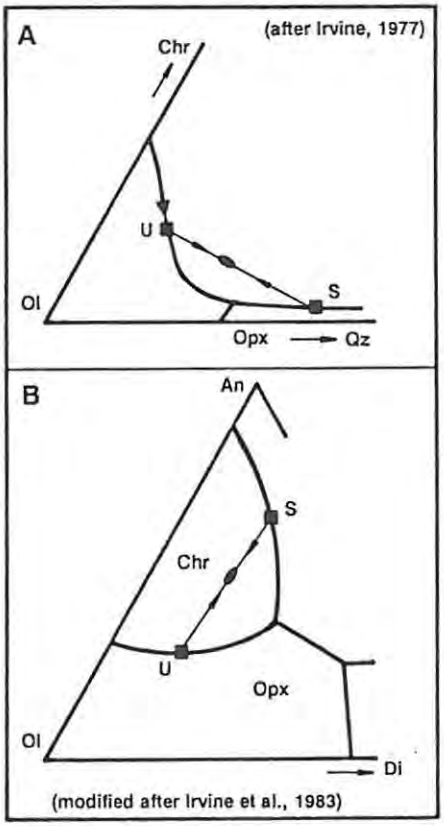

Fig. 57 Chromite precipitation triggered by magma mixing : A) early mixing (predominantly in the lCZ); B) late mixing (in the uCZ), where pla (An) is a cumulus phase. (Note "U" denotes primitive magma and "S" supernatant resident liquid).

The compositional differences between U- and S-liquid were more pronounced after long periods of uninterrupted fractional crystallization (massive chromitite layers occur only in the CZ in the NG-sequence where the latter process was dominant). This complex interplay caused the variations in foot- and hangingwall lithologies and the thickness differences of the chromitite layers.

In summary, the cumulate pile of the NG-sequence was formed by successive influxes of magmas of the U-type lineage into the chamber. During times of high magmatic activity rejuvenation was the major operating process in the chamber, while fractional crystallization took over during times of low magmatic activity, which eventually led to the origin of pla - opx cumulates without involvement of A-type liquids. The formation of massive chromitite layers is ascribed to a mixing of a Cr-rich parental magma of the lCZ with the fractionated residual liquid of the previous influxes.

PART B : OTHER SEQUENCES STUDIED

AND COMPARISONS ALONG STRIKE

CHAPTER 9 : INTRODUCTION

9.1. Introduction and Rationale

Part B of this thesis deals with two other sequences under investigation and a comparison along strike based on data presented here as well as published data from the western and other compartments of the complex. Additional to the NG-sequence two other boreholes, situated in the southern part of the Western BIC were investigated. The borehole KD-86/2 (hereafter KD) was drilled on the farm Kroondal 304 JQ, ca. 8 km east of Rustenburg, into the footwall of the LG1-chromitite (Fig. 58; see also Fig. 1). The samples were kindly provided by Millsell Chrome Mines Ltd., (Rand Mines).

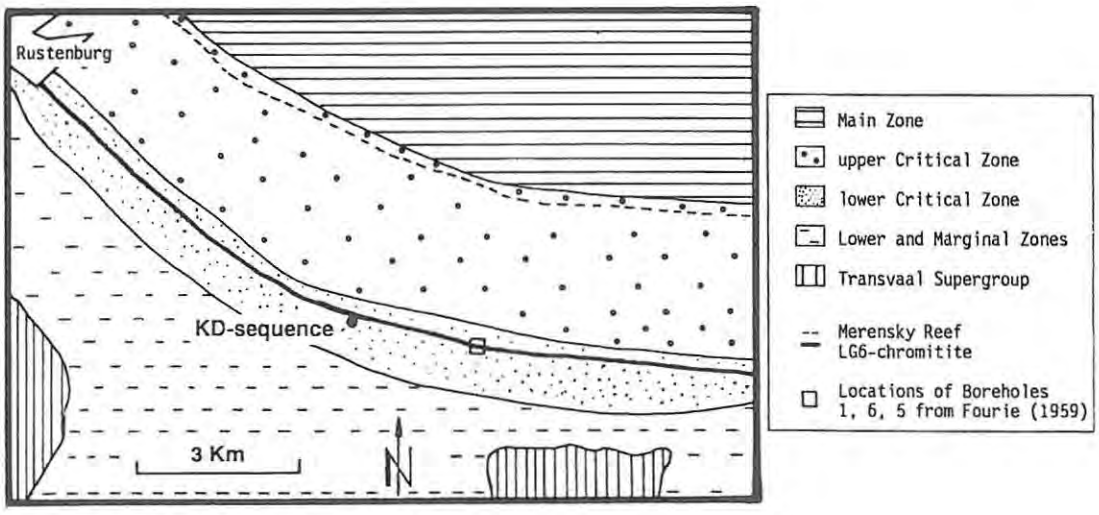

Fig. 58 Simplified geological map showing the collar position of the KD-borehole (see also Fig. 1; source: Worst, 1986).

Further towards the east near Brits (ca. 55 km east of Rustenburg) borehole SF-7 (hereafter SF), drilled on the farm Sandfontein 447 JQ within the "Brits Graben", was made available for sampling and studying in the year 1987 by Golden Dumps Exploration Ltd.. The collar position of this diamond drillhole is in the hangingwall of the UG1-chromitite (Fig. 59; see also Fig. 1). Both boreholes were stopped in the marginal norite without intersecting the contact of the floor and the RLS. Both sequences of the ultramafic and mafic cumulates below the cumulates which are exposed in the mining operations (LG6-chromitite at Kroondal and UG2-chromitite at Sandfontein) provide excellent information for correlation purposes.

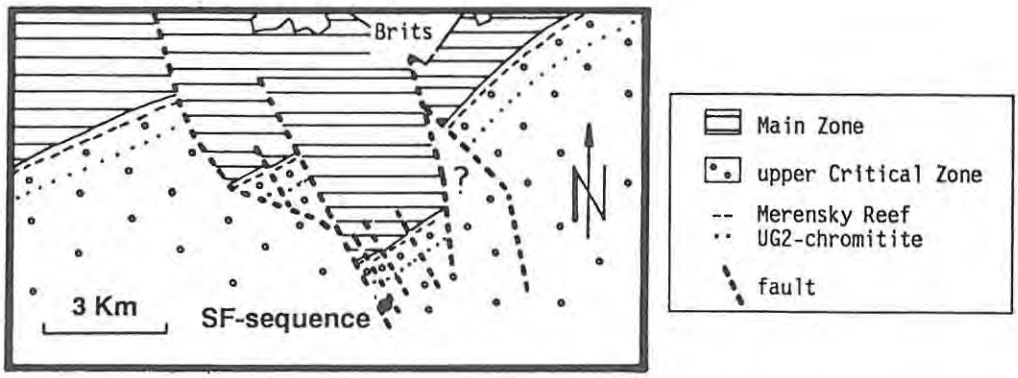

Fig. 59 Simplified geological map showing the collar position of the SF-borehole (see also Fig. 1; source: Visitors Brochure, Crocodile River Mine).

9.2. Regional Geology of the Southern Part of the Western BIC

In contrast to the NW sector of the Western BIC (Union and Amandelbult sections) the ultramafic cumulates of the southern sector are rimmed by a marginal norite (up to 260 m thick) with abundant cpx (Kolobeng Norite, SACS (1980). As shown in Fig. 4 the general stratigraphy above this marginal norite appears to be very similar in the separate sequences. However, the type section selected by SACS (op.cit.) is derived from mapping west of the Pilanesberg and in this part of the thesis major differences between the type section and sections further east will be revealed.

The strike direction is generally E-W and the general dip is between 10 and 15° towards N (Fourie, 1959). Fourie (op.cit.) reported the presence of 25 chromitite layers and divided this part into two sectors (Marikana-Rustenburg sector and Boshoek-Rustenburg sector), which are characterized by different thicknesses of the cumulate pile. The vertical distance between the Merensky Reef and the UG-, MG- and LG-chromitites, is after Fourie (op.cit.):

	UG	MG	LG6-chromitite
Boshoek-Rustenburg	171 - 250 m	296 - 558 m	347 - 668 m
Rustenburg-Marikana	168 - 274 m	369 - 765 m	634 - 960 m

From Cousins and Feringa's work (1964) a decrease in the abundance of ol-rich rocks in a easterly direction can be inferred, but no further information is available from published work. Two structural features are prominent in the region, which might have had some control on the formation of the cumulates (Hatton, 1986):

a)the Spruitfontein upfold, or Kafferskraal arch, straddles a sector in which an important change in the development of the chromitite layers occurs: west of the structure (towards Rustenburg) the LG-chromitite layers are well developed (the LG6-chromitite is the orebody), while east of the upfold the MG-chromitites are better developed (the MG1- and MG2-chromitites are subjects of intensive mining operations), while the LG-chromitites thin out or disappear;

b) the "Brits Graben" is a graben structure with associated sub-graben blocks (Crocodile River Mine, Visitors Brochure; Fig. 59). The main block is bounded by two roughly NW-striking faults with a displacement of up to 600 m (op.cit.). Minor faults occur within and outside the major graben segment. The strike direction and the dip of the layering change slightly within the graben (Fig. 59). Several fault-controlled dykes cut across the graben structure.

The collar position of the KD-borehole is in a pyroxenite below the LG1-chromitite ca. 44 m below the LG6-chromitite (Bristow, pers.com.). The final depth of the borehole is 124.69 m. In Fig. 60 the lithostratigraphy of the KD-sequence is illustrated; the detailed log is attached in the Appendix.

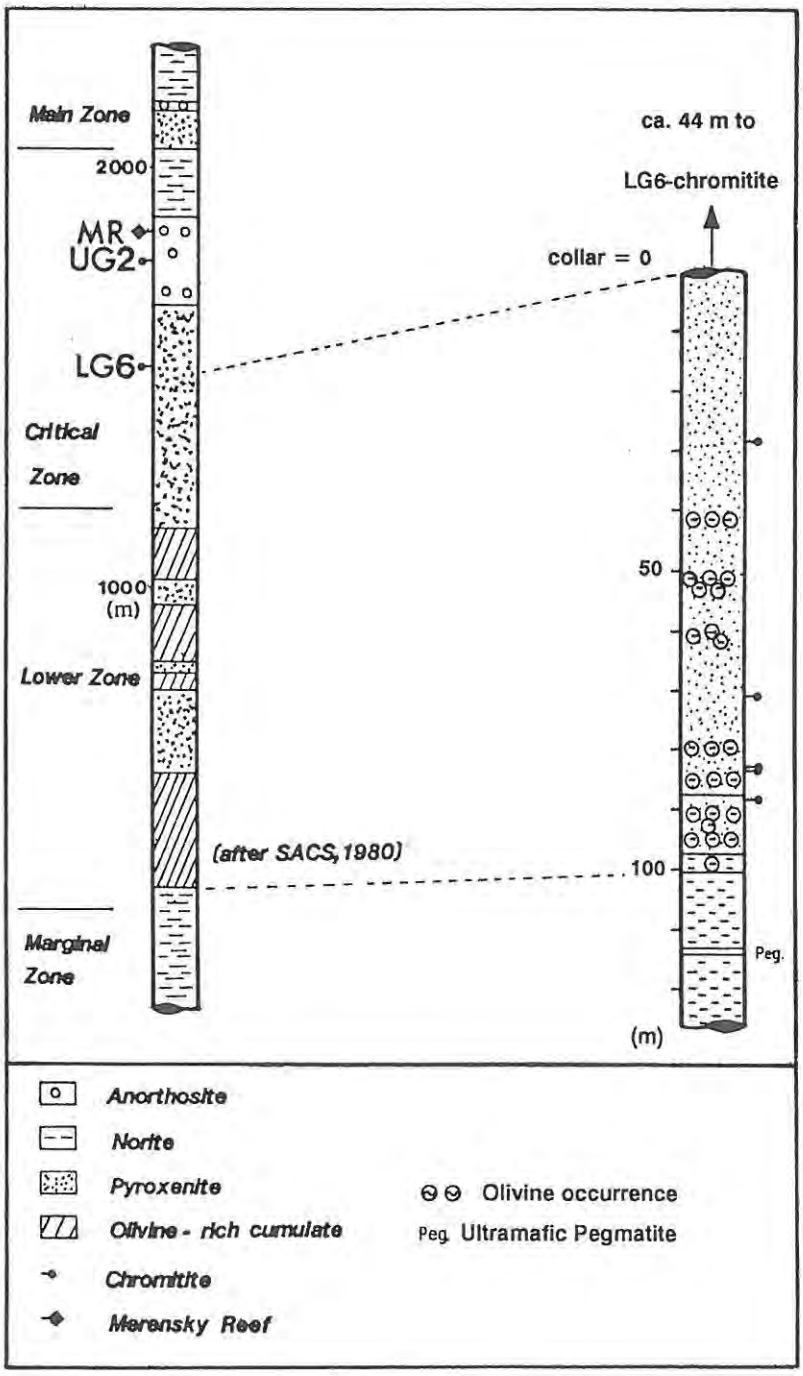

Fig. 60 The KD-sequence and its stratigraphic position in the RLS (note different scales).

10.1. The Lithostratigraphy and Petrography

From the bottom of the borehole to a depth of 100 m the sequence comprises noritic rocks, which grade from a leucocratic variety at the bottom to a more melanocratic variety towards the top. Within the norite (between 101.10 and 105.00 m) and also in the overlying pyroxenite several partly pegmatoidal ol-rich pods, schlieren, lenses or layers were intersected. These ol-rich pods or layers are between 2 and 10 cm thick. Ol and opx are present as large (up to 3 cm) anhedral crystals with an almost amoeboid appearance, which commonly display optical continuity. Lath-like as well as rounded pla inclusions are ubiquitous in both phases. Above this ol-bearing unit a gradational transition from melanorite to pyroxenite takes place within a 3 m interval. Interlayering of pyroxenite and ol-bearing laminae or pods with a similar habit dominates the next interval. A thin chromitite layer at 88.46 m terminates this package. Above this level ol becomes less abundant but is still present sporadically in pods or schlieren up to depth of 44.02 m. The dominant rock type is pyroxenite, which is conspicuously rich in modal postcumulus pla. Within this feldspathic pyroxenite several thin chromitiferous layers (1 - 8 cm thick) were intersected (Fig. 60). These chr disseminations grade in three places into massive chromitite layers at the base (ca. 0.5 cm thick at 71.00, 82.42 and 82.60 m). A massive chromitite, 7 cm thick, layer occurs at 28.38 m and is interpreted as a marker layer in the footwall of the LG1-chromitite. Textures within the pyroxenites and norites are very similar to those encountered in the NG-sequence. The cumulates are cut by pegmatites. Two types can be distinguished: a) an ultramafic, possibly iron-rich, pegmatite (0.96 cm) at a depth of 112.40 m, and b) pegmatitic plagioclase biotite veins (1 - 8 cm) at 52.46 m, 70.88 m and 86.86 m.

10.2. Geochemistry

No whole-rock analyses were executed for this sequence, but the mineral chemistry of the four major constituents (opx, ol, chr and pla) provide the basis for the interpretation given later in this section.

10.2.1. Orthopyroxene

Nineteen samples were selected for the study of opx (83 core-domain analyses). The results are summarized in Fig. 61. Orthopyroxene displays mostly cumulus habit, but might also be a replacement phase in the ol-bearing pods. In the samples KD-71.10, KD-73.10 and KD-88.46 chr is a major phase and the effects of subsolidus re-equilibration are evident. In the triangular diagram (Fig. 61), depicting the cationic % of Ca, Mg and Fe+Mn, this is demonstrated by the two samples which plot outside the field of the remaining samples (towards the Mg-apex).

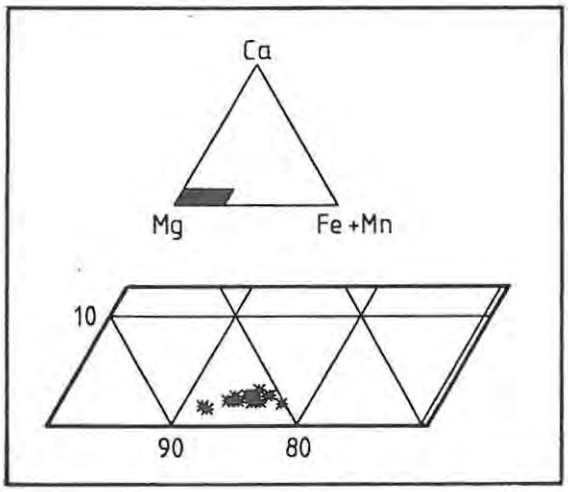

Fig. 61 Compositional range of orthopyroxene in the KD-sequence.

By means of major and minor elements plotted against the Mg# (Fig. 62) compositional variations are illustrated. The levels of Al_2O_3 and Cr_2O_3 are positively linked with the Mg# and linear regression yields:

Al_2O_3 (wt.%) = 21.7 $Mg\#_{opx}$ - 16.6 in ol-bearing norite (n=3)

Al_2O_3 (wt.%) = 10.8 $Mg\#_{opx}$ - 7.8 cc:0.882 in pyroxenite (n=7)
(sample KD-28.28 and
ol-bearing pyroxenites omitted).

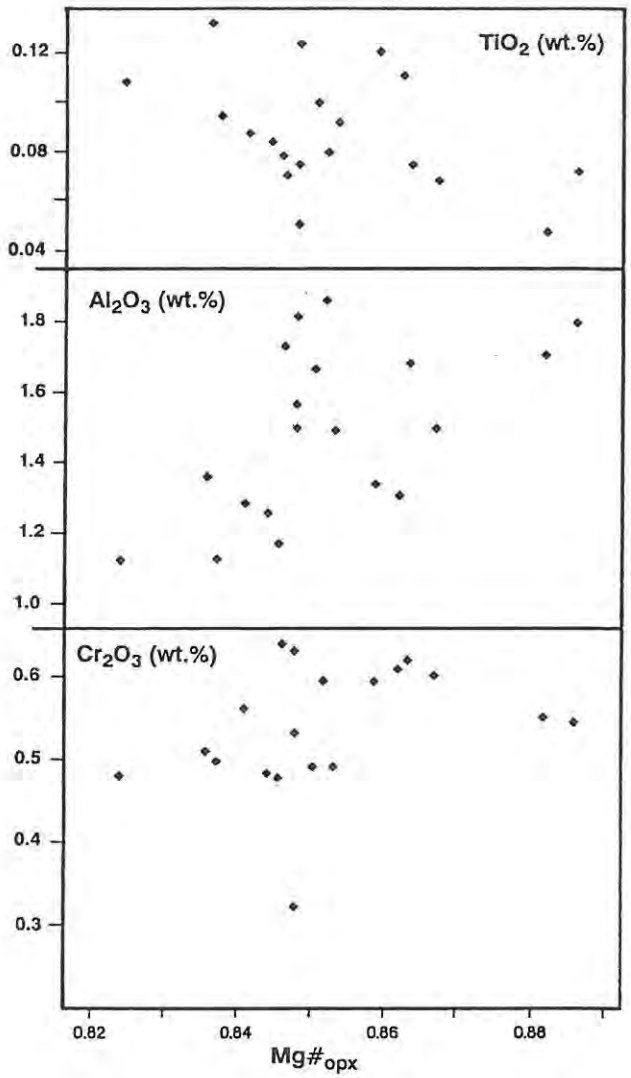

Fig. 62 Orthopyroxene mineralogy in the KD-sequence (note scale breaks).

For the noritic cumulates (4 samples only) no unequivocal conclusion can be drawn. The expression

Cr_2O_3 (wt.%) = 3.7 $Mg\#_{opx}$ - 2.6 cc:0.969

is obtained for pyroxenites (n=6) after omission of the samples KD-71.10 and KD-73.10.

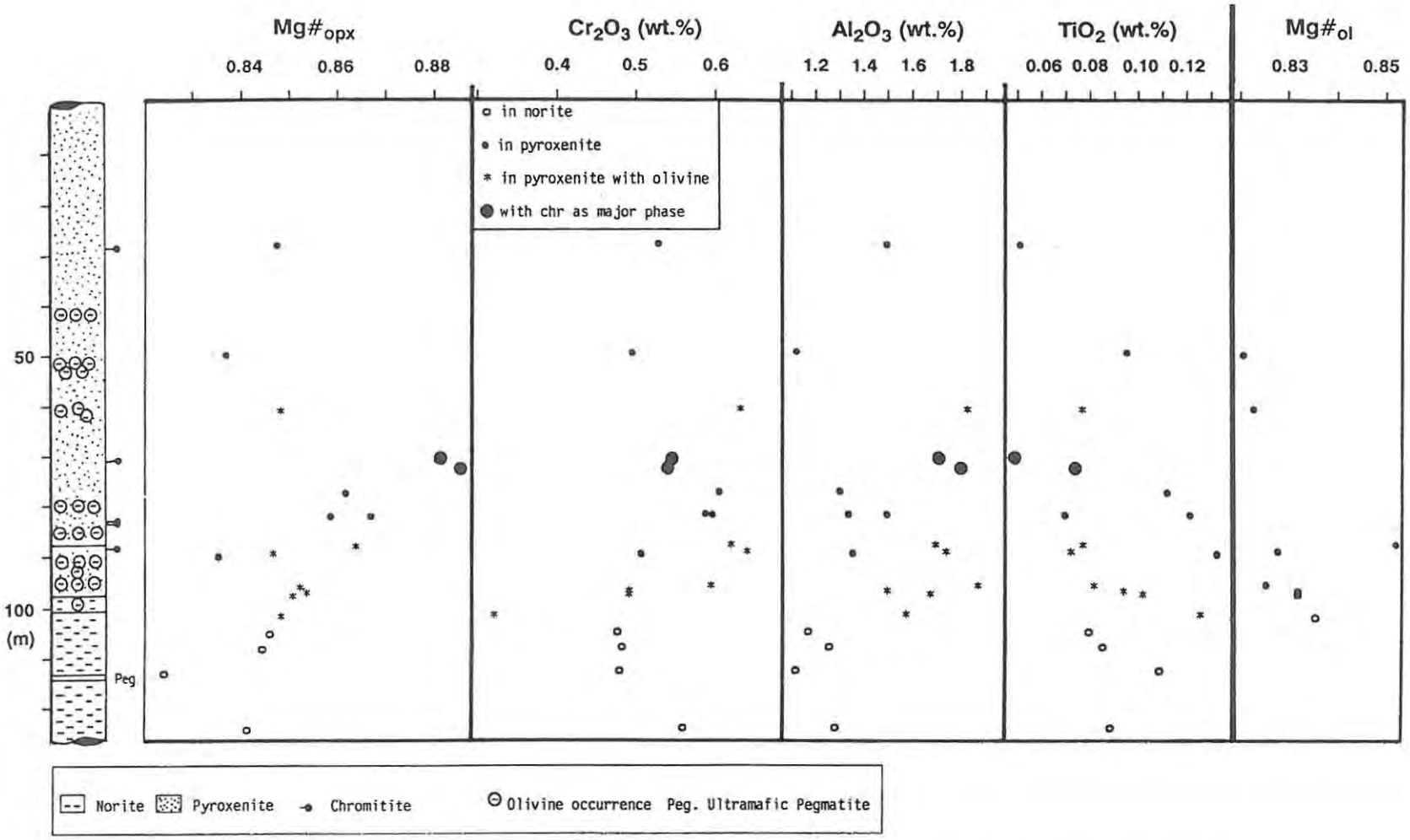

Fig. 63 Cryptic variations of orthopyroxene and olivine through the KD-sequence.

The elements Ti and Ca display a negative correlation with the Mg# and for Ti linear regression yields the following equations:

TiO_2 (wt.%) = -1.3 $Mg\#_{opx}$ + 1.2 cc:-0.991 in norite (n=4)

TiO_2 (wt.%) = -1.1 $Mg\#_{opx}$ + 1.1 cc:-0.730 in pyroxenite (n=7)
(sample KD-28.28 and
ol-bearing pyroxenites omitted).

TiO_2 (wt.%) = -5.9 $Mg\#_{opx}$ + 5.2 in ol-bearing norite (n=3).

Significant cryptic variations with height are shown in Fig. 63. The lower part of the sequence exhibits an upwardly increasing trend of $Mg\#_{opx}$ up to a depth of ca. 85 m. This trend is also evident in opx of the marginal norite, although sample KD-113.63 deviates from the general pattern, which might be due to its closeness to the ultramafic pegmatite, shifting the composition to a more evolved level. The Cr concentrations follow the $Mg\#_{opx}$ as expected from Fig. 62. No general pattern through the sequence is displayed by the TiO_2 levels.

10.2.2. Olivine

Olivine is present only in the described schlieren or laminae. Eight samples were analysed (39 analyses) and the average compositions are tabulated in Table 23. Three of the samples are hosted by norite (the last three of Table 23), while the remainder are associated with pyroxenite.

Ol shows Fo contents of 0.821 - 0.853; the latter value is influenced by subsolidus re-equilibration with chr (sample KD-88.46; see also Fig. 64B). The NiO levels range from 0.19 to 0.32 wt.%; no relationship with the MgO content can be observed (Fig. 64A).

TABLE 23 Olivine Compositions in the KD-sequence

Sample:	KD-50.50	KD-61.20	KD-88.40	KD-89.70	KD-96.30	KD-97.44	KD-97.93	KD-102.50
wt.%								
SiO_2	38.40	38.57	39.03	38.86	39.21	38.53	39.09	38.97
FeO	17.16	16.79	14.13	16.52	16.57	16.11	16.05	15.72
MnO	0.22	0.21	0.18	0.22	0.20	0.20	0.18	0.20
NiO	0.20	0.19	0.28	0.21	0.31	0.24	0.32	0.29
MgO	44.28	43.95	46.00	44.80	44.23	44.88	44.74	44.97
CaO	0.03	0.02	0.02	0.01	0.02	0.03	0.01	0.01
Total	100.28	99.73	99.65	100.62	100.54	99.99	100.40	100.16
cations (based on 4 oxygens):								
Si	0.9751	0.9824	0.9828	0.9796	0.9886	0.9765	0.9852	0.9833
Fe^{2+}	0.3645	0.3576	0.2976	0.3483	0.3494	0.3415	0.3383	0.3318
Mn	0.0047	0.0045	0.0039	0.0047	0.0042	0.0042	0.0039	0.0042
Ni	0.0040	0.0040	0.0056	0.0043	0.0064	0.0049	0.0066	0.0059
Mg	1.6758	1.6685	1.7265	1.6833	1.6623	1.6956	1.6805	1.6913
Ca	0.0008	0.0007	0.0006	0.0003	0.0006	0.0007	0.0003	0.0004
Total	3.0249	3.0176	3.0172	3.0204	3.0114	3.0235	3.0148	3.0167
a	5	4	5	5	5	5	5	5
Fo	0.8214	0.8235	0.8530	0.8286	0.8263	0.8323	0.8324	0.8360
standard deviation:								
wt.%								
SiO_2	0.0361	0.1247	0.1665	0.2540	0.1664	0.1768	0.1032	0.1161
FeO	0.1418	0.1139	0.2655	0.1140	0.1386	0.0582	0.1074	0.1592
MnO	0.0087	0.0089	0.0106	0.0123	0.0106	0.0071	0.0100	0.0144
NiO	0.0401	0.0252	0.0329	0.0278	0.0329	0.0354	0.0125	0.0113
MgO	0.1535	0.1993	0.2067	0.1325	0.2770	0.2222	0.0819	0.1091
CaO	0.0047	0.0075	0.0053	0.0076	0.0054	0.0062	0.0087	0.0094

Notes: 1) a: number of analyses

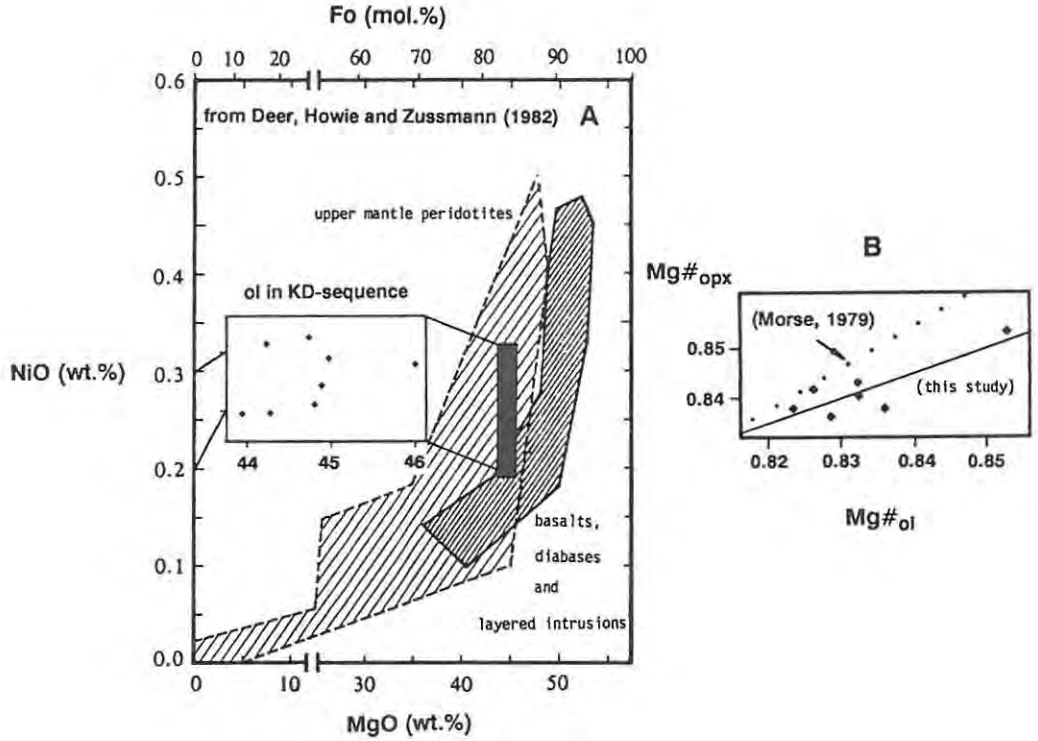

Fig. 64 Olivine mineralogy in the KD-sequence : A) Variation of MgO and NiO in olivine; B) Coexisting orthopyroxene and olivine.

The Mg#s of the coexisting ferromagnesian phases ol and opx were regressed and the equation

$$Mg\#_{opx} = 0.50\ Mg\#_{ol} + 0.43 \text{ (cc: 0.841, n=7)}$$

is derived from this comparison (Fig. 64B). The equation is significantly different from the expression found by Morse (1979) and those obtained for the opx-ol pairs in the NG-sequence. The measured $Mg\#_{opx}$ is generally too low or $Mg\#_{ol}$ too high and disequilibrium of ol and opx is evident. Two different explanations might resolve this problem:

a) the ol-bearing schlieren are xenolithic, i.e. they did not crystallize together with the surrounding opx;

b) the compositions of the assemblage do not represent magmatic compositions, implying a postmagmatic overprint.
The described textures might point to an increased activity of volatiles during and/or after the formation of the ol-rich schlieren. It is therefore suggested that the primary composition of ol was modified by a late-stage reaction causing the disequilibrium between ol and opx.

10.2.3. Chromite

Chromite was analysed in 9 samples (40 analyses) and the data are summarized in Table 24. In samples KD-71.10, KD-73.10 and KD-88.46 chr is a major component, while sample KD-28.38 was taken just below the 7 cm massive chromitite layer.

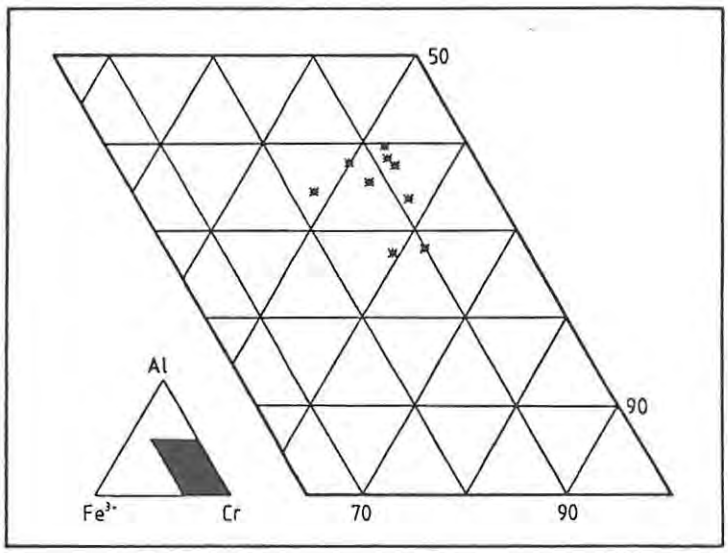

Fig. 65 Triangular diagram of the trivalent cations Cr, Fe^{3+} and Al (in cation %) of chromite in the KD-sequence.

In the conventional triangle depicting the trivalent cations Al, Fe^{3+} and Cr (Fig. 65) the compositional variation of chr in the KD-sequence is wide with two samples enriched in Cr (KD-28.38; KD-82.70). The ranges of the respective elements are:

Al_2O_3: 14.00 - 21.46 wt.%; Al : 27.4 - 39.4 cationic %,

Fe_2O_3: 6.94 - 14.05 wt.% Fe^{3+}: 8.2 - 17.5 cationic %,

Cr_2O_3: 36.92 - 46.56 wt.%; Cr : 48.2 - 62.0 cationic %.

TABLE 24 Chromite Compositions in the KD-sequence (Core Domains only)

Sample:	KD-28.38	KD-71.10	KD-73.10	KD-78.00	KD-82.60	KD-82.70	KD-88.40	KD-89.70	KD-97.93
wt.%									
TiO_2	0.47	0.33	0.39	0.13	0.57	0.70	0.48	0.69	0.56
Al_2O_3	14.01	21.46	20.28	17.36	19.86	14.07	18.22	17.65	19.66
Cr_2O_3	44.99	42.45	42.21	44.51	43.21	46.56	40.52	36.92	38.86
FeO	21.94	17.26	17.76	22.05	16.93	21.44	21.48	22.91	21.17
Fe_2O_3	10.73	6.95	7.19	7.24	6.94	8.01	9.40	14.05	10.27
MnO	0.32	0.28	0.32	0.32	0.30	0.36	0.35	0.32	0.28
NiO	0.15	0.09	0.12	0.10	0.12	0.06	0.09	0.16	0.16
MgO	8.08	11.93	11.21	8.01	11.91	8.38	8.52	7.90	9.11
Total	100.70	100.75	99.48	99.73	99.84	99.58	99.05	100.58	100.07
cations (based on 32 oxygens):									
Ti	0.0933	0.0610	0.0748	0.0249	0.1081	0.1402	0.0947	0.1350	0.1076
Al	4.3364	6.2656	6.0426	5.3389	5.8836	4.3828	5.6038	5.3998	5.9356
Cr	9.3537	8.3163	8.4400	9.1895	8.5874	9.7414	8.3605	7.5837	7.8703
Fe^{2+}	4.8249	3.5767	3.7555	4.8156	3.5588	4.7441	4.6921	4.9795	4.5358
Fe^{3+}	2.1234	1.2961	1.3677	1.4219	1.3130	1.5955	1.8463	2.7465	1.9790
Mn	0.0714	0.0593	0.0681	0.0710	0.0635	0.0802	0.0765	0.0696	0.0598
Ni	0.0312	0.0180	0.0243	0.0220	0.0236	0.0136	0.0180	0.0325	0.0331
Mg	3.1658	4.4071	4.2270	3.1162	4.4622	3.3023	3.3081	3.0534	3.4789
a	4	6	4	4	6	4	5	4	3
cationic ratios:									
Cr/Al	2.1570	1.3273	1.3967	1.7213	1.4596	2.2227	1.4919	1.4044	1.3259
$Mg\#_{chr}$	0.3962	0.5520	0.5295	0.3929	0.5563	0.4104	0.4135	0.3801	0.4341
FFE	0.3056	0.2660	0.2670	0.2280	0.2695	0.2517	0.2824	0.3555	0.3038
Cr/(Cr+Al)	0.6832	0.5703	0.5828	0.6325	0.5934	0.6897	0.5987	0.5841	0.5701
weight ratio of metals:									
Cr/Fe	1.25	1.59	1.53	1.37	1.64	1.43	1.19	0.91	1.12
standard deviation:									
wt.%									
TiO_2	0.0341	0.0548	0.0319	0.0734	0.0138	0.0900	0.0697	0.2557	0.0171
Al_2O_3	1.3566	0.2486	0.2765	1.3289	0.2322	1.1811	0.7097	1.2264	0.1343
Cr_2O_3	1.1870	0.4620	0.2189	1.1301	0.3041	0.6326	0.4795	0.3870	0.1837
FeO	0.3738	0.2039	0.6000	0.4640	0.2391	0.5472	1.4817	1.1546	0.1526
Fe_2O_3	0.3352	0.2405	0.3287	0.3884	0.1068	0.3961	0.1647	0.2274	0.1345
MnO	0.0220	0.0151	0.0247	0.0135	0.0153	0.0255	0.0397	0.0178	0.0132
NiO	0.0120	0.0222	0.0229	0.0225	0.0191	0.0072	0.0233	0.0087	0.0092
MgO	0.4248	0.1667	0.3370	0.4491	0.1284	0.4837	1.0692	0.7738	0.1214

Notes: 1) $Mg\#_{chr}$: cationic ratio of $Mg/(Mg + Fe^{2+})$
2) FFE : cationic ratio of $Fe^{3+}/(Fe^{3+} + Fe^{2+})$
3) Cr/Fe : weight ratio of Cr metal to Fe metal
4) a : number of analyses

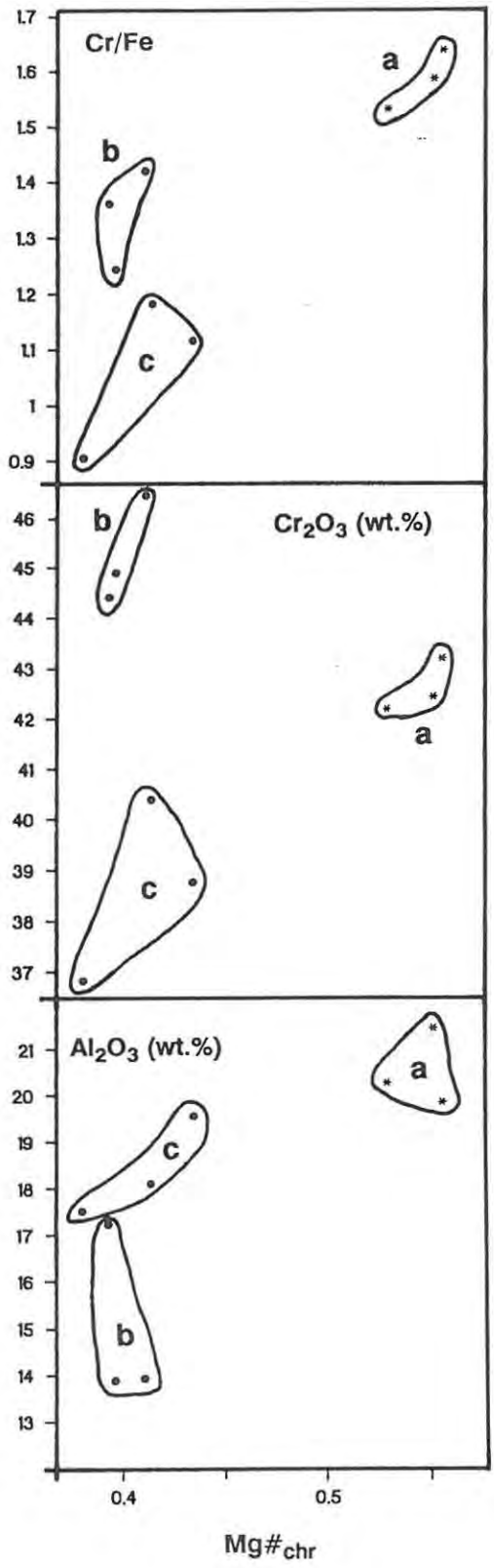

Fig. 66 Chromite mineralogy - variation diagrams (KD-sequence).

In simple variation diagrams with the $Mg\#_{chr}$ as abscissa (Fig. 66) the dependence of chr mineralogy upon host cumulate and modal abundance is clearly demonstrated. Here the datum points fall into three fields:

a) cumulates with chr as major phase (field "a");

b) pyroxenites with chr as accessory phase (field "b");

c) ol-bearing cumulates with accessory chr (field "c").

The conspicuously low Cr_2O_3 levels (<40 wt.%) in the samples KD-89.70 and KD-97.93 are accompanied with cuspate or lobate textural forms of chr, similar to those described as typical for the Pseudo-, Merensky and Bastard Reefs (Eales and Reynolds, 1986).

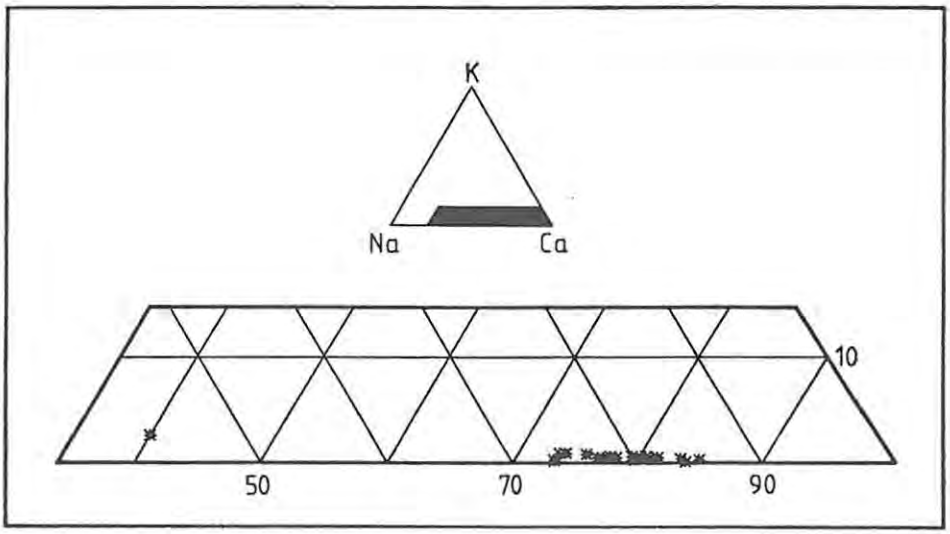

Fig. 67 Compositional range of plagioclase in the KD-sequence.

10.2.4. Plagioclase

Plagioclase occurs as a cumulus phase in noritic rocks and as a postcumulus phase in pyroxenite. In the pegmatoidal ol-bearing schlieren pla displays anhedral shapes similar to those of ol. In twenty one samples (76 analyses) the composition of pla was determined by microprobe.

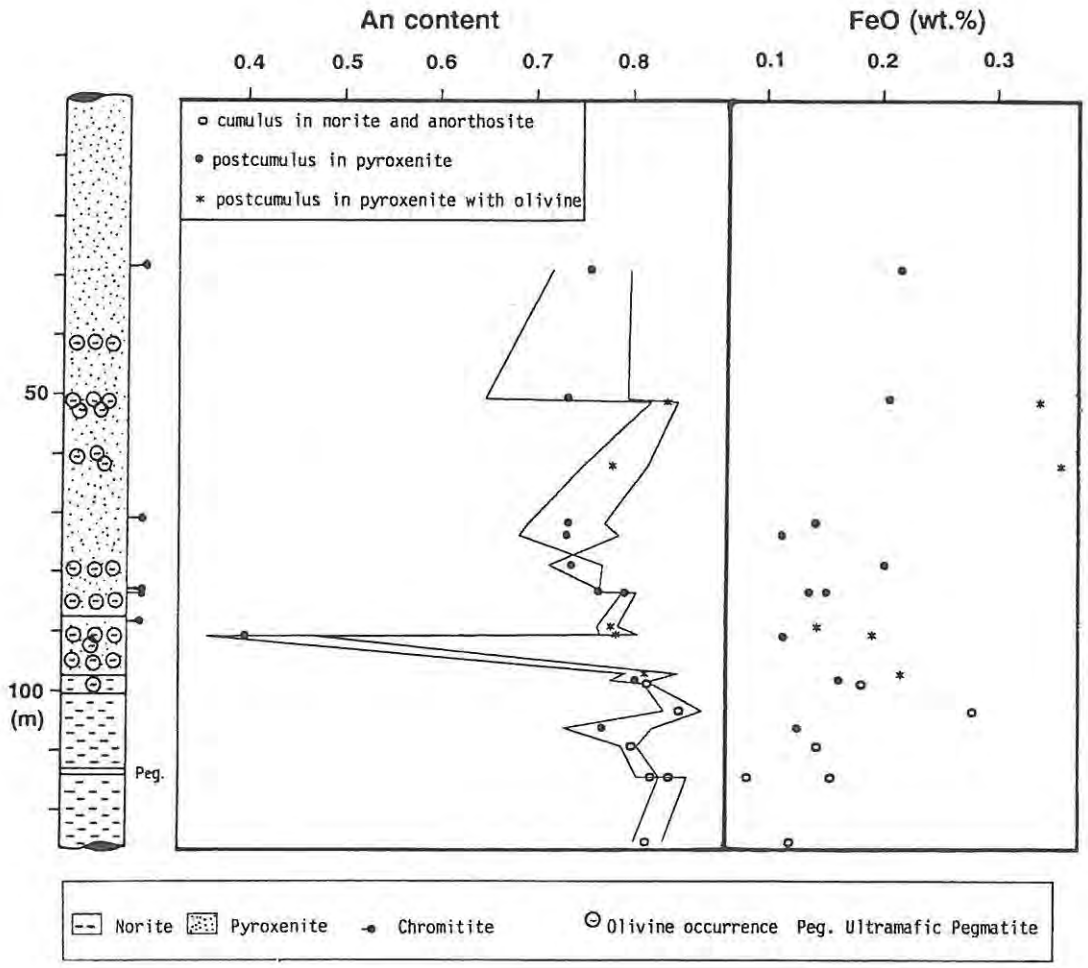

Fig. 68 Cryptic variations of plagioclase through the KD-sequence, solid lines show maximum and minimum An values.

In one sample (KD-90.30) feldspar of andesine composition was found ($An_{40.5}Ab_{56.9}Or_{2.6}$), but the remaining samples cluster in a field between $An_{73.7}$ and $An_{85.3}$, thus are bytownite plagioclase (Fig. 67) regardless of their textural appearance. The generally lower An content of postcumulus pla is not pronounced in the KD-sequence. Postcumulus pla in the pyroxenites exhibits only slightly lower An contents than the cumulus variety in the noritic rocks. Anhedral, amoeboid pla within the pegmatoidal ol-bearing schlieren is characterized by high An values ($>An_{78}$) indicating a cumulus origin. The amount of Fe in the feldspar ranges from 0.09 to 0.35 wt.% oxide (see also Fig. 68). The very limited variations with height are illustrated in Fig. 68. An overall decrease in An content might be indicated.

10.3. Discussion and Conclusions

The KD-sequence is interpreted as the lower, telescoped part of the RLS comprising the MZ, LZ and lower half of the lCZ as developed east of Rustenburg; this correlation (see also Fig. 69) is based on the stratigraphic, petrographic and geochemical data presented. The MZ of the KD-sequence (up to a depth of 105.50 m) is composed of the marginal norite with limited occurrences of ol in its upper portion. The full thickness of the marginal norite here is not known. This marginal norite is overlain here by the ol-rich cumulates of the LZ, which are here only 17.1 m thick, comprising norite with abundant ol-bearing schlieren passing upwards into ol-bearing pyroxenite interlayered with ol-rich laminae. The LZ - lCZ-boundary (at a depth of 88.46 m) is defined by the reversal of the trend displayed by the $Mg\#_{opx}$ and the occurrence of thin chromitite layers with chr as the sole cumulus phase. As in the NG-sequence, pyroxenite is the dominant rock type in the lCZ.

A combined sequence of the lower part of the RLS (including the upper part of the lCZ) was constructed using the data of Fourie (1959) and the KD-sequence (Fig. 69) to demonstrate the condensation (i.e. telescoping) of the sequence. The stratigraphic level of the collar position of the KD-borehole ca. 45 m below the LG6-chromitite layer was calculated using an average dip and the borehole location (Bristow, pers.com.). Unfortunately, Fourie (op.cit.) included only limited petrographic descriptions of the silicate cumulates, and ol-bearing cumulates were not mentioned by him. According to this combined sequence the entire lCZ at Kroondal is ca. 205 m thick, and pyroxenite is by far the most abundant rock type. It appears from the KD-borehole that the thick ol-rich intervals of the LZ in the NG-sequence deteriorate to thin laminae or discontinuous schlieren of ol hosted in norite or pyroxenite. However, the reversed fractionation trend in the lower part of the KD-sequence can be equated with the overall reversed fractionation trend of the LZ in the NG-sequence. Hence, despite considerable stratigraphic differences, the newly defined LZ - lCZ boundary (Eales et al.,1990b) is here still valid.

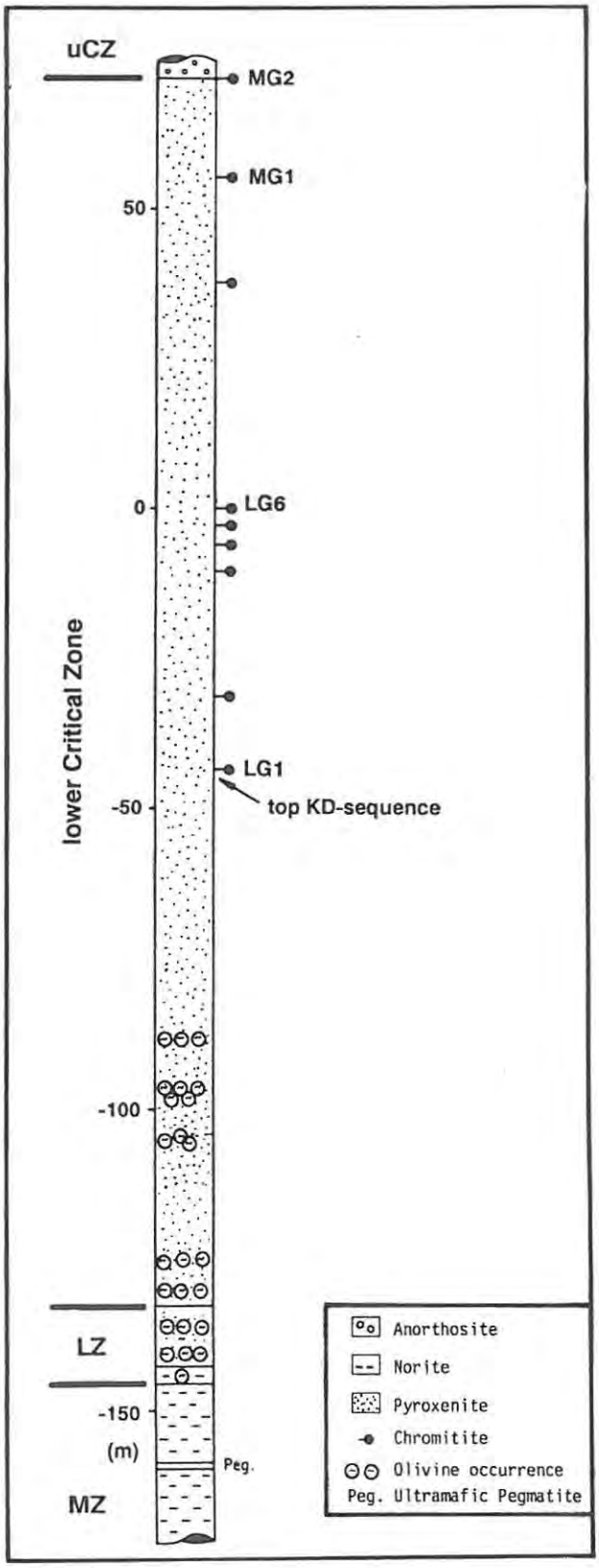

Fig. 69 Combined sequence of the lCZ, LZ and MZ at Kroondal using the KD-sequence and boreholes 1, 6 and 5 from Fourie (1959).

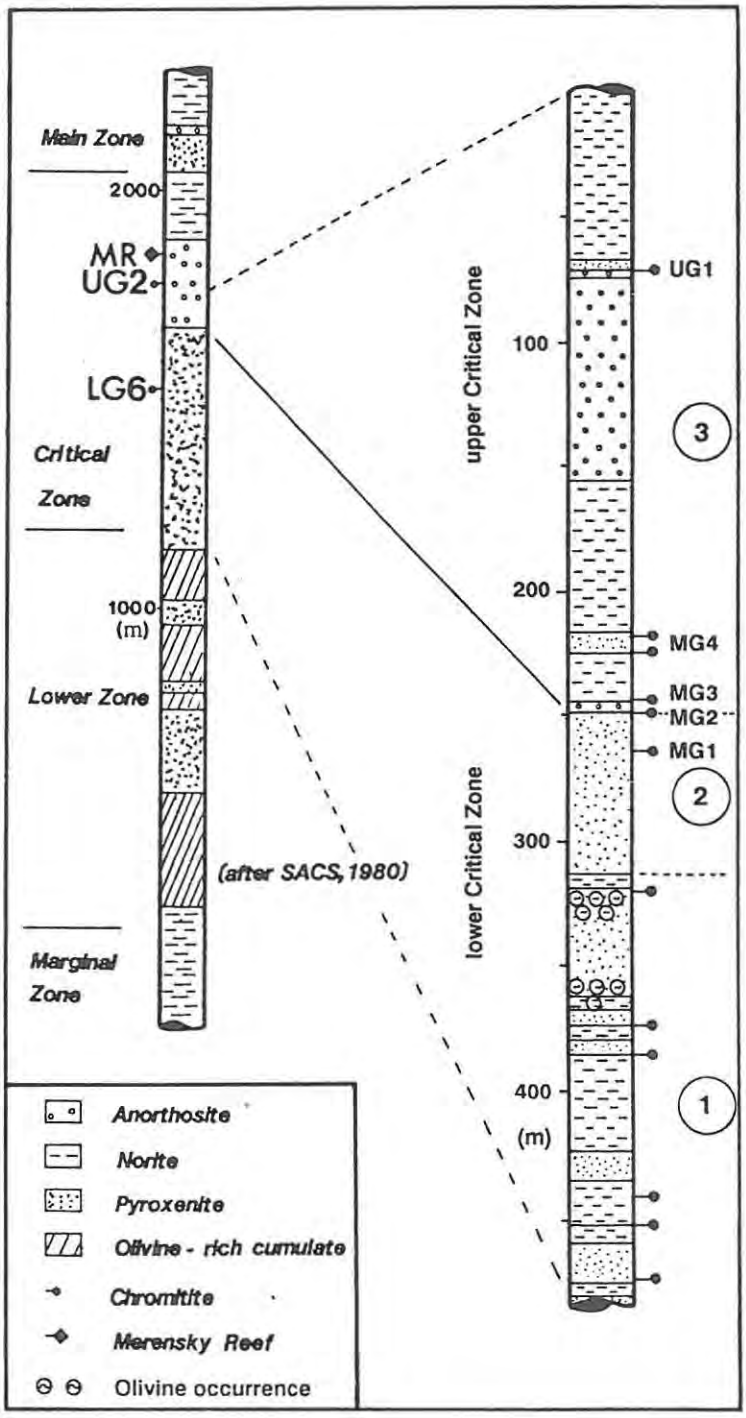

Fig. 70 The SF-sequence and its stratigraphic position in the RLS (note different scales).

CHAPTER 11 : THE SF-SEQUENCE

Mining operations in the Lefkochrysos Mine (now Crocodile River Mine) are directed to exploit solely the UG2-chromitite; underground exposures are therefore restricted to the chromitite layer and its immediate foot- and hangingwall. Borehole SF-7 was drilled for study and correlation purposes into the deep footwall of the orebody (Fig. 59); its final depth was 485.75 m below collar. Because of the thrust of this thesis, microprobe and petrographic sampling started at a depth of ca. 219.00 m (in the hangingwall of the MG4-chromitite) apart from 5 samples covering the UG1- and UG2-chromitites. However, Golden Dumps Expl. Ltd. generously provided whole-rock XRF-data for the entire sequence, which were incorporated in some of the diagrams. The cumulate pile intersected by SF-7 is a sequence commencing with the noritic hangingwall of the UG1-chromitite and ending in ultramafic cumulates of the lCZ. Unfortunately, the borehole was stopped before reaching the contact between the RLS and the sedimentary floor rocks.

11.1. The Lithostratigraphy and Petrography

The SF-sequence is dominated by leucocratic cumulates but includes also ultramafic rocks; both rock types host several chromitite layers (Table 25). The detailed log is attached in the Appendix. The sequence can be subdivided into 3 segments (based on the relative proportions of the major lithologies, prominent marker layers and geochemistry), which are (Fig. 70):

a) from the bottom of the hole to a depth of 312.95 m (segment 1) the cumulate pile is dominated by noritic rocks intercalated with layers of pyroxenite and chromitite. In this segment 6 minor chromitite layers occur. These are either hosted entirely in pyroxenite or associated with an anorthositic footwall and a pyroxenitic hangingwall. Only sample SF-453.28 shows a chromitite sandwiched between leucocratic lithologies. The chromitite layers hosted by pla-rich cumulates form schlieren or lenses with very irregular contacts.

TABLE 25 Chromitite Layers in the SF-sequence

Layer No	Distance to UG1 in m	Thickness in cm	Characteristic features	Host rocks	Correlation with Cousins and Feringa, 1964
1	0.0	156	m	p/a	UG1
2	- 0.8	23	m	p/a	UG1
3	- 2.3	39	m	a	UG1
4	- 3.0	11	m	a	UG1
5	-148.7	106	d	p	MG4B
6	-153.5	225	m	p/n	MG4A
7	-172.9	90	m	n/a	MG3
8	-177.7	39	m	a/p	MG2
9	-178.5	52	m	p	MG2
10	-179.4	40	m	p	MG2
11	-180.1	26	m	P	MG2
12	-192.3	146	m	p	MG1
13	-195.1	31	m	p	MG1
14	-196.4	54	m	p	MG1
15	-197.4	10	d	p	MG1
16	-248.7	4	m	n/p	LG
17	-301.6	16	m	p/n	LG
18	-314.3	10	m	p	LG
19	-369.8	10	m	n/p	LG
20	-382.2	5	m	p/n	LG
21	-404.4	14	m	p	LG

Notes: 1) datum: UG1-chromitite, bottom contact of main layer

2) massive (m): chromite is the only cumulus phase

3) disseminated (d): chromite and silicate phases are cumulus minerals

4) host rocks denoted are hangingwall and footwall: p=pyroxenite, d=dunite, n=norite, a=anorthosite

The rock at the bottom of SF-7 is a highly feldspathic pyroxenite, fine- to medium-grained (≤2 mm), with abundant mica, quartz and cpx as postcumulus phases. It is overlain by a norite, which is capped by a further pyroxenitic layer. Such cyclicity, i.e. the interlayering of pyroxenite and norite with or without chromitite layers, is repeated 6 times in this segment. Within the noritic layer at a depth of ca. 364 m and in two horizons (357.65 - 360.15 and 318.00 - 337.00 m) within the overlying, thick pyroxenite package ol occurs in layers, schlieren and pegmatoidal pods in a similar habit to that found in the KD-sequence. A 4 cm massive chromitite layer with some thin leader stringers at 319.58 m forms the uppermost ultramafic member just beneath the base of the norite at 318.33 m;

b) up to a depth of 248.46 m (segment 2) the sequence comprises only pyroxenites and chromitites. The MG1- and MG2-chromitites are located within this segment;

c) the remainder of the SF-sequence (segment 3, i.e. the lower part of the uCZ) is dominated by leucocratic cumulates, which host the MG3-, MG4- and the UG1-chromitites. Pyroxenites form thin packages (up to 3.74 m thick) below, above or in between chromitite layers. A conspicuous mottled anorthosite (3.86 m) between the MG2- and MG3-chromitites defines the boundary of lCZ and uCZ. Between 216.66 and 71.56 m all cumulates are noritic or anorthositic; in this interval pyroxenites were not intersected.

The compositional differences of the three segments is also illustrated by the relative proportions of the major lithologies:

	segment			total SF-sequence
	1	2	3	
% anorthosite	0.3	0.0	35.2	18.0
% norite	40.7	0.0	58.1	47.7
% pyroxenite	58.7	93.8	4.1	32.0
% chromitite	0.3	6.2	2.6	2.3

Alteration in the SF-sequence is generally higher in degree than in the other cores studied. However, the degree is variable and very often localised. At some levels complete serpentinization of the ferromagnesian phases discouraged microprobe work. Pla displays different stages of saussuritization, which is in some samples concentrated in the core domains giving rise to a cloudy appearance, while the margins are clear.

11.2. Mineralogy

All major phases were analysed by electron microprobe. However, despite the abundance of ol in the described horizons only in three samples (SF-336.97; SF-360.90; SF-362.12) was ol unserpentinized, allowing determination of the mineral composition. The average compositions were calculated according to the technique used in the previous sections.

11.2.1. Orthopyroxene

In all samples investigated (38 samples, 171 analyses) opx is a cumulus phase, apart from two samples from massive chromitite layers. The average compositions are listed in the Appendix.

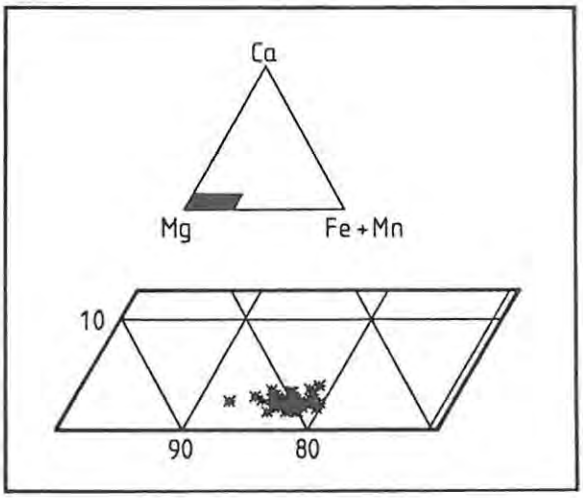

Fig. 71 Compositional range of orthopyroxene in the SF-sequence.

In the ternary diagram (Fig. 71) depicting the elements Ca, Mg and Fe+Mn the field of the samples under investigation is very limited. The ranges are:

	cationic %	or	wt.% oxide	
Ca	1.7 - 4.4		0.9 - 2.1	
Mg	77.0 - 84.9		28.3 - 32.0	
Fe + Mn	12.5 - 19.7		8.2 - 13.0	FeO
			0.2 - 0.3	MnO

Hence, all opx are of enstatitic composition with $Mg\#_{opx}$ in the range of 0.801 to 0.875, with the highest ratios being displayed by opx in chromitiferous cumulates, probably caused by subsolidus re-equilibration. The Cr_2O_3 contents vary between 0.3 and 0.6 wt.%.

In scattergrams (Fig. 72) of Cr_2O_3, Al_2O_3 and TiO_2 versus the $Mg\#_{opx}$ the following features can be observed:

a) for the entire opx population general trends are only weakly developed and in the case of Ti no pattern is apparent;

b) Al_2O_3 and Cr_2O_3 appear to be positively linked with the $Mg\#_{opx}$. Under the assumption that repeated replenishment by a primitive liquid took place during the formation of the cumulate column, thus concealing distribution patterns hidden within the entire opx population, limited intervals were tested. In two of the tested intervals acceptable correlations after linear regression were found:

interval 69.30 - 268.41 m (n=6)
Cr_2O_3 (wt.%) = 3.25 $Mg\#_{opx}$ - 2.15 (cc: 0.992; SF- 69.30 omitted)
Al_2O_3 (wt.%) = 18.74 $Mg\#_{opx}$ - 14.21 (cc: 0.900; SF-223.68 omitted)

interval 305.35 - 318.52 m (n=4)
Cr_2O_3 (wt.%) = 14.49 $Mg\#_{opx}$ - 11.61 cc: 0.890
Cr_2O_3 (wt.%) = 32.11 $Mg\#_{opx}$ - 25.60 cc: 0.950 .

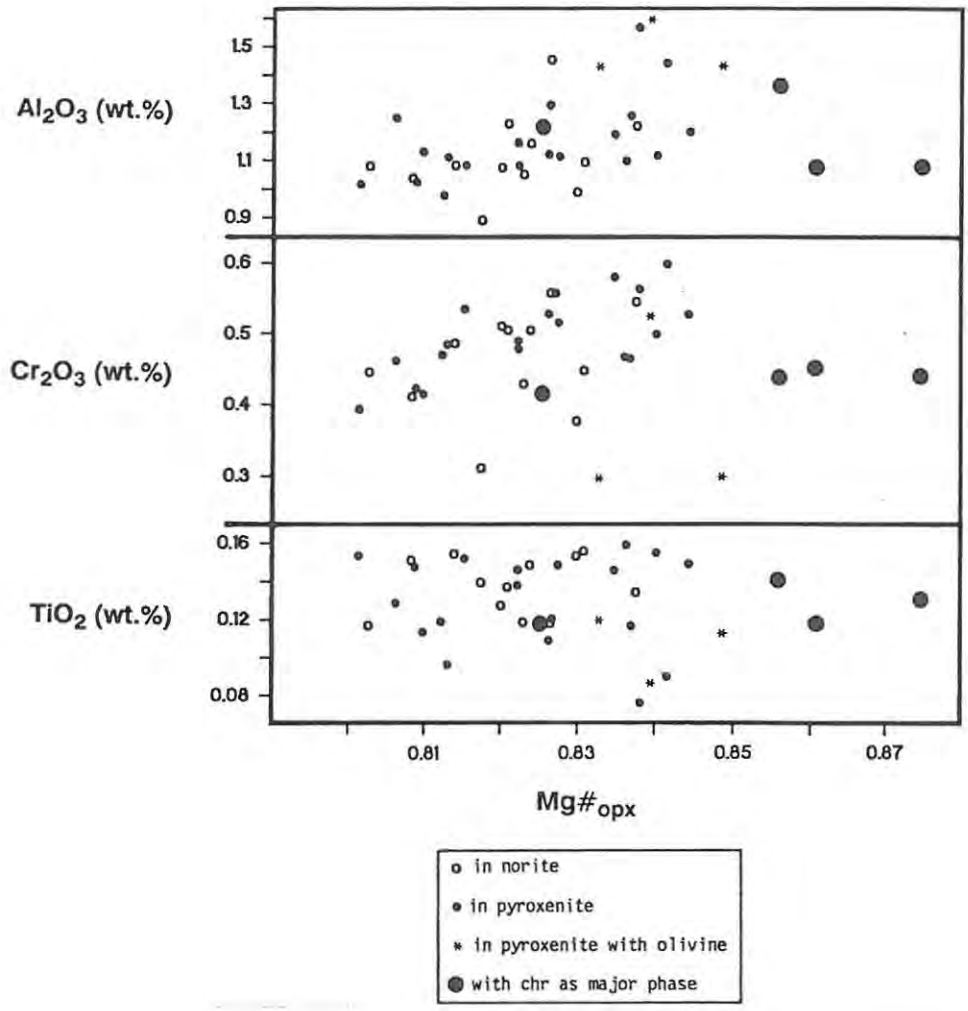

Fig. 72 Orthopyroxene mineralogy in the SF-sequence (note scale breaks).

However, it might pointed out here that the first interval spans three massive chromitite layers (MG2-, MG3- and MG4-chromitites), which are probably formed by magma mixing of a newly emplaced primitive liquid and the fractionated resident liquid. Therefore it is suggested that the equations obtained might be a resultant of several very similar expressions, pointing to a broad similarity of the compositions of the replenishing magmas.

Cryptic variations with height are shown in Fig. 73. The trend outlined by the $Mg\#_{opx}$ displays a steady increase up to ca. 316 m, with perhaps short intervals of normal fractionation trends in norite (see also Fig. 82). Unusually high $Mg\#_{opx}$ at the bottom of the sequence and at 319.54 m are almost certainly due to subsolidus re-equilibration with chr. Above 336 m a regular decline is apparent. No clear patterns are evident in plots depicting TiO_2 and Cr_2O_3 in opx.

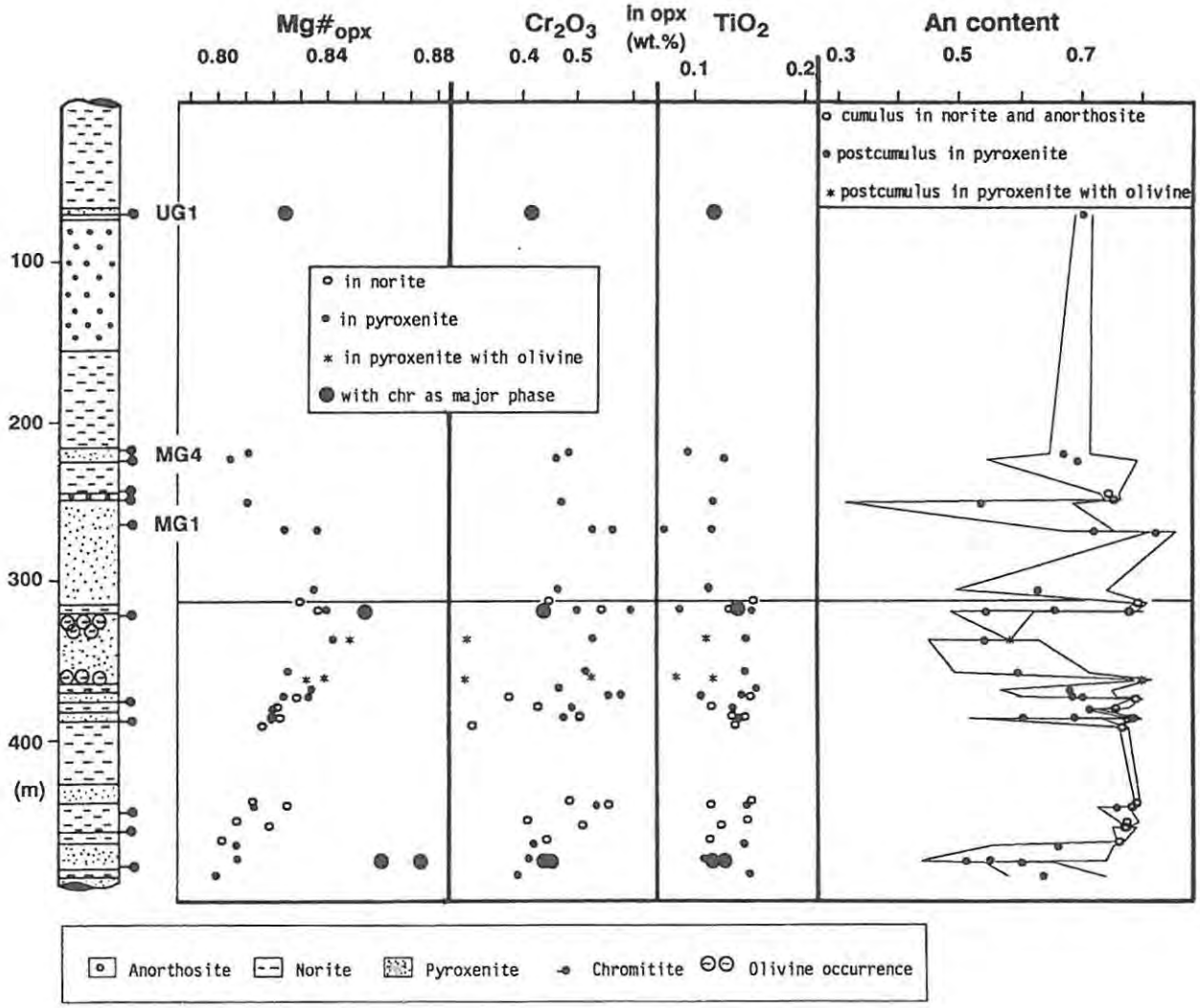

Fig. 73 Cryptic variations of orthopyroxene and plagioclase through the SF-sequence, solid lines show maximum and minimum An values.

11.2.2. Olivine

The compositions of ol in the three samples containing this phase (see log in Fig. 73) are tabulated in Table 26. The NiO content ranges from 0.21 to 0.27 wt.% with MgO levels between 42.97 and 44.32 wt.%. Hence, the forsterite content varies from $Fo_{81.5}$ to $Fo_{83.4}$. After linear regression of $Mg\#_{opx}$ and $Mg\#_{ol}$ (Fig. 74) the equation

$$Mg\#_{opx} = 0.83\ Mg\#_{ol} + 0.15$$

is obtained, which is very similar to the one found by Morse (1979), and the present writer in earlier chapters. Equilibrium is indicated.

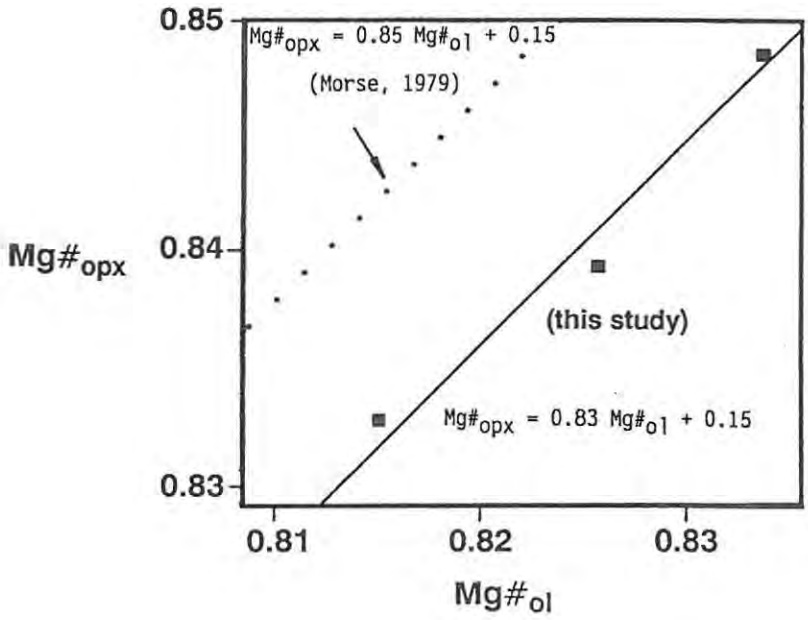

Fig. 74 Coexisting orthopyroxene and olivine in the SF-sequence.

TABLE 26 Olivine Composition in the SF-sequence

Sample:	SF-336.97	SF-360.90	SF-362.12
wt.%			
SiO_2	39.57	39.24	39.48
FeO	15.77	16.57	17.38
MnO	0.17	0.22	0.22
NiO	0.27	0.21	0.26
MgO	44.32	44.03	42.97
CaO	0.02	0.03	0.01
Total	100.10	100.30	100.32
cations (based on 4 oxygens):			
Si	0.9970	0.9912	0.9998
Fe^{2+}	0.3322	0.3500	0.3681
Mn	0.0035	0.0048	0.0047
Ni	0.0054	0.0042	0.0052
Mg	1.6644	1.6578	1.6220
Ca	0.0006	0.0008	0.0004
Total	3.0030	3.0088	3.0002
a	5	7	3
Fo	0.8336	0.8257	0.8150
standard deviation:			
wt.%			
SiO_2	0.0183	0.1957	0.1217
FeO	0.0926	0.1967	0.1485
MnO	0.0065	0.0129	0.0122
NiO	0.0326	0.0362	0.0160
MgO	0.1114	0.1766	0.1556
CaO	0.0078	0.0084	0.0038

Notes: 1) a: number of analyses

11.2.3. Chromite

Chr compositions were investigated in 34 samples (169 analyses; listed in the Appendix) , of which 27 are either from massive chromitite layers or chromitiferous cumulates. In the remaining samples chr is an accessory phase.

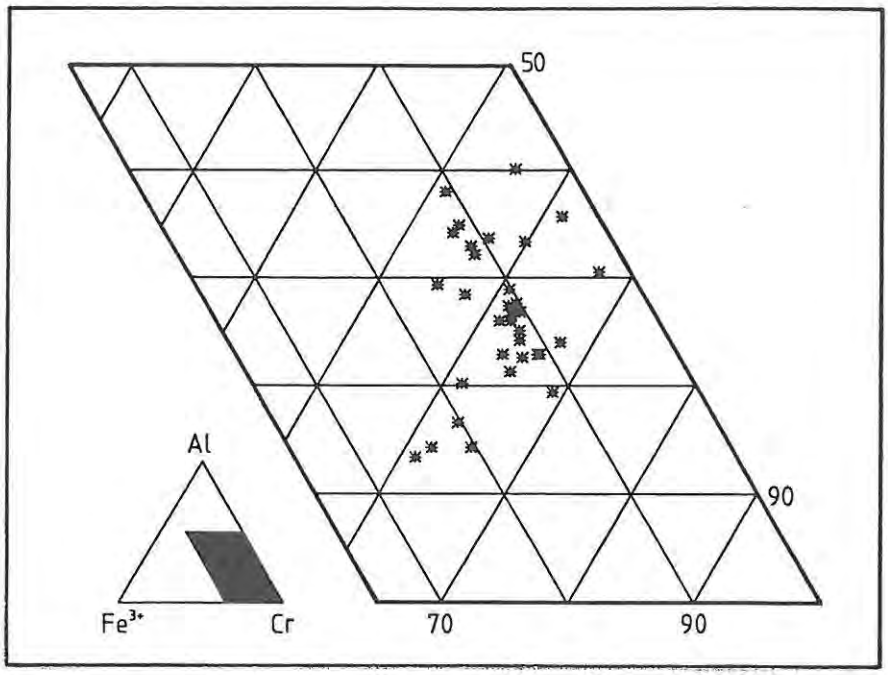

Fig. 75 Triangular diagram of the trivalent cations Cr, Fe^{3+} and Al (in cation %) of chromite in the SF-sequence.

In the triangular diagram showing the trivalent cations (Fig. 75) the compositional field is wide, which is also expressed in the ranges of composition:

	wt.%
TiO_2	0.27 - 1.89
Al_2O_3	6.36 - 21.36
Cr_2O_3	40.92 - 50.13
FeO	17.73 - 28.53
Fe_2O_3	2.04 - 15.05
NiO	0.05 - 0.20
MgO	3.20 - 11.56

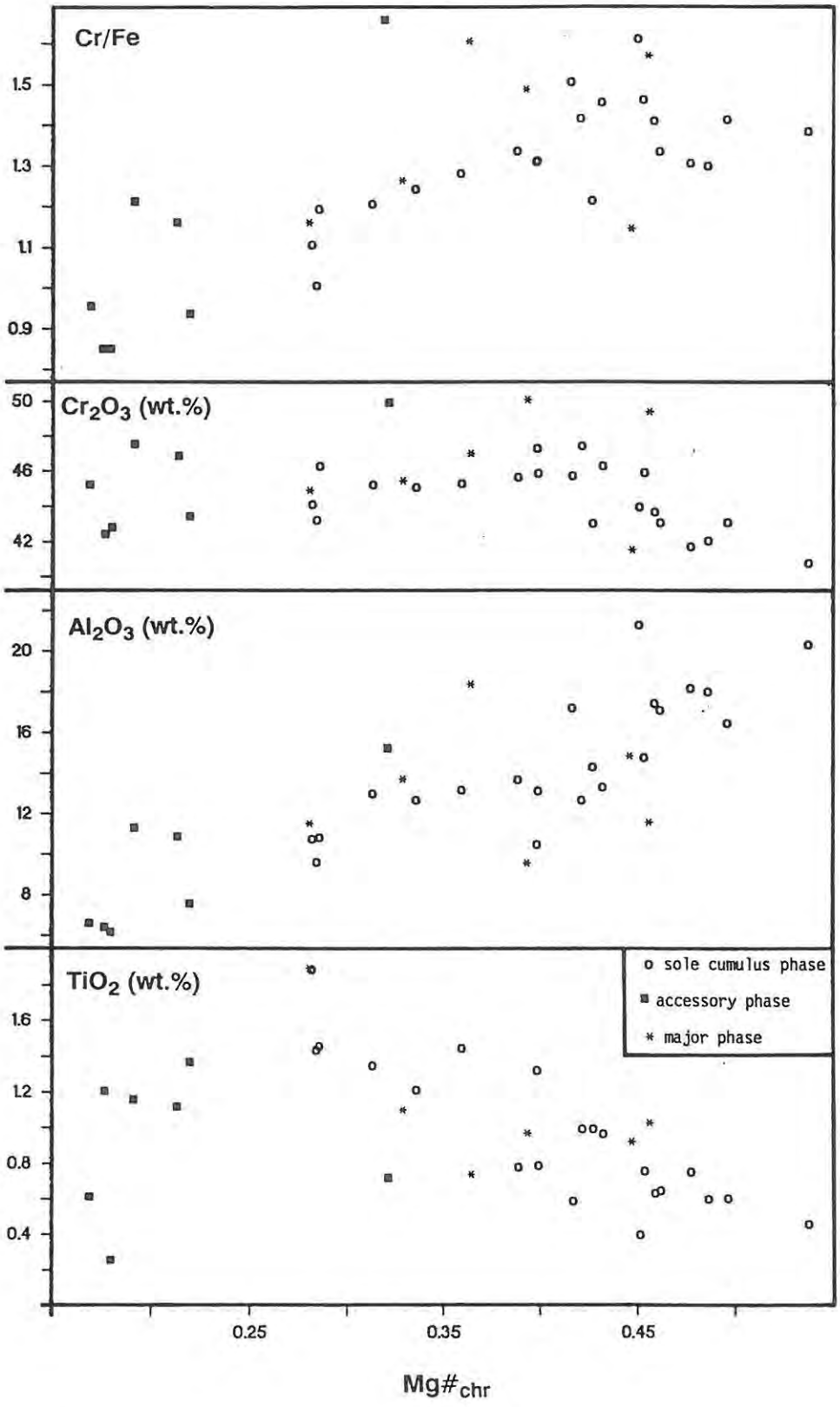

Fig. 76 Chromite mineralogy in the SF-sequence (note scale breaks).

In variation diagrams (Fig. 76) of selected elements against $Mg\#_{chr}$ the following trends can be observed:

a) accessory chr has generally lower $Mg\#_{chr}$ probably attributable to subsolidus re-equilibration with opx or longer residence time in the liquid (Botha, 1987);

b) a positive relationship of the entire chr population with the $Mg\#_{chr}$ is displayed by Al_2O_3 and the Cr/Fe ratio.

c) negative correlations with TiO_2, MnO and Cr/Al ratio (the latter two not depicted) are exhibited;

d) a complex pattern arises from the plot Cr_2O_3 vs. $Mg\#_{chr}$. A general three-field distribution appears to be present. Accessory chr shows wide scatter in its Cr levels, but plots mainly in the left side of the diagram due to its low Mg# (field 1). The second or intermediate field is formed by chr from the UG1- and MG4B-chromitites, while chr from the remaining massive chromitite layers or chromitiferous cumulates plots in the third field.

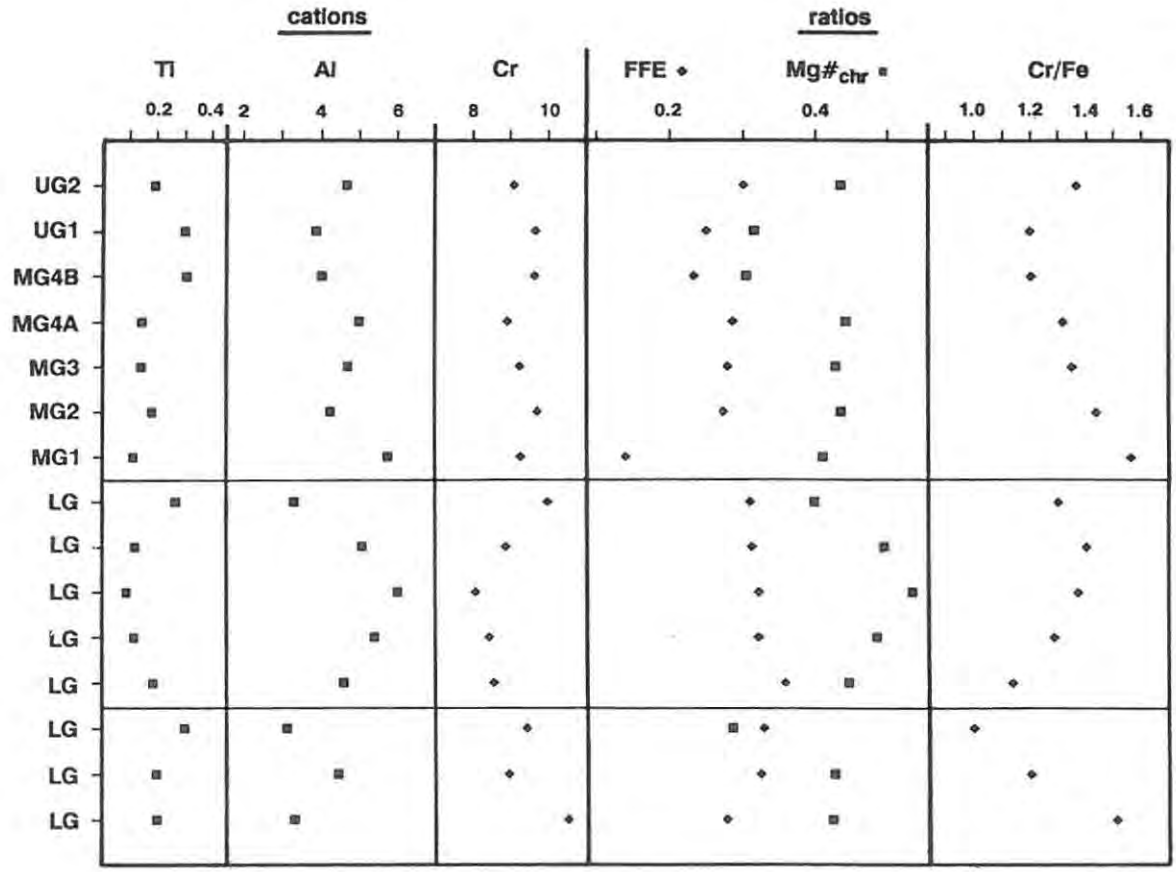

Fig. 77 Compositions of chromitite layers in the SF-sequence.

TABLE 27 Composition of Chromite in the Massive Chromitite Layers (SF-sequence)

Layer:	UG2	UG1	MG4B	MG4A	MG3	MG2	MG1	LG	LG	LG	LG	LG	LG	LG	LG
wt.%															
TiO_2	0.98	1.47	1.50	0.73	0.71	0.91	0.58	1.33	0.61	0.46	0.60	0.95	1.44	1.00	0.99
Al_2O_3	15.27	12.16	12.63	16.41	15.36	13.67	19.02	10.55	16.58	20.43	18.11	15.03	9.68	14.39	10.58
Cr_2O_3	44.33	45.29	45.22	43.60	44.91	46.67	45.65	47.42	43.23	40.92	42.16	41.75	43.31	43.14	49.79
FeO	19.94	24.83	25.26	20.70	21.05	20.72	22.02	22.06	18.60	17.73	19.46	20.62	25.49	21.18	20.82
Fe_2O_3	9.53	9.25	8.58	9.24	9.03	8.65	3.97	10.96	9.35	9.31	10.21	12.76	13.80	11.27	8.87
MnO	0.31	0.35	0.34	0.29	0.33	0.33	0.30	0.33	0.31	0.28	0.32	0.31	0.38	0.32	0.33
NiO	0.14	0.15	0.14	0.14	0.14	0.13	0.09	0.13	0.14	0.15	0.12	0.13	0.09	0.05	0.18
MgO	9.76	6.43	6.22	9.27	8.91	9.00	8.64	8.22	10.31	11.56	10.36	9.38	5.69	8.88	8.67
Total	100.26	99.94	99.87	100.37	100.44	100.07	100.27	100.99	99.11	100.84	101.34	100.92	99.86	100.24	100.22
cations (based on 32 oxygens):															
Ti	0.1914	0.2994	0.3046	0.1421	0.1398	0.1796	0.1115	0.2650	0.1185	0.0871	0.1148	0.1848	0.2976	0.1963	0.1994
Al	4.6668	3.8617	4.0088	4.9932	4.7004	4.2320	5.7454	3.3072	5.0678	6.0073	5.3972	4.5896	3.1346	4.4463	3.3215
Cr	9.0895	9.6605	9.6405	8.9250	9.2481	9.6991	9.2640	9.9689	8.8698	8.0712	8.4305	8.5523	9.4137	8.9387	10.4999
Fe^{2+}	4.3240	5.6038	5.6986	4.4832	4.5860	4.5549	4.7282	4.9050	4.0367	3.7001	4.1162	4.4691	5.8603	4.6431	4.6472
Fe^{3+}	1.8609	1.8789	1.7414	1.7976	1.7720	1.7098	0.7674	2.1938	1.8253	1.7474	1.9426	2.4886	2.8564	2.2223	1.7798
Mn	0.0673	0.0807	0.0776	0.0625	0.0719	0.0724	0.0648	0.0733	0.0673	0.0586	0.0685	0.0674	0.0875	0.0716	0.0734
Ni	0.0292	0.0330	0.0299	0.0286	0.0294	0.0281	0.0182	0.0278	0.0293	0.0308	0.0245	0.0263	0.0192	0.0108	0.0376
Mg	3.7709	2.5819	2.4986	3.5677	3.4525	3.5242	3.3004	3.2589	3.9852	4.2976	3.9055	3.6220	2.3306	3.4708	3.4411
n	6	5	2	3	2	3	3	1	1	1	1	1	1	1	2
a	24	28	10	15	10	14	13	5	5	5	5	5	6	5	10
cationic ratios:															
Cr/Al	1.9477	2.5016	2.4049	1.7874	1.9675	2.2919	1.6124	3.0143	1.7502	1.3436	1.5620	1.8634	3.0032	2.0104	3.1612
$Mg\#_{chr}$	0.4360	0.3154	0.3048	0.4431	0.4295	0.4362	0.4111	0.3992	0.4968	0.5374	0.4869	0.4477	0.2845	0.4278	0.4254
FFE	0.3009	0.2511	0.2341	0.2862	0.2787	0.2729	0.1396	0.3090	0.3114	0.3208	0.3206	0.3577	0.3277	0.3237	0.2769
Cr/(Cr + Al)	0.6608	0.7144	0.7063	0.6412	0.6630	0.6962	0.6172	0.7509	0.6364	0.5733	0.6097	0.6508	0.7502	0.6678	0.7597
weight ratio of metals:															
Cr/Fe	1.37	1.21	1.21	1.32	1.36	1.44	1.57	1.31	1.41	1.38	1.30	1.14	1.01	1.21	1.52
standard deviation:															
wt.%															
TiO_2	0.1532	0.2258	0.3975	0.0576	0.0763	0.1044	0.1367								0.0294
Al_2O_3	0.7112	1.0683	1.1006	1.9126	2.1646	0.8770	1.7173								1.0181
Cr_2O_3	0.7832	0.6918	0.2791	1.6218	1.0959	0.6400	1.2225								0.3408
FeO	0.3538	0.9347	0.8624	1.0644	0.8508	0.4866	1.2034								0.8269
Fe_2O_3	0.8139	0.6172	0.3592	0.2479	1.0084	0.3797	1.3756								0.1477
MnO	0.0163	0.0316	0.0024	0.0179	0.0203	0.0025	0.0123								0.0037
NiO	0.0165	0.0260	0.0037	0.0197	0.0225	0.0244	0.0371								0.0005
MgO	0.2706	0.6459	0.5006	0.9589	0.7103	0.2927	0.8064								0.7666

Notes: 1) notation after Cousins and Feringa (1964)
2) $Mg\#_{chr}$: cationic ratio of $Mg/(Mg + Fe^{2+})$
3) FFE : cationic ratio of $Fe^{3+}/(Fe^{3+} + Fe^{2+})$
4) Cr/Fe : weight ratio of Cr metal to Fe metal
5) n : number of samples
a : number of analyses
6) standard deviation calculated only where sample populations exceed one; see Appendix for intra-sample standard deviations

Because of the small number of samples with accessory chr, computed average compositions of the chromitite layers (Table 27) were chosen to show cryptic variations with height. In Fig. 77 the compositional variations of the chromitite layers of the SF-sequence are illustrated:

a) abrupt compositional changes break the different chromitite layers up into three groups. Group 1 comprises the lower three layers at 440.67, 453.28 and 475.23 m. Group 2 is made of the remaining LG-chromitite layers below the MG1-chromitite and the MG- and UG-chromitites fall into group 3.

b) through the sequence of chromitite layers as a whole no general trend can be observed.

c) a comparison with the massive chromitite layers in the NG-sequence (although hampered by the poor development of the MG1-chromitite in the NG-sequence) shows that both groups "3" display similar compositional ranges, but generally contrasting trends with height, while groups "2" and "1" are not comparable. It appears that the group "3" chromitites in the SF-sequence are generally more evolved with regard to $Mg\#_{chr}$, but contain more Cr_2O_3. These differences might be explained by the significant differences in the underlying cumulate pile as well as the immediate footwall. Smaller proportions of opx components in the S-liquid might cause the lower $Mg\#_{chr}$ but the consequently poor development of pyroxenites in the CZ of the SF-sequence also causes less depletion of Cr in the S-liquid.

The Cr/Fe ratio of the chromitite layers in group 3 shows a regular decrease up to the UG1-chromitite, while the UG2-chromitite is characterized by an higher ratio. In contrast to this pattern the $Mg\#_{chr}$ increases with height. However, the UG1- and MG4B-chromitites, similar in composition, differ significantly in most parameters from the other chromitite layers, thus exhibiting major deflections from the overall trends in group 3. The chromitites below the MG1-chromitite exhibit a wide compositional range, whereas the reversals seen above the layer at 440.67 m represent justification for grouping the lowermost three chromitite layers together.

11.2.4. Plagioclase

Average compositions of postcumulus as well as cumulus pla in 39 samples were calculated using 162 analyses; the results are listed in in the Appendix. Zonation was not investigated, although it is evident in some thin sections. The ranges of compositions are:

	cumulus	postcumulus	
SiO_2	47.4 - 49.4	47.3 - 54.5	wt.%
Al_2O_3	32.2 - 33.4	29.3 - 34.5	
FeO	0.2 - 0.3	0.1 - 0.3	
CaO	15.5 - 17.3	11.3 - 15.3	
Na_2O	1.9 - 2.7	3.0 - 5.4	
K_2O	0.1 - 0.2	0.0 - 0.3	
An	75.4 - 80.9	53.0 - 83.4	

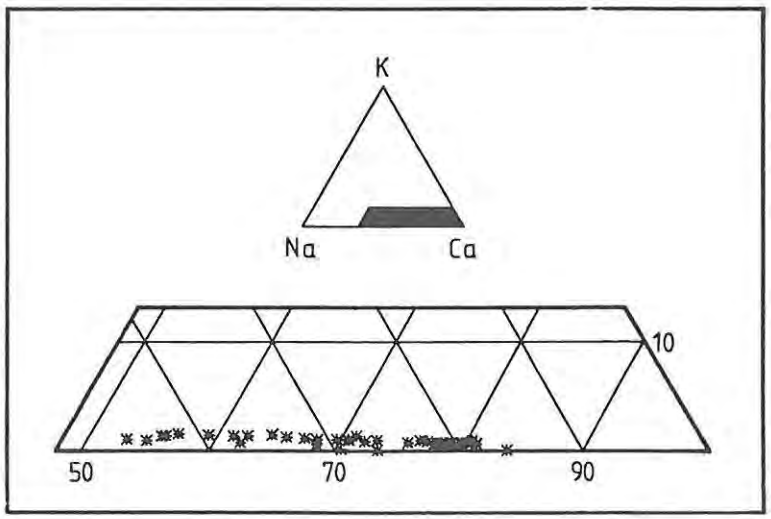

Fig. 78 Compositional range of plagioclase in the SF-sequence.

In the triangular diagram showing K, Na and Ca (cationic %) all datum points plot roughly parallel to the base line in the labradorite and bytownite fields (Fig. 78). Cumulus pla clusters extremely close together ($An_{75.4}$ - $An_{80.9}$) regardless of stratigraphic position. Sample SF-268.41, a pyroxenite immediately below the MG1-chromitite, yielded anomalously high An contents ($An_{82.1}$ - $An_{86.3}$), which can possibly be ascribed to a higher degree of alteration noticeable under the microscope.

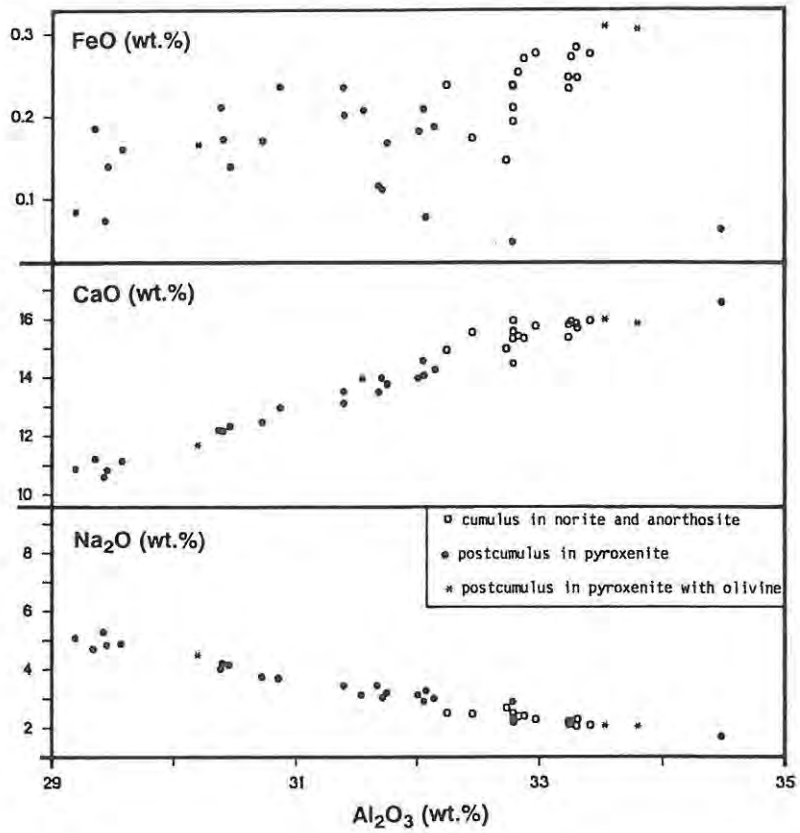

Fig. 79 Plagioclase mineralogy in the SF-sequence (note scale breaks).

Interelement relationships are depicted in Fig. 79 with Al_2O_3 (wt.%) as abscissa. The FeO concentrations appear to be positively correlated with Al. However, the relationship is weak with scatter in the datum points of postcumulus pla and clustering in cumulus pla. Because of the repeated intercalations of pyroxenite with norite or anorthosite a general trend with stratigraphic height is not detectable (Fig. 73). The intrasample variation in cumulus pla is, as expected, small while within the postcumulus variety the range increases to 37 % in An molecule (sample SF-250.88: $An_{32.1}$ - $An_{69.3}$).

11.3. Whole-rock Geochemistry

The whole-rock data (51 samples), analysed by Rocklabs using conventional XRF-techniques, cover all major lithologies apart from chromitites; the analyses are listed in the Appendix (NiO and Cr_2O_3 are included as minor elements and Fe_2O_3 is stated as FeO*0.1). From the whole-rock data CIPW-norms were calculated using the same program as for the NG-samples.

In the normative anorthite - forsterite - quartz triangle (Fig. 80) the major element distribution is summarized. All samples plot roughly parallel the tieline enstatite - anorthite with a slight shift into the left field apart from one sample (SF-481.70). Also in Fig. 80 is shown the plot of normative feldspar (an + ab + or) in wt.% versus Al_2O_3 (wt.%) used by Eales et al. (1988) to classify pyroxene - pla cumulates. The levels of Al in the pyroxenites are noteworthy. While Eales et al. (op.cit.) defined the boundary between pyroxenites and melanorites at 6.5 wt.% Al_2O_3 in pyroxenites in the Union Section area, pyroxenites in the SF-sequence have up to 8.8 wt.% Al_2O_3. Linear regression yields the expression

$$FSP = 3.05\ Al_2O_3 + 0.70 \quad (cc: 0.999;\ n=51),$$

which is almost identical to that found by Eales et al. (op.cit.). A conspicuous gap appears between the pyroxenites and norites of the diagram, which points to the absence of melanorite.

The ranges of composition of the major rock types are listed in Table 28. The Sr levels (see Figs. 81 and 82) are remarkably constant for anorthosites apart from sample SF-461.60, which might be caused by its stratigraphic position in the lower part of the sequence.

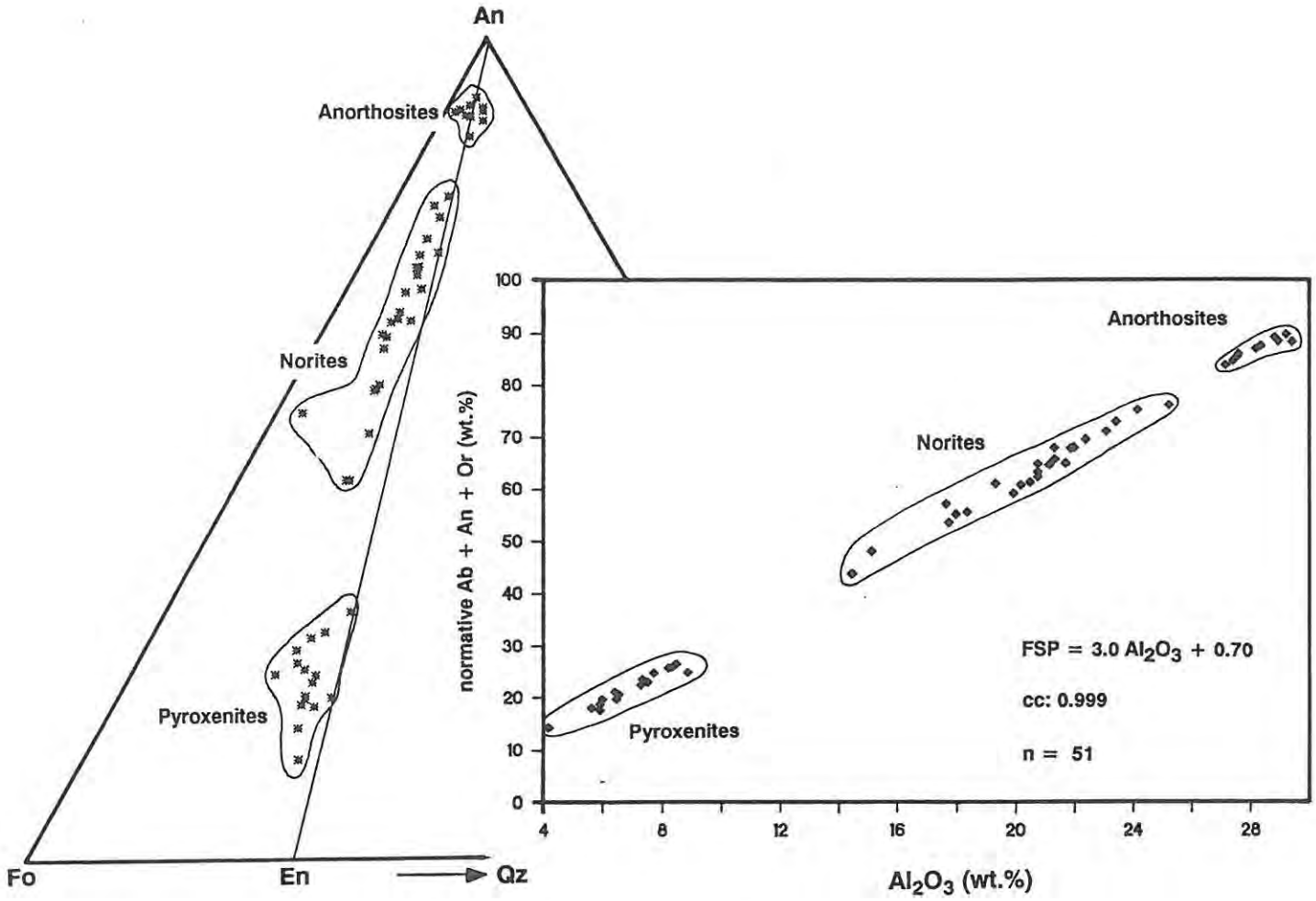

Fig. 80 Normative compositions of whole-rock samples (SF-sequence) in the system An - Fo - Q, and plot of normative feldspar against whole-rock Al_2O_3.

TABLE 28 Range of Compositions of the Major Lithologies in the SF-sequence

Lithology:	Anorthosite	Norite	Pyroxenite
wt.%			
SiO_2	47.13 - 50.63	47.14 - 51.23	47.85 - 52.41
TiO_2	0.05 - 0.15	0.05 - 0.21	0.12 - 0.49
Al_2O_3	27.16 - 29.38	14.45 - 25.24	4.17 - 8.83
FeO	1.68 - 3.05	3.49 - 8.80	8.43 - 11.89
Fe_2O_3	0.17 - 0.30	0.35 - 0.88	0.84 - 1.19
MnO	0.02 - 0.06	0.08 - 0.20	0.18 - 0.27
MgO	2.06 - 3.59	5.91 - 18.37	21.62 - 27.34
CaO	13.36 - 14.19	7.27 - 12.07	2.81 - 5.29
Na_2O	1.69 - 2.53	0.98 - 2.15	0.09 - 0.87
K_2O	0.17 - 1.07	0.06 - 0.61	0.02 - 0.25
P_2O_5	0.03 - 0.07	0.02 - 0.06	0.01 - 0.09
Cr_2O_3	0.00 - 1.58	0.08 - 2.74	0.41 - 7.54
NiO	0.00	0.00 - 0.05	0.05 - 0.12
$Mg\#_{WR}$	0.6190 - 0.7704	0.6984 - 0.8490	0.7769 - 0.8465
Sr (ppm)	397 - 450	160 - 394	33 - 106

Notes: 1) $Mg\#_{WR}$: $Mg/(Mg + Fe^{2+})$

2) Analytical data from Rocklabs

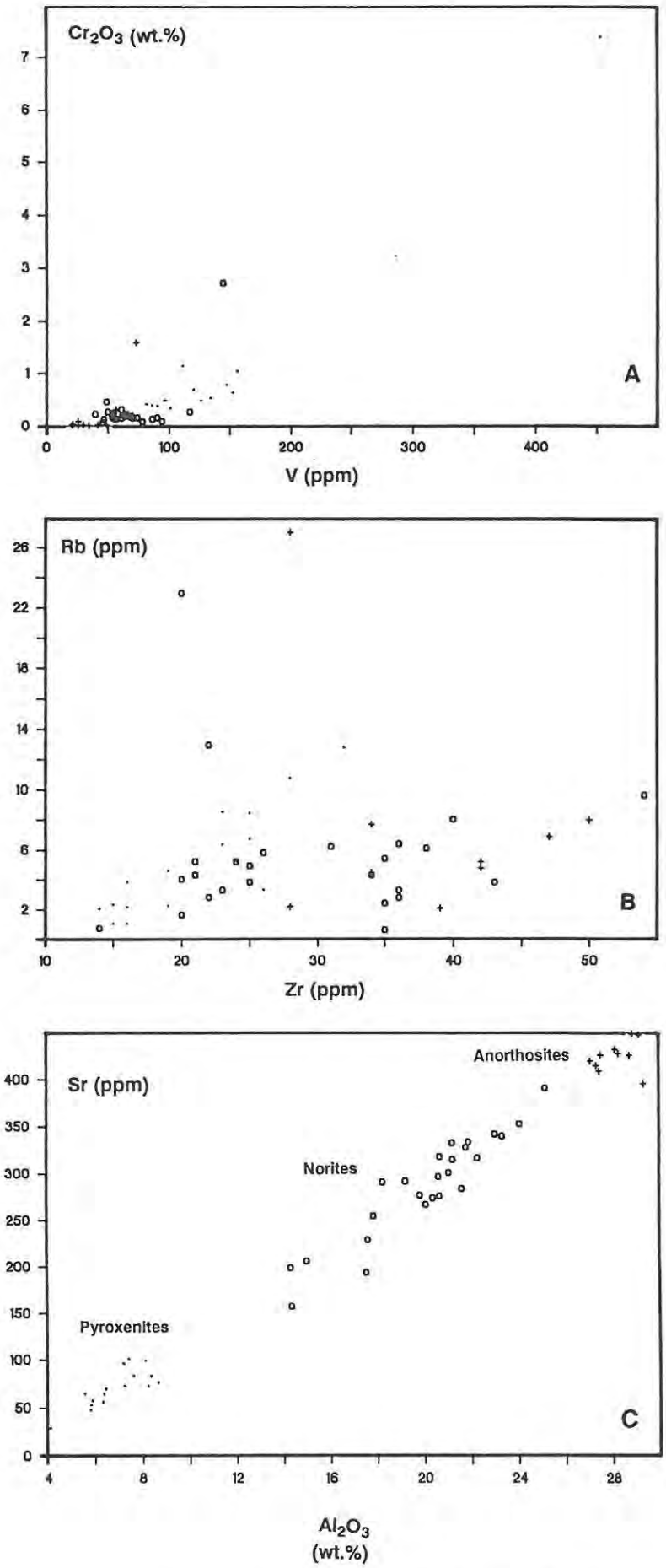

Fig. 81 Interelement relationships of A) Cr_2O_3 vs. V; B) Rb vs. Zr, and C) Sr vs. Al_2O_3 (all whole-rock data, SF-sequence).

The relationship between Sr (ppm) and Al_2O_3 (wt.%) is illustrated in Fig. 81C; the following equations in the form y = mx + c, where y = Sr, and x = Al_2O_3, are derived by linear regression:

Sample	Number of Samples	m	c	cc
all	51	16.4	-39.4	0.983
all norites	25	18.6	-85.8	0.936
norites above the MG2-chromitite	15	16.0	-23.9	0.927
norites below the MG2-chromitite	10	17.4	-77.5	0.912
all pyroxenites	16	12.5	-11.4	0.796

For Cr_2O_3 (wt.%) versus V (ppm) the expression

$Cr_2O_3 = 0.015\ V - 0.752$ (cc: 0.917; n=51)

is obtained for all datum points; and for all pyroxenites linear regression yields the equation

$Cr_2O_3 = 0.018\ V - 1.412$ (cc: 0.973; n=16).

However, as shown in Fig. 81A the equations found are greatly dependent upon the position of the three V-rich (i.e. chr-rich) samples. In Fig. 81B Rb is plotted against Zr, demonstrating a weak positive relationship between these incompatible elements, or some degree of inaccuracy in the data.

Variations with height are shown in Fig. 82. Although for the upper part of the sequence no microprobe or petrographic samples are available, all whole-rock data are displayed. The Mg# displays a wide spread with well defined trends matching the trend set by the microprobe data, where available (see Fig. 73). The lower part of the sequence is characterized by an increase of the Mg# up to the level of ca. 316 m, just above the uppermost horizon with abundant ol. The overlying interval up to 120 m displays a steady decline of the ratio followed by a reversal culminating at the level of the UG1-chromitite at ca. 70 m. Above this position the

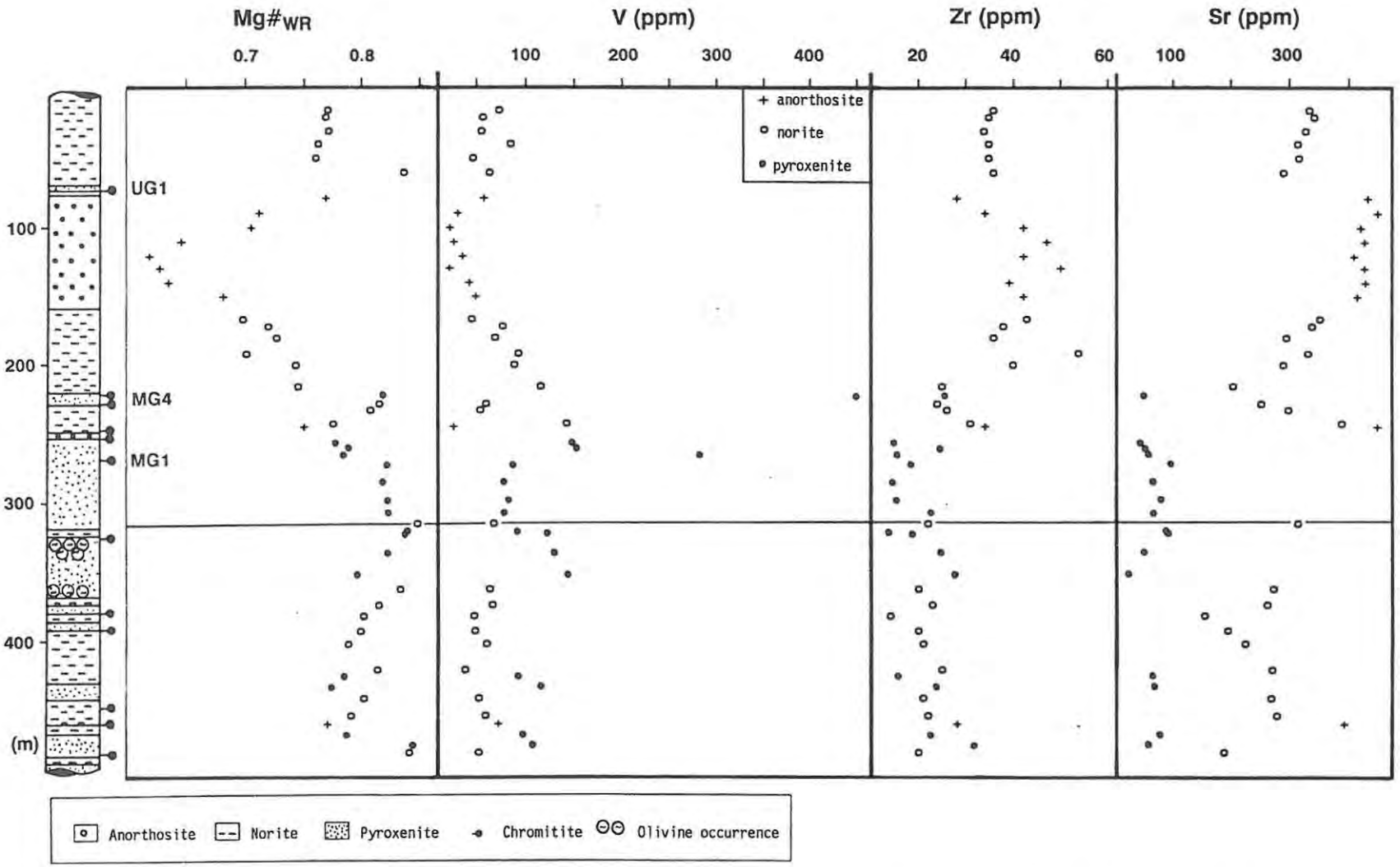

Fig. 82 Selected whole-rock data plotted against stratigraphic height (SF-sequence).

$Mg\#_{WR}$ remains more or less steady after an initial drop. Minor deviations from this general pattern occur between the MG3- and MG4A-chromitites and at the level of the lowermost chromitite intersected at ca. 475 m.

Despite the dependence of the levels of incompatible trace elements on the residual porosity of cumulate rocks, some general conclusions can be drawn from Fig. 82. The Zr levels vary around a value of 23 ppm for all rocks below ca. 216 m, while above this level an average of 38 ppm is obtained for norites and anorthosites, which might point to a generally higher fractionation stage of the cumulates above 216 m. The compatible trace elements V and Sr display contrasting distribution patterns due to their different partition coefficients for the two major phases opx and pla. The partitioning of V into the opx lattice also finds expression in the absolute values in the different rock types:

Lithology	V (ppm)
anorthosite	34
norite	67
pyroxenite	126

However, the effect of copious amounts of chr in the whole-rock sample might also have some influence on this distribution pattern. In contrast, Sr partitions strongly into pla, which is clearly evident in Fig. 82. Pyroxenites (average 76 ppm) show no general trend through the sequence, whilst the Sr distribution in the pla-rich cumulates might indicate a slight general enrichment in the upper part of the SF-sequence. Cu (not depicted)shows no general trend through the entire sequence. The concentrations are independent of the rock type; the average background level is 21 ppm Cu with four samples containing more than 35 ppm and four samples less than 12 ppm. These low levels indicate a paucity of BMS throughout the entire sequence.

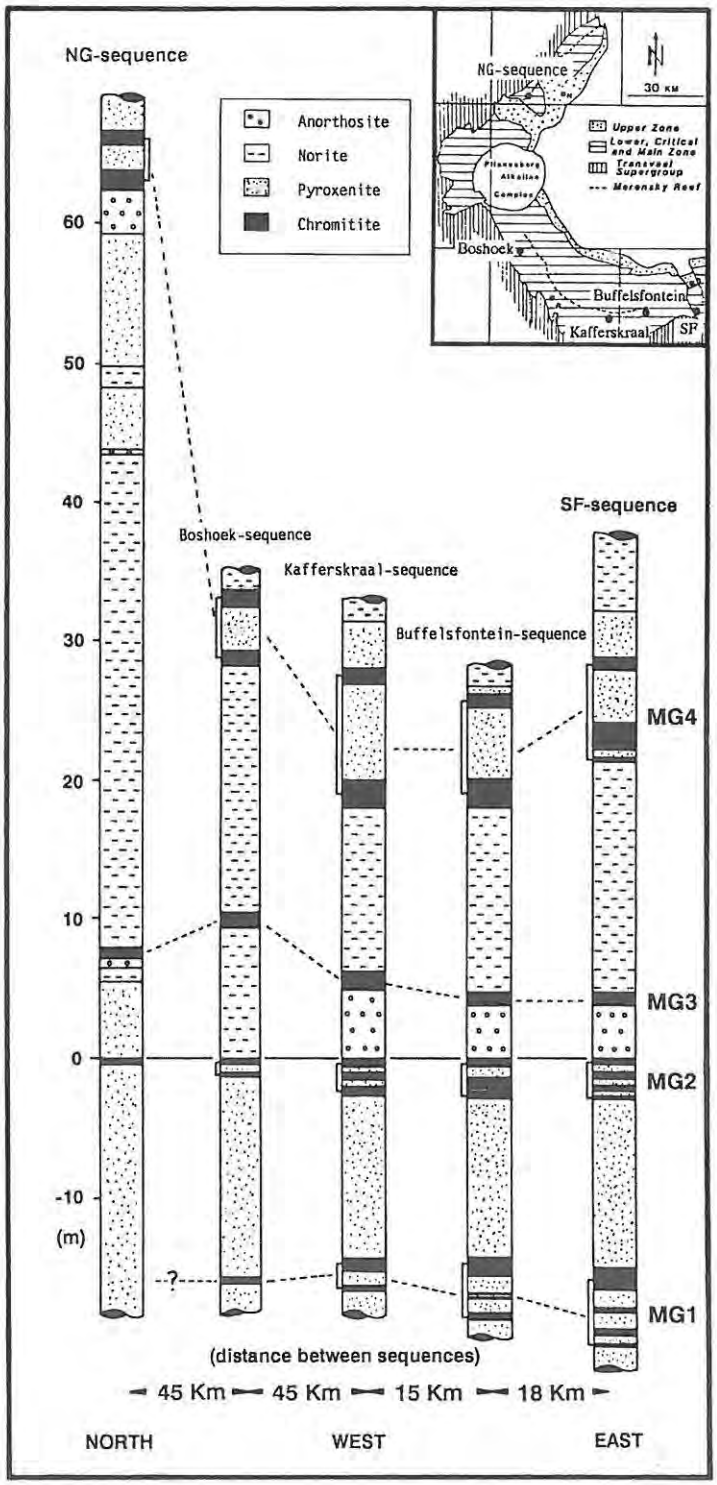

Fig. 83 The MG-chromitites and their variations along strike in the western BIC (Boshoek-, Kafferskraal-, and Buffelsfontein-sequences from Gruenewaldt et al. (1986); note all sequences on the same scale).

11.4. Discussion and Conclusions

Borehole SF-7 has intersected a sequence which is crucial to the understanding of the development of the RLS in the western limb. To the author's knowledge no other borehole covering the deep footwall of the MG1-chromitite in the eastern part of the southern limb of the Western BIC has been recorded or described, and therefore for the first time the cumulate pile below the MG1-chromitite here has been the subject of detailed investigations.

The UG1-chromitite, as well as the MG-chromitite layers, are all well developed and can easily be correlated with sequences further west (Fig. 83). Consequently, the cumulates below the MG1-chromitite (see Fig. 70 and 73) have to be situated in the lCZ. This conclusion is corroborated by the presence of several chromitite layers which are traditionally grouped within the lCZ. The number of layers in the SF-sequence, and their spacing, suggest strongly that most of the LG-chromitites are present (see Fig. 70). However, different host rock lithologies as well as the poor development of these chromitites prevent any meaningful correlation. If this correlation of the cumulates below the MG1-chromitite is correct, then it is significant that cumulus pla can be found ca. 235 m below the accepted lCZ - uCZ-boundary (Fig. 70). Hatton and von Gruenewaldt (1987) reported the presence of pla cumulates with poorly developed chromitite layers in the lCZ in the Brits/Marikana area. Cyclic units in the lCZ of the SF-sequence have the order pyroxenite - norite with or without chromitite layers in their basal part. Despite this intercalation of noritic and pyroxenitic rocks in the lCZ of the SF-sequence, a superimposed overall increase in the $Mg\#_{opx}$, regardless of the lithology, up to the level of the uppermost ol-rich horizon indicates an origin of all cumulates from parental liquids of the U-magma-lineage.

A model for the formation of a cyclic unit in the lCZ of the SF-sequence is suggested by the data. A fractionated derivative (resident liquid) of a primitive liquid crystallized opx - pla cumulates. Mixing of the resident liquid with the fresh magma (with a higher Mg#) triggered copious precipitation of chr leading to the chromitite layers followed by pyroxenite. The poor development of the chromitite layers and the lithological variations of the silicate cumulates in the lCZ of the SF-sequence will be discussed in the next chapter.

CHAPTER 12 : REGIONAL VARIATIONS ALONG STRIKE - A SYNTHESIS

The emphasis of this chapter lies on a comparison of stratigraphy and geochemistry of the NG-sequence with other sequences along strike within the western limb of the BIC, to establish common features as well as significant differences.

12.1. Petrography

No attempt is made to compare textures of individual rock types. It is a justifiable assumption that the common textural features described in Part A are present in the cumulates throughout the complex. Therefore, this section concentrates on two measurable petrographic features, which are grain size and modal compositions.

Two sequences covering the lCZ on the farms Zandspruit and Ruighoek were investigated for grain size variations (Botha, 1987; McDonald, 1967). Though different techniques were applied a comparison should reveal similar trends, if grain size varies systematically in response to processes operating in the entire magma chamber. Local controls might be superimposed and complicate any pattern and interpretation thereof.

Figure 84 shows the grain size distribution within the lCZ of the NG-sequence compared with the results of Botha's work (1987) and McDonald's study (1967). In all three investigations drill core samples were used. McDonald (op.cit.) applied a very similar technique of grain size determination to that in this study, whilst Botha (op.cit.) counted the number of cumulus silicate crystals per cm^3 of rock (crystallinity), i.e. coarse-grained rocks have a low crystallinity. For comparison the reciprocal value of crystallinity is used here. McDonald (1967) described a general decrease from the base of the Ruighoek-sequence (ca. 35 m below the LG1-chromitite) to the bottom of the LG6-chromitite, above which the grain size gradually increases. However, through the entire NG-sequence no general trend is apparent, although a conspicuous decline in grain size below the LG6-chromitite can be observed. The same is evident in the Zandspruit-sequence.

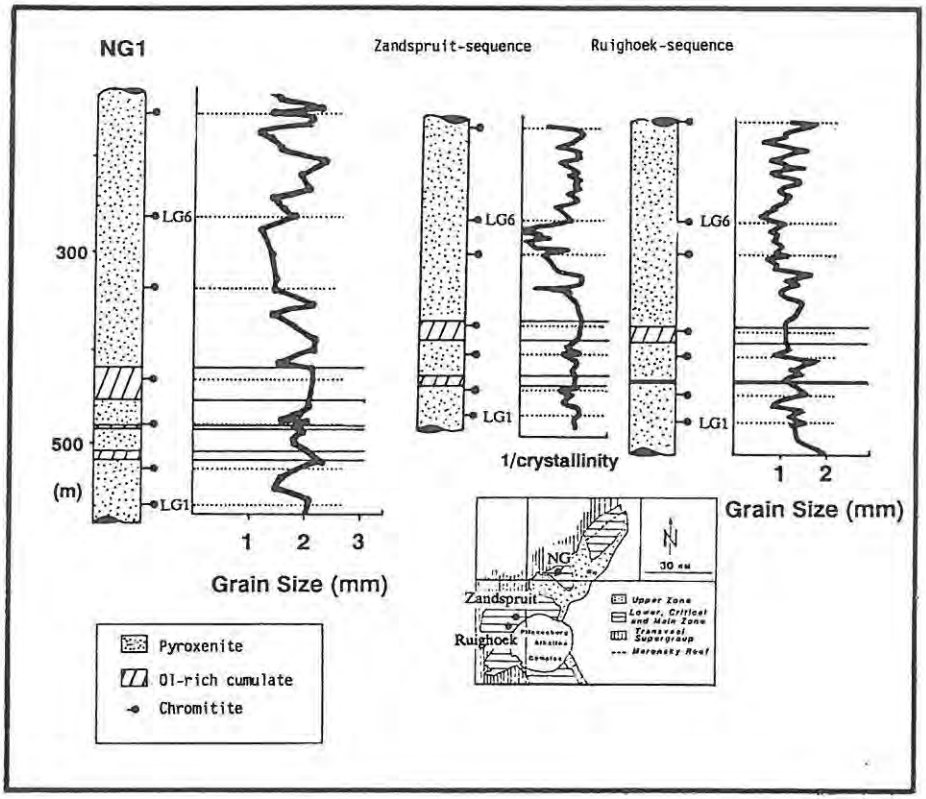

Fig. 84 Grain size variations of opx in NG1 in comparison with the Zandspruit- (Botha, 1987) and Ruighoek- (McDonald, 1967) sequences.

Coarse-grained cumulates appear to be located at similar stratigraphic positions, which are generally juxtaposed to lithological interfaces. The correspondence of the relative grain size variations in spite of the fact that three borehole intersections from widely separated localities were studied and different analytical methods used, indicates that crystal growth was largely controlled by conditions operating contemporaneously on a regional scale. It is an interesting feature that the cumulates in the NG-sequence appear to be generally coarser-grained than their counterparts further south (Ruighoek-sequence). This might point to slightly higher temperatures at Union Section, if the temperature - grain size relationship of Fig. 55 is applied.

Although neither Cameron (1978, 1980) nor McDonald (1967) gave absolute values of modal proportions in tabulated form, the relative variations through the lCZ in the Ruighoek sequence can be gauged from a published diagram.

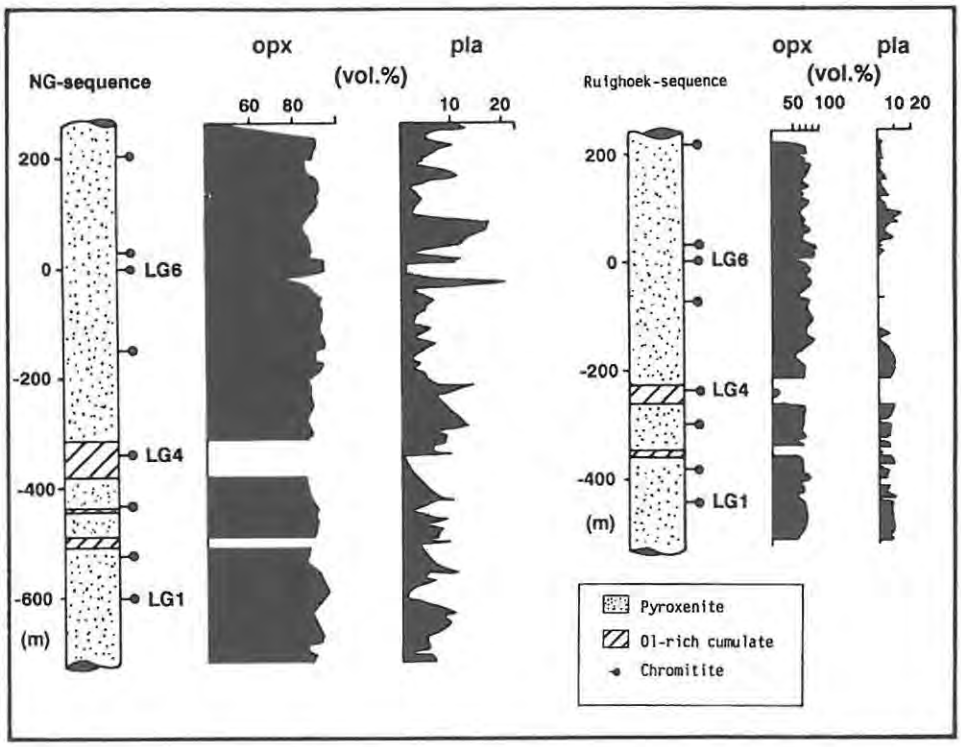

Fig. 85 Comparison of modal compositions in the lCZ of the NG-sequence with the Ruighoek-sequence (McDonald, 1967).

As demonstrated in Fig. 85 the modal compositions of the cumulates in the lCZ of the NG- and Ruighoek-sequences are very similar with good correspondence in limited intervals, especially in the foot- and hangingwall of the LG6-chromitite. The average proportion of opx in both sequences is 89.5 vol.%, while chr ranges in the Ruighoek-sequence between 1 - 2 vol.% and the average in the NG-sequence is 0.8 vol.%. Cameron (op.cit.) calculated bulk modal compositions for the LZ and lCZ in the sequence in the Olifants river trough. His data set was recalculated to fit the newly defined lCZ - LZ-boundary (Eales et al., 1990b), i.e. Cameron's Upper Bronzitite unit was incorporated into the lCZ.

The bulk compositions are tabulated below together with those of the NG-sequence:

	LZ			lCZ	
	Olifants river	NG-sequence		Olifants river	NG-sequence
pla	3.7	4.5	wt.%	4.7	4.9
cpx	0.4	2.1		1.5	2.1
opx	83.9	56.7		89.7	83.8
ol	11.6	34.6		1.3	6.4
chr	0.4	1.4		2.1	1.9
mica	0.0	0.6		0.5	0.5
qtz	0.0	0.1		0.1	0.4
perthite	0.0	0.1		0.0	0.0

The salient features are:

a) pla is present in both sequences in similar proportions;

b) the LZ of the NG-sequence is enriched in modal ol, and hence contains less opx. However, the sum of the ferromagnesian phases (opx, ol, cpx) is very similar (92.5 and 92.3 wt.%, respectively);

c) ol is also more abundant in the lCZ of the NG-sequence;

d) the LZ of the NG-sequence contains more modal chr, while the lCZ in the separate areas shows comparable proportions.

12.2. Geochemistry and Stratigraphy

Only limited whole-rock data are available and therefore emphasis is laid upon mineral chemistry. However, Botha (1987) analysed some silicate cumulates of the lCZ; no significant differences were detected in samples from similar stratigraphic levels in the NG- and Zandspruit-sequences.

For the western BIC FeO concentrations of opx of the lCZ of four sequences are compared. From Fig. 86 it is evident that the general trends in the northwestern sequences are very similar: a decline in FeO up to the level of the LG4-chromitite is followed by an irregular but steady increase in FeO above.

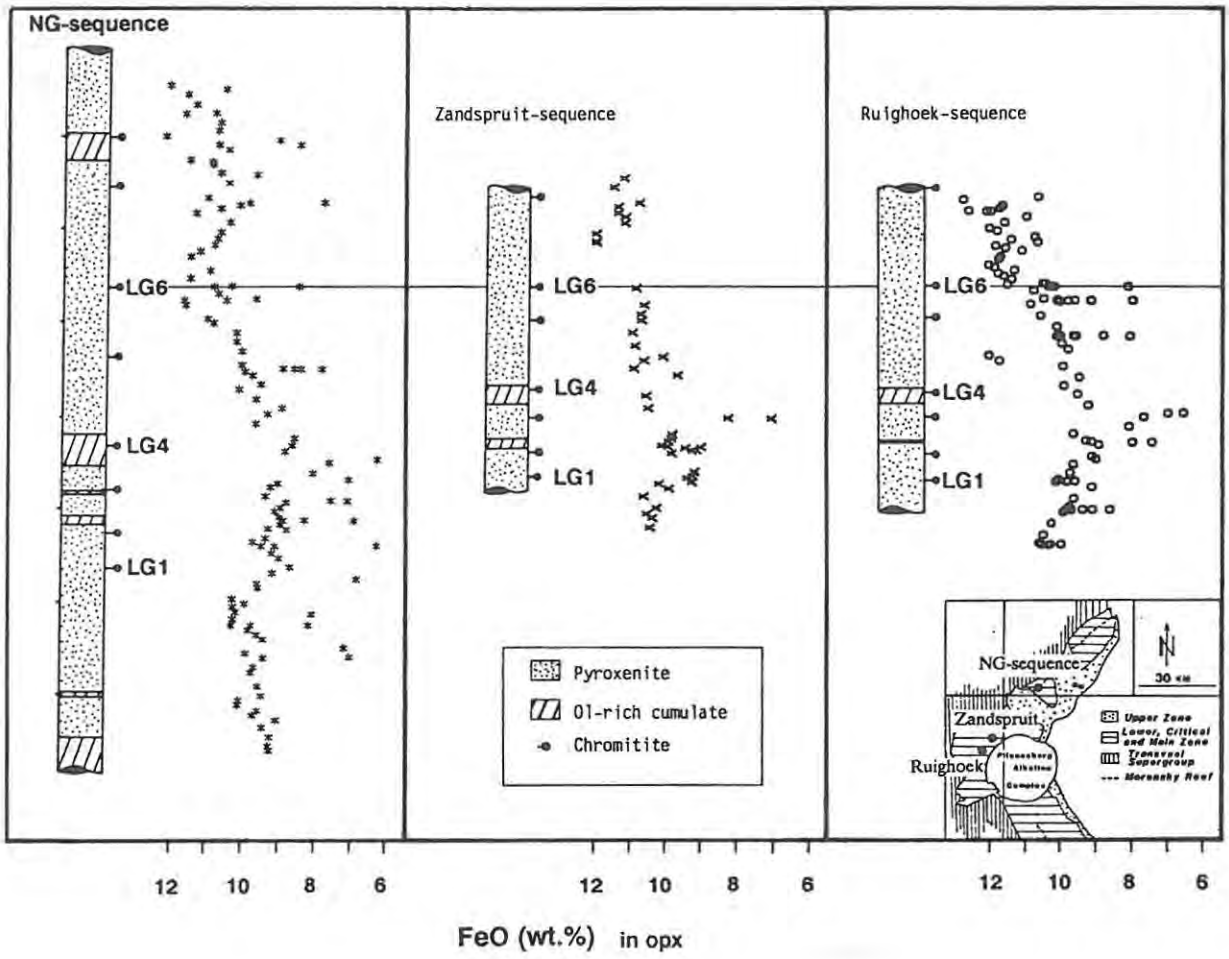

Fig. 86 Comparison of orthopyroxene compositions of the NG-sequence with those from the Zandspruit- (Botha, 1987) and Ruighoek- (McDonald, 1967) sequence. (Datum: LG6-chromitite).

In the SF-sequence (not depicted; see Fig. 73) a similar pattern can be deduced by the trend of $Mg\#_{opx}$. Although McDonald's data were obtained applying wet chemistry techniques, trends and ranges are similar to those derived from microprobe analyses. Unusually low FeO levels in all sequences are probably caused by subsolidus re-equilibration with chr. Closer examination shows that opx in the lCZ of the NG-sequence is generally poorer in FeO, hence more rich in MgO (or more primitive) than opx of the Zandspruit- or Ruighoek-sequence.

The average FeO concentrations in opx of the lCZ, $Mg\#_{opx}$ and Fo contents of ol are tabulated below:

	opx			ol	
	FeO (wt.%)	$Mg\#_{opx}$		Fo content	
	lCZ	LZ	lCZ	LZ	lCZ
NG	8.80	0.857	0.849	0.858	0.851
Zandspruit	10.38	0.843	0.840	0.840	0.846
Ruighoek	10.19				
KD		0.846	0.844	0.831	0.823
SF	11.04		0.826		0.825

Note: 1) LZ data from Zandspruit are based on 4 opx and 2 ol analyses from Botha (1987).

2) $Mg\#_{opx}$ in the KD-sequence represents lower part of lCZ which displays generally higher values.

A comparison with microprobe data from the sequence in the Olifants River trough (Cameron, 1978, 1980) covering the entire LZ and lCZ reveals remarkable adherence to the same overall pattern. In both sequences $Mg\#_{opx}$ rises with height reaching peak values of ca. 0.88 at the top of the LZ (Harzburgite Subzone, Cameron (op.cit.)). Decline to ratios of ca. 0.84 follows within the succeeding pyroxenites of both sequences, until the ol-rich cumulates within the lCZ (Cameron's C1- and C3-units) are approached. High $Mg\#_{opx}$ (ca. 0.86) are again recorded here. Overall decline in $Mg\#_{opx}$ to 0.81 at the top of the lCZ follows in both sequences.

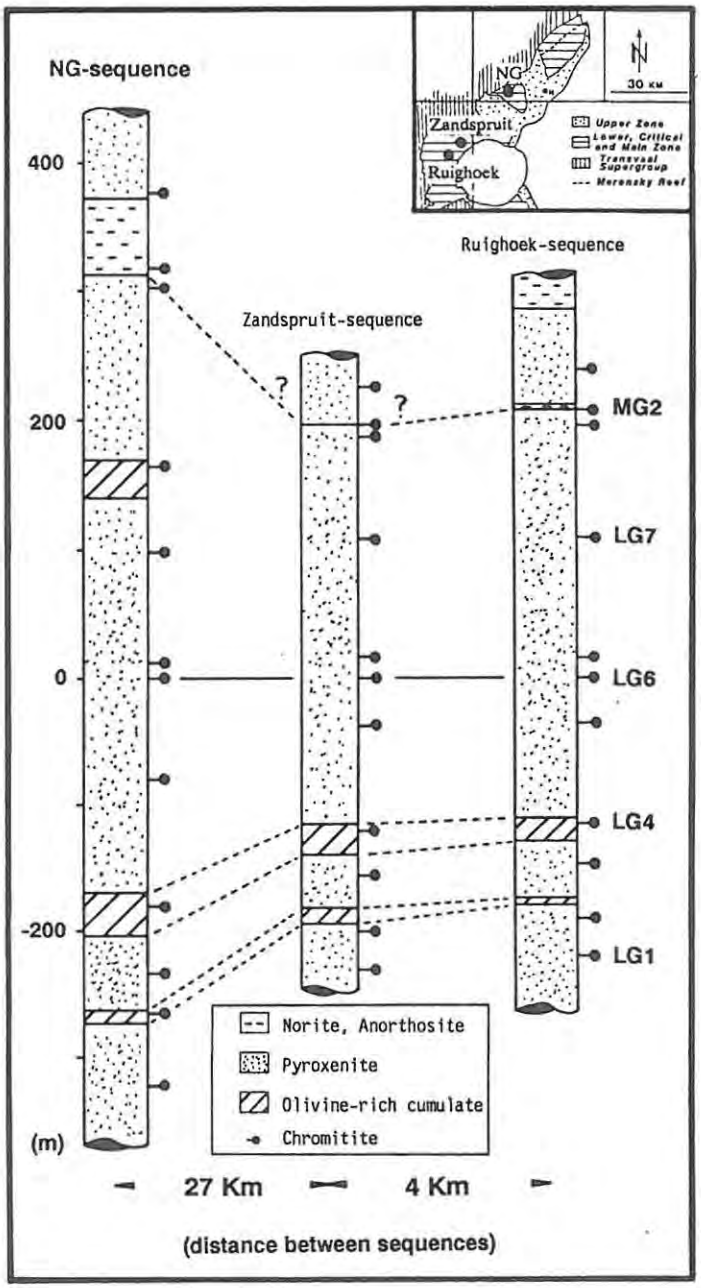

Fig. 87 The lCZ in the NG-sequence in comparison with those from the Zandspruit- (Botha, 1987) and Ruighoek- (McDonald, 1967) sequences. (Note all sequences are in the same scale).

Significant variations along strike in the western compartment can be also detected in the thickness of the ol-rich units in the lCZ (partly shown in Fig. 87):

	upper unit with LG4-chromitite		lower unit	source
NG	34.0	(in m)	18.3	own data
Zandspruit	23.9		11.9	Botha (1987)
Ruighoek	19.5		6.1	McDonald (1967)
Amandelbult	10.7		3.5	von Gruenewaldt and Worst (1986)
Boshoek	8.8		/	Hatton and von Gruenewaldt (1987)
Olifants River	18.2		16.2	Cameron (1980)

In the SF-sequence in the far east of the southern limb the ol-rich cumulates are probably degraded to two horizons (17 m and 5 m thick, respectively), in which ol occurs in minor proportions as laminae or schlieren associated with pyroxenites as well as plagioclase cumulates. Dunites or harzburgites were not intersected in the SF-sequence. The evolved traits of the lCZ in the SF-sequence are also displayed by the average whole-rock composition of pyroxenite, which yields a $Mg\#_{WR}$ of 0.811. This ratio is considerably lower than the one obtained from the average whole-rock value for pyroxenite in the lCZ of the NG-sequence (0.841). A similar decrease in the abundance of ol can also be noticed in the LZ although only limited information is available. The thick ol-rich packages in the LZ of the NG-sequence (Cameron's Harzburgite Subzone) seem to thin out along strike and are probably replaced by pla-opx cumulates.

Other interesting variations along strike are the cumulative thicknesses of the LG- and MG-chromitites:

	LG	MG	remarks and source
NG	3.8	3.7	no MG1-chromitite; own data
Zandspruit	2.9	?	Botha (1987)
Ruighoek	3.2	2.6	no MG3-chromitite; McDonald (1967)
Amandelbult	2.8	3.1	without LG7-chromitite; von Gruenewaldt and Worst (1986)
Boshoek	2.6	3.8	Cousins and Feringa (1964); von Gruenewaldt et al. (1986)
Rustenburg	2.5	3.8	Hatton and von Gruenewaldt (1987)
Kroondal	2.9	4.9	without LG1-chromitite; Fourie (1959)
Kafferskraal	?	7.3	von Gruenewaldt et al. (1986)
Elandsdrift	?	6.8	Bristow (pers.com.)
Buffelsfontein	?	8.2	von Gruenewaldt et al. (1986)
SF	0.6	8.2	own data

(in m)

For locations see Fig. 1.

In summation, the sequences in the northwestern sector are characterized by thick LG-chromitites, while the MG-chromitites are rather poorly developed. This relationship appears to be reversed in the sequences east of the Spruitfontein upfold.

12.3. Discussion and Conclusions

Any model for the petrogenesis of the LZ and lCZ of the western compartment of the BIC is constrained by the following features:

a) zones, subzones, units and individual layers can be traced along strike throughout the entire compartment (a strike length of ca. 200 km). However, significant changes in thickness, lithological composition, modes and mineralogy are evident;

b) the NG-sequence is the most primitive in composition; the thickest ultramafic cumulate pile with abundant ol is associated with high $Mg\#_{opx}$ and Fo contents of ol;

c) the cumulative thickness of the LG-chromitites appears to be highest in the northwestern sector and decreases towards the S and then E, while the MG-chromitites display the opposite trend;

d) in the southern part of the western BIC the lCZ and LZ contain rocks with abundant cumulus pla intercalated with pyroxenite and chromitiferous lithologies.

The increasing abundance of noritic rocks hosting the MG-chromitites and their thickness variations were also noticed by Hatton (1986) and Hatton and von Gruenewaldt (1987), who ascribed this feature to the thickening of the Kaapvaal craton southwards, which supposedly caused a greater degree of contamination and differentiation of a primitive mantle-derived magma.

In 1988 Eales et al. presented a model based on their work in the uCZ (UG2-chromitite - Bastard unit interval) explaining thickening of units and superposition of leucocratic rocks on ultramafic rocks. They concluded that the ol-rich and compositionally more primitive cumulates at Union Section represent a proximal facies with reference to a feeder zone from which primitive liquids intruded as basal flows along the interface between the crystal pile and residual or supernatant liquid. The thickness variations along strike of cyclic units in the uCZ were explained as the result of various degrees of thermal erosion of pla-rich lithologies,

which is strongest close to the feeder zone (proximal facies), and loses influence with distance (distal facies). Thus, the uCZ in proximal facies is depleted in pla-cumulates and therefore thinner, while in distal facies the preservation of pla-cumulate packages led to an increased thickness. Other facies models (Hatton, 1986; Bristow, 1988) related the stratigraphic changes in the different facies primarily to tectonic structures, which caused a compartmentalization of the magma chamber. However, the data presented in the present work show the existence of a gradational change along strike mainly due to fractional crystallization with only minor influence of tectonic features. Hence, it is proposed here that the concept of a proximal and distal facies is also suitable to explain the differences along strike of the LZ and lCZ in the western limb of the complex. The LZ and lCZ in the NG-sequence at Union Section represent a proximal facies, while sequences further south and east are representative of a gradually developing distal facies. The proximity of Union Section to a feeder zone could explain the thickness of the ultramafic cumulates by virtue of a sustained supply of U-type magma, from which the cumulates were derived. With distance from the feeder three processes probably took place:

a) the supply of primitive magma decreased;

b) the primitive liquid fractionated along strike because of the continuous crystallization, loss of heat and accumulation of ferromagnesian phases;

c) mixing with expelled interstitial liquid and/or incorporation of residual liquid, as well as eroded footwall material, shifted the composition of the intruding liquid gradually towards a composition similar to that of the supernatant liquid.

If it is accepted that the parental liquid of the LZ and the lower part of the lCZ is of the U-lineage with the crystallization sequence ol (± chr) - opx - pla - cpx then a four-stage model can be developed to explain the petrogenesis of the cumulate pile up to the lower part of the uCZ in the Western BIC:

Stage 1:

The initial emplacement of a U-magma-type liquid led to the less well understood formation of the MZ, including the marginal norite, with its considerable thickness differences along strike.

Stage 2 :

During multiple replenishing events (manifested in the reversals in the segments 1 and 3 of the NG-sequence as well as in the LZ of the KD-sequence), ultramafic cumulates were accumulated in a proximal facies thinning out with distance from a hypothetical feeder zone in the vicinity of Union Section; hence the telescoping of the LZ in the KD-sequence. In the chamber a layer of supernatant liquid developed. Its composition was greatly dependent upon the type of cumulates deposited at the floor.

Stage 3 :

After continued replenishment (segment 5 of the NG-sequence) the size of the magma chamber had increased by emplacement along a regional unconformity or inhomogeneity within the Transvaal sediments. Close to the feeder zone ultramafic cumulates continued to accumulate (segments 6 and 7 of the NG-sequence) while in the more distal areas the above-described processes shifted the composition of the crystallizing liquid towards the pla - opx cotectic, thus forming noritic rocks in the lCZ of the SF-sequence.

One of the most pronounced facies change of the lCZ and LZ is associated with the Spruitfontein upfold, which might indicate that tectonic features, e.g., folds, might have influenced the development of the different sectors of the magma chamber by impeding the flow of earlier pulses of the U-type, Cr-rich parental liquid of the lCZ. While copious chr precipitation in the proximal facies of the NG-sequence formed thick LG-chromitites, this was hampered by limited volumes of the primitive liquid in the distal facies (SF-sequence) leading to thinly developed chromitites, or even disappearance of LG-chromitite layers.

Stage 4 :

With time the magmatic activity decreased and fractionation became the dominant process in the upper part of the lCZ (segment 8 and lower part of segment 10 in the NG-sequence), apart from a short period leading to the formation of segment 9 in the NG-sequence. This led eventually to the appearance of cumulus pla in the proximal facies, the lCZ/uCZ boundary in the NG-sequence. In the more distal facies, cumulus pla is already well represented in the lCZ, as in the SF-sequence, i.e. it appeared at lower stratigraphic levels.

The distal facies is now characterized by well-developed MG-chromitites (e.g. SF-sequence), which indicate a greater supply of primitive liquid, which implies in turn that regional tectonic structures had lost control over the spreading of the basal flows formed by the replenishing liquid. The greater thickness of the chromitite layers might be attributable to the enhanced compositional contrast of resident and replenishing liquid in the distal facies.

CHAPTER 13 : SUMMARY

In **Part A** of this thesis the lower part of the RLS (as intersected by the boreholes NG1, NG2 and NG3, drilled on the farm Nooitgedacht 406 KQ at Union Section, R.P.M., in the northwestern Bushveld Complex) is described and studied. The study included the following aspects:

a) stratigraphy of the NG-sequence and correlation with other sequences;

b) petrography of the silicate rocks by analyses of modal proportions and grain size variations;

c) mineralogical investigations of the silicate phases and chromite by electron microprobe;

d) whole-rock geochemistry of the silicate cumulates by the XRF-technique;

e) PGE distribution through the NG-sequence and in the massive chromitite layers;

f) Sr isotope variations.

From these studies the following main conclusions are drawn:

Stratigraphy and Correlation:

The stratigraphic succession of the NG-sequence is very similar to that defined by earlier workers. However, there is closer correlation with sequences situated in the northern parts of the complex than with those in the south. The sequence of chromitite layers can be readily correlated with the MG- and LG-chromitites of Cousins and Feringa (1964). The boundary between the LZ and lCZ is re-defined in the present work.

Petrography:

Good correlation was yielded between modal proportions derived from a point-counting technique and the CIPW-norms. The LZ and lCZ vary significantly in their modal compositions. The LZ is dominated by ol-rich rocks, while the lCZ is essentially pyroxenitic with an irregular increase in modal postcumulus plagioclase with height. Significant variations in grain size are generally associated with lithological breaks. Fine-grained pyroxenites are more primitive in composition than coarse-grained varieties.

Mineralogy:

Orthopyroxene shows no zoning structures with regard to $Mg\#_{opx}$, but limited variations in minor elements (Al_2O_3, Cr_2O_3 and TiO_2) do exist. Olivine was found to be in equilibrium with orthopyroxene throughout the sequence. Subsolidus re-equilibration between ferromagnesian phases and spinels occurs only in the immediate vicinity of the interface between contiguous grains. Chromite as an accessory phase shows distinctly different compositions than chromite present in major proportions. Massive chromitite layers display a chemistry coupled with the petrogenetic evolution of the surrounding silicate cumulates. The chromitite layers are geochemically classified into three groups, which are: Group 1 (LG1- to LG4-chromitites), Group 2 (LG5- to LG7-chromitites) and Group 3 (MG2- to MG4-chromitites and the UG1- and UG2-chromitites). Postcumulus plagioclase contains 10 - 15 % less An molecule than the cumulus species. A general increase of An content with height is evident in the CZ, while the values of $Mg\#_{opx}$ show a general decrease. By means of the cryptic variations of $Mg\#_{opx}$ the NG-sequence can be divided into 10 segments, five of which are characterized by reversed fractionation trends. All ferromagnesian phases of the lCZ are enriched in Cr. No significant geochemical break is associated with the lCZ/uCZ boundary, but such a break is established at the LZ/CZ boundary.

Whole-rock geochemistry:

Good agreement exists between whole-rock and microprobe data. Pyroxenites in different stratigraphic intervals differ in their composition in response to the degree of fractionation at this stage of the evolution of the cumulate pile. No evidence was found in support of the addition of an A-type liquid with a contrasting composition and different crystallization order.

PGE distribution:

No significant differences exist between PGE concentration of the silicate cumulates in different stratigraphic intervals. All massive chromitite layers are enriched in PGEs with a distribution pattern corresponding to their spinel chemistry. Chromitite layers of group 1 are enriched in Ru, Os and Ir, while group 2 chromitites contain almost equal proportions of ΣRu and ΣPt. Group 3 chromitite layers display a dominance of Pt, Pd and Rh over Ru, Os and Ir.

Sr isotope data:

Variations in initial $^{87}Sr/^{86}Sr$ ratios are limited apart from one major deviation towards the top of the LZ. No explanation can be offered for these very high values at this stage of the investigation. Unequivocal isotopic evidence for the addition of an A-type liquid during lCZ-times was not found.

All findings lead to a self-consistent model for the evolution of the cumulate pile of the NG-sequence. All cumulates are thought to be derived from liquids of the U-type lineage. The interplay between rejuvenation and fractional crystallization controls the bulk composition of the liquid and its liquidus phases.

From the comparison along strike it is concluded that:

a) grain size variations are comparable in other sequences;

b) bulk modal composition of the lCZ of the NG-sequence is similar to that in the Olifants River trough, while the Lower Zone is distinctly different in modal amounts of orthopyroxene and chromite;

c) the proportion of olivine decreases with distance from the NG-sequence;

d) cryptic variations of orthopyroxene and olivine from similar stratigraphic positions show most primitive compositions associated with the NG-sequence, while a gradational change towards evolved traits takes place with distance from the NG-sequence;

e) the cumulative thicknesses of individual groups of chromitite layers vary along strike. However, the total thickness of LG- and MG-chromitites combined is similar in all sequences;

The conclusions of Part A and B of this thesis lead to a facies model for the evolution of the western BIC, in which the NG-sequence represents a proximal and the SF-sequence a distal facies in terms of a feeder system.

Part B of this work offers descriptions of two other sequences studied and a comparison along strike with other published sequences. The petrography and mineral chemistry were investigated in samples of the KD-sequence, drilled ca. 8 km east of Rustenburg, while whole-rock data are also available for the SF-sequence, situated ca. 55 km east of Rustenburg.

The salient features of the KD- and SF-sequences are:

Stratigraphy and Correlation

The KD-sequence comprises a condensed or telescoped LZ and lCZ succession with a significant decrease in the thickness of ultramafic cumulates. The lCZ in the SF-sequence is characterized by the occurrence of plagioclase - orthopyroxene cumulates together with thin chromitite layers. The MG-chromitites and the UG1-chromitite can be correlated with the sequence of Cousins and Feringa (1964).

Petrography

Both sequences contain intervals with schlieren or pods of olivine. In these intervals partially resorbed plagioclase inclusions are found in both orthopyroxene and olivine.

Mineralogy

Disequilibrium is indicated for coexisting olivine and orthopyroxene in the KD-sequence, but not in the SF-sequence. The MG-chromitites have a compositional range similar to that of their equivalents in the NG-sequence.

Whole-rock Geochemistry

The data yield regression equations similar to those obtained from the NG-data. No evidence was found for the involvement of an A-type liquid in the formation of the lCZ.

REFERENCES

Atkins, F.B. (1969). Pyroxenes of the Bushveld Intrusion, South Africa. *J. Petrol.*, **10**, 222 - 249.

Ballhaus, C.G. (1988). Potholes of the Merensky Reef at Brakspruit Shaft, Rustenburg Platinum Mines: Primary Disturbances in the Magmatic Stratigraphy. *Econ. Geol.*, **83**, 1140 - 1158.

Barnes, Sarah-J., Naldrett, A.J. and Gorton, M.P. (1985). The origin of the fractionation of platinum-group elements in terrestrial magmas. *Chem. Geol.*, **53**, 303 - 323.

Barnes, Stephen J. and Campbell, I.H. (1988). Role of late magmatic fluids in Merensky-type platinum deposits: A discussion. *Geology*, **16**, 488 - 491.

---------- and Naldrett, A.J. (1986). Geochemistry of the J-M Reef of the Stillwater Complex, Minneapolis Adit Area II. Silicate Mineral Chemistry and Petrogenesis. *J. Petrol.*, **27**, 791 - 825.

Botha, M.J. (1987). *Petrology and geochemistry of the lower group chromitites and host rocks on the farm Zandspruit 168 JP, western Bushveld Complex*. M.Sc. thesis (unpubl.), Rhodes University, 216 pp.

Bowen, N.L. (1915). Crystallization differentiation in silicate liquids. *Am. J. Sci.*, **39**, 175 - 191.

Bristow, D.M. (1988). *Visitors Brochure Millsell Chrome Mines*. 5 pp.

Buntin, T.J., Grandstaff, D.E., Ulmer, G.C. and Gold, D.P. (1985). A Pilot Study of Geochemical and Redox Relationships between Potholes and Adjacent Normal Merensky Reef of the Bushveld Complex. *Econ. Geol.*, 80, 975 - 987.

Burger, A.J. and Coertze, F.J. (1973). Radiometric age measurements on rocks from Southern Africa to the end of 1971. *Geol. Surv. S. Afr.*, **Bull. 58**, 46 pp.

Cameron, E.N. (1969). Postcumulus changes in the Eastern Bushveld Complex. *Am. Mineralogist*, **54**, 754 - 779.

---------- (1975). Postcumulus and subsolidus equilibration of chromite and coexisting silicates in the Eastern Bushveld Complex. *Geochim. Cosmochim. Acta*, **39**, 1021 - 1033.

---------- (1977). Chromite in the central sector of the Eastern Bushveld Complex, South Africa. *Am. Mineralogist*, **62**, 1082 - 1096.

---------- (1978). The Lower Zone of the Eastern Bushveld Complex in the Olifants River Trough. *J. Petrol.*, **19**, 437 - 462.

---------- (1980). Evolution of the Lower Critical Zone, Central Sector, and Its Chromite Deposits. *Econ. Geol.*, **75**, 845 - 871.

---------- (1982). The Upper Critical Zone of the Eastern Bushveld Complex - Precursor of the Merensky Reef. *Econ. Geol.*, **77**, 1307 - 1327.

---------- and Desborough, G.A. (1969). Occurrence and Characteristics of Chromite Deposits - Eastern Bushveld Complex, South Africa. *Econ. Geol.*, **Monogr. 4**, 23 - 40.

Campbell, I.H. (1978). Some problems with the cumulus theory. *Lithos*, **11**, 311 - 323.

---------- (1986). A Fluid Dynamic Model for the Potholes of the Merensky Reef. *Econ. Geol.*, **81**, 1118 - 1125.

---------- and Naldrett, A.J. (1979). The influence of silicate : sulfide ratios on the geochemistry of magmatic sulfides. *Econ. Geol.*, **74**, 1503 - 1506.

----------, Naldrett, A.J. and Barnes, S.J. (1983). A Model for the Origin of the Platinum-rich Sulfide Horizons in the Bushveld and Stillwater Complexes. *J. Petrol.*, **24**, 133 - 165.

Campbell, I.H. and Turner, J.S. (1986a). The Influence of Viscosity on Fountains in Magma Chambers. *J. Petrol.*, **27**, 1 - 30.

Campbell, I.H. and Turner, J.S. (1986b). The Role of Convection in the Formation of Platinum and Chromitite Deposits in Layered Intrusions, 236 - 278. *In* Scarfe, C.M., Ed., *Silicate Melts: their Properties and Structure Applied to Problems in Geochemistry, Petrology, Economic Geology and Planetary Geology*. Short Course Handbook, Mineral. Association of Canada, Edmonton, 319 pp.

Campbell, I.H. and Turner, J.S. (1989). Fountains in Magma Chambers. *J. Petrol.*, **30**, 825 -923.

Cawthorn, R.G. and McCarthy, T.S. (1985). Incompatible Trace Element Behaviour in the Bushveld Complex. *Econ. Geol.*, **80**, 1016 - 1026.

Coertze, F.J. (1958). Intrusive Relationship and Ore Deposits in the Western Part of the Bushveld Igneous Complex. *Trans. Geol. Soc. S. Afr.*, **61**, 387 - 392.

---------- (1974). The Geology of the Basic Portion of the Western Bushveld Igneous Complex. *Geol. Surv. S. Afr.*, **Mem. 66**, 148 pp.

Coertze, F.J., Burger, A.J., Walraven, F., Marlow, A.G. and McCaskie, D.R. (1978). Field relations and age determinations in the Bushveld Complex. *Trans. Geol. Soc. S. Afr.*, **81**, 1 - 11.

---------- and Schumann, F.W. (1962). The Basic Portion and Associated Minerals of the Bushveld Igneous Complex North of Pilanesberg. *Geol. Surv. S. Afr.*, **Bull. 38**, 48 pp.

Cousins, C.A. (1959). The Structure of the Mafic Portion of the Bushveld Igneous Complex. *Trans. Geol. Soc. S. Afr.*, **62**, 179 - 189.

---------- and Feringa, G. (1964). The Chromite Deposits of the Western Belt of the Bushveld Complex, 183 - 202. *In* Haughton, S.H., Ed., *The geology of some ore deposits in Southern Africa.* Vol. II. Geological Society of South Africa, Johannesburg, 739 pp.

Davies, G. and Tredoux, M. (1985). Platinum-group Element and Gold Contents of the Marginal Rocks and Sills of the Bushveld Complex. *Econ. Geol.*, **80**, 838 - 848.

Deer, W.A., Howie, P.A. and Zussman, J. (1966). *An Introduction to the Rock Forming Minerals.* Longman Group Limited, London, 528 pp.

---------- (1978). *Rock forming minerals.* Vol.2a, Single chain silicates. Longman Group Limited, London - New York, 668 pp.

---------- (1982). *Rock forming minerals.* Vol.1a, Orthosilicates. Longman Group Limited, London - New York, 919 pp.

De Klerk, W.J. (1982). *The geology, geochemistry and silicate mineralogy of the upper critical zone of the north-western Bushveld complex, at Rustenburg Platinum Mines, Union Section.* M.Sc. thesis (unpubl.), Rhodes University, 210 pp.

De Villiers, J.S. (1970). The structure and the petrology of the mafic rocks of the Bushveld Complex south of Potgietersrust. *Geol. Soc. S. Afr.*, **Spec. Publn. 1**, 23 - 35.

Dietz, R.S. (1963). Vredefort Ring - Bushveld Complex impact event and lunar maria (abstr.). *Geol. Soc. Am.*, **Spec. Pap. 73**, 35 pp.

Eales, H.V. (1987). Upper Critical Zone Chromitite Layers at R.P.M. Union Section Mine, Western Bushveld Complex, 144 - 168. *In* Stowe, C.W., Ed., *Evolution of chromium ore fields.* Van Nostrand Reinhold Company inc., Stroudsburg, Pennssylvania, 340 pp.

----------, Reynolds, I.M. and Gouws, D.A. (1980). The spinel-group minerals of the central Karoo tholeiitic province. *Trans. Geol. Soc. S. Afr.*, **83**, 243 - 253.

---------- and Reynolds, I.M. (1986). Cryptic Variations within Chromitites of the Upper Critical Zone, Northwestern Bushveld complex. *Econ. Geol.*, **81**, 1056 - 1066.

----------, Marsh, J.S., Mitchell, A.A., De Klerk, W.J., Kruger, F.J. and Field, M. (1986). Some geochemical constraints upon models for the crystallization of the upper critical zone - main zone interval, north-western Bushveld complex. *Mineralog. Mag.*, **50**, 567 - 582.

----------, Field, M., De Klerk, W.J. and Scoon, R.N. (1988). Regional trends of chemical variation and thermal erosion in the Upper Critical Zone , western Bushveld complex. *Mineralog. Mag.*, **52**, 63 - 79.

----------, De Klerk, W.J., Butcher, A.R. and Kruger, F.J. (1990a). The cyclic unit beneath the UG1 chromitite (UG1FW unit) at RPM Union Section Platinum Mine - Rosetta Stone of the Bushveld Upper Critical Zone?. *Mineralog. Mag.*, **54**, 23 - 43.

----------, De Klerk and Teigler, B. (1990b). Evidence for magma mixing processes within the Critical and Lower Zones of the northwestern Bushveld Complex. *Chem. Geol.*, **88**, in press.

Ferguson, J. and Botha, E. (1963). Some Aspects of Igneous Layering in the Basic Zones of the Bushveld Complex. *Trans. Geol. Soc. S. Afr.*, **66**, 259 - 278.

Feringa, G. (1959). The Geological Succession in a Portion of the North-Western Bushveld (Union Section) and its Interpretation. *Trans. Geol. Soc. S. Afr.*, **62**, 219 - 232.

Field, M. (1987). *The petrology and geochemistry of the upper critical zone of the Bushveld Complex at Amandelbult Section of Rustenburg Platinum Mines Ltd., Northwestern Transvaal, South Africa.* M.Sc. thesis (unpubl.), Rhodes University, 129 pp.

Fisk, M.R. and Bence, A.E. (1980). Experimental crystallization of chrome spinel in FAMOUS basalt 527-1-1. *Earth Plan. Sci. Lett.*, **48**, 111 - 123.

Fourie, G.P. (1959). The chromite deposits in the Rustenburg area. *Geol. Surv. S. Afr.*, **Bull. 27**, 45 pp.

Haikney, S. (1990). *The nature of Mg-rich Dunites in the Western Bushveld Complex.*, M.Sc. thesis (unpubl.), Rhodes University., in prep.

Hall, A.L. (1932). The Bushveld Igneous Complex of the Central Transvaal. *Geol. Soc. S. Afr.*, **Mem. 28**, 544 pp.

Hamilton , P.J. (1977). Sr Isotope and Trace Element Studies of the Great Dyke and Bushveld Mafic Phase and their Relation to Early Proterozoic Magma Genesis in South Africa. *J. Petrol.*, **18**, 28 - 52.

Harmer, R.E. and Sharpe, M.R. (1985). Field Relations and Strontium Isotope Systematics of the Marginal Rocks of the Eastern Bushveld Complex. *Econ. Geol.*, **80**, 813 - 837.

Hatton, C.J. (1986). Regional Variations in the Middle Group of chromitite layers, Bushveld Complex (abstr.), 595 - 598. In *Extended Abstracts Geocongress '86*. Geological Society of South Africa, Marshalltown, 1056 pp.

Hatton, C.J. and Von Gruenewaldt, G. (1987). The geological setting and petrogenesis of the Bushveld chromitite layers, 109 - 143. *In* Stowe, C.W., Ed., *Evolution of chromium ore fields*. Van Nostrand Reinhold Company inc., Stroudsburg, Pennssylvania, 340 pp.

Henderson, P. (1975). Geochemical indicator of the efficiency of fractionation of the Skaergaard intrusion, east Greenland. *Mineral. Mag.*, **40**, 285 - 291.

Hess, H.H. (1960). Stillwater Igneous Complex, Montana : A quantitative mineralogical study. *Geol. Soc. Am.*, **Mem. 80**, 230 pp.

Hill, R. and Roeder, P.L. (1974). The crystallization of spinel from basaltic liquid as a function of oxygen fugacity. *J. Geol.*, **82**, 709 - 729.

Huppert, H.E. and Sparks, R.S.J. (1980). The Fluid Dynamics of a Basaltic Magma Chamber Replenished by Influx of Hot, Dense Ultrabasic Magma. *Contr. Miner. Petrol.*, **75**, 279 - 289.

Huppert, H.E. and Turner, J.S. (1981). A Laboratory Model of a Replenished Magma Chamber. *Earth Plan. Sci. Lett.*, **54**, 144 - 152.

Huppert, H.E. and Sparks, R.S.J. (1989). Chilled margins in igneous rocks. *Earth Plan. Sci. Lett.*, **92**, 397 - 405.

Irvine, T.N. (1965). Chromian spinel as a petrogenetic indicator. *Can. J. Earth Sci.*, **2**, 648 - 672.

---------- (1967). Chromian spinel as a petrogenetic indicator, Part 2. Petrologic applications. *Can. J. Earth Sci.*, **4**, 71 -103.

---------- (1974). Petrology of the Duke Island Ultramafic Complex Southeastern Alaska. *Geol. Soc. Am.*, **Mem. 138**, 240 pp.

---------- (1975). Crystallization sequences in the Muskox intrusion and other layered intrusions - II. Origin of chromitite layers and similar deposits of other magmatic ores. *Geochim. Cosmochim. Acta*, **39**, 991 - 1020.

---------- (1977). Origin of chromitite layers in the Muskox intrusion and other stratiform intrusions: A new interpretation. *Geology*, **5**, 273 - 277.

---------- (1980). Magmatic infiltration metasomatism, double diffusive fractional crystallization, and adcumulus growth in the Muskox Intrusion and other layered intrusions, 325 - 383. *In* Hargraves, R.B., Ed., *Physics of magmatic processes*. Princeton University Press, Princeton, 585 pp.

---------- (1982). Terminology for Layered Intrusions. *J. Petrol.*, **23**, 127 - 162.

---------- (1987a). Appendix I. Glossary of terms for layered intrusions, 641 - 647. *In* Parsons, I., Ed., *Origins of Igneous Layering*. D. Reidel Publishing Company, Dordrecht, 666 pp.

---------- (1987b). Appendix II. Processes involved in the formation and development of layered igneous rocks, 649 - 656. *In* Parsons, I., Ed., *Origins of Igneous Layering*. D. Reidel Publishing Company, Dordrecht, 666 pp.

----------, Keith, D.W. and Todd, S.G. (1983). The J-M Platinum - Palladium Reef of the Stillwater Complex, Montana, II: Origin by Double-Diffusive Convective Magma Mixing and Implications for the Bushveld Complex. *Econ. Geol.*, **78**, 1287 - 1334.

Jackson, E.D. (1961). Primary Textures and Mineral Associations in the Ultramafic Zone of the Stillwater Complex, Montana. *Geol. Surv. Am.*, **Prof. Pap. 358**, 106 pp.

---------- (1967). Ultramafic cumulates in the Stillwater, Great Dyke, and Bushveld Intrusions, 20 - 38. *In* Wyllie, P.J., Ed., *Ultramafic and related rocks*. John Wiley and Sons, Inc., New York, 464 pp.

---------- (1969). Chemical Variation in Coexisting Chromite and Olivine in Chromitite Zones of the Stillwater Complex. *Econ. Geol.*, **Monogr. 4**, 41 - 71.

Kelsey, C.H. (1965). Calculation of the C.I.P.W. norm. *Mineralog. Mag.*, **34**, 276 - 282.

Kruger, F.J. and Marsh, J.S. (1982). Significance of $^{87}Sr/^{86}Sr$ ratios in the Merensky cyclic unit of the Bushveld Complex. *Nature*, **298**, 53 - 55.

---------- and Mitchell, A.A. (1985). Discontinuities and variations of Sr-isotope systematics in the Main Zone of the Bushveld Complex, and their relevance to PGE mineralization (abstr.). *Can. Mineralogist*, **23**, 306 - 307.

Kruger, F.J., Cawthorn, R.G. and Walsh, K.L. (1987). Strontium isotopic evidence against magma addition in the Upper Zone of the Bushveld Complex. *Earth Plan. Sci. Lett.*, **84**, 51 - 58.

Kupferbuerger, W., Lombaard, B.V., Wasserstein, B. and Schwellnus, C.M. (1937). The chromite deposits of the Bushveld Igneous Complex Transvaal. *Geol. Surv. S. Afr.*, **Bull. 10**, 48 pp.

Lee, C.A. and Parry, S.J. (1988). Platinum-Group Element Geochemistry of the Lower and Middle Group Chromitites of the Eastern Bushveld Complex. *Econ. Geol.*, **83**, 1127 - 1139.

---------, Sharpe, M.R. and Viljoen, E.A. (1983). The chemistry of minor chromite layers in the Bushveld Complex, with special reference to chromite-plagioclase reaction (abstr.). *Symposium on the Bushveld Complex*. Inst. Geological Research on the Bushveld Complex, Pretoria, 103 pp.

--------- and Tredoux, M. (1986). Platinum-Group Element Abundances in the Lower and the Lower Critical Zones of the Eastern Bushveld Complex. *Econ. Geol.*, **81**, 1087 - 1095.

--------- and Butcher, A.R. (1990). Cyclicity in the Sr-isotope stratigraphy through the Merensky and Bastard Reef units, Atok Section, Eastern Bushveld Complex. *Econ. Geol.*, **85**, in press.

Lindsley, D.H. (1983). Pyroxene thermometry. *Am. Mineralogist*, **68**, 477 - 493.

Marsh, J.S. (1979). *A manual for X-ray fluorescence determination of major and trace elements in natural silicate rock materials.* Manual (unpubl.), Rhodes University, 41 pp.

Marsh B.D. (1988). Crystal capture, sorting, and retention in convecting magma. *Geol. Soc. Am.*, **Bull. 100**, 1720 - 1737.

---------- (1989). On Convective Style and Vigor in Sheet-like Magma Chambers. *J. Petrol.*, **30**, 479 - 530.

McDonald, J.A. (1965). Liquid immiscibility as one factor in chromitite seam formation in the Bushveld Igneous Complex. *Econ. Geol.*, **60**, 1674 - 1685.

---------- (1967). Evolution of Part of the Lower Critical Zone, Farm Ruighoek, Western Bushveld. *J. Petrol.*, **8**, 165 - 209.

Meyer, R. and De Beer, J.H. (1987). Structure of the Bushveld Complex from resistivity measurements. *Nature*, **325**, 610 - 612.

Mitchell, A.A. (1986). *The Petrology, Mineralogy and Geochemistry of the Main Zone of the Bushveld Complex at Rustenburg Platinum Mines, Union Section*. Ph.D. thesis (unpubl.), Rhodes University, 104 pp.

Molyneux, T.G. (1970). The geology of the area in the vicinity of Magnet Heights, Eastern Transvaal, with special reference to the magnetic iron ore. *Geol. Soc. S. Afr.*, **Spec. Publn. 1**, 228 - 241.

Mori, T. and Green, D.H. (1978). Laboratory duplication of phase equilibria observed in natural garnet lherzolites. *J. Geol.*, **86**, 83 - 97.

Morse, S.A. (1979). Reaction constants for En-Fo-Sil-equilibria: an adjustment and some applications. *Am. J. Sci.*, **279**, 1060 - 1069.

---------- (1986). Convection in Aid of Adcumulus Growth. *J. Petrol.*, **27**, 1183 - 1214.

---------- and Nolan, K.M. (1984). Origin of strongly reversed rims on plagioclase in cumulates. *Earth Plan. Sci. Lett.*, **68**, 485 - 498.

Mullin, J.W. (1961). *Crystallization*. Butterworths, London, 268 pp.

Murck, B.W. and Campbell, I.H. (1986). The effects of temperature, oxygen fugacity and melt composition on the behaviour of chromium in basic and ultrabasic melts. *Geochim. Cosmochim. Acta*, **50**, 1871 - 1887.

Naldrett, A.J. and Barnes, S.J. (1986). The behaviour of platinum group elements during fractional crystallization and partial melting with special reference to the composition of magmatic sulfide ores. *Fortschr. Miner.*, **64**, 113 - 133.

---------- and Duke, J.M. (1980). Platinum Metals in Magmatic Sulfide Ores. *Science*, **208**, 1417 - 1424.

---------- and Von Gruenewaldt, G. (1988). Association of Platinum-Group Elements with Chromitite in layered intrusions and ophiolite complexes. *Econ. Geol.*, **84**, 180 - 187.

Norrish, K. and Hutton, J.T. (1969). An accurate X-ray spectrographic method for the analysis of a wide range of geological samples. *Geochim. Cosmochim. Acta*, **33**, 431 - 453.

Osborn, E.F. (1978). Changes in phase relations in response to change in pressure from 1 atm. to 10 kbar for the system Mg_2SiO_4 - iron oxide - $CaAl_2Si_2O_8$ - SiO_2. *Carnegie Inst. Washington Year Book*, **77**, 784 - 790.

Roeder, P.L., Campbell, I.H. and Jamieson, H.E. (1979). A Re-Evaluation of the Olivine-Spinel Geothermometer. *Contr. Miner. Petrol.*, **68**, 325 - 334.

---------- and Campbell, I.H. (1985). The Effect of Postcumulus Reactions on Composition of Chrome-spinels from the Jimberlana Intrusion. *J. Petrol.*, **26**, 763 - 786.

Sampson, E. (1932). Magmatic chromite deposits in Southern Africa. *Econ. Geol.*, **27**, 113 - 144.

Schmidt, E.R. (1952). The Structure and Composition of the Merensky Reef and Associated Rocks in the Rustenburg Platinum Mine. *Trans. Geol. Soc. S. Afr.*, **55**, 233 -279.

Scoates, R.F.J., Eckstrand, O.R. and Cabri, L.J. (1988). Inter-element Correlation, Stratigraphic Variation, and Distribution of PGE in the Ultramafic Series of the Bird River sill, Canada, 239 -249. *In* Prichard, H.M., Potts, P.J., Bowles, J.F.W. and Cribb, S.J., Eds., *Geo-Platinum '87*. Elsevier Science Publishers Ltd., Barking, England, 422 pp.

Scoon, R.N. (1985). *Discordant bodies of postcumulus, ultramafic rock in the upper critical zone of the Bushveld Complex: iron-rich ultramafic pegmatite bodies at Amandelbult and the Driekop platiniferous ultramafic pipe*. Ph.D. thesis (unpubl.), Rhodes University, 265 pp.

---------- and De Klerk, W.J. (1987). The relationship of olivine cumulates and mineralization to cyclic units in part of the upper critical zone of the western Bushveld Complex. *Can. Mineralogist*, **25**, 51 -77.

Sharpe, M.R. (1982). Noble Metals in the Marginal Rocks of the Bushveld Complex. *Econ. Geol.*, **77**, 1286 - 1295.

---------- (1985). Strontium isotope evidence for preserved density stratification in the main zone of the Bushveld complex, South Africa. *Nature*, **316**, 119 - 126.

---------- (1986). *Bushveld Complex - Excursion Guidebook, Geocongress '86*. Geological Society of South Africa, Marshalltown, 143 pp.

---------- and Irvine, T.N. (1983). Melting relations of two Bushveld chilled margin rocks and implications for the origin of chromitite. *Carnegie Inst. Washington Year Book*, **82**, 295 - 300.

----------, Bahat, D. and Von Gruenewaldt, G. (1981). The concentric elliptical structure of the Bushveld Complex and possible economic implications. *Trans. Geol. Soc. S. Afr.*, **84**, 239 - 244.

Smit, P.J., Hales, A.L. and Gough, D.I. (1962). *The gravity survey of the Republic of South Africa*. Geological Survey of South Africa, **Handbook 3**, Pretoria, 477 pp.

Stockman, H.W. and Hlava, P.F. (1984). Platinum-group Minerals in Alpine Chromitites from Southwestern Oregon. *Econ. Geol.*, **79**, 491 - 508.

Streckeisen, A. (1974). Classification and nomenclature of plutonic rocks. *Geol. Rdsch.*, **63**, 773 - 786.

Stumpfl, E.F. (1974). The genesis of platinum deposits: further thoughts. *Minerals Sci. Engng.*, **6**, 120 - 141.

Subcommittee on the Amphibole Group (1978). Nomenclature of amphiboles. *Can. Mineralogist*, **16**, 501 - 520.

Subcommittee on Pyroxenes (1989). Nomenclature of pyroxenes. *Can. Mineralogist*, **27**, 143 - 156.

South African Committee for Stratigraphy (SACS), (1980). *Stratigraphy of South Africa. Part 1 (Comp. L.E. Kent). Lithostratigraphy of the Republic of South Africa, South West Africa / Namibia, and the Republic of Bophuthatswana, Transkei and Venda*, Geological Survey of South Africa, **Handbook 8**, Pretoria, 690 pp.

Tankard, A.J., Jackson, M.P.A., Eriksson, K.A., Hobday, D.K., Hunter, D.R. and Minter, W.E.L. (1982). *Crustal evolution of Southern Africa*, Springer-Verlag, New York, Heidelberg, Berlin, 523 pp.

Teigler, B. (1990). Platinum Group Element Distribution in the Lower and Middle Group Chromitites in the Western Bushveld Complex. *Mineral. Petrol.*, **42**, 165 - 179.

Textoris, D.A. (1971). Grain size measurement in thin-section, 95 -107. *In* Carver, R.E., Ed., *Procedures in Sedimentary Petrology*. Wiley - Interscience & Sons, Inc., New York, 653 pp.

Tucker, M. (1988). *Techniques in Sedimentology*. Blackwell Scientific Publications, London, 394 pp.

Turner, J.S. and Gustafson, L.B. (1978). The Flow of Hot, Saline Solutions from Vents in the Sea Floor - some Implications for Exhalative Sulfide and Other Ore Deposits. *Econ. Geol.*, **73**, 1082 - 1100.

Ulmer, G.C. (1969). Experimental Investigation of Chromite Spinels. *Econ. Geol.*, **Monogr. 4**, 114 - 131.

Van Der Plas, L. and Tobi, A. (1965). A chart for judging the reliability of point counting results. *Am. J. Sci.*, **263**, 87 - 90.

Van Zyl, J.P. (1970). The petrology of the Merensky Reef and the associated rocks on Swartklip 988, Rustenburg District. *Geol. Soc. Afr.*, **Spec. Publn. 1**, 80 - 107.

Vermaak, C.F. (1970). The geology of the lower portion of the Bushveld Complex and its relationship to the floor rocks in the area west of Pilanesberg, Western Transvaal. *Geol. Soc. S. Afr.*, **Spec. Publn. 1**, 242 - 265.

Vermaak, C.F. (1976). The Merensky Reef - Thoughts on its Environment and Genesis. *Econ. Geol.*, **71**, 1270 -1298.

Vermaak, C.F. (1986). Summary aspects of the economics of chromium with special reference to southern Africa, 1155 - 1181. *In* Anhaeusser, C.R. and Maske, S., Eds., *Mineral deposits of Southern Africa*. Vol. 2. Geological Society of South Africa, 2376 pp.

Viljoen, M.J. and Scoon, R.N. (1985). The Distribution and Main Geological Features of Discordant Bodies of Iron-rich Ultramafic Pegmatite in the Bushveld Complex. *Econ. Geol.*, **80**, 1109 - 1128.

---------- and De Klerk, W.J., Coetzer, P.M., Hatch, N.P., Kinloch, E. and Peyerl, W. (1986a). The Union Section of Rustenburg Platinum Mines Limited, with reference to the Merensky Reef, 1061 - 1090. *In* Anhaeusser, C.R. and Maske, S., Eds., *Mineral deposits of Southern Africa*. Vol. 2. Geological Society of South Africa, 2376 pp.

---------- and Theron, J., Underwood, B., Walters, B.M., Weaver, J. and Peyerl, W. (1986b). The Amandelbult Section of Rustenburg Platinum Mines Limited, with reference to the Merensky Reef, 1041 - 1060. *In* Anhaeusser, C.R. and Maske, S., Eds., *Mineral deposits of southern Africa*. Vol. 2. Geological Society of South Africa, 2376 pp.

Visitors Brochure. *Crocodile River Mine*, Barplats Mine Limited, Geology Department, 15 pp.

Von Gruenewaldt, G. (1973). The Main and Upper Zones of the Bushveld Complex in the Roossenekal area, Eastern Transvaal. *Trans. Geol. Soc. S. Afr.*, **76**, 207 - 227.

---------- and Worst, B.G. (1986). Chromite deposits at Zwartkop Chrome Mine, western Bushveld Complex, 1217 - 1227. *In* Anhaeusser, C.R. and Maske, S., Eds., *Mineral deposits of Southern Africa*. Vol. 2. Geological Society of South Africa, 2376 pp.

----------, Sharpe, M.R. and Hatton, C.J. (1985). The Bushveld Complex: Introduction and Review. *Econ. Geol.*, **80**, 803 - 812.

----------, Hatton, C.J., Merkle, R.K.W. and Gain, S.B. (1986). Platinum-Group Element - Chromitite Associations in the Bushveld Complex. *Econ. Geol.*, **81**, 1067 - 1079.

Wager, L.R., Brown, G.M. and Wadsworth, W.J. (1960). Types of Igneous Cumulates. *J. Petrol.*, **1**, 73 - 85.

Wager, L.R. and Brown, G.M. (1968). *Layered igneous rocks*. Oliver and Boyd, Edinburgh and London, 588 pp.

Wagner, P.A. (1929). *The platinum deposits and mines of South Africa.* Oliver and Boyd, Edinburgh and London, 326 pp.

Walraven, F. and Darracott, B.W. (1976). Quantitative interpretation of a gravity profile across the western Bushveld Complex. *Trans. Geol. Soc. S. Afr.*, **79**, 22 - 26.

Wasserstein, B. (1936). Some notes on the Critical Zone of the Bushveld Gabbro at the Swartkop Chrome Mine in the Rustenburg District. *Trans. Geol. Soc. S. Afr.*, **39**, 215 - 222.

Wells, P.R.A. (1977). Pyroxene Thermometry in Simple and Complex Systems. *Contr. Miner. Petrol.*, **62**, 129 - 139.

Willemse, J. (1964). A Brief Outline of the Geology of the Bushveld Igneous Complex, 91 - 128. *In* Haughton, S.H., Ed., *The geology of some ore deposits in Southern Africa.* Vol. II. Geological Society of South Africa, Johannesburg, 739 pp.

---------- (1969). The Geology of the Bushveld Igneous Complex, the Largest Repository of Magmatic Ore Deposits in the World. *Econ. Geol.*, **Monogr. 4**, 1 - 22.

Wilson, A.H. (1982). The Geology of the Great Dyke, Zimbabwe: the Ultramafic Rocks. *J. Petrol.*, **23**, 240 - 292.

Wood, B.J. and Banno, S. (1973). Garnet-Orthopyroxene and Orthopyroxene-Clinopyroxene Relationships in Simple and Complex Systems. *Contr. Miner. Petrol.*, **42**, 109 -124.

Worst, B.G. (1986). The Chromite Deposits at Kroondal Chrome Mine, Western Bushveld Complex, 1209 - 1215. *In* Anhaeusser, C.R. and Maske, S., Eds., *Mineral deposits of Southern Africa*. Vol. 2. Geological Society of South Africa, 2376 pp.

Young, D.R. (1978). Explanatory notes for 1:50000 Sheets 2526BA (Kayakulu), 2526BB (Mabeskraal) and 2526BC (Lindleyspoort), *Geol. Surv. S. Afr.*, unpubl. report.

APPENDIX I

1) Log of NG1

Logged by: H.V. Eales, W.J. de Klerk, R.N. Scoon, B. Teigler, S.A. Haikney

Depth in metres	Petrographic description
0.00 - 2.00	Overburden: black turf soil.
2.00 - 3.50	Fragmented and weathered pyroxenite.
3.50 - 6.15	Fresher pyroxenite, finer-grained; pyroxenite with disseminated chromite stringers (5.20 - 5.90); probably some core loss.
6.15 - 6.50	Chromitite layer (ca. 40 % dissemination); more massive towards the base.
6.50 - 7.00	Caliche (weathering) mainly magnesite with sporadic, pyroxenitic sandy layers.
8.05 - 16.10	Medium-grained pyroxenite, partially weathered; chromite disseminations (9.40 - 9.50; wispy stringers); numerous small fractures with associated alteration.
16.10 - 55.90	Fresh medium- to fine-grained pyroxenite; thin chromitite lenses at 20.90, 29.80, 40.15 and 46.20; igneous lamination occurs from 54.80 - 55.90; pyroxenite is more medium grained and feldspathic towards the base.
55.90 - 65.19	Medium- to coarse-grained pyroxenite with large intercumulus plagioclase crystals (up to 3 cm in diameter); no igneous lamination; much more feldspathic than the pyroxenite above. Isolated chromitite lenses at 56.55, 56.70, 56.85, 57.12, 57.35 and 58.30; sporadic occurrence of large clinopyroxene oikocrysts; from 61.71 onwards pyroxenite is finer-grained.
65.19 - 89.95	Medium- to fine-grained pyroxenite; thin chromitite blebs occur at 71.46 and 78.50; at 82.10 - 82.75 and 84.85 - 85.20 chromite disseminations (10 - 20 %).
89.95 - 90.30	Pyroxenite with layers of heavy dissemination of chromite.
90.30 - 90.70	Medium- to coarse-grained pyroxenite.
90.70 - 91.42	Pyroxenite with heavy dissemination of chromite in layers and a massive chromitite (3 cm) at the base; dip ca. 20°.
91.42 - 92.02	Core loss associated with a serpentinised shear zone.
92.02 - 95.00	Medium-grained pyroxenite.
95.00 - 95.85	Harzburgite interlayered with pyroxenite; harzburgite layers range from only a few mm to 45 cm in thickness; sharp basal contacts.
95.85 - 100.50	Massive pyroxenite with sporadic olivine and rather abundant phlogopite; at 96.75 thin chromitite lens in somewhat coarser pyroxenite; a layer of harzburgite occurs between 99.50 and 99.76; from 100.00 the pyroxenite is finer-grained.
100.50 - 100.80	Harzburgite.
100.80 - 108.26	Medium- to coarse-grained pyroxenite with phlogopite.
108.26 - 108.76	Harzburgite, serpentinised.
108.76 - 122.61	Coarse-grained pyroxenite with sporadic olivine; thin lenses of chromitite at 114.36 (3 mm) and 118.54 (1 cm); harzburgite layer (25 cm) at 118.70.
122.61 - 122.98	Highly feldspathic harzburgite.

122.98 - 152.51	Coarse-grained pyroxenite with igneous lamination.
152.51 - 152.54	Massive chromitite layer (LG7-chromitite); dipping at ca. 15°.
152.54 - 159.40	Medium- to coarse-grained pyroxenite with ca. 5 cm of harzburgite at 155.00; chromitite lens at 159.32.
159.40 - 160.25	Pyroxenite with 15 - 20% disseminated chromite at 159.85 and 160.25.
160.25 - 242.18	Medium-to fine-grained massive pyroxenite; chromitite lenses at 162.78, 163.27, 173.39, 174.15 and 174.95.
242.18 - 242.24	Pyroxenite with disseminated chromite layers dipping at ca. 20°.
242.24 - 242.42	Massive chromitite layer (LG6A-chromitite).
242.42 - 242.74	Pyroxenite with disseminated chromite.
242.74 - 255.46	Medium-grained pyroxenite with a probably increase in grain size.
255.46 - 255.91	Pyroxenite with disseminated chromite.
255.91 - 256.95	Massive chromitite layer (LG6-chromitite); base of chromitite dips at ca. 25°.
256.95 - 351.16	Medium-to coarse-grained pyroxenite; thin chromitite lens at 301.08.
331.16 - 331.71	Massive chromitite layers (LG5-chromitite) interlayered with pyroxenite; basal part of chromitite displays abundant orthopyroxene oikocrysts.
331.71 - 332.02	Pyroxenite.
332.02 - 332.34	Massive chromitite layer with orthopyroxene oikocrysts towards the base; underlying 0.5 cm of pyroxenite is highly altered.
332.34 - 332.70	Pyroxenite, highly altered; chromitite layer (1 cm) at 332.70.
332.70 - 417.10	Medium-grained pyroxenite; chromitite lens (0.5 cm) at 337.20.
417.10 - 418.20	Pyroxenite grading into a harzburgite.
418.20 - 420.82	Olivine pyroxenite grading into harzburgite at the base.
420.82 - 421.36	Pyroxenite with olivine coming in at 421.20 to harzburgite.
421.36 - 425.24	Olivine pyroxenite grading into harzburgite and dunite at 422.50.
425.24 - 425.34	Pyroxenite with a basal chromitite layer (1-2 cm).
425.34 - 429.43	Dunite with abundant large (3 -5 cm) oikocrysts of orthopyroxene; at 428.00 chromitiferous dunite over 20 cm.
429.43 - 429.70	Chromitite layer with olivine (LG4-chromitite).
429.70 - 434.90	Dunite with a heavy dissemination of chromite; gradation into chromitite at base.
434.90 - 452.06	Dunite with minor disseminations of chromite; chromitite stringer at 435.75.
452.06 - 452.52	Pyroxenite, partly feldspathic.
452.52 - 452.63	Massive chromitite layer.
452.63 - 475.02	Medium-grained pyroxenite; chromitite lamina (2mm) at 474.40.
475.02 - 475.51	Massive chromitite with abundant orthopyroxene oikocrysts and pyroxenite partings (LG3-chromitite).
475.51 - 481.25	Medium- to coarse-grained pyroxenite with disseminated chromite; olivine-rich lamina (ca. 5 mm-thick) occur from 480.45-480.70.
481.25 - 481.32	Chromitite layer.
481.32 - 496.35	Medium- to coarse-grained pyroxenite with a chromite dissemination; chromitiferous pyroxenite at the base (25 cm).
496.35 - 496.43	Massive chromitite layer; dip ca. 25°.
496.43 - 505.64	Medium- to coarse-grained pyroxenite; thin layers of dunite (1 - 2 mm) at 498.10 - 498.25.
505.64 - 506.50	Dunite with disseminated chromite.
506.50 - 506.70	Chromitite layer (LG2B-chromitite); very friable with abundant orthopyroxene oikocrysts.

506.70 - 512.72	Dunite and harzburgite layers with thin pyroxenite interlayers.
512.72 - 513.20	Medium- to coarse-grained pyroxenite.
513.20 - 515.00	Harzburgite and dunite.
515.00 - 523.98	Harzburgite and dunite layers (1 cm thick) alternating with pyroxenite; thin chromitite layer at 517.25; dipping at 20°.
523.98 - 524.18	Massive chromitite layer (LG2A-chromitite).
524.18 - 559.92	Coarse- to medium grained pyroxenite; chromitite lenses occur at 525.96, 526.41 and 535.91; pyroxenite is chromitiferous between 533.00 to 534.50; chromitite layer (1.5 cm) at 546.90; basal part with heavy chromite dissemination.
559.92 - 560.28	Massive chromitite layer (LG1-chromitite).
560.28 - 597.65	Pyroxenite with sporadic green clinopyroxene; chromitite lens at 595.05 (0.8x1.5 cm).
597.65 - 597.70	Chromitiferous pyroxenite grades into chromitite layer at the base.
597.70 - 609.57	Pyroxenite.
609.57 - 609.63	Massive chromitite layer with sharp upper and lower contacts; dip of ca. 25°.
609.63 - 643.10	Pyroxenite, fine-grained.
643.10 - 644.26	Chromitiferous pyroxenite with some chromitite laminae.
644.26 - 697.80	Pyroxenite.
697.80 - 699.73	Dunite; sharp contact.
699.73 - 700.37	Pyroxenite.
700.37 - 701.10	Chromitiferous dunite to 700.70 underlain by dunite.
701.10 - 744.80	Medium-grained pyroxenite.
744.80 - 745.10	Medium-grained pyroxenite with sporadic olivine; gradation into harzburgite at 745.10.
745.10 - 745.20	Harzburgite.
745.20 - 762.60	Coarse- to medium-grained chromitiferous dunite.
762.60 - 773.67	Poikilitic harzburgite (mottled dunite).
773.67 - 774.44	Medium-grained dunite.
774.44 - 793.72	Very coarse-grained dunite with some poikilitic orthopyroxene and sporadic dissemination of chromite.
793.72 - 803.52	Poikilitic harzburgite (mottled dunite).
803.52 - 831.06	Coarse-grained dunite with some poikilitic orthopyroxene; sporadic dissemination of chromite.

End of hole at 831.06 m.

2) Log of NG2

Logged by: B. Teigler, W.J. de Klerk, R.N. Scoon, S.A. Haikney, W.D. Maier

Depth in metres	Petrographic description
0.00 - 3.00	Overburden: black turf soil.
3.00 - 12.50	Highly weathered material with some magnesite.
12.50 - 38.00	Medium-grained dunite, but heavily weathered.
38.00 - 51.60	Medium-grained dunite with some poikilitic orthopyroxene.
51.60 - 52.50	Medium- to coarse-grained pyroxenite.
52.50 - 91.00	Medium-grained dunite; contact is sheared and serpentinised; a thin layer of medium-grained pyroxenite occurs at 69.40 - 69.70; between 70.45 - 71.55 olivine pyroxenite, at about 77.00 gradation into harzburgite, which grades into dunite at ca. 83.30.
91.00 - 120.60	Medium-grained pyroxenite with sporadic clinopyroxene oikocrysts; harzburgite lens at 119.45.
120.60 - 123.15	Coarse-grained granular harzburgite.
123.15 - 159.20	Medium- to coarse-grained poikilitic harzburgite; chromitite lens (15 cm) at 158.50.
159.20 - 197.30	Medium-grained pyroxenite with sporadic olivine; at 161.00 harzburgite layers at 161.00 (10 cm) and 165.60 (52 cm).
197.30 - 199.65	Medium-grained granular harzburgite.
199.65 - 202.00	Olivine pyroxenite with gradations into harzburgite.
202.00 - 206.45	Medium-grained pyroxenite.
206.45 - 208.75	Olivine pyroxenite with gradations into harzburgite.
208.75 - 211.00	Medium-grained pyroxenite.
211.00 - 212.60	Olivine pyroxenite.
212.60 - 221.43	Poikilitic harzburgite.
221.43 - 225.65	Medium-grained pyroxenite.
225.65 - 228.05	Poikilitic harzburgite with gradations into dunite.
228.05 - 229.12	Granular harzburgite with conspicuous amount of phlogopite.
229.12 - 233.00	Medium-grained pyroxenite.
233.00 - 234.20	Granular harzburgite.
234.20 - 234.90	Medium-grained pyroxenite.
234.90 - 237.00	Granular harzburgite with inch scale layering of poikilitic harzburgite and dunite.
237.00 - 241.05	Medium-grained feldspathic poikilitic harzburgite and dunite
241.05 - 297.13	Medium-grained pyroxenite.
297.13 - 300.00	Norite with sheared upper contact.
300.00 - 326.56	Medium-grained pyroxenite; pegmatoidal development at 323.86 (17 cm).
326.56 - 327.73	Dunite and poikilitic harzburgite.
327.73 - 337.02	Medium-grained pyroxenite.
337.02 - 337.59	Poikilitic harzburgite and dunite.
337.59 - 358.66	Medium-grained feldspathic pyroxenite.
358.66 - 360.20	Harzburgite.
360.20 - 372.60	Medium-grained pyroxenite.
372.60 - 374.26	Harzburgite grading downwards into dunite.
374.26 - 374.85	Pyroxenite.
374.85 - 375.68	Dunite grading into harzburgite.
375.68 - 376.10	Pyroxenite - olivine pyroxenite - harzburgite.
376.10 - 376.62	Harzburgite.
376.62 - 377.38	Olivine pyroxenite.
377.38 - 380.22	Harzburgite grading into dunite.

380.22 - 382.94 Dunite.
382.94 - 384.37 Harzburgite.
384.37 - 397.68 Pyroxenite.
397.68 - 399.50 Harzburgite.
399.50 - 410.60 Pyroxenite.
410.60 - 411.74 Harzburgite with a basal dunite layer.
411.74 - 415.86 Pyroxenite.
415.86 - 418.55 Harzburgite.
418.55 - 418.95 Olivine pyroxenite.
418.95 - 420.01 Dunite.
420.01 - 421.50 Pyroxenite.
421.50 - 424.10 Harzburgite.
424.10 - 426.05 Pyroxenite.
426.05 - 436.58 Harzburgite with gradations into olivine pyroxenite and dunite at 428.00 and 430.00 .
436.58 - 437.04 Pyroxenite.
437.04 - 437.50 Harzburgite.
437.50 - 438.29 Pyroxenite.
438.29 - 438.43 Harzburgite.
438.43 - 439.30 Pyroxenite.
439.30 - 439.42 Harzburgite.
439.42 - 449.45 Pyroxenite.
449.45 - 450.00 Dunite with gradational contact to underlying harzburgite.
450.00 - 450.70 Harzburgite.
450.70 - 451.71 Pyroxenite.
451.71 - 452.85 Harzburgite.
452.85 - 454.44 Dunite.
454.44 - 466.10 Pyroxenite.
466.10 - 467.65 Harzburgite.
467.85 - 478.46 Dunite.
478.46 - 479.47 Pyroxenite.
479.47 - 480.80 Harzburgite.
480.80 - 481.40 Dunite.
481.40 - 488.87 Pyroxenite.
488.87 - 489.25 Dunite, highly altered .
489.25 - 489.95 Harzburgite.
489.95 - 531.02 Dunite.
531.02 - 531.23 Pegmatoidal pyroxenite.
531.23 - 546.26 Medium-grained pyroxenite with sporadic olivine.
546.26 - 548.16 Harzburgite.
548.16 - 550.05 Dunite.
550.05 - 553.22 Harzburgite.
553.22 - 557.16 Pyroxenite.
557.16 - 564.65 Harzburgite; with dunite at 561.90.

564.65 - 617.25 Pyroxenite with multiple intercalations of dunites and harzburgites.

Dunite layers at:

565.58 - 565.76	577.84 - 578.60
565.83 - 565.94	578.73 - 578.89
565.97 - 566.23	580.29 - 581.14
566.32 - 566.42	582.14 - 582.41
566.45 - 566.51	584.92 - 584-56
567.03 - 567.22	584.90 - 584.99
567.70 - 568.00	585.37 - 585.48
568.53 - 569.34	585.57 - 586.44
571.38 - 571.53	587.22 - 587.90
571.65 - 571.75	588.30 - 589.19
572.54 - 573.00	589.68 - 590.22
573.05 - 573.06	590.41 - 590.44
573.23 - 573.31	590.83 - 590.92
573.42 - 573.46	591.15 - 591.28
573.72 - 573.80	591.37 - 591.66
573.91 - 574.26	592.09 - 592.17
574.35 - 574.36	592.23 - 593.15
574.53 - 574.73	593.45 - 593.68
575.40 - 575.60	595.14 - 595.45
575.68 - 575.70	595.68 - 596.40
575.85 - 576.37	

Harzburgite layers at:

604.45 - 604.55	607.48 - 607.61
604.86 - 605.35	607.62 - 607.76
605.53 - 605.76	608.09 - 608.18
605.84 - 605.85	608.29 - 608.36
606.45 - 607.05	608.48 - 608.53
607.30 - 607.44	

Dunite layers at:

608.94 - 608.95	612.36 - 612.62
609.00 - 609.05	612.85 - 612.89
610.67 - 610.95	613.05 - 613.43
611.03 - 611.53	613.53 - 614.00
611.82 - 612.12	614.14 - 614.84
612.15 - 612.31	615.01 - 615.62

617.25 - 622.61 Harzburgite.

622.61 - 639.94 Olivine pyroxenite with harzburgite layers at:

626.13 - 627.10	632.93 - 633.15
627.50 - 627.68	633.27 - 633.35
628.31 - 628.61	633.58 - 633.81
629.83 - 629.88	633.90 - 634.06
630.15 - 630.56	634.16 - 634.34
630.64 - 630.86	634.55 - 636.10
631.22 - 631.62	636.43 - 636.44
631.74 - 632.74	636.66 - 639.71

639.94 - 674.00 Dunite and harzburgite interlayering.

674.00 - 694.14 Dunite with olivine pyroxenite layers and lamina at:

676.06 - 676.25	683.59 - 683.67
676.28 - 676.32	683.72 - 683.88
678.93 - 678.98	683.97 - 684.35
679.75 - 680.32	684.42 - 684.54
681.27 - 681.30	684.64 - 684.81
681.40 - 681.56	685.32 - 685.46
681.60 - 681.89	685.65 - 685.76
682.00 - 682.09	685.90 - 686.00
682.21 - 682.32	686.33 - 686.38
682.36 - 683.59	686.90 - 687.36
682.63 - 682.68	689.21 - 689.90
682.73 - 683.78	690.06 - 690.11
683.08 - 683.57	

694.14 - 696.06 Pyroxenite with dunite layers at:

694.34 - 694.48	695.09 - 695.09
694.57 - 694.65	695.26 - 695.54
694.79 - 694.84	695.75 - 696.06
694.98 - 695.02	

696.36 - 697.30 Dunite with very thin (1 cm) pyroxenite laminae.

697.30 - 701.00 Pyroxenite with dunite layers or lenses at:

697.40 - 697.45	698.77 - 699.43
697.86 - 698.48	

701.00 - 711.00 Dunite with pyroxenite layer at 701.55-702.31 .

711.00 - 736.75 Poikilitic harzburgite and dunite;
at 733.61 - 733.81 occurrence of sulfides.

736.75 - 763.45 Pyroxenite with dunite and harzburgite at:

737.87 - 738.09	750.28 - 750.32
738.79 - 738.95	750.28 - 750.32
740.16 - 740.58	750.36 - 750.45
741.44 - 741.55	750.96 - 750.99
742.55 - 742.67	751.67 - 751.81

763.45 - 773.20 Fine-grained dunite; at 766.33 - 766.91 quartzite xenolith.

773.20 - 773.60 Gabbronorite.

773.60 - 774.70 Hornfels.

End of hole at 774.70 m.

3) Log of NG3

Logged by: B. Teigler, W.D. Maier

Depth in metres	Petrographic description
0.00 - 1.50	Overburden: black turf soil.
1.50 - 3.60	Weathered pyroxenite.
3.69 - 134.48	Pyroxenite with variable proportions of plagioclase; an anorthositic lens occurs at 98.00; melanorite layers might be present.
134.48 - 136.68	Pegmatoidal pyroxenite.
136.68 - 151.41	Pyroxenite.
151.41 - 151.70	Pegmatoidal pyroxenite.
151.70 - 151.87	Pyroxenite with disseminations of chromite and chromitite laminae.
151.87 - 152.85	Massive chromitite layer (MG4B-chromitite) with pyroxenite parting (10 cm) at 152.07 .
152.85 - 154.62	Coarse-grained almost pegmatoidal pyroxenite.
154.62 - 156.10	Massive chromitite layer (MG4A-chromitite).
156.10 - 159.20	Anorthosite with heavy chromite dissemination and sporadic schlieren or layers; basal layer is a massive chromitite 5 cm thick.
159.20 - 168.33	Pyroxenite.
168.33 - 170.34	Melanorite and norite.
170.34 - 174.77	Pyroxenite.
174.77 - 175.05	Chromitiferous anorthosite and leuconorite.
175.88 - 179.88	Norite grading into pyroxenite at the base.
179.88 - 183.00	Pyroxenite with gradation into norite at the base.
183.00 - 211.45	Norite.
211.45 - 212.20	Massive chromitite layer (MG3-chromitite).
212.20 - 212.93	Anorthosite with 4 cm chromite dissemination at 212.36 .
212.93 - 213.95	Leuconorite, basal part more noritic.
213.95 - 219.07	Pyroxenite with a chromitite lamina (2 mm) and sulfides at the basal contact.
219.07 - 219.40	Chromitiferous pyroxenite.
219.40 - 219.95	Massive chromitite layer (MG2-chromitite); lower contact sheared (5cm).
219.95 - 220.17	Pyroxenite, completely serpentinised.
220.17 - 260.41	Pyroxenite, fine- to medium-grained; chromite dissemination at 236.20 (lens 0.5 - 3.0 cm), 248.25 and 252.65 (1 cm lamina).

End of hole at 260.41 m.

4) Log of **KD86/2**

Logged by: B. Teigler

Depth in metres	Petrographic description
0.00 - 38.00	Pyroxenite, heavily weathered.
38.00 - 87.02	Pyroxenite with olivine occurrences at: 44.02 - 44.03 60.53 - 60.57 50.63 - 50.67 63.50 - 63.52 54.08 - 54.11 80.73 - 80.75 59.84 85.10 - 85.13 60.11 - 60.15 chromitiferous pyroxenite at: 70.53 - 70.61 73.05 - 73.10 70.20 - 70.21 71.90 - 71.91 70.49 - 70.50 82.33 - 82.34 massive chromitite laminae at: 71.00 - 71.01 82.42 0.5 cm massive chromitite pegmatitic veins with plagioclase and mica at: 52.46 - 52.54 86.86 - 86.87 70.88 - 70.90
87.02 - 100.00	Pyroxenite and dunite interlayered; below 97.00 pyroxenite grades into a norite; pegmatitic vein at: 99.57 - 99.62 .
100.00 - 124.69	Norite, upper part more melanocratic, lower part leucocratic; at 108.52 anorthosite lens (3cm). olivine occurrences at: 101.10 - 101.14 103.39 - 103.44 102.06 - 102.07 104.98 - 105.00 102.26 - 102.36 pyroxenite lamina at: 113.80 - 114.70 ultramafic pegmatite at: 112.40 - 113.36 .

End of hole at 124.69 m.

5) Log of SF-7

Logged by: R.N. Scoon, B. Teigler

Depth in metres	Petrographic description
0.00 - 13.20	No core.
13.20 - 67.40	Norite; basal part (65 cm) more melanocratic.
67.40 - 69.30	Pyroxenite; feldspathic.
69.30 - 70.86	Massive chromitite layer (UG1-chromitite).
70.86 - 71.59	Chromitiferous pyroxenite.
71.59 - 71.82	Massive chromitite layer.
71.82 - 73.12	Anorthosite, mottled.
73.12 - 73.51	Massive chromitite layer.
73.51 - 73.79	Anorthosite, mottled.
73.79 - 73.90	Massive chromitite layer.
73.80 - 174.65	Anorthosite and leuconorite.
174.65 - 216.26	Norite.
216.26 - 219.54	Pyroxenite.
219.54 - 220.60	Massive chromitite layer (MG4B-chromitite) with pyroxenite parting (5cm) at 220.25 .
220.60 - 224.34	Pyroxenite, feldspathic.
224.34 - 227.08	Massive chromitite layer (MG4A-chromitite) with pyroxenite parting 224.62 - 225.11 .
227.08 - 243.70	Norite.
243.70 - 244.60	Massive chromitite layer (MG3-chromitite).
244.60 - 248.46	Anorthosite, mottled.
248.46 - 248.85	Massive chromitite layer (MG2D-chromitite).
248.85 - 249.29	Pyroxenite.
249.29 - 249.81	Massive chromitite layer (MG2C-chromitite).
249.81 - 250.21	Pyroxenite.
250.21 - 250.61	Massive chromitite layer (MG2B-chromitite).
250.61 - 250.90	Pyroxenite.
250.90 - 251.16	Massive chromitite layer (MG2A-chromitite).
251.16 - 263.10	Pyroxenite.
263.10 - 264.56	Massive chromitite layer (MG1D-chromitite).
264.56 - 265.87	Pyroxenite.
265.87 - 266.18	Massive chromitite layer (MG1C-chromitite).
266.18 - 267.21	Pyroxenite.
267.21 - 267.75	Massive chromitite layer (MG1B-chromitite).
267.75 - 268.21	Pyroxenite.
268.21 - 268.31	Massive chromitite layer (MG1A-chromitite).
268.31 - 312.95	Pyroxenite.
312.95 - 318.50	Norite; chromitite stringer (1 mm) at 318.33 .
318.50 - 319.48	Pyroxenite with abundant olivine and chromitite stringers.
319.48 - 319.54	Chromitite layer.
319.54 - 360.15	Pyroxenite with olivine occurrences at: 318.00 - 337.00 357.65 - 360.15
360.15 - 363.75	Norite with olivine occurrence at 362.15 .
363.75 - 364.20	Pyroxenite.
364.20 - 366.20	Norite with some minor pyroxenite.
366.20 - 372.41	Pyroxenite.
372.41 - 372.57	Massive chromitite layer.
372.57 - 372.63	Anorthosite.
372.63 - 379.45	Norite.
379.45 - 385.15	Pyroxenite.

385.15 - 385.25	Chromitite layer; very irregular contacts with the anorthositic host rock.
385.25 - 385.36	Pyroxenite.
385.36 - 387.10	Norite.
387.10 - 388.63	Pyroxenite.
388.63 - 423.67	Norite.
423.67 - 435.38	Pyroxenite.
435.38 - 440.66	Norite.
440.66 - 440.81	Chromitite layer; very irregular contacts with the anorthositic host rock.
440.81 - 440.86	Pyroxenite.
440.86 - 452.90	Norite.
452.90 - 453.05	Pyroxenite.
453.05 - 453.07	Massive chromitite layer.
453.07 - 453.16	Chromitiferous anorthosite with thin pyroxenite laminae.
453.16 - 461.19	Norite; at 453.28 chromitite layer 3 cm-thick.
461.19 - 461.85	Anorthosite and leuconorite with abundant chromitite stringers.
461.85 - 475.16	Pyroxenite.
475.16 - 475.30	Chromitite layer.
475.30 - 476.94	Pyroxenite; upper part pegmatoidal.
476.94 - 483.20	Norite.
483.20 - 485.75	Pyroxenite.

End of hole at 485.75 m.

APPENDIX II

Modal compositions (in vol.%) as determined by the point-counting technique are listed hereafter. Samples analysed by Haikney are included. Note that no distinction is made in the table for the textural habits of the phases.

The abbreviations for the phases are:

pla	plagioclase
cpx	clinopyroxene
opx	orthopyroxene
ol	olivine
chr	chromite
phl	phlogopite
qtz	quartz
others	amphibole, rutile, apatite, base metal sulphides and alteration phases

Modal compositions in the NG-sequence

Sample:	Depth (m):	pla	cpx	opx	ol	chr	phl	qtz	others	Total
NG3										
3.98	3.98	14.7	4.1	81.1	0.0	0.0	0.0	0.0	0.1	100.0
28.62	28.62	23.1	3.8	72.9	0.0	0.0	0.0	0.0	0.2	100.0
55.13	55.13	18.9	2.3	78.6	0.0	0.0	0.0	0.0	0.2	100.0
79.60	79.60	9.4	5.3	85.3	0.0	0.0	0.0	0.0	0.0	100.0
99.60	99.60	12.4	2.1	85.5	0.0	0.0	0.0	0.0	0.0	100.0
126.05	126.05	7.8	1.7	90.5	0.0	0.0	0.0	0.0	0.0	100.0
146.50	146.50	4.9	2.2	92.9	0.0	0.0	0.0	0.0	0.0	100.0
153.15	153.15	11.8	0.5	83.6	0.0	1.0	2.0	1.0	0.1	100.0
159.40	159.40	15.0	1.7	79.8	0.0	3.2	0.3	0.0	0.0	100.0
176.45	176.45	58.5	1.3	40.2	0.0	0.0	0.0	0.0	0.0	100.0
181.70	181.70	34.4	2.8	62.5	0.0	0.0	0.0	0.0	0.3	100.0
194.74	194.74	63.5	3.0	33.5	0.0	0.0	0.0	0.0	0.0	100.0
213.18	213.18	42.0	2.2	55.2	0.0	0.0	0.0	0.0	0.6	100.0
214.25	214.25	32.5	4.5	61.7	0.0	0.5	0.0	0.0	0.8	100.0
221.30	221.30	6.3	2.4	89.2	0.0	1.0	0.6	0.0	0.5	100.0
232.00	232.00	9.7	0.6	85.5	0.0	0.3	1.9	1.4	0.6	100.0
260.05	260.05	16.4	1.2	77.8	0.0	2.6	0.2	0.5	1.3	100.0
NG1										
17.00	267.00	9.2	6.3	84.0	0.0	0.0	0.4	0.0	0.1	100.0
21.00	271.00	12.4	7.4	78.6	0.0	0.5	0.0	0.0	1.1	100.0
25.00	275.00	12.1	3.6	83.5	0.0	0.0	0.8	0.0	0.0	100.0
29.80	279.80	23.9	3.3	72.8	0.0	0.0	0.0	0.0	0.0	100.0
35.00	285.00	7.2	5.7	86.1	0.0	1.0	0.0	0.0	0.0	100.0
46.25	296.25	12.8	3.2	84.0	0.0	0.0	0.0	0.0	0.0	100.0
49.75	299.75	8.1	4.5	87.4	0.0	0.0	0.0	0.0	0.0	100.0
55.40	305.40	12.8	4.3	82.9	0.0	0.0	0.0	0.0	0.0	100.0
56.00	306.00	5.9	0.8	83.1	0.0	0.0	5.1	4.2	0.9	100.0
56.60	306.60	7.7	1.1	82.5	0.0	1.1	3.3	2.7	1.6	100.0
61.71	311.71	5.2	0.5	78.4	0.0	0.9	4.2	9.9	0.9	100.0
65.19	315.19	9.8	3.7	84.8	0.0	1.6	0.0	0.0	0.1	100.0
65.25	315.25	7.9	3.2	87.5	0.0	1.1	0.0	0.0	0.3	100.0
69.20	319.20	8.4	3.2	88.0	0.0	0.4	0.0	0.0	0.0	100.0
B71.46	321.46	7.7	1.8	90.5	0.0	0.0	0.0	0.0	0.0	100.0
74.40	324.40	9.5	4.7	85.8	0.0	0.0	0.0	0.0	0.0	100.0
79.75	329.75	5.7	3.9	89.7	0.0	0.7	0.0	0.0	0.0	100.0
82.75	332.75	11.0	0.7	68.7	0.0	19.3	0.0	0.0	0.3	100.0
84.90	334.90	3.8	1.7	73.4	0.0	21.0	0.0	0.0	0.1	100.0
85.85	335.85	5.0	3.4	87.2	0.0	0.0	2.7	1.7	0.0	100.0
89.55	339.55	6.6	3.6	88.5	0.0	1.3	0.0	0.0	0.0	100.0
A90.33	340.23	0.0	0.8	23.5	4.4	64.5	0.0	0.0	6.8	100.0
B90.33	340.33	1.5	1.5	54.6	0.0	38.7	0.6	0.0	3.1	100.0
C90.33	340.43	2.6	1.5	71.1	0.0	24.8	0.0	0.0	0.0	100.0
94.60	344.60	9.1	2.9	84.5	0.0	0.6	0.0	0.0	2.9	100.0
95.00	345.00	12.7	0.0	0.0	74.7	0.8	1.2	0.0	10.6	100.0
96.75	346.75	12.0	7.5	77.2	0.6	0.0	1.2	0.0	1.5	100.0
A100.30	350.30	6.0	1.8	91.9	0.0	0.0	0.0	0.0	0.3	100.0
B100.30	350.35	5.0	4.3	90.3	0.0	0.3	0.0	0.0	0.1	100.0
100.70	350.70	3.7	11.9	14.8	61.7	0.0	0.0	0.0	7.9	100.0
105.45	355.45	7.3	12.0	80.4	0.0	0.0	0.3	0.0	0.0	100.0
108.30	358.30	0.4	2.3	59.8	27.2	0.0	0.0	0.0	10.3	100.0
108.30	358.30	3.0	1.6	0.3	74.1	0.0	3.0	0.0	18.0	100.0
110.52	360.52	7.8	10.2	79.6	0.0	0.0	1.7	0.7	0.0	100.0
115.10	365.10	9.5	1.5	87.1	0.0	0.4	0.8	0.0	0.7	100.0
118.80	368.80	12.3	2.8	7.5	57.1	1.2	0.4	0.0	18.7	100.0
118.87	368.87	11.0	3.7	49.2	29.7	5.3	0.0	0.0	1.1	100.0
119.90	369.90	8.3	2.2	89.1	0.0	0.0	0.3	0.0	0.1	100.0
122.80	372.80	5.4	4.5	0.4	72.7	0.8	0.0	0.0	16.2	100.0
126.00	376.00	4.2	1.6	91.9	0.0	0.7	0.3	0.0	1.3	100.0
130.60	380.60	5.5	4.1	90.4	0.0	0.0	0.0	0.0	0.0	100.0
136.30	386.30	9.4	1.7	88.8	0.0	0.0	0.0	0.0	0.1	100.0
146.50	396.50	3.8	2.4	93.8	0.0	0.0	0.0	0.0	0.0	100.0
148.20	398.20	4.7	2.6	84.7	0.0	0.4	2.1	4.7	0.8	100.0
152.20	402.20	2.3	2.7	87.3	0.4	1.3	0.7	0.0	5.3	100.0
158.20	408.20	8.3	0.7	82.1	0.0	4.0	0.0	0.3	4.6	100.0
163.27	413.27	10.4	1.0	87.2	0.0	0.3	0.7	0.0	0.4	100.0
168.15	418.15	4.5	2.3	90.2	0.0	1.9	0.0	0.0	1.1	100.0
173.37	423.37	1.5	2.3	94.7	0.0	1.5	0.0	0.0	0.0	100.0
178.45	428.45	2.8	2.4	91.7	0.0	0.4	0.0	2.0	0.7	100.0
183.70	433.70	3.7	0.0	90.0	0.0	1.7	0.3	0.0	4.3	100.0
191.00	441.00	2.8	2.8	89.8	0.0	0.0	0.9	0.0	3.7	100.0
197.50	447.50	1.6	2.2	93.3	0.0	1.0	0.0	0.0	1.9	100.0
204.50	454.50	15.8	0.0	84.2	0.0	0.0	0.0	0.0	0.0	100.0
210.30	460.30	16.0	0.0	82.5	0.0	0.0	0.0	0.6	0.9	100.0
218.60	468.60	12.0	0.9	85.2	0.0	0.3	0.0	0.0	1.6	100.0
225.90	475.90	10.9	0.8	87.9	0.0	0.0	0.4	0.0	0.0	100.0
233.60	483.60	1.1	1.9	89.3	0.0	0.8	4.6	2.3	0.0	100.0
237.50	487.50	10.9	0.0	87.5	0.0	1.5	0.0	0.0	0.1	100.0
242.00	492.00	2.2	3.0	86.6	0.0	8.2	0.0	0.0	0.0	100.0
A242.15	492.15	4.4	0.7	85.2	0.0	9.6	0.0	0.0	0.1	100.0
242.70	492.70	4.8	0.0	80.7	0.0	13.8	0.0	0.0	0.7	100.0
242.72	492.72	9.8	0.8	89.4	0.0	0.0	0.0	0.0	0.0	100.0
245.25	495.25	0.8	1.7	97.1	0.0	0.4	0.0	0.0	0.0	100.0
250.15	500.15	0.8	2.1	95.8	0.0	1.3	0.0	0.0	0.0	100.0
255.25	505.25	5.5	1.2	90.5	0.0	2.5	0.0	0.0	0.3	100.0
257.10	507.10	12.4	4.8	76.0	0.0	5.2	0.8	0.0	0.8	100.0
257.70	507.70	18.8	1.8	74.3	0.0	5.0	0.0	0.0	0.1	100.0
262.17	512.17	14.3	1.6	70.6	0.0	11.9	1.6	0.0	0.0	100.0
267.00	517.00	2.0	2.8	95.2	0.0	0.0	0.0	0.0	0.0	100.0
277.25	527.25	6.0	2.5	91.1	0.0	0.4	0.0	0.0	0.0	100.0
282.25	532.25	4.5	3.0	92.4	0.0	0.0	0.0	0.0	0.1	100.0
287.15	537.15	4.4	4.4	90.6	0.0	0.4	0.0	0.0	0.2	100.0
292.30	542.30	2.4	0.7	94.8	0.0	0.7	0.0	0.0	1.4	100.0
297.40	547.40	1.9	2.5	94.6	0.0	0.9	0.0	0.0	0.1	100.0
302.00	552.00	5.4	3.3	89.5	0.0	1.8	0.0	0.0	0.0	100.0
307.30	557.30	4.0	3.2	90.6	0.0	1.8	0.4	0.0	0.0	100.0
312.10	562.10	2.0	0.8	96.7	0.0	0.4	0.0	0.0	0.1	100.0
317.60	567.60	6.1	1.6	92.3	0.0	0.0	0.0	0.0	0.0	100.0
322.75	572.75	3.9	2.8	93.3	0.0	0.0	0.0	0.0	0.0	100.0
327.45	577.45	2.2	1.5	94.8	0.0	0.7	0.4	0.4	0.0	100.0
331.13	581.13	1.7	1.4	80.5	0.0	2.5	0.0	0.0	13.9	100.0

Sample:	Depth (m):	pla	cpx	opx	ol	chr	phl	qtz	others	Total
334.30	584.30	3.3	0.4	94.4	0.0	1.9	0.0	0.0	0.0	100.0
338.45	588.45	2.0	2.3	94.4	0.0	0.7	0.0	0.0	0.6	100.0
343.40	593.40	4.1	3.7	91.7	0.0	0.0	0.4	0.0	0.1	100.0
348.20	598.20	4.6	2.5	92.5	0.0	0.4	0.0	0.0	0.0	100.0
A353.40	603.30	7.0	0.6	86.9	0.0	0.0	4.9	0.6	0.0	100.0
B353.40	603.40	13.2	1.6	83.2	0.0	0.0	1.9	0.0	0.1	100.0
C353.40	603.50	9.7	2.0	88.3	0.0	0.0	0.0	0.0	0.0	100.0
358.75	608.75	10.4	0.0	88.2	0.0	0.0	0.9	0.5	0.0	100.0
364.25	614.25	6.3	5.1	87.8	0.0	0.0	0.4	0.4	0.0	100.0
374.35	624.35	8.5	2.8	87.1	0.0	0.0	0.7	1.7	0.0	100.0
380.35	630.35	3.6	1.0	91.3	0.0	0.5	0.8	2.8	0.0	100.0
385.40	635.40	8.1	2.5	85.6	0.0	0.0	1.3	2.2	0.3	100.0
B390.60	640.60	12.1	1.4	83.6	0.0	0.4	0.7	1.8	0.0	100.0
396.00	646.00	6.3	4.3	88.0	0.0	0.0	0.7	0.7	0.0	100.0
396.70	646.70	6.5	1.8	90.6	0.0	0.0	0.4	0.7	0.0	100.0
401.38	651.38	8.3	3.0	84.9	0.0	0.4	1.1	2.3	0.0	100.0
406.40	656.40	8.0	1.5	90.5	0.0	0.0	0.0	0.0	0.0	100.0
411.12	661.12	6.0	8.7	84.5	0.0	0.0	0.4	0.0	0.4	100.0
414.85	664.85	5.9	1.4	92.0	0.0	0.7	0.0	0.0	0.0	100.0
418.10	668.10	1.0	1.0	36.5	59.6	0.5	1.0	0.0	0.4	100.0
418.30	668.30	4.3	0.0	72.8	19.6	1.1	0.0	0.0	2.2	100.0
418.30	668.30	9.0	0.7	90.3	0.0	0.0	0.0	0.0	0.0	100.0
419.80	669.80	11.5	1.9	85.9	0.0	0.4	0.0	0.0	0.3	100.0
420.20	670.20	10.3	0.0	87.8	0.0	0.7	1.1	0.0	0.1	100.0
420.75	670.75	2.9	12.6	46.4	33.3	0.5	3.9	0.0	0.4	100.0
421.00	671.00	0.0	6.4	83.7	0.0	0.0	7.5	0.7	1.7	100.0
422.15	672.15	3.0	10.6	40.3	37.4	1.5	7.2	0.0	0.0	100.0
423.60	673.60	3.5	8.1	0.0	78.2	10.1	0.0	0.0	0.1	100.0
425.20	675.20	0.0	0.0	13.7	71.3	15.0	0.0	0.0	0.0	100.0
427.00	677.00	8.7	0.0	0.0	83.2	2.7	0.0	0.0	5.4	100.0
430.55	680.55	0.0	0.0	63.9	22.1	13.5	0.5	0.0	0.0	100.0
439.30	689.30	1.4	0.0	36.6	50.5	9.3	2.2	0.0	0.0	100.0
445.45	695.45	0.0	0.0	57.0	41.9	1.1	0.0	0.0	0.0	100.0
451.25	701.25	4.1	0.0	60.8	23.4	9.3	0.0	0.0	2.4	100.0
452.00	702.00	3.9	1.4	64.4	22.8	6.0	0.0	0.0	1.5	100.0
455.65	705.65	6.3	1.7	91.7	0.0	0.0	0.3	0.0	0.0	100.0
459.30	709.30	9.4	2.6	85.8	0.0	1.6	0.6	0.0	0.0	100.0
459.70	709.70	6.2	2.9	88.0	0.0	0.0	1.2	1.5	0.2	100.0
464.10	714.10	4.3	1.0	87.7	0.0	0.7	2.3	4.0	0.0	100.0
A469.40	719.40	1.8	1.0	91.7	0.0	0.8	2.3	1.3	1.1	100.0
474.45	724.45	5.0	0.0	93.1	0.0	1.9	0.0	0.0	0.0	100.0
476.40	726.40	8.0	0.6	87.2	0.0	3.8	0.0	0.0	0.4	100.0
478.90	728.90	6.6	1.4	89.0	0.0	0.3	1.2	1.4	0.1	100.0
480.60	730.60	2.30	0.50	63.40	31.40	0.80	0.00	0.00	1.6	100.0
481.90	731.90	3.3	1.7	94.7	0.0	0.3	0.0	0.0	0.0	100.0
486.55	736.55	7.2	1.5	89.8	0.0	0.6	0.9	0.0	0.0	100.0
492.15	742.15	6.6	3.3	88.9	0.0	0.3	0.6	0.3	0.0	100.0
495.90	745.90	2.9	2.9	89.3	0.0	3.9	0.0	0.0	1.0	100.0
496.43	746.43	8.7	0.3	90.7	0.0	0.3	0.0	0.0	0.0	100.0
500.50	750.50	3.2	8.2	86.1	0.0	0.4	2.1	0.0	0.0	100.0
506.05	756.05	4.3	2.6	34.8	55.7	2.2	0.0	0.0	0.4	100.0
508.01	758.01	4.4	2.8	15.8	72.2	4.8	0.0	0.0	0.0	100.0
509.86	759.86	2.2	0.0	24.5	71.6	1.3	0.2	0.0	0.2	100.0
511.35	761.35	0.0	0.0	23.8	71.5	2.6	1.3	0.0	0.8	100.0
512.60	762.60	3.3	0.0	17.1	77.6	2.0	0.0	0.0	0.0	100.0
515.35	765.35	3.2	8.8	59.7	26.9	0.9	0.5	0.0	0.0	100.0
519.26	769.26	6.7	1.0	88.9	0.0	1.5	0.5	0.3	1.1	100.0
523.90	773.90	10.3	0.7	83.7	0.0	1.8	0.7	2.8	0.0	100.0
524.35	774.35	5.1	1.0	91.1	0.0	1.6	0.6	0.6	0.0	100.0
A527.62	777.62	3.1	0.3	95.6	0.0	0.9	0.0	0.0	0.1	100.0
528.50	778.50	4.5	2.1	90.3	0.0	0.6	0.9	1.5	0.1	100.0
532.14	782.14	5.8	2.8	90.0	0.0	0.8	0.3	0.3	0.0	100.0
536.95	786.95	3.3	0.5	95.6	0.0	0.0	0.3	0.3	0.0	100.0
543.23	793.23	1.2	0.0	96.7	0.0	1.8	0.0	0.0	0.3	100.0
546.85	796.85	0.5	0.5	96.0	0.0	2.8	0.2	0.0	0.0	100.0
553.33	803.33	5.9	0.6	92.5	0.0	0.6	0.3	0.0	0.1	100.0
558.75	808.75	9.8	1.0	87.5	0.0	0.7	0.3	0.7	0.0	100.0
564.45	814.45	7.3	1.3	89.2	0.0	0.0	0.8	1.3	0.1	100.0
569.20	819.20	8.8	1.0	88.9	0.0	0.0	0.3	0.8	0.2	100.0
575.35	825.35	7.3	1.4	89.9	0.0	0.0	0.0	0.6	0.8	100.0
581.00	831.00	4.6	0.8	93.8	0.0	0.0	0.8	0.0	0.0	100.0
586.00	836.00	4.7	1.1	94.1	0.0	0.0	0.0	0.0	0.1	100.0
589.60	839.60	5.2	0.9	93.0	0.0	0.0	0.0	0.9	0.0	100.0
595.05	845.05	4.3	2.6	91.8	0.0	0.5	0.5	0.3	0.0	100.0
B597.62	847.62	0.0	0.0	74.6	0.0	25.4	0.0	0.0	0.0	100.0
597.77	847.77	5.4	2.5	92.1	0.0	0.0	0.0	0.0	0.0	100.0
603.10	853.10	6.2	2.3	89.6	0.0	0.3	0.6	1.0	0.0	100.0
608.25	858.25	6.7	1.4	89.8	0.0	0.2	1.2	0.7	0.0	100.0
609.47	859.47	11.0	0.5	85.3	0.0	1.8	0.9	0.5	0.0	100.0
609.68	859.68	4.8	0.8	93.6	0.0	0.0	0.5	0.3	0.0	100.0
614.76	864.76	5.8	0.5	92.1	0.0	0.0	0.5	1.0	0.1	100.0
619.85	869.85	5.2	1.5	91.7	0.0	0.0	0.0	0.3	1.3	100.0
624.70	874.70	4.0	1.7	94.0	0.0	0.0	0.0	0.0	0.3	100.0
635.25	885.25	7.2	1.0	90.1	0.0	0.0	1.0	0.7	0.0	100.0
639.95	889.95	6.0	1.0	92.2	0.0	0.7	0.0	0.0	0.1	100.0
A644.00	894.00	2.6	1.0	90.5	0.0	5.2	0.7	0.0	0.0	100.0
645.17	895.17	6.6	0.6	88.7	0.0	1.2	1.7	1.2	0.0	100.0
649.66	899.66	6.4	2.0	91.2	0.0	0.4	0.0	0.0	0.0	100.0
A655.15	905.15	5.2	1.4	91.0	0.0	0.0	1.6	0.8	0.0	100.0
B655.20	905.20	3.0	1.4	95.3	0.0	0.0	0.0	0.3	0.0	100.0
660.40	910.40	5.6	0.4	86.3	0.0	0.0	2.2	5.2	0.3	100.0
670.10	920.10	5.8	0.6	90.0	0.0	0.0	1.6	1.6	0.4	100.0
675.25	925.25	3.1	1.5	93.9	0.0	0.0	0.5	0.5	0.5	100.0
680.17	930.17	2.9	0.7	96.4	0.0	0.0	0.0	0.0	0.0	100.0
685.40	935.40	4.6	2.2	90.2	0.0	0.3	0.8	1.9	0.0	100.0
690.30	940.30	5.7	1.5	92.5	0.0	0.0	0.3	0.0	0.0	100.0
695.50	945.50	7.0	0.9	90.4	0.0	0.0	0.6	1.1	0.0	100.0
698.00	948.00	1.7	3.8	55.1	33.1	6.3	0.0	0.0	0.0	100.0
699.45	949.45	7.1	1.0	5.2	82.8	1.3	0.3	0.0	2.3	100.0
700.65	950.65	0.0	0.0	51.0	28.6	20.4	0.0	0.0	0.0	100.0
701.75	951.75	3.5	0.5	95.7	0.0	0.3	0.0	0.0	0.0	100.0
702.75	952.75	4.2	1.2	94.3	0.0	0.0	0.3	0.0	0.0	100.0
706.90	956.90	6.6	0.6	89.5	0.0	3.0	0.0	0.3	0.0	100.0
711.60	961.60	1.5	0.6	95.5	0.0	2.4	0.0	0.0	0.0	100.0
715.35	965.35	2.1	1.2	95.9	0.0	0.6	0.0	0.0	0.2	100.0
720.15	970.15	2.8	1.4	88.5	0.0	0.0	3.9	2.8	0.6	100.0
725.35	975.35	4.5	1.4	94.1	0.0	0.0	0.0	0.0	0.0	100.0
730.35	980.35	5.1	1.0	93.8	0.0	0.0	0.0	0.0	0.1	100.0

Sample:	Depth (m):	pla	cpx	opx	ol	chr	phl	qtz	others	Total
735.10	985.10	1.4	1.1	96.9	0.0	0.6	0.0	0.0	0.0	100.0
739.80	989.80	3.1	3.3	92.4	0.0	0.0	0.7	0.5	0.0	100.0
744.70	994.70	1.8	0.9	95.1	1.5	0.6	0.0	0.0	0.1	100.0
745.45	995.45	2.2	11.4	80.3	1.3	3.9	0.9	0.0	0.0	100.0
745.65	995.65	3.9	2.1	18.2	69.3	5.0	0.4	0.0	1.1	100.0
749.30	999.30	1.2	1.6	55.3	39.1	2.4	0.4	0.0	0.0	100.0
752.40	1002.40	3.7	0.9	18.7	72.9	3.3	0.5	0.0	0.0	100.0
752.54	1002.54	1.6	0.0	2.6	94.3	0.8	0.0	0.0	0.7	100.0
753.09	1003.09	0.5	4.5	9.0	83.0	2.5	0.0	0.0	0.5	100.0
761.95	1011.95	0.0	0.0	0.0	100.0	0.0	0.0	0.0	0.0	100.0
762.75	1012.75	0.0	0.0	0.0	100.0	0.0	0.0	0.0	0.0	100.0
773.74	1023.74	0.0	0.0	0.0	100.0	0.0	0.0	0.0	0.0	100.0
774.25	1024.25	0.0	0.0	0.0	97.0	1.5	0.0	0.0	1.5	100.0
776.10	1026.10	2.4	4.1	0.0	88.8	0.6	4.1	0.0	0.0	100.0
777.43	1027.43	8.0	0.0	0.0	89.2	2.4	0.4	0.0	0.0	100.0
779.59	1029.59	6.0	8.8	1.2	79.5	1.6	2.8	0.0	0.1	100.0
781.37	1031.37	4.7	0.0	0.0	94.7	0.6	0.0	0.0	0.0	100.0
782.05	1032.05	7.7	0.4	4.7	82.1	4.3	0.4	0.0	0.4	100.0
784.06	1034.06	1.6	1.2	45.4	46.8	5.0	0.0	0.0	0.0	100.0
784.64	1034.64	2.4	13.4	8.7	72.4	3.1	0.0	0.0	0.0	100.0
786.60	1036.60	7.1	3.2	0.0	86.5	0.0	3.2	0.0	0.0	100.0
787.00	1037.00	10.0	0.0	0.4	88.7	0.4	0.4	0.0	0.1	100.0
791.35	1041.35	0.4	0.0	42.8	54.9	0.8	0.8	0.0	0.3	100.0
793.60	1043.60	0.0	12.8	0.0	84.9	2.3	0.0	0.0	0.0	100.0
793.80	1043.80	0.0	0.9	0.0	89.6	1.8	0.0	0.0	7.7	100.0
796.04	1046.04	0.0	0.5	0.0	99.0	0.5	0.0	0.0	0.0	100.0
802.23	1052.23	0.0	0.0	0.8	98.0	1.2	0.0	0.0	0.0	100.0
803.41	1053.41	0.4	0.0	16.6	81.7	0.4	0.0	0.0	0.9	100.0
803.69	1053.69	0.5	2.0	0.0	90.2	1.0	2.9	0.0	3.4	100.0
806.80	1056.80	2.4	3.6	0.0	91.9	1.2	0.8	0.0	0.1	100.0
814.00	1064.00	2.2	0.0	30.5	66.1	0.0	1.1	0.0	0.1	100.0
816.10	1066.10	0.0	5.7	5.7	88.6	0.0	0.0	0.0	0.0	100.0
816.20	1066.20	2.6	11.9	7.7	77.8	0.0	0.0	0.0	0.0	100.0
822.44	1072.44	4.1	0.0	26.1	69.8	0.0	0.0	0.0	0.0	100.0
824.23	1074.23	5.7	0.9	1.9	88.7	1.4	1.4	0.0	0.0	100.0
830.15	1080.15	1.5	12.4	8.6	76.9	0.3	0.3	0.0	0.0	100.0
NG2										
39.35	1079.35	4.4	5.5	16.5	69.1	1.8	2.6	0.0	0.1	100.0
42.55	1082.55	6.6	0.0	12.4	79.5	1.1	0.4	0.0	0.0	100.0
46.40	1086.40	0.4	2.3	2.0	86.0	0.4	6.6	0.0	2.3	100.0
51.50	1091.50	1.9	0.4	7.8	80.5	1.2	1.9	0.0	6.3	100.0
A51.90	1091.90	3.8	1.0	94.2	0.0	0.0	1.0	0.0	0.0	100.0
B51.90	1092.00	5.4	1.0	87.5	0.0	0.0	2.0	0.2	3.9	100.0
53.50	1093.50	0.0	3.8	19.3	74.2	1.5	0.4	0.0	0.8	100.0
55.50	1095.50	2.3	3.2	54.4	39.3	0.8	0.0	0.0	0.0	100.0
59.10	1099.10	0.7	1.1	26.1	70.3	0.7	0.7	0.0	0.4	100.0
63.35	1103.35	4.6	4.2	47.2	40.7	0.9	0.9	0.0	1.5	100.0
69.42	1109.42	3.0	4.0	45.5	47.0	0.0	0.5	0.0	0.0	100.0
71.50	1111.50	0.0	6.4	66.4	26.0	1.1	0.0	0.0	0.1	100.0
73.60	1113.60	2.4	4.7	53.5	38.6	0.8	0.0	0.0	0.0	100.0
77.20	1117.20	7.6	5.3	29.2	56.8	1.1	0.0	0.0	0.0	100.0
80.35	1120.35	3.5	0.0	28.6	67.3	0.5	0.0	0.0	0.1	100.0
83.75	1123.75	6.3	1.6	18.0	72.9	0.4	0.8	0.0	0.0	100.0

Sample:	Depth (m):	pla	cpx	opx	ol	chr	phl	qtz	others	Total
86.20	1126.20	1.5	1.5	31.1	64.6	0.4	0.8	0.0	0.1	100.0
89.30	1129.30	0.0	0.0	29.4	70.1	0.4	0.0	0.0	0.1	100.0
89.95	1129.95	0.0	9.9	22.9	64.9	1.5	0.8	0.0	0.0	100.0
91.40	1131.40	2.9	1.4	94.8	0.0	0.0	0.9	0.0	0.0	100.0
98.00	1138.00	4.0	9.5	85.5	0.0	0.0	0.6	0.3	0.1	100.0
A102.60	1142.60	1.2	2.3	95.5	0.0	0.0	0.9	0.0	0.1	100.0
B102.60	1142.70	11.1	2.2	85.5	0.0	0.0	0.7	0.4	0.1	100.0
106.60	1146.60	6.3	2.6	90.6	0.0	0.0	0.3	0.0	0.2	100.0
110.80	1150.80	2.0	1.3	95.3	0.0	0.0	0.7	0.7	0.0	100.0
115.25	1155.25	3.1	1.0	95.8	0.0	0.0	0.0	0.0	0.1	100.0
119.10	1159.10	0.0	0.0	71.1	28.9	0.0	0.0	0.0	0.0	100.0
120.40	1160.40	13.8	0.9	84.6	0.0	0.0	0.6	0.0	0.1	100.0
122.30	1162.30	1.9	5.7	38.7	51.8	0.0	1.9	0.0	0.0	100.0
123.40	1163.40	0.0	4.2	19.1	72.5	2.3	1.9	0.0	0.0	100.0
127.15	1167.15	4.4	1.6	19.9	70.5	0.4	0.5	0.0	2.7	100.0
130.20	1170.20	5.3	1.6	18.3	74.4	0.4	0.0	0.0	0.0	100.0
134.40	1174.40	7.8	3.1	19.1	67.9	1.0	1.0	0.0	0.1	100.0
138.80	1178.80	5.7	3.4	1.5	86.7	1.1	1.5	0.0	0.1	100.0
143.30	1183.30	2.5	0.0	24.7	71.7	0.5	0.4	0.0	0.2	100.0
143.35	1183.35	6.3	0.0	6.8	85.6	1.3	0.0	0.0	0.0	100.0
152.35	1192.35	7.9	5.8	14.5	70.5	1.2	0.0	0.0	0.1	100.0
157.30	1197.30	0.0	0.0	18.3	79.9	0.6	1.2	0.0	0.0	100.0
159.35	1199.35	2.7	0.4	92.4	4.5	0.0	0.0	0.0	0.0	100.0
161.65	1201.65	4.1	0.0	91.0	4.1	0.8	0.0	0.0	0.0	100.0
165.40	1205.40	0.0	0.0	92.3	5.3	0.0	2.4	0.0	0.0	100.0
165.62	1205.62	0.4	0.0	76.7	21.1	0.8	0.8	0.0	0.2	100.0
A176.00	1216.00	5.5	0.8	93.6	0.0	0.0	0.0	0.0	0.1	100.0
B176.00	1216.10	3.2	0.0	96.4	0.0	0.0	0.4	0.0	0.0	100.0
180.55	1220.55	4.1	1.7	92.5	0.0	0.0	1.7	0.0	0.0	100.0
185.40	1225.40	5.9	1.5	92.1	0.0	0.0	0.5	0.0	0.0	100.0
189.40	1229.40	5.6	1.7	91.6	0.0	0.0	1.0	0.0	0.1	100.0
194.20	1234.20	5.4	0.4	94.2	0.0	0.0	0.0	0.0	0.0	100.0
197.00	1237.00	1.7	0.0	92.7	5.5	0.0	0.0	0.0	0.1	100.0
197.75	1237.75	0.8	1.3	61.5	35.1	0.8	0.4	0.0	0.1	100.0
198.85	1238.85	1.4	0.0	41.7	56.2	0.0	0.7	0.0	0.0	100.0
200.50	1240.50	1.7	0.0	54.7	43.2	0.4	0.0	0.0	0.0	100.0
204.40	1244.40	5.0	0.8	86.2	7.9	0.0	0.0	0.0	0.1	100.0
206.30	1246.30	1.9	0.0	93.0	4.6	0.0	0.5	0.0	0.0	100.0
208.40	1248.40	3.8	0.0	92.0	4.2	0.0	0.0	0.0	0.0	100.0
210.50	1250.50	1.9	6.4	80.8	10.9	0.0	0.0	0.0	0.0	100.0
212.20	1252.20	3.4	0.8	65.7	30.1	0.0	0.0	0.0	0.0	100.0
213.30	1253.30	4.9	7.8	9.9	74.9	2.5	0.0	0.0	0.0	100.0
217.60	1257.60	0.5	0.0	49.8	48.3	0.5	0.9	0.0	0.0	100.0
220.50	1260.50	4.1	6.0	9.3	79.5	0.7	0.4	0.0	0.0	100.0
225.51	1265.51	0.4	2.6	94.8	1.5	0.0	0.7	0.0	0.0	100.0
228.75	1268.75	3.4	0.4	43.2	51.7	0.4	0.9	0.0	0.0	100.0
231.80	1271.80	5.0	0.8	81.1	11.2	1.9	0.0	0.0	0.0	100.0
233.85	1273.85	8.7	0.0	81.3	9.5	0.4	0.0	0.0	0.1	100.0
234.85	1274.85	6.1	0.0	86.6	6.1	1.1	0.0	0.0	0.1	100.0
238.90	1278.90	0.0	23.4	18.8	52.6	5.2	0.0	0.0	0.0	100.0
241.27	1281.27	1.8	0.5	71.0	12.9	13.8	0.0	0.0	0.0	100.0
A241.27	1281.37	4.9	1.6	68.4	9.4	15.2	0.4	0.0	0.1	100.0
A241.55	1281.55	10.9	0.8	87.9	0.0	0.0	0.4	0.0	0.0	100.0
B241.55	1281.65	13.1	0.7	68.8	17.0	0.0	0.4	0.0	0.0	100.0

Sample:	Depth (m):	pla	cpx	opx	ol	chr	phl	qtz	others	Total
284.66	1324.66	19.3	0.0	79.8	0.0	0.0	0.9	0.0	0.0	100.0
289.90	1329.90	15.3	0.6	83.4	0.0	0.0	0.6	0.0	0.1	100.0
293.60	1333.60	28.3	0.0	71.7	0.0	0.0	0.0	0.0	0.0	100.0
294.12	1334.12	15.7	0.0	76.6	0.0	0.0	4.2	1.5	2.0	100.0
294.30	1334.30	11.1	2.1	86.8	0.0	0.0	0.0	0.0	0.0	100.0
294.65	1334.65	19.1	0.7	78.1	0.0	0.0	2.1	0.0	0.0	100.0
A296.95	1336.95	9.8	0.6	88.6	0.0	0.0	0.6	0.0	0.4	100.0
B296.95	1337.00	13.2	0.4	85.5	0.0	0.0	0.4	0.0	0.5	100.0
A299.89	1340.89	43.3	0.0	56.7	0.0	0.0	0.0	0.0	0.0	100.0
305.75	1345.75	11.4	1.8	86.3	0.0	0.0	0.0	0.5	0.0	100.0
307.10	1347.10	6.6	0.5	90.7	0.0	1.6	0.5	0.0	0.1	100.0
313.18	1353.18	1.5	2.4	84.9	0.0	0.0	7.7	3.5	0.0	100.0
320.15	1360.15	13.8	2.0	83.2	0.0	0.0	0.5	0.5	0.0	100.0
B326.28	1366.28	9.7	4.3	81.6	0.0	0.3	0.3	0.0	3.8	100.0
B327.73	1367.73	2.0	0.5	65.3	24.8	7.3	0.0	0.0	0.1	100.0
A332.25	1372.25	5.0	0.9	89.2	0.0	1.7	0.0	2.6	0.6	100.0
B332.25	1372.35	15.7	0.8	80.3	0.0	0.8	1.5	0.5	0.4	100.0
339.13	1379.13	0.3	4.5	81.0	0.0	0.0	6.2	6.2	1.8	100.0
A344.39	1384.39	10.2	1.8	87.4	0.0	0.3	0.3	0.0	0.0	100.0
350.48	1390.48	14.8	1.0	83.8	0.0	0.2	0.0	0.0	0.2	100.0
355.70	1395.70	13.4	4.3	79.8	0.0	0.3	0.0	2.0	0.2	100.0
B358.66	1398.66	5.2	1.9	52.5	37.8	2.5	0.0	0.0	0.1	100.0
A360.20	1400.20	1.1	0.3	80.5	14.1	3.7	0.3	0.0	0.0	100.0
B360.20	1400.30	13.2	0.2	83.9	0.0	0.2	0.7	0.0	1.8	100.0
366.00	1406.00	12.8	4.3	82.3	0.0	0.3	0.3	0.0	0.0	100.0
372.60	1412.60	6.0	0.2	72.3	19.2	2.2	0.0	0.0	0.1	100.0
377.38	1417.38	7.9	1.8	88.1	0.9	1.1	0.2	0.0	0.0	100.0
A382.65	1422.65	1.3	1.1	3.5	92.0	2.1	0.0	0.0	0.0	100.0
397.68	1437.68	1.8	0.0	81.8	12.6	2.5	1.3	0.0	0.0	100.0
398.65	1438.65	1.2	0.0	51.9	43.3	3.3	0.2	0.0	0.1	100.0
405.00	1445.00	7.0	0.2	91.3	0.0	1.0	0.5	0.0	0.0	100.0
411.10	1451.10	5.0	0.4	52.6	38.4	3.3	0.2	0.0	0.1	100.0
A420.00	1460.00	4.0	3.3	34.7	55.6	2.4	0.0	0.0	0.0	100.0
424.44	1464.44	8.6	1.9	86.4	1.7	0.7	0.7	0.0	0.0	100.0
426.60	1466.60	7.40	0.70	77.40	13.8	0.5	0.2	0.0	0.0	100.0
428.15	1468.15	8.0	2.9	86.9	0.0	0.2	1.2	0.0	0.8	100.0
429.47	1469.47	7.5	4.2	45.0	40.2	1.9	0.2	0.0	1.0	100.0
436.58	1476.58	10.3	0.8	76.5	9.6	2.3	0.5	0.0	0.0	100.0
B438.29	1478.29	7.1	2.5	30.0	59.8	0.5	0.0	0.0	0.1	100.0
438.57	1478.57	9.8	6.8	83.0	0.0	0.2	0.2	0.0	0.0	100.0
442.00	1482.00	12.0	3.4	82.7	0.0	0.7	1.2	0.0	0.0	100.0
447.00	1487.00	5.3	3.2	89.1	0.0	0.2	1.2	0.7	0.3	100.0
449.40	1489.40	6.8	1.0	24.8	65.8	1.0	0.5	0.0	0.1	100.0
450.70	1490.70	8.5	2.6	88.1	0.0	0.0	0.8	0.0	0.0	100.0
452.00	1492.00	7.3	2.1	74.8	13.4	1.2	1.2	0.0	0.0	100.0
454.26	1494.26	5.5	1.1	19.0	71.9	2.5	0.0	0.0	0.0	100.0
458.00	1498.00	6.0	3.0	87.8	0.0	0.0	0.7	1.8	0.7	100.0
467.65	1507.65	6.3	1.6	55.5	33.4	2.5	0.7	0.0	0.0	100.0
480.80	1520.80	5.1	5.6	51.6	35.5	1.3	0.9	0.0	0.0	100.0
481.00	1521.00	4.9	2.3	32.0	59.5	0.5	0.8	0.0	0.0	100.0
488.35	1528.35	8.6	4.4	85.4	0.0	0.0	0.7	0.0	0.9	100.0
490.05	1530.05	4.9	3.7	33.4	55.5	2.0	0.5	0.0	0.0	100.0
520.00	1560.00	4.1	0.7	20.1	69.9	2.2	1.7	0.0	1.3	100.0
530.95	1570.95	8.9	1.4	11.2	77.6	0.0	0.2	0.0	0.7	100.0
531.10	1571.10	10.3	1.2	84.2	1.0	0.0	1.4	0.0	1.9	100.0
546.00	1586.00	1.4	1.6	90.9	0.0	0.5	1.6	0.0	4.0	100.0
A550.05	1590.05	7.8	1.1	4.3	83.8	0.5	2.5	0.0	0.0	100.0
551.90	1591.90	5.2	1.4	83.0	8.0	0.7	1.7	0.0	0.0	100.0
557.10	1597.10	5.6	1.6	87.5	4.7	0.2	0.4	0.0	0.0	100.0
A591.00	1631.00	7.8	4.0	85.1	0.0	0.0	2.4	0.0	0.7	100.0
595.05	1635.05	7.4	4.3	87.7	0.0	0.0	0.5	0.0	0.1	100.0
654.56	1694.56	9.1	1.7	12.9	73.9	1.7	0.7	0.0	0.0	100.0
706.53	1746.53	6.5	2.5	13.5	74.6	1.1	1.7	0.0	0.1	100.0
723.22	1763.22	4.2	2.1	18.5	73.1	1.3	0.8	0.0	0.0	100.0
737.00	1777.00	9.8	6.3	82.4	0.0	0.0	1.5	0.0	0.0	100.0
743.62	1783.62	16.2	3.2	75.1	0.0	0.0	2.9	2.3	0.3	100.0
754.00	1794.00	19.3	4.9	71.5	0.0	0.0	3.2	0.9	0.2	100.0
760.12	1800.12	22.0	7.3	64.0	0.0	0.5	3.1	3.0	0.1	100.0
762.27	1802.27	16.1	8.4	68.0	0.0	0.0	6.1	1.4	0.0	100.0
763.45	1803.45	7.0	5.5	71.8	3.7	0.7	6.0	0.0	5.3	100.0
772.36	1812.36	18.5	5.0	40.6	30.9	0.6	4.4	0.0	0.0	100.0
773.60	1813.60	36.9	7.0	46.7	0.0	0.7	6.0	2.4	0.3	100.0

APPENDIX III

A) Operating conditions for Jeol CXA-733 Superprobe

All electron microprobe data were determined on a Jeol CXA-733 Superprobe operating at 15 kV and a beam current of 25 nA, using a ZAF-correction routine provided by the manufacturer. International standards and pure synthetic crystals were used for calibration. The standards used are: Stillwater chromite, Orapa ilmenite, ilmenite (A236), St. John's Island olivine, fayalite (8526), jadeite (Rhodes), orthoclase (JVPL), orthoclase (PSU-1A), rhodonite (U.K.), rhodonite (Rhodes) and Ni-magnetite (Rhodes). LiF 200, PET and TAP were employed as diffracting crystals. For the analyses of the ferromagnesian phases (opx, ol, cpx) and plagioclase a defocused 10 μm beam was used, while most analyses of chromite were done with a focused beam. The counting times were set 30 sec for peak position and 10 sec for background position.

B) Analytical details for the X-ray fluorescence spectrometry

All samples were analysed using a Philips PW 1410 XRF spectrometer. Major elements were determined in duplicate sets employing the fusion-disc technique of Norrish and Hutton (1969),while trace elements and Na were analysed in 5 g pressed powder briquettes with corrections for instrumental drift, absorption, background and spectral interference. Counting times were as follows:

Si, Al and P	40 sec
Fe and Mn	20 sec
Ti, Ca and K	10 sec
Mg	200 sec
Na and all trace elements	200 sec
Background positions for Na and trace elements	100 sec .

Mass absorption coefficients were calculated using major element data and the data set from Heinrich (1966). USGS, NIMROC and other international standards were used for calibration.

For each trace element analysis counting error, lower limit of detection and lower limit of determination, i.e. defined as twice the detection limit, were calculated after the equations (Marsh, 1979):

a) counting error (c.e.):

$$c.e. = \frac{\left[\frac{R_P}{T_P} - \frac{R_B}{T_B}\right]^{\frac{1}{2}}}{R_P - R_P} * \text{concentration}$$

where R_P and R_B are count rates at Peak and Background positions and T_P and T_B are counting times at Peak and Background positions;

b) lower limit of detection (d.l.):

$$d.l. = \frac{3}{M} * \left[\frac{R_B}{T_B}\right]^{\frac{1}{2}}$$

where M is equal the counts per second per unit concentration;

c) lower limit of determination (l.l.d):

$$d.l. = \frac{6}{M} * \left[\frac{R_B}{T_B}\right]^{\frac{1}{2}} .$$

Approximate c.e.s and l.l.d.s are listed below:

element	c.e.	l.l.d.	concentration
	(all in ppm)		
Nb	0.6	1.6	150
Zr	0.5	1.4	100
Y	0.5	1.5	60
Sr	0.6	1.4	100
Rb	0.6	1.4	100
Zn	0.8	1.7	100
Cu	1.0	2.4	100
Ni	1.3	3.1	100
Co	0.8	3.0	40
Cr	1.3	2.7	350
V	0.8	2.8	60 .

Heinrich, K.F.J. (1966). X-ray absorption uncertainty, 296 - 377. In McKinley, T.D., Heinrich, K.F.J. and Wittry, D.B., Eds., The Electron Microprobe. John Wiley & Sons, Inc., New York, London, Sydney, 1035 pp.

Marsh, J.S. (1979). A manual for X-ray fluorescence determination of major and trace elements in natural silicate rock materials. Manual (unpubl.), Rhodes University, 41 pp.

Norrish, K. and Hutton, J.T. (1969). An accurate X-ray spectrographic method for the analysis of a wide range of geological samples. Geochim. Cosmochim. Acta, 33, 431 - 453.

APPENDIX IV

In the following pages the compositions of opx, cpx, ol, chr and pla, which were determined by the author (included are also some of Haikney's opx analyses) are listed. Standard deviations are quoted at the 1σ level.

Notes:

A) ortho- and clinopyroxene

Habit: cum denotes opx as cumulus phase
pcum denotes opx as postcumulus or replacement phase
n : number of analyses used to calculate composition and standard deviation
Mg# : cationic ratio of Mg/(Mg + Fe)
en : cationic ratio of Mg/(Mg + Fe + Ca)
wo : cationic ratio of Ca/(Mg + Fe + Ca)
fs : cationic ratio of Fe/(Mg + Fe + Ca)

B) olivine

n : number of analyses used to calculate composition and standard deviation
Fo : cationic ratio of Mg/(Mg + Fe)

C) chromite

Mode : acc denotes chr as accessory phase
maj denotes chr as major phase
ML denotes chr as sole cumulus phase
(P) : value from microprobe analysis
(C) : recalculated value assuming stoichiometry
n : number of analyses used to calculate composition and standard deviation
Cr/Al : cationic ratio of Cr/Al
Mg# : cationic ratio of $Mg/(Mg + Fe^{2+})$
FFE : cationic ratio of $Fe^{3+}/(Fe^{3+} + Fe^{2+})$
Cr/Cr+Al: cationic ratio of Cr/(Cr + Al)
Cr/Fe : weight ratio of Cr metal to Fe metal

D) plagioclase

Habit: cum denotes pla as cumulus phase
pcum denotes pla as postcumulus phase
n : number of analyses used to calculate composition and standard deviation
An : cationic ratio of Ca/(Ca + Na + K)

Total number of microprobe analyses completed by the author:

phase	number of samples	number of analyses
orthopyroxene	292	1786
clinopyroxene	95	433
olivine	36	220
amphibole	12	26
feldspar	264	1272
mica	8	11
chromite	216	1198

MICROPROBE DATA: Composition of orthopyroxene in the NG-sequence (NG3-borehole)

Sample:	3.98	28.62	55.00	79.60	99.60	126.05	146.50	151.90	152.90	153.15	153.20	154.72
Depth in NG-sequence in m:	3.98	28.62	55.00	79.60	99.60	126.05	146.50	151.90	152.90	153.15	153.20	154.72
Habit:	cum	cum	cum	cum	cum	cum	cum	cum	cum	cum	cum	cum
wt.%												
SiO2	54.57	54.78	55.16	55.30	55.01	54.75	54.56	54.56	55.77	54.76	55.14	55.76
TiO2	0.14	0.15	0.14	0.13	0.11	0.13	0.11	0.13	0.12	0.09	0.11	0.09
Al2O3	0.94	0.91	0.88	0.95	1.06	1.06	1.19	1.49	1.36	1.24	1.32	1.48
Cr2O3	0.35	0.33	0.34	0.33	0.41	0.37	0.39	0.52	0.49	0.47	0.54	0.50
FeO	13.70	13.61	13.25	13.11	12.94	12.78	12.39	11.29	11.16	12.27	12.31	9.60
MnO	0.29	0.27	0.27	0.27	0.32	0.27	0.27	0.24	0.22	0.29	0.27	0.21
NiO	0.07	0.09	0.10	0.14	0.10	0.05	0.08	0.02	0.09	0.05	0.09	0.08
MgO	28.53	28.21	28.64	29.16	28.52	29.39	29.06	29.63	29.36	29.39	28.69	30.16
CaO	0.85	1.18	0.84	0.92	1.19	1.24	1.22	1.72	1.76	0.80	1.56	1.85
Na2O	0.01	0.01	0.00	0.01	0.01	0.02	0.00	0.01	0.02	0.01	0.03	0.02
Total	99.44	99.54	99.63	100.33	99.67	100.05	99.26	99.61	100.35	99.36	100.05	99.75
cations (based on 6 oxygens):												
Si	1.9652	1.9706	1.9761	1.9674	1.9704	1.9540	1.9588	1.9458	1.9686	1.9602	1.9638	1.9669
Ti	0.0037	0.0040	0.0039	0.0036	0.0029	0.0034	0.0030	0.0034	0.0032	0.0024	0.0030	0.0024
Al	0.0397	0.0385	0.0374	0.0399	0.0447	0.0445	0.0503	0.0626	0.0567	0.0523	0.0554	0.0614
Cr	0.0100	0.0094	0.0096	0.0092	0.0117	0.0106	0.0110	0.0145	0.0136	0.0133	0.0152	0.0141
Fe	0.4126	0.4094	0.3970	0.3900	0.3875	0.3814	0.3720	0.3369	0.3295	0.3673	0.3668	0.2831
Mn	0.0087	0.0083	0.0083	0.0082	0.0097	0.0081	0.0083	0.0074	0.0066	0.0086	0.0081	0.0062
Ni	0.0021	0.0026	0.0029	0.0040	0.0028	0.0014	0.0023	0.0007	0.0027	0.0014	0.0025	0.0022
Mg	1.5313	1.5129	1.5293	1.5465	1.5226	1.5636	1.5550	1.5748	1.5449	1.5679	1.5228	1.5858
Ca	0.0327	0.0456	0.0322	0.0352	0.0458	0.0475	0.0468	0.0657	0.0666	0.0308	0.0595	0.0701
Na	0.0005	0.0009	0.0001	0.0009	0.0005	0.0011	0.0003	0.0008	0.0013	0.0005	0.0019	0.0014
Total	4.0065	4.0020	3.9967	4.0049	3.9987	4.0156	4.0077	4.0126	3.9937	4.0048	3.9989	3.9936
n	5	6	5	6	5	5	3	2	5	2	4	4
Mg#	0.7878	0.7870	0.7939	0.7986	0.7971	0.8039	0.8070	0.8238	0.8242	0.8102	0.8059	0.8485
en	77.5	76.9	78.1	78.4	77.8	78.5	78.8	79.6	79.6	79.8	78.1	81.8
wo	1.7	2.3	1.6	1.8	2.3	2.4	2.4	3.3	3.4	1.6	3.1	3.6
fs	20.9	20.8	20.3	19.8	19.8	19.1	18.8	17.0	17.0	18.7	18.8	14.6
standard deviation:												
wt.%												
SiO2	0.16	0.15	0.21	0.29	0.09	0.18	0.09	0.12	0.20	0.26	0.16	0.20
TiO2	0.01	0.01	0.01	0.01	0.01	0.01	0.01	0.01	0.01	0.01	0.02	0.01
Al2O3	0.02	0.05	0.05	0.07	0.03	0.03	0.02	0.17	0.08	0.01	0.09	0.08
Cr2O3	0.02	0.02	0.03	0.02	0.00	0.01	0.01	0.05	0.04	0.00	0.04	0.02
FeO	0.09	0.11	0.23	0.10	0.10	0.10	0.12	0.49	0.53	0.20	0.36	0.40
MnO	0.00	0.02	0.02	0.01	0.03	0.02	0.01	0.03	0.02	0.01	0.02	0.02
NiO	0.01	0.01	0.01	0.02	0.01	0.02	0.03	0.01	0.01	0.00	0.03	0.01
MgO	0.18	0.17	0.20	0.26	0.23	0.11	0.12	0.31	0.44	0.17	0.29	0.06
CaO	0.07	0.18	0.11	0.30	0.26	0.16	0.28	0.00	0.20	0.07	0.18	0.41
Na2O	0.00	0.01	0.00	0.01	0.00	0.00	0.01	0.00	0.00	0.00	0.00	0.01

Sample:	156.10	158.55	159.20	159.40	163.45	168.75	170.74	173.55	174.77	174.87	175.05	176.45
Depth in NG-sequence in m:	156.10	158.55	159.20	159.40	163.45	168.75	170.74	173.55	174.77	174.87	175.05	176.45
Habit:	cum	cum	cum	cum	cum	cum	cum	cum	cum	pcum	cum	cum
wt.%												
SiO2	56.67	56.21	56.01	54.86	55.00	55.81	55.39	55.55	55.73	56.10	55.75	55.36
TiO2	0.09	0.09	0.11	0.12	0.18	0.10	0.11	0.12	0.12	0.10	0.10	0.13
Al2O3	1.47	1.43	1.34	1.25	1.17	1.28	1.18	1.24	1.39	1.59	1.36	1.14
Cr2O3	0.42	0.40	0.46	0.47	0.44	0.47	0.49	0.36	0.45	0.44	0.47	0.54
FeO	7.46	10.45	10.71	11.99	12.61	11.95	11.85	11.66	10.48	9.18	10.40	11.86
MnO	0.17	0.21	0.20	0.27	0.23	0.21	0.24	0.22	0.24	0.23	0.22	0.23
NiO	0.03	0.06	0.08	0.07	0.09	0.04	0.08	0.07	0.07	0.07	0.12	0.10
MgO	32.97	30.94	29.46	29.01	29.27	29.24	29.92	29.46	30.37	31.98	31.22	29.38
CaO	0.64	0.40	1.70	1.41	1.12	1.01	0.96	1.14	1.24	0.74	0.74	0.95
Na2O	0.02	0.01	0.01	0.01	0.01	0.00	0.01	0.01	0.02	0.00	0.00	0.01
Total	99.95	100.20	100.08	99.45	100.11	100.13	100.24	99.82	100.11	100.43	100.37	99.70
cations (based on 6 oxygens):												
Si	1.9674	1.9713	1.9766	1.9625	1.9584	1.9759	1.9615	1.9718	1.9639	1.9562	1.9571	1.9704
Ti	0.0023	0.0025	0.0028	0.0031	0.0047	0.0028	0.0029	0.0032	0.0031	0.0027	0.0026	0.0034
Al	0.0601	0.0591	0.0558	0.0525	0.0492	0.0536	0.0492	0.0521	0.0579	0.0653	0.0562	0.0477
Cr	0.0116	0.0111	0.0127	0.0133	0.0123	0.0132	0.0136	0.0100	0.0125	0.0121	0.0131	0.0153
Fe	0.2167	0.3066	0.3162	0.3588	0.3755	0.3537	0.3511	0.3461	0.3090	0.2678	0.3053	0.3531
Mn	0.0049	0.0061	0.0061	0.0080	0.0069	0.0064	0.0073	0.0066	0.0072	0.0069	0.0066	0.0069
Ni	0.0009	0.0018	0.0021	0.0021	0.0026	0.0012	0.0024	0.0020	0.0020	0.0020	0.0034	0.0028
Mg	1.7061	1.6173	1.5491	1.5467	1.5533	1.5427	1.5793	1.5585	1.5949	1.6619	1.6338	1.5583
Ca	0.0239	0.0150	0.0643	0.0540	0.0428	0.0384	0.0364	0.0434	0.0467	0.0278	0.0277	0.0362
Na	0.0014	0.0004	0.0009	0.0005	0.0009	0.0003	0.0008	0.0004	0.0014	0.0000	0.0002	0.0010
Total	3.9952	3.9912	3.9868	4.0017	4.0066	3.9881	4.0045	3.9942	3.9985	4.0025	4.0058	3.9951
n	5	3	5	4	5	5	5	5	5	5	5	5
Mg#	0.8873	0.8406	0.8305	0.8117	0.8053	0.8135	0.8181	0.8183	0.8377	0.8612	0.8426	0.8153
en	87.6	83.4	80.3	78.9	78.8	79.7	80.3	80.0	81.8	84.9	83.1	80.0
wo	1.2	0.8	3.3	2.8	2.2	2.0	1.9	2.2	2.4	1.4	1.4	1.9
fs	11.1	15.8	16.4	18.3	19.0	18.3	17.8	17.8	15.8	13.7	15.5	18.1
standard deviation:												
wt.%												
SiO2	0.37	0.06	0.44	0.25	0.43	0.10	0.09	0.37	0.27	0.22	0.18	0.24
TiO2	0.01	0.01	0.01	0.01	0.02	0.01	0.01	0.01	0.01	0.00	0.01	0.01
Al2O3	0.05	0.04	0.09	0.04	0.06	0.05	0.08	0.09	0.11	0.02	0.07	0.14
Cr2O3	0.07	0.01	0.02	0.01	0.02	0.02	0.02	0.01	0.02	0.03	0.03	0.05
FeO	0.43	0.19	1.02	0.17	0.22	0.10	0.17	0.11	0.36	0.35	0.14	0.15
MnO	0.03	0.00	0.02	0.02	0.02	0.03	0.01	0.02	0.01	0.01	0.02	0.02
NiO	0.01	0.02	0.03	0.01	0.02	0.01	0.03	0.01	0.02	0.01	0.02	0.01
MgO	0.49	0.04	0.85	0.20	0.35	0.18	0.24	0.16	0.38	0.29	0.11	0.30
CaO	0.13	0.04	0.79	0.31	0.42	0.15	0.28	0.20	0.33	0.16	0.13	0.19
Na2O	0.01	0.00	0.01	0.01	0.01	0.00	0.01	0.00	0.01	0.00	0.00	0.01

Sample:	181.70	194.74	208.15	212.93	213.18	214.05	214.07	214.25	219.20	219.30	220.17	221.30
Depth in NG-sequence in m:	181.70	194.74	208.15	212.93	213.18	214.05	214.07	214.25	219.20	219.30	220.17	221.30
Habit:	cum	cum	cum	cum	cum	cum	cum	cum	cum	cum	cum	cum
wt.%												
SiO2	55.22	54.99	56.13	55.00	54.71	55.10	55.34	54.92	55.71	55.91	55.70	55.64
TiO2	0.14	0.15	0.10	0.14	0.13	0.16	0.15	0.14	0.13	0.13	0.16	0.21
Al2O3	1.18	1.17	1.04	1.17	1.29	1.25	1.26	1.24	1.15	1.35	1.12	1.19
Cr2O3	0.49	0.53	0.58	0.50	0.52	0.53	0.48	0.50	0.46	0.47	0.35	0.46
FeO	12.03	11.81	10.74	13.00	11.69	11.56	11.74	11.79	10.83	10.66	11.86	11.42
MnO	0.24	0.25	0.24	0.21	0.26	0.27	0.23	0.26	0.22	0.20	0.26	0.21
NiO	0.08	0.10	0.06	0.10	0.06	0.08	0.07	0.05	0.06	0.10	0.06	0.04
MgO	29.97	29.72	29.74	28.58	29.90	29.01	29.25	29.85	29.49	29.63	29.80	29.97
CaO	0.86	0.88	1.15	1.24	1.02	1.18	1.09	1.13	1.63	1.40	1.23	0.93
Na2O	0.01	0.02	0.01	0.01	0.01	0.00	0.02	0.02	0.02	0.02	0.02	0.01
Total	100.21	99.61	99.80	99.96	99.59	99.14	99.62	99.89	99.71	99.87	100.57	100.08
cations (based on 6 oxygens):												
Si	1.9577	1.9601	1.9840	1.9649	1.9513	1.9709	1.9700	1.9536	1.9753	1.9755	1.9660	1.9675
Ti	0.0038	0.0041	0.0027	0.0037	0.0034	0.0042	0.0041	0.0037	0.0034	0.0036	0.0044	0.0055
Al	0.0491	0.0492	0.0434	0.0493	0.0543	0.0526	0.0527	0.0521	0.0481	0.0563	0.0464	0.0496
Cr	0.0138	0.0149	0.0162	0.0142	0.0146	0.0149	0.0135	0.0141	0.0130	0.0132	0.0099	0.0130
Fe	0.3567	0.3521	0.3175	0.3885	0.3486	0.3458	0.3494	0.3508	0.3211	0.3148	0.3501	0.3377
Mn	0.0072	0.0074	0.0071	0.0064	0.0080	0.0083	0.0068	0.0078	0.0065	0.0061	0.0079	0.0064
Ni	0.0022	0.0027	0.0017	0.0027	0.0018	0.0023	0.0020	0.0016	0.0016	0.0027	0.0017	0.0011
Mg	1.5839	1.5790	1.5669	1.5221	1.5893	1.5466	1.5521	1.5825	1.5585	1.5605	1.5678	1.5793
Ca	0.0325	0.0335	0.0436	0.0473	0.0391	0.0454	0.0416	0.0429	0.0621	0.0528	0.0466	0.0352
Na	0.0007	0.0011	0.0010	0.0008	0.0010	0.0002	0.0010	0.0011	0.0016	0.0012	0.0017	0.0009
Total	4.0074	4.0042	3.9841	4.0000	4.0114	3.9913	3.9933	4.0101	3.9914	3.9868	4.0024	3.9961
n	6	5	4	3	6	5	5	5	5	4	3	4
Mg#	0.8162	0.8177	0.8315	0.7967	0.8201	0.8173	0.8162	0.8186	0.8292	0.8321	0.8174	0.8238
en	80.3	80.4	81.3	77.7	80.4	79.8	79.9	80.1	80.3	80.9	79.8	80.9
wo	1.6	1.7	2.3	2.4	2.0	2.3	2.1	2.2	3.2	2.7	2.4	1.8
fs	18.1	17.9	16.5	19.8	17.6	17.8	18.0	17.7	16.5	16.3	17.8	17.3
standard deviation:												
wt.%												
SiO2	0.14	0.15	0.06	0.32	0.20	0.20	0.17	0.16	0.12	0.17	0.05	0.10
TiO2	0.01	0.00	0.01	0.00	0.01	0.02	0.03	0.02	0.01	0.00	0.01	0.10
Al2O3	0.07	0.11	0.07	0.02	0.07	0.05	0.07	0.02	0.07	0.03	0.06	0.03
Cr2O3	0.02	0.09	0.04	0.01	0.03	0.03	0.02	0.03	0.04	0.03	0.02	0.04
FeO	0.09	0.14	0.13	0.13	0.16	0.27	0.14	0.23	0.16	0.50	0.24	0.07
MnO	0.02	0.04	0.01	0.01	0.02	0.02	0.01	0.01	0.01	0.03	0.04	0.02
NiO	0.03	0.02	0.00	0.02	0.02	0.00	0.02	0.01	0.02	0.01	0.01	0.02
MgO	0.12	0.15	0.24	0.03	0.25	0.35	0.32	0.19	0.26	0.33	0.18	0.20
CaO	0.10	0.10	0.37	0.12	0.39	0.47	0.37	0.35	0.26	0.37	0.45	0.22
Na2O	0.00	0.01	0.01	0.01	0.01	0.00	0.01	0.00	0.00	0.01	0.01	0.01

Sample:	232.00	248.25	255.20	260.05
Depth in NG-sequence in m:	232.00	248.25	255.20	260.05
Habit:	cum	cum	cum	cum
wt.%				
SiO2	54.78	55.68	55.68	55.21
TiO2	0.16	0.17	0.13	0.11
Al2O3	1.21	1.16	1.23	1.31
Cr2O3	0.46	0.46	0.52	0.48
FeO	11.85	11.03	10.96	10.99
MnO	0.24	0.20	0.24	0.25
NiO	0.11	0.07	0.08	0.08
MgO	29.75	30.19	30.39	29.78
CaO	1.13	1.29	1.06	1.56
Na2O	0.01	0.02	0.01	0.02
Total	99.71	100.28	100.30	99.80
cations (based on 6 oxygens):				
Si	1.9534	1.9642	1.9625	1.9598
Ti	0.0042	0.0046	0.0035	0.0030
Al	0.0510	0.0484	0.0512	0.0549
Cr	0.0131	0.0128	0.0144	0.0136
Fe	0.3533	0.3255	0.3229	0.3263
Mn	0.0072	0.0060	0.0072	0.0074
Ni	0.0033	0.0020	0.0023	0.0024
Mg	1.5813	1.5876	1.5966	1.5755
Ca	0.0431	0.0488	0.0399	0.0594
Na	0.0010	0.0012	0.0009	0.0016
Total	4.0109	4.0012	4.0015	4.0065
n	6	5	8	9
Mg#	0.8174	0.8298	0.8318	0.8284
en	80.0	80.9	81.5	80.3
wo	2.2	2.5	2.0	3.0
fs	17.9	16.6	16.5	16.6
standard deviation:				
wt.%				
SiO2	0.09	0.19	0.26	0.16
TiO2	0.03	0.03	0.02	0.02
Al2O3	0.06	0.08	0.07	0.05
Cr2O3	0.04	0.02	0.01	0.02
FeO	0.27	0.04	0.23	0.18
MnO	0.03	0.02	0.03	0.03
NiO	0.01	0.01	0.02	0.02
MgO	0.31	0.13	0.27	0.37
CaO	0.46	0.20	0.41	0.44
Na2O	0.01	0.01	0.01	0.01

MICROPROBE DATA: Composition of orthopyroxene in the NG-sequence (NG1-borehole)

Sample:	17.00	25.00	29.80	35.00	46.25	55.40	56.00	65.19	74.45	79.75	84.90	89.55
Depth in NG-sequence in m:	267.00	275.00	279.80	285.00	296.25	305.40	306.00	315.19	324.45	329.75	334.90	339.55
Habit:	cum	cum	cum	cum	cum	cum	cum	cum	cum	cum	cum	cum
wt.%												
SiO2	54.65	55.42	55.75	55.33	55.13	55.48	55.54	55.88	55.77	55.50	56.22	55.89
TiO2	0.14	0.14	0.13	0.14	0.12	0.08	0.10	0.09	0.13	0.13	0.12	0.12
Al2O3	1.24	1.17	1.29	1.24	1.22	1.34	1.15	1.28	1.19	1.19	1.47	1.17
Cr2O3	0.51	0.44	0.49	0.49	0.48	0.51	0.44	0.47	0.47	0.46	0.46	0.43
FeO	12.36	12.03	10.45	11.53	11.28	10.74	11.59	10.60	10.65	12.14	8.96	10.65
MnO	0.26	0.27	0.22	0.24	0.23	0.25	0.23	0.24	0.24	0.26	0.21	0.23
NiO	0.08	0.08	0.07	0.07	0.07	0.08	0.09	0.07	0.08	0.08	0.07	0.06
MgO	29.69	28.83	30.01	29.22	29.85	29.82	29.31	29.64	29.87	29.00	31.49	30.57
CaO	0.94	1.31	1.38	1.23	1.30	1.38	1.39	1.57	1.31	1.09	1.39	0.88
Na2O	0.01	0.02	0.03	0.01	0.01	0.02	0.03	0.01	0.02	0.02	0.02	0.02
Total	99.85	99.69	99.81	99.50	99.70	99.70	99.86	99.86	99.75	99.88	100.40	100.01
cations (based on 6 oxygens):												
Si	1.9496	1.9750	1.9703	1.9712	1.9601	1.9666	1.9725	1.9756	1.9738	1.9738	1.9620	1.9701
Ti	0.0037	0.0037	0.0034	0.0037	0.0033	0.0021	0.0026	0.0025	0.0034	0.0036	0.0031	0.0032
Al	0.0522	0.0489	0.0539	0.0520	0.0513	0.0561	0.0482	0.0532	0.0496	0.0501	0.0603	0.0485
Cr	0.0143	0.0124	0.0137	0.0137	0.0134	0.0144	0.0124	0.0132	0.0132	0.0131	0.0128	0.0121
Fe	0.3688	0.3585	0.3089	0.3434	0.3355	0.3183	0.3441	0.3133	0.3154	0.3611	0.2615	0.3138
Mn	0.0077	0.0081	0.0066	0.0073	0.0068	0.0074	0.0070	0.0071	0.0071	0.0077	0.0063	0.0070
Ni	0.0022	0.0022	0.0019	0.0020	0.0021	0.0024	0.0025	0.0020	0.0022	0.0022	0.0020	0.0016
Mg	1.5790	1.5313	1.5807	1.5515	1.5817	1.5756	1.5515	1.5619	1.5759	1.5375	1.6380	1.6061
Ca	0.0358	0.0499	0.0522	0.0471	0.0495	0.0523	0.0527	0.0595	0.0498	0.0415	0.0520	0.0333
Na	0.0024	0.0012	0.0026	0.0009	0.0009	0.0016	0.0019	0.0010	0.0015	0.0019	0.0011	0.0011
Total	4.0156	3.9913	3.9942	3.9927	4.0047	3.9968	3.9954	3.9893	3.9920	3.9924	3.9989	3.9969
n	24	10	12	9	7	4	8	9	10	12	10	7
Mg#	0.8107	0.8103	0.8365	0.8188	0.8250	0.8319	0.8185	0.8329	0.8333	0.8098	0.8623	0.8365
en	79.6	78.9	81.4	79.9	80.4	81.0	79.6	80.7	81.2	79.2	83.9	82.2
wo	1.8	2.6	2.7	2.4	2.5	2.7	2.7	3.1	2.6	2.1	2.7	1.7
fs	18.6	18.5	15.9	17.7	17.1	16.4	17.7	16.2	16.2	18.6	13.4	16.1
standard deviation:												
wt.%												
SiO2	0.26	0.14	0.25	0.22	0.22	0.11	0.23	0.20	0.30	0.15	0.26	0.35
TiO2	0.02	0.02	0.01	0.01	0.01	0.01	0.03	0.03	0.02	0.01	0.06	0.01
Al2O3	0.11	0.15	0.11	0.09	0.07	0.05	0.20	0.13	0.18	0.07	0.09	0.10
Cr2O3	0.03	0.05	0.02	0.05	0.03	0.01	0.08	0.04	0.05	0.03	0.04	0.04
FeO	0.21	0.18	0.27	0.31	0.07	0.19	0.28	0.26	0.29	0.22	0.36	0.22
MnO	0.02	0.02	0.02	0.03	0.02	0.02	0.03	0.02	0.02	0.03	0.02	0.02
NiO	0.02	0.04	0.02	0.02	0.03	0.02	0.02	0.03	0.03	0.02	0.02	0.02
MgO	0.30	0.30	0.30	0.24	0.15	0.12	0.18	0.44	0.46	0.17	0.36	0.25
CaO	0.33	0.38	0.43	0.38	0.27	0.21	0.33	0.61	0.76	0.21	0.35	0.35
Na2O	0.01	0.01	0.02	0.01	0.01	0.00	0.02	0.01	0.01	0.01	0.01	0.01

Sample:	90.33	94.60	105.45	110.52	119.90	130.60	146.50	152.20	152.25	158.20	163.27	173.37
Depth in NG-sequence in m:	340.33	344.60	355.45	360.52	369.90	380.60	396.50	402.20	402.25	408.20	413.27	423.37
Habit:	cum	cum	cum	cum	cum	cum	cum	cum	cum	cum	cum	cum
wt.%												
SiO2	55.33	56.17	55.90	56.18	56.03	55.25	55.65	55.81	56.67	56.02	55.59	55.83
TiO2	0.06	0.08	0.15	0.17	0.10	0.09	0.09	0.08	0.07	0.09	0.11	0.08
Al2O3	1.47	1.49	1.05	1.26	1.36	1.21	1.31	1.35	1.25	1.20	1.12	1.18
Cr2O3	0.46	0.49	0.39	0.43	0.40	0.47	0.48	0.44	0.42	0.44	0.50	0.47
FeO	8.40	10.36	11.45	10.80	10.58	10.35	10.94	9.79	7.73	10.58	11.28	10.34
MnO	0.22	0.22	0.23	0.22	0.21	0.26	0.24	0.24	0.19	0.22	0.25	0.23
NiO	0.08	0.05	0.06	0.06	0.08	0.07	0.09	0.10	0.08	0.05	0.06	0.09
MgO	32.00	30.20	30.28	29.82	30.10	30.03	29.54	30.11	32.54	29.45	29.74	30.42
CaO	1.43	1.51	1.23	1.43	1.21	0.98	1.34	1.50	0.86	1.37	1.20	1.30
Na2O	0.02	0.01	0.02	0.02	0.02	0.01	0.03	0.02	0.01	0.01	0.02	0.02
Total	99.45	100.57	100.76	100.39	100.09	98.71	99.70	99.44	99.83	99.43	99.88	99.97
cations (based on 6 oxygens):												
Si	1.9482	1.9686	1.9657	1.9757	1.9735	1.9723	1.9730	1.9741	1.9737	1.9859	1.9705	1.9692
Ti	0.0016	0.0021	0.0040	0.0045	0.0026	0.0024	0.0025	0.0020	0.0019	0.0023	0.0030	0.0022
Al	0.0608	0.0614	0.0434	0.0520	0.0564	0.0508	0.0547	0.0565	0.0513	0.0500	0.0468	0.0493
Cr	0.0127	0.0135	0.0108	0.0119	0.0111	0.0133	0.0133	0.0123	0.0117	0.0123	0.0141	0.0132
Fe	0.2474	0.3037	0.3367	0.3176	0.3117	0.3091	0.3243	0.2896	0.2251	0.3138	0.3344	0.3049
Mn	0.0064	0.0065	0.0068	0.0066	0.0064	0.0079	0.0071	0.0072	0.0057	0.0066	0.0074	0.0070
Ni	0.0022	0.0015	0.0017	0.0018	0.0023	0.0020	0.0025	0.0030	0.0022	0.0015	0.0018	0.0026
Mg	1.[illegible]94	1.5774	1.5867	1.5630	1.5799	1.5978	1.5612	1.5875	1.6888	1.5560	1.5715	1.5990
Ca	0.0538	0.0566	0.0465	0.0539	0.0455	0.0373	0.0508	0.0567	0.0323	0.0520	0.0457	0.0492
Na	0.0017	0.0010	0.0015	0.0017	0.0013	0.0005	0.0019	0.0012	0.0005	0.0006	0.0016	0.0013
Total	4.0143	3.9923	4.0039	3.9887	3.9907	3.9935	3.9914	3.9901	3.9932	3.9809	3.9969	3.9980
n	4	8	12	11	10	4	12	6	10	9	4	7
Mg#	0.8716	0.8386	0.8250	0.8311	0.8352	0.8379	0.8280	0.8457	0.8824	0.8322	0.8245	0.8398
en	84.8	81.4	80.5	80.8	81.6	82.2	80.6	82.1	86.8	81.0	80.5	81.9
wo	2.7	2.9	2.4	2.8	2.3	1.9	2.6	2.9	1.7	2.7	2.3	2.5
fs	12.5	15.7	17.1	16.4	16.1	15.9	16.7	15.0	11.6	16.3	17.1	15.6
standard deviation:												
wt.%												
SiO2	0.08	0.13	0.30	0.22	0.15	0.18	0.32	0.40	0.26	0.23	0.18	0.35
TiO2	0.00	0.01	0.06	0.04	0.02	0.01	0.01	0.01	0.01	0.02	0.01	0.02
Al2O3	0.02	0.06	0.25	0.17	0.13	0.04	0.07	0.06	0.09	0.06	0.04	0.10
Cr2O3	0.03	0.02	0.07	0.06	0.02	0.02	0.03	0.04	0.13	0.04	0.04	0.03
FeO	0.33	0.30	0.17	0.24	0.16	0.11	0.40	0.58	0.27	0.24	0.19	0.25
MnO	0.01	0.02	0.02	0.02	0.02	0.02	0.02	0.02	0.02	0.02	0.01	0.01
NiO	0.02	0.02	0.02	0.04	0.01	0.03	0.02	0.02	0.02	0.02	0.01	0.02
MgO	0.64	0.30	0.42	0.39	0.23	0.18	0.55	0.60	0.54	0.35	0.22	0.58
CaO	0.38	0.46	0.39	0.29	0.29	0.21	0.83	0.38	0.20	0.51	0.35	0.71
Na2O	0.01	0.01	0.01	0.01	0.01	0.00	0.02	0.01	0.01	0.01	0.01	0.01

Sample:	183.70	191.00	197.50	204.50	210.30	225.90	233.60	242.15	242.45	242.70	250.15	255.88
Depth in NG-sequence in m:	433.70	441.00	447.50	454.50	460.30	475.90	483.60	492.15	492.45	492.70	500.15	505.88
Habit:	cum	cum	cum	cum	cum	cum	cum	cum	cum	cum	cum	cum
wt.%												
SiO2	56.09	56.02	56.01	55.47	55.68	55.50	56.11	55.99	56.62	55.82	55.85	55.99
TiO2	0.11	0.09	0.09	0.10	0.11	0.10	0.08	0.05	0.08	0.07	0.06	0.06
Al2O3	1.15	1.26	1.20	1.20	1.21	1.09	1.06	1.24	1.31	1.14	1.30	1.23
Cr2O3	0.44	0.49	0.49	0.49	0.49	0.48	0.44	0.50	0.47	0.52	0.52	0.47
FeO	10.58	10.67	10.75	11.16	11.43	10.87	11.44	10.28	8.42	10.76	10.63	9.61
MnO	0.22	0.22	0.23	0.24	0.24	0.25	0.23	0.22	0.18	0.22	0.22	0.22
NiO	0.08	0.10	0.07	0.08	0.06	0.06	0.06	0.08	0.08	0.07	0.09	0.05
MgO	29.94	29.56	29.60	29.04	28.77	29.59	29.11	30.12	31.19	29.56	29.54	30.80
CaO	1.23	1.47	1.17	1.57	1.51	1.24	1.37	1.25	1.36	1.40	1.35	1.21
Na2O	0.01	0.03	0.02	0.03	0.03	0.01	0.04	0.02	0.04	0.03	0.03	0.01
Total	99.85	99.91	99.63	99.38	99.52	99.20	99.95	99.74	99.74	99.59	99.59	99.65
cations (based on 6 oxygens):												
Si	1.9802	1.9791	1.9826	1.9766	1.9820	1.9769	1.9867	1.9769	1.9812	1.9794	1.9787	1.9729
Ti	0.0028	0.0024	0.0024	0.0027	0.0028	0.0027	0.0023	0.0014	0.0020	0.0019	0.0015	0.0016
Al	0.0480	0.0524	0.0500	0.0502	0.0506	0.0459	0.0441	0.0514	0.0541	0.0475	0.0544	0.0511
Cr	0.0122	0.0136	0.0137	0.0138	0.0136	0.0136	0.0123	0.0139	0.0131	0.0147	0.0147	0.0131
Fe	0.3123	0.3153	0.3183	0.3324	0.3401	0.3239	0.3388	0.3035	0.2464	0.3191	0.3150	0.2833
Mn	0.0065	0.0066	0.0069	0.0073	0.0072	0.0074	0.0070	0.0065	0.0054	0.0066	0.0067	0.0064
Ni	0.0022	0.0027	0.0019	0.0023	0.0018	0.0018	0.0018	0.0022	0.0023	0.0020	0.0025	0.0015
Mg	1.5756	1.5564	1.5620	1.5421	1.5265	1.5709	1.5365	1.5852	1.6267	1.5625	1.5596	1.6174
Ca	0.0467	0.0556	0.0444	0.0600	0.0576	0.0474	0.0521	0.0474	0.0508	0.0533	0.0513	0.0457
Na	0.0009	0.0022	0.0015	0.0023	0.0019	0.0009	0.0025	0.0012	0.0024	0.0019	0.0021	0.0010
Total	3.9873	3.9865	3.9839	3.9898	3.9840	3.9912	3.9841	3.9897	3.9844	3.9887	3.9863	3.9939
n	8	6	11	11	8	8	11	5	4	5	7	4
Mg#	0.8346	0.8315	0.8307	0.8227	0.8178	0.8291	0.8194	0.8393	0.8685	0.8304	0.8320	0.8510
en	81.4	80.8	81.2	79.7	79.3	80.9	79.7	81.9	84.6	80.8	81.0	83.1
wo	2.4	2.9	2.3	3.1	3.0	2.4	2.7	2.4	12.8	2.8	2.7	2.3
fs	16.1	16.4	16.5	17.2	17.7	16.7	17.6	15.7	2.6	16.5	16.4	14.6
standard deviation:												
wt.%												
SiO2	0.23	0.06	0.19	0.24	0.26	0.33	0.20	0.22	0.08	0.18	0.25	0.09
TiO2	0.02	0.02	0.01	0.03	0.01	0.02	0.03	0.01	0.01	0.01	0.01	0.01
Al2O3	0.11	0.04	0.08	0.13	0.16	0.13	0.15	0.06	0.03	0.07	0.05	0.03
Cr2O3	0.07	0.01	0.03	0.03	0.03	0.02	0.07	0.02	0.03	0.03	0.03	0.03
FeO	0.25	0.17	0.15	0.49	0.21	0.23	0.32	0.21	0.33	0.13	0.23	0.41
MnO	0.03	0.03	0.02	0.03	0.02	0.02	0.02	0.02	0.01	0.02	0.01	0.01
NiO	0.02	0.02	0.03	0.03	0.03	0.02	0.01	0.02	0.00	0.02	0.03	0.02
MgO	0.37	0.22	0.25	0.70	0.30	0.31	0.39	0.18	0.42	0.20	0.48	0.50
CaO	0.55	0.34	0.41	0.97	0.21	0.50	0.44	0.29	0.46	0.18	0.44	0.61
Na2O	0.01	0.00	0.01	0.02	0.01	0.01	0.02	0.00	0.01	0.01	0.01	0.01

Sample:	257.10	257.70	262.17	277.25	282.25	292.30	302.00	312.10	327.45	331.35	331.65	331.81
Depth in NG-sequence in m:	507.10	507.70	512.17	527.25	532.25	542.30	552.00	562.10	577.45	581.35	581.65	581.81
Habit:	cum	cum	cum	cum	cum	cum	cum	cum	cum	cum	cum	cum
wt.%												
SiO2	55.92	55.70	55.59	55.31	56.42	56.50	56.43	56.63	55.99	56.43	56.29	56.73
TiO2	0.07	0.08	0.06	0.07	0.08	0.08	0.07	0.09	0.08	0.07	0.08	0.08
Al2O3	1.17	1.11	1.05	1.13	1.14	1.08	1.22	1.10	1.09	1.14	1.14	1.08
Cr2O3	0.48	0.49	0.44	0.50	0.48	0.52	0.52	0.53	0.52	0.52	0.50	0.49
FeO	10.42	11.61	11.57	10.93	10.77	10.14	10.14	9.99	9.99	8.86	8.54	8.37
MnO	0.23	0.22	0.24	0.20	0.24	0.22	0.22	0.22	0.22	0.24	0.22	0.19
NiO	0.05	0.08	0.05	0.08	0.08	0.11	0.07	0.07	0.09	0.06	0.08	0.11
MgO	29.69	29.05	28.89	30.05	30.03	30.27	30.06	30.38	30.62	31.64	31.74	31.50
CaO	1.49	1.49	1.34	1.34	1.05	1.09	1.32	1.15	1.18	0.69	1.42	1.27
Na2O	0.01	0.04	0.03	0.04	0.02	0.03	0.02	0.02	0.03	0.00	0.03	0.03
Total	99.52	99.87	99.27	99.67	100.32	100.04	100.06	100.18	99.82	99.65	100.02	99.85
cations (based on 6 oxygens):												
Si	1.9809	2.0284	1.9842	1.9640	1.9826	1.9858	1.9836	1.9859	1.9739	1.9781	1.9688	1.9827
Ti	0.0018	0.0021	0.0017	0.0018	0.0022	0.0022	0.0019	0.0023	0.0021	0.0017	0.0020	0.0021
Al	0.0487	0.0443	0.0442	0.0475	0.0473	0.0446	0.0504	0.0454	0.0455	0.0472	0.0472	0.0447
Cr	0.0135	0.0131	0.0124	0.0141	0.0135	0.0144	0.0145	0.0148	0.0144	0.0145	0.0137	0.0136
Fe	0.3087	0.3278	0.3453	0.3247	0.3164	0.2979	0.2981	0.2929	0.2944	0.2596	0.2497	0.2446
Mn	0.0069	0.0063	0.0074	0.0061	0.0073	0.0065	0.0065	0.0066	0.0066	0.0072	0.0064	0.0056
Ni	0.0014	0.0021	0.0014	0.0024	0.0023	0.0030	0.0020	0.0021	0.0026	0.0016	0.0022	0.0030
Mg	1.5674	1.4616	1.5371	1.5902	1.5729	1.5859	1.5751	1.5880	1.6088	1.6532	1.6547	1.6411
Ca	0.0565	0.0538	0.0512	0.0512	0.0397	0.0410	0.0495	0.0430	0.0447	0.0260	0.0531	0.0476
Na	0.0008	0.0025	0.0021	0.0024	0.0016	0.0024	0.0013	0.0010	0.0021	0.0003	0.0018	0.0022
Total	3.9866	3.9421	3.9869	4.0045	3.9857	3.9837	3.9828	3.9821	3.9951	3.9895	3.9997	3.9872
n	4	6	3	7	13	9	11	8	8	4	6	4
Mg#	0.8355	0.8168	0.8166	0.8304	0.8325	0.8418	0.8409	0.8443	0.8453	0.8643	0.8689	0.8703
en	81.1	79.3	79.5	80.9	81.5	82.4	81.9	82.5	82.6	85.3	84.5	84.9
wo	2.9	2.9	2.6	2.6	2.1	2.1	2.6	2.2	2.3	1.3	2.7	2.5
fs	16.0	17.8	17.9	16.5	16.4	15.5	15.5	15.2	15.1	13.4	12.8	12.7
standard deviation:												
wt.%												
SiO2	0.18	0.17	0.30	0.17	0.30	0.15	0.27	0.12	0.27	0.06	0.31	0.14
TiO2	0.01	0.01	0.00	0.01	0.03	0.01	0.02	0.01	0.02	0.01	0.01	0.01
Al2O3	0.06	0.09	0.02	0.10	0.16	0.09	0.14	0.06	0.09	0.05	0.06	0.06
Cr2O3	0.01	0.04	0.07	0.03	0.05	0.03	0.04	0.02	0.04	0.03	0.02	0.02
FeO	0.44	0.14	0.35	0.28	0.20	0.19	0.16	0.20	0.16	0.08	0.61	0.21
MnO	0.02	0.03	0.02	0.03	0.03	0.03	0.02	0.02	0.02	0.02	0.01	0.01
NiO	0.03	0.01	0.03	0.02	0.02	0.01	0.01	0.01	0.02	0.01	0.01	0.01
MgO	0.50	0.11	0.50	0.33	0.38	0.35	0.48	0.37	0.44	0.24	0.60	0.69
CaO	0.71	0.18	0.45	0.55	0.34	0.34	0.45	0.45	0.46	0.12	0.48	0.78
Na2O	0.01	0.01	0.01	0.02	0.03	0.01	0.01	0.01	0.01	0.01	0.01	0.02

Sample:	331.85	334.30	338.45	348.20	353.40	364.25	374.35	380.35	390.60	406.40	414.85	421.00
Depth in												
NG-sequence in m:	581.85	584.30	588.45	598.20	603.40	614.25	624.35	630.35	640.60	656.40	664.85	671.00
Habit:	cum	cum	cum	cum	cum	cum	cum	cum	cum	cum	cum	cum
wt.%												
SiO2	56.31	55.80	55.89	56.54	56.27	55.90	56.24	56.41	55.48	56.35	56.31	55.83
TiO2	0.09	0.10	0.08	0.08	0.08	0.08	0.08	0.12	0.09	0.08	0.06	0.08
Al2O3	1.25	0.97	1.10	1.12	0.99	1.01	1.09	1.00	0.97	1.09	1.08	1.20
Cr2O3	0.47	0.47	0.51	0.50	0.44	0.46	0.50	0.42	0.45	0.51	0.49	0.44
FeO	7.79	9.90	9.69	9.46	10.06	9.59	8.89	9.28	9.60	8.55	8.61	8.79
MnO	0.19	0.20	0.22	0.20	0.22	0.20	0.21	0.20	0.19	0.23	0.18	0.21
NiO	0.05	0.05	0.04	0.05	0.05	0.06	0.09	0.06	0.03	0.06	0.06	0.08
MgO	32.07	31.55	31.30	31.11	30.52	30.78	31.00	30.97	30.86	31.80	31.75	31.73
CaO	1.08	1.04	1.31	1.18	1.38	1.45	1.39	1.19	0.92	1.35	1.44	1.34
Na2O	0.02	0.02	0.02	0.02	0.03	0.03	0.03	0.02	0.01	0.03	0.04	0.05
Total	99.31	100.10	100.14	100.26	100.04	99.56	99.56	99.67	98.60	100.05	100.01	99.74
cations (based on 6 oxygens):												
Si	1.9735	1.9615	1.9630	1.9775	1.9793	1.9735	1.9788	1.9829	1.9750	1.9700	1.9701	1.9612
Ti	0.0023	0.0026	0.0021	0.0021	0.0021	0.0022	0.0022	0.0033	0.0024	0.0022	0.0015	0.0021
Al	0.0515	0.0400	0.0455	0.0463	0.0411	0.0420	0.0453	0.0413	0.0407	0.0450	0.0445	0.0499
Cr	0.0130	0.0132	0.0141	0.0137	0.0122	0.0128	0.0138	0.0117	0.0125	0.0140	0.0135	0.0123
Fe	0.2284	0.2911	0.2845	0.2767	0.2960	0.2831	0.2615	0.2727	0.2859	0.2501	0.2518	0.2583
Mn	0.0055	0.0060	0.0065	0.0060	0.0065	0.0059	0.0062	0.0060	0.0057	0.0067	0.0052	0.0062
Ni	0.0013	0.0014	0.0010	0.0014	0.0014	0.0016	0.0026	0.0016	0.0010	0.0018	0.0017	0.0022
Mg	1.6753	1.6534	1.6384	1.6219	1.6001	1.6197	1.6256	1.6224	1.6375	1.6572	1.6559	1.6613
Ca	0.0404	0.0394	0.0495	0.0443	0.0522	0.0550	0.0522	0.0448	0.0350	0.0504	0.0538	0.0504
Na	0.0014	0.0014	0.0011	0.0013	0.0022	0.0020	0.0017	0.0013	0.0007	0.0019	0.0025	0.0033
Total	3.9927	4.0100	4.0057	3.9911	3.9931	3.9979	3.9902	3.9880	3.9964	3.9992	4.0006	4.0072
n	5	7	6	9	10	10	7	8	1	8	4	6
Mg#	0.8800	0.8503	0.8520	0.8543	0.8439	0.8512	0.8614	0.8561	0.8513	0.8689	0.8680	0.8654
en	86.2	83.3	83.1	83.5	82.1	82.7	83.8	83.6	83.6	84.7	84.4	84.3
wo	2.1	2.0	2.5	2.3	2.7	2.8	2.7	2.3	1.8	2.6	2.7	2.6
fs	11.7	14.7	14.4	14.2	15.2	14.5	13.5	14.1	14.6	12.8	12.8	13.1
standard deviation:												
wt.%												
SiO2	0.16	0.32	0.26	0.22	0.24	0.26	0.19	0.23		0.27	0.17	0.10
TiO2	0.00	0.02	0.02	0.01	0.02	0.02	0.02	0.04		0.03	0.01	0.04
Al2O3	0.15	0.10	0.08	0.11	0.13	0.12	0.14	0.17		0.11	0.03	0.11
Cr2O3	0.06	0.02	0.04	0.02	0.07	0.07	0.03	0.08		0.03	0.01	0.04
FeO	0.59	0.17	0.08	0.24	0.09	0.31	0.13	0.15		0.14	0.18	0.09
MnO	0.02	0.02	0.01	0.02	0.02	0.01	0.03	0.02		0.02	0.01	0.01
NiO	0.00	0.02	0.02	0.02	0.01	0.02	0.02	0.02		0.01	0.01	0.01
MgO	0.22	0.41	0.19	0.27	0.34	0.52	0.18	0.37		0.59	0.29	0.21
CaO	0.50	0.39	0.20	0.44	0.55	0.77	0.33	0.45		0.54	0.50	0.14
Na2O	0.01	0.01	0.01	0.01	0.01	0.02	0.01	0.01		0.02	0.01	0.01

Sample:	429.90	433.60	455.65	459.70	469.40	475.10	475.45	476.40	481.90	486.55	492.15	495.90
Depth in												
NG-sequence in m:	679.90	683.60	705.65	709.70	719.40	725.10	725.45	726.40	731.90	736.55	742.15	745.90
Habit:	cum	cum	cum	cum	cum	cum	cum	cum	cum	cum	cum	cum
wt.%												
SiO2	57.26	57.14	56.29	55.99	56.43	57.01	57.35	56.17	55.86	56.69	56.35	56.79
TiO2	0.05	0.06	0.08	0.07	0.09	0.06	0.04	0.07	0.07	0.09	0.07	0.06
Al2O3	1.09	1.11	1.13	1.07	0.95	1.10	1.12	1.09	1.11	1.13	1.11	1.16
Cr2O3	0.43	0.45	0.49	0.50	0.47	0.51	0.49	0.49	0.47	0.45	0.45	0.45
FeO	6.24	7.59	9.00	9.20	9.32	7.54	7.06	8.77	8.93	9.08	8.95	8.26
MnO	0.16	0.21	0.19	0.18	0.21	0.20	0.18	0.18	0.17	0.21	0.19	0.19
NiO	0.06	0.05	0.07	0.06	0.04	0.05	0.07	0.06	0.07	0.05	0.07	0.07
MgO	32.59	31.81	31.47	31.52	31.23	31.95	32.59	31.60	31.02	30.96	31.09	31.30
CaO	1.60	1.18	1.34	1.31	1.07	1.60	0.97	1.40	1.44	1.16	1.32	1.07
Na2O	0.06	0.04	0.02	0.02	0.03	0.03	0.02	0.02	0.04	0.02	0.02	0.02
Total	99.52	99.63	100.06	99.92	99.84	100.05	99.89	99.85	99.18	99.84	99.62	99.37
cations (based on 6 oxygens):												
Si	1.9885	1.9917	1.9708	1.9661	1.9805	1.9826	1.9883	1.9697	1.9736	1.9861	1.9798	1.9903
Ti	0.0014	0.0016	0.0020	0.0019	0.0025	0.0016	0.0009	0.0019	0.0018	0.0023	0.0018	0.0016
Al	0.0445	0.0454	0.0465	0.0442	0.0391	0.0451	0.0457	0.0449	0.0462	0.0465	0.0459	0.0480
Cr	0.0118	0.0123	0.0135	0.0140	0.0130	0.0140	0.0135	0.0136	0.0130	0.0126	0.0125	0.0126
Fe	0.1812	0.2212	0.2636	0.2700	0.2737	0.2193	0.2048	0.2571	0.2638	0.2661	0.2630	0.2420
Mn	0.0046	0.0061	0.0056	0.0052	0.0061	0.0058	0.0054	0.0053	0.0051	0.0063	0.0055	0.0057
Ni	0.0016	0.0013	0.0019	0.0018	0.0011	0.0014	0.0020	0.0017	0.0021	0.0014	0.0020	0.0019
Mg	1.6869	1.6528	1.6425	1.6496	1.6337	1.6558	1.6841	1.6517	1.6337	1.6166	1.6281	1.6349
Ca	0.0594	0.0442	0.0501	0.0493	0.0402	0.0596	0.0359	0.0524	0.0545	0.0435	0.0498	0.0403
Na	0.0041	0.0025	0.0014	0.0016	0.0020	0.0019	0.0012	0.0017	0.0024	0.0013	0.0016	0.0012
Total	3.9840	3.9791	3.9979	4.0037	3.9919	3.9871	3.9818	4.0000	3.9962	3.9827	3.9900	3.9784
n	2	3	9	6	11	3	6	6	3	9	11	5
Mg#	0.9030	0.8819	0.8617	0.8593	0.8565	0.8831	0.8916	0.8653	0.8610	0.8587	0.8609	0.8711
en	87.5	86.2	84.0	83.8	83.9	85.6	87.5	84.2	83.7	83.9	83.9	85.3
wo	3.1	2.3	2.6	2.5	2.1	3.1	1.9	2.7	2.8	2.3	2.6	2.1
fs	9.4	11.5	13.5	13.7	14.1	11.3	10.6	13.1	13.5	13.8	13.6	12.6
standard deviation:												
wt.%												
SiO2	0.03	0.43	0.34	0.08	0.16	0.19	0.21	0.10	0.10	0.47	0.15	0.18
TiO2	0.01	0.00	0.03	0.01	0.04	0.02	0.01	0.02	0.01	0.05	0.02	0.01
Al2O3	0.04	0.04	0.08	0.06	0.10	0.04	0.07	0.06	0.09	0.08	0.06	0.04
Cr2O3	0.03	0.01	0.03	0.01	0.05	0.00	0.04	0.03	0.00	0.04	0.03	0.03
FeO	0.05	0.07	0.26	0.11	0.21	0.39	0.53	0.10	0.05	0.25	0.14	0.23
MnO	0.00	0.01	0.02	0.02	0.02	0.03	0.01	0.02	0.01	0.03	0.02	0.02
NiO	0.01	0.01	0.02	0.02	0.03	0.02	0.01	0.01	0.02	0.02	0.01	0.01
MgO	0.22	0.10	0.30	0.19	0.36	0.59	0.49	0.21	0.07	0.38	0.25	0.12
CaO	0.16	0.17	0.35	0.17	0.30	0.09	0.30	0.28	0.08	0.31	0.23	0.21
Na2O	0.01	0.00	0.01	0.01	0.02	0.00	0.01	0.01	0.01	0.01	0.01	0.01

Sample:	496.43	496.53	500.50	519.26	523.90	523.95	524.26	532.14	536.95	546.85	553.33	560.10
Depth in NG-sequence in m:	746.43	746.53	750.50	769.26	773.90	773.95	774.26	782.14	786.95	796.85	803.33	810.10
Habit:	cum	cum	cum	cum	cum	cum	cum	cum	cum	cum	cum	cum
wt.%												
SiO2	56.14	56.92	56.50	56.17	56.19	56.25	57.54	55.92	56.47	56.25	56.38	56.82
TiO2	0.08	0.04	0.05	0.04	0.09	0.04	0.05	0.06	0.06	0.06	0.04	0.05
Al2O3	1.17	1.04	1.24	1.11	0.97	1.10	1.02	1.09	1.17	1.20	1.12	1.15
Cr2O3	0.45	0.48	0.45	0.49	0.46	0.47	0.48	0.53	0.51	0.52	0.48	0.50
FeO	8.86	6.90	8.93	9.68	9.45	9.07	6.27	9.17	8.97	8.66	9.14	6.82
MnO	0.21	0.14	0.19	0.20	0.24	0.20	0.16	0.22	0.20	0.19	0.20	0.20
NiO	0.08	0.04	0.07	0.08	0.06	0.05	0.03	0.10	0.07	0.08	0.09	0.08
MgO	31.08	33.23	31.07	31.15	30.81	31.27	33.20	31.05	31.48	31.82	31.29	33.15
CaO	1.29	0.80	1.22	1.33	1.34	0.75	0.56	1.50	1.24	1.02	1.29	1.37
Na2O	0.04	0.02	0.04	0.03	0.03	0.01	0.00	0.03	0.04	0.02	0.02	0.01
Total	99.39	99.60	99.75	100.26	99.63	99.22	99.31	99.67	100.22	99.84	100.06	100.14
cations (based on 6 oxygens):												
Si	1.9770	1.9785	1.9809	1.9691	1.9796	1.9819	1.9954	1.9697	1.9729	1.9696	1.9747	1.9688
Ti	0.0021	0.0010	0.0012	0.0012	0.0023	0.0012	0.0012	0.0015	0.0017	0.0017	0.0011	0.0014
Al	0.0485	0.0425	0.0512	0.0457	0.0402	0.0456	0.0416	0.0452	0.0481	0.0495	0.0464	0.0468
Cr	0.0125	0.0132	0.0125	0.0135	0.0127	0.0131	0.0132	0.0148	0.0140	0.0145	0.0133	0.0138
Fe	0.2609	0.2007	0.2617	0.2837	0.2784	0.2673	0.1820	0.2702	0.2622	0.2536	0.2676	0.1976
Mn	0.0063	0.0041	0.0057	0.0058	0.0071	0.0060	0.0046	0.0065	0.0060	0.0058	0.0061	0.0060
Ni	0.0021	0.0012	0.0021	0.0021	0.0016	0.0015	0.0009	0.0028	0.0021	0.0023	0.0026	0.0021
Mg	1.6313	1.7211	1.6237	1.6280	1.6180	1.6424	1.7161	1.6304	1.6395	1.6608	1.6334	1.7119
Ca	0.0485	0.0299	0.0460	0.0498	0.0507	0.0283	0.0209	0.0565	0.0465	0.0383	0.0485	0.0508
Na	0.0024	0.0011	0.0024	0.0021	0.0021	0.0004	0.0003	0.0023	0.0027	0.0013	0.0010	0.0005
Total	3.9916	3.9932	3.9873	4.0011	3.9927	3.9878	3.9762	3.9999	3.9957	3.9974	3.9947	3.9997
n	7	6	7	11	5	3	2	6	5	9	6	6
Mg#	0.8621	0.8956	0.8612	0.8516	0.8532	0.8600	0.9041	0.8578	0.8621	0.8675	0.8592	0.8965
en	84.1	88.2	84.1	83.0	83.1	84.7	89.4	83.3	84.2	85.0	83.8	87.3
wo	2.5	1.5	2.4	2.5	2.6	1.5	1.1	2.9	2.4	2.0	2.5	2.6
fs	13.4	10.3	13.5	14.5	14.3	13.8	9.5	13.8	13.5	13.0	13.7	10.1
standard deviation:												
wt.%												
SiO2	0.14	0.46	0.34	0.37	0.08	0.16	0.48	0.21	0.21	0.25	0.17	0.08
TiO2	0.02	0.01	0.01	0.01	0.02	0.01	0.02	0.02	0.01	0.02	0.02	0.01
Al2O3	0.05	0.11	0.06	0.06	0.08	0.06	0.02	0.05	0.03	0.05	0.02	0.06
Cr2O3	0.01	0.05	0.02	0.02	0.05	0.02	0.01	0.01	0.03	0.02	0.01	0.03
FeO	0.25	1.26	0.12	0.11	0.18	0.19	1.18	0.17	0.07	0.10	0.19	0.47
MnO	0.02	0.03	0.02	0.02	0.01	0.03	0.04	0.02	0.02	0.02	0.02	0.02
NiO	0.01	0.02	0.04	0.02	0.02	0.01	0.01	0.02	0.03	0.01	0.02	0.02
MgO	0.25	1.33	0.21	0.42	0.43	0.08	0.75	0.23	0.26	0.27	0.20	0.41
CaO	0.42	0.44	0.21	0.29	0.37	0.22	0.06	0.17	0.35	0.28	0.26	0.12
Na2O	0.01	0.02	0.01	0.01	0.02	0.01	0.00	0.01	0.02	0.02	0.01	0.01

Sample:	564.45	569.20	581.00	586.00	589.60	595.05	597.62	603.10	609.47	609.57	609.68	614.76
Depth in NG-sequence in m:	814.45	819.20	831.00	836.00	839.60	845.05	847.62	853.10	859.47	859.57	859.68	864.76
Habit:	cum	cum	cum	cum	cum	cum	cum	cum	cum	cum	cum	cum
wt.%												
SiO2	55.80	56.21	56.02	55.84	55.87	55.57	55.96	55.85	56.25	56.75	56.43	56.26
TiO2	0.05	0.06	0.05	0.08	0.10	0.06	0.05	0.07	0.07	0.06	0.06	0.07
Al2O3	1.14	1.14	1.10	1.12	1.05	1.14	1.24	1.07	1.06	1.25	1.17	1.16
Cr2O3	0.49	0.47	0.49	0.50	0.46	0.50	0.51	0.50	0.44	0.50	0.53	0.50
FeO	9.57	9.54	10.25	9.91	10.22	10.15	8.06	10.23	10.27	8.15	9.72	9.81
MnO	0.23	0.21	0.23	0.22	0.21	0.20	0.19	0.23	0.24	0.20	0.22	0.24
NiO	0.07	0.07	0.06	0.07	0.10	0.06	0.08	0.06	0.07	0.09	0.10	0.07
MgO	30.98	30.51	30.50	30.53	30.52	30.79	32.21	30.64	30.54	31.76	30.44	30.40
CaO	1.32	1.44	0.88	1.40	1.23	1.21	1.43	1.27	1.06	1.27	1.37	1.33
Na2O	0.03	0.03	0.02	0.03	0.02	0.02	0.03	0.02	0.01	0.02	0.03	0.04
Total	99.67	99.68	99.60	99.71	99.79	99.69	99.76	99.94	100.00	100.04	100.07	99.87
cations (based on 6 oxygens):												
Si	1.9679	1.9800	1.9786	1.9716	1.9725	1.9642	1.9597	1.9696	1.9795	1.9778	1.9810	1.9799
Ti	0.0012	0.0015	0.0014	0.0021	0.0027	0.0015	0.0014	0.0017	0.0018	0.0017	0.0016	0.0019
Al	0.0474	0.0475	0.0457	0.0466	0.0438	0.0474	0.0511	0.0445	0.0438	0.0512	0.0484	0.0481
Cr	0.0138	0.0130	0.0136	0.0140	0.0129	0.0139	0.0142	0.0141	0.0122	0.0139	0.0148	0.0138
Fe	0.2822	0.2810	0.3027	0.2925	0.3018	0.3002	0.2360	0.3016	0.3022	0.2375	0.2855	0.2886
Mn	0.0067	0.0063	0.0068	0.0066	0.0064	0.0059	0.0056	0.0070	0.0072	0.0059	0.0065	0.0070
Ni	0.0020	0.0020	0.0018	0.0021	0.0028	0.0016	0.0023	0.0018	0.0019	0.0024	0.0027	0.0021
Mg	1.6284	1.6015	1.6057	1.6065	1.6061	1.6223	1.6812	1.6106	1.6017	1.6495	1.5928	1.5945
Ca	0.0500	0.0544	0.0334	0.0530	0.0465	0.0457	0.0538	0.0480	0.0401	0.0474	0.0516	0.0501
Na	0.0018	0.0019	0.0014	0.0020	0.0015	0.0016	0.0019	0.0014	0.0008	0.0015	0.0021	0.0025
Total	4.0012	3.9892	3.9910	3.9970	3.9972	4.0044	4.0072	4.0002	3.9912	3.9887	3.9869	3.9885
n	5	17	5	16	8	6	16	6	6	6	5	6
Mg#	0.8523	0.8507	0.8414	0.8460	0.8418	0.8439	0.8769	0.8423	0.8413	0.8741	0.8480	0.8467
en	83.1	82.7	82.7	82.3	82.2	82.4	85.3	82.2	82.4	85.3	82.5	82.5
wo	2.5	2.8	1.7	2.7	2.4	2.3	2.7	2.4	2.1	2.4	2.7	2.6
fs	14.4	14.5	15.6	15.0	15.4	15.3	12.0	15.4	15.5	12.3	14.8	14.9
standard deviation:												
wt.%												
SiO2	0.15	0.27	0.09	0.10	0.12	0.33	0.14	0.20	0.19	0.20	0.18	0.20
TiO2	0.01	0.02	0.02	0.02	0.05	0.02	0.01	0.02	0.01	0.01	0.03	0.01
Al2O3	0.05	0.06	0.04	0.05	0.04	0.07	0.06	0.07	0.21	0.04	0.05	0.06
Cr2O3	0.03	0.02	0.02	0.02	0.02	0.01	0.03	0.02	0.10	0.03	0.02	0.01
FeO	0.03	0.25	0.16	0.16	0.15	0.12	0.16	0.18	0.20	1.20	0.15	0.18
MnO	0.02	0.02	0.03	0.01	0.02	0.02	0.03	0.01	0.01	0.03	0.02	0.01
NiO	0.02	0.03	0.01	0.03	0.02	0.01	0.02	0.02	0.02	0.02	0.01	0.02
MgO	0.23	0.42	0.26	0.23	0.26	0.41	0.14	0.31	0.33	0.60	0.32	0.11
CaO	0.33	0.53	0.30	0.30	0.37	0.29	0.24	0.34	0.41	0.34	0.16	0.16
Na2O	0.02	0.01	0.01	0.01	0.01	0.01	0.01	0.01	0.01	0.01	0.01	0.01

Sample:	619.85	624.70	634.20	639.95	644.20	645.17	655.10	660.40	675.25	685.40	690.90	695.50
Depth in												
NG-sequence in m:	869.85	874.70	884.20	889.95	894.20	895.17	905.10	910.40	925.25	935.40	940.90	945.50
Habit:	cum	cum	cum	cum	cum	cum	cum	cum	cum	cum	cum	cum
wt.%												
SiO2	56.06	56.45	57.04	56.02	56.82	56.58	56.60	56.18	56.54	56.66	56.48	56.03
TiO2	0.07	0.07	0.05	0.07	0.08	0.07	0.09	0.08	0.08	0.07	0.08	0.08
Al2O3	1.13	1.14	1.17	1.15	1.17	1.12	1.03	1.14	1.19	1.17	1.16	1.17
Cr2O3	0.52	0.50	0.46	0.50	0.42	0.49	0.46	0.47	0.48	0.49	0.48	0.46
FeO	9.57	9.39	7.17	9.88	7.01	9.39	9.65	9.72	9.53	9.43	10.07	10.10
MnO	0.22	0.22	0.15	0.20	0.15	0.20	0.20	0.20	0.22	0.21	0.21	0.23
NiO	0.06	0.09	0.03	0.05	0.06	0.07	0.06	0.06	0.05	0.08	0.07	0.05
MgO	30.62	30.38	32.71	31.33	32.27	30.74	30.52	30.99	31.07	30.89	30.77	30.34
CaO	1.35	1.28	0.94	1.12	1.47	1.24	1.29	1.26	1.28	1.20	1.16	1.19
Na2O	0.03	0.02	0.01	0.03	0.05	0.02	0.03	0.04	0.02	0.03	0.03	0.03
Total	99.62	99.54	99.74	100.36	99.48	99.93	99.94	100.14	100.48	100.22	100.52	99.68
cations (based on 6 oxygens):												
Si	1.9765	1.9876	1.9818	1.9636	1.9814	1.9843	1.9871	1.9716	1.9746	1.9816	1.9761	1.9775
Ti	0.0017	0.0019	0.0014	0.0019	0.0020	0.0019	0.0023	0.0021	0.0020	0.0018	0.0021	0.0021
Al	0.0471	0.0474	0.0478	0.0477	0.0479	0.0464	0.0427	0.0471	0.0492	0.0483	0.0476	0.0488
Cr	0.0144	0.0140	0.0127	0.0137	0.0116	0.0136	0.0126	0.0130	0.0134	0.0136	0.0133	0.0128
Fe	0.2821	0.2764	0.2083	0.2896	0.2045	0.2754	0.2833	0.2854	0.2785	0.2759	0.2946	0.2981
Mn	0.0065	0.0065	0.0045	0.0060	0.0044	0.0061	0.0061	0.0061	0.0066	0.0062	0.0063	0.0069
Ni	0.0017	0.0025	0.0009	0.0015	0.0016	0.0018	0.0018	0.0018	0.0015	0.0021	0.0019	0.0015
Mg	1.6090	1.5944	1.6938	1.6366	1.6770	1.6069	1.5972	1.6207	1.6176	1.6101	1.6046	1.5960
Ca	0.0509	0.0484	0.0348	0.0421	0.0549	0.0467	0.0487	0.0473	0.0479	0.0451	0.0436	0.0449
Na	0.0022	0.0014	0.0007	0.0023	0.0031	0.0013	0.0023	0.0025	0.0016	0.0020	0.0023	0.0021
Total	3.9921	3.9805	3.9869	4.0049	3.9883	3.9844	3.9840	3.9975	3.9929	3.9867	3.9925	3.9907
n	6	5	5	9	8	9	7	10	8	8	9	5
Mg#	0.8508	0.8522	0.8905	0.8497	0.8913	0.8537	0.8494	0.8503	0.8531	0.8537	0.8449	0.8426
en	82.9	83.1	87.4	83.1	86.6	83.3	82.8	83.0	83.2	83.4	82.6	82.3
wo	2.6	2.5	1.8	2.1	2.8	2.4	2.5	2.4	2.5	2.3	2.2	2.3
fs	14.5	14.4	10.8	14.7	10.6	14.3	14.7	14.6	14.3	14.3	15.2	15.4
standard deviation:												
wt.%												
SiO2	0.13	0.13	0.15	0.18	0.16	0.17	0.23	0.21	0.25	0.29	0.11	0.20
TiO2	0.01	0.01	0.01	0.03	0.01	0.02	0.02	0.03	0.03	0.04	0.03	0.02
Al2O3	0.05	0.12	0.04	0.08	0.03	0.06	0.14	0.13	0.09	0.08	0.11	0.04
Cr2O3	0.01	0.02	0.03	0.02	0.04	0.02	0.08	0.05	0.04	0.03	0.03	0.02
FeO	0.22	0.08	0.22	0.39	0.16	0.14	0.23	0.26	0.15	0.13	0.20	0.08
MnO	0.03	0.02	0.02	0.03	0.02	0.02	0.02	0.01	0.03	0.02	0.02	0.03
NiO	0.02	0.01	0.01	0.03	0.03	0.02	0.02	0.03	0.02	0.01	0.04	0.01
MgO	0.22	0.09	0.10	0.45	0.55	0.33	0.44	0.32	0.46	0.37	0.29	0.17
CaO	0.34	0.21	0.16	0.31	0.27	0.39	0.56	0.40	0.35	0.32	0.38	0.26
Na2O	0.01	0.01	0.01	0.01	0.01	0.01	0.02	0.01	0.01	0.01	0.01	0.01

Sample:	701.75	706.90	711.60	720.15	730.38	739.80	744.70
Depth in							
NG-sequence in m:	951.75	956.90	961.60	970.15	980.38	989.80	994.70
Habit:	cum	cum	cum	cum	cum	cum	cum
wt.%							
SiO2	55.78	56.21	56.30	55.72	56.28	55.71	56.18
TiO2	0.07	0.09	0.08	0.08	0.09	0.10	0.07
Al2O3	1.09	1.14	1.28	1.15	1.11	1.13	1.14
Cr2O3	0.47	0.48	0.51	0.50	0.48	0.48	0.48
FeO	9.56	9.68	9.05	9.41	9.20	9.26	9.23
MnO	0.26	0.21	0.22	0.21	0.20	0.20	0.21
NiO	0.05	0.07	0.08	0.08	0.08	0.05	0.06
MgO	30.57	31.10	30.92	31.12	31.03	31.75	31.05
CaO	1.49	1.00	1.34	1.25	1.33	1.15	1.29
Na2O	0.01	0.03	0.02	0.02	0.02	0.04	0.03
Total	99.35	100.00	99.79	99.54	99.83	99.88	99.75
cations (based on 6 oxygens):							
Si	1.9736	1.9731	1.9761	1.9663	1.9764	1.9582	1.9748
Ti	0.0018	0.0024	0.0020	0.0021	0.0023	0.0025	0.0019
Al	0.0456	0.0471	0.0529	0.0477	0.0461	0.0470	0.0474
Cr	0.0132	0.0133	0.0141	0.0139	0.0134	0.0134	0.0133
Fe	0.2828	0.2842	0.2656	0.2776	0.2703	0.2721	0.2713
Mn	0.0078	0.0063	0.0064	0.0062	0.0058	0.0060	0.0062
Ni	0.0014	0.0018	0.0022	0.0023	0.0021	0.0015	0.0018
Mg	1.6121	1.6271	1.6176	1.6367	1.6243	1.6637	1.6268
Ca	0.0564	0.0378	0.0506	0.0472	0.0500	0.0433	0.0485
Na	0.0007	0.0019	0.0012	0.0017	0.0016	0.0025	0.0020
Total	3.9955	3.9952	3.9889	4.0017	3.9924	4.0103	3.9940
n	1	8	8	10	9	7	16
Mg#	0.8508	0.8513	0.8590	0.8550	0.8573	0.8595	0.8571
en	82.6	83.5	83.6	83.4	83.5	84.1	83.6
wo	2.9	1.9	2.6	2.4	2.6	2.2	2.5
fs	14.5	14.6	13.7	14.2	13.9	13.7	13.9
standard deviation:							
wt.%							
SiO2		0.23	0.30	0.19	0.21	0.18	0.29
TiO2		0.02	0.02	0.04	0.01	0.01	0.01
Al2O3		0.07	0.15	0.09	0.15	0.02	0.02
Cr2O3		0.01	0.02	0.02	0.05	0.01	0.02
FeO		0.24	0.36	0.28	0.29	0.27	0.76
MnO		0.01	0.03	0.02	0.02	0.02	0.03
NiO		0.01	0.02	0.02	0.02	0.00	0.01
MgO		0.39	0.89	0.37	0.38	0.41	0.55
CaO		0.46	1.29	0.40	0.47	0.10	0.11
Na2O		0.01	0.03	0.01	0.01	0.01	0.01

MICROPROBE DATA: Composition of orthopyroxene in the NG-sequence (NG2-borehole)

Sample:	80.35	91.40	94.30	98.00	102.60	102.65	106.60	115.25	120.40	171.50	180.55	189.40
Depth in NG-sequence in m:	1120.35	1131.40	1134.30	1138.00	1142.60	1142.65	1146.60	1155.25	1160.40	1211.50	1220.55	1229.40
Habit:	pcum	cum	cum	cum	cum	cum	cum	cum	cum	cum	cum	cum
wt.%												
SiO2	56.01	56.40	55.71	56.15	56.07	55.36	55.79	56.22	56.29	55.36	55.40	55.88
TiO2	0.07	0.07	0.05	0.08	0.06	0.09	0.08	0.08	0.08	0.08	0.09	0.09
Al2O3	1.20	0.98	1.11	1.00	1.05	0.90	1.06	1.27	1.25	1.17	1.18	1.17
Cr2O3	0.44	0.39	0.39	0.40	0.44	0.38	0.46	0.51	0.43	0.42	0.45	0.46
FeO	8.89	9.48	9.30	9.47	9.25	9.52	9.51	7.47	8.41	9.83	9.84	9.64
MnO	0.20	0.20	0.21	0.19	0.23	0.22	0.20	0.18	0.16	0.20	0.21	0.20
NiO	0.08	0.09	0.10	0.08	0.07	0.08	0.12	0.12	0.10	0.09	0.14	0.12
MgO	31.80	30.78	30.75	30.31	30.80	31.88	31.54	32.30	32.04	31.70	31.67	31.80
CaO	1.69	1.06	1.18	1.49	1.68	1.43	1.72	1.59	1.02	1.06	1.43	1.19
Na2O	0.05	0.02	0.02	0.01	0.04	0.03	0.05	0.02	0.04	0.03	0.04	0.02
Total	100.42	99.48	98.81	99.19	99.69	99.90	100.52	99.77	99.83	99.94	100.45	100.56
cations (based on 6 oxygens):												
Si	1.9574	1.9870	1.9770	1.9865	1.9750	1.9516	1.9549	1.9637	1.9685	1.9506	1.9456	1.9547
Ti	0.0018	0.0018	0.0014	0.0021	0.0016	0.0024	0.0020	0.0022	0.0020	0.0021	0.0025	0.0025
Al	0.0494	0.0408	0.0465	0.0417	0.0435	0.0375	0.0437	0.0522	0.0514	0.0486	0.0489	0.0483
Cr	0.0121	0.0108	0.0108	0.0113	0.0122	0.0107	0.0127	0.0140	0.0120	0.0117	0.0124	0.0126
Fe	0.2600	0.2792	0.2759	0.2803	0.2725	0.2806	0.2787	0.2181	0.2460	0.2897	0.2889	0.2819
Mn	0.0058	0.0060	0.0064	0.0058	0.0068	0.0067	0.0059	0.0055	0.0049	0.0059	0.0062	0.0060
Ni	0.0021	0.0027	0.0030	0.0022	0.0020	0.0024	0.0035	0.0035	0.0027	0.0026	0.0040	0.0034
Mg	1.6567	1.6164	1.6263	1.5982	1.6172	1.6749	1.6476	1.6815	1.6704	1.6648	1.6575	1.6579
Ca	0.0633	0.0398	0.0449	0.0565	0.0634	0.0541	0.0646	0.0597	0.0384	0.0402	0.0539	0.0445
Na	0.0032	0.0017	0.0012	0.0008	0.0027	0.0019	0.0031	0.0014	0.0029	0.0021	0.0026	0.0013
Total	4.0117	3.9862	3.9934	3.9854	3.9969	4.0228	4.0165	4.0017	3.9992	4.0183	4.0226	4.0131
n	9	6	6	5	6	6	5	6	8	6	6	6
Mg#	0.8644	0.8527	0.8550	0.8508	0.8558	0.8565	0.8553	0.8852	0.8716	0.8518	0.8516	0.8547
en	83.7	83.5	83.5	82.6	82.8	83.3	82.8	85.8	85.4	83.5	82.9	83.6
wo	3.2	2.1	2.3	2.9	3.2	2.7	3.2	3.0	2.0	2.0	2.7	2.2
fs	13.1	14.4	14.2	14.5	14.0	14.0	14.0	11.1	12.6	14.5	14.4	14.2
standard deviation:												
wt.%												
SiO2	0.20	0.11	0.17	0.17	0.18	0.24	0.08	0.16	1.39	0.41	0.29	0.24
TiO2	0.02	0.04	0.01	0.03	0.02	0.04	0.01	0.01	0.03	0.02	0.02	0.03
Al2O3	0.14	0.13	0.05	0.06	0.03	0.11	0.09	0.07	0.38	0.13	0.11	0.13
Cr2O3	0.04	0.02	0.03	0.02	0.01	0.06	0.02	0.02	0.08	0.05	0.03	0.01
FeO	0.14	0.23	0.23	0.15	0.07	0.25	0.12	0.12	0.39	0.28	0.14	0.12
MnO	0.02	0.01	0.02	0.03	0.01	0.01	0.01	0.02	0.02	0.02	0.02	0.01
NiO	0.02	0.02	0.01	0.02	0.02	0.01	0.02	0.02	0.02	0.02	0.02	0.03
MgO	0.29	0.34	0.32	0.26	0.17	0.44	0.23	0.35	1.37	0.42	0.30	0.16
CaO	0.26	0.49	0.45	0.53	0.15	0.66	0.22	0.41	0.54	0.50	0.37	0.24
Na2O	0.02	0.02	0.01	0.01	0.01	0.01	0.01	0.01	0.03	0.02	0.01	0.01

Sample:	194.20	200.50	223.86	247.82	253.05	269.92	272.40	277.15	293.60	294.12	298.80	299.87
Depth in NG-sequence in m:	1234.20	1240.50	1263.86	1287.82	1293.05	1309.92	1312.40	1317.15	1333.60	1334.12	1338.80	1339.87
Habit:	cum	cum	cum	cum	cum	cum	cum	cum	cum	cum	cum	cum
wt.%												
SiO2	56.03	56.17	55.36	55.00	55.62	55.67	55.47	55.74	55.09	55.10	56.19	55.46
TiO2	0.12	0.07	0.07	0.07	0.09	0.06	0.06	0.10	0.09	0.08	0.08	0.08
Al2O3	1.08	1.36	1.13	1.05	1.02	1.25	1.33	1.22	1.54	1.53	1.13	1.52
Cr2O3	0.48	0.44	0.42	0.46	0.43	0.42	0.51	0.47	0.59	0.57	0.29	0.58
FeO	9.16	9.06	9.27	10.26	10.03	9.27	9.62	9.74	10.35	10.23	9.96	10.19
MnO	0.20	0.22	0.17	0.19	0.18	0.20	0.18	0.23	0.23	0.22	0.21	0.20
NiO	0.09	0.11	0.08	0.10	0.09	0.08	0.09	0.08	0.10	0.10	0.10	0.09
MgO	32.24	31.98	31.77	31.29	30.60	31.58	32.37	31.67	30.74	30.73	31.68	30.82
CaO	1.12	1.23	0.96	1.28	1.52	1.45	0.87	1.27	1.01	1.06	0.89	1.14
Na2O	0.02	0.03	0.02	0.03	0.02	0.03	0.01	0.02	0.01	0.03	0.01	0.02
Total	100.54	100.67	99.25	99.71	99.62	100.01	100.51	100.54	99.76	99.63	100.54	100.11
cations (based on 6 oxygens):												
Si	1.9558	1.9568	1.9575	1.9486	1.9679	1.9559	1.9411	1.9519	1.9490	1.9507	1.9645	1.9532
Ti	0.0031	0.0018	0.0020	0.0018	0.0023	0.0017	0.0017	0.0025	0.0023	0.0022	0.0022	0.0022
Al	0.0442	0.0559	0.0469	0.0437	0.0426	0.0518	0.0547	0.0505	0.0644	0.0637	0.0468	0.0631
Cr	0.0133	0.0121	0.0119	0.0128	0.0121	0.0116	0.0142	0.0130	0.0165	0.0159	0.0079	0.0160
Fe	0.2675	0.2639	0.2741	0.3040	0.2968	0.2724	0.2814	0.2852	0.3064	0.3028	0.2912	0.3002
Mn	0.0058	0.0066	0.0050	0.0058	0.0055	0.0058	0.0055	0.0068	0.0069	0.0065	0.0063	0.0060
Ni	0.0025	0.0030	0.0021	0.0029	0.0027	0.0022	0.0026	0.0023	0.0027	0.0027	0.0028	0.0025
Mg	1.6775	1.6604	1.6743	1.6525	1.6140	1.6538	1.6887	1.6532	1.6213	1.6216	1.6507	1.6179
Ca	0.0419	0.0459	0.0365	0.0485	0.0577	0.0546	0.0326	0.0477	0.0383	0.0400	0.0332	0.0430
Na	0.0015	0.0020	0.0014	0.0018	0.0015	0.0018	0.0006	0.0015	0.0010	0.0018	0.0008	0.0015
Total	4.0131	4.0084	4.0119	4.0223	4.0032	4.0116	4.0230	4.0146	4.0087	4.0081	4.0064	4.0057
n	5	5	4	6	6	6	6	6	6	11	6	6
Mg#	0.8625	0.8629	0.8593	0.8446	0.8447	0.8586	0.8572	0.8529	0.8411	0.8427	0.8501	0.8435
en	84.4	84.3	84.3	82.4	82.0	83.5	84.3	83.2	82.5	82.5	83.6	82.5
wo	2.1	2.3	1.8	2.4	2.9	2.8	1.6	2.4	1.9	2.0	1.7	2.2
fs	13.5	13.4	13.8	15.2	15.1	13.8	14.1	14.4	15.6	15.4	14.7	15.3
standard deviation:												
wt.%												
SiO2	0.16	0.16	0.08	0.30	0.22	0.12	0.09	0.15	0.37	0.17	0.28	0.25
TiO2	0.01	0.01	0.01	0.01	0.02	0.02	0.01	0.04	0.02	0.03	0.01	0.02
Al2O3	0.07	0.09	0.10	0.11	0.12	0.10	0.08	0.21	0.26	0.24	0.20	0.28
Cr2O3	0.03	0.02	0.02	0.02	0.01	0.04	0.02	0.02	0.03	0.05	0.02	0.03
FeO	0.07	0.12	0.06	0.11	0.19	0.19	0.28	0.15	0.35	0.48	0.26	0.23
MnO	0.03	0.04	0.01	0.02	0.02	0.02	0.02	0.02	0.02	0.02	0.03	0.02
NiO	0.03	0.02	0.00	0.02	0.02	0.02	0.02	0.02	0.02	0.03	0.02	0.01
MgO	0.28	0.34	0.19	0.20	0.29	0.20	0.35	0.10	0.40	0.32	0.31	0.13
CaO	0.36	0.32	0.40	0.42	0.43	0.30	0.46	0.10	0.40	0.43	0.30	0.29
Na2O	0.01	0.01	0.01	0.01	0.01	0.01	0.01	0.01	0.01	0.01	0.01	0.01

Sample:	299.89	299.91	307.10	320.15	332.35	350.50	358.66	358.70	360.20	360.23	376.65	397.68
Depth in NG-sequence in m:	1339.89	1339.91	1347.10	1360.15	1372.35	1390.50	1398.66	1398.70	1400.20	1400.23	1416.65	1437.68
Habit:	cum	cum	cum	cum	cum	cum	cum	cum	pcum	cum	cum	cum
wt.%												
SiO2	54.98	55.10	55.12	55.43	55.84	55.45	55.71	55.65	55.42	55.83	55.66	55.41
TiO2	0.09	0.11	0.07	0.09	0.07	0.09	0.06	0.08	0.09	0.09	0.07	0.06
Al2O3	1.71	1.18	1.24	1.09	0.99	1.28	1.23	1.33	1.56	1.25	1.13	1.33
Cr2O3	0.60	0.54	0.51	0.50	0.43	0.42	0.48	0.41	0.51	0.46	0.48	0.40
FeO	10.07	10.44	10.90	10.58	10.47	9.07	9.90	9.22	8.57	9.74	9.46	8.93
MnO	0.22	0.25	0.21	0.21	0.23	0.21	0.19	0.20	0.18	0.20	0.18	0.18
NiO	0.14	0.14	0.09	0.08	0.07	0.10	0.10	0.11	0.10	0.02	0.09	0.09
MgO	31.27	31.47	30.70	30.92	30.99	32.16	31.40	31.19	31.90	31.68	31.83	31.54
CaO	1.03	0.96	1.32	1.30	1.38	1.55	1.10	1.29	1.16	0.92	1.17	1.38
Na2O	0.02	0.03	0.02	0.04	0.02	0.05	0.03	0.03	0.04	0.03	0.04	0.03
Total	100.14	100.22	100.19	100.24	100.49	100.37	100.20	99.53	99.52	100.24	100.10	99.36
cations (based on 6 oxygens):												
Si	1.9370	1.9434	1.9488	1.9550	1.9624	1.9426	1.9574	1.9626	1.9496	1.9574	1.9546	1.9562
Ti	0.0024	0.0028	0.0019	0.0024	0.0019	0.0024	0.0015	0.0020	0.0024	0.0024	0.0018	0.0017
Al	0.0711	0.0490	0.0517	0.0451	0.0408	0.0527	0.0507	0.0554	0.0648	0.0517	0.0467	0.0553
Cr	0.0168	0.0152	0.0143	0.0139	0.0120	0.0116	0.0132	0.0115	0.0141	0.0129	0.0132	0.0113
Fe	0.2968	0.3078	0.3222	0.3120	0.3075	0.2657	0.2908	0.2720	0.2520	0.2857	0.2778	0.2636
Mn	0.0064	0.0074	0.0062	0.0062	0.0070	0.0062	0.0057	0.0061	0.0053	0.0060	0.0052	0.0055
Ni	0.0040	0.0039	0.0026	0.0024	0.0019	0.0027	0.0030	0.0032	0.0029	0.0007	0.0026	0.0027
Mg	1.6424	1.6548	1.6177	1.6256	1.6230	1.6792	1.6445	1.6391	1.6726	1.6556	1.6662	1.6596
Ca	0.0387	0.0363	0.0501	0.0493	0.0520	0.0581	0.0415	0.0489	0.0438	0.0346	0.0439	0.0521
Na	0.0017	0.0018	0.0016	0.0028	0.0016	0.0034	0.0018	0.0023	0.0024	0.0023	0.0026	0.0020
Total	4.0174	4.0225	4.0171	4.0146	4.0101	4.0246	4.0100	4.0031	4.0099	4.0092	4.0149	4.0099
n	3	5	6	6	6	5	7	5	6	6	6	4
Mg#	0.8469	0.8432	0.8339	0.8390	0.8407	0.8634	0.8498	0.8577	0.8691	0.8528	0.8571	0.8629
en	83.0	82.8	81.3	81.8	81.9	83.8	83.2	83.6	85.0	83.8	83.8	84.0
wo	2.0	1.8	2.5	2.5	2.6	2.9	2.1	2.5	2.2	1.7	2.2	2.6
fs	15.0	15.4	16.2	15.7	15.5	13.3	14.7	13.9	12.8	14.5	14.0	13.3
standard deviation:												
wt.%												
SiO2	0.49	0.43	0.13	0.28	0.23	0.31	0.28	0.18	0.22	0.38	0.08	0.13
TiO2	0.02	0.03	0.02	0.04	0.03	0.02	0.04	0.02	0.02	0.02	0.04	0.02
Al2O3	0.23	0.15	0.12	0.15	0.20	0.11	0.04	0.12	0.12	0.15	0.06	0.05
Cr2O3	0.04	0.03	0.02	0.03	0.09	0.03	0.02	0.04	0.03	0.02	0.04	0.05
FeO	0.34	0.04	0.20	0.17	0.40	0.07	0.27	0.21	0.09	0.16	0.36	0.22
MnO	0.02	0.03	0.01	0.01	0.03	0.02	0.02	0.02	0.02	0.01	0.03	0.03
NiO	0.01	0.01	0.02	0.01	0.01	0.02	0.01	0.01	0.03	0.01	0.02	0.02
MgO	0.23	0.27	0.19	0.35	0.57	0.31	0.22	0.09	0.20	0.16	0.28	0.51
CaO	0.04	0.37	0.34	0.45	0.86	0.32	0.16	0.24	0.29	0.09	0.31	0.52
Na2O	0.00	0.01	0.01	0.01	0.02	0.00	0.01	0.01	0.01	0.01	0.01	0.03

Sample:	410.61	420.00	420.05	426.60	428.15	439.40	447.00	451.00	454.45	488.33	509.05	520.00
Depth in NG-sequence in m:	1450.61	1460.00	1460.05	1466.60	1468.15	1479.40	1487.00	1491.00	1494.45	1528.33	1549.05	1560.00
Habit:	cum	cum	cum	cum	cum	cum	cum	cum	cum	cum	pcum	pcum
wt.%												
SiO2	56.43	56.22	56.37	55.61	56.45	56.33	56.68	56.47	56.34	56.36	56.81	56.51
TiO2	0.07	0.08	0.09	0.10	0.08	0.10	0.08	0.14	0.09	0.09	0.11	0.19
Al2O3	1.22	1.23	1.20	1.25	1.16	1.23	1.08	1.13	1.20	1.25	1.21	1.07
Cr2O3	0.43	0.44	0.46	0.47	0.43	0.46	0.43	0.46	0.43	0.43	0.51	0.31
FeO	8.67	8.77	9.01	8.82	9.31	8.61	9.37	9.01	8.94	8.07	6.95	8.52
MnO	0.22	0.19	0.18	0.21	0.21	0.21	0.19	0.19	0.18	0.16	0.18	0.24
NiO	0.08	0.10	0.11	0.08	0.09	0.11	0.08	0.07	0.06	0.10	0.08	0.05
MgO	31.75	31.83	31.60	31.70	31.09	32.20	31.22	30.78	32.53	32.31	32.87	31.81
CaO	1.52	1.34	1.37	1.18	1.08	1.00	1.16	0.95	1.30	1.44	1.24	0.95
Na2O	0.02	0.03	0.03	0.03	0.03	0.03	0.03	0.02	0.02	0.04	0.05	0.03
Total	100.40	100.23	100.44	99.45	99.93	100.27	100.32	99.21	101.09	100.23	100.02	99.67
cations (based on 6 oxygens):												
Si	1.9673	1.9641	1.9672	1.9595	1.9792	1.9642	1.9800	1.9889	1.9537	1.9630	1.9711	1.9784
Ti	0.0019	0.0022	0.0024	0.0027	0.0020	0.0026	0.0020	0.0037	0.0024	0.0023	0.0028	0.0049
Al	0.0501	0.0507	0.0492	0.0518	0.0481	0.0504	0.0445	0.0467	0.0491	0.0511	0.0493	0.0440
Cr	0.0118	0.0121	0.0128	0.0130	0.0120	0.0125	0.0118	0.0127	0.0118	0.0118	0.0141	0.0085
Fe	0.2527	0.2561	0.2631	0.2599	0.2730	0.2512	0.2738	0.2655	0.2592	0.2349	0.2017	0.2495
Mn	0.0064	0.0057	0.0053	0.0064	0.0061	0.0061	0.0056	0.0056	0.0053	0.0048	0.0053	0.0071
Ni	0.0023	0.0027	0.0031	0.0023	0.0024	0.0031	0.0022	0.0020	0.0018	0.0028	0.0023	0.0014
Mg	1.6499	1.6574	1.6439	1.6647	1.6245	1.6737	1.6255	1.6159	1.6816	1.6775	1.7000	1.6600
Ca	0.0568	0.0502	0.0514	0.0444	0.0406	0.0372	0.0433	0.0358	0.0482	0.0536	0.0461	0.0356
Na	0.0016	0.0022	0.0021	0.0020	0.0017	0.0020	0.0023	0.0015	0.0011	0.0029	0.0031	0.0019
Total	4.0007	4.0034	4.0004	4.0065	3.9897	4.0028	3.9910	3.9784	4.0141	4.0047	3.9959	3.9914
n	6	8	6	7	5	6	6	6	6	5	5	5
Mg#	0.8672	0.8661	0.8620	0.8649	0.8561	0.8695	0.8558	0.8589	0.8665	0.8772	0.8939	0.8693
en	84.2	84.4	83.9	84.5	83.8	85.3	83.7	84.3	84.5	85.3	87.3	85.3
wo	2.9	2.6	2.6	2.3	2.1	1.9	2.2	1.9	2.4	2.7	2.4	1.8
fs	12.9	13.0	13.4	13.2	14.1	12.8	14.1	13.8	13.0	11.9	10.4	12.8
standard deviation:												
wt.%												
SiO2	0.11	0.19	0.15	0.29	0.13	0.09	0.12	0.15	0.16	0.29	0.15	0.31
TiO2	0.02	0.03	0.02	0.05	0.03	0.03	0.02	0.07	0.03	0.01	0.06	0.06
Al2O3	0.05	0.09	0.08	0.10	0.06	0.08	0.05	0.09	0.06	0.05	0.11	0.14
Cr2O3	0.04	0.04	0.03	0.05	0.07	0.03	0.03	0.04	0.03	0.03	0.10	0.07
FeO	0.15	0.11	0.14	0.13	0.13	0.14	0.17	0.12	0.11	0.18	0.21	0.21
MnO	0.02	0.02	0.01	0.01	0.03	0.02	0.02	0.03	0.02	0.02	0.02	0.01
NiO	0.02	0.02	0.02	0.03	0.03	0.01	0.02	0.01	0.02	0.02	0.02	0.02
MgO	0.19	0.20	0.21	0.22	0.26	0.28	0.23	0.21	0.33	0.36	0.20	0.36
CaO	0.21	0.21	0.27	0.30	0.08	0.32	0.41	0.26	0.36	0.40	0.26	0.37
Na2O	0.00	0.01	0.01	0.01	0.01	0.01	0.01	0.02	0.01	0.01	0.01	0.01

Sample:	530.95	531.10	561.35	561.37	590.97	591.03	591.05	591.10	591.12	591.14	591.25	604.30
Depth in NG-sequence in m:	1570.95	1571.10	1601.35	1601.37	1630.97	1631.03	1631.05	1631.10	1631.12	1631.14	1631.25	1644.30
Habit:	cum	cum	cum	cum	cum	pcum	cum	cum	pcum	pcum	pcum	cum
wt.%												
SiO2	56.42	56.93	56.52	56.26	55.89	56.01	56.23	55.89	55.79	56.50	56.63	55.66
TiO2	0.09	0.09	0.08	0.13	0.10	0.28	0.06	0.08	0.18	0.17	0.08	0.10
Al2O3	1.10	1.06	1.31	1.15	1.16	1.19	1.02	1.08	1.20	1.23	1.08	1.15
Cr2O3	0.34	0.35	0.45	0.43	0.49	0.36	0.47	0.46	0.32	0.35	0.45	0.46
FeO	8.73	8.77	9.91	9.80	9.24	9.12	8.99	9.45	9.28	9.27	9.08	9.55
MnO	0.20	0.20	0.21	0.20	0.18	0.18	0.18	0.21	0.19	0.20	0.20	0.18
NiO	0.07	0.07	0.09	0.09	0.06	0.02	0.07	0.08	0.07	0.08	0.05	0.11
MgO	32.62	31.83	31.11	31.23	31.30	30.79	31.21	31.57	31.25	30.80	31.11	31.53
CaO	0.90	1.02	0.92	0.77	1.21	1.53	0.94	1.01	1.28	1.20	1.08	1.12
Na2O	0.01	0.04	0.03	0.02	0.03	0.04	0.02	0.03	0.03	0.03	0.03	0.02
Total	100.48	100.35	100.63	100.07	99.66	99.51	99.19	99.86	99.60	99.83	99.79	99.88
cations (based on 6 oxygens):												
Si	1.9631	1.9813	1.9725	1.9730	1.9671	1.9730	1.9825	1.9648	1.9654	1.9818	1.9849	1.9589
Ti	0.0023	0.0022	0.0020	0.0034	0.0027	0.0074	0.0016	0.0022	0.0049	0.0044	0.0022	0.0027
Al	0.0453	0.0436	0.0537	0.0477	0.0481	0.0494	0.0423	0.0449	0.0498	0.0510	0.0445	0.0477
Cr	0.0093	0.0097	0.0125	0.0119	0.0137	0.0099	0.0131	0.0128	0.0089	0.0097	0.0125	0.0129
Fe	0.2539	0.2551	0.2893	0.2874	0.2721	0.2685	0.2649	0.2778	0.2734	0.2718	0.2661	0.2811
Mn	0.0059	0.0058	0.0061	0.0059	0.0054	0.0053	0.0053	0.0062	0.0058	0.0059	0.0058	0.0053
Ni	0.0019	0.0019	0.0026	0.0025	0.0018	0.0005	0.0019	0.0023	0.0020	0.0022	0.0015	0.0031
Mg	1.6915	1.6509	1.6183	1.6325	1.6419	1.6168	1.6402	1.6543	1.6409	1.6104	1.6250	1.6538
Ca	0.0337	0.0381	0.0345	0.0291	0.0455	0.0578	0.0354	0.0379	0.0482	0.0452	0.0405	0.0420
Na	0.0006	0.0024	0.0019	0.0011	0.0022	0.0024	0.0016	0.0023	0.0022	0.0023	0.0024	0.0012
Total	4.0076	3.9910	3.9934	3.9944	4.0004	3.9911	3.9890	4.0054	4.0015	3.9847	3.9856	4.0088
n	6	6	5	5	6	1	3	4	3	6	6	8
Mg#	0.8695	0.8662	0.8484	0.8503	0.8579	0.8576	0.8609	0.8562	0.8572	0.8556	0.8593	0.8547
en	85.5	84.9	83.3	83.8	83.8	83.2	84.5	84.0	83.6	83.5	84.1	83.7
wo	1.7	2.0	1.8	1.5	2.3	3.0	1.8	1.9	2.5	2.3	2.1	2.1
fs	12.8	13.1	14.9	14.7	13.9	13.8	13.7	14.1	13.9	14.1	13.8	14.2
standard deviation:												
wt.%												
SiO2	0.47	0.22	0.09	0.23	0.16		0.10	0.16	0.05	0.19	0.13	0.29
TiO2	0.03	0.02	0.02	0.08	0.03		0.00	0.01	0.06	0.03	0.03	0.04
Al2O3	0.11	0.11	0.22	0.09	0.08		0.09	0.09	0.13	0.08	0.09	0.09
Cr2O3	0.11	0.13	0.07	0.04	0.03		0.02	0.02	0.11	0.10	0.03	0.05
FeO	0.20	0.40	0.24	0.12	0.04		0.38	0.18	0.17	0.13	0.28	0.23
MnO	0.02	0.02	0.01	0.01	0.02		0.03	0.02	0.02	0.02	0.02	0.02
NiO	0.02	0.03	0.02	0.02	0.01		0.01	0.02	0.02	0.02	0.02	0.02
MgO	0.41	0.87	0.28	0.11	0.21		0.39	0.41	0.26	0.50	0.26	0.31
CaO	0.39	0.91	0.49	0.17	0.21		0.06	0.68	0.52	0.53	0.42	0.56
Na2O	0.01	0.03	0.02	0.01	0.01		0.00	0.01	0.01	0.02	0.02	0.02

Sample:	618.25	618.27	654.56	678.64	691.95	702.60	709.10	723.22	736.66	738.90	739.10	743.62
Depth in NG-sequence in m:	1658.25	1658.27	1694.56	1718.64	1731.95	1742.60	1749.10	1763.22	1776.66	1778.90	1779.10	1783.62
Habit:	cum	cum	pcum	cum	cum	pcum	pcum	pcum	cum	pcum	cum	cum
wt.%												
SiO2	55.67	55.81	56.13	56.56	56.07	57.21	57.51	56.81	55.94	56.99	56.33	55.61
TiO2	0.06	0.05	0.08	0.08	0.06	0.06	0.13	0.15	0.07	0.09	0.09	0.12
Al2O3	1.25	1.12	1.21	1.12	1.09	1.17	0.92	1.49	1.21	1.08	1.07	0.93
Cr2O3	0.43	0.46	0.47	0.44	0.44	0.48	0.28	0.50	0.45	0.36	0.48	0.38
FeO	9.11	9.41	8.25	8.99	8.76	7.52	7.71	7.61	9.10	9.08	9.34	11.60
MnO	0.20	0.21	0.19	0.19	0.21	0.17	0.17	0.19	0.18	0.17	0.21	0.23
NiO	0.10	0.09	0.09	0.08	0.07	0.04	0.05	0.04	0.09	0.07	0.09	0.10
MgO	31.43	31.47	32.62	31.79	33.40	32.64	33.42	31.66	31.53	31.34	31.33	29.70
CaO	0.92	0.69	1.24	0.91	0.71	0.99	1.02	1.68	0.77	1.04	1.19	0.71
Na2O	0.04	0.02	0.03	0.05	0.03	0.04	0.02	0.11	0.03	0.01	0.03	0.01
Total	99.20	99.33	100.30	100.23	100.83	100.33	101.25	100.25	99.36	100.24	100.15	99.38
cations (based on 6 oxygens):												
Si	1.9664	1.9698	1.9560	1.9741	1.9468	1.9799	1.9745	1.9734	1.9706	1.9870	1.9728	1.9800
Ti	0.0015	0.0014	0.0020	0.0022	0.0016	0.0016	0.0035	0.0040	0.0017	0.0023	0.0023	0.0033
Al	0.0522	0.0464	0.0497	0.0463	0.0447	0.0475	0.0374	0.0611	0.0500	0.0446	0.0442	0.0391
Cr	0.0120	0.0130	0.0130	0.0122	0.0120	0.0132	0.0077	0.0138	0.0125	0.0098	0.0132	0.0107
Fe	0.2689	0.2776	0.2404	0.2624	0.2545	0.2177	0.2214	0.2212	0.2681	0.2649	0.2737	0.3455
Mn	0.0061	0.0062	0.0056	0.0056	0.0061	0.0051	0.0049	0.0056	0.0054	0.0049	0.0062	0.0070
Ni	0.0028	0.0026	0.0024	0.0023	0.0020	0.0013	0.0015	0.0012	0.0025	0.0020	0.0025	0.0028
Mg	1.6544	1.6554	1.6942	1.6533	1.7283	1.6837	1.7104	1.6388	1.6555	1.6286	1.6355	1.5761
Ca	0.0347	0.0261	0.0463	0.0343	0.0264	0.0367	0.0374	0.0625	0.0290	0.0390	0.0447	0.0269
Na	0.0025	0.0017	0.0022	0.0034	0.0018	0.0030	0.0014	0.0072	0.0022	0.0010	0.0019	0.0005
Total	4.0013	4.0000	4.0118	3.9962	4.0242	3.9896	4.0001	3.9888	3.9975	3.9840	3.9971	3.9921
n	3	4	5	6	8	4	3	5	4	5	5	7
Mg#	0.8602	0.8564	0.8757	0.8630	0.8716	0.8855	0.8854	0.8811	0.8606	0.8601	0.8566	0.8202
en	84.5	84.5	85.5	84.8	86.0	86.9	86.9	85.2	84.8	84.3	83.7	80.9
wo	1.8	1.3	2.3	1.8	1.3	1.9	1.9	3.3	1.5	2.0	2.3	1.4
fs	13.7	14.2	12.1	13.5	12.7	11.2	11.2	11.5	13.7	13.7	14.0	17.7
standard deviation:												
wt.%												
SiO2	0.11	0.06	0.37	0.43	0.21	0.32	0.43	0.63	0.41	0.06	0.43	0.20
TiO2	0.02	0.02	0.03	0.06	0.02	0.01	0.11	0.08	0.03	0.04	0.04	0.01
Al2O3	0.21	0.05	0.30	0.37	0.16	0.10	0.29	0.47	0.23	0.10	0.23	0.14
Cr2O3	0.02	0.04	0.13	0.13	0.04	0.06	0.09	0.16	0.02	0.12	0.11	0.06
FeO	0.18	0.28	0.17	0.41	0.25	0.14	0.11	0.13	0.19	0.25	0.27	0.11
MnO	0.01	0.01	0.02	0.03	0.01	0.02	0.02	0.02	0.02	0.03	0.00	0.02
NiO	0.02	0.02	0.02	0.01	0.01	0.01	0.01	0.02	0.03	0.02	0.02	0.01
MgO	0.18	0.34	0.58	0.84	0.24	0.30	0.53	0.94	0.10	0.16	0.78	0.33
CaO	0.21	0.24	0.53	0.64	0.19	0.15	0.29	0.72	0.22	0.15	0.63	0.34
Na2O	0.01	0.01	0.02	0.08	0.01	0.01	0.01	0.12	0.01	0.01	0.02	0.01

Sample:	754.00	762.27	763.45	772.36	773.60	773.70	773.71	774.00
Depth in								
MG-sequence in m:	1794.00	1802.27	1803.45	1812.36	1813.60	1813.70	1813.71	1814.00
Habit:	cum	cum	cum	cum	cum	cum	cum	cum
wt.%								
SiO2	55.42	55.82	56.03	55.47	54.34	54.80	54.44	54.50
TiO2	0.11	0.12	0.08	0.18	0.15	0.15	0.16	0.10
Al2O3	0.99	0.95	1.25	1.32	1.08	1.11	0.88	0.69
Cr2O3	0.41	0.37	0.54	0.35	0.28	0.39	0.23	0.16
FeO	12.39	11.88	10.04	10.37	16.72	13.32	16.57	16.76
MnO	0.25	0.23	0.20	0.20	0.28	0.24	0.30	0.33
NiO	0.07	0.09	0.06	0.06	0.08	0.08	0.04	0.05
MgO	29.41	29.09	30.52	30.87	26.30	28.79	26.25	26.66
CaO	0.70	0.73	0.99	1.11	0.66	0.65	0.58	0.40
Na2O	0.01	0.01	0.02	0.03	0.02	0.02	0.01	0.01
Total	99.76	99.30	99.72	99.97	99.90	99.55	99.46	99.66
cations (based on 6 oxygens):								
Si	1.9737	1.9899	1.9752	1.9566	1.9720	1.9654	1.9815	1.9809
Ti	0.0030	0.0033	0.0021	0.0049	0.0040	0.0041	0.0043	0.0027
Al	0.0415	0.0400	0.0518	0.0551	0.0462	0.0471	0.0379	0.0296
Cr	0.0115	0.0105	0.0150	0.0098	0.0082	0.0112	0.0065	0.0046
Fe	0.3690	0.3541	0.2959	0.3059	0.5074	0.3994	0.5044	0.5095
Mn	0.0077	0.0070	0.0060	0.0060	0.0086	0.0073	0.0094	0.0101
Ni	0.0020	0.0025	0.0016	0.0016	0.0023	0.0024	0.0012	0.0013
Mg	1.5615	1.5457	1.6036	1.6230	1.4221	1.5391	1.4239	1.4445
Ca	0.0267	0.0280	0.0373	0.0421	0.0256	0.0249	0.0225	0.0155
Na	0.0006	0.0010	0.0016	0.0021	0.0012	0.0011	0.0010	0.0009
Total	3.9971	3.9820	3.9901	4.0071	3.9975	4.0019	3.9925	3.9997
n	9	12	6	11	8	12	7	5
Mg#	0.8089	0.8136	0.8442	0.8414	0.7370	0.7940	0.7384	0.7393
en	79.8	80.2	82.8	82.3	72.7	78.4	73.0	73.3
wo	1.4	1.5	1.9	2.1	1.3	1.3	1.2	0.8
fs	18.9	18.4	15.3	15.5	26.0	20.3	25.9	25.9
standard deviation:								
wt.%								
SiO2	0.29	0.31	0.23	0.37	0.21	0.30	0.17	0.29
TiO2	0.03	0.03	0.03	0.12	0.04	0.06	0.02	0.02
Al2O3	0.15	0.27	0.15	0.17	0.23	0.23	0.13	0.04
Cr2O3	0.10	0.12	0.06	0.17	0.16	0.06	0.02	0.01
FeO	0.21	0.42	0.22	0.28	0.77	0.43	0.23	0.21
MnO	0.03	0.02	0.04	0.02	0.05	0.02	0.03	0.03
NiO	0.03	0.03	0.02	0.03	0.02	0.01	0.01	0.02
MgO	0.23	0.34	0.32	0.31	0.58	0.22	0.20	0.20
CaO	0.30	0.45	0.22	0.42	0.22	0.28	0.09	0.06
Na2O	0.01	0.02	0.01	0.02	0.01	0.01	0.00	0.02

MICROPROBE DATA: Composition of orthopyroxene in the KD-sequence

Sample:	28.38	50.05	61.20	71.10	73.10	78.00	82.60	82.70	88.40	89.70	90.30	96.30	97.40
Habit:	all cumulus												
wt.%													
SiO2	55.90	55.40	54.80	55.83	56.31	56.21	56.28	55.39	55.74	55.12	54.64	55.80	55.70
TiO2	0.05	0.10	0.08	0.05	0.08	0.11	0.12	0.07	0.08	0.07	0.13	0.08	0.09
Al2O3	1.51	1.13	1.82	1.72	1.81	1.32	1.35	1.51	1.69	1.74	1.37	1.87	1.50
Cr2O3	0.53	0.50	0.63	0.55	0.54	0.61	0.59	0.60	0.62	0.64	0.51	0.59	0.49
FeO	9.82	10.55	9.65	7.78	7.47	9.01	9.18	8.81	8.76	9.92	10.66	9.42	9.63
MnO	0.23	0.25	0.22	0.21	0.22	0.21	0.22	0.22	0.23	0.21	0.22	0.27	0.22
NiO	0.06	0.08	0.05	0.04	0.09	0.06	0.08	0.05	0.06	0.05	0.03	0.09	0.06
MgO	30.71	30.41	30.18	32.52	32.52	31.56	31.29	32.21	31.05	30.63	30.40	30.38	31.39
CaO	1.41	1.45	1.47	0.86	1.01	1.19	1.22	1.26	1.47	1.44	1.53	1.51	1.51
Na2O	0.02	0.02	0.03	0.01	0.01	0.02	0.02	0.02	0.03	0.02	0.04	0.03	0.02
Total	100.24	99.89	98.92	99.57	100.06	100.29	100.35	100.14	99.73	99.84	99.52	100.04	100.63
cations (based on 6 oxygens):													
Si	1.9622	1.9605	1.9506	1.9526	1.9568	1.9638	1.9665	1.9407	1.9582	1.9464	1.9443	1.9597	1.9487
Ti	0.0014	0.0026	0.0021	0.0013	0.0020	0.0030	0.0032	0.0019	0.0020	0.0019	0.0036	0.0022	0.0025
Al	0.0623	0.0473	0.0765	0.0710	0.0743	0.0543	0.0555	0.0623	0.0702	0.0724	0.0573	0.0774	0.0619
Cr	0.0147	0.0139	0.0177	0.0152	0.0150	0.0168	0.0164	0.0167	0.0172	0.0179	0.0143	0.0165	0.0136
Fe	0.2883	0.3122	0.2873	0.2276	0.2171	0.2632	0.2682	0.2581	0.2574	0.2930	0.3172	0.2769	0.2819
Mn	0.0067	0.0074	0.0065	0.0061	0.0064	0.0064	0.0066	0.0065	0.0070	0.0062	0.0065	0.0080	0.0066
Ni	0.0018	0.0023	0.0014	0.0012	0.0026	0.0017	0.0023	0.0014	0.0017	0.0014	0.0008	0.0025	0.0017
Mg	1.6068	1.6043	1.6011	1.6955	1.6845	1.6433	1.6293	1.6823	1.6262	1.6121	1.6126	1.5902	1.6370
Ca	0.0530	0.0551	0.0560	0.0321	0.0376	0.0445	0.0455	0.0472	0.0553	0.0544	0.0584	0.0568	0.0568
Na	0.0012	0.0016	0.0018	0.0008	0.0008	0.0013	0.0015	0.0016	0.0017	0.0015	0.0026	0.0018	0.0010
Total	3.9985	4.0071	4.0010	4.0034	3.9970	3.9983	3.9951	4.0187	3.9970	4.0073	4.0176	3.9920	4.0116
n	5	5	3	3	4	5	4	5	5	3	4	3	5
Mg#	0.8479	0.8371	0.8479	0.8817	0.8858	0.8619	0.8587	0.8670	0.8634	0.8462	0.8356	0.8517	0.8531
en	82.5	81.4	82.3	86.7	86.9	84.2	83.9	84.6	83.9	82.3	81.1	82.7	82.9
wo	2.7	2.8	2.9	1.6	1.9	2.3	2.3	2.4	2.9	2.8	2.9	3.0	2.9
fs	14.8	15.8	14.8	11.6	11.2	13.5	13.8	13.0	13.3	15.0	16.0	14.4	14.3
standard deviation:													
wt.%													
SiO2	0.19	0.18	0.19	0.09	0.19	0.25	0.17	0.25	0.06	0.15	0.25	0.13	0.13
TiO2	0.02	0.01	0.01	0.01	0.01	0.02	0.04	0.01	0.01	0.01	0.03	0.02	0.02
Al2O3	0.11	0.08	0.06	0.07	0.09	0.08	0.28	0.12	0.03	0.13	0.23	0.22	0.10
Cr2O3	0.03	0.01	0.04	0.02	0.03	0.03	0.08	0.02	0.01	0.04	0.05	0.05	0.04
FeO	0.11	0.11	0.16	0.13	0.16	0.14	0.37	0.16	0.13	0.11	0.17	0.42	0.19
MnO	0.01	0.01	0.01	0.03	0.02	0.01	0.01	0.03	0.03	0.01	0.02	0.01	0.01
NiO	0.01	0.02	0.02	0.00	0.02	0.01	0.01	0.02	0.02	0.01	0.02	0.01	0.02
MgO	0.20	0.15	0.13	0.14	0.18	0.22	0.19	0.12	0.24	0.09	0.42	0.44	0.10
CaO	0.20	0.12	0.28	0.23	0.12	0.28	0.29	0.19	0.12	0.12	0.53	0.12	0.18
Na2O	0.01	0.01	0.01	0.01	0.01	0.00	0.01	0.01	0.00	0.00	0.02	0.01	0.01

Sample:	97.97	102.00	105.50	108.50	113.16	124.48
Habit:	all cumulus					
wt.%						
SiO2	55.36	55.95	55.46	55.61	55.87	55.93
TiO2	0.10	0.13	0.08	0.09	0.11	0.09
Al2O3	1.68	1.57	1.18	1.27	1.13	1.29
Cr2O3	0.49	0.32	0.48	0.48	0.48	0.56
FeO	9.71	9.82	9.96	10.27	11.52	10.34
MnO	0.26	0.26	0.21	0.25	0.27	0.23
NiO	0.06	0.08	0.10	0.06	0.06	0.09
MgO	30.94	30.68	30.61	31.19	30.26	30.68
CaO	1.35	1.14	1.78	1.20	1.09	1.17
Na2O	0.01	0.01	0.02	0.01	0.00	0.01
Total	99.96	99.95	99.88	100.41	100.79	100.39
cations (based on 6 oxygens):						
Si	1.9495	1.9665	1.9595	1.9538	1.9643	1.9643
Ti	0.0027	0.0033	0.0021	0.0023	0.0029	0.0024
Al	0.0695	0.0652	0.0491	0.0524	0.0467	0.0535
Cr	0.0137	0.0089	0.0133	0.0134	0.0133	0.0156
Fe	0.2860	0.2885	0.2942	0.3017	0.3390	0.3037
Mn	0.0078	0.0076	0.0063	0.0075	0.0080	0.0068
Ni	0.0017	0.0022	0.0028	0.0016	0.0017	0.0024
Mg	1.6241	1.6074	1.6117	1.6332	1.5854	1.6059
Ca	0.0508	0.0430	0.0673	0.0450	0.0412	0.0439
Na	0.0009	0.0003	0.0015	0.0004	0.0003	0.0007
Total	4.0067	3.9932	4.0079	4.0112	4.0029	3.9992
n	5	3	5	5	5	6
Mg#	0.8503	0.8478	0.8456	0.8441	0.8238	0.8410
en	82.8	82.9	81.7	82.5	80.7	82.2
wo	2.6	2.2	3.4	2.3	2.1	2.2
fs	14.6	14.9	14.9	15.2	17.2	15.5
standard deviation:						
wt.%						
SiO2	0.11	0.06	0.13	0.19	0.46	0.25
TiO2	0.05	0.03	0.01	0.01	0.02	0.01
Al2O3	0.13	0.02	0.10	0.17	0.06	0.13
Cr2O3	0.14	0.04	0.04	0.02	0.05	0.02
FeO	0.21	0.18	0.41	0.11	1.03	0.19
MnO	0.04	0.01	0.02	0.02	0.04	0.02
NiO	0.04	0.01	0.01	0.02	0.03	0.01
MgO	0.27	0.39	0.44	0.11	0.84	0.36
CaO	0.40	0.28	0.70	0.08	0.26	0.42
Na2O	0.01	0.00	0.02	0.01	0.00	0.01

MICROPROBE DATA: Composition of orthopyroxene in the SF-sequence

Sample:	69.30	219.55	223.68	250.88	268.22	268.41	305.35	313.00	318.50	318.52	319.18	319.54	336.97
Habit:	pcum	cum	cum	cum	cum	cum	cum	cum	cum	cum	cum	pcum	cum
wt.%													
SiO2	55.07	55.35	55.12	55.15	55.91	55.65	55.35	55.21	55.29	55.45	55.63	55.65	55.85
TiO2	0.12	0.10	0.13	0.12	0.08	0.12	0.12	0.16	0.13	0.09	0.16	0.14	0.11
Al2O3	1.22	1.13	1.26	0.99	1.58	1.14	1.27	1.10	1.23	1.46	1.13	1.38	1.43
Cr2O3	0.42	0.49	0.47	0.48	0.57	0.53	0.47	0.45	0.55	0.60	0.51	0.45	0.30
FeO	11.21	11.95	12.12	11.87	10.38	11.05	10.42	10.99	10.57	10.38	10.34	9.36	9.83
MnO	0.23	0.23	0.25	0.23	0.21	0.22	0.21	0.25	0.22	0.21	0.22	0.21	0.19
NiO	0.07	0.02	0.07	0.06	0.04	0.06	0.04	0.07	0.09	0.09	0.08	0.09	0.07
MgO	29.74	29.10	28.26	28.83	30.13	29.47	29.97	30.32	30.60	30.91	30.51	31.18	30.92
CaO	1.52	1.31	2.09	1.96	1.40	1.40	1.52	1.21	1.22	0.91	1.51	1.64	1.47
Na2O	0.02	0.01	0.01	0.04	0.00	0.02	0.03	0.00	0.02	0.02	0.02	0.01	0.01
Total	99.61	99.68	99.79	99.74	100.32	99.66	99.39	99.76	99.91	100.11	100.09	100.12	100.20
cations (based on 6 oxygens):													
Si	1.9602	1.9718	1.9685	1.9687	1.9650	1.9751	1.9658	1.9591	1.9556	1.9534	1.9622	1.9548	1.9610
Ti	0.0032	0.0026	0.0035	0.0032	0.0021	0.0032	0.0032	0.0042	0.0036	0.0024	0.0042	0.0038	0.0030
Al	0.0513	0.0473	0.0532	0.0418	0.0656	0.0477	0.0534	0.0461	0.0513	0.0605	0.0471	0.0572	0.0594
Cr	0.0118	0.0138	0.0132	0.0135	0.0158	0.0150	0.0132	0.0126	0.0153	0.0168	0.0141	0.0125	0.0083
Fe	0.3338	0.3559	0.3620	0.3544	0.3053	0.3281	0.3094	0.3263	0.3127	0.3058	0.3051	0.2751	0.2887
Mn	0.0069	0.0070	0.0077	0.0071	0.0061	0.0067	0.0062	0.0074	0.0065	0.0063	0.0065	0.0062	0.0055
Ni	0.0021	0.0005	0.0021	0.0018	0.0011	0.0016	0.0011	0.0020	0.0025	0.0025	0.0021	0.0027	0.0021
Mg	1.5776	1.5454	1.5044	1.5339	1.5785	1.5589	1.5866	1.6038	1.6131	1.6229	1.6040	1.6323	1.6183
Ca	0.0578	0.0502	0.0799	0.0748	0.0528	0.0532	0.0579	0.0459	0.0464	0.0343	0.0570	0.0617	0.0555
Na	0.0043	0.0017	0.0025	0.0101	0.0013	0.0016	0.0084	0.0007	0.0053	0.0052	0.0047	0.0038	0.0034
Total	4.0089	3.9965	3.9969	4.0093	3.9934	3.9899	4.0051	4.0080	4.0122	4.0101	4.0071	4.0100	4.0051
n	4	2	5	5	5	4	4	5	3	4	5	4	5
Mg#	0.8254	0.8128	0.8060	0.8123	0.8380	0.8261	0.8368	0.8309	0.8376	0.8415	0.8402	0.8558	0.8486
en	80.1	79.2	77.3	78.1	81.5	80.4	81.2	81.2	81.8	82.7	81.6	82.9	82.5
wo	2.9	2.6	4.1	3.8	2.7	2.7	3.0	2.3	2.4	1.7	2.9	3.1	2.8
fs	16.9	18.2	18.6	18.1	15.8	16.9	15.8	16.5	15.9	15.6	15.5	14.0	14.7
standard deviation:													
wt.%													
SiO2	0.10	0.31	0.22	0.19	0.15	0.09	0.21	0.16	0.25	0.28	0.33	0.05	0.20
TiO2	0.01	0.00	0.01	0.03	0.02	0.02	0.02	0.01	0.02	0.03	0.01	0.03	0.02
Al2O3	0.10	0.05	0.11	0.06	0.16	0.02	0.18	0.05	0.09	0.23	0.04	0.13	0.12
Cr2O3	0.02	0.04	0.05	0.02	0.04	0.02	0.02	0.02	0.02	0.03	0.02	0.04	0.11
FeO	0.17	0.12	0.23	0.28	0.56	0.19	0.13	0.20	0.06	0.32	0.10	0.54	0.26
MnO	0.03	0.00	0.04	0.02	0.02	0.01	0.03	0.01	0.02	0.01	0.01	0.02	0.02
NiO	0.03	0.00	0.02	0.02	0.01	0.02	0.02	0.01	0.00	0.01	0.01	0.02	0.01
MgO	0.18	0.66	0.16	0.43	0.23	0.20	0.13	0.15	0.15	0.19	0.19	0.11	0.28
CaO	0.11	0.45	0.35	0.45	0.40	0.19	0.33	0.24	0.22	0.15	0.25	0.18	0.28
Na2O	0.01	0.01	0.01	0.02	0.00	0.01	0.01	0.00	0.01	0.00	0.00	0.01	0.01

Sample:	337.00	357.30	360.90	362.12	368.10	372.16	372.38	373.00	379.10	380.00	385.20	385.94	385.96
Habit:	cum	cum	cum	cum	cum	cum	cum	cum	cum	cum	cum	cum	cum
wt.%													
SiO2	55.95	56.03	55.32	55.70	56.05	55.75	54.75	56.19	55.76	55.04	55.45	55.52	55.19
TiO2	0.15	0.15	0.09	0.12	0.16	0.15	0.11	0.15	0.12	0.14	0.14	0.15	0.15
Al2O3	1.22	1.13	1.60	1.43	1.12	1.21	1.31	1.00	1.06	1.18	1.23	1.16	1.09
Cr2O3	0.53	0.52	0.53	0.30	0.47	0.59	0.56	0.38	0.43	0.50	0.51	0.51	0.48
FeO	9.94	10.99	10.32	10.89	10.70	10.58	11.04	11.19	11.29	11.36	11.37	11.31	11.43
MnO	0.22	0.18	0.20	0.25	0.21	0.23	0.26	0.22	0.20	0.21	0.24	0.24	0.25
NiO	0.07	0.08	0.01	0.08	0.05	0.07	0.07	0.04	0.06	0.07	0.04	0.08	0.08
MgO	30.25	29.56	30.27	30.44	30.65	29.99	29.44	30.65	29.44	29.45	29.25	29.69	29.63
CaO	1.95	1.79	1.66	1.50	1.10	1.44	1.79	1.41	1.47	1.45	1.28	1.09	1.16
Na2O	0.03	0.02	0.03	0.00	0.02	0.02	0.04	0.02	0.02	0.03	0.01	0.01	0.01
Total	100.31	100.46	100.02	100.69	100.53	100.03	99.38	101.26	99.84	99.43	99.52	99.77	99.48
cations (based on 6 oxygens):													
Si	1.9669	1.9737	1.9530	1.9565	1.9676	1.9686	1.9553	1.9645	1.9771	1.9635	1.9733	1.9700	1.9668
Ti	0.0040	0.0040	0.0023	0.0031	0.0043	0.0039	0.0030	0.0040	0.0032	0.0038	0.0037	0.0040	0.0040
Al	0.0505	0.0470	0.0665	0.0592	0.0462	0.0502	0.0551	0.0410	0.0442	0.0497	0.0518	0.0487	0.0460
Cr	0.0149	0.0146	0.0147	0.0083	0.0131	0.0164	0.0159	0.0105	0.0121	0.0140	0.0143	0.0142	0.0136
Fe	0.2922	0.3237	0.3046	0.3198	0.3141	0.3125	0.3298	0.3271	0.3347	0.3389	0.3383	0.3357	0.3405
Mn	0.0067	0.0055	0.0061	0.0073	0.0064	0.0069	0.0078	0.0066	0.0059	0.0062	0.0071	0.0073	0.0074
Ni	0.0019	0.0023	0.0002	0.0022	0.0014	0.0019	0.0019	0.0011	0.0015	0.0019	0.0011	0.0024	0.0022
Mg	1.5850	1.5524	1.5928	1.5937	1.6033	1.5785	1.5672	1.5971	1.5562	1.5662	1.5511	1.5703	1.5740
Ca	0.0734	0.0675	0.0629	0.0563	0.0412	0.0544	0.0687	0.0532	0.0560	0.0555	0.0489	0.0416	0.0444
Na	0.0071	0.0062	0.0073	0.0013	0.0067	0.0056	0.0115	0.0046	0.0051	0.0077	0.0038	0.0015	0.0040
Total	4.0026	3.9969	4.0105	4.0077	4.0043	3.9991	4.0162	4.0097	3.9960	4.0076	3.9933	3.9958	4.0030
n	5	5	5	6	5	4	4	5	5	5	5	7	3
Mg#	0.8443	0.8274	0.8395	0.8329	0.8362	0.8347	0.8261	0.8300	0.8230	0.8221	0.8210	0.8239	0.8221
en	81.3	79.9	81.3	80.9	81.9	81.1	79.7	80.8	79.9	79.9	80.0	80.6	80.4
wo	3.8	3.5	3.2	2.9	2.1	2.8	3.5	2.7	2.9	2.8	2.5	2.1	2.3
fs	15.0	16.7	15.5	16.2	16.0	16.1	16.8	16.5	17.2	17.3	17.5	17.2	17.4
standard deviation:													
wt.%													
SiO2	0.23	0.14	0.21	0.12	0.25	0.11	0.12	1.78	0.09	0.15	0.27	0.22	0.29
TiO2	0.03	0.02	0.02	0.02	0.05	0.02	0.02	0.02	0.01	0.03	0.02	0.03	0.05
Al2O3	0.10	0.10	0.12	0.06	0.15	0.07	0.06	0.07	0.03	0.10	0.26	0.23	0.13
Cr2O3	0.04	0.02	0.03	0.06	0.01	0.03	0.03	0.02	0.01	0.02	0.09	0.06	0.04
FeO	0.12	0.18	0.26	0.17	0.34	0.24	0.18	0.41	0.18	0.27	0.32	0.43	0.23
MnO	0.03	0.03	0.01	0.01	0.02	0.01	0.01	0.01	0.01	0.01	0.02	0.02	0.02
NiO	0.01	0.01	0.01	0.02	0.02	0.01	0.01	0.03	0.01	0.02	0.02	0.02	0.01
MgO	0.20	0.46	0.42	0.26	0.30	0.26	0.13	1.08	0.15	0.20	0.28	0.19	0.50
CaO	0.30	0.57	0.58	0.33	0.14	0.39	0.26	0.45	0.29	0.43	0.29	0.29	0.60
Na2O	0.01	0.01	0.01	0.01	0.01	0.01	0.01	0.00	0.00	0.01	0.01	0.01	0.02

Sample:	390.70	438.00	440.67	440.69	450.00	453.28	462.00	465.00	474.12	475.17	475.30	484.00
Habit:	cum	cum	cum	cum	cum	cum	cum	cum	cum	cum	cum	cum
wt.%												
SiO2	54.97	55.06	55.45	55.36	55.31	54.87	56.11	54.83	54.82	56.55	55.89	54.78
TiO2	0.14	0.16	0.12	0.15	0.15	0.13	0.12	0.15	0.12	0.13	0.12	0.16
Al2O3	0.90	1.09	1.46	1.10	1.04	1.08	1.09	1.04	1.15	1.08	1.08	1.03
Cr2O3	0.31	0.49	0.56	0.54	0.41	0.51	0.45	0.43	0.42	0.44	0.45	0.40
FeO	11.93	12.09	11.32	11.95	12.32	11.80	12.99	12.36	12.12	8.17	9.01	12.81
MnO	0.26	0.26	0.30	0.32	0.27	0.25	0.28	0.27	0.25	0.20	0.21	0.24
NiO	0.07	0.06	0.06	0.06	0.06	0.07	0.05	0.06	0.05	0.07	0.09	0.05
MgO	29.98	29.70	30.26	29.56	29.15	30.17	29.66	29.32	28.92	31.97	31.23	28.98
CaO	0.91	1.41	0.86	1.08	1.24	0.94	1.06	1.47	1.73	1.40	1.77	1.30
Na2O	0.02	0.01	0.02	0.03	0.02	0.01	0.01	0.02	0.03	0.03	0.04	0.01
Total	99.49	100.31	100.40	100.16	99.96	99.81	101.80	99.94	99.60	100.04	99.89	99.75
cations (based on 6 oxygens):												
Si	1.9618	1.9546	1.9557	1.9643	1.9689	1.9532	1.9650	1.9566	1.9613	1.9731	1.9647	1.9606
Ti	0.0038	0.0041	0.0031	0.0041	0.0041	0.0034	0.0031	0.0040	0.0031	0.0034	0.0031	0.0042
Al	0.0378	0.0455	0.0606	0.0460	0.0437	0.0454	0.0448	0.0437	0.0483	0.0446	0.0447	0.0435
Cr	0.0088	0.0137	0.0156	0.0152	0.0116	0.0144	0.0124	0.0121	0.0119	0.0122	0.0126	0.0113
Fe	0.3561	0.3590	0.3338	0.3546	0.3667	0.3511	0.3805	0.3688	0.3627	0.2382	0.2649	0.3836
Mn	0.0080	0.0078	0.0088	0.0097	0.0082	0.0076	0.0084	0.0082	0.0075	0.0059	0.0061	0.0073
Ni	0.0019	0.0017	0.0016	0.0018	0.0016	0.0019	0.0014	0.0018	0.0015	0.0018	0.0027	0.0013
Mg	1.5955	1.5714	1.5904	1.5634	1.5469	1.6005	1.5477	1.5596	1.5420	1.6627	1.6365	1.5459
Ca	0.0347	0.0535	0.0326	0.0409	0.0472	0.0357	0.0398	0.0562	0.0661	0.0524	0.0669	0.0497
Na	0.0056	0.0023	0.0059	0.0091	0.0042	0.0018	0.0018	0.0049	0.0092	0.0070	0.0025	0.0036
Total	4.0150	4.0136	4.0083	4.0090	4.0031	4.0150	4.0049	4.0158	4.0135	4.0012	4.0029	4.0110
n	5	5	4	3	4	4	5	5	4	5	4	4
Mg#	0.8175	0.8140	0.8265	0.8151	0.8084	0.8201	0.8027	0.8088	0.8096	0.8747	0.8607	0.8012
en	80.3	79.2	81.3	79.8	78.9	80.5	78.6	78.6	78.2	85.1	83.1	78.1
wo	1.7	2.7	1.7	2.1	2.4	1.8	2.0	2.8	3.4	2.7	3.4	2.5
fs	17.9	18.1	17.1	18.1	18.7	17.7	19.3	18.6	18.4	12.2	13.5	19.4
standard deviation:												
wt.%												
SiO2	0.16	0.16	0.30	0.26	0.11	0.10	1.85	0.10	0.11	0.18	0.26	0.27
TiO2	0.03	0.01	0.01	0.01	0.03	0.01	0.01	0.02	0.01	0.02	0.02	0.03
Al2O3	0.09	0.05	0.06	0.04	0.03	0.09	0.06	0.03	0.06	0.04	0.11	0.09
Cr2O3	0.03	0.03	0.02	0.03	0.02	0.04	0.02	0.04	0.03	0.02	0.03	0.05
FeO	0.13	0.20	0.25	0.09	0.15	0.15	0.39	0.33	0.33	0.49	0.28	0.21
MnO	0.03	0.02	0.02	0.01	0.02	0.01	0.03	0.01	0.02	0.01	0.01	0.02
NiO	0.02	0.01	0.02	0.01	0.00	0.02	0.02	0.01	0.01	0.02	0.02	0.01
MgO	0.17	0.20	0.20	0.06	0.49	0.25	1.14	0.25	0.20	0.21	0.43	0.42
CaO	0.26	0.20	0.19	0.21	0.44	0.31	0.28	0.42	0.49	0.15	0.59	0.53
Na2O	0.01	0.00	0.01	0.00	0.00	0.01	0.01	0.01	0.02	0.00	0.01	0.01

MICROPROBE DATA: Composition of chromite in the NG-sequence (NG3-borehole)

Sample:	151.85	151.90	152.25	152.60	152.90	153.15	154.72	154.74	155.30	155.85	156.10	156.12
Mode:	acc	ML	ML	ML	maj	acc	acc	ML	ML	ML	ML	maj
Depth in NG-sequence in m:	151.85	151.90	152.25	152.60	152.90	153.15	154.72	154.74	155.30	155.85	156.10	156.12
wt.%												
TiO2	1.00	0.79	0.74	0.74	1.06	1.16	1.10	0.78	0.80	0.88	0.87	0.82
Al2O3	12.25	18.13	18.47	17.95	14.06	10.33	13.06	18.10	18.43	17.94	17.22	16.19
Cr2O3	44.37	42.42	41.79	42.25	43.01	44.65	43.89	41.51	41.63	41.42	41.47	42.84
FeO(P)	34.99	27.60	26.33	27.81	32.51	34.97	33.24	28.78	27.44	27.82	29.23	29.17
FeO(C)	25.42	19.90	19.02	19.43	23.58	24.92	23.66	20.72	19.83	20.00	20.36	20.51
Fe2O3	10.64	8.56	8.12	9.31	9.92	11.17	10.65	8.96	8.46	8.69	9.85	9.61
MnO	0.38	0.29	0.28	0.29	0.30	0.38	0.32	0.26	0.29	0.28	0.29	0.29
NiO	0.10	0.13	0.13	0.13	0.14	0.14	0.15	0.11	0.13	0.11	0.12	0.14
MgO	5.78	9.98	10.28	10.26	7.07	5.65	7.06	9.38	9.90	9.72	9.51	9.27
Total(P)	98.87	99.34	98.02	99.45	98.15	97.28	98.83	98.92	98.62	98.16	98.72	98.71
Total(C)	99.94	100.20	98.84	100.38	99.14	98.40	99.89	99.82	99.47	99.03	99.70	99.68
cations (based on 32 oxygens):												
Ti	0.2038	0.1527	0.1436	0.1429	0.2146	0.2430	0.2215	0.1509	0.1549	0.1708	0.1694	0.1609
Al	3.9131	5.4663	5.6145	5.4006	4.4414	3.3777	4.1144	5.4991	5.5860	5.4773	5.2537	4.9685
Cr	9.5088	8.5810	8.5214	8.5250	9.1252	9.8023	9.2954	8.4617	8.4666	8.4860	8.4889	8.8252
Fe2+	5.7616	4.2578	4.1030	4.1481	5.2922	5.7877	5.3009	4.4665	4.2662	4.3334	4.4088	4.4693
Fe3+	2.1705	1.6473	1.5768	1.7886	2.0043	2.3339	2.1471	1.7375	1.6377	1.6952	1.9186	1.8846
Mn	0.0863	0.0621	0.0607	0.0635	0.0691	0.0893	0.0737	0.0578	0.0640	0.0620	0.0639	0.0642
Ni	0.0217	0.0276	0.0279	0.0277	0.0295	0.0310	0.0327	0.0237	0.0274	0.0225	0.0258	0.0295
Mg	2.3342	3.8052	3.9521	3.9035	2.8238	2.3351	2.8142	3.6028	3.7972	3.7528	3.6710	3.5979
n	4	6	5	8	5	5	4	6	6	6	4	4
Cr/Al	2.4300	1.5698	1.5177	1.5785	2.0546	2.9020	2.2593	1.5387	1.5157	1.5493	1.6158	1.7762
Mg#	0.2883	0.4719	0.4906	0.4848	0.3479	0.2875	0.3468	0.4465	0.4709	0.4641	0.4543	0.4460
FFE	0.2736	0.2790	0.2776	0.3013	0.2747	0.2874	0.2883	0.2801	0.2774	0.2812	0.3032	0.2966
Cr/(Cr+Al)	0.7085	0.6109	0.6028	0.6122	0.6726	0.7437	0.6932	0.6061	0.6025	0.6077	0.6177	0.6398
Cr/Fe	1.1162	1.3530	1.3969	1.3370	1.1648	1.1239	1.1624	1.2699	1.3352	1.3106	1.2492	1.2931
standard deviation:												
wt.%												
TiO2	0.14	0.03	0.03	0.03	0.23	0.06	0.13	0.05	0.08	0.01	0.03	0.08
Al2O3	2.12	0.23	0.08	0.22	1.49	0.79	1.53	0.25	0.24	0.19	0.38	0.78
Cr2O3	1.89	0.16	0.24	0.24	0.47	0.64	0.82	0.41	0.20	0.39	0.55	0.82
FeO(P)	0.66	0.07	0.23	0.20	1.16	0.88	1.48	0.40	0.37	0.46	0.51	0.30
FeO(C)	0.82	0.07	0.10	0.15	0.75	0.86	1.19	0.29	0.14	0.19	0.33	0.15
Fe2O3	0.86	0.12	0.18	0.19	0.55	0.25	0.41	0.31	0.33	0.59	0.23	0.16
MnO	0.03	0.02	0.02	0.02	0.02	0.02	0.03	0.01	0.03	0.01	0.02	0.01
NiO	0.08	0.02	0.02	0.02	0.01	0.03	0.01	0.01	0.01	0.02	0.01	0.02
MgO	1.19	0.09	0.06	0.10	0.52	0.67	0.87	0.19	0.07	0.10	0.18	0.09

Sample:	158.54	158.55	158.56	159.20	159.22	159.40	168.75	170.34	174.77	175.05	176.45	194.74
Mode:	acc	ML	acc	ML	acc	acc	acc	acc	maj	maj	acc	acc
Depth in NG-sequence in m:	158.54	158.55	158.56	159.20	159.22	159.40	168.75	170.34	174.77	175.05	176.45	194.74
wt.%												
TiO2	0.72	0.73	0.84	0.83	1.12	1.06	1.16	0.86	1.00	0.92	0.74	0.75
Al2O3	15.11	16.82	14.09	16.27	10.29	7.72	10.48	8.33	11.05	13.33	7.59	7.12
Cr2O3	44.01	42.75	44.10	42.46	44.45	45.32	41.62	45.47	43.21	43.21	46.16	44.70
FeO(P)	30.43	28.82	30.48	29.36	35.68	39.15	37.83	38.50	35.93	32.12	38.53	40.83
FeO(C)	21.81	20.80	22.00	21.04	25.27	26.66	25.30	26.15	23.93	22.52	25.88	27.00
Fe2O3	9.58	8.91	9.43	9.24	11.56	13.88	13.93	13.72	13.34	10.66	14.06	15.37
MnO	0.31	0.30	0.31	0.30	0.36	0.40	0.34	0.37	0.32	0.30	0.41	0.36
NiO	0.12	0.18	0.10	0.13	0.14	0.18	0.19	0.20	0.20	0.12	0.18	0.18
MgO	8.32	9.04	7.93	8.81	5.45	4.36	5.37	4.69	6.48	7.47	4.69	3.86
Total(P)	99.02	98.62	97.85	98.16	97.49	98.19	96.99	98.42	98.19	97.48	98.30	97.81
Total(C)	99.98	99.52	98.79	99.09	98.65	99.58	98.38	99.80	99.53	98.55	99.71	99.35
cations (based on 32 oxygens):												
Ti	0.1425	0.1423	0.1685	0.1630	0.2345	0.2241	0.2421	0.1799	0.2043	0.1870	0.1551	0.1607
Al	4.6791	5.1631	4.4403	5.0348	3.3524	2.5551	3.4365	2.7373	3.5461	4.2378	2.5057	2.3796
Cr	9.1425	8.8055	9.3246	8.8135	9.7584	10.0632	9.1603	10.0238	9.3100	9.2214	10.2211	10.0197
Fe2+	4.7920	4.5310	4.9194	4.6197	5.8744	6.2633	5.8902	6.0983	5.4548	5.0852	6.0629	6.4004
Fe3+	1.8933	1.7467	1.8980	1.8257	2.4201	2.9335	2.9190	2.8792	2.7353	2.1668	2.9630	3.2794
Mn	0.0683	0.0661	0.0697	0.0668	0.0842	0.0951	0.0798	0.0877	0.0746	0.0692	0.0972	0.0860
Ni	0.0243	0.0371	0.0205	0.0283	0.0308	0.0411	0.0429	0.0452	0.0438	0.0268	0.0399	0.0413
Mg	3.2579	3.5081	3.1589	3.4482	2.2451	1.8245	2.2292	1.9487	2.6311	3.0058	1.9551	1.6330
n	5	5	5	6	3	4	5	5	5	5	3	9
Cr/Al	1.9539	1.7055	2.1000	1.7505	2.9109	3.9385	2.6656	3.6619	2.6254	2.1760	4.0791	4.2107
Mg#	0.4047	0.4364	0.3910	0.4274	0.2765	0.2256	0.2746	0.2422	0.3254	0.3715	0.2438	0.2033
FFE	0.2832	0.2782	0.2784	0.2833	0.2918	0.3190	0.3314	0.3207	0.3340	0.2988	0.3283	0.3388
Cr/(Cr+Al)	0.6615	0.6304	0.6774	0.6364	0.7443	0.7975	0.7272	0.7855	0.7242	0.6851	0.8031	0.8081
Cr/Fe	1.2734	1.3060	1.2736	1.2732	1.0967	1.0189	0.9684	1.0396	1.0586	1.1842	1.0547	0.9639
standard deviation:												
wt.%												
TiO2	0.17	0.04	0.12	0.06	0.01	0.18	0.08	0.08	0.05	0.05	0.05	0.07
Al2O3	0.50	0.34	0.67	0.25	1.91	0.59	0.45	0.10	0.78	0.64	0.30	0.55
Cr2O3	0.17	0.23	0.15	0.31	0.37	0.62	0.42	0.17	0.30	0.37	0.41	0.50
FeO(P)	0.70	0.30	0.75	0.25	2.22	0.91	1.06	0.30	1.03	0.42	0.91	0.60
FeO(C)	0.33	0.16	0.37	0.13	1.36	0.40	0.50	0.17	0.67	0.19	0.64	0.24
Fe2O3	0.52	0.17	0.56	0.20	0.96	0.83	0.64	0.28	0.48	0.30	0.30	0.78
MnO	0.01	0.02	0.02	0.01	0.03	0.02	0.02	0.02	0.03	0.03	0.00	0.02
NiO	0.05	0.00	0.02	0.01	0.02	0.03	0.03	0.02	0.02	0.02	0.01	0.02
MgO	0.16	0.10	0.28	0.12	1.21	0.22	0.38	0.15	0.49	0.33	0.50	0.14

Sample:	208.15	211.45	212.20	212.30	214.05	214.25	219.22	219.32	219.34	219.42	219.65	221.70
Mode:	acc	ML	ML	ML	acc	acc	acc	acc	ML	ML	ML	acc
Depth in NG-sequence in m:	208.15	211.45	212.20	212.30	214.05	214.25	219.22	219.32	219.34	219.42	219.65	221.70
wt.%												
TiO2	0.55	0.68	0.67	0.72	0.89	0.93	1.27	0.80	1.22	0.78	0.80	1.16
Al2O3	8.40	18.63	18.56	17.43	8.91	9.24	9.43	16.86	10.40	17.67	17.28	8.14
Cr2O3	46.20	40.47	41.52	41.70	44.45	44.35	43.05	42.49	42.89	41.83	41.42	43.89
FeO(P)	37.69	27.15	27.85	28.14	38.50	38.34	38.13	27.29	36.91	27.89	27.06	40.35
FeO(C)	26.47	18.89	19.43	19.19	25.91	25.77	25.57	18.99	24.70	18.79	18.43	27.01
Fe2O3	12.47	9.17	9.36	9.95	14.00	13.97	13.96	9.23	13.57	10.11	9.59	14.83
MnO	0.38	0.28	0.28	0.26	0.38	0.34	0.32	0.24	0.35	0.26	0.31	0.37
NiO	0.20	0.11	0.16	0.13	0.21	0.18	0.17	0.12	0.15	0.14	0.16	0.19
MgO	4.10	10.28	10.24	10.21	4.88	5.13	5.33	10.22	6.00	10.65	10.44	4.30
Total(P)	97.52	97.59	99.28	98.60	98.21	98.52	97.69	98.03	97.92	99.22	97.46	98.40
Total(C)	98.76	98.51	100.21	99.59	99.61	99.92	99.09	98.96	99.28	100.24	98.42	99.89
cations (based on 32 oxygens):												
Ti	0.1159	0.1314	0.1285	0.1400	0.1857	0.1942	0.2652	0.1570	0.2520	0.1493	0.1571	0.2443
Al	2.7971	5.6775	5.5767	5.2951	2.9210	3.0091	3.0883	5.1598	3.3673	5.3162	5.2948	2.6836
Cr	10.3202	8.2744	8.3703	8.4959	9.7763	9.6951	9.4606	8.7230	9.3179	8.4425	8.5153	9.7061
Fe2+	6.2547	4.0857	4.1437	4.1349	6.0285	5.9580	5.9438	4.1228	5.6832	4.0104	4.0086	6.3197
Fe3+	2.6510	1.7853	1.7959	1.9289	2.9313	2.9075	2.9207	1.8033	2.8107	1.9428	1.8758	3.1217
Mn	0.0921	0.0620	0.0606	0.0571	0.0884	0.0806	0.0751	0.0532	0.0808	0.0569	0.0674	0.0870
Ni	0.0443	0.0230	0.0332	0.0275	0.0468	0.0410	0.0389	0.0257	0.0341	0.0287	0.0328	0.0433
Mg	1.7247	3.9608	3.8910	3.9205	2.0219	2.1146	2.2074	3.9553	2.4539	4.0533	4.0482	1.7943
n	4	8	5	5	3	4	5	6	4	8	9	4
Cr/Al	3.6897	1.4574	1.5009	1.6045	3.3469	3.2219	3.0634	1.6906	2.7671	1.5881	1.6082	3.6168
Mg#	0.2161	0.4922	0.4843	0.4867	0.2512	0.2619	0.2708	0.4896	0.3016	0.5027	0.5025	0.2211
FFE	0.2977	0.3041	0.3024	0.3181	0.3272	0.3280	0.3295	0.3043	0.3309	0.3263	0.3188	0.3306
Cr/ (Cr+Al)	0.7868	0.5931	0.6002	0.6160	0.7700	0.7631	0.7539	0.6283	0.7345	0.6136	0.6166	0.7834
Cr/Fe	1.0790	1.3123	1.3122	1.3046	1.0162	1.0184	0.9938	1.3705	1.0230	1.3204	1.3474	0.9573
standard deviation:												
wt.%												
TiO2	0.09	0.04	0.06	0.02	0.16	0.04	0.08	0.05	0.14	0.05	0.03	0.13
Al2O3	0.52	0.30	0.13	0.15	0.48	0.41	0.50	0.61	0.85	0.08	0.17	0.28
Cr2O3	0.31	0.50	0.24	0.20	0.90	0.79	0.58	1.09	2.02	0.32	0.28	1.15
FeO(P)	0.78	0.51	0.28	0.16	1.33	0.70	0.57	0.52	3.66	0.22	0.39	0.65
FeO(C)	0.53	0.27	0.17	0.07	1.05	0.31	0.21	0.48	1.96	0.11	0.19	0.27
Fe2O3	0.38	0.34	0.20	0.11	0.57	0.92	0.44	0.29	1.98	0.17	0.26	0.97
MnO	0.02	0.02	0.01	0.01	0.01	0.03	0.03	0.02	0.04	0.01	0.02	0.04
NiO	0.02	0.02	0.02	0.02	0.04	0.02	0.02	0.02	0.03	0.03	0.01	0.03
MgO	0.39	0.11	0.09	0.08	0.59	0.25	0.21	0.20	1.27	0.08	0.08	0.25

Sample:	232.00	255.30	260.05
Mode:	acc	acc	acc
Depth in NG-sequence in m:	232.00	255.30	260.05
wt.%			
TiO2	0.78	0.72	1.25
Al2O3	8.37	10.56	10.25
Cr2O3	43.94	42.39	41.65
FeO(P)	40.55	37.67	39.78
FeO(C)	27.03	25.04	26.11
Fe2O3	15.03	14.04	15.19
MnO	0.34	0.32	0.36
NiO	0.13	0.22	0.13
MgO	4.12	5.34	5.27
Total(P)	98.24	97.22	98.70
Total(C)	99.75	98.63	100.22
cations (based on 32 oxygens):			
Ti	0.1649	0.1497	0.2574
Al	2.7648	3.4572	3.3131
Cr	9.7361	9.3082	9.0331
Fe2+	6.3339	5.8148	5.9912
Fe3+	3.1694	2.9352	3.1391
Mn	0.0812	0.0760	0.0842
Ni	0.0286	0.0496	0.0295
Mg	1.7212	2.2093	2.1525
n	4	6	5
Cr/Al	3.5215	2.6924	2.7265
Mg#	0.2137	0.2753	0.2643
FFE	0.3335	0.3355	0.3438
Cr/ (Cr+Al)	0.7788	0.7292	0.7317
Cr/Fe	0.9537	0.9906	0.9217
standard deviation:			
wt.%			
TiO2	0.14	0.21	0.17
Al2O3	0.74	0.79	0.71
Cr2O3	1.91	1.91	1.03
FeO(P)	0.79	0.76	1.62
FeO(C)	0.25	1.07	0.58
Fe2O3	1.11	0.98	1.23
MnO	0.03	0.03	0.03
NiO	0.02	0.03	0.03
MgO	0.23	0.61	0.53

MICROPROBE DATA: Composition of chromite in the NG-sequence (NG1-borehole)

Sample:	17.00	25.00	29.80	46.25	56.00	65.19	74.45	79.75	84.90	89.55	90.33	94.60
Mode:	acc	acc	acc	acc	acc	acc	acc	acc	maj	acc	ML	acc
Depth in NG-sequence in m:	267.00	275.00	279.80	296.25	306.00	315.19	324.45	329.75	334.90	339.55	340.33	344.60
wt.%												
TiO2	0.62	1.06	0.73	0.64	0.71	1.24	0.90	0.54	0.99	0.88	0.74	0.88
Al2O3	8.37	7.79	9.71	8.73	6.50	10.22	10.02	7.31	13.93	11.73	17.69	9.95
Cr2O3	42.05	42.97	46.06	44.28	45.06	41.39	44.48	44.54	42.61	43.97	40.72	43.67
FeO(P)	43.90	41.39	36.73	38.67	40.87	38.76	37.17	41.04	32.15	36.45	28.68	37.74
FeO(C)	28.39	29.64	26.02	28.75	29.16	25.10	25.95	27.97	22.16	25.26	18.43	25.93
Fe2O3	17.20	13.05	11.90	11.03	13.02	15.19	12.47	14.52	11.10	12.44	11.39	13.12
MnO	0.41	0.37	0.37	0.40	0.39	0.33	0.37	0.39	0.32	0.36	0.26	0.36
NiO	0.00	0.16	0.13	0.18	0.18	0.17	0.17	0.16	0.15	0.17	0.14	0.17
MgO	3.25	3.26	4.91	3.69	3.11	5.74	4.96	2.91	7.92	5.86	10.85	5.08
Total(P)	98.59	97.00	98.64	96.59	96.81	97.85	98.07	96.89	98.07	99.42	99.08	97.85
Total(C)	100.29	98.31	99.84	97.70	98.11	99.37	99.32	98.35	99.18	100.66	100.22	99.17
cations (based on 32 oxygens):												
Ti	0.1294	0.2340	0.1510	0.1417	0.1570	0.2570	0.1878	0.1171	0.1993	0.1789	0.1415	0.1828
Al	2.7658	2.6922	3.1585	3.0147	2.2565	3.3188	3.2732	2.4800	4.3821	3.7269	5.3184	3.2396
Cr	9.3365	9.9607	10.0642	10.2668	10.5298	9.0195	9.7498	10.1405	8.9904	9.3858	8.2130	9.6360
Fe2+	6.6756	7.2669	6.0136	7.0512	7.2098	5.7836	6.0158	6.7372	4.9455	5.7051	3.9317	6.0662
Fe3+	3.6390	2.8791	2.4753	2.4351	2.8996	3.1478	2.6013	3.1453	2.2290	2.5295	2.1856	2.7587
Mn	0.0977	0.0878	0.0866	0.0947	0.0933	0.0764	0.0873	0.0958	0.0722	0.0816	0.0567	0.0844
Ni	0.0000	0.0700	0.0294	0.0793	0.0774	0.0378	0.0374	0.0379	0.0323	0.0360	0.0284	0.0431
Mg	1.3561	0.8093	2.0215	0.9165	0.7765	2.3591	2.3432	1.2461	3.1066	2.3174	4.1247	2.0248
n	13	8	8	5	9	7	6	4	15	6	6	6
Cr/Al	3.3757	3.6998	3.1864	3.4055	4.6663	2.7177	2.9787	4.0889	2.0516	2.5184	1.5443	2.9744
Mg#	0.1688	0.1002	0.2516	0.1150	0.0972	0.2897	0.2803	0.1561	0.3858	0.2889	0.5120	0.2503
FFE	0.3528	0.2838	0.2916	0.2567	0.2868	0.3524	0.3019	0.3183	0.3107	0.3072	0.3573	0.3126
Cr/(Cr+Al)	0.7715	0.7872	0.7611	0.7730	0.8235	0.7310	0.7487	0.8035	0.6723	0.7158	0.6070	0.7484
Cr/Fe	0.8432	0.9139	1.1039	1.0079	0.9704	0.9399	1.0534	0.9555	1.1669	1.0617	1.2501	1.0187
standard deviation:												
wt.%												
TiO2	0.23	0.15	0.18	0.11	0.23	0.04	0.18	0.24	0.13	0.23	0.03	0.22
Al2O3	0.67	0.51	1.50	1.02	1.69	0.11	0.64	0.25	0.16	1.60	0.31	2.52
Cr2O3	1.22	1.11	1.61	0.67	1.24	0.26	1.10	1.96	0.59	1.10	0.72	1.27
FeO(P)	1.92	2.03	1.24	1.19	2.34	1.24	0.43	2.16	0.45	1.49	0.28	3.03
FeO(C)	0.87	0.44	0.69	0.22	0.40	0.35	0.55	0.43	0.43	0.79	0.30	2.24
Fe2O3	1.39	1.86	0.90	1.20	2.22	1.04	0.44	2.19	0.28	1.22	0.42	1.37
MnO	0.05	0.04	0.03	0.03	0.03	0.01	0.02	0.04	0.03	0.02	0.01	0.03
NiO	0.00	0.03	0.03	0.04	0.03	0.03	0.01	0.05	0.03	0.02	0.03	0.01
MgO	0.83	0.26	0.52	0.29	0.56	0.19	0.50	0.47	0.37	0.56	0.14	1.72

Sample:	119.90	152.20	158.20	163.27	173.37	183.70	191.00	197.50	225.90	233.60	242.15	242.40
Mode:	acc	ML	acc	acc	acc	acc	acc	acc	acc	acc	maj	ML
Depth in NG-sequence in m:	369.90	402.20	408.20	413.27	423.37	433.70	441.00	447.50	475.90	483.60	492.15	492.40
wt.%												
TiO2	1.01	0.71	0.71	0.76	0.70	1.00	0.31	0.54	0.75	0.18	0.70	0.54
Al2O3	9.11	15.39	10.54	7.97	10.08	8.38	8.02	10.47	9.22	6.07	10.20	14.13
Cr2O3	46.15	43.32	45.42	47.11	48.04	48.54	47.55	46.97	47.64	47.49	47.82	47.38
FeO(P)	38.34	30.33	35.77	39.41	32.92	35.71	37.02	34.89	34.03	41.80	33.39	26.41
FeO(C)	27.19	21.61	25.89	28.16	23.86	26.05	26.54	25.61	24.69	28.48	24.90	19.24
Fe2O3	12.39	9.69	10.98	12.51	10.07	10.74	11.65	10.32	10.37	14.80	9.44	7.97
MnO	0.37	0.30	0.37	0.40	0.35	0.34	0.37	0.30	0.34	0.46	0.36	0.27
NiO	0.16	0.14	0.13	0.11	0.13	0.11	0.09	0.13	0.16	0.05	0.07	0.10
MgO	4.43	8.36	4.89	3.49	6.32	5.03	3.88	5.14	5.52	2.65	5.59	9.70
Total(P)	99.56	98.56	97.83	99.25	98.55	99.10	97.25	98.43	97.65	98.70	98.15	98.53
Total(C)	100.80	99.53	98.93	100.50	99.56	100.18	98.41	99.47	98.69	100.19	99.09	99.32
cations (based on 32 oxygens):												
Ti	0.2088	0.1401	0.1475	0.1603	0.1453	0.2070	0.0663	0.1120	0.1576	0.0390	0.1458	0.1057
Al	2.9541	4.7781	3.4415	2.6266	3.2361	2.7305	2.6835	3.3981	3.0188	2.0395	3.3179	4.3755
Cr	10.0602	9.0218	9.9692	10.4203	10.3993	10.6194	10.6897	10.2362	10.4913	10.7055	10.4321	9.8384
Fe2+	6.2688	4.7623	6.0134	6.5881	5.4691	6.0316	6.3108	5.9025	5.7538	6.7938	5.7442	4.2264
Fe3+	2.5681	1.9199	2.2944	2.6326	2.0741	2.2360	2.4942	2.1418	2.1748	3.1769	1.9584	1.5747
Mn	0.0863	0.0677	0.0865	0.0947	0.0823	0.0804	0.0889	0.0700	0.0806	0.1118	0.0847	0.0603
Ni	0.0345	0.0291	0.0282	0.0244	0.0291	0.0238	0.0214	0.0287	0.0348	0.0112	0.0162	0.0212
Mg	1.8193	3.2674	2.0194	1.4532	2.5647	2.0713	1.6452	2.1108	2.2884	1.1223	2.3006	3.7979
n	6	37	6	2	7	6	10	5	5	8	6	5
Cr/Al	3.4055	1.8882	2.8968	3.9672	3.2135	3.8892	3.9834	3.0124	3.4753	5.2490	3.1442	2.2485
Mg#	0.2249	0.4069	0.2514	0.1807	0.3192	0.2556	0.2068	0.2634	0.2845	0.1418	0.2860	0.4733
FFE	0.2906	0.2873	0.2762	0.2855	0.2750	0.2705	0.2833	0.2662	0.2743	0.3186	0.2543	0.2714
Cr/(Cr+Al)	0.7730	0.6538	0.7434	0.7987	0.7627	0.7955	0.7993	0.7508	0.7766	0.8400	0.7587	0.6922
Cr/Fe	1.0596	1.2574	1.1177	1.0522	1.2847	1.1963	1.1307	1.1849	1.2323	1.0000	1.2608	1.5792
standard deviation:												
wt.%												
TiO2	0.21	0.10	0.16	0.47	0.13	0.05	0.22	0.27	0.10	0.17	0.04	0.03
Al2O3	1.18	0.58	1.94	0.25	2.08	0.48	0.99	1.71	1.37	0.58	0.57	0.15
Cr2O3	1.89	0.83	1.69	1.18	1.26	0.30	0.92	0.68	0.65	0.46	0.54	0.44
FeO(P)	1.05	1.66	2.42	0.24	1.99	1.46	1.97	0.67	1.08	1.15	0.81	0.36
FeO(C)	0.48	0.97	2.07	0.37	1.71	1.11	1.34	0.42	0.63	0.88	0.35	0.14
Fe2O3	1.13	1.03	0.80	0.14	0.56	0.49	0.87	1.11	0.59	0.40	0.84	0.29
MnO	0.02	0.03	0.04	0.03	0.03	0.03	0.04	0.02	0.03	0.03	0.02	0.01
NiO	0.03	0.03	0.02	0.04	0.02	0.02	0.04	0.03	0.02	0.03	0.03	0.01
MgO	0.47	0.72	1.31	0.50	1.35	0.80	0.81	0.17	0.66	0.64	0.18	0.10

Sample:	242.45	245.40	250.15	255.82	255.95	256.70	257.10	257.70	262.17	277.25	292.30	302.00
Mode:	ML	ML	acc	maj	ML	ML	ML	acc	maj	acc	acc	acc
Depth in NG-sequence in m:	492.45	495.40	500.15	505.82	505.95	506.70	507.10	507.70	512.17	527.25	542.30	552.00
wt.%												
TiO2	0.58	0.49	0.49	0.61	0.58	0.60	0.79	0.91	0.96	0.62	0.68	0.78
Al2O3	13.63	14.20	12.21	11.63	13.12	12.88	11.57	7.48	8.34	8.86	8.82	8.11
Cr2O3	47.27	46.95	49.12	47.89	48.11	47.83	48.01	47.12	46.70	48.13	49.33	49.68
FeO(P)	27.01	26.18	30.63	30.48	26.93	27.05	29.85	38.94	35.94	35.39	34.30	33.62
FeO(C)	19.53	18.80	24.62	21.71	19.21	18.94	21.54	27.52	25.64	26.00	25.19	24.96
Fe2O3	8.32	8.20	6.67	9.74	8.58	9.02	9.23	12.69	11.44	10.43	10.13	9.62
MnO	0.31	0.27	0.34	0.34	0.25	0.26	0.32	0.41	0.37	0.35	0.35	0.36
NiO	0.10	0.13	0.09	0.13	0.10	0.14	0.12	0.10	0.12	0.10	0.13	0.11
MgO	9.43	9.86	5.98	7.93	9.73	9.81	8.10	3.85	4.88	4.68	5.41	5.32
Total(P)	98.33	98.07	98.85	98.99	98.82	98.57	98.75	98.81	97.32	98.12	99.03	97.97
Total(C)	99.17	98.89	99.52	99.97	99.68	99.48	99.68	100.08	98.47	99.17	100.05	98.93
cations (based on 32 oxygens):												
Ti	0.1156	0.0973	0.1006	0.1218	0.1153	0.1180	0.1591	0.1925	0.2027	0.1295	0.1414	0.1630
Al	4.2416	4.4058	3.9027	3.6645	4.0669	4.0031	3.6473	2.4728	2.7624	2.9131	2.8638	2.6712
Cr	9.8733	9.7754	10.5342	10.1299	10.0047	9.9717	10.1709	10.4603	10.4028	10.6337	10.7524	10.9793
Fe2+	4.3142	4.1403	5.5860	4.8576	4.2256	4.1754	4.8323	6.4623	6.0487	6.0770	5.8068	5.8351
Fe3+	1.6538	1.6242	1.3619	1.9619	1.6977	1.7892	1.8635	2.6818	2.4295	2.1943	2.1009	2.0235
Mn	0.0696	0.0600	0.0788	0.0774	0.0546	0.0590	0.0727	0.0974	0.0890	0.0827	0.0828	0.0852
Ni	0.0214	0.0269	0.0189	0.0275	0.0220	0.0296	0.0255	0.0234	0.0264	0.0232	0.0298	0.0250
Mg	3.7103	3.8701	2.4169	3.1593	3.8132	3.8539	3.2287	1.6094	2.0387	1.9465	2.2221	2.2177
n	5	7	5	6	6	6	8	12	6	6	6	6
Cr/Al	2.3277	2.2188	2.6992	2.7643	2.4601	2.4910	2.7886	4.2301	3.7659	3.6503	3.7545	4.1103
Mg#	0.4624	0.4831	0.3020	0.3941	0.4744	0.4800	0.4005	0.1994	0.2521	0.2426	0.2768	0.2754
FFE	0.2771	0.2818	0.1960	0.2877	0.2866	0.3000	0.2783	0.2933	0.2866	0.2653	0.2657	0.2575
Cr/(Cr+Al)	0.6995	0.6893	0.7297	0.7343	0.7110	0.7135	0.7360	0.8088	0.7902	0.7850	0.7897	0.8043
Cr/Fe	1.5404	1.5790	1.4117	1.3833	1.5727	1.5566	1.4157	1.0653	1.1440	1.1970	1.2661	1.3008
standard deviation:												
wt.%												
TiO2	0.01	0.03		0.05	0.03	0.01	0.19	0.15	0.30	0.08	0.14	0.14
Al2O3	0.69	0.10		0.78	0.16	0.09	1.70	0.53	1.11	1.28	0.71	0.26
Cr2O3	0.74	0.28		0.46	0.23	0.16	0.62	0.44	0.65	0.85	0.81	0.50
FeO(P)	0.50	0.14		0.99	0.15	0.15	2.83	1.25	1.61	1.02	0.47	1.01
FeO(C)	0.41	0.12		0.80	0.14	0.04	1.98	0.88	0.98	0.55	0.30	0.50
Fe2O3	0.25	0.18		0.30	0.06	0.15	1.01	0.62	0.88	0.55	0.32	0.68
MnO	0.02	0.02		0.02	0.02	0.01	0.03	0.03	0.03	0.02	0.02	0.01
NiO	0.02	0.02		0.02	0.02	0.02	0.01	0.04	0.02	0.03	0.03	0.02
MgO	0.33	0.06		0.55	0.05	0.06	1.28	0.58	1.15	0.44	0.30	0.28

Sample:	312.10	327.45	331.35	331.36	331.55	331.65	331.66	331.80	331.81	331.85	332.20	334.30
Mode:	acc	acc	acc	ML	ML	ML	acc	ML	maj	ML	ML	acc
Depth in NG-sequence in m:	562.10	577.45	581.35	581.36	581.55	581.65	581.66	581.80	581.81	581.85	582.20	584.30
wt.%												
TiO2	0.73	0.65	0.73	0.57	0.56	0.55	0.58	0.48	0.59	0.53	0.55	0.69
Al2O3	8.54	9.33	10.00	13.96	13.48	13.04	10.11	13.26	9.66	11.95	14.02	7.96
Cr2O3	49.69	48.86	49.96	49.27	49.40	50.25	50.14	50.19	50.90	48.96	48.88	50.72
FeO(P)	32.73	33.82	30.95	24.82	24.40	25.09	30.96	23.39	29.69	28.21	24.50	33.47
FeO(C)	24.80	25.45	22.69	17.71	17.78	18.02	22.88	17.82	23.14	20.36	17.67	25.38
Fe2O3	8.81	9.31	9.18	7.90	7.36	7.87	8.98	6.19	7.27	8.72	7.60	8.99
MnO	0.35	0.38	0.39	0.28	0.24	0.28	0.38	0.31	0.38	0.29	0.27	0.37
NiO	0.11	0.15	0.21	0.15	0.12	0.12	0.13	0.12	0.14	0.10	0.05	0.11
MgO	5.34	5.08	7.20	10.98	10.68	10.69	7.02	10.37	6.48	8.80	10.88	5.05
Total(P)	97.50	98.27	99.44	100.04	98.89	100.03	99.32	98.12	97.84	98.84	99.15	98.39
Total(C)	98.39	99.21	100.36	100.83	99.63	100.82	100.22	98.74	98.57	99.71	99.91	99.29
cations (based on 32 oxygens):												
Ti	0.1539	0.1370	0.1487	0.1099	0.1107	0.1072	0.1178	0.0960	0.1225	0.1056	0.1065	0.1446
Al	2.8212	3.0496	3.1809	4.2326	4.1438	3.9760	3.2220	4.1202	3.1422	3.7427	4.2840	2.6203
Cr	11.0130	10.7312	10.6580	10.0180	10.1893	10.2784	10.7157	10.4590	11.1036	10.2990	10.0209	11.2006
Fe2+	5.8131	5.9118	5.1198	3.8089	3.8779	3.8979	5.1730	3.9277	5.3399	4.5340	3.8309	5.9272
Fe3+	1.8578	1.9452	1.8638	1.5295	1.4456	1.5311	1.8267	1.2287	1.5092	1.7473	1.4821	1.8899
Mn	0.0833	0.0888	0.0896	0.0619	0.0539	0.0622	0.0875	0.0683	0.0881	0.0659	0.0602	0.0879
Ni	0.0253	0.0342	0.0448	0.0309	0.0256	0.0249	0.0281	0.0256	0.0302	0.0206	0.0096	0.0256
Mg	2.2323	2.1021	2.8945	4.2082	4.1532	4.1221	2.8292	4.0745	2.6643	3.4850	4.2058	2.1038
n	6	6	1	5	6	3	2	4	2	5	4	6
Cr/Al	3.9036	3.5189	3.3507	2.3669	2.4589	2.5851	3.3258	2.5385	3.5337	2.7518	2.3392	4.2745
Mg#	0.2775	0.2623	0.3612	0.5249	0.5171	0.5140	0.3536	0.5092	0.3329	0.4346	0.5233	0.2620
FFE	0.2422	0.2476	0.2669	0.2865	0.2716	0.2820	0.2610	0.2383	0.2204	0.2782	0.2790	0.2418
Cr/(Cr+Al)	0.7961	0.7787	0.7702	0.7030	0.7109	0.7211	0.7688	0.7174	0.7794	0.7335	0.7005	0.8104
Cr/Fe	1.3366	1.2715	1.4210	1.7473	1.7821	1.7628	1.4255	1.8886	1.5095	1.5275	1.7562	1.3339
standard deviation:												
wt.%												
TiO2	0.09	0.08		0.05	0.04	0.01	0.10	0.03	0.08	0.03	0.03	0.08
Al2O3	0.59	1.01		0.10	0.10	0.14	0.05	0.10	0.02	1.18	0.11	0.30
Cr2O3	0.66	0.84		0.32	0.15	0.19	0.43	0.18	0.02	0.52	0.22	0.61
FeO(P)	0.64	0.73		0.11	0.13	0.12	0.08	0.22	0.13	1.46	0.09	1.28
FeO(C)	0.27	0.33		0.09	0.10	0.09	0.15	0.11	0.09	1.21	0.14	0.75
Fe2O3	0.56	0.66		0.16	0.15	0.18	0.08	0.14	0.05	0.41	0.11	0.67
MnO	0.02	0.01		0.01	0.02	0.02	0.02	0.03	0.02	0.03	0.02	0.02
NiO	0.01	0.02		0.01	0.02	0.01	0.01	0.01	0.00	0.01	0.03	0.02
MgO	0.16	0.36		0.09	0.05	0.05	0.14	0.07	0.10	0.95	0.04	0.39

Sample:	338.45	380.35	406.40	414.85	421.00	429.55	429.91	433.61	455.65	459.70	469.40	469.45
Mode:	acc	acc	acc	acc	acc	ML	ML	maj	acc	acc	acc	acc
Depth in NG-sequence in m:	588.45	630.35	656.40	664.85	671.00	679.55	679.91	683.61	705.65	709.70	719.40	719.45
wt.%												
TiO2	0.58	0.48	0.41	0.50	0.32	0.39	0.37	0.50	0.52	0.42	0.22	0.50
Al2O3	8.20	7.96	11.30	9.48	4.89	13.58	14.14	14.95	8.36	9.07	8.35	8.35
Cr2O3	50.21	51.86	50.42	50.95	51.70	51.70	48.91	47.89	51.56	50.38	50.74	51.73
FeO(P)	34.27	32.69	29.93	30.74	38.09	21.27	23.58	25.23	32.44	33.23	33.34	32.36
FeO(C)	25.65	25.33	23.10	23.68	27.82	15.76	17.19	18.96	24.99	25.18	24.80	24.87
Fe2O3	9.58	8.18	7.60	7.84	11.42	6.13	7.10	6.97	8.29	8.95	9.50	8.32
MnO	0.36	0.39	0.35	0.36	0.42	0.31	0.29	0.30	0.38	0.41	0.40	0.36
NiO	0.12	0.07	0.09	0.11	0.03	0.06	0.09	0.10	0.10	0.07	0.08	0.06
MgO	4.90	4.98	6.96	6.19	2.98	11.97	10.87	10.01	5.30	5.23	5.19	5.44
Total(P)	98.64	98.42	99.47	98.34	98.44	99.28	98.24	98.98	98.67	98.81	98.33	98.79
Total(C)	99.60	99.24	100.23	99.12	99.58	99.90	98.95	99.68	99.50	99.70	99.28	99.63
cations (based on 32 oxygens):												
Ti	0.1225	0.1015	0.0824	0.1034	0.0688	0.0751	0.0726	0.0987	0.1088	0.0866	0.0455	0.1041
Al	2.6902	2.6194	3.5798	3.0744	1.6548	4.1266	4.3535	4.5836	2.7341	2.9513	2.7379	2.7239
Cr	11.0564	11.4575	10.7177	11.0943	11.7407	10.5347	10.1052	9.8548	11.3173	11.0137	11.1782	11.3323
Fe2+	5.9758	5.9215	5.1931	5.4552	6.6819	3.3967	3.7570	4.1271	5.8013	5.8230	5.7780	5.7609
Fe3+	2.0084	1.7201	1.5378	1.6245	2.4668	1.1884	1.3961	1.3642	1.7309	1.8618	1.9929	1.7357
Mn	0.0851	0.0918	0.0805	0.0849	0.1030	0.0678	0.0639	0.0662	0.0901	0.0957	0.0952	0.0839
Ni	0.0259	0.0150	0.0189	0.0249	0.0062	0.0131	0.0189	0.0209	0.0226	0.0148	0.0173	0.0136
Mg	2.0356	2.0733	2.7898	2.5383	1.2777	4.5975	4.2328	3.8845	2.1948	2.1531	2.1549	2.2456
n	7	6	5	8	3	6	4	8	5	7	8	5
Cr/Al	4.1099	4.3741	2.9940	3.6087	7.0949	2.5529	2.3212	2.1500	4.1393	3.7319	4.0828	4.1603
Mg#	0.2541	0.2593	0.3495	0.3175	0.1605	0.5751	0.5298	0.4849	0.2745	0.2699	0.2716	0.2805
FFE	0.2515	0.2251	0.2285	0.2295	0.2696	0.2592	0.2709	0.2484	0.2298	0.2423	0.2565	0.2315
Cr/ (Cr+Al)	0.8043	0.8139	0.7496	0.7830	0.8765	0.7185	0.6989	0.6825	0.8054	0.7887	0.8033	0.8062
Cr/Fe	1.2894	1.3963	1.4826	1.4592	1.1948	2.1393	1.8260	1.6709	1.3990	1.3348	1.3396	1.4074
standard deviation:												
wt.%												
TiO2	0.14	0.18	0.11	0.12	0.02	0.03	0.01	0.05	0.11	0.25	0.15	0.21
Al2O3	0.66	0.77	0.65	1.07	0.11	0.13	0.20	0.67	0.27	1.23	1.36	1.23
Cr2O3	0.48	0.92	0.57	0.88	0.28	0.27	0.44	0.91	0.55	1.30	0.87	1.41
FeO(P)	0.87	1.25	0.32	1.03	0.86	0.23	0.35	0.17	0.59	1.34	1.17	0.44
FeO(C)	0.29	0.85	0.40	0.88	0.25	0.30	0.30	0.25	0.24	0.95	0.59	0.51
Fe2O3	0.72	0.66	0.33	0.40	0.80	0.31	0.14	0.33	0.72	0.48	0.85	0.33
MnO	0.03	0.03	0.02	0.04	0.02	0.01	0.01	0.01	0.02	0.02	0.04	0.04
NiO	0.03	0.03	0.02	0.03	0.02	0.01	0.02	0.02	0.03	0.02	0.02	0.03
MgO	0.21	0.65	0.29	0.59	0.10	0.22	0.25	0.25	0.16	0.78	0.53	0.40

Sample:	475.10	475.11	475.41	475.49	475.50	476.40	481.30	486.55	492.15	496.40	496.41	496.49
Mode:	acc	maj	ML	maj	maj	acc	maj	acc	acc	acc	ML	ML
Depth in NG-sequence in m:	725.10	725.11	725.41	725.49	725.50	726.40	731.30	736.55	742.15	746.40	746.41	746.49
wt.%												
TiO2	0.43	0.50	0.37	0.46	0.42	0.53	0.50	0.53	0.61	0.60	0.41	0.37
Al2O3	9.64	13.58	11.78	10.41	13.35	10.34	15.48	7.43	8.91	12.49	12.50	12.31
Cr2O3	53.04	49.57	53.43	51.68	50.77	49.61	45.62	51.85	49.86	45.23	52.38	52.67
FeO(P)	28.46	25.62	21.74	28.50	24.48	31.48	28.19	33.43	32.57	32.06	22.45	22.63
FeO(C)	22.50	18.79	15.88	21.81	18.49	23.74	19.75	25.11	24.87	22.93	16.49	16.72
Fe2O3	6.63	7.60	6.51	7.44	6.65	8.61	9.38	9.25	8.56	10.15	6.63	6.56
MnO	0.32	0.30	0.27	0.33	0.27	0.35	0.29	0.35	0.40	0.29	0.28	0.27
NiO	0.08	0.12	0.12	0.10	0.03	0.09	0.16	0.09	0.10	0.15	0.08	0.11
MgO	7.13	10.16	11.72	7.69	10.30	6.39	9.76	5.22	5.29	6.99	11.47	11.27
Total(P)	99.11	99.86	99.43	99.17	99.63	98.79	100.00	98.90	97.74	97.82	99.58	99.62
Total(C)	99.77	100.62	100.08	99.92	100.30	99.65	100.94	99.83	98.60	98.84	100.24	100.27
cations (based on 32 oxygens):												
Ti	0.0876	0.0975	0.0725	0.0931	0.0824	0.1084	0.0970	0.1103	0.1285	0.1228	0.0804	0.0716
Al	3.0826	4.1529	3.6081	3.3044	4.0932	3.3210	4.6941	2.4356	2.9249	3.9886	3.8174	3.7648
Cr	11.3888	10.1687	10.9744	11.0024	10.4403	10.6953	9.2947	11.4070	11.0188	9.6952	10.7303	10.8102
Fe2+	5.1098	4.0765	3.4506	4.9120	4.0223	5.4138	4.2565	5.8423	5.8132	5.1989	3.5732	3.6298
Fe3+	1.3535	1.4835	1.2725	1.5069	1.3017	1.7670	1.8172	1.9369	1.7994	2.0705	1.2916	1.2818
Mn	0.0739	0.0660	0.0596	0.0754	0.0598	0.0809	0.0630	0.0818	0.0938	0.0673	0.0613	0.0589
Ni	0.0184	0.0242	0.0259	0.0206	0.0072	0.0198	0.0336	0.0203	0.0228	0.0337	0.0157	0.0223
Mg	2.8854	3.9308	4.5364	3.0851	3.9931	2.5939	3.7439	2.1660	2.1988	2.8229	4.4301	4.3605
n	3	2	6	4	2	7	6	6	5	6	6	4
Cr/Al	3.6946	2.4486	3.0416	3.3297	2.5507	3.2205	1.9801	4.6835	3.7673	2.4307	2.8109	2.8714
Mg#	0.3609	0.4909	0.5680	0.3858	0.4982	0.3239	0.4680	0.2705	0.2744	0.3519	0.5535	0.5457
FFE	0.2094	0.2668	0.2694	0.2348	0.2445	0.2461	0.2992	0.2490	0.2364	0.2848	0.2655	0.2610
Cr/ (Cr+Al)	0.7870	0.7100	0.7526	0.7690	0.7184	0.7631	0.6644	0.8241	0.7902	0.7085	0.7376	0.7417
Cr/Fe	1.6405	1.7029	2.1635	1.5959	1.8261	1.3872	1.4246	1.3652	1.3478	1.2420	2.0537	2.0494
standard deviation:												
wt.%												
TiO2	0.08	0.00	0.02	0.08	0.03	0.17	0.04	0.05	0.09	0.21	0.03	0.03
Al2O3	0.61	0.10	0.21	0.25	0.17	0.67	1.17	0.49	1.89	0.37	0.08	0.16
Cr2O3	0.56	0.11	0.28	0.45	0.51	0.57	0.99	1.01	1.70	1.02	0.19	0.57
FeO(P)	0.43	0.06	0.25	0.02	0.34	1.12	0.65	0.51	1.04	0.87	0.10	0.05
FeO(C)	0.34	0.01	0.07	0.14	0.06	0.83	0.36	0.18	0.83	0.48	0.14	0.30
Fe2O3	0.20	0.07	0.30	0.15	0.44	0.47	0.44	0.68	0.53	0.90	0.21	0.33
MnO	0.01	0.01	0.03	0.01	0.01	0.02	0.04	0.02	0.03	0.04	0.02	0.01
NiO	0.01	0.00	0.02	0.01	0.00	0.03	0.02	0.02	0.05	0.02	0.01	0.01
MgO	0.24	0.00	0.07	0.15	0.02	0.60	0.47	0.17	0.71	0.41	0.08	0.18

Sample:	496.50	500.50	519.26	523.90	523.95	523.99	524.26	524.27	532.14	536.95	546.85	546.91
Mode:	maj	acc	acc	maj	ML	ML	ML	acc	acc	acc	acc	acc
Depth in NG-sequence in m:	746.50	750.50	769.26	773.90	773.95	773.99	774.26	774.27	782.14	786.95	796.85	796.91
wt.%												
TiO2	0.45	0.46	0.69	0.73	0.45	0.43	0.43	0.39	0.61	0.70	0.52	0.48
Al2O3	6.42	9.34	9.87	8.37	11.51	12.15	12.69	8.13	8.94	8.33	9.53	10.05
Cr2O3	52.67	49.52	48.67	49.81	52.28	51.74	52.11	51.74	50.43	51.50	51.24	51.96
FeO(P)	33.52	32.61	33.34	34.48	24.76	23.66	23.75	33.59	32.33	31.83	30.86	28.88
FeO(C)	24.91	24.92	24.53	25.45	18.54	17.19	17.76	26.30	24.12	24.79	23.89	22.78
Fe2O3	9.56	8.55	9.80	10.03	6.90	7.18	6.67	8.10	9.13	7.82	7.75	6.77
MnO	0.39	0.37	0.38	0.38	0.31	0.28	0.27	0.44	0.37	0.32	0.36	0.36
NiO	0.14	0.09	0.10	0.09	0.12	0.14	0.05	0.04	0.12	0.09	0.12	0.10
MgO	5.10	5.20	5.94	5.24	9.97	10.89	10.81	4.34	6.02	5.49	6.17	6.91
Total(P)	98.67	97.59	99.00	99.10	99.40	99.28	100.13	98.68	98.82	98.26	98.80	98.73
Total(C)	99.63	98.45	99.98	100.10	100.09	100.00	100.79	99.49	99.74	99.04	99.57	99.40
cations (based on 32 oxygens):												
Ti	0.0943	0.0956	0.1412	0.1513	0.0896	0.0844	0.0841	0.0812	0.1255	0.1458	0.1082	0.0975
Al	2.1199	3.0526	3.1764	2.7217	3.5709	3.7378	3.8709	2.6825	2.8971	2.7337	3.0786	3.2240
Cr	11.6761	10.9582	10.5249	10.8876	10.8827	10.6822	10.6625	11.4489	10.9625	11.3357	11.1062	11.1947
Fe2+	5.8422	5.8332	5.6117	5.8858	4.0833	3.7548	3.8427	6.1550	5.5463	5.7728	5.4776	5.1918
Fe3+	2.0155	1.7980	2.0164	2.0880	1.3672	1.4112	1.2983	1.7063	1.8894	1.6391	1.5989	1.3863
Mn	0.0922	0.0875	0.0884	0.0883	0.0692	0.0614	0.0593	0.1045	0.0864	0.0757	0.0825	0.0828
Ni	0.0311	0.0211	0.0229	0.0205	0.0256	0.0295	0.0114	0.0101	0.0254	0.0204	0.0270	0.0216
Mg	2.1288	2.1538	2.4182	2.1568	3.9115	4.2386	4.1707	1.8117	2.4674	2.2769	2.5211	2.8012
n	2	6	20	7	6	6	3	3	7	4	13	3
Cr/Al	5.5078	3.5899	3.3135	4.0003	3.0476	2.8578	2.7545	4.2680	3.7840	4.1466	3.6075	3.4723
Mg#	0.2671	0.2697	0.3011	0.2682	0.4893	0.5303	0.5205	0.2274	0.3079	0.2829	0.3152	0.3505
FFE	0.2565	0.2356	0.2643	0.2619	0.2508	0.2732	0.2525	0.2170	0.2541	0.2211	0.2259	0.2107
Cr/(Cr+Al)	0.8463	0.7821	0.7682	0.8000	0.7529	0.7408	0.7337	0.8102	0.7910	0.8057	0.7830	0.7764
Cr/Fe	1.3833	1.3369	1.2849	1.2718	1.8589	1.9253	1.9311	1.3561	1.3730	1.4241	1.4615	1.5840
standard deviation:												
wt.%												
TiO2	0.01	0.19	0.24	0.08	0.09	0.01	0.03	0.14	0.18	0.20	0.08	0.03
Al2O3	0.12	2.87	1.21	1.54	0.59	0.06	0.10	0.13	0.60	0.08	0.55	0.81
Cr2O3	0.96	2.61	1.09	0.88	1.12	0.14	0.26	0.35	0.59	0.45	0.62	1.17
FeO(P)	0.81	1.47	1.02	1.34	0.23	0.18	0.03	1.01	1.22	1.15	0.95	0.20
FeO(C)	0.29	1.27	0.78	0.87	0.65	0.03	0.10	0.82	0.93	0.50	0.40	0.67
Fe2O3	1.22	0.54	0.59	0.59	0.71	0.19	0.11	0.32	0.68	0.75	0.77	0.90
MnO	0.01	0.06	0.03	0.03	0.01	0.01	0.02	0.01	0.02	0.06	0.03	0.03
NiO	0.00	0.04	0.03	0.02	0.02	0.01	0.02	0.02	0.03	0.06	0.04	0.04
MgO	0.27	1.24	0.74	0.76	0.39	0.06	0.05	0.58	0.65	0.42	0.29	0.62

Sample:	546.92	553.33	559.95	560.09	560.10	569.20	581.00	586.00	589.60	595.05	597.62	603.10
Mode:	ML	acc	ML	ML	maj	acc	acc	acc	acc	acc	acc	acc
Depth in NG-sequence in m:	796.92	803.33	809.95	810.09	810.10	819.20	831.00	836.00	839.60	845.05	847.62	853.10
wt.%												
TiO2	0.45	0.48	0.49	0.44	0.48	0.28	0.53	0.34	0.59	0.73	0.56	0.62
Al2O3	13.05	8.31	13.11	12.79	12.79	7.69	8.50	8.10	8.94	8.73	12.02	7.88
Cr2O3	50.86	50.12	50.97	51.39	51.15	50.32	49.03	48.75	48.70	48.60	48.30	48.69
FeO(P)	23.67	34.49	23.16	23.36	24.80	33.69	35.31	36.99	34.98	33.73	30.19	36.84
FeO(C)	17.40	26.03	16.83	16.57	18.26	25.35	26.25	26.91	25.82	25.02	22.55	26.67
Fe2O3	6.96	9.40	7.04	7.54	7.27	9.28	10.07	11.20	10.18	9.68	8.49	11.31
MnO	0.26	0.36	0.29	0.30	0.29	0.36	0.39	0.41	0.36	0.35	0.34	0.40
NiO	0.12	0.08	0.06	0.12	0.11	0.09	0.07	0.06	0.05	0.10	0.09	0.10
MgO	10.88	4.59	11.33	11.50	10.47	4.53	4.46	3.94	4.90	5.23	7.38	4.27
Total(P)	99.29	98.43	99.41	99.90	100.09	96.97	98.28	98.58	98.52	97.47	98.88	98.80
Total(C)	99.98	99.37	100.12	100.66	100.81	97.90	99.29	99.70	99.54	98.44	99.73	99.93
cations (based on 32 oxygens):												
Ti	0.0874	0.1013	0.0953	0.0859	0.0941	0.0593	0.1122	0.0709	0.1234	0.1548	0.1131	0.1311
Al	4.0010	2.7379	4.0028	3.8858	3.9073	2.5769	2.8038	2.6791	2.9239	2.8816	3.8044	2.5941
Cr	10.4611	11.0805	10.4355	10.4784	10.4863	11.3178	10.8511	10.8138	10.6991	10.7676	10.2539	10.7636
Fe2+	3.7860	6.0867	3.6446	3.5745	3.9608	6.0296	6.1447	6.3143	5.9996	5.8632	5.0642	6.2360
Fe3+	1.3630	1.9790	1.3712	1.4641	1.4182	1.9867	2.1207	2.3654	2.1302	2.0412	1.7156	2.3801
Mn	0.0577	0.0843	0.0646	0.0646	0.0635	0.0872	0.0925	0.0969	0.0851	0.0830	0.0781	0.0945
Ni	0.0246	0.0171	0.0133	0.0248	0.0221	0.0206	0.0153	0.0130	0.0120	0.0226	0.0192	0.0218
Mg	4.2191	1.9132	4.3728	4.4219	4.0476	1.9219	1.8597	1.6465	2.0268	2.1859	2.9515	1.7788
n	5	7	6	6	6	6	1	6	5	6	8	8
Cr/Al	2.6146	4.0470	2.6071	2.6966	2.6838	4.3921	3.8702	4.0364	3.6592	3.7367	2.6953	4.1493
Mg#	0.5271	0.2392	0.5454	0.5530	0.5054	0.2417	0.2323	0.2068	0.2525	0.2716	0.3682	0.2219
FFE	0.2647	0.2454	0.2734	0.2906	0.2637	0.2478	0.2566	0.2725	0.2620	0.2582	0.2530	0.2762
Cr/(Cr+Al)	0.7233	0.8019	0.7228	0.7295	0.7285	0.8145	0.7947	0.8014	0.7854	0.7889	0.7294	0.8058
Cr/Fe	1.8917	1.2792	1.9372	1.9364	1.8152	1.3147	1.2224	1.1601	1.2256	1.2684	1.4082	1.1632
standard deviation:												
wt.%												
TiO2	0.01	0.17	0.01	0.02	0.03	0.22		0.24	0.10	0.09	0.05	0.13
Al2O3	0.09	0.70	0.15	0.12	0.22	0.05		0.28	1.25	0.66	0.20	0.72
Cr2O3	0.38	0.70	0.25	0.25	0.23	0.70		0.76	0.60	0.67	0.49	0.87
FeO(P)	0.13	0.88	0.13	0.26	0.65	0.40		1.24	1.51	1.10	0.57	1.13
FeO(C)	0.18	0.82	0.04	0.29	0.40	0.23		0.76	0.73	0.68	0.52	0.62
Fe2O3	0.16	0.70	0.17	0.12	0.32	0.50		0.64	0.90	0.51	0.50	0.73
MnO	0.03	0.07	0.02	0.02	0.02	0.03		0.05	0.03	0.03	0.02	0.02
NiO	0.02	0.03	0.01	0.02	0.01	0.04		0.02	0.02	0.01	0.03	0.04
MgO	0.07	0.50	0.07	0.19	0.23	0.11		0.57	0.48	0.44	0.38	0.46

Sample:	609.47	609.53	609.54	609.68	609.69	614.76	624.70	639.95	644.00	644.20	695.50	711.60	Sample:	739.80	744.70
Mode:	acc	maj	ML	ML	acc	acc	acc	acc	maj	maj	acc	acc	Mode:	acc	acc
Depth in NG-sequence in m:	859.47	859.53	859.54	859.68	859.69	864.76	874.70	889.95	894.00	894.20	945.50	961.60	Depth in NG-sequence in m:	989.80	994.70
wt.%													wt.%		
TiO2	0.58	0.92	0.52	0.51	0.55	0.64	0.55	0.54	0.56	0.54	0.53	0.39	TiO2	0.66	0.68
Al2O3	9.99	10.34	13.18	13.25	9.88	10.25	8.54	9.04	13.55	13.81	9.95	10.40	Al2O3	8.96	14.88
Cr2O3	47.79	48.43	50.40	50.38	51.39	47.62	51.05	50.09	49.68	48.09	47.75	49.79	Cr2O3	49.37	43.34
FeO(P)	34.89	32.87	24.39	24.53	30.94	34.41	31.63	32.02	25.79	23.97	33.90	30.27	FeO(P)	32.70	30.76
FeO(C)	25.73	23.96	17.93	17.75	23.73	25.35	24.52	23.88	19.35	17.67	25.21	23.54	FeO(C)	24.85	21.79
Fe2O3	10.18	9.90	7.18	7.53	8.01	10.06	7.90	9.05	7.16	7.00	9.66	7.48	Fe2O3	8.72	9.96
MnO	0.40	0.40	0.31	0.26	0.35	0.41	0.35	0.33	0.32	0.28	0.38	0.34	MnO	0.39	0.33
NiO	0.09	0.12	0.09	0.14	0.16	0.14	0.08	0.13	0.07	0.09	0.09	0.08	NiO	0.11	0.13
MgO	5.07	6.62	10.63	10.84	6.51	5.34	5.46	6.03	9.83	10.41	5.15	6.15	MgO	5.28	8.09
Total(P)	98.80	99.69	99.52	99.91	99.79	98.80	97.66	98.17	99.79	97.18	97.76	97.43	Total(P)	97.46	98.21
Total(C)	99.82	100.68	100.24	100.66	100.59	99.81	98.45	99.08	100.51	97.89	98.73	98.18	Total(C)	98.34	99.21
cations (based on 32 oxygens):													cations (based on 32 oxygens):		
Ti	0.1199	0.1858	0.1018	0.0994	0.1114	0.1324	0.1155	0.1119	0.1087	0.1083	0.1107	0.0814	Ti	0.1391	0.1353
Al	3.2319	3.2871	4.0377	4.0369	3.1495	3.3142	2.8131	2.9434	4.1568	4.3128	3.2493	3.3878	Al	2.9551	4.6486
Cr	10.4170	10.3306	10.3553	10.2988	10.9963	10.3411	11.2913	10.9498	10.2237	10.0741	10.5072	10.8914	Cr	10.9284	9.0951
Fe2+	5.9310	5.4061	3.8966	3.8374	5.3720	5.8243	5.7391	5.5233	4.2116	3.9145	5.8674	5.4455	Fe2+	5.8207	4.8362
Fe3+	2.1114	2.0107	1.4035	1.4657	1.6312	2.0798	1.6646	1.8831	1.4021	1.3965	2.0221	1.5579	Fe3+	1.8384	1.9857
Mn	0.0931	0.0913	0.0688	0.0570	0.0806	0.0947	0.0838	0.0764	0.0696	0.0620	0.0907	0.0804	Mn	0.0927	0.0740
Ni	0.0197	0.0271	0.0198	0.0289	0.0344	0.0301	0.0175	0.0284	0.0150	0.0186	0.0207	0.0187	Ni	0.0253	0.0282
Mg	2.0762	2.6613	4.1165	4.1761	2.6245	2.1832	2.2751	2.4837	3.8125	4.1132	2.1319	2.5368	Mg	2.2003	3.1969
n	7	1	4	3	2	8	6	6	6	8	5	5	n	3	6
Cr/Al	3.2232	3.1428	2.5646	2.5512	3.4914	3.1202	4.0138	3.7202	2.4595	2.3359	3.2337	3.2149	Cr/Al	3.6982	1.9565
Mg#	0.2593	0.3299	0.5137	0.5211	0.3282	0.2726	0.2839	0.3102	0.4751	0.5124	0.2665	0.3178	Mg#	0.2743	0.3980
FFE	0.2625	0.2711	0.2648	0.2764	0.2329	0.2631	0.2248	0.2543	0.2498	0.2629	0.2563	0.2224	FFE	0.2400	0.2911
Cr/(Cr+Al)	0.7632	0.7586	0.7195	0.7184	0.7774	0.7573	0.8006	0.7881	0.7109	0.7002	0.7638	0.7627	Cr/(Cr+Al)	0.7872	0.6618
Cr/Fe	1.2060	1.2969	1.8192	1.8083	1.4620	1.2184	1.4209	1.3770	1.6957	1.7661	1.2400	1.4481	Cr/Fe	1.3290	1.2405
standard deviation:													standard deviation:		
wt.%													wt.%		
TiO2	0.17		0.02	0.02	0.05	0.14	0.23	0.18	0.04	0.03	0.24	0.21	TiO2	0.12	0.24
Al2O3	2.40		0.07	0.01	1.03	1.37	0.65	0.73	0.15	0.19	2.34	1.32	Al2O3	0.22	1.38
Cr2O3	1.89		0.13	0.05	1.34	0.71	0.71	0.59	0.36	0.74	1.63	1.21	Cr2O3	0.64	2.65
FeO(P)	1.36		0.12	0.09	0.66	0.94	1.24	1.41	0.38	0.38	1.17	1.13	FeO(P)	0.95	1.06
FeO(C)	0.81		0.05	0.03	0.99	0.60	0.87	1.16	0.20	0.34	0.81	0.58	FeO(C)	0.39	0.71
Fe2O3	0.67		0.09	0.12	0.37	0.53	0.56	0.54	0.23	0.30	0.42	0.63	Fe2O3	0.62	1.25
MnO	0.04		0.02	0.01	0.01	0.03	0.03	0.02	0.02	0.01	0.03	0.02	MnO	0.03	0.02
NiO	0.03		0.01	0.01	0.01	0.03	0.03	0.03	0.01	0.01	0.02	0.01	NiO	0.04	0.02
MgO	0.74		0.05	0.02	0.75	0.50	0.74	0.87	0.10	0.09	0.74	0.48	MgO	0.44	0.65

MICROPROBE DATA: Composition of chromite in the NG-sequence (NG2-borehole)

Sample:	120.40	219.90	294.12	299.89	307.10	320.15	358.66	360.20	424.44	428.15	451.00	509.05
Mode:	acc	acc	acc	maj	acc	acc	acc	acc	acc	acc	acc	acc
Depth in NG-sequence in m:	1160.40	1259.90	1334.12	1339.89	1347.10	1360.15	1398.66	1400.20	1464.44	1468.15	1491.00	1549.05
wt.%												
TiO2	0.25	0.71	0.08	0.37	0.86	0.12	0.62	0.47	0.75	0.46	0.45	0.62
Al2O3	7.91	8.19	9.35	16.75	8.13	8.30	11.66	15.73	11.82	10.51	10.69	12.86
Cr2O3	50.47	51.40	47.41	41.91	46.25	47.87	43.92	37.07	44.41	43.23	47.60	43.24
FeO(P)	31.93	32.04	37.01	30.80	37.44	37.92	35.39	36.47	35.56	36.06	33.34	33.28
FeO(C)	23.94	24.76	26.70	21.54	26.23	27.71	24.78	22.83	25.77	25.62	24.55	21.99
Fe2O3	8.88	8.09	11.46	10.29	12.46	11.35	11.78	15.16	10.88	13.83	9.77	12.54
MnO	0.36	0.36	0.39	0.29	0.36	0.42	0.33	0.32	0.36	0.38	0.35	0.35
NiO	0.08	0.13	0.09	0.11	0.18	0.09	0.23	0.23	0.19	0.16	0.08	0.16
MgO	5.33	5.46	3.99	8.40	4.47	3.12	5.64	7.24	5.19	4.90	5.75	7.72
Total(P)	96.32	98.28	98.33	98.63	97.69	97.84	97.80	97.53	98.28	97.70	98.24	98.23
Total(C)	97.21	99.09	99.47	99.67	98.94	98.98	98.98	99.05	99.37	99.08	99.22	99.48
cations (based on 32 oxygens):												
Ti	0.0532	0.1488	0.0177	0.0730	0.1820	0.0247	0.1288	0.0952	0.1552	0.0951	0.0919	0.1259
Al	2.6463	2.6873	3.0632	5.1632	2.6981	2.7763	3.7734	4.9466	3.8206	3.4353	3.4576	4.0561
Cr	11.3468	11.3201	10.4866	8.6652	10.2979	10.7500	9.5342	7.8202	9.6237	9.4860	10.3386	9.1612
Fe2+	5.6928	5.7695	6.2475	4.7099	6.1794	6.5833	5.6920	5.0932	5.9109	5.9490	5.6412	4.9314
Fe3+	1.9005	1.6949	2.4149	2.0255	2.6400	2.4244	2.4349	3.0429	2.2454	2.8885	2.0200	2.5309
Mn	0.0858	0.0839	0.0934	0.0653	0.0857	0.1020	0.0769	0.0716	0.0829	0.0883	0.0811	0.0804
Ni	0.0176	0.0295	0.0208	0.0226	0.0414	0.0212	0.0516	0.0497	0.0414	0.0357	0.0167	0.0339
Mg	2.2570	2.2660	1.6559	3.2753	1.8755	1.3183	2.3082	2.8806	2.1200	2.0222	2.3530	3.0803
n	3	4	6	5	5	4	4	4	3	4	4	7
Cr/Al	4.2878	4.2124	3.4234	1.6782	3.8167	3.8721	2.5267	1.5809	2.5189	2.7614	2.9901	2.2586
Mg#	0.2839	0.2820	0.2095	0.4102	0.2328	0.1668	0.2885	0.3613	0.2640	0.2537	0.2943	0.3845
FFE	0.2503	0.2271	0.2788	0.3007	0.2993	0.2691	0.2996	0.3740	0.2753	0.3268	0.2637	0.3392
Cr/(Cr+Al)	0.8109	0.8081	0.7739	0.6266	0.7924	0.7948	0.7164	0.6125	0.7158	0.7341	0.7494	0.6931
Cr/Fe	1.3915	1.4120	1.1276	1.1979	1.0873	1.1113	1.0925	0.8948	1.0994	0.9998	1.2565	1.1438
standard deviation:												
wt.%												
TiO2	0.20	0.10	0.05	0.03	0.12	0.04	0.20	0.04	0.26	0.14	0.10	0.28
Al2O3	1.32	0.58	2.47	0.42	0.34	0.34	0.86	0.80	0.93	0.77	1.00	1.96
Cr2O3	1.00	0.72	1.41	0.66	0.56	0.53	0.80	1.29	2.43	0.07	1.32	1.29
FeO(P)	0.76	0.26	1.86	0.30	0.62	0.80	1.08	1.02	2.22	1.00	0.51	1.90
FeO(C)	0.79	0.21	0.98	0.42	0.59	0.92	0.63	0.38	1.26	0.83	0.64	1.44
Fe2O3	0.92	0.31	1.02	0.14	0.21	0.33	0.59	0.77	1.07	0.41	0.49	1.08
MnO	0.02	0.02	0.02	0.03	0.01	0.01	0.01	0.03	0.04	0.03	0.01	0.04
NiO	0.01	0.02	0.04	0.02	0.03	0.02	0.04	0.03	0.02	0.03	0.02	0.04
MgO	0.58	0.15	0.93	0.26	0.42	0.63	0.37	0.16	0.95	0.78	0.50	1.05

Sample:	561.35	591.00	604.30	618.25	654.56	678.64	709.10	723.22	738.90	743.62	754.00	763.45
Mode:	acc	acc	acc	acc	acc	acc	acc	acc	acc	acc	acc	acc
Depth in NG-sequence in m:	1601.35	1631.00	1644.30	1658.25	1694.56	1718.64	1749.10	1763.22	1778.90	1783.62	1794.00	1803.45
wt.%												
TiO2	1.32	1.31	0.92	0.67	0.67	0.23	0.54	0.41	0.34	0.68	0.46	1.18
Al2O3	11.46	12.00	8.90	13.05	17.75	10.76	15.35	16.02	25.39	6.94	8.04	13.58
Cr2O3	36.95	35.42	33.69	41.22	39.84	44.54	42.20	40.45	27.38	45.10	46.74	29.49
FeO(P)	43.17	40.97	46.25	35.86	31.97	36.33	32.70	32.80	37.52	39.96	39.17	47.47
FeO(C)	27.43	24.56	25.80	24.19	22.50	24.53	23.16	22.36	24.36	27.09	27.81	26.44
Fe2O3	17.50	18.24	22.72	12.96	10.53	13.11	10.61	11.60	14.63	14.30	12.63	23.36
MnO	0.38	0.36	0.37	0.36	0.34	0.46	0.39	0.35	0.35	0.34	0.44	0.32
NiO	0.25	0.15	0.43	0.23	0.14	0.14	0.10	0.09	0.24	0.16	0.09	0.28
MgO	4.34	6.00	4.20	6.14	8.03	5.51	7.21	7.61	7.35	3.52	3.32	5.10
Total(P)	97.88	96.22	94.76	97.52	98.73	97.96	98.49	97.72	98.56	96.71	98.26	97.42
Total(C)	99.63	98.05	97.03	98.82	99.79	99.27	99.55	98.88	100.03	98.14	99.53	99.76
cations (based on 32 oxygens):												
Ti	0.2758	0.2741	0.1999	0.1375	0.1306	0.0469	0.1086	0.0831	0.0652	0.1477	0.0974	0.2426
Al	3.7334	3.9103	2.9965	4.1841	5.4574	3.4849	4.7920	5.0122	7.5829	2.3535	2.6778	4.3500
Cr	8.0729	7.7433	7.6360	8.8771	8.2147	9.6912	8.8655	8.5027	5.4930	10.2566	10.4414	6.3611
Fe2+	6.3429	5.6827	6.2205	5.5170	4.9094	5.6556	5.1444	4.9700	5.1664	6.5175	6.5713	6.0349
Fe3+	3.6421	3.7982	4.9678	2.6639	2.0668	2.7302	2.1254	2.3189	2.7936	3.0946	2.6859	4.8037
Mn	0.0901	0.0850	0.0898	0.0826	0.0741	0.1071	0.0881	0.0783	0.0742	0.0836	0.1059	0.0744
Ni	0.0552	0.0338	0.1001	0.0500	0.0295	0.0312	0.0210	0.0184	0.0482	0.0373	0.0199	0.0624
Mg	1.7875	2.4726	1.7895	2.4879	3.1176	2.2529	2.8550	3.0164	2.7765	1.5093	1.4004	2.0708
n	5	3	4	6	6	5	4	4	5	1	1	7
Cr/Al	2.1624	1.9802	2.5483	2.1216	1.5052	2.7809	1.8501	1.6964	0.7244	4.3581	3.8993	1.4623
Mg#	0.2199	0.3032	0.2234	0.3108	0.3884	0.2849	0.3569	0.3777	0.3496	0.1880	0.1757	0.2555
FFE	0.3648	0.4006	0.4440	0.3256	0.2963	0.3256	0.2924	0.3181	0.3510	0.3219	0.2901	0.4432
Cr/(Cr+Al)	0.6838	0.6645	0.7182	0.6797	0.6008	0.7355	0.6491	0.6291	0.4201	0.8134	0.7959	0.5939
Cr/Fe	0.7533	0.7610	0.6412	1.0120	1.0969	1.0792	1.1358	1.0855	0.6423	0.9935	1.0502	0.5469
standard deviation:												
wt.%												
TiO2	0.81	0.58	0.26	0.27	0.16	0.09	0.46	0.13	0.10	0.11	0.04	0.49
Al2O3	0.39	0.99	2.47	1.38	1.30	1.62	2.94	1.78	1.94	1.72	0.85	3.00
Cr2O3	5.28	2.99	10.14	2.05	2.03	3.06	1.00	1.96	1.70	1.28	0.51	2.52
FeO(P)	5.19	4.29	11.24	2.74	1.55	4.77	1.31	0.85	0.85	1.19	0.83	3.60
FeO(C)	2.09	1.12	1.13	1.05	1.71	1.28	0.13	0.71	0.99	1.00	0.57	1.08
Fe2O3	3.68	3.53	11.67	1.95	0.30	4.17	1.51	0.20	1.24	0.24	0.32	2.94
MnO	0.02	0.02	0.07	0.03	0.05	0.10	0.02	0.02	0.01	0.03	0.01	0.01
NiO	0.04	0.04	0.23	0.03	0.04	0.05	0.03	0.02	0.00	0.02	0.02	0.04
MgO	0.87	0.79	1.21	0.93	1.14	1.11	0.09	0.36	0.64	0.94	0.43	0.71

Sample:	772.36	773.70
Mode:	acc	acc
Depth in MG-sequence in m:	1812.36	1813.70
wt.%		
TiO2	0.91	0.58
Al2O3	17.65	8.24
Cr2O3	33.08	46.13
FeO(P)	41.29	40.11
FeO(C)	26.99	30.37
Fe2O3	15.90	10.82
MnO	0.36	0.38
NiO	0.20	0.06
MgO	5.22	1.52
Total(P)	98.71	97.01
Total(C)	100.30	98.10
cations (based on 32 oxygens):		
Ti	0.1824	0.1268
Al	5.5067	2.8099
Cr	6.9443	10.5691
Fe2+	5.9955	7.3681
Fe3+	3.1842	2.3673
Mn	0.0811	0.0933
Ni	0.0435	0.0132
Mg	2.0624	0.6523
n	4	4
Cr/Al	1.2611	3.7614
Mg#	0.2559	0.0813
FFE	0.3469	0.2432
Cr/ (Cr+Al)	0.5577	0.7900
Cr/Fe	0.7051	1.0125
standard deviation:		
wt.%		
TiO2	0.39	0.21
Al2O3	2.87	1.03
Cr2O3	0.71	1.85
FeO(P)	2.74	2.70
FeO(C)	0.94	0.78
Fe2O3	2.06	2.20
MnO	0.02	0.04
NiO	0.04	0.03
MgO	0.72	0.72

MICROPROBE DATA: Composition of chromite in the SF-sequence

Sample:	69.30	69.61	70.81	71.82	73.90	219.55	220.32	223.68	224.34	226.10	227.07	244.10	244.60
Mode:	ML	ML	ML	ML	ML	maj	maj	acc	ML	ML	ML	ML	ML
wt.%													
TiO2	1.22	1.46	1.45	1.89	1.35	1.89	1.10	1.18	0.78	0.65	0.76	0.64	0.79
Al2O3	12.74	10.90	13.25	10.83	13.07	11.53	13.73	11.50	13.78	17.19	18.27	17.53	13.20
Cr2O3	45.19	46.37	45.40	44.19	45.32	44.94	45.50	47.71	45.76	43.19	41.85	43.81	46.00
FeO(P)	32.05	34.21	31.23	35.18	33.09	34.16	31.79	34.51	30.19	28.57	28.28	27.41	30.93
FeO(C)	23.97	25.68	23.52	25.88	25.11	26.12	24.39	28.53	22.19	20.15	19.76	20.19	21.90
Fe2O3	8.99	9.49	8.58	10.33	8.86	8.94	8.22	6.65	8.89	9.35	9.47	8.02	10.04
MnO	0.31	0.39	0.33	0.39	0.34	0.34	0.34	0.37	0.30	0.29	0.26	0.31	0.35
NiO	0.15	0.16	0.20	0.13	0.12	0.13	0.14	0.11	0.11	0.14	0.16	0.16	0.12
MgO	6.81	5.76	7.42	5.71	6.44	5.72	6.72	3.80	7.94	9.72	10.15	9.63	8.20
Total(P)	98.49	99.25	99.28	98.31	99.73	98.72	99.31	99.18	98.86	99.75	99.72	99.48	99.59
Total(C)	99.39	100.20	100.14	99.35	100.62	99.61	100.14	99.85	99.75	100.69	100.67	100.29	100.59
cations (based on 32 oxygens):													
Ti	0.2468	0.2985	0.2898	0.3900	0.2719	0.3887	0.2206	0.2450	0.1564	0.1252	0.1447	0.1231	0.1565
Al	4.0498	3.4936	4.1535	3.5013	4.1104	3.7026	4.3149	3.7317	4.3095	5.1920	5.4781	5.3061	4.0946
Cr	9.6334	9.9687	9.5499	9.5852	9.5653	9.6861	9.5950	10.3979	9.6017	8.7536	8.4196	8.8972	9.5990
Fe2+	5.4038	5.8389	5.2318	5.9371	5.6073	5.9554	5.4418	6.5770	4.9247	4.3199	4.2050	4.3379	4.8341
Fe3+	1.8231	1.9407	1.7170	2.1335	1.7804	1.8338	1.6490	1.3803	1.7761	1.8039	1.8129	1.5505	1.9934
Mn	0.0713	0.0890	0.0752	0.0915	0.0766	0.0789	0.0762	0.0866	0.0684	0.0630	0.0563	0.0664	0.0774
Ni	0.0332	0.0344	0.0423	0.0286	0.0268	0.0294	0.0304	0.0242	0.0239	0.0293	0.0327	0.0337	0.0251
Mg	2.7385	2.3363	2.9406	2.3329	2.5612	2.3250	2.6722	1.5572	3.1393	3.7131	3.8508	3.6850	3.2199
n	7	5	4	4	8	5	5	6	5	5	5	5	5
Cr/Al	2.3788	2.8534	2.2993	2.7376	2.3271	2.6160	2.2237	2.7864	2.2281	1.6860	1.5369	1.6768	2.3443
Mg#	0.3363	0.2858	0.3598	0.2821	0.3136	0.2808	0.3293	0.1914	0.3893	0.4622	0.4780	0.4593	0.3998
FFE	0.2523	0.2495	0.2471	0.2644	0.2410	0.2354	0.2326	0.1735	0.2651	0.2946	0.3013	0.2633	0.2920
Cr/ (Cr+Al)	0.7040	0.7405	0.6969	0.7324	0.6994	0.7235	0.6898	0.7359	0.6902	0.6277	0.6058	0.6264	0.7010
Cr/Fe	1.2412	1.1930	1.2796	1.1059	1.2057	1.1580	1.2599	1.2170	1.3342	1.3309	1.3027	1.4069	1.3093
standard deviation:													
wt.%													
TiO2	0.05	0.20	0.09	0.09	0.15	0.23	0.02	0.03	0.05	0.08	0.02	0.08	0.11
Al2O3	0.25	0.15	0.16	0.22	0.64	0.63	0.40	1.10	0.54	0.19	0.09	0.11	1.72
Cr2O3	0.46	0.26	0.12	0.28	1.36	0.53	0.83	0.60	0.59	0.39	0.24	0.18	1.28
FeO(P)	0.23	0.33	0.33	0.46	0.92	0.53	0.27	1.07	0.47	0.18	0.09	0.29	1.19
FeO(C)	0.20	0.18	0.19	0.54	0.68	0.24	0.25	0.85	0.34	0.11	0.12	0.19	1.00
Fe2O3	0.24	0.23	0.20	0.10	0.31	0.41	0.54	0.52	0.22	0.19	0.12	0.19	0.24
MnO	0.02	0.03	0.01	0.03	0.01	0.03	0.03	0.04	0.02	0.02	0.02	0.03	0.03
NiO	0.02	0.03	0.01	0.01	0.02	0.02	0.01	0.02	0.01	0.02	0.01	0.01	0.02
MgO	0.17	0.10	0.02	0.35	0.23	0.12	0.28	0.67	0.24	0.10	0.05	0.11	0.94

Sample:	248.46	249.76	250.88	251.16	266.10	267.72	268.22	268.41	319.18	319.54	357.30	372.38	372.56
Mode:	ML	ML	acc	ML	ML	ML	maj	acc	ML	ML	acc	acc	ML
wt.%													
TiO2	1.00	0.97	1.14	0.76	0.59	0.40	0.73	0.74	1.33	0.61	0.27	0.63	0.46
Al2O3	12.75	13.40	11.05	14.85	17.30	21.36	18.40	15.42	10.55	16.58	6.36	6.79	20.43
Cr2O3	47.55	46.42	47.03	46.05	45.84	44.07	47.04	50.12	47.42	43.23	42.95	45.42	40.92
FeO(P)	29.61	28.12	35.51	27.77	26.85	24.12	25.83	26.52	31.92	27.01	44.11	41.63	26.11
FeO(C)	21.36	20.63	27.83	20.17	21.65	20.77	23.65	24.69	22.06	18.60	27.17	27.96	17.73
Fe2O3	9.18	8.32	8.53	8.44	5.77	3.72	2.43	2.04	10.96	9.35	18.83	15.19	9.31
MnO	0.32	0.32	0.41	0.33	0.32	0.29	0.29	0.37	0.33	0.31	0.52	0.47	0.28
NiO	0.11	0.17	0.11	0.12	0.04	0.13	0.10	0.07	0.13	0.14	0.12	0.09	0.15
MgO	8.75	8.83	4.24	9.41	8.70	9.59	7.62	6.55	8.22	10.31	3.33	3.20	11.56
Total(P)	100.10	98.22	99.49	99.29	99.64	99.96	100.02	99.78	99.89	98.18	97.66	98.22	99.90
Total(C)	101.02	99.05	100.35	100.13	100.22	100.33	100.26	99.99	100.99	99.11	99.55	99.74	100.84
cations (based on 32 oxygens):													
Ti	0.1963	0.1933	0.2362	0.1491	0.1155	0.0761	0.1430	0.1465	0.2650	0.1185	0.0586	0.1334	0.0871
Al	3.9395	4.1958	3.5674	4.5607	5.2723	6.3515	5.6125	4.8105	3.3072	5.0678	2.1389	2.2722	6.0073
Cr	9.8570	9.7535	10.1999	9.4869	9.3737	8.7897	9.6286	10.4905	9.9689	8.8698	9.6937	10.2085	8.0712
Fe2+	4.6828	4.5856	6.3845	4.3962	4.6835	4.3818	5.1192	5.4655	4.9050	4.0367	6.4860	6.6498	3.7001
Fe3+	1.8109	1.6641	1.7603	1.6542	1.1230	0.7065	0.4728	0.4061	2.1938	1.8253	4.0501	3.2525	1.7474
Mn	0.0717	0.0728	0.0942	0.0725	0.0691	0.0620	0.0632	0.0822	0.0733	0.0673	0.1261	0.1125	0.0586
Ni	0.0230	0.0356	0.0247	0.0258	0.0080	0.0258	0.0209	0.0158	0.0278	0.0293	0.0286	0.0210	0.0308
Mg	3.4188	3.4993	1.7328	3.6546	3.3548	3.6065	2.9398	2.5829	3.2699	3.9852	1.4179	1.3502	4.2976
n	5	5	5	4	5	3	5	4	5	5	4	7	5
Cr/Al	2.5021	2.3246	2.8592	2.0801	1.7779	1.3839	1.7155	2.1807	3.0143	1.7502	4.5320	4.4928	1.3436
Mg#	0.4220	0.4328	0.2135	0.4539	0.4174	0.4515	0.3648	0.3209	0.3992	0.4968	0.1794	0.1688	0.5374
FFE	0.2789	0.2663	0.2161	0.2734	0.1934	0.1389	0.0846	0.0692	0.3090	0.3114	0.3844	0.3285	0.3208
Cr/ (Cr+Al)	0.7145	0.6992	0.7409	0.6753	0.6400	0.5805	0.6318	0.6856	0.7509	0.6364	0.8192	0.8179	0.5733
Cr/Fe	1.4135	1.4532	1.1659	1.4599	1.5031	1.6085	1.6031	1.6635	1.3076	1.4090	0.8571	0.9604	1.3796
standard deviation:													
wt.%													
TiO2	0.04	0.02	0.30	0.01	0.06	0.07	0.08	0.08	0.11	0.10	0.16	0.36	0.04
Al2O3	0.85	0.12	1.13	0.28	0.38	0.33	0.18	0.32	0.04	0.67	1.11	0.94	0.15
Cr2O3	0.51	0.23	1.08	0.35	0.13	0.14	0.19	0.71	0.33	0.46	4.90	0.50	0.14
FeO(P)	0.83	0.37	0.54	0.23	0.73	0.18	0.37	0.33	0.27	0.48	3.54	1.85	0.23
FeO(C)	0.57	0.41	0.58	0.14	0.24	0.19	0.20	0.10	0.16	0.27	2.19	1.04	0.11
Fe2O3	0.32	0.36	0.33	0.21	0.57	0.07	0.28	0.28	0.27	0.29	6.34	0.95	0.19
MnO	0.01	0.02	0.02	0.02	0.02	0.00	0.02	0.01	0.02	0.01	0.06	0.06	0.01
NiO	0.02	0.02	0.02	0.01	0.02	0.02	0.01	0.01	0.03	0.03	0.02	0.05	0.01
MgO	0.43	0.31	0.47	0.07	0.12	0.15	0.14	0.08	0.04	0.25	1.27	0.99	0.07

Sample:	372.65	385.20	385.94	438.00	440.67	453.28	475.17	475.30
Mode:	ML	acc	acc	acc	ML	ML	maj	maj
wt.%								
TiO2	0.60	0.95	1.22	1.39	1.44	1.00	1.02	0.97
Al2O3	18.11	15.03	6.65	7.76	9.68	14.39	11.60	9.56
Cr2O3	42.16	41.75	42.62	43.60	43.31	43.14	49.45	50.13
FeO(P)	28.65	32.11	43.78	40.72	37.91	31.32	27.84	29.76
FeO(C)	19.46	20.62	28.23	27.18	25.49	21.18	20.00	21.65
Fe2O3	10.21	12.76	17.28	15.05	13.80	11.27	8.72	9.01
MnO	0.32	0.31	0.38	0.40	0.38	0.32	0.33	0.32
NiO	0.12	0.13	0.16	0.14	0.09	0.05	0.17	0.18
MgO	10.36	9.38	3.39	4.29	5.69	8.88	9.43	7.90
Total(P)	100.32	99.64	98.19	98.30	98.48	99.11	99.85	98.82
Total(C)	101.34	100.92	99.93	99.81	99.86	100.24	100.72	99.72
cations (based on 32 oxygens):								
Ti	0.1148	0.1848	0.2610	0.2938	0.2976	0.1963	0.2024	0.1964
Al	5.3972	4.5896	2.2243	2.5663	3.1346	4.4463	3.5937	3.0492
Cr	8.4305	8.5523	9.5637	9.6695	9.4137	8.9387	10.2771	10.7228
Fe2+	4.1162	4.4691	6.7005	6.3757	5.8603	4.6431	4.3959	4.8986
Fe3+	1.9426	2.4886	3.6900	3.1766	2.8564	2.2223	1.7243	1.8352
Mn	0.0685	0.0674	0.0912	0.0944	0.0875	0.0716	0.0732	0.0737
Ni	0.0245	0.0263	0.0355	0.0312	0.0192	0.0108	0.0369	0.0382
Mg	3.9055	3.6220	1.4337	1.7924	2.3306	3.4708	3.6963	3.1859
n	5	5	3	4	6	5	5	5
Cr/Al	1.5620	1.8634	4.2997	3.7678	3.0032	2.0104	2.8597	3.5166
Mg#	0.4869	0.4477	0.1763	0.2194	0.2845	0.4278	0.4568	0.3941
FFE	0.3206	0.3577	0.3551	0.3325	0.3277	0.3237	0.2817	0.2725
Cr/ (Cr+Al)	0.6097	0.6508	0.8113	0.7903	0.7502	0.6678	0.7409	0.7786
Cr/Fe	1.2956	1.1446	0.8570	0.9426	1.0057	1.2123	1.5635	1.4828
standard deviation:								
wt.%								
TiO2	0.06	0.06	0.03	0.15	0.06	0.05	0.03	0.13
Al2O3	0.41	0.15	0.08	0.48	0.62	0.12	0.10	0.25
Cr2O3	0.58	0.77	0.64	0.40	0.88	0.23	0.24	0.49
FeO(P)	0.21	0.79	0.76	0.70	1.04	0.18	0.28	0.44
FeO(C)	0.12	0.33	0.10	0.21	0.33	0.08	0.10	0.13
Fe2O3	0.15	0.67	0.75	0.78	0.81	0.15	0.30	0.45
MnO	0.01	0.01	0.01	0.02	0.02	0.02	0.02	0.02
NiO	0.02	0.03	0.01	0.01	0.02	0.01	0.02	0.02
MgO	0.12	0.18	0.09	0.12	0.26	0.03	0.03	0.14

MICROPROBE DATA: Composition of olivine in the NG-sequence (NG1- and NG2-boreholes)

	NG1	NG2										
Sample:	744.70	80.35	200.50	242.55	358.66	376.65	387.37	397.68	410.61	420.00	420.05	421.50
Depth in NG-sequence in m:	994.70	1120.35	1240.50	1282.55	1398.66	1416.65	1427.37	1437.68	1450.61	1460.00	1460.05	1461.50
wt.%												
SiO2	39.57	39.77	39.23	39.98	38.98	39.72	39.82	39.31	39.58	39.86	39.55	39.68
FeO	14.04	14.28	14.43	12.34	15.27	14.61	13.64	15.18	14.24	13.86	12.85	14.58
MnO	0.16	0.17	0.15	0.17	0.20	0.17	0.15	0.15	0.15	0.16	0.15	0.18
NiO	0.33	0.30	0.35	0.29	0.34	0.36	0.35	0.35	0.42	0.37	0.41	0.42
MgO	46.32	46.11	46.04	47.07	45.40	45.86	46.05	45.65	45.94	46.25	46.75	45.67
CaO	0.02	0.02	0.03	0.02	0.01	0.01	0.02	0.02	0.02	0.02	0.01	0.00
Total	100.45	100.65	100.23	99.87	100.20	100.73	100.02	100.65	100.34	100.52	99.71	100.53
cations (based on 4 oxygens):												
Si	0.9871	0.9904	0.9833	0.9942	0.9816	0.9901	0.9948	0.9840	0.9893	0.9922	0.9888	0.9912
Fe	0.2929	0.2974	0.3024	0.2568	0.3215	0.3045	0.2850	0.3178	0.2977	0.2885	0.2687	0.3047
Mn	0.0034	0.0036	0.0031	0.0036	0.0042	0.0037	0.0033	0.0032	0.0032	0.0035	0.0033	0.0038
Ni	0.0067	0.0060	0.0071	0.0059	0.0069	0.0073	0.0070	0.0071	0.0084	0.0075	0.0082	0.0084
Mg	1.7223	1.7117	1.7198	1.7448	1.7040	1.7041	1.7148	1.7033	1.7117	1.7158	1.7421	1.7007
Ca	0.0004	0.0006	0.0008	0.0005	0.0002	0.0002	0.0004	0.0004	0.0005	0.0004	0.0002	0.0001
Total	3.0129	3.0096	3.0167	3.0058	3.0184	3.0099	3.0052	3.0160	3.0107	3.0078	3.0112	3.0088
n	2	5	4	7	4	4	5	5	4	4	5	4
Fo	0.8546	0.8520	0.8504	0.8717	0.8413	0.8484	0.8575	0.8427	0.8518	0.8561	0.8664	0.8481
standard deviation:												
wt.%												
SiO2	0.00	0.14	0.07	0.13	0.09	0.20	0.06	0.11	0.06	0.02	0.15	0.08
FeO	0.03	0.13	0.20	0.15	0.21	0.10	0.09	0.19	0.19	0.05	0.09	0.10
MnO	0.01	0.02	0.01	0.01	0.00	0.01	0.01	0.01	0.00	0.01	0.01	0.01
NiO	0.01	0.03	0.01	0.03	0.01	0.02	0.02	0.02	0.02	0.02	0.03	0.03
MgO	0.30	0.12	0.23	0.15	0.13	0.14	0.19	0.13	0.21	0.25	0.12	0.09
CaO	0.00	0.01	0.01	0.01	0.01	0.01	0.00	0.01	0.01	0.01	0.01	0.00

Sample:	426.60	438.29	454.45	509.05	520.00	530.95	550.05	561.35	591.05	591.10	591.25	604.30
Depth in NG-sequence in m:	1466.60	1478.29	1494.45	1549.05	1560.00	1570.95	1590.05	1601.35	1631.05	1631.10	1631.25	1644.30
wt.%												
SiO2	39.72	39.43	39.75	40.13	39.24	39.49	39.60	39.00	39.13	39.44	39.23	39.29
FeO	14.18	13.01	13.57	11.31	13.38	14.04	15.49	15.57	14.33	14.71	14.55	13.93
MnO	0.16	0.14	0.13	0.11	0.17	0.17	0.19	0.15	0.15	0.15	0.18	0.15
NiO	0.30	0.46	0.37	0.37	0.35	0.27	0.30	0.39	0.32	0.31	0.31	0.56
MgO	45.94	46.99	46.13	47.82	46.31	46.56	45.20	44.56	44.55	44.84	46.20	45.55
CaO	0.02	0.01	0.01	0.02	0.01	0.02	0.03	0.02	0.01	0.01	0.01	0.01
Total	100.32	100.04	99.96	99.76	99.47	100.55	100.81	99.69	98.49	99.47	100.48	99.49
cations (based on 4 oxygens):												
Si	0.9919	0.9841	0.9937	0.9945	0.9864	0.9842	0.9902	0.9879	0.9966	0.9959	0.9813	0.9902
Fe	0.2962	0.2716	0.2836	0.2345	0.2813	0.2925	0.3240	0.3299	0.3052	0.3106	0.3045	0.2936
Mn	0.0033	0.0030	0.0028	0.0022	0.0035	0.0036	0.0040	0.0033	0.0033	0.0033	0.0038	0.0032
Ni	0.0060	0.0092	0.0075	0.0075	0.0072	0.0055	0.0061	0.0079	0.0065	0.0063	0.0062	0.0113
Mg	1.7101	1.7479	1.7184	1.7662	1.7350	1.7296	1.6848	1.6825	1.6913	1.6876	1.7227	1.7112
Ca	0.0004	0.0001	0.0003	0.0006	0.0003	0.0004	0.0007	0.0006	0.0004	0.0004	0.0003	0.0004
Total	3.0081	3.0159	3.0063	3.0055	3.0136	3.0158	3.0098	3.0121	3.0034	3.0041	3.0187	3.0098
n	5	4	5	7	3	4	4	5	5	5	5	5
Fo	0.8524	0.8655	0.8583	0.8828	0.8605	0.8553	0.8387	0.8361	0.8471	0.8446	0.8498	0.8536
standard deviation:												
wt.%												
SiO2	0.13	0.12	0.13	0.24	0.23	0.16	0.07	0.12	0.10	0.13	0.09	0.08
FeO	0.11	0.20	0.14	0.22	0.14	0.05	0.15	0.19	0.11	0.05	0.24	0.37
MnO	0.01	0.01	0.01	0.01	0.01	0.01	0.01	0.01	0.01	0.01	0.00	0.01
NiO	0.02	0.01	0.02	0.04	0.01	0.01	0.02	0.03	0.04	0.02	0.01	0.03
MgO	0.23	0.26	0.34	0.15	0.31	0.12	0.13	0.22	0.12	0.15	0.24	0.52
CaO	0.01	0.00	0.01	0.01	0.01	0.01	0.01	0.00	0.00	0.01	0.00	0.00

Sample:	618.25	654.56	678.64	691.95	702.60	709.10	723.22	736.66	738.90	739.10	763.45	772.36
Depth in												
NG-sequence in m:	1658.25	1694.56	1718.64	1731.95	1742.60	1749.10	1763.22	1776.66	1778.90	1779.10	1803.45	1812.36
wt.%												
SiO2	39.45	39.27	39.71	39.82	39.57	40.16	39.65	39.18	39.67	39.71	39.26	39.23
FeO	14.74	13.04	14.02	13.64	12.87	11.75	12.47	14.65	14.76	14.63	16.30	14.43
MnO	0.13	0.18	0.16	0.15	0.14	0.13	0.14	0.13	0.15	0.17	0.19	0.15
NiO	0.38	0.35	0.37	0.35	0.35	0.36	0.28	0.50	0.37	0.38	0.26	0.35
MgO	45.25	46.90	45.97	46.05	47.45	47.56	47.35	45.78	45.08	45.53	43.78	46.04
CaO	0.01	0.02	0.01	0.02	0.01	0.01	0.02	0.01	0.01	0.02	0.01	0.03
Total	99.96	99.77	100.23	100.02	100.40	99.97	99.91	100.25	100.03	100.44	99.80	100.23
cations (based on 4 oxygens):												
Si	0.9919	0.9829	0.9922	0.9948	0.9829	0.9949	0.9870	0.9834	0.9961	0.9929	0.9953	0.9833
Fe	0.3098	0.2729	0.2928	0.2850	0.2673	0.2435	0.2597	0.3074	0.3098	0.3059	0.3456	0.3024
Mn	0.0029	0.0039	0.0033	0.0033	0.0030	0.0028	0.0030	0.0028	0.0033	0.0036	0.0041	0.0031
Ni	0.0076	0.0071	0.0074	0.0070	0.0071	0.0071	0.0056	0.0101	0.0074	0.0077	0.0054	0.0071
Mg	1.6957	1.7498	1.7118	1.7148	1.7567	1.7564	1.7571	1.7126	1.6871	1.6966	1.6542	1.7198
Ca	0.0002	0.0005	0.0002	0.0004	0.0002	0.0003	0.0005	0.0002	0.0002	0.0005	0.0002	0.0008
Total	3.0081	3.0171	3.0078	3.0052	3.0171	3.0051	3.0130	3.0166	3.0039	3.0071	3.0047	3.0167
n	4	4	5	5	5	4	5	3	7	5	4	5
Fo	0.8455	0.8651	0.8539	0.8575	0.8679	0.8782	0.8712	0.8478	0.8448	0.8472	0.8272	0.8504
standard deviation:												
wt.%												
SiO2	0.08	0.05	0.09	0.06	0.10	0.15	0.17	0.31	0.26	0.16	0.05	0.07
FeO	0.18	0.22	0.17	0.09	0.11	0.25	0.07	0.29	0.27	0.43	0.04	0.20
MnO	0.01	0.00	0.01	0.01	0.02	0.00	0.01	0.01	0.01	0.01	0.01	0.01
NiO	0.03	0.03	0.05	0.02	0.02	0.02	0.02	0.01	0.02	0.03	0.01	0.01
MgO	0.33	0.20	0.12	0.19	0.14	0.14	0.14	0.37	0.54	0.23	0.33	0.23
CaO	0.01	0.01	0.00	0.00	0.01	0.01	0.01	0.01	0.00	0.00	0.01	0.01

MICROPROBE DATA: Composition of plagioclase in the NG-sequence (NG3-borehole)

Sample:	3.98	28.62	55.00	79.60	99.60	126.05	146.50	151.90	152.90	153.15	153.20	154.72
Depth in NG-sequence in m:	3.98	28.62	55.00	79.60	99.60	126.05	146.50	151.90	152.90	153.15	153.20	154.72
Habit:	pcum	pcum	pcum	pcum	pcum	pcum	pcum	pcum	pcum	pcum	pcum	pcum
wt.%												
SiO2	50.55	49.74	50.30	50.98	49.36	50.28	49.86	50.05	49.34	49.46	52.87	48.95
Al2O3	30.96	31.19	30.12	30.93	32.04	31.24	31.56	30.99	31.99	31.84	29.70	32.09
FeO	0.32	0.31	0.23	0.33	0.30	0.30	0.21	0.22	0.14	0.18	0.15	0.17
CaO	14.08	14.57	14.65	13.85	15.21	14.58	14.76	14.59	15.46	15.34	12.44	15.44
Na2O	3.50	3.22	3.26	3.58	2.95	3.29	3.21	3.34	3.16	2.85	4.36	3.17
K2O	0.24	0.18	0.22	0.25	0.18	0.20	0.24	0.26	0.16	0.20	0.28	0.18
Total	99.64	99.23	98.78	99.91	100.03	99.89	99.83	99.46	100.26	99.88	99.80	100.01
cations (based on 32 oxygens):												
Si	9.2585	9.1617	9.3023	9.3017	9.0317	9.1955	9.1288	9.1994	9.0162	9.0606	9.6066	8.9763
Al	6.6821	6.7705	6.5644	6.6510	6.9107	6.7331	6.8115	6.7118	6.8924	6.8740	6.3613	6.9354
Fe	0.0488	0.0480	0.0362	0.0499	0.0458	0.0454	0.0316	0.0341	0.0216	0.0276	0.0225	0.0265
Ca	2.7620	2.8761	2.9020	2.7074	2.9814	2.8568	2.8965	2.8739	3.0286	3.0115	2.4229	3.0328
Na	1.2423	1.1506	1.1701	1.2675	1.0445	1.1666	1.1371	1.1892	1.1199	1.0101	1.5344	1.1280
K	0.0561	0.0429	0.0512	0.0581	0.0425	0.0477	0.0568	0.0617	0.0379	0.0474	0.0647	0.0420
Total	20.0497	20.0498	20.0262	20.0356	20.0565	20.0451	20.0624	20.0701	20.1166	20.0312	20.0123	20.1410
n	5	4	4	5	5	5	4	3	5	4	3	5
An	0.6802	0.7067	0.7038	0.6713	0.7328	0.7017	0.7081	0.6967	0.7234	0.7401	0.6024	0.7216
standard deviation:												
wt.%												
SiO2	0.76	0.61	0.18	0.62	0.54	0.64	0.96	0.22	1.75	0.15	1.09	0.43
Al2O3	0.52	0.37	0.49	0.46	0.23	0.50	0.34	0.14	1.17	0.13	0.81	0.53
FeO	0.08	0.11	0.08	0.11	0.16	0.07	0.03	0.04	0.02	0.02	0.03	0.02
CaO	0.63	0.53	0.18	0.53	0.31	0.45	0.49	0.05	1.49	0.14	0.96	0.53
Na2O	0.29	0.29	0.11	0.26	0.14	0.25	0.28	0.03	0.74	0.05	0.50	0.20
K2O	0.06	0.02	0.06	0.04	0.04	0.02	0.04	0.03	0.09	0.01	0.03	0.10

Sample:	156.10	158.55	159.20	159.40	163.45	168.75	170.34	173.55	174.77	174.87	175.05	176.45
Depth in NG-sequence in m:	156.10	158.55	159.20	159.40	163.45	168.75	170.34	173.55	174.77	174.87	175.05	176.45
Habit:	pcum	pcum	pcum	pcum	pcum	pcum	cum	cum	cum	cum	cum	cum
wt.%												
SiO2	48.32	48.06	48.69	50.49	49.98	49.13	48.71	48.32	48.31	48.56	48.41	48.64
Al2O3	32.22	32.65	31.86	30.87	31.56	32.08	32.12	32.19	32.83	32.73	32.43	32.48
FeO	0.19	0.17	0.21	0.21	0.16	0.20	0.22	0.21	0.24	0.19	0.18	0.25
CaO	15.55	16.16	15.92	14.53	14.64	15.76	15.93	16.22	15.89	16.33	16.02	16.11
Na2O	2.88	2.75	3.11	3.31	3.55	2.98	2.71	2.83	2.52	2.84	2.92	2.52
K2O	0.24	0.15	0.18	0.19	0.24	0.15	0.13	0.33	0.14	0.10	0.14	0.13
Total	99.41	99.94	99.97	99.59	100.13	100.30	99.81	100.09	99.95	100.76	100.10	100.13
cations (based on 32 oxygens):												
Si	8.9190	8.8353	8.9510	9.2512	9.1306	8.9834	8.9503	8.8838	8.8630	8.8563	8.8832	8.9100
Al	7.0094	7.0751	6.9036	6.6686	6.7945	6.9133	6.9550	6.9749	7.0989	7.0356	7.0139	7.0126
Fe	0.0293	0.0266	0.0316	0.0318	0.0241	0.0303	0.0331	0.0317	0.0372	0.0284	0.0277	0.0381
Ca	3.0757	3.1833	3.1356	2.8529	2.8666	3.0881	3.1360	3.1948	3.1240	3.1918	3.1494	3.1608
Na	1.0295	0.9790	1.1092	1.1751	1.2569	1.0551	0.9647	1.0085	0.8956	1.0038	1.0393	0.8950
K	0.0563	0.0345	0.0418	0.0450	0.0557	0.0344	0.0309	0.0784	0.0331	0.0241	0.0319	0.0295
Total	20.1192	20.1339	20.1727	20.0245	20.1285	20.1047	20.0700	20.1722	20.0519	20.1398	20.1455	20.0460
n	3	4	5	3	4	4	6	5	5	5	4	6
An	0.7391	0.7585	0.7315	0.7005	0.6859	0.7392	0.7590	0.7462	0.7708	0.7564	0.7462	0.7737
standard deviation:												
wt.%												
SiO2	0.46	0.75	1.09	0.99	0.77	0.29	0.37	0.61	0.83	0.47	0.46	0.27
Al2O3	0.11	0.35	0.74	0.47	0.33	0.18	0.42	0.34	0.65	0.31	0.44	0.23
FeO	0.02	0.02	0.06	0.04	0.01	0.02	0.06	0.02	0.04	0.02	0.02	0.04
CaO	0.23	0.44	0.90	0.61	0.36	0.16	0.36	0.40	0.66	0.36	0.27	0.19
Na2O	0.09	0.25	0.47	0.34	0.22	0.09	0.17	0.25	0.38	0.19	0.16	0.13
K2O	0.14	0.03	0.06	0.05	0.03	0.00	0.02	0.25	0.04	0.02	0.01	0.01

Sample:	181.70	194.74	208.15	212.25	212.93	212.95	213.18	214.05	214.07	214.25	219.22	220.17
Depth in NG-sequence in m:	181.70	194.74	208.15	212.25	212.93	212.95	213.18	214.05	214.07	214.25	219.22	220.17
Habit:	cum	cum	cum	cum	cum	cum	cum	cum	pcum	pcum	pcum	pcum
wt.%												
SiO2	48.43	48.09	47.86	48.11	47.37	47.24	47.80	48.50	48.81	50.14	50.65	53.22
Al2O3	32.09	32.42	33.13	32.08	32.85	33.17	32.49	32.45	31.58	31.74	31.08	29.66
FeO	0.24	0.21	0.24	0.37	0.34	0.28	0.27	0.22	0.19	0.21	0.19	0.21
CaO	15.84	15.86	16.83	16.21	17.10	17.06	16.43	16.00	15.00	14.91	14.53	12.46
Na2O	2.70	2.53	2.44	2.44	2.35	2.35	2.42	2.54	2.84	3.09	3.76	4.46
K2O	0.15	0.20	0.12	0.15	0.13	0.13	0.13	0.17	0.21	0.18	0.26	0.28
Total	99.44	99.32	100.62	99.36	100.14	100.23	99.53	99.89	98.63	100.27	100.47	100.29
cations (based on 32 oxygens):												
Si	8.9346	8.8824	8.7536	8.8950	8.7225	8.6891	8.8264	8.9055	9.0510	9.1330	9.2206	9.6269
Al	6.9768	7.0571	7.1417	6.9916	7.1300	7.1888	7.0707	7.0231	6.9010	6.8158	6.6682	6.3239
Fe	0.0363	0.0328	0.0372	0.0566	0.0522	0.0431	0.0420	0.0335	0.0295	0.0323	0.0283	0.0312
Ca	3.1299	3.1397	3.2975	3.2106	3.3730	3.3614	3.2503	3.1477	2.9809	2.9128	2.8349	2.4156
Na	0.9646	0.9071	0.8638	0.8741	0.8391	0.8384	0.8665	0.9054	1.0221	1.0881	1.3261	1.5632
K	0.0344	0.0473	0.0272	0.0364	0.0304	0.0298	0.0313	0.0409	0.0499	0.0424	0.0605	0.0637
Total	20.0765	20.0663	20.1210	20.0644	20.1473	20.1506	20.0872	20.0560	20.0345	20.0243	20.1386	20.0246
n	5	5	4	4	5	4	6	5	5	3	6	4
An	0.7580	0.7669	0.7873	0.7791	0.7950	0.7947	0.7835	0.7689	0.7355	0.7204	0.6715	0.5975
standard deviation:												
wt.%												
SiO2	0.19	0.17	0.30	0.38	0.70	0.26	0.56	0.40	0.65	1.79	1.30	0.53
Al2O3	0.08	0.19	0.17	0.18	0.42	0.23	0.27	0.22	0.52	0.97	0.90	0.26
FeO	0.02	0.02	0.02	0.02	0.05	0.01	0.05	0.02	0.02	0.04	0.04	0.02
CaO	0.07	0.13	0.12	0.29	0.33	0.28	0.33	0.31	0.56	1.25	1.16	0.30
Na2O	0.02	0.10	0.07	0.15	0.07	0.08	0.17	0.15	0.32	0.63	0.59	0.17
K2O	0.01	0.14	0.01	0.02	0.02	0.01	0.02	0.02	0.05	0.02	0.07	0.01

Sample:	221.30	232.00	248.25	255.20	260.05
Depth in NG-sequence in m:	221.30	232.00	248.25	255.20	260.05
Habit:	pcum	pcum	pcum	pcum	pcum
wt.%					
SiO2	50.76	53.91	50.56	49.24	50.87
Al2O3	30.44	29.31	30.99	31.37	30.07
FeO	0.20	0.14	0.22	0.20	0.17
CaO	14.02	12.01	14.24	15.27	13.53
Na2O	3.60	4.66	3.86	3.45	3.87
K2O	0.18	0.32	0.28	0.18	0.18
Total	99.20	100.36	100.15	99.69	98.70
cations (based on 32 oxygens):					
Si	9.3289	9.7286	9.2307	9.0602	9.3874
Al	6.5924	6.2316	6.6690	6.8023	6.5399
Fe	0.0302	0.0214	0.0341	0.0305	0.0258
Ca	2.7608	2.3211	2.7851	3.0100	2.6757
Na	1.2834	1.6319	1.3671	1.2291	1.3853
K	0.0416	0.0739	0.0649	0.0422	0.0426
Total	20.0373	20.0085	20.1508	20.1743	20.0567
n	4	3	4	3	5
An	0.6757	0.5764	0.6604	0.7031	0.6520
standard deviation:					
wt.%					
SiO2	1.51	0.28	0.84	0.46	0.45
Al2O3	1.48	0.51	0.55	0.20	0.55
FeO	0.04	0.02	0.09	0.02	0.02
CaO	1.26	0.67	0.81	0.09	0.46
Na2O	0.66	0.29	0.38	0.07	0.25
K2O	0.04	0.04	0.06	0.02	0.03

MICROPROBE DATA: Composition of plagioclase in the NG-sequence (NG1-borehole)

Sample:	17.00	25.00	29.80	35.00	46.25	55.40	56.00	65.19	74.45	79.75	84.90	89.55
Depth in NG-sequence in m:	267.00	275.00	279.80	285.00	296.25	305.40	306.00	315.19	324.45	329.75	334.90	339.55
Habit: all postcumulus												
wt.%												
SiO2	51.24	53.33	55.00	51.90	52.37	50.40	58.55	52.37	52.91	51.35	52.95	51.45
Al2O3	30.81	29.60	28.60	30.38	31.26	31.01	26.26	31.26	30.12	30.84	30.35	31.63
FeO	0.23	0.18	0.24	0.24	0.21	0.29	0.11	0.21	0.17	0.23	0.21	0.22
CaO	14.07	12.64	11.10	13.38	13.34	14.76	8.00	13.34	12.38	13.95	12.75	14.07
Na2O	3.39	4.27	5.08	3.75	3.87	3.25	6.97	3.87	4.53	3.37	4.54	3.58
K2O	0.03	0.02	0.06	0.01	0.03	0.02	0.06	0.03	0.03	0.03	0.02	0.02
Total	99.77	100.03	100.08	99.65	101.07	99.72	99.95	101.07	100.14	99.77	100.81	100.97
cations (based on 32 oxygens):												
Si	9.3373	9.6505	9.9086	9.4531	9.4028	9.2245	10.4685	9.4028	9.5715	9.3547	9.5309	9.2717
Al	6.6243	6.3135	6.0730	6.5218	6.6137	6.6906	5.5332	6.6137	6.4217	6.6220	6.4371	6.7191
Fe	0.0351	0.0274	0.0357	0.0363	0.0308	0.0437	0.0164	0.0308	0.0263	0.0344	0.0314	0.0327
Ca	2.7513	2.4511	2.1430	2.6113	2.5661	2.8938	1.5320	2.5661	2.4009	2.7240	2.4579	2.7183
Na	1.1984	1.4959	1.7749	1.3241	1.3475	1.1511	2.4166	1.3475	1.5886	1.1908	1.5827	1.2485
K	0.0065	0.0045	0.0143	0.0030	0.0065	0.0041	0.0131	0.0065	0.0058	0.0077	0.0034	0.0054
Total	19.9530	19.9429	19.9495	19.9495	19.9673	20.0078	19.9798	19.9673	20.0149	19.9336	20.0436	19.9957
n	21	5	15	5	5	5	7	6	5	11	6	4
An	0.6954	0.6203	0.5450	0.6630	0.6546	0.7147	0.3867	0.6546	0.6009	0.6945	0.6078	0.6843
standard deviation:												
wt.%												
SiO2	1.16	1.75	0.59	1.17	0.55	0.62	0.66	0.55	1.28	1.07	0.40	1.10
Al2O3	0.73	1.23	0.44	0.69	0.50	0.41	0.62	0.50	0.82	0.64	0.29	0.70
FeO	0.07	0.03	0.05	0.03	0.05	0.03	0.02	0.05	0.03	0.02	0.03	0.05
CaO	0.81	1.40	0.51	0.86	0.57	0.47	0.57	0.57	0.93	0.78	0.25	0.77
Na2O	0.42	0.80	0.27	0.45	0.30	0.27	0.32	0.30	0.50	0.39	0.16	0.46
K2O	0.01	0.01	0.01	0.01	0.02	0.01	0.02	0.02	0.01	0.01	0.00	0.01

Sample:	94.60	105.45	110.52	119.90	130.60	146.50	152.20	158.20	163.27	173.37	183.70	191.00
Depth in NG-sequence in m:	344.60	355.45	360.52	369.90	380.60	396.50	402.20	408.20	413.27	423.37	433.70	441.00
Habit: all postcumulus												
wt.%												
SiO2	51.79	58.44	61.58	55.39	52.04	52.55	52.53	52.33	53.62	53.03	53.24	54.83
Al2O3	31.46	26.48	25.40	29.25	30.30	30.68	30.70	30.66	29.14	31.02	30.67	28.54
FeO	0.21	0.13	0.10	0.34	0.26	0.19	0.18	0.16	0.09	0.27	0.17	0.20
CaO	13.67	8.23	6.52	10.73	12.81	13.06	13.01	13.06	12.27	12.86	12.93	11.28
Na2O	3.74	6.89	7.76	5.22	4.07	4.11	4.34	4.12	4.69	4.13	4.21	5.06
K2O	0.01	0.05	0.05	0.04	0.03	0.02	0.01	0.03	0.03	0.03	0.03	0.05
Total	100.87	100.22	101.40	100.96	99.51	100.61	100.87	100.35	99.84	101.33	101.25	99.97
cations (based on 32 oxygens):												
Si	9.3297	10.4289	10.7875	9.8821	9.4865	9.4747	9.4626	9.4610	9.7163	9.4828	9.5293	9.8947
Al	6.6781	5.5679	5.2432	6.1514	6.5093	6.5191	6.5183	6.5330	6.2273	6.5402	6.4688	6.0719
Fe	0.0322	0.0197	0.0140	0.0504	0.0393	0.0291	0.0267	0.0242	0.0143	0.0397	0.0250	0.0299
Ca	2.6378	1.5726	1.2231	2.0514	2.5021	2.5226	2.5119	2.5296	2.3860	2.4655	2.4801	2.1822
Na	1.3055	2.3842	2.6347	1.8058	1.4371	1.4358	1.5154	1.4422	1.6455	1.4307	1.4598	1.7702
K	0.0015	0.0121	0.0115	0.0081	0.0062	0.0049	0.0023	0.0073	0.0069	0.0071	0.0067	0.0112
Total	19.9847	19.9854	19.9140	19.9492	19.9805	19.9861	20.0372	19.9973	19.9963	19.9660	19.9696	19.9601
n	2	4	2	1	6	5	3	5	6	2	4	6
An	0.6687	0.3962	0.3161	0.5307	0.6342	0.6365	0.6234	0.6357	0.5908	0.6316	0.6284	0.5505
standard deviation:												
wt.%												
SiO2	0.63	0.58	0.28		0.79	1.23	0.97	0.28	2.75	2.16	0.41	1.27
Al2O3	0.53	0.63	0.12		0.57	0.94	0.50	0.15	1.85	1.39	0.33	0.75
FeO	0.02	0.03	0.01		0.04	0.04	0.03	0.02	0.03	0.01	0.02	0.06
CaO	0.60	0.70	0.07		0.68	1.07	0.63	0.10	2.21	1.64	0.45	0.89
Na2O	0.23	0.37	0.03		0.39	0.55	0.35	0.06	1.28	0.99	0.26	0.50
K2O	0.01	0.01	0.01		0.01	0.00	0.00	0.01	0.01	0.00	0.01	0.01

Sample:	197.50	204.50	210.30	225.90	242.15	242.70	257.10	257.70	262.17	277.25	282.25	292.30
Depth in NG-sequence in m:	447.50	454.50	460.30	475.90	492.15	492.70	507.10	507.70	512.17	527.25	532.25	542.30
Habit: all postcumulus												
wt.%												
SiO2	51.95	51.61	52.23	50.73	52.99	54.34	52.02	53.69	50.00	52.87	52.54	52.85
Al2O3	31.26	31.24	30.89	31.40	29.86	28.91	31.07	29.43	31.78	30.43	30.96	30.10
FeO	0.21	0.19	0.15	0.17	0.21	0.15	0.23	0.13	0.12	0.32	0.24	0.30
CaO	13.42	13.32	13.09	14.10	12.75	11.76	13.00	12.30	14.39	12.71	13.19	12.45
Na2O	3.76	3.86	3.99	3.39	4.12	4.73	3.98	4.35	3.28	4.22	3.97	4.45
K2O	0.03	0.02	0.02	0.02	0.03	0.03	0.00	0.02	0.01	0.03	0.02	0.02
Total	100.62	100.24	100.37	99.81	99.97	99.92	100.31	99.91	99.58	100.57	100.92	100.18
cations (based on 32 oxygens):												
Si	9.3725	9.3477	9.4373	9.2488	9.6004	9.8179	9.4073	9.7101	9.1485	9.5298	9.4445	9.5638
Al	6.6470	6.6731	6.5786	6.7471	6.3767	6.1558	6.6219	6.2743	6.8538	6.4652	6.5599	6.4195
Fe	0.0317	0.0292	0.0224	0.0261	0.0317	0.0225	0.0354	0.0200	0.0183	0.0477	0.0355	0.0451
Ca	2.5931	2.5869	2.5354	2.7541	2.4756	2.2771	2.5191	2.3845	2.8207	2.4551	2.5405	2.4148
Na	1.3136	1.3529	1.3959	1.1986	1.4467	1.6559	1.3951	1.5234	1.1634	1.4729	1.3849	1.5609
K	0.0060	0.0048	0.0038	0.0045	0.0070	0.0058	0.0007	0.0041	0.0033	0.0067	0.0053	0.0057
Total	19.9638	19.9546	19.9733	19.9793	19.9381	19.9350	19.9796	19.9165	20.0080	19.9774	19.9706	20.0098
n	5	8	6	5	6	6	3	8	3	6	2	6
An	0.6628	0.6558	0.6443	0.6960	0.6300	0.5781	0.6435	0.6095	0.7074	0.6240	0.6463	0.6065
standard deviation:												
wt.%												
SiO2	0.37	2.11	1.35	0.57	0.60	0.56	0.38	1.87	0.73	0.82	0.25	0.86
Al2O3	0.24	1.44	0.89	0.45	0.44	0.36	0.09	1.20	0.25	0.68	0.29	0.61
FeO	0.02	0.06	0.04	0.02	0.03	0.03	0.02	0.02	0.01	0.11	0.03	0.07
CaO	0.38	1.53	1.10	0.58	0.51	0.42	0.20	1.45	0.41	0.89	0.26	0.51
Na2O	0.12	0.92	0.66	0.27	0.25	0.22	0.13	0.80	0.22	0.42	0.13	0.26
K2O	0.01	0.01	0.01	0.01	0.01	0.00	0.00	0.01	0.01	0.00	0.00	0.01

Sample:	302.00	312.10	327.45	331.65	331.80	334.30	338.45	348.20	353.40	364.25	374.35	380.35
Depth in NG-sequence in m:	552.00	562.10	577.45	581.65	581.80	584.30	588.45	598.20	603.40	614.25	624.35	630.35
Habit: all postcumulus												
wt.%												
SiO2	53.66	54.46	54.62	53.04	52.73	52.73	53.33	53.03	55.71	55.60	52.93	53.52
Al2O3	30.28	29.67	29.16	29.85	30.27	30.39	30.59	30.49	28.47	28.43	30.33	29.70
FeO	0.22	0.23	0.19	0.11	0.28	0.23	0.23	0.23	0.14	0.20	0.12	0.16
CaO	12.23	11.56	11.23	12.58	12.70	11.94	13.00	12.47	10.28	10.40	12.46	11.85
Na2O	4.54	4.96	5.03	4.56	4.38	4.55	4.27	4.41	5.89	5.52	4.20	4.72
K2O	0.02	0.02	0.02	0.28	0.29	0.02	0.03	0.03	0.02	0.03	0.03	0.02
Total	100.95	100.89	100.25	100.42	100.64	99.86	101.43	100.65	100.52	100.18	100.07	99.96
cations (based on 32 oxygens):												
Si	9.6164	9.7480	9.8263	9.5876	9.5200	9.5545	9.5333	9.5439	9.9808	9.9866	9.5688	9.6780
Al	6.3967	6.2607	6.1830	6.3596	6.4412	6.4908	6.4451	6.4680	6.0121	6.0204	6.4610	6.3299
Fe	0.0336	0.0339	0.0280	0.0168	0.0424	0.0348	0.0339	0.0343	0.0205	0.0296	0.0187	0.0239
Ca	2.3482	2.2174	2.1654	2.4370	2.4566	2.3188	2.4894	2.4041	1.9746	2.0023	2.4126	2.2966
Na	1.5765	1.7198	1.7536	1.5994	1.5318	1.5973	1.4784	1.5378	2.0452	1.9210	1.4731	1.6527
K	0.0041	0.0036	0.0056	0.0636	0.0669	0.0051	0.0066	0.0059	0.0052	0.0075	0.0061	0.0046
Total	19.9755	19.9834	19.9619	20.0641	20.0588	20.0013	19.9867	19.9940	20.0384	19.9674	19.9403	19.9857
n	2	2	6	3	3	5	2	2	5	6	5	5
An	0.5977	0.5627	0.5517	0.5944	0.6058	0.5914	0.6264	0.6090	0.4906	0.5094	0.6199	0.5808
standard deviation:												
wt.%												
SiO2	0.35	1.27	0.84	0.44	0.28	0.73	0.31	0.30	1.29	1.61	0.87	0.45
Al2O3	0.13	0.70	0.57	0.34	0.12	0.37	0.11	0.10	0.84	1.00	0.65	0.18
FeO	0.04	0.01	0.06	0.02	0.01	0.08	0.04	0.00	0.05	0.07	0.04	0.04
CaO	0.20	0.85	0.63	0.35	0.17	0.49	0.32	0.53	0.92	1.26	0.72	0.40
Na2O	0.10	0.49	0.36	0.19	0.04	0.29	0.08	0.14	0.56	0.72	0.38	0.24
K2O	0.00	0.00	0.01	0.02	0.04	0.01	0.00	0.00	0.01	0.01	0.01	0.01

Sample:	406.40	414.85	455.65	459.70	469.40	475.10	476.40	486.55	492.15	496.40	496.43	500.50
Depth in												
NG-sequence in m:	656.40	664.85	705.65	709.70	719.40	725.10	726.40	736.55	742.15	746.40	746.43	750.50
Habit: all postcumulus												
wt.%												
SiO2	53.98	56.41	54.04	52.97	57.28	55.32	53.60	54.83	56.51	53.51	65.53	57.88
Al2O3	30.08	27.28	29.22	29.59	27.15	28.91	29.08	28.93	27.19	29.13	19.44	27.19
FeO	0.13	0.14	0.11	0.12	0.10	0.19	0.13	0.11	0.12	0.15	0.05	0.15
CaO	11.98	10.05	12.09	12.68	9.14	11.19	12.18	11.05	9.90	11.60	0.90	8.72
Na2O	4.67	5.92	4.75	4.38	6.37	5.03	4.41	5.18	5.97	5.00	4.75	6.47
K2O	0.02	0.01	0.03	0.03	0.02	0.12	0.03	0.02	0.02	0.02	9.47	0.04
Total	100.87	99.81	100.24	99.78	100.07	100.76	99.43	100.12	99.72	99.40	100.13	100.44
cations (based on 32 oxygens):												
Si	9.6681	10.1587	9.7473	9.6199	10.2607	9.8977	9.7415	9.8693	10.1802	9.7329	11.8425	10.3121
Al	6.3530	5.7922	6.2125	6.3333	5.7324	6.0965	6.2298	6.1380	5.7764	6.2447	4.1400	5.7111
Fe	0.0195	0.0214	0.0162	0.0187	0.0152	0.0281	0.0193	0.0164	0.0174	0.0225	0.0069	0.0227
Ca	2.3023	1.9394	2.3364	2.4672	1.7559	2.1456	2.3726	2.1323	1.9129	2.2616	0.1748	1.6654
Na	1.6205	2.0650	1.6606	1.5415	2.2127	1.7458	1.5550	1.8068	2.0835	1.7608	1.6642	2.2339
K	0.0046	0.0019	0.0076	0.0074	0.0050	0.0264	0.0060	0.0047	0.0056	0.0053	2.1825	0.0082
Total	19.9679	19.9787	19.9805	19.9879	19.9819	19.9401	19.9242	19.9675	19.9761	20.0277	20.0109	19.9534
n	6	6	8	6	8	3	4	6	6	6	2	6
An	0.5862	0.4841	0.5834	0.6143	0.4419	0.5476	0.6032	0.5407	0.4780	0.5615	0.0435	0.4262
standard deviation:												
wt.%												
SiO2	2.26	1.16	0.58	0.13	1.99	0.19	0.20	1.34	2.49	1.18	0.16	2.33
Al2O3	1.43	0.72	0.44	0.11	1.60	0.31	0.22	0.98	1.74	0.89	0.01	1.67
FeO	0.02	0.05	0.03	0.02	0.03	0.08	0.01	0.05	0.03	0.03	0.01	0.10
CaO	1.72	0.83	0.44	0.12	1.49	0.29	0.18	1.07	1.95	1.03	0.01	1.87
Na2O	0.94	0.50	0.25	0.03	0.87	0.35	0.11	0.61	1.10	0.64	0.06	0.96
K2O	0.01	0.01	0.01	0.01	0.01	0.02	0.00	0.01	0.01	0.01	0.00	0.01

Sample:	519.26	523.90	523.95	523.96	532.14	536.95	553.33	569.20	581.00	586.00	589.60	595.05
Depth in												
NG-sequence in m:	769.26	773.90	773.95	773.96	782.14	786.95	803.33	819.20	831.00	836.00	839.60	845.05
Habit: all postcumulus												
wt.%												
SiO2	56.98	54.53	58.70	53.90	54.45	54.47	52.97	54.36	54.84	54.91	52.91	54.55
Al2O3	26.83	28.88	26.27	29.87	28.69	29.04	29.80	29.47	28.57	28.58	29.70	28.73
FeO	0.12	0.12	0.17	0.10	0.10	0.18	0.10	0.16	0.15	0.13	0.14	0.13
CaO	9.06	11.53	8.24	12.32	11.80	11.56	12.80	11.57	11.44	11.30	12.75	10.76
Na2O	5.30	4.83	6.99	4.71	4.87	4.81	4.09	4.90	4.81	5.07	4.18	5.35
K2O	1.60	0.03	0.38	0.14	0.04	0.03	0.02	0.03	0.05	0.04	0.02	0.03
Total	99.87	99.92	100.74	101.04	99.95	100.10	99.78	100.50	99.85	100.04	99.70	99.55
cations (based on 32 oxygens):												
Si	10.2797	9.8430	10.4442	9.6606	9.8385	9.8194	9.6090	9.7653	9.9000	9.8987	9.6090	9.8763
Al	5.7067	6.1443	5.5110	6.3100	6.1102	6.1712	6.3711	6.2404	6.0788	6.0727	6.3602	6.1319
Fe	0.0175	0.0184	0.0254	0.0148	0.0156	0.0265	0.0157	0.0247	0.0221	0.0189	0.0206	0.0192
Ca	1.7533	2.2307	1.5725	2.3650	2.2854	2.2331	2.4890	2.2273	2.2130	2.1836	2.4831	2.0887
Na	1.8507	1.6904	2.4092	1.6358	1.7052	1.6823	1.4364	1.7058	1.6824	1.7726	1.4703	1.8772
K	0.3687	0.0069	0.0852	0.0321	0.0084	0.0071	0.0051	0.0077	0.0112	0.0093	0.0056	0.0063
Total	19.9766	19.9336	20.0475	20.0183	19.9633	19.9397	19.9262	19.9712	19.9074	19.9558	19.9488	19.9996
n	6	11	3	4	8	6	6	6	9	5	7	6
An	0.4413	0.5679	0.3867	0.5864	0.5715	0.5693	0.6333	0.5652	0.5665	0.5506	0.6272	0.5258
standard deviation:												
wt.%												
SiO2	4.13	1.47	1.76	0.14	1.26	0.44	1.23	1.02	1.48	0.61	1.98	1.41
Al2O3	3.41	1.01	1.00	0.07	0.89	0.26	0.87	0.62	0.97	0.45	1.32	0.87
FeO	0.04	0.03	0.07	0.04	0.02	0.04	0.02	0.05	0.02	0.02	0.04	0.05
CaO	3.82	1.25	1.20	0.05	1.08	0.30	1.02	0.81	1.06	0.56	1.62	1.02
Na2O	0.71	0.76	0.75	0.05	0.56	0.16	0.63	0.37	0.51	0.31	0.91	0.61
K2O	3.52	0.01	0.04	0.05	0.01	0.00	0.01	0.01	0.01	0.01	0.01	0.01

Sample:	603.10	609.47	609.50	614.76	619.85	624.70	639.95	645.17	655.10	660.40	675.25	685.40
Depth in NG-sequence in m:	853.10	859.47	859.50	864.76	869.85	874.70	889.95	895.17	905.10	910.40	925.25	935.40
Habit: all postcumulus												
wt.%												
SiO2	54.14	56.12	51.29	53.40	54.59	53.61	53.50	55.18	54.81	56.69	53.92	52.91
Al2O3	29.13	27.95	30.91	29.83	28.93	29.87	29.86	28.58	29.29	28.01	29.49	30.33
FeO	0.14	0.13	0.12	0.16	0.11	0.13	0.18	0.16	0.16	0.11	0.12	0.18
CaO	11.74	10.48	13.96	12.48	11.87	12.12	12.05	10.58	11.10	9.73	11.63	12.36
Na2O	4.75	5.46	3.67	4.26	4.78	4.57	4.56	5.55	5.21	6.02	5.05	4.54
K2O	0.03	0.02	0.10	0.02	0.03	0.03	0.02	0.02	0.04	0.04	0.03	0.03
Total	99.93	100.17	100.06	100.14	100.32	100.33	100.18	100.07	100.60	100.60	100.24	100.34
cations (based on 32 oxygens):												
Si	9.7825	10.0710	9.3306	9.6439	9.8262	9.6612	9.6560	9.9330	9.8254	10.1171	9.7231	9.5525
Al	6.2037	5.9124	6.6276	6.3511	6.1360	6.3444	6.3530	6.0650	6.1891	5.8946	6.2687	6.4537
Fe	0.0211	0.0200	0.0183	0.0236	0.0171	0.0192	0.0276	0.0238	0.0233	0.0168	0.0184	0.0275
Ca	2.2740	2.0167	2.7197	2.4146	2.2889	2.3405	2.3308	2.0417	2.1329	1.8627	2.2465	2.3904
Na	1.6610	1.8999	1.2950	1.4896	1.6679	1.5953	1.5956	1.9367	1.8102	2.0804	1.7649	1.5867
K	0.0075	0.0053	0.0236	0.0050	0.0071	0.0073	0.0045	0.0050	0.0082	0.0084	0.0069	0.0062
Total	19.9498	19.9254	20.0149	19.9278	19.9433	19.9679	19.9676	20.0053	19.9892	19.9799	20.0285	20.0171
n	7	7	3	7	2	6	5	6	5	6	6	5
An	0.5768	0.5142	0.6735	0.6177	0.5774	0.5936	0.5929	0.5126	0.5398	0.4714	0.5591	0.6001
standard deviation:												
wt.%												
SiO2	0.78	1.28	0.48	1.23	0.01	0.55	0.96	1.42	1.35	1.73	0.71	0.97
Al2O3	0.49	0.75	0.44	0.85	0.07	0.37	0.63	1.01	0.72	0.94	0.57	0.61
FeO	0.02	0.03	0.00	0.04	0.01	0.05	0.03	0.09	0.08	0.03	0.06	0.08
CaO	0.70	0.93	0.58	0.98	0.17	0.43	0.72	1.15	0.91	1.14	0.61	0.75
Na2O	0.42	0.50	0.24	0.55	0.00	0.26	0.36	0.64	0.56	0.71	0.36	0.42
K2O	0.01	0.01	0.02	0.01	0.00	0.01	0.01	0.01	0.00	0.01	0.00	0.01

Sample:	690.90	695.50	706.90	711.60	720.15	730.38	739.80	744.70
Depth in NG-sequence in m:	940.90	945.50	956.90	961.60	970.15	980.38	989.80	994.70
Habit: all postcumulus								
wt.%								
SiO2	53.51	53.25	52.57	53.43	55.98	52.38	55.13	54.03
Al2O3	30.03	29.55	30.09	29.75	28.16	30.93	28.05	29.23
FeO	0.14	0.14	0.16	0.21	0.17	0.15	0.11	0.16
CaO	11.84	12.57	12.57	11.86	9.64	12.94	10.86	11.34
Na2O	4.64	4.36	4.37	4.72	5.78	4.03	5.50	5.11
K2O	0.02	0.03	0.04	0.04	0.03	0.02	0.03	0.02
Total	100.19	99.89	99.80	100.00	99.75	100.45	99.68	99.89
cations (based on 32 oxygens):								
Si	9.6480	9.6488	9.5475	9.6628	10.0730	9.4512	9.9712	9.7692
Al	6.3854	6.3139	6.4410	6.3428	5.9724	6.5783	5.9797	6.2281
Fe	0.0217	0.0206	0.0244	0.0315	0.0259	0.0224	0.0166	0.0239
Ca	2.2911	2.4426	2.4458	2.2976	1.8589	2.5013	2.1043	2.1979
Na	1.6210	1.5305	1.5379	1.6539	2.0153	1.4083	1.9271	1.7909
K	0.0051	0.0061	0.0084	0.0083	0.0060	0.0046	0.0071	0.0044
Total	19.9724	19.9625	20.0051	19.9969	19.9514	19.9662	20.0060	20.0144
n	6	9	5	7	6	6	2	6
An	0.5849	0.6139	0.6126	0.5802	0.4791	0.6390	0.5211	0.5504
standard deviation:								
wt.%								
SiO2	2.56	2.12	0.26	0.75	1.16	0.69	0.01	1.17
Al2O3	1.70	1.40	0.26	0.34	0.88	0.30	0.03	0.94
FeO	0.05	0.04	0.02	0.05	0.09	0.03	0.01	0.03
CaO	1.92	1.68	0.23	0.30	0.80	0.42	0.09	0.93
Na2O	1.11	0.95	0.09	0.18	0.54	0.26	0.07	0.55
K2O	0.01	0.01	0.01	0.01	0.00	0.01	0.01	0.01

MICROPROBE DATA: Composition of plagioclase in the NG-sequence (NG2-borehole)

Sample:	80.35	91.40	98.00	106.60	115.25	120.40	171.50	180.55	189.40	194.20	200.50	219.90
Depth in NG-sequence in m:	1120.35	1131.40	1138.00	1146.60	1155.25	1160.40	1211.50	1220.55	1229.40	1234.20	1240.50	1259.90
Habit:	pcum	pcum	pcum	pcum	pcum	pcum	pcum	pcum	pcum	pcum	pcum	pcum
wt.%												
SiO2	51.42	57.68	56.48	52.46	53.32	55.45	57.10	54.86	51.86	52.68	53.03	52.87
Al2O3	31.09	26.66	27.98	29.87	29.25	28.17	27.39	28.09	30.49	29.36	29.30	29.21
FeO	0.13	0.15	0.18	0.13	0.19	0.08	0.22	0.17	0.15	0.19	0.10	0.13
CaO	14.46	9.14	10.44	13.42	12.57	10.46	9.43	10.80	13.08	12.46	12.41	12.55
Na2O	3.64	6.43	5.65	4.11	4.55	5.41	6.25	5.49	3.92	4.52	4.81	4.66
K2O	0.12	0.40	0.38	0.29	0.31	0.28	0.34	0.32	0.27	0.31	0.07	0.23
Total	100.87	100.46	101.09	100.27	100.18	99.85	100.73	99.73	99.78	99.52	99.73	99.65
cations (based on 32 oxygens):												
Si	9.2946	10.3180	10.0706	9.5169	9.6633	9.9965	10.1970	9.9398	9.4435	9.6128	9.6445	9.6352
Al	6.6254	5.6198	5.8797	6.3877	6.2471	5.9946	5.7654	5.9985	6.5426	6.3151	6.2808	6.2731
Fe	0.0202	0.0230	0.0265	0.0190	0.0283	0.0128	0.0321	0.0257	0.0227	0.0294	0.0156	0.0194
Ca	2.8021	1.7515	1.9940	2.6094	2.4401	2.0276	1.8051	2.0967	2.5527	2.4367	2.4182	2.4511
Na	1.2732	2.2275	1.9512	1.4446	1.5975	1.8863	2.1627	1.9255	1.3849	1.5985	1.6955	1.6456
K	0.0274	0.0923	0.0865	0.0678	0.0710	0.0634	0.0785	0.0750	0.0625	0.0729	0.0166	0.0533
Total	20.0430	20.0320	20.0085	20.0454	20.0474	19.9811	20.0409	20.0612	20.0089	20.0654	20.0712	20.0777
n	5	7	6	4	4	6	4	3	4	5	4	4
An	0.6830	0.4302	0.4946	0.6331	0.5939	0.5098	0.4461	0.5117	0.6382	0.5931	0.5855	0.5906
standard deviation:												
wt.%												
SiO2	1.78	0.99	1.01	1.12	0.62	3.84	1.08	0.97	0.29	0.97	1.40	0.63
Al2O3	1.17	0.63	0.80	0.67	0.42	2.54	0.64	0.43	0.28	0.76	0.95	0.50
FeO	0.02	0.07	0.09	0.02	0.05	0.03	0.03	0.04	0.05	0.04	0.02	0.02
CaO	1.40	0.64	0.92	0.87	0.54	3.04	0.85	0.62	0.21	0.90	1.19	0.58
Na2O	0.79	0.36	0.57	0.45	0.31	1.67	0.39	0.40	0.16	0.42	0.67	0.31
K2O	0.05	0.07	0.05	0.04	0.07	0.13	0.10	0.02	0.03	0.04	0.02	0.03

Sample:	223.86	242.55	247.82	253.05	269.92	272.40	277.15	294.12	298.80	299.89	299.91	301.10
Depth in NG-sequence in m:	1263.86	1282.55	1287.82	1293.05	1309.92	1312.40	1317.15	1334.12	1338.80	1339.89	1339.91	1341.10
Habit:	pcum	pcum	pcum	pcum	pcum	pcum	pcum	pcum	cum	cum	cum	pcum
wt.%												
SiO2	53.71	51.01	52.37	52.67	52.51	48.10	53.70	55.07	46.75	47.46	47.38	49.01
Al2O3	28.07	30.80	29.70	29.56	29.51	32.22	29.33	27.97	33.21	33.44	33.67	32.21
FeO	0.17	0.14	0.15	0.15	0.20	0.11	0.14	0.14	0.18	0.17	0.29	0.21
CaO	10.40	14.12	12.64	12.34	12.54	15.92	12.05	10.98	18.08	17.43	17.27	16.06
Na2O	5.26	3.73	4.13	4.44	4.42	2.53	4.67	5.45	1.62	1.85	1.82	2.52
K2O	0.25	0.08	0.20	0.29	0.22	0.11	0.27	0.29	0.07	0.08	0.09	0.14
Total	97.87	99.88	99.20	99.45	99.39	98.98	100.16	99.90	99.91	100.44	100.51	100.16
cations (based on 32 oxygens):												
Si	9.8990	9.3071	9.5737	9.6064	9.5892	8.9058	9.7069	9.9589	8.6303	8.6937	8.6715	8.9675
Al	6.1003	6.6238	6.3989	6.3566	6.3534	7.0316	6.2534	5.9625	7.2256	7.2182	7.2622	6.9469
Fe	0.0270	0.0221	0.0222	0.0227	0.0311	0.0167	0.0219	0.0218	0.0271	0.0268	0.0440	0.0328
Ca	2.0557	2.7605	2.4762	2.4120	2.4533	3.1579	2.3368	2.1284	3.5754	3.4212	3.3864	3.1485
Na	1.8776	1.3174	1.4641	1.5680	1.5640	0.9076	1.6325	1.9092	0.5802	0.6555	0.6465	0.8943
K	0.0599	0.0176	0.0476	0.0673	0.0502	0.0250	0.0622	0.0671	0.0167	0.0191	0.0201	0.0324
Total	20.0196	20.0485	19.9827	20.0329	20.0412	20.0447	20.0137	20.0479	20.0553	20.0345	20.0307	20.0224
n	3	4	4	4	6	3	6	4	8	7	4	5
An	0.5148	0.6740	0.6209	0.5960	0.6032	0.7720	0.5796	0.5185	0.8569	0.8353	0.8355	0.7726
standard deviation:												
wt.%												
SiO2	1.79	0.95	0.67	1.49	1.10	0.32	2.87	1.39	0.52	0.28	0.65	0.44
Al2O3	1.11	0.63	0.52	1.05	0.76	0.09	1.97	0.95	0.39	0.30	0.33	0.28
FeO	0.07	0.01	0.03	0.02	0.04	0.01	0.07	0.05	0.06	0.03	0.08	0.03
CaO	1.21	0.81	0.37	1.17	0.87	0.24	2.29	1.17	0.46	0.29	0.49	0.34
Na2O	0.78	0.39	0.30	0.78	0.50	0.15	1.28	0.70	0.21	0.16	0.28	0.19
K2O	0.03	0.02	0.02	0.05	0.05	0.01	0.09	0.05	0.02	0.01	0.03	0.02

Sample:	307.10	320.15	332.35	350.50	358.66	358.76	360.20	360.30	376.65	376.67	387.37	397.68
Depth in NG-sequence in m:	1347.10	1360.15	1372.35	1390.50	1398.66	1398.76	1400.20	1400.30	1416.65	1416.67	1427.37	1437.68
Habit:	pcum	pcum	pcum	pcum	pcum	pcum	pcum	pcum	pcum	pcum	pcum	pcum
wt.%												
SiO2	49.42	52.33	56.27	51.73	50.13	49.43	52.92	55.16	48.62	54.66	51.00	55.58
Al2O3	31.70	29.30	27.94	29.99	31.64	31.74	29.25	28.13	32.68	28.80	30.75	28.42
FeO	0.22	0.15	0.12	0.15	0.19	0.35	0.11	0.13	0.21	0.17	0.22	0.14
CaO	15.64	12.71	10.28	13.43	15.01	15.33	12.28	10.55	16.16	11.44	14.25	10.85
Na2O	2.90	4.50	5.87	4.21	3.20	2.94	4.95	5.65	2.61	5.10	3.67	5.80
K2O	0.12	0.19	0.26	0.09	0.11	0.06	0.07	0.32	0.01	0.19	0.12	0.10
Total	100.01	99.18	100.74	99.61	100.28	99.85	99.59	99.93	100.28	100.35	100.01	100.91
cations (based on 32 oxygens):												
Si	9.0512	9.5850	10.0588	9.4521	9.1340	9.0600	9.6407	9.9626	8.8870	9.8410	9.3012	9.9420
Al	6.8437	6.3269	5.8963	6.4587	6.7963	6.8577	6.2814	5.9913	7.0425	6.1152	6.6106	5.9968
Fe	0.0335	0.0234	0.0181	0.0233	0.0284	0.0543	0.0165	0.0197	0.0327	0.0252	0.0341	0.0211
Ca	3.0704	2.4966	1.9768	2.6283	2.9313	3.0103	2.3978	2.0445	3.1673	2.2098	2.7859	2.0839
Na	1.0282	1.5956	2.0278	1.4897	1.1305	1.0428	1.7479	1.9745	0.9220	1.7766	1.2959	2.0080
K	0.0282	0.0439	0.0583	0.0221	0.0253	0.0150	0.0165	0.0728	0.0022	0.0437	0.0276	0.0239
Total	20.0552	20.0714	20.0361	20.0744	20.0457	20.0401	20.1008	20.0654	20.0538	20.0115	20.0553	20.0756
n	5	5	5	4	5	4	4	5	3	3	3	4
An	0.7440	0.6036	0.4865	0.6348	0.7172	0.7400	0.5761	0.4997	0.7741	0.5483	0.6779	0.5063
standard deviation:												
wt.%												
SiO2	1.05	1.71	4.02	0.51	0.56	1.10	0.78	2.56	1.89	1.94	1.22	2.58
Al2O3	0.41	1.11	2.65	0.45	0.34	0.59	0.40	1.71	1.31	1.07	0.88	1.57
FeO	0.04	0.02	0.02	0.05	0.03	0.40	0.03	0.07	0.05	0.04	0.07	0.02
CaO	0.75	1.40	3.21	0.45	0.38	0.66	0.52	1.95	1.51	1.38	0.99	1.95
Na2O	0.41	0.72	1.84	0.24	0.25	0.44	0.35	1.10	0.92	0.75	0.49	1.18
K2O	0.03	0.03	0.14	0.01	0.01	0.01	0.02	0.12	0.01	0.08	0.03	0.02

Sample:	410.61	420.00	420.10	421.50	421.52	424.44	426.60	428.15	439.40	447.00	451.00	454.45
Depth in NG-sequence in m:	1450.61	1460.00	1460.10	1461.50	1461.52	1464.44	1466.60	1468.15	1479.40	1487.00	1491.00	1494.45
Habit:	pcum	pcum	pcum	pcum	pcum	pcum	pcum	pcum	pcum	pcum	pcum	pcum
wt.%												
SiO2	50.93	50.00	50.30	52.27	50.90	49.79	50.42	60.34	51.41	52.27	58.20	49.51
Al2O3	31.21	31.52	31.63	29.69	30.55	31.27	31.05	24.60	30.85	29.82	26.20	32.30
FeO	0.18	0.19	0.12	0.14	0.17	0.15	0.17	0.15	0.17	0.11	0.10	0.19
CaO	14.39	14.95	15.01	12.99	14.16	14.85	14.88	6.68	14.20	12.93	8.48	15.61
Na2O	3.57	3.46	3.31	4.42	3.89	3.26	3.42	8.05	3.76	4.31	6.89	2.83
K2O	0.07	0.03	0.08	0.19	0.06	0.10	0.06	0.38	0.07	0.17	0.41	0.04
Total	100.36	100.15	100.45	99.69	99.74	99.42	100.00	100.20	100.45	99.60	100.28	100.47
cations (based on 32 oxygens):												
Si	9.2536	9.1293	9.1453	9.5333	9.3110	9.1500	9.2113	10.7557	9.3261	9.5317	10.4099	9.0140
Al	6.6844	6.7812	6.7823	6.3809	6.5863	6.7738	6.6853	5.1700	6.5956	6.4088	5.5299	6.9308
Fe	0.0266	0.0291	0.0181	0.0218	0.0259	0.0230	0.0255	0.0227	0.0255	0.0165	0.0156	0.0288
Ca	2.8023	2.9243	2.9266	2.5372	2.7761	2.9247	2.9115	1.2777	2.7611	2.5259	1.6311	3.0443
Na	1.2574	1.2250	1.1643	1.5620	1.3790	1.1606	1.2103	2.7808	1.3202	1.5233	2.3839	0.9970
K	0.0172	0.0073	0.0181	0.0438	0.0138	0.0227	0.0145	0.0857	0.0153	0.0388	0.0934	0.0084
Total	20.0415	20.0963	20.0548	20.0791	20.0922	20.0547	20.0584	20.0926	20.0438	20.0450	20.0638	20.0233
n	3	4	4	3	3	3	4	6	3	4	5	7
An	0.6874	0.7035	0.7122	0.6124	0.6659	0.7120	0.7039	0.3083	0.6740	0.6179	0.3970	0.7517
standard deviation:												
wt.%												
SiO2	1.44	0.60	2.09	0.38	0.61	1.17	0.43	2.57	0.95	1.08	3.31	1.13
Al2O3	0.86	0.58	1.18	0.52	0.13	0.62	0.42	1.69	0.47	0.87	2.09	0.87
FeO	0.02	0.03	0.03	0.02	0.02	0.02	0.01	0.08	0.06	0.03	0.03	0.03
CaO	1.13	0.68	1.41	0.48	0.29	1.06	0.35	2.10	0.71	1.01	2.50	1.01
Na2O	0.65	0.40	0.83	0.21	0.14	0.50	0.23	1.15	0.43	0.56	1.34	0.43
K2O	0.02	0.02	0.05	0.01	0.02	0.02	0.01	0.12	0.02	0.02	0.19	0.02

Sample:	509.05	520.00	530.95	531.10	550.05	561.35	591.00	591.02	591.10	591.20	591.22	591.30
Depth in												
NG-sequence in m:	1549.05	1560.00	1570.95	1571.10	1590.05	1601.35	1631.00	1631.02	1631.10	1631.20	1631.22	1631.30
Habit:	pcum	pcum	pcum	pcum	pcum	pcum	pcum	pcum	pcum	pcum	pcum	pcum
wt.%												
SiO2	54.80	54.84	51.93	52.25	53.32	55.46	59.69	50.72	51.27	57.81	56.47	54.89
Al2O3	28.38	27.96	30.05	30.14	29.27	27.89	25.46	31.75	30.29	26.52	27.27	28.15
FeO	0.12	0.09	0.12	0.09	0.10	0.13	0.08	0.12	0.11	0.09	0.17	0.10
CaO	11.03	10.68	12.80	13.13	12.40	10.60	7.42	14.74	13.49	8.76	9.44	10.72
Na2O	5.46	5.70	4.38	4.32	4.91	5.84	7.32	3.28	3.93	6.51	6.30	5.76
K2O	0.10	0.07	0.04	0.12	0.07	0.15	0.42	0.13	0.12	0.40	0.04	0.06
Total	99.89	99.34	99.32	100.05	100.08	100.07	100.38	100.74	99.21	100.10	99.69	99.68
cations (based on 32 oxygens):												
Si	9.9048	9.9570	9.4890	9.4896	9.6637	9.9986	10.6255	9.1846	9.4006	10.3582	10.1780	9.9390
Al	6.0456	5.9880	6.4760	6.4522	6.2524	5.9307	5.3416	6.7752	6.5467	5.6056	5.7932	6.0062
Fe	0.0178	0.0143	0.0182	0.0135	0.0159	0.0196	0.0116	0.0187	0.0175	0.0139	0.0256	0.0146
Ca	2.1368	2.0809	2.5104	2.5554	2.4084	2.0502	1.4157	2.8590	2.6501	1.6865	1.8229	2.0799
Na	1.9110	2.0021	1.5505	1.5200	1.7231	2.0387	2.5244	1.1515	1.3953	2.2590	2.2016	2.0225
K	0.0237	0.0156	0.0081	0.0271	0.0161	0.0352	0.0943	0.0293	0.0273	0.0906	0.0100	0.0139
Total	20.0397	20.0578	20.0523	20.0579	20.0797	20.0730	20.0131	20.0182	20.0374	20.0138	20.0312	20.0761
n	4	4	3	4	3	4	3	2	3	3	3	2
An	0.5248	0.5077	0.6169	0.6229	0.5807	0.4971	0.3509	0.7077	0.6507	0.4178	0.4518	0.5053
standard deviation:												
wt.%												
SiO2	0.41	2.34	2.18	0.79	1.11	2.48	1.64	0.57	0.22	2.93	0.61	0.27
Al2O3	0.31	1.35	1.07	0.65	0.76	1.55	1.29	0.30	0.18	1.88	0.40	0.16
FeO	0.05	0.04	0.05	0.01	0.03	0.01	0.01	0.03	0.02	0.02	0.12	0.01
CaO	0.40	1.71	1.44	0.76	0.97	1.81	1.49	0.15	0.16	2.28	0.50	0.07
Na2O	0.24	0.96	0.79	0.41	0.59	1.10	0.74	0.22	0.09	1.19	0.29	0.08
K2O	0.03	0.01	0.01	0.04	0.02	0.07	0.10	0.02	0.05	0.19	0.02	0.01

Sample:	591.32	604.30	604.32	618.25	654.16	678.64	691.95	691.97	702.60	709.10	723.22	738.90
Depth in												
NG-sequence in m:	1631.32	1644.30	1644.32	1658.25	1694.16	1718.64	1731.95	1731.97	1742.60	1749.10	1763.22	1778.90
Habit:	pcum	pcum	pcum	pcum	pcum	pcum	pcum	pcum	pcum	pcum	pcum	pcum
wt.%												
SiO2	51.73	50.01	51.89	56.99	52.31	56.24	58.16	54.82	55.41	56.38	43.22	50.09
Al2O3	30.15	30.60	29.54	26.64	29.57	27.21	26.70	30.81	28.71	27.28	24.06	31.93
FeO	0.15	0.21	0.19	0.16	0.11	0.10	0.10	0.09	0.10	0.06	1.43	0.18
CaO	13.27	14.07	12.72	8.73	12.80	9.79	8.93	13.25	11.21	9.96	26.69	15.21
Na2O	4.18	3.66	4.37	6.42	4.57	6.26	6.54	4.52	5.34	6.34	0.05	3.14
K2O	0.15	0.09	0.15	0.27	0.03	0.21	0.29	0.16	0.14	0.10	0.01	0.05
Total	99.64	98.64	98.85	99.21	99.39	99.81	100.72	103.64	100.90	100.12	95.45	100.60
cations (based on 32 oxygens):												
Si	9.4450	9.2506	9.5328	10.3056	9.5552	10.1479	10.3553	9.6009	9.9081	10.1406	8.7091	9.0990
Al	6.4882	6.6730	6.4019	5.6784	6.3687	5.7855	5.6055	6.3474	6.0522	5.7832	5.7124	6.8369
Fe	0.0229	0.0319	0.0295	0.0237	0.0166	0.0144	0.0145	0.0137	0.0147	0.0088	0.2427	0.0276
Ca	2.5967	2.7902	2.5081	1.6911	2.5077	1.8933	1.7051	2.4765	2.1506	1.9184	5.7605	2.9612
Na	1.4810	1.3126	1.5526	2.2507	1.6168	2.1883	2.2569	1.5388	1.8480	2.2104	0.0182	1.1053
K	0.0352	0.0216	0.0353	0.0620	0.0076	0.0483	0.0662	0.0352	0.0320	0.0232	0.0017	0.0105
Total	20.0689	20.0799	20.0602	20.0116	20.0726	20.0777	20.0036	20.0125	20.0057	20.0846	20.4447	20.0404
n	3	4	4	3	5	4	3	3	4	3	3	3
An	0.6314	0.6765	0.6123	0.4224	0.6069	0.4584	0.4233	0.6114	0.5336	0.4620	0.9966	0.7263
standard deviation:												
wt.%												
SiO2	0.10	1.97	2.67	0.91	2.26	0.40	1.89	3.46	2.08	1.05	0.63	0.72
Al2O3	0.20	1.43	1.52	0.59	1.45	0.21	1.21	3.51	1.24	0.91	0.26	0.41
FeO	0.06	0.04	0.05	0.06	0.02	0.05	0.01	0.02	0.02	0.02	0.99	0.02
CaO	0.23	1.81	2.02	0.60	1.84	0.25	1.36	3.54	1.83	1.16	0.83	0.52
Na2O	0.14	1.02	1.16	0.43	1.03	0.10	0.71	1.70	0.94	0.68	0.03	0.29
K2O	0.07	0.04	0.06	0.06	0.01	0.02	0.10	0.08	0.07	0.04	0.00	0.01

Sample:	739.10	743.62	754.00	762.27	763.45	772.36	773.60	773.70	773.72
Depth in									
MG-sequence in m:	1779.10	1783.62	1794.00	1802.27	1803.45	1812.36	1813.60	1813.70	1813.72
Habit:	pcum	pcum	pcum	pcum	pcum	pcum	cum	pcum	cum
wt.%									
SiO2	50.94	52.07	53.85	58.38	53.94	54.91	53.55	51.10	55.30
Al2O3	31.02	30.41	29.10	27.06	29.21	28.80	29.16	31.47	28.40
FeO	0.11	0.11	0.15	0.14	0.23	0.08	0.13	0.24	0.17
CaO	14.48	13.82	12.04	9.32	12.12	11.20	11.98	14.33	10.74
Na2O	3.58	3.79	4.91	6.67	5.11	5.46	4.80	3.47	5.47
K2O	0.17	0.19	0.25	0.41	0.08	0.09	0.28	0.16	0.22
Total	100.31	100.38	100.29	101.99	100.69	100.54	99.90	100.78	100.30
cations (based on 32 oxygens):									
Si	9.2671	9.4341	9.7291	10.2932	9.7128	9.8628	9.7127	9.2453	9.9470
Al	6.6505	6.4962	6.1994	5.6284	6.2003	6.0974	6.2341	6.7117	6.0214
Fe	0.0173	0.0163	0.0222	0.0211	0.0348	0.0120	0.0204	0.0364	0.0249
Ca	2.8213	2.6846	2.3332	1.7656	2.3389	2.1557	2.3280	2.7784	2.0700
Na	1.2628	1.3300	1.7180	2.2774	1.7828	1.9002	1.6855	1.2174	1.9077
K	0.0404	0.0434	0.0565	0.0914	0.0178	0.0209	0.0644	0.0364	0.0503
Total	20.0592	20.0045	20.0584	20.0770	20.0874	20.0491	20.0452	20.0256	20.0213
n	5	6	8	6	3	3	4	6	4
An	0.6840	0.6616	0.5680	0.4270	0.5650	0.5288	0.5709	0.6891	0.5139
standard deviation:									
wt.%									
SiO2	0.74	1.62	2.46	2.72	1.28	1.42	0.93	0.89	0.48
Al2O3	0.62	1.11	1.60	0.82	0.83	1.05	0.58	0.61	0.52
FeO	0.03	0.02	0.03	0.08	0.01	0.01	0.02	0.06	0.02
CaO	0.82	1.30	1.92	0.71	1.04	1.19	0.71	0.90	0.49
Na2O	0.45	0.74	1.05	0.62	0.67	0.71	0.37	0.42	0.31
K2O	0.04	0.07	0.08	0.09	0.02	0.00	0.04	0.11	0.02

MICROPROBE DATA: Composition of plagioclase in the KD-sequence

Sample:	28.38	50.05	50.50	61.20	71.10	73.10	78.00	82.60	82.70	88.40	89.70	90.30	96.30
Habit:	pcum	pcum	pcum	pcum	pcum	pcum	pcum	pcum	pcum	pcum	pcum	pcum	pcum
wt.%													
SiO2	48.49	48.50	46.49	48.10	49.00	48.30	49.09	48.35	47.32	48.11	47.94	59.15	47.33
Al2O3	32.61	31.84	32.84	32.03	32.12	31.96	32.13	32.43	32.43	32.80	32.88	25.81	33.11
FeO	0.22	0.21	0.34	0.36	0.15	0.12	0.21	0.16	0.14	0.15	0.19	0.12	0.22
CaO	15.78	15.21	17.04	16.10	15.31	15.36	15.51	16.15	16.49	16.18	16.33	7.82	16.95
Na2O	2.65	2.87	1.78	2.42	2.98	2.99	2.85	2.59	2.23	2.47	2.40	6.05	2.08
K2O	0.14	0.16	0.07	0.11	0.03	0.06	0.17	0.08	0.10	0.07	0.09	0.42	0.06
Total	99.89	98.79	98.57	99.13	99.59	98.80	99.96	99.75	98.72	99.78	99.84	99.37	99.74
cations (based on 32 oxygens):													
Si	8.8983	8.9888	8.6814	8.9075	9.0001	8.9553	8.9948	8.8909	8.8044	8.8426	8.8137	10.5997	8.7243
Al	7.0527	6.9565	7.2284	6.9913	6.9537	6.9837	6.9382	7.0277	7.1112	7.1055	7.1254	5.4522	7.1941
Fe	0.0338	0.0327	0.0529	0.0553	0.0227	0.0183	0.0318	0.0242	0.0222	0.0225	0.0298	0.0181	0.0337
Ca	3.1026	3.0212	3.4103	3.1948	3.0133	3.0513	3.0456	3.1814	3.2879	3.1858	3.2164	1.5021	3.3484
Na	0.9428	1.0296	0.6454	0.8697	1.0597	1.0749	1.0126	0.9224	0.8055	0.8801	0.8545	2.1087	0.7429
K	0.0330	0.0378	0.0173	0.0261	0.0065	0.0134	0.0389	0.0195	0.0231	0.0161	0.0220	0.0957	0.0134
Total	20.0632	20.0667	20.0357	20.0448	20.0561	20.0970	20.0619	20.0662	20.0543	20.0527	20.0619	19.7764	20.0568
n	4	5	3	3	4	2	3	2	3	4	4	3	4
An	0.7607	0.7389	0.8373	0.7810	0.7386	0.7371	0.7434	0.7716	0.7987	0.7805	0.7858	0.4053	0.8157
standard deviation:													
wt.%													
SiO2	0.94	1.12	0.29	0.78	0.93	0.95	0.54	0.32	0.17	0.33	0.28	1.65	0.62
Al2O3	0.62	0.85	0.15	0.52	0.49	0.77	0.50	0.07	0.12	0.08	0.22	0.29	0.27
FeO	0.01	0.05	0.01	0.02	0.01	0.01	0.01	0.01	0.01	0.00	0.01	0.02	0.02
CaO	0.74	1.10	0.21	0.52	0.67	1.06	0.43	0.07	0.16	0.16	0.32	0.33	0.37
Na2O	0.35	0.56	0.13	0.32	0.30	0.60	0.26	0.03	0.07	0.10	0.16	1.19	0.24
K2O	0.04	0.04	0.01	0.03	0.02	0.00	0.01	0.00	0.00	0.01	0.02	0.03	0.02

Sample:	97.44	97.93	102.50	105.50	108.50	113.63	113.65	124.48
Habit:	pcum	cum	cum	pcum	cum	cum	cum	cum
wt.%								
SiO2	47.35	46.68	46.02	48.50	47.24	47.11	46.36	47.35
Al2O3	33.07	32.97	33.42	32.79	32.89	33.56	33.90	33.36
FeO	0.17	0.19	0.28	0.13	0.15	0.09	0.16	0.12
CaO	16.65	16.92	17.72	16.14	16.69	17.16	17.53	17.11
Na2O	2.10	2.00	1.66	2.53	2.20	1.99	1.79	2.04
K2O	0.10	0.08	0.05	0.08	0.07	0.04	0.02	0.08
Total	99.45	98.85	99.16	100.17	99.24	99.96	99.77	100.07
cations (based on 32 oxygens):								
Si	8.7462	8.6880	8.5627	8.8744	8.7471	8.6645	8.5601	8.7008
Al	7.1985	7.2326	7.3278	7.0715	7.1781	7.2764	7.3756	7.2256
Fe	0.0262	0.0290	0.0441	0.0203	0.0230	0.0134	0.0247	0.0192
Ca	3.2958	3.3747	3.5331	3.1657	3.3114	3.3827	3.4681	3.3680
Na	0.7529	0.7229	0.5984	0.8979	0.7908	0.7105	0.6415	0.7279
K	0.0229	0.0199	0.0128	0.0181	0.0177	0.0104	0.0056	0.0179
Total	20.0425	20.0671	20.0790	20.0479	20.0681	20.0578	20.0757	20.0593
n	3	2	3	5	4	5	3	6
An	0.8095	0.8196	0.8525	0.7756	0.8038	0.8243	0.8427	0.8187
standard deviation:								
wt.%								
SiO2	0.53	0.21	0.44	0.92	0.19	0.37	0.24	0.33
Al2O3	0.23	0.10	0.37	0.59	0.14	0.13	0.29	0.28
FeO	0.03	0.01	0.02	0.01	0.02	0.02	0.03	0.05
CaO	0.48	0.03	0.35	0.74	0.12	0.13	0.36	0.24
Na2O	0.20	0.05	0.20	0.41	0.09	0.10	0.14	0.11
K2O	0.03	0.01	0.01	0.02	0.01	0.01	0.01	0.01

MICROPROBE DATA: Composition of plagioclase in the SF-sequence

Sample:	69.30	219.55	223.68	244.60	248.46	250.88	268.22	268.41	305.35	313.00	318.50	318.52	319.18
Habit:	pcum	pcum	pcum	cum	cum	pcum	pcum	pcum	pcum	cum	cum	pcum	pcum
wt.%													
SiO2	49.91	50.85	49.86	48.84	49.41	54.05	49.37	47.27	51.88	47.78	48.28	51.42	53.19
Al2O3	31.71	31.67	32.06	32.73	32.24	29.17	32.77	34.47	30.71	33.41	33.23	31.39	29.55
FeO	0.14	0.14	0.10	0.17	0.26	0.11	0.07	0.09	0.20	0.30	0.27	0.23	0.19
CaO	14.67	14.20	14.78	15.60	15.54	11.56	15.15	17.32	13.18	16.56	15.99	13.83	11.87
Na2O	3.15	3.59	3.41	2.73	2.56	5.22	3.05	1.86	3.91	2.13	2.26	3.63	5.01
K2O	0.24	0.11	0.04	0.14	0.17	0.18	0.01	0.02	0.26	0.14	0.13	0.21	0.25
Total	99.83	100.56	100.25	100.21	100.19	100.28	100.43	101.03	100.13	100.32	100.16	100.70	100.06
cations (based on 32 oxygens):													
Si	9.1301	9.2160	9.0821	8.9235	9.0207	9.7474	8.9794	8.5985	9.4153	8.7484	8.8314	9.2949	9.6422
Al	6.8369	6.7649	6.8854	7.0483	6.9371	6.2114	7.0255	7.3894	6.5721	7.2090	7.1643	6.6904	6.3154
Fe	0.0209	0.0213	0.0156	0.0259	0.0396	0.0164	0.0110	0.0136	0.0299	0.0456	0.0412	0.0345	0.0281
Ca	2.8758	2.7564	2.8862	3.0550	3.0404	2.2417	2.9535	3.3757	2.5644	3.2494	3.1332	2.6806	2.3062
Na	1.1184	1.2603	1.2028	0.9657	0.9063	1.8199	1.0738	0.6556	1.3731	0.7573	0.8021	1.2704	1.7590
K	0.0571	0.0254	0.0090	0.0335	0.0397	0.0402	0.0034	0.0036	0.0607	0.0319	0.0304	0.0485	0.0574
Total	20.0392	20.0444	20.0811	20.0519	19.9838	20.0770	20.0465	20.0363	20.0155	20.0416	20.0026	20.0193	20.1083
n	3	5	5	5	5	4	3	4	5	5	3	5	5
An	0.7099	0.6819	0.7043	0.7535	0.7627	0.5465	0.7327	0.8366	0.6414	0.8046	0.7901	0.6702	0.5594
standard deviation:													
wt.%													
SiO2	0.37	0.60	2.11	0.48	0.05	3.84	0.88	0.32	2.52	0.24	0.22	2.40	1.24
Al2O3	0.18	0.49	1.42	0.20	0.24	2.35	0.66	0.26	1.78	0.18	0.06	1.73	0.71
FeO	0.02	0.01	0.03	0.04	0.03	0.04	0.01	0.03	0.06	0.02	0.01	0.06	0.02
CaO	0.25	0.53	1.65	0.21	0.28	3.02	0.70	0.41	2.08	0.24	0.18	1.84	0.94
Na2O	0.13	0.31	1.04	0.15	0.10	1.78	0.46	0.17	1.11	0.10	0.07	1.13	0.56
K2O	0.03	0.04	0.03	0.01	0.01	0.07	0.00	0.01	0.11	0.02	0.01	0.07	0.03

Sample:	336.97	337.00	357.30	360.90	362.12	368.10	372.16	372.38	373.00	379.10	380.00	385.20	385.22
Habit:	pcum	pcum	pcum	cum	cum	pcum	pcum	pcum	cum	cum	pcum	cum	pcum
wt.%													
SiO2	53.30	53.47	52.61	48.03	46.92	50.46	49.83	49.76	47.94	48.57	49.46	48.68	50.66
Al2O3	30.20	29.44	30.39	33.80	33.53	31.75	31.54	32.13	33.24	32.78	32.04	33.26	32.00
FeO	0.19	0.17	0.20	0.33	0.33	0.19	0.23	0.21	0.26	0.26	0.23	0.29	0.21
CaO	12.26	11.54	12.88	16.43	16.57	14.45	14.64	14.96	16.42	15.95	15.27	16.54	14.68
Na2O	4.50	4.93	4.36	2.06	2.08	3.37	3.27	3.13	2.15	2.54	3.03	2.25	3.27
K2O	0.25	0.24	0.26	0.13	0.13	0.19	0.19	0.15	0.13	0.16	0.18	0.12	0.17
Total	100.70	99.79	100.70	100.77	99.55	100.42	99.70	100.36	100.14	100.25	100.21	101.13	101.00
cations (based on 32 oxygens):													
Si	9.5931	9.6973	9.4940	8.7443	8.6665	9.1691	9.1322	9.0635	8.7855	8.8830	9.0360	8.8321	9.1553
Al	6.4051	6.2946	6.4662	7.2518	7.2991	6.8016	6.8142	6.8996	7.1789	7.0673	6.8983	7.1115	6.8150
Fe	0.0281	0.0251	0.0298	0.0496	0.0510	0.0295	0.0357	0.0325	0.0392	0.0397	0.0358	0.0446	0.0314
Ca	2.3644	2.2441	2.4912	3.2048	3.2797	2.8146	2.8764	2.9212	3.2238	3.1252	2.9880	3.2149	2.8431
Na	1.5693	1.7323	1.5245	0.7286	0.7454	1.1857	1.1604	1.1038	0.7640	0.8998	1.0728	0.7914	1.1453
K	0.0581	0.0564	0.0589	0.0297	0.0298	0.0450	0.0440	0.0359	0.0312	0.0366	0.0408	0.0267	0.0394
Total	20.0181	20.0498	20.0646	20.0089	20.0716	20.0455	20.0629	20.0565	20.0227	20.0516	20.0717	20.0211	20.0295
n	3	4	5	4	4	7	4	5	4	4	5	3	4
An	0.5923	0.5565	0.6114	0.8087	0.8088	0.6958	0.7049	0.7193	0.8021	0.7695	0.7285	0.7972	0.7059
standard deviation:													
wt.%													
SiO2	0.09	1.91	2.18	0.25	0.38	1.72	1.53	1.62	0.39	0.54	0.29	0.19	0.45
Al2O3	0.11	1.29	1.53	0.19	0.10	1.17	1.09	1.10	0.10	0.24	0.19	0.17	0.25
FeO	0.04	0.05	0.02	0.01	0.04	0.01	0.02	0.04	0.02	0.02	0.03	0.04	0.01
CaO	0.05	1.56	1.82	0.22	0.06	1.40	1.23	1.33	0.15	0.19	0.19	0.17	0.27
Na2O	0.02	0.96	1.02	0.14	0.10	0.81	0.70	0.78	0.09	0.15	0.10	0.09	0.13
K2O	0.02	0.07	0.05	0.02	0.01	0.07	0.05	0.03	0.02	0.02	0.01	0.01	0.02

Sample:	385.94	385.96	390.70	438.00	440.67	440.69	450.00	453.28	453.29	462.00	465.00	474.12	475.17	Sample:	475.30	484.00
Habit:	cum	pcum	cum	cum	cum	pcum	cum	cum	cum	cum	pcum	pcum	pcum	Habit:	pcum	pcum
wt.%														wt.%		
SiO2	48.45	52.57	47.97	48.02	47.36	48.08	47.81	47.62	48.01	48.22	51.20	53.28	54.52	SiO2	52.14	51.37
Al2O3	33.31	30.37	32.83	33.30	32.79	32.45	32.97	32.79	32.79	32.87	31.39	29.33	29.41	Al2O3	30.45	30.86
FeO	0.27	0.24	0.28	0.31	0.26	0.20	0.30	0.23	0.22	0.29	0.26	0.21	0.10	FeO	0.16	0.26
CaO	16.32	12.91	16.04	16.45	16.57	16.17	16.39	16.22	16.16	15.96	14.22	11.93	11.28	CaO	13.03	13.68
Na2O	2.34	4.17	2.42	2.10	2.25	2.52	2.33	2.37	2.34	2.44	3.59	4.84	5.40	Na2O	4.32	3.84
K2O	0.13	0.25	0.12	0.16	0.13	0.12	0.15	0.12	0.10	0.14	0.19	0.29	0.19	K2O	0.15	0.23
Total	100.82	100.52	99.65	100.34	99.35	99.54	99.95	99.36	99.62	99.93	100.85	99.90	100.91	Total	100.24	100.23
cations (based on 32 oxygens):														cations (based on 32 oxygen		
Si	8.8171	9.4976	8.8312	8.7849	8.7642	8.8653	8.7898	8.8007	8.8383	8.8501	9.2565	9.6699	9.7694	Si	9.4533	9.3359
Al	7.1430	6.4716	7.1235	7.1785	7.1513	7.0532	7.1433	7.1417	7.1147	7.1106	6.6926	6.2798	6.2126	Al	6.5082	6.6133
Fe	0.0409	0.0357	0.0424	0.0468	0.0400	0.0302	0.0459	0.0359	0.0333	0.0447	0.0395	0.0319	0.0147	Fe	0.0249	0.0396
Ca	3.1826	2.5028	3.1641	3.2242	3.2864	3.1950	3.2280	3.2105	3.1882	3.1387	2.7594	2.3248	2.1675	Ca	2.5312	2.6658
Na	0.8243	1.4595	0.8646	0.7444	0.8056	0.9002	0.8289	0.8499	0.8356	0.8682	1.2546	1.7007	1.8760	Na	1.5164	1.3527
K	0.0312	0.0580	0.0274	0.0385	0.0311	0.0285	0.0344	0.0292	0.0241	0.0327	0.0441	0.0669	0.0440	K	0.0338	0.0531
Total	20.0392	20.0253	20.0530	20.0173	20.0785	20.0724	20.0702	20.0680	20.0342	20.0450	20.0466	20.0740	20.0843	Total	20.0678	20.0604
n	4	4	4	4	4	5	5	2	4	5	4	4	3	n	3	3
An	0.7881	0.6225	0.7801	0.8046	0.7971	0.7748	0.7890	0.7850	0.7876	0.7770	0.6800	0.5681	0.5303	An	0.6202	0.6547
standard deviation:														standard deviation:		
wt.%														wt.%		
SiO2	0.51	2.53	0.17	0.18	0.20	0.50	0.26	0.05	0.26	0.24	2.33	2.85	1.48	SiO2	1.24	1.94
Al2O3	0.44	1.57	0.11	0.24	0.24	0.31	0.21	0.05	0.33	0.07	1.24	1.87	0.81	Al2O3	0.85	1.11
FeO	0.01	0.02	0.04	0.04	0.04	0.02	0.02	0.01	0.03	0.01	0.04	0.03	0.02	FeO	0.04	0.04
CaO	0.49	1.86	0.14	0.11	0.18	0.43	0.16	0.08	0.34	0.08	1.71	2.18	1.11	CaO	0.93	1.32
Na2O	0.24	1.00	0.07	0.08	0.07	0.19	0.11	0.06	0.17	0.04	0.99	1.29	0.66	Na2O	0.61	0.81
K2O	0.01	0.08	0.01	0.05	0.01	0.03	0.04	0.00	0.01	0.01	0.08	0.08	0.04	K2O	0.02	0.07

MICROPROBE DATA: Composition of clinopyroxene in the NG-sequence (NG3-borehole)

Sample:	163.45	219.22	232.00	260.05	248.25
Depth in NG-sequence in m:	163.45	219.22	232.00	260.05	248.25
wt.%					
SiO2	52.50	52.45	53.14	52.86	52.40
TiO2	0.30	0.21	0.31	0.32	0.33
Al2O3	1.91	1.48	2.06	2.23	1.97
Cr2O3	0.70	0.65	0.86	0.93	0.92
FeO	4.88	3.69	4.93	4.37	4.71
MnO	0.14	0.11	0.14	0.15	0.10
NiO	0.02	0.04	0.03	0.01	0.05
MgO	16.15	16.73	16.82	16.93	17.10
CaO	21.94	23.26	21.55	22.34	21.78
Na2O	0.38	0.29	0.43	0.40	0.39
Total	98.92	98.92	100.27	100.54	99.74
cations (based on 6 oxygens):					
Si	1.9465	1.9431	1.9412	1.9268	1.9273
Ti	0.0083	0.0060	0.0085	0.0087	0.0091
Al	0.0835	0.0647	0.0886	0.0960	0.0854
Cr	0.0206	0.0191	0.0249	0.0267	0.0267
Fe	0.1514	0.1144	0.1508	0.1331	0.1446
Mn	0.0043	0.0034	0.0042	0.0048	0.0031
Ni	0.0006	0.0012	0.0010	0.0004	0.0014
Mg	0.8929	0.9234	0.9160	0.9199	0.9371
Ca	0.8716	0.9232	0.8434	0.8726	0.8588
Na	0.0270	0.0210	0.0302	0.0282	0.0279
Total	4.0067	4.0195	4.0087	4.0172	4.0215
n	7	4	5	2	4
Mg#	0.8550	0.8898	0.8587	0.8736	0.8663
en	46.6	47.1	48.0	47.8	48.3
wo	45.5	47.1	44.2	45.3	44.3
fs	7.9	5.8	7.9	6.9	7.5
standard deviation:					
wt.%					
SiO2	0.21	0.63	0.46	0.07	0.19
TiO2	0.02	0.11	0.02	0.01	0.02
Al2O3	0.10	0.65	0.12	0.11	0.19
Cr2O3	0.03	0.31	0.03	0.08	0.06
FeO	0.59	0.59	0.52	0.11	1.06
MnO	0.03	0.01	0.01	0.00	0.04
NiO	0.02	0.02	0.02	0.01	0.02
MgO	0.62	0.61	0.48	0.52	1.30
CaO	1.36	0.92	1.17	0.76	2.27
Na2O	0.03	0.14	0.03	0.05	0.05

MICROPROBE DATA: Composition of clinopyroxene in the NG-sequence (NG1-borehole)

Sample:	17.00	25.00	29.80	35.00	46.25	55.40	56.00	74.45	79.75	84.90	89.55	94.60
Depth in NG-sequence in m:	267.00	275.00	279.80	285.00	296.25	305.40	306.00	324.45	329.75	334.90	339.55	344.60
wt.%												
SiO2	52.45	53.09	53.59	53.06	52.91	53.36	52.95	53.45	53.57	53.00	53.38	52.78
TiO2	0.31	0.31	0.31	0.30	0.29	0.21	0.43	0.32	0.32	0.28	0.37	0.33
Al2O3	1.90	1.65	1.91	2.12	2.13	1.85	2.30	1.86	1.85	2.04	1.93	2.26
Cr2O3	0.96	0.76	0.88	0.90	0.95	0.91	1.07	0.89	0.86	0.84	0.85	0.91
FeO	4.69	4.57	4.05	5.07	4.87	4.19	4.36	4.17	4.73	3.48	4.40	4.68
MnO	0.14	0.14	0.12	0.10	0.15	0.12	0.14	0.13	0.14	0.09	0.13	0.11
NiO	0.04	0.04	0.05	0.06	0.05	0.06	0.02	0.05	0.04	0.05	0.04	0.04
MgO	16.16	16.55	17.07	17.00	17.33	17.07	16.06	17.42	16.86	17.65	17.89	17.77
CaO	22.42	21.88	21.66	20.75	20.70	22.03	22.01	21.34	21.28	22.14	20.20	20.94
Na2O	0.39	0.39	0.41	0.37	0.41	0.37	0.75	0.44	0.36	0.37	0.48	0.47
Total	99.45	99.38	100.06	99.73	99.78	100.16	100.10	100.07	100.01	99.94	99.66	100.28
cations (based on 6 oxygens):												
Si	1.9378	1.9551	1.9528	1.9451	1.9384	1.9469	1.9382	1.9481	1.9564	1.9339	1.9492	1.9247
Ti	0.0086	0.0087	0.0085	0.0082	0.0079	0.0059	0.0118	0.0089	0.0088	0.0076	0.0102	0.0089
Al	0.0826	0.0716	0.0820	0.0914	0.0919	0.0797	0.0991	0.0800	0.0795	0.0876	0.0829	0.0969
Cr	0.0280	0.0222	0.0253	0.0260	0.0275	0.0264	0.0310	0.0255	0.0247	0.0243	0.0245	0.0263
Fe	0.1449	0.1408	0.1235	0.1555	0.1493	0.1277	0.1336	0.1270	0.1445	0.1062	0.1343	0.1428
Mn	0.0044	0.0043	0.0036	0.0030	0.0045	0.0036	0.0044	0.0041	0.0045	0.0028	0.0040	0.0035
Ni	0.0013	0.0012	0.0016	0.0019	0.0014	0.0018	0.0007	0.0016	0.0011	0.0016	0.0010	0.0010
Mg	0.8899	0.9082	0.9274	0.9290	0.9459	0.9282	0.8763	0.9464	0.9178	0.9600	0.9733	0.9659
Ca	0.8872	0.8632	0.8457	0.8150	0.8126	0.8610	0.8633	0.8331	0.8327	0.8655	0.7906	0.8183
Na	0.0279	0.0276	0.0288	0.0263	0.0294	0.0261	0.0531	0.0310	0.0251	0.0263	0.0338	0.0329
Total	4.0124	4.0031	3.9994	4.0012	4.0088	4.0072	4.0115	4.0057	3.9952	4.0158	4.0039	4.0212
n	4	5	10	3	9	9	1	4	11	4	5	5
Mg#	0.8600	0.8658	0.8824	0.8566	0.8637	0.8791	0.8677	0.8816	0.8640	0.9004	0.8787	0.8712
en	46.3	47.5	48.9	48.9	49.6	48.4	46.8	49.6	48.4	49.7	51.3	50.1
wo	46.2	45.1	44.6	42.9	42.6	44.9	46.1	43.7	43.9	44.8	41.6	42.5
fs	7.5	7.4	6.5	8.2	7.8	6.7	7.1	6.7	7.6	5.5	7.1	7.4
standard deviation:												
wt.%												
SiO2	0.13	0.24	0.27	0.31	0.19	0.18		0.23	0.44	0.40	0.12	0.25
TiO2	0.01	0.05	0.03	0.02	0.02	0.03		0.03	0.06	0.04	0.09	0.05
Al2O3	0.16	0.22	0.11	0.06	0.12	0.11		0.14	0.21	0.25	0.45	0.07
Cr2O3	0.06	0.15	0.04	0.01	0.02	0.03		0.04	0.08	0.15	0.10	0.08
FeO	0.58	0.28	0.13	0.31	0.67	0.26		0.30	0.69	0.36	0.44	0.56
MnO	0.02	0.01	0.03	0.02	0.02	0.01		0.02	0.02	0.02	0.02	0.02
NiO	0.01	0.01	0.02	0.01	0.01	0.03		0.01	0.01	0.01	0.01	0.01
MgO	0.20	0.38	0.32	0.39	0.92	0.22		0.39	0.78	0.33	0.84	0.80
CaO	0.86	0.45	0.51	0.75	1.54	0.69		1.03	1.40	0.67	1.63	1.30
Na2O	0.01	0.04	0.02	0.01	0.03	0.01		0.01	0.03	0.02	0.06	0.04

Sample:	105.45	110.52	119.90	163.27	173.37	183.70	191.00	197.50	204.50	210.30	242.70	257.70
Depth in NG-sequence in m:	355.45	360.52	369.90	413.27	423.37	433.70	441.00	447.50	454.50	460.30	492.70	507.70
wt.%												
SiO2	53.29	53.57	52.89	53.37	53.49	53.21	54.01	53.18	53.41	53.52	54.06	54.45
TiO2	0.51	0.48	0.33	0.35	0.18	0.24	0.24	0.17	0.37	0.33	0.15	0.22
Al2O3	1.87	1.76	1.67	1.68	1.61	1.79	1.63	1.57	1.76	1.56	1.31	1.24
Cr2O3	0.72	0.75	0.74	0.87	0.84	0.91	0.81	0.90	0.92	0.83	0.81	0.69
FeO	4.48	4.51	4.11	4.38	3.92	4.02	4.32	3.82	4.45	4.59	4.42	3.96
MnO	0.11	0.10	0.12	0.14	0.15	0.11	0.14	0.13	0.12	0.14	0.12	0.12
NiO	0.03	0.04	0.02	0.05	0.04	0.05	0.05	0.04	0.02	0.05	0.03	0.05
MgO	16.88	17.27	17.24	17.38	17.20	17.20	17.94	17.18	17.01	17.30	17.57	17.15
CaO	21.74	21.28	22.15	20.98	21.98	21.68	20.67	22.47	21.52	21.06	21.57	22.48
Na2O	0.55	0.55	0.44	0.43	0.36	0.40	0.37	0.36	0.43	0.42	0.34	0.32
Total	100.19	100.30	99.72	99.62	99.80	99.60	100.18	99.83	100.02	99.81	100.38	100.68
cations (based on 6 oxygens):												
Si	1.9454	1.9501	1.9406	1.9538	1.9559	1.9494	1.9611	1.9477	1.9510	1.9575	1.9649	2.0376
Ti	0.0141	0.0130	0.0091	0.0097	0.0051	0.0066	0.0066	0.0047	0.0102	0.0092	0.0041	0.0055
Al	0.0803	0.0755	0.0724	0.0725	0.0694	0.0773	0.0699	0.0677	0.0757	0.0673	0.0562	0.0496
Cr	0.0207	0.0215	0.0216	0.0251	0.0244	0.0263	0.0232	0.0259	0.0266	0.0240	0.0233	0.0186
Fe	0.1368	0.1372	0.1262	0.1341	0.1199	0.1231	0.1312	0.1171	0.1361	0.1404	0.1344	0.1123
Mn	0.0035	0.0032	0.0037	0.0043	0.0047	0.0035	0.0042	0.0040	0.0037	0.0044	0.0035	0.0035
Ni	0.0010	0.0012	0.0006	0.0014	0.0013	0.0016	0.0016	0.0013	0.0007	0.0014	0.0009	0.0013
Mg	0.9185	0.9373	0.9430	0.9485	0.9372	0.9393	0.9706	0.9377	0.9263	0.9433	0.9519	0.8668
Ca	0.8502	0.8299	0.8708	0.8230	0.8614	0.8510	0.8045	0.8819	0.8422	0.8253	0.8401	0.8168
Na	0.0390	0.0386	0.0310	0.0305	0.0258	0.0281	0.0264	0.0255	0.0303	0.0299	0.0242	0.0211
Total	4.0095	4.0076	4.0188	4.0029	4.0051	4.0062	3.9990	4.0135	4.0028	4.0026	4.0034	3.9333
n	4	4	4	7	5	5	4	5	4	4	6	2
Mg#	0.8703	0.8723	0.8820	0.8761	0.8866	0.8841	0.8809	0.8890	0.8719	0.8704	0.8763	0.8853
en	48.2	49.2	48.6	49.8	48.9	49.1	50.9	48.4	48.6	49.4	49.4	48.3
wo	44.6	43.6	44.9	43.2	44.9	44.5	42.2	45.5	44.2	43.2	43.6	45.5
fs	7.2	7.2	6.5	7.0	6.2	6.4	6.9	6.0	7.1	7.4	7.0	6.3
standard deviation:												
wt.%												
SiO2	0.21	0.24	0.32	0.09	0.30	0.10	0.17	0.30	0.13	0.21	0.09	0.12
TiO2	0.04	0.06	0.01	0.01	0.03	0.02	0.02	0.01	0.02	0.02	0.01	0.01
Al2O3	0.23	0.34	0.19	0.09	0.24	0.14	0.27	0.10	0.13	0.18	0.17	0.02
Cr2O3	0.11	0.12	0.06	0.03	0.08	0.05	0.14	0.02	0.02	0.07	0.07	0.02
FeO	0.34	0.29	0.29	0.40	0.66	0.34	0.81	0.11	0.22	0.45	0.27	0.27
MnO	0.02	0.02	0.02	0.03	0.07	0.01	0.02	0.02	0.02	0.01	0.01	0.00
NiO	0.02	0.02	0.01	0.01	0.01	0.03	0.01	0.01	0.02	0.02	0.02	0.00
MgO	0.34	0.22	0.23	0.36	1.03	0.42	1.40	0.18	0.25	0.38	0.33	0.02
CaO	0.72	0.42	0.66	0.58	0.68	0.72	2.04	0.20	0.71	0.83	0.71	0.25
Na2O	0.01	0.05	0.03	0.03	0.04	0.02	0.04	0.02	0.03	0.02	0.03	0.00

Sample:	277.25	282.25	292.30	302.00	312.10	332.20	338.45	348.20	364.25	374.35	380.35	406.40
Depth in NG-sequence in m:	527.25	532.25	542.30	552.00	562.10	582.20	588.45	598.20	614.25	624.35	630.35	656.40
wt.%												
SiO2	53.62	53.65	53.74	53.49	54.05	52.94	53.81	53.60	53.07	53.10	53.06	53.44
TiO2	0.16	0.19	0.18	0.18	0.18	0.23	0.22	0.18	0.21	0.28	0.32	0.27
Al2O3	1.50	1.29	1.39	1.43	1.58	2.43	1.43	1.60	1.67	1.59	1.79	1.61
Cr2O3	0.92	0.67	0.77	0.83	0.90	1.01	0.86	0.96	0.95	1.00	1.06	0.99
FeO	3.80	3.86	3.78	3.62	3.71	2.85	3.55	4.31	3.81	3.51	3.73	3.45
MnO	0.14	0.10	0.12	0.10	0.11	0.13	0.13	0.12	0.14	0.09	0.16	0.09
NiO	0.03	0.02	0.04	0.02	0.02	0.10	0.05	0.03	0.03	0.05	0.05	0.05
MgO	17.23	17.08	17.04	17.54	17.20	16.65	17.90	19.59	17.34	17.41	17.32	17.32
CaO	22.24	22.14	22.48	22.41	21.89	22.54	21.77	19.84	22.07	22.49	21.49	22.47
Na2O	0.37	0.33	0.37	0.35	0.37	0.51	0.35	0.34	0.46	0.42	0.44	0.45
Total	100.02	99.33	99.90	99.97	100.02	99.38	100.07	100.57	99.75	99.93	99.42	100.13
cations (based on 6 oxygens):												
Si	1.9567	1.9691	1.9630	1.9525	1.9668	1.9397	1.9571	1.9378	1.9439	1.9413	1.9462	1.9477
Ti	0.0045	0.0052	0.0050	0.0049	0.0050	0.0062	0.0060	0.0050	0.0058	0.0077	0.0087	0.0073
Al	0.0644	0.0560	0.0599	0.0614	0.0675	0.1048	0.0613	0.0683	0.0723	0.0683	0.0775	0.0693
Cr	0.0267	0.0194	0.0223	0.0240	0.0259	0.0293	0.0247	0.0274	0.0274	0.0289	0.0308	0.0284
Fe	0.1159	0.1184	0.1155	0.1104	0.1130	0.0874	0.1081	0.1303	0.1166	0.1072	0.1143	0.1051
Mn	0.0044	0.0031	0.0037	0.0030	0.0033	0.0040	0.0041	0.0037	0.0045	0.0028	0.0050	0.0028
Ni	0.0008	0.0007	0.0012	0.0007	0.0006	0.0028	0.0013	0.0008	0.0007	0.0013	0.0014	0.0014
Mg	0.9372	0.9342	0.9277	0.9543	0.9329	0.9096	0.9706	1.0556	0.9470	0.9489	0.9468	0.9407
Ca	0.8695	0.8704	0.8797	0.8765	0.8534	0.8850	0.8483	0.7686	0.8661	0.8811	0.8444	0.8773
Na	0.0263	0.0233	0.0259	0.0246	0.0263	0.0359	0.0249	0.0236	0.0325	0.0296	0.0316	0.0319
Total	4.0064	3.9997	4.0038	4.0123	3.9947	4.0049	4.0064	4.0211	4.0167	4.0172	4.0067	4.0120
n	6	3	6	5	5	3	8	2	6	6	1	3
Mg#	0.8899	0.8876	0.8893	0.8963	0.8920	0.9123	0.8998	0.8901	0.8904	0.8985	0.8923	0.8995
en	48.7	48.6	48.2	49.2	49.1	48.3	50.4	54.0	49.1	49.0	49.7	48.9
wo	45.2	45.3	45.7	45.2	44.9	47.0	44.0	39.3	44.9	45.5	44.3	45.6
fs	6.0	6.2	6.0	5.7	5.9	4.6	5.6	6.7	6.0	5.5	6.0	5.5
standard deviation:												
wt.%												
SiO2	0.09	0.08	0.27	0.20	0.16	0.58	0.11	0.15	0.33	0.25		0.03
TiO2	0.01	0.01	0.01	0.01	0.02	0.01	0.01	0.00	0.03	0.02		0.03
Al2O3	0.08	0.16	0.18	0.12	0.11	0.23	0.11	0.03	0.12	0.16		0.21
Cr2O3	0.03	0.08	0.10	0.08	0.05	0.12	0.04	0.01	0.03	0.03		0.05
FeO	0.27	0.09	0.28	0.38	0.47	0.10	0.26	0.25	0.38	0.31		0.19
MnO	0.02	0.02	0.02	0.01	0.01	0.06	0.01	0.02	0.03	0.02		0.01
NiO	0.03	0.01	0.01	0.01	0.02	0.12	0.02	0.01	0.01	0.03		0.04
MgO	0.13	0.33	0.20	0.11	0.65	0.04	0.41	0.89	0.27	0.39		0.09
CaO	0.37	0.27	0.48	0.66	1.07	0.26	0.75	1.38	0.69	0.73		0.53
Na2O	0.01	0.02	0.03	0.02	0.03	0.04	0.02	0.02	0.02	0.01		0.04

Sample:	414.85	421.00	455.65	459.70	469.40	476.40	486.55	492.15	496.43	500.50	519.26	523.90
Depth in NG-sequence in m:	664.85	671.00	705.65	709.70	719.40	726.40	736.55	742.15	746.43	750.50	769.26	773.90
wt.%												
SiO2	53.82	53.78	54.11	53.89	53.36	53.82	53.40	53.66	53.83	52.83	53.69	53.96
TiO2	0.22	0.34	0.29	0.20	0.28	0.22	0.26	0.28	0.26	0.32	0.26	0.28
Al2O3	1.55	1.88	1.36	0.91	1.61	1.48	1.99	1.73	1.99	2.06	1.56	1.78
Cr2O3	0.87	0.85	0.90	0.56	1.02	0.84	1.01	0.93	0.94	0.97	0.82	1.01
FeO	3.42	3.42	3.63	3.41	3.77	3.30	4.51	3.69	3.94	3.88	3.72	3.70
MnO	0.13	0.10	0.11	0.11	0.09	0.09	0.13	0.11	0.10	0.11	0.12	0.14
NiO	0.01	0.01	0.01	0.06	0.03	0.05	0.06	0.04	0.05	0.04	0.05	0.03
MgO	18.16	17.47	18.05	18.13	17.73	18.01	18.49	17.58	18.22	17.31	17.78	18.03
CaO	21.55	21.64	21.21	22.30	22.17	21.65	19.84	21.41	20.47	21.46	21.32	20.80
Na2O	0.42	0.62	0.39	0.34	0.45	0.43	0.43	0.47	0.45	0.55	0.40	0.49
Total	100.15	100.12	100.06	99.90	100.50	99.88	100.11	99.90	100.25	99.53	99.71	100.20
cations (based on 6 oxygens):												
Si	1.9537	1.9534	1.9644	1.9644	1.9397	1.9581	1.9412	1.9548	1.9500	1.9371	1.9586	1.9558
Ti	0.0059	0.0092	0.0080	0.0054	0.0075	0.0060	0.0070	0.0076	0.0072	0.0089	0.0072	0.0075
Al	0.0664	0.0806	0.0582	0.0393	0.0688	0.0637	0.0850	0.0741	0.0850	0.0892	0.0670	0.0758
Cr	0.0250	0.0245	0.0257	0.0163	0.0294	0.0240	0.0290	0.0269	0.0268	0.0281	0.0235	0.0288
Fe	0.1038	0.1039	0.1101	0.1040	0.1146	0.1003	0.1371	0.1122	0.1194	0.1188	0.1136	0.1122
Mn	0.0039	0.0032	0.0035	0.0033	0.0026	0.0026	0.0041	0.0035	0.0030	0.0034	0.0036	0.0042
Ni	0.0003	0.0003	0.0004	0.0016	0.0009	0.0013	0.0016	0.0012	0.0014	0.0012	0.0014	0.0008
Mg	0.9827	0.9456	0.9766	0.9851	0.9606	0.9768	1.0019	0.9545	0.9837	0.9462	0.9668	0.9742
Ca	0.8383	0.8423	0.8252	0.8709	0.8634	0.8441	0.7726	0.8358	0.7946	0.8430	0.8333	0.8079
Na	0.0294	0.0438	0.0271	0.0241	0.0320	0.0300	0.0302	0.0331	0.0313	0.0388	0.0281	0.0345
Total	4.0094	4.0067	3.9992	4.0144	4.0196	4.0071	4.0098	4.0037	4.0025	4.0147	4.0030	4.0017
n	5	6	5	5	6	7	5	8	2	5	2	6
Mg#	0.9045	0.9010	0.8987	0.9045	0.8934	0.9068	0.8796	0.8948	0.8918	0.8884	0.8949	0.8967
en	51.1	50.0	51.1	50.3	49.6	50.8	52.4	50.2	51.8	49.6	50.5	51.4
wo	43.6	44.5	43.2	44.4	44.5	43.9	40.4	43.9	41.9	44.2	43.5	42.6
fs	5.4	5.5	5.8	5.3	5.9	5.2	7.2	5.9	6.3	6.2	5.9	5.9
standard deviation:												
wt.%												
SiO2	0.49	0.37	0.31	0.29	0.30	0.23	0.18	0.29	0.22	0.38	0.44	0.11
TiO2	0.08	0.07	0.01	0.08	0.04	0.02	0.08	0.03	0.03	0.06	0.02	0.02
Al2O3	0.37	0.31	0.13	0.26	0.23	0.04	0.32	0.35	0.13	0.30	0.41	0.14
Cr2O3	0.17	0.11	0.04	0.19	0.11	0.03	0.08	0.12	0.07	0.06	0.13	0.02
FeO	0.41	0.32	0.22	0.35	0.40	0.16	0.32	0.38	0.17	0.46	0.63	0.19
MnO	0.02	0.03	0.02	0.02	0.04	0.01	0.02	0.02	0.02	0.02	0.01	0.02
NiO	0.01	0.02	0.01	0.01	0.02	0.00	0.02	0.02	0.01	0.03	0.02	0.01
MgO	0.56	0.34	0.51	0.35	0.63	0.37	1.01	0.46	0.23	0.37	0.67	0.42
CaO	0.92	0.86	0.99	1.02	1.18	0.49	1.71	0.94	0.21	1.02	1.27	0.90
Na2O	0.03	0.06	0.02	0.05	0.02	0.01	0.04	0.04	0.00	0.03	0.02	0.01

Sample:	532.14	536.95	553.33	569.20	581.00	586.00	589.60	595.05	603.10	609.47	614.76	639.95
Depth in NG-sequence in m:	782.14	786.95	803.33	819.20	831.00	836.00	839.60	845.05	853.10	859.47	864.76	889.95
wt.%												
SiO2	53.61	53.87	53.53	53.22	53.74	54.05	53.94	53.59	53.51	53.52	53.68	52.70
TiO2	0.26	0.22	0.33	0.26	0.30	0.16	0.23	0.27	0.33	0.28	0.28	0.30
Al2O3	1.43	1.49	1.71	1.90	1.58	1.24	1.41	1.15	1.68	1.90	1.62	1.68
Cr2O3	0.92	0.94	0.98	0.92	0.93	0.83	0.78	0.69	0.93	0.96	0.93	1.01
FeO	3.63	3.32	4.12	4.56	3.74	3.75	3.26	3.41	3.89	4.32	3.74	3.83
MnO	0.14	0.11	0.14	0.14	0.12	0.14	0.10	0.07	0.12	0.12	0.12	0.13
NiO	0.05	0.05	0.06	0.05	0.02	0.04	0.03	0.00	0.09	0.04	0.04	0.05
MgO	17.88	17.60	18.08	18.40	16.79	17.84	17.41	17.26	17.54	17.79	17.30	18.05
CaO	21.47	22.12	20.71	20.57	22.31	21.58	22.46	23.34	21.40	20.52	21.87	21.51
Na2O	0.41	0.40	0.42	0.39	0.44	0.40	0.40	0.39	0.44	0.40	0.42	0.39
Total	99.79	100.12	100.06	100.40	99.96	100.02	100.04	100.18	99.94	99.86	100.02	99.66
cations (based on 6 oxygens):												
Si	1.9558	1.9583	1.9480	1.9342	1.9610	1.9667	1.9627	1.9551	1.9515	1.9509	1.9560	1.9315
Ti	0.0072	0.0061	0.0089	0.0071	0.0081	0.0044	0.0063	0.0074	0.0092	0.0077	0.0078	0.0083
Al	0.0613	0.0640	0.0733	0.0813	0.0678	0.0531	0.0606	0.0493	0.0723	0.0816	0.0697	0.0726
Cr	0.0264	0.0270	0.0281	0.0265	0.0269	0.0238	0.0224	0.0200	0.0268	0.0278	0.0269	0.0292
Fe	0.1106	0.1010	0.1252	0.1385	0.1142	0.1140	0.0993	0.1040	0.1186	0.1318	0.1141	0.1174
Mn	0.0044	0.0033	0.0043	0.0042	0.0036	0.0042	0.0031	0.0023	0.0036	0.0038	0.0038	0.0041
Ni	0.0015	0.0013	0.0017	0.0014	0.0006	0.0013	0.0009	0.0000	0.0028	0.0013	0.0012	0.0014
Mg	0.9722	0.9534	0.9806	0.9968	0.9134	0.9674	0.9443	0.9387	0.9536	0.9664	0.9397	0.9859
Ca	0.8392	0.8615	0.8076	0.8011	0.8722	0.8414	0.8757	0.9122	0.8361	0.8014	0.8539	0.8449
Na	0.0288	0.0284	0.0295	0.0275	0.0311	0.0282	0.0282	0.0277	0.0308	0.0280	0.0296	0.0279
Total	4.0075	4.0044	4.0071	4.0185	3.9990	4.0045	4.0036	4.0168	4.0052	4.0007	4.0027	4.0232
n	6	8	6	5	6	2	7	2	5	10	8	4
Mg#	0.8978	0.9042	0.8867	0.8780	0.8888	0.8945	0.9048	0.9002	0.8894	0.8800	0.8917	0.8936
en	50.6	49.8	51.2	51.5	48.1	50.3	49.2	48.0	50.0	50.9	49.3	50.6
wo	43.7	45.0	42.2	41.4	45.9	43.8	45.6	46.7	43.8	42.2	44.8	43.4
fs	5.8	5.3	6.5	7.2	6.0	5.9	5.2	5.3	6.2	6.9	6.0	6.0
standard deviation:												
wt.%												
SiO2	0.28	0.23	0.13	0.29	0.14	0.12	0.24	0.19	0.13	0.23	0.26	0.27
TiO2	0.02	0.01	0.04	0.02	0.02	0.13	0.05	0.06	0.02	0.06	0.05	0.02
Al2O3	0.19	0.18	0.22	0.07	0.13	0.30	0.27	0.03	0.17	0.37	0.13	0.21
Cr2O3	0.08	0.12	0.06	0.05	0.06	0.15	0.16	0.01	0.04	0.13	0.06	0.05
FeO	0.24	0.41	0.37	0.59	0.14	0.35	0.21	0.24	0.28	0.57	0.24	0.43
MnO	0.02	0.02	0.01	0.02	0.01	0.02	0.02	0.02	0.01	0.02	0.01	0.02
NiO	0.01	0.02	0.02	0.01	0.01	0.00	0.01	0.00	0.01	0.02	0.01	0.01
MgO	0.34	0.54	0.48	0.97	0.08	0.24	0.25	0.14	0.54	0.75	0.30	0.62
CaO	0.57	0.88	0.98	1.57	0.23	0.76	0.49	0.22	0.99	1.41	0.45	1.22
Na2O	0.04	0.03	0.03	0.05	0.02	0.03	0.05	0.03	0.01	0.03	0.03	0.03

MICROPROBE DATA: Composition of clinopyroxene in the NG-sequence (NG2-borehole)

Sample:	645.17	655.10	660.40	675.25	685.40	690.90	695.50	720.15	730.38	739.80	744.70
Depth in NG-sequence in m:	895.17	905.10	910.40	925.25	935.40	940.90	945.50	970.15	980.38	989.80	994.70
wt.%											
SiO2	53.49	52.53	52.96	53.92	53.32	52.70	53.55	52.98	53.23	52.91	52.84
TiO2	0.32	0.37	0.37	0.37	0.37	0.41	0.29	0.34	0.29	0.40	0.32
Al2O3	1.36	1.72	1.65	1.59	1.61	1.77	1.84	1.72	1.45	1.94	1.82
Cr2O3	0.87	0.99	0.93	0.91	0.90	0.92	0.85	0.97	0.86	0.97	0.72
FeO	3.60	3.61	3.95	3.67	3.83	3.88	3.53	3.82	3.30	3.83	3.74
MnO	0.11	0.10	0.11	0.09	0.12	0.13	0.07	0.09	0.11	0.09	0.12
NiO	0.05	0.05	0.08	0.01	0.03	0.03	0.03	0.03	0.02	0.02	0.01
MgO	17.61	17.34	17.77	17.52	17.81	17.73	16.99	17.18	16.94	18.02	17.65
CaO	22.62	22.98	21.89	22.19	21.80	22.04	22.26	22.17	23.20	20.94	22.39
Na2O	0.36	0.45	0.41	0.44	0.43	0.48	0.47	0.41	0.37	0.48	0.47
Total	100.39	100.15	100.13	100.70	100.22	100.08	99.86	99.71	99.77	99.59	100.09
cations (based on 6 oxygens):											
Si	1.9466	1.9232	1.9340	1.9520	1.9418	1.9267	1.9538	1.9416	1.9497	1.9352	1.9305
Ti	0.0088	0.0101	0.0102	0.0100	0.0100	0.0113	0.0081	0.0093	0.0081	0.0111	0.0088
Al	0.0583	0.0743	0.0711	0.0677	0.0693	0.0761	0.0790	0.0745	0.0624	0.0835	0.0782
Cr	0.0250	0.0286	0.0268	0.0260	0.0260	0.0267	0.0244	0.0280	0.0250	0.0279	0.0209
Fe	0.1096	0.1104	0.1205	0.1111	0.1165	0.1186	0.1076	0.1170	0.1012	0.1171	0.1144
Mn	0.0035	0.0031	0.0033	0.0028	0.0038	0.0039	0.0021	0.0029	0.0033	0.0027	0.0038
Ni	0.0013	0.0015	0.0023	0.0001	0.0008	0.0008	0.0008	0.0009	0.0006	0.0005	0.0004
Mg	0.9554	0.9464	0.9674	0.9452	0.9663	0.9661	0.9239	0.9384	0.9248	0.9825	0.9612
Ca	0.8819	0.9014	0.8567	0.8607	0.8508	0.8635	0.8702	0.8707	0.9102	0.8207	0.8763
Na	0.0251	0.0322	0.0290	0.0307	0.0302	0.0339	0.0332	0.0294	0.0264	0.0338	0.0334
Total	4.0155	4.0313	4.0213	4.0065	4.0156	4.0276	4.0030	4.0126	4.0117	4.0149	4.0279
n	3	2	6	5	5	4	5	5	5	5	2
Mg#	0.8971	0.8955	0.8892	0.8948	0.8924	0.8906	0.8957	0.8891	0.9014	0.8935	0.8936
en	49.1	48.3	49.7	49.3	50.0	49.6	48.6	48.7	47.8	51.2	49.2
wo	45.3	46.0	44.1	44.9	44.0	44.3	45.8	45.2	47.0	42.7	44.9
fs	5.6	5.6	6.2	5.8	6.0	6.1	5.7	6.1	5.2	6.1	5.9
standard deviation:											
wt.%											
SiO2	0.06	0.05	0.32	0.13	0.51	0.30	0.43	0.21	0.39	0.10	0.32
TiO2	0.00	0.01	0.03	0.02	0.02	0.02	0.08	0.02	0.05	0.03	0.03
Al2O3	0.12	0.10	0.12	0.20	0.07	0.07	0.51	0.11	0.12	0.02	0.15
Cr2O3	0.07	0.01	0.02	0.09	0.05	0.02	0.12	0.02	0.10	0.03	0.05
FeO	0.25	0.34	0.52	0.40	0.44	0.27	0.19	0.32	0.20	0.32	0.10
MnO	0.01	0.00	0.01	0.02	0.03	0.02	0.01	0.02	0.01	0.01	0.01
NiO	0.01	0.02	0.03	0.01	0.02	0.02	0.01	0.03	0.02	0.01	0.01
MgO	0.31	0.36	0.73	0.72	0.78	0.27	0.34	0.57	0.15	0.54	0.15
CaO	0.58	0.51	1.29	1.18	1.13	0.63	0.32	1.01	0.34	0.83	0.16
Na2O	0.01	0.03	0.03	0.05	0.04	0.03	0.07	0.01	0.02	0.03	0.00

Sample:	80.35	98.00	115.25	120.40	194.20	219.90	277.15	293.60	307.10	320.15	350.50	376.65
Depth in NG-sequence in m:	1120.35	1138.00	1155.25	1160.40	1234.20	1259.90	1317.15	1333.60	1347.10	1360.15	1390.50	1416.65
wt.%												
SiO2	53.67	52.71	54.00	53.16	53.51	53.19	53.21	53.84	53.32	52.86	52.55	53.32
TiO2	0.20	0.13	0.18	0.27	0.29	0.26	0.31	0.33	0.28	0.37	0.38	0.36
Al2O3	2.17	2.11	1.68	1.53	1.71	1.73	1.28	1.37	1.60	1.52	2.17	1.90
Cr2O3	1.04	0.93	0.77	0.80	0.83	0.89	0.68	0.72	0.82	0.78	0.78	0.81
FeO	4.34	3.80	4.25	3.15	3.70	3.80	3.86	4.29	4.28	4.35	4.26	4.34
MnO	0.09	0.11	0.12	0.12	0.12	0.11	0.13	0.11	0.11	0.10	0.12	0.07
NiO	0.07	0.07	0.07	0.03	0.05	0.03	0.11	0.07	0.03	0.06	0.09	0.03
MgO	18.10	17.57	20.02	16.81	17.35	17.64	17.57	17.16	16.92	16.97	17.56	17.89
CaO	20.52	21.78	19.12	23.15	22.22	21.23	22.52	22.37	22.71	22.23	21.62	20.74
Na2O	0.50	0.40	0.28	0.59	0.38	0.50	0.33	0.35	0.41	0.36	0.56	0.52
Total	100.71	99.62	100.49	99.61	100.16	99.37	100.00	100.61	100.48	99.61	100.10	99.98
cations (based on 6 oxygens):												
Si	1.9406	1.9320	1.9465	1.9500	1.9490	1.9496	1.9464	1.9569	1.9447	1.9443	1.9218	1.9437
Ti	0.0054	0.0036	0.0050	0.0073	0.0078	0.0070	0.0085	0.0091	0.0076	0.0101	0.0105	0.0099
Al	0.0925	0.0912	0.0711	0.0662	0.0734	0.0749	0.0552	0.0588	0.0689	0.0659	0.0937	0.0815
Cr	0.0299	0.0270	0.0220	0.0231	0.0239	0.0257	0.0196	0.0206	0.0236	0.0227	0.0225	0.0232
Fe	0.1313	0.1164	0.1276	0.0966	0.1127	0.1165	0.1180	0.1304	0.1305	0.1339	0.1303	0.1324
Mn	0.0027	0.0035	0.0037	0.0038	0.0038	0.0033	0.0042	0.0033	0.0033	0.0031	0.0039	0.0023
Ni	0.0020	0.0021	0.0021	0.0009	0.0016	0.0008	0.0032	0.0020	0.0010	0.0019	0.0026	0.0009
Mg	0.9755	0.9599	1.0739	0.9190	0.9416	0.9639	0.9581	0.9296	0.9199	0.9304	0.9574	0.9718
Ca	0.7954	0.8554	0.7402	0.9101	0.8674	0.8338	0.8827	0.8713	0.8876	0.8758	0.8470	0.8100
Na	0.0352	0.0285	0.0198	0.0420	0.0270	0.0352	0.0233	0.0247	0.0290	0.0260	0.0398	0.0369
Total	4.0104	4.0196	4.0119	4.0190	4.0081	4.0107	4.0193	4.0067	4.0160	4.0142	4.0294	4.0125
n	4	4	2	3	3	3	2	3	3	3	3	3
Mg#	0.8814	0.8919	0.8938	0.9049	0.8931	0.8922	0.8903	0.8770	0.8758	0.8742	0.8802	0.8801
en	51.3	49.7	55.3	47.7	49.0	50.4	48.9	48.1	47.5	48.0	49.5	50.8
wo	41.8	44.3	38.1	47.3	45.1	43.6	45.1	45.1	45.8	45.1	43.8	42.3
fs	6.9	6.0	6.6	5.0	5.9	6.1	6.0	6.8	6.7	6.9	6.7	6.9
standard deviation:												
wt.%												
SiO2	0.32	0.11	0.44	0.37	0.29	0.10	0.03	0.12	0.19	0.24	0.30	0.24
TiO2	0.05	0.03	0.01	0.09	0.01	0.01	0.02	0.01	0.02	0.03	0.03	0.02
Al2O3	0.09	0.15	0.12	0.44	0.02	0.07	0.04	0.07	0.14	0.21	0.07	0.12
Cr2O3	0.16	0.05	0.02	0.15	0.01	0.02	0.01	0.01	0.08	0.07	0.08	0.06
FeO	0.47	0.41	1.26	0.13	0.19	0.09	0.48	0.22	0.14	0.39	0.11	0.06
MnO	0.01	0.04	0.02	0.01	0.01	0.02	0.02	0.02	0.00	0.03	0.01	0.01
NiO	0.01	0.02	0.02	0.02	0.02	0.01	0.01	0.01	0.01	0.03	0.04	0.02
MgO	1.04	0.63	2.86	0.38	0.48	0.28	0.42	0.22	0.21	0.38	0.09	0.23
CaO	1.56	1.04	4.29	0.24	0.71	0.25	1.04	0.50	0.16	1.12	0.35	0.49
Na2O	0.07	0.03	0.05	0.04	0.01	0.02	0.03	0.02	0.03	0.01	0.03	0.02

Sample:	420.05	428.15	590.97	591.03	618.25	678.64	691.95
Depth in							
NG-sequence in m:	1460.05	1468.15	1630.97	1631.03	1658.25	1718.64	1731.95
wt.%							
SiO2	53.71	53.48	53.15	54.12	54.59	53.03	54.07
TiO2	0.32	0.40	0.46	0.33	0.08	0.38	0.36
Al2O3	2.00	2.01	1.74	1.35	0.94	2.14	1.83
Cr2O3	0.92	0.75	0.80	0.65	0.41	0.72	0.82
FeO	3.91	4.02	3.61	3.73	3.28	3.39	3.35
MnO	0.11	0.09	0.10	0.08	0.08	0.11	0.07
NiO	0.06	0.09	0.03	0.04	0.05	0.06	0.05
MgO	17.18	17.26	16.78	17.32	16.45	17.16	17.93
CaO	21.82	21.24	22.68	22.25	23.61	21.58	21.12
Na2O	0.51	0.53	0.52	0.48	0.49	0.60	0.55
Total	100.52	99.88	99.86	100.35	99.98	99.16	100.14
cations (based on 6 oxygens):							
Si	1.9482	1.9504	1.9451	1.9651	1.9900	1.9460	1.9582
Ti	0.0088	0.0110	0.0127	0.0090	0.0021	0.0105	0.0098
Al	0.0854	0.0865	0.0749	0.0577	0.0404	0.0925	0.0781
Cr	0.0264	0.0218	0.0230	0.0188	0.0120	0.0209	0.0234
Fe	0.1185	0.1227	0.1104	0.1134	0.1000	0.1039	0.1014
Mn	0.0032	0.0028	0.0031	0.0024	0.0023	0.0035	0.0021
Ni	0.0017	0.0026	0.0008	0.0012	0.0015	0.0017	0.0014
Mg	0.9289	0.9380	0.9152	0.9376	0.8938	0.9383	0.9677
Ca	0.8480	0.8300	0.8895	0.8657	0.9221	0.8484	0.8199
Na	0.0357	0.0377	0.0368	0.0335	0.0350	0.0423	0.0384
Total	4.0049	4.0034	4.0116	4.0045	3.9992	4.0080	4.0004
n	3	4	3	2	1	3	3
Mg#	0.8868	0.8843	0.8924	0.8921	0.8994	0.9003	0.9052
en	49.0	49.6	47.8	48.9	46.7	49.6	51.2
wo	44.7	43.9	46.4	45.2	48.1	44.9	43.4
fs	6.3	6.5	5.8	5.9	5.2	5.5	5.4
standard deviation:							
wt.%							
SiO2	0.06	0.36	0.21	0.40		0.05	0.43
TiO2	0.02	0.04	0.03	0.14		0.07	0.05
Al2O3	0.24	0.39	0.14	0.39		0.09	0.07
Cr2O3	0.05	0.20	0.06	0.06		0.03	0.05
FeO	0.40	0.32	0.13	0.35		0.32	0.34
MnO	0.02	0.02	0.02	0.03		0.01	0.02
NiO	0.01	0.02	0.00	0.03		0.01	0.01
MgO	0.54	0.33	0.46	0.30		0.57	1.04
CaO	0.94	1.14	0.61	1.10		0.85	1.60
Na2O	0.02	0.09	0.02	0.04		0.06	0.01

APPENDIX V

All whole-rock XRF analyses used in the thesis are tabulated hereafter. Samples analysed by Haikney and Rocklabs (closed corporation) are included. All data were recalculated to 100 % L.O.I.-free, whereas Cr_2O_3 were included as major elements. Fe_2O_3 has been stated assuming a constant ratio of $FeO/Fe_2O_3 = 10$. The Mg# is the atomic ratio of $Mg/(Mg + Fe^{2+})$. As evident from Appendix IIB trace element concentrations below 2 ppm are generally below the lower limit of determination.

The abbreviations for the normative minerals are as follows:

AP	apatite	DIEN	diopside-enstatite
CM	chromite	DIFS	diopside-ferrosilite
IL	ilmenite	DIWO	diopside-wollastonite
OR	orthoclase	HYEN	hypersthene-enstatite
AB	albite	HYFS	hypersthene-ferrosilite
AN	anorthite	Q	quartz
C	corundum	FO	forsterite
MT	magnetite	FA	fayalite

WHOLE-ROCK XRF-ANALYSES: NG-sequence (NG3-borehole)

Sample:	3.98	28.62	55.00	79.60	99.60	126.05	146.50	153.15	159.40	176.45	181.70	194.74	212.20	213.18	214.25	220.17	220.20	232.00	260.05
Depth in NG-sequence in m:	3.98	28.62	55.00	79.60	99.60	126.05	146.50	153.15	159.40	176.45	181.70	194.74	212.20	213.18	214.25	220.17	220.20	232.00	260.05
wt.%																			
SiO2	54.2	53.9	54.6	54.3	54.1	54.4	54.4	53.0	52.2	51.1	52.8	51.3	48.1	50.7	54.4	55.6	54.2	54.9	53.2
TiO2	0.1	0.1	0.1	0.1	0.1	0.1	0.1	0.2	0.2	0.1	0.1	0.1	0.0	0.1	0.2	0.3	0.2	0.2	0.3
Al2O3	4.2	5.9	3.3	3.0	4.3	2.7	2.4	5.2	5.0	18.4	10.6	18.0	30.2	18.2	3.6	4.5	4.1	3.8	3.7
Fe2O3	1.1	1.1	1.1	1.1	1.1	1.1	1.1	1.0	1.1	0.5	0.8	0.5	0.1	0.5	1.0	0.8	1.0	1.0	1.0
FeO	11.3	10.6	11.2	11.4	10.9	11.3	11.2	10.4	10.9	5.3	7.8	5.4	1.0	5.3	10.0	8.3	9.9	9.9	10.4
MnO	0.2	0.2	0.3	0.2	0.2	0.3	0.2	0.2	0.2	0.1	0.2	0.1	0.0	0.1	0.2	0.1	0.2	0.2	0.2
MgO	24.2	22.8	25.4	25.9	24.8	26.6	27.3	24.0	24.4	13.2	20.2	13.4	3.8	13.7	26.6	25.7	25.7	25.7	25.4
CaO	3.5	4.2	3.0	2.9	3.4	2.7	2.5	3.4	3.2	9.5	6.0	9.4	14.3	9.6	3.0	3.1	3.3	3.0	3.1
Na2O	0.5	0.7	0.4	0.3	0.4	0.3	0.2	0.7	0.5	1.5	0.9	1.4	2.3	1.4	0.3	0.2	0.5	0.5	0.6
K2O	0.0	0.1	0.1	0.0	0.0	0.0	0.0	0.2	0.1	0.1	0.1	0.1	0.1	0.1	0.0	0.1	0.1	0.1	0.1
P2O5	0.0	0.0	0.0	0.0	0.0	0.0	0.0	0.0	0.0	0.0	0.0	0.0	0.0	0.0	0.0	0.0	0.1	0.0	0.0
Cr2O3	0.4	0.3	0.4	0.5	0.5	0.5	0.4	1.6	2.1	0.3	0.4	0.3	0.1	0.3	0.6	1.2	0.7	0.6	1.8
NiO	0.1	0.1	0.1	0.1	0.1	0.1	0.1	0.1	0.1	0.0	0.1	0.0	0.0	0.0	0.1	0.1	0.1	0.1	0.1
Total	100.0	100.0	100.0	100.0	100.0	100.0	100.0	100.0	100.0	100.0	100.0	100.0	100.0	100.0	100.0	100.0	100.0	100.0	100.0
Mg#	0.7920	0.7925	0.8015	0.8017	0.8014	0.8080	0.8128	0.8052	0.7996	0.8163	0.8216	0.8172	0.8766	0.8216	0.8262	0.8467	0.8230	0.8228	0.8125
Trace elements																			
ppm																			
Zr	6	5	8	5	3	3	1	13	10	1	5	2	0	0	5	21	28	12	19
Y	2	4	4	2	0	2	1	1	4	0	1	0	2	0	3	5	0	2	5
Sr	54	82	36	32	47	25	18	62	53	273	158	268	411	247	32	9	43	40	41
Rb	4	3	3	1	3	1	0	5	4	2	3	2	2	1	3	10	4	7	4
Co	105	101	110	109	101	109	111	84	104	55	82	63	7	54	98	86	99	102	102
Cr	2750	2252	2715	3247	3404	3103	2910	10913	14263	1937	2841	2050	471	1912	4207	8392	4731	4115	12130
V	165	155	172	196	153	157	179	190	230	56	93	52	15	68	135	197	144	134	194
Zn	87	80	88	89	85	93	84	81	92	36	61	39	2	41	83	22	70	72	87
Cu	11	14	13	13	11	17	7	26	18	9	12	9	16	12	13	7	22	17	27
Ni	538	511	570	604	579	578	593	500	549	277	429	286	77	270	534	625	517	525	566
Sc	34	31	34	36	33	35	35	33	32	20	25	17	4	15	35	41	35	35	35
CIPW-norm																			
wt.%																			
AP	0.00	0.00	0.00	0.00	0.00	0.00	0.00	0.00	0.00	0.00	0.00	0.00	0.02	0.00	0.00	0.00	0.28	0.07	0.05
CM	0.59	0.49	0.59	0.69	0.74	0.66	0.63	2.34	3.06	0.41	0.62	0.44	0.10	0.41	0.90	1.81	1.02	0.88	2.61
IL	0.26	0.26	0.28	0.26	0.21	0.24	0.21	0.36	0.34	0.13	0.23	0.15	0.08	0.15	0.30	0.49	0.34	0.34	0.54
OR	0.24	0.41	0.35	0.30	0.18	0.12	0.06	0.89	0.47	0.47	0.35	0.53	0.83	0.59	0.18	0.83	0.71	0.83	0.83
AB	4.57	5.75	3.47	2.62	3.55	2.12	1.61	5.84	4.57	12.27	7.95	12.01	19.71	11.59	2.88	1.35	4.48	4.48	4.91
AN	8.95	12.90	7.12	6.51	9.76	6.16	5.75	10.79	10.98	43.36	24.47	42.48	70.78	43.11	8.18	11.07	8.40	7.52	7.13
C	0.00	0.00	0.00	0.00	0.00	0.00	0.00	0.00	0.00	0.00	0.00	0.00	0.26	0.00	0.00	0.00	0.00	0.00	0.00
MT	1.64	1.55	1.62	1.65	1.58	1.64	1.62	1.51	1.58	0.77	1.13	0.78	0.14	0.77	1.45	1.20	1.44	1.44	1.51
DIEN	2.46	2.28	2.32	2.37	2.10	2.20	2.04	1.79	1.49	1.17	1.59	1.21	0.00	1.32	2.06	1.30	2.09	2.15	2.47
DIFS	0.81	0.75	0.72	0.73	0.65	0.66	0.59	0.51	0.43	0.33	0.43	0.34	0.00	0.36	0.54	0.27	0.55	0.57	0.66
DIWO	3.56	3.30	3.32	3.39	3.01	3.12	2.88	2.52	2.10	1.64	2.21	1.69	0.00	1.84	2.86	1.74	2.90	2.99	3.43
HYEN	57.76	54.12	60.83	62.20	59.58	63.99	65.00	55.00	55.49	28.86	46.20	29.95	0.52	27.69	63.56	62.80	60.45	61.95	57.94
HYFS	19.04	17.83	18.90	19.25	18.49	19.08	18.83	15.64	16.05	8.04	12.45	8.31	0.09	7.43	16.48	13.11	15.95	16.46	15.41
Q	0.14	0.00	0.46	0.01	0.14	0.02	0.00	0.00	0.00	0.00	0.00	0.00	0.00	0.00	0.00	4.03	0.00	0.33	0.00
FO	0.00	0.29	0.00	0.00	0.00	0.00	0.59	2.14	2.60	1.94	1.82	1.62	6.32	3.65	0.46	0.00	1.10	0.00	1.94
FA	0.00	0.10	0.00	0.00	0.00	0.00	0.19	0.67	0.83	0.60	0.54	0.49	1.15	1.08	0.13	0.00	0.32	0.00	0.57
TOTAL	100.00	100.02	100.00	100.00	100.00	100.01	100.00	99.98	100.00	99.98	99.99	100.01	100.00	99.99	99.99	100.00	100.02	100.01	99.99

WHOLE-ROCK XRF-ANALYSES: NG-sequence (NG1-borehole; including Haikney's analyses)

Sample:	25.00	49.75	79.75	95.50	108.33	115.10	122.80	126.00	152.20	163.27	178.45	204.50	233.60	245.25	257.70	292.30	327.45	338.45	380.35	414.85	420.75	421.00	430.55	445.45
Depth in NG-sequence in m:	275.00	299.75	329.75	345.50	358.33	365.10	372.80	376.00	402.20	413.27	428.45	454.50	483.60	495.25	507.70	542.30	577.45	588.45	630.35	664.85	670.75	671.00	680.55	695.45
wt.%																								
SiO2	55.3	54.9	55.3	43.7	45.1	55.0	44.8	54.9	52.4	54.7	55.9	54.9	54.9	55.2	52.9	55.5	55.2	55.8	56.0	56.1	47.9	55.3	39.1	44.5
TiO2	0.2	0.2	0.2	0.1	0.2	0.3	0.0	0.2	0.2	0.2	0.1	0.1	0.2	0.1	0.3	0.1	0.1	0.2	0.2	0.1	0.3	0.2	0.1	0.1
Al2O3	3.6	3.1	2.6	4.4	2.6	2.8	3.3	2.3	2.6	3.8	2.1	4.3	3.2	2.3	5.2	2.0	2.9	2.4	2.7	2.5	2.6	2.6	3.8	1.6
Fe2O3	1.1	1.0	1.0	1.2	1.3	1.0	1.2	0.9	1.1	1.0	1.0	1.0	1.0	1.0	1.1	1.0	0.9	0.9	0.8	0.8	1.1	0.8	1.2	1.1
FeO	10.6	10.1	9.7	12.5	13.3	10.0	11.9	9.2	10.9	9.7	9.9	9.8	10.2	10.1	10.5	9.8	9.4	9.0	8.4	8.2	10.8	8.0	11.7	11.1
MnO	0.2	0.2	0.2	0.1	0.2	0.2	0.2	0.2	0.2	0.2	0.2	0.2	0.2	0.2	0.2	0.2	0.2	0.2	0.2	0.2	0.1	0.2	0.2	0.2
MgO	24.8	26.6	27.3	35.1	34.5	26.4	36.2	28.7	28.1	26.0	27.5	25.2	26.2	28.1	24.0	28.4	27.5	28.2	27.4	28.7	33.8	28.7	38.2	39.3
CaO	3.2	2.8	2.5	2.1	1.7	2.5	1.9	2.3	2.2	2.9	1.9	3.3	2.4	2.1	3.0	2.0	2.6	2.2	2.3	2.3	1.3	2.5	1.5	1.2
Na2O	0.4	0.4	0.3	0.1	0.1	0.5	0.1	0.2	0.2	0.6	0.3	0.6	0.4	0.0	0.5	0.2	0.3	0.3	0.4	0.4	0.1	0.6	0.5	0.3
K2O	0.0	0.0	0.1	0.0	0.0	0.5	0.0	0.0	0.0	0.0	0.2	0.0	0.1	0.0	0.1	0.0	0.0	0.0	0.2	0.0	0.4	0.3	0.0	0.0
P2O5	0.0	0.0	0.0	0.0	0.0	0.0	0.0	0.0	0.0	0.0	0.0	0.0	0.0	0.0	0.0	0.0	0.0	0.0	0.1	0.0	0.0	0.1	0.0	0.0
Cr2O3	0.6	0.6	0.7	0.6	0.8	0.7	0.3	1.0	1.9	0.9	0.7	0.6	1.1	0.7	2.2	0.7	0.8	0.8	1.2	0.6	1.6	0.7	3.6	0.5
NiO	0.1	0.1	0.1	0.2	0.2	0.1	0.2	0.1	0.1	0.1	0.1	0.1	0.1	0.1	0.1	0.1	0.1	0.1	0.1	0.1	0.1	0.1	0.2	0.2
Total	100.0	100.0	100.0	100.0	100.0	100.0	100.0	100.0	100.0	100.0	100.0	100.0	100.0	100.0	100.0	100.0	100.0	100.0	100.0	100.0	100.0	100.0	100.0	100.0
Mg#	0.8064	0.8239	0.8344	0.8339	0.8223	0.8246	0.8443	0.8482	0.8209	0.8270	0.8316	0.8217	0.8199	0.8322	0.8025	0.8383	0.8397	0.8481	0.8539	0.8625	0.8484	0.8652	0.8533	0.8636
Trace elements																								
ppm																								
Zr	10	7	14	3	13	28	5	7	9	9	13	9	11	1	7	5	5	7	21	5	22	22	3	3
Y	5	4	4	4	5	7	4	3	4	4	2	4	3	2	4	3	2	3	4	3	5	4	4	0
Sr	33	25	18	49	20	15	44	11	18	37	12	46	21	2	40	14	19	20	22	23	9	19	39	19
Rb	3	2	6	0	0	14	0	2	1	4	6	3	5	0	4	1	2	2	9	2	17	13	0	0
Co	95	92	94	112	175	94	156	96	192	95	97	89	176	101	90	98	93	91	83	79	129	79	127	142
Cr	4140	4212	4671	3804	5365	4701	1957	6846	13088	6380	5042	3758	7206	5076	15363	4680	5701	5155	7880	4059	10723	4645	24819	3106
V	152	145	122	46	101	115	3	107	235	135	129	118	131	137	272	116	118	100	112	86	118	93	177	58
Zn	80	75	68	68	136	74	74	74	78	74	75	75	82	86	93	68	70	64	60	56	73	56	83	67
Cu	18	16	17	7	44	16	12	12	16	14	11	18	17	8	22	12	18	17	16	16	17	18	20	13
Ni	498	566	510	1485	1367	558	1784	572	629	574	555	476	521	543	490	510	481	491	427	478	1054	514	1437	1257
Sc	34	34	32	0	0	33	0	29	26	30	30	30	33	34	33	30	29	25	25	24	0	23	0	0
CIPW-norm																								
wt.%																								
AP	0.00	0.00	0.02	0.00	0.00	0.09	0.17	0.00	0.02	0.00	0.00	0.02	0.00	0.00	0.02	0.00	0.02	0.05	0.17	0.02	0.00	0.21	0.12	0.02
CM	0.90	0.91	1.02	0.82	1.15	1.02	0.37	1.50	2.83	1.38	1.09	0.82	1.56	1.09	3.28	1.02	1.22	1.12	1.72	0.90	2.31	1.00	5.35	1.09
IL	0.32	0.30	0.34	0.13	0.32	0.47	0.11	0.30	0.28	0.30	0.26	0.28	0.34	0.17	0.51	0.19	0.23	0.34	0.32	0.23	0.49	0.34	0.21	0.13
OR	0.12	0.00	0.77	0.00	0.00	2.66	0.00	0.06	0.00	0.24	0.89	0.18	0.77	0.00	0.30	0.00	0.00	0.06	1.06	0.00	2.13	1.65	0.00	0.00
AB	3.64	3.13	2.88	1.10	0.93	4.32	0.93	1.95	2.03	4.65	2.79	4.91	3.30	0.00	4.40	1.78	2.62	2.20	3.64	3.22	1.18	4.82	4.65	2.37
AN	7.94	6.69	5.21	10.32	6.60	4.05	9.07	5.19	6.04	7.76	3.83	9.15	6.71	6.30	11.74	4.57	6.49	5.33	5.02	5.14	5.32	3.71	7.02	3.22
C	0.00	0.00	0.00	0.40	0.00	0.00	0.01	0.00	0.00	0.00	0.00	0.00	0.00	0.00	0.00	0.00	0.00	0.00	0.00	0.00	0.00	0.00	0.28	0.00
MT	1.54	1.46	1.41	1.81	1.93	1.45	1.73	1.33	1.58	1.41	1.44	1.42	1.48	1.46	1.52	1.42	1.36	1.30	1.22	1.19	1.57	1.16	1.70	1.61
DIEN	2.26	2.21	2.14	0.00	0.55	2.51	0.00	1.96	1.53	1.96	1.76	2.12	1.52	1.26	0.89	1.62	1.99	1.67	1.90	1.98	0.41	2.57	0.00	0.93
DIFS	0.67	0.58	0.52	0.00	0.15	0.65	0.00	0.42	0.39	0.50	0.44	0.57	0.40	0.32	0.25	0.39	0.46	0.37	0.39	0.39	0.09	0.49	0.00	0.19
DIWO	3.21	3.07	2.93	0.00	0.77	3.48	0.00	2.64	2.11	2.71	2.42	2.95	2.11	1.74	1.25	2.21	2.71	2.26	2.54	2.63	0.55	3.41	0.00	1.24
HYEN	59.40	63.98	65.97	20.53	28.07	62.25	23.98	69.49	61.09	62.76	66.63	60.72	63.61	68.74	58.78	69.13	66.45	68.65	66.43	69.49	39.75	64.86	1.03	22.12
HYFS	17.59	16.92	16.06	5.13	7.51	16.13	5.73	14.97	15.53	15.92	16.57	16.28	16.86	17.14	16.33	16.50	15.49	15.00	13.51	13.64	8.31	12.32	0.19	4.43
Q	2.42	0.73	0.74	0.00	0.00	0.00	0.00	0.19	0.00	0.41	1.87	0.61	1.34	1.77	0.74	1.18	0.94	1.66	2.08	1.19	0.00	0.00	0.00	0.00
FO	0.00	0.00	0.00	46.87	40.17	0.72	45.85	0.00	5.13	0.00	0.00	0.00	0.00	0.00	0.00	0.00	0.00	0.00	0.00	0.00	30.81	2.87	65.87	51.31
FA	0.00	0.00	0.00	12.90	11.85	0.21	12.07	0.00	1.44	0.00	0.00	0.00	0.00	0.00	0.00	0.00	0.00	0.00	0.00	0.00	7.09	0.60	13.63	11.33
TOTAL	100.01	99.99	100.01	100.00	100.00	100.01	100.00	100.00	99.99	99.99	99.98	100.02	99.99	100.00	100.00	100.00	99.99	100.00	100.00	100.01	100.01	100.01	100.05	100.00

Sample:	464.00	480.60	486.55	500.50	506.05	509.86	528.50	558.78	575.35	603.10	619.85	645.17	670.10	695.50	698.00	699.45	701.75	720.15	739.80	753.09	773.74	784.64	793.80	803.41
Depth in																								
MG-sequence in m:	714.00	730.60	736.55	750.50	756.05	759.86	778.50	808.78	825.35	853.10	869.85	895.17	920.10	945.50	948.00	949.45	951.75	970.15	989.80	1003.09	1023.74	1034.64	1043.80	1053.41
wt.%																								
SiO2	55.5	51.0	55.3	55.2	47.1	41.8	54.7	55.9	55.1	55.7	55.6	54.3	55.6	54.8	47.1	40.6	54.8	55.4	54.9	39.6	40.1	42.1	40.4	40.6
TiO2	0.1	0.1	0.1	0.1	0.1	0.1	0.1	0.2	0.1	0.2	0.1	0.1	0.2	0.1	0.1	0.0	0.1	0.1	0.1	0.0	0.0	0.1	0.0	0.0
Al2O3	2.8	2.6	3.2	2.9	2.6	1.9	3.0	2.7	2.5	2.6	2.3	2.5	2.5	2.8	2.2	1.4	2.2	2.8	3.1	0.4	0.2	1.2	0.5	0.5
Fe2O3	0.8	1.0	0.8	0.8	1.1	1.3	0.9	0.9	0.9	0.9	0.9	0.9	0.8	0.9	1.2	1.4	0.9	0.8	0.8	1.2	1.1	1.1	1.1	1.1
FeO	8.3	9.6	8.3	8.3	10.8	12.7	8.7	8.6	9.0	9.0	8.8	8.8	8.4	9.1	11.8	13.6	9.0	8.4	8.1	11.8	10.9	10.6	10.7	10.8
MnO	0.2	0.2	0.2	0.2	0.2	0.2	0.2	0.2	0.2	0.2	0.4	0.6	0.2	0.2	0.2	0.2	0.2	0.2	0.2	0.2	0.2	0.2	0.2	0.2
MgO	28.5	32.5	28.2	28.9	34.2	39.7	28.4	27.9	28.7	27.8	28.8	29.0	28.9	28.8	34.5	41.1	29.5	28.9	29.1	45.8	46.5	41.9	45.7	45.5
CaO	2.3	1.8	2.4	2.3	1.8	1.2	2.2	2.1	2.3	2.2	2.1	2.0	2.2	2.2	1.4	1.0	1.9	2.3	2.4	0.3	0.4	1.8	0.4	0.6
Na2O	0.4	0.2	0.5	0.5	0.3	0.3	0.4	0.4	0.4	0.4	0.3	0.3	0.4	0.4	0.1	0.3	0.3	0.4	0.5	0.0	0.0	0.3	0.0	0.1
K2O	0.0	0.0	0.0	0.0	0.0	0.0	0.0	0.1	0.0	0.1	0.1	0.0	0.1	0.1	0.0	0.0	0.0	0.0	0.0	0.0	0.0	0.1	0.0	0.0
P2O5	0.1	0.0	0.0	0.1	0.0	0.0	0.1	0.0	0.1	0.1	0.1	0.1	0.1	0.1	0.0	0.0	0.1	0.1	0.0	0.0	0.0	0.0	0.0	0.0
Cr2O3	0.7	0.9	0.7	0.6	1.7	0.8	1.2	0.9	0.6	0.7	0.6	1.4	0.5	0.6	1.3	0.3	0.8	0.5	0.7	0.5	0.3	0.4	0.7	0.3
NiO	0.1	0.1	0.1	0.1	0.1	0.2	0.1	0.1	0.1	0.1	0.1	0.1	0.1	0.1	0.1	0.2	0.1	0.1	0.1	0.2	0.3	0.3	0.3	0.3
Total	100.0	100.0	100.0	100.0	100.0	100.0	100.0	100.0	100.0	100.0	100.0	100.0	100.0	100.0	100.0	100.0	100.0	100.0	100.0	100.0	100.0	100.0	100.0	100.0
Mg#	0.8590	0.8576	0.8577	0.8618	0.8492	0.8478	0.8539	0.8526	0.8501	0.8458	0.8534	0.8542	0.8598	0.8501	0.8389	0.8432	0.8539	0.8594	0.8646	0.8741	0.8839	0.8756	0.8841	0.8821
Trace elements																								
ppm																								
Zr	6	5	8	4	3	3	7	17	7	13	11	6	11	12	6	4	6	8	6	0	0	11	0	2
Y	3	4	3	3	5	0	3	4	3	2	2	2	4	4	3	0	3	2	3	0	0	3	0	0
Sr	30	20	32	34	26	24	29	23	21	22	20	18	20	29	19	25	18	27	33	6	3	20	4	8
Rb	1	0	3	1	0	0	2	5	3	6	4	3	4	3	0	0	2	2	3	0	0	6	0	0
Co	87	111	86	87	118	158	90	85	87	92	94	87	86	88	127	172	96	86	82	161	162	151	151	159
Cr	5011	6439	4887	4073	11721	5276	8203	6203	3762	5025	4044	9595	3613	3789	9018	1889	5681	3673	4457	3408	2088	2802	5070	1844
V	96	82	89	80	108	64	100	107	92	106	96	123	100	97	114	32	102	95	94	24	18	40	34	21
Zn	61	50	63	61	78	83	65	64	66	66	64	66	64	67	81	87	67	64	62	69	69	60	67	57
Cu	17	18	18	19	21	16	17	16	18	14	15	17	14	18	14	14	12	16	17	10	6	15	11	12
Ni	470	770	459	492	896	1422	498	483	467	471	487	479	482	500	1022	1540	545	509	466	1666	2254	2031	2522	2296
Sc	22	0	22	25	0	0	23	24	26	27	26	24	25	26	0	0	26	24	24	0	0	0	0	0
CIPW-norm																								
wt.%																								
AP	0.12	0.00	0.07	0.24	0.00	0.00	0.12	0.09	0.26	0.17	0.14	0.26	0.17	0.17	0.00	0.00	0.26	0.12	0.09	0.00	0.00	0.09	0.00	0.12
CM	1.09	1.38	1.08	0.88	2.52	1.13	1.80	1.34	0.82	1.10	0.88	2.09	0.78	0.82	1.94	0.41	1.24	0.80	0.96	0.74	0.40	0.60	1.09	0.40
IL	0.21	0.19	0.23	0.21	0.19	0.11	0.23	0.30	0.24	0.28	0.23	0.24	0.34	0.26	0.21	0.08	0.23	0.24	0.26	0.02	0.00	0.11	0.04	0.04
OR	0.18	0.00	0.18	0.00	0.00	0.00	0.18	0.65	0.24	0.53	0.30	0.12	0.65	0.35	0.00	0.00	0.00	0.06	0.18	0.00	0.00	0.35	0.00	0.00
AB	3.81	1.52	4.32	4.15	2.37	2.54	3.47	3.72	2.96	3.22	2.54	2.28	3.30	3.05	1.10	2.37	2.20	3.30	3.89	0.24	0.00	2.45	0.42	0.85
AN	5.64	6.37	6.30	5.66	5.89	3.76	6.20	5.07	5.19	5.18	4.75	5.44	4.77	5.87	5.56	2.48	4.92	5.94	6.33	0.96	0.19	1.93	1.09	1.00
C	0.00	0.00	0.00	0.00	0.00	0.00	0.00	0.00	0.00	0.00	0.00	0.00	0.00	0.00	0.00	0.00	0.00	0.00	0.00	0.00	0.00	0.00	0.00	0.00
MT	1.20	1.39	1.20	1.20	1.57	1.84	1.26	1.25	1.30	1.30	1.28	1.28	1.22	1.32	1.71	1.97	1.30	1.22	1.17	1.71	1.59	1.54	1.55	1.57
DIEN	1.70	0.85	1.75	1.60	0.91	0.55	1.42	1.54	1.64	1.63	1.57	1.11	1.72	1.37	0.37	0.73	1.23	1.59	1.63	0.15	0.00	2.09	0.26	0.51
DIFS	0.34	0.17	0.36	0.32	0.19	0.12	0.29	0.32	0.36	0.36	0.34	0.23	0.35	0.30	0.08	0.17	0.26	0.32	0.31	0.03	0.00	0.38	0.04	0.09
DIWO	2.27	1.13	2.34	2.13	1.23	0.75	1.89	2.06	2.22	2.20	2.12	1.49	2.29	1.85	0.50	0.99	1.64	2.13	2.16	0.20	0.00	2.75	0.33	0.67
HYEN	69.37	53.13	67.84	67.99	35.64	9.39	68.10	67.94	68.80	67.68	70.22	69.29	70.17	67.20	37.76	2.83	70.43	69.54	66.77	0.00	0.00	4.98	2.97	2.02
HYFS	13.93	10.75	13.77	13.49	7.49	2.11	13.95	14.23	15.07	15.13	15.19	14.57	14.12	14.69	8.78	0.67	14.79	14.11	12.85	0.00	0.00	0.90	0.49	0.35
Q	0.13	0.00	0.00	0.00	0.00	0.00	0.00	1.49	0.00	1.20	0.42	0.00	0.00	0.00	0.00	0.00	0.00	0.00	0.00	0.00	0.00	0.00	0.00	0.00
FO	0.00	18.91	0.48	1.76	34.10	62.26	0.90	0.00	0.72	0.00	0.00	1.29	0.11	2.19	33.44	69.20	1.23	0.52	2.79	79.86	82.32	68.19	77.49	77.60
FA	0.00	4.22	0.11	0.38	7.89	15.40	0.20	0.00	0.17	0.00	0.00	0.30	0.02	0.53	8.57	18.09	0.29	0.12	0.59	16.09	15.34	13.66	14.22	14.84
TOTAL	99.99	100.00	100.01	100.00	100.00	99.97	100.00	100.00	100.01	99.99	99.99	100.00	100.00	99.97	100.00	100.01	100.01	100.00	99.98	100.00	100.01	100.03	100.01	100.03

WHOLE-ROCK XRF-ANALYSES: NG-sequence (NG2-borehole; including Haikney's analyses)

Sample:	809.31	816.10	830.15
Depth in NG-sequence in m:	1059.31	1066.10	1080.15
wt.%			
SiO2	42.0	40.6	42.0
TiO2	0.0	0.0	0.0
Al2O3	1.1	1.5	1.2
Fe2O3	1.1	1.1	1.1
FeO	10.8	11.2	11.4
MnO	0.2	0.2	0.2
MgO	42.8	43.6	41.5
CaO	0.8	0.8	1.4
Na2O	0.3	0.3	0.2
K2O	0.0	0.0	0.0
P2O5	0.0	0.0	0.0
Cr2O3	0.6	0.3	0.5
NiO	0.3	0.3	0.3
Total	100.0	100.0	100.0
Mg#	0.8764	0.8737	0.8666
Trace elements			
ppm			
Zr	11	0	6
Y	3	0	3
Sr	17	0	19
Rb	3	0	0
Co	154	156	145
Cr	4001	1969	3606
V	35	22	41
Zn	63	64	73
Cu	15	15	16
Ni	2123	2086	1988
Sc	0	0	0
CIPW-norm			
wt.%			
AP	0.12	0.12	0.02
CM	0.85	0.43	0.78
IL	0.09	0.04	0.09
OR	0.06	0.00	0.00
AB	2.62	2.28	1.95
AN	1.58	2.80	2.35
C	0.00	0.00	0.00
MT	1.57	1.62	1.65
DIEN	0.65	0.33	1.39
DIFS	0.12	0.06	0.27
DIWO	0.86	0.43	1.85
HYEN	7.41	1.18	7.65
HYFS	1.33	0.22	1.50
Q	0.00	0.00	0.00
FO	69.08	75.08	66.16
FA	13.67	15.44	14.32
TOTAL	100.01	100.04	100.00

Sample:	39.35	42.55	50.20	65.25	80.35	83.75	91.40	102.60	115.25	122.30	134.40	143.35
Depth in NG-sequence in m:	1079.35	1082.55	1090.20	1105.25	1120.35	1123.75	1131.40	1142.60	1155.25	1162.30	1174.40	1183.35
wt.%												
SiO2	40.7	42.6	41.3	49.0	43.8	41.2	55.9	56.0	55.6	44.5	40.7	43.5
TiO2	0.1	0.0	0.1	0.1	0.1	0.0	0.1	0.1	0.1	0.1	0.0	0.1
Al2O3	1.8	2.3	2.3	1.5	2.0	2.3	2.1	2.3	1.9	1.9	2.6	2.0
Fe2O3	1.1	1.1	1.1	1.0	1.1	1.2	0.8	0.9	0.8	1.1	1.2	1.1
FeO	11.2	10.5	11.2	9.6	11.3	11.9	7.7	8.6	7.6	10.7	11.5	11.2
MnO	0.2	0.2	0.2	0.2	0.2	0.2	0.2	0.2	0.2	0.2	0.2	0.2
MgO	41.9	40.8	40.9	36.1	39.0	40.4	28.6	27.7	31.4	38.9	41.2	39.5
CaO	1.4	1.5	1.6	1.6	1.6	1.8	3.5	3.2	1.6	1.5	1.6	1.4
Na2O	0.2	0.4	0.3	0.1	0.2	0.3	0.4	0.3	0.2	0.2	0.5	0.4
K2O	0.1	0.0	0.0	0.0	0.0	0.0	0.0	0.1	0.0	0.1	0.0	0.0
P2O5	0.0	0.0	0.0	0.0	0.0	0.0	0.0	0.0	0.0	0.0	0.0	0.0
Cr2O3	0.9	0.4	0.7	0.7	0.4	0.4	0.5	0.5	0.6	0.7	0.3	0.5
NiO	0.2	0.2	0.2	0.2	0.2	0.2	0.1	0.1	0.1	0.2	0.3	0.3
Total	100.0	100.0	100.0	100.0	100.0	100.0	100.0	100.0	100.0	100.0	100.0	100.0
Mg#	0.8696	0.8737	0.8669	0.8702	0.8596	0.8581	0.8688	0.8522	0.8801	0.8668	0.8644	0.8629
Trace elements												
ppm												
Zr	18	3	5	0	7	4	10	15	6	8	0	3
Y	3	0	0	0	3	3	4	3	2	2	3	2
Sr	29	42	38	16	43	45	19	20	12	27	48	31
Rb	8	3	2	0	5	0	4	8	1	6	0	0
Co	154	138	146	118	136	151	90	86	88	134	156	150
Cr	6261	3038	4701	4605	2894	2429	3422	3405	3824	5057	2155	3113
V	53	36	48	67	44	37	88	89	78	70	36	41
Zn	66	66	65	76	73	68	55	59	53	69	90	68
Cu	19	10	22	11	16	16	14	16	11	33	27	20
Ni	1776	1705	1815	1304	1737	1925	581	628	704	1658	2114	2145
Sc	0	0	0	0	0	0	25	24	20	0	0	0
CIPW-norm												
wt.%												
AP	0.00	0.00	0.02	0.00	0.02	0.00	0.00	0.02	0.02	0.02	0.00	0.00
CM	1.35	0.65	1.02	0.99	0.62	0.53	0.74	0.74	0.82	1.09	0.47	0.68
IL	0.15	0.08	0.11	0.11	0.11	0.08	0.23	0.23	0.17	0.17	0.09	0.11
OR	0.77	0.00	0.00	0.00	0.00	0.00	0.06	0.65	0.00	0.41	0.00	0.00
AB	2.12	3.05	2.62	1.10	1.86	2.71	3.72	2.71	1.69	1.86	2.93	3.05
AN	3.54	4.66	4.94	3.54	4.58	4.84	3.86	4.43	4.31	3.85	4.91	3.90
C	0.00	0.00	0.00	0.00	0.00	0.00	0.00	0.00	0.00	0.00	0.00	0.00
MT	1.62	1.52	1.62	1.39	1.65	1.73	1.12	1.25	1.10	1.55	1.67	1.62
DIEN	1.12	0.88	0.91	1.47	0.96	1.26	4.26	3.51	1.11	1.06	0.92	0.88
DIFS	0.21	0.16	0.18	0.27	0.20	0.27	0.80	0.76	0.19	0.20	0.18	0.18
DIWO	1.48	1.16	1.20	1.94	1.29	1.69	5.64	4.73	1.44	1.41	1.22	1.17
HYEN	1.38	8.43	4.20	42.34	16.89	2.92	66.96	65.55	74.06	20.08	0.00	13.79
HYFS	0.26	1.56	0.81	7.90	3.52	0.62	12.58	14.17	12.55	3.86	0.00	2.80
Q	0.00	0.00	0.00	0.00	0.00	0.00	0.00	1.27	0.00	0.00	0.00	0.00
FO	71.30	64.68	67.88	32.29	55.55	67.58	0.02	0.00	2.12	53.14	71.17	58.69
FA	14.71	13.16	14.47	6.64	12.74	15.80	0.00	0.00	0.40	11.27	15.81	13.14
TOTAL	100.01	99.99	99.98	99.98	99.99	100.03	99.99	100.01	99.99	99.97	99.37	100.01

Sample:	253.05	267.92	272.40	293.60	294.12	298.80	301.66	307.10	320.15	326.86	332.25	372.00	157.30	171.50	180.55	194.20	200.50	212.20	223.86	228.75	236.86	238.90	241.55	247.32
Depth in																								
NG-sequence in m:	1293.05	1307.92	1312.40	1333.60	1334.12	1338.80	1341.66	1347.10	1360.15	1366.86	1372.25	1412.00	1197.30	1211.50	1220.55	1234.20	1240.50	1252.20	1263.86	1268.75	1276.86	1278.90	1281.55	1287.32
wt.%																								
SiO2	55.4	55.6	55.2	53.8	54.0	51.5	54.4	54.3	55.2	44.1	54.7	55.6	40.5	54.6	55.3	54.8	50.0	50.2	55.5	44.5	46.9	41.4	56.0	55.2
TiO2	0.1	0.1	0.1	0.1	0.1	0.1	0.1	0.1	0.1	0.1	0.1	0.1	0.0	0.1	0.1	0.1	0.1	0.1	0.1	0.1	0.1	0.1	0.1	0.1
Al2O3	3.1	2.3	4.1	5.7	5.7	15.0	6.0	3.4	4.1	2.3	4.4	4.1	2.1	2.2	3.3	2.5	2.4	2.6	2.6	2.9	3.8	2.4	3.0	3.6
Fe2O3	0.9	0.9	0.8	0.9	0.9	0.5	0.8	1.0	0.9	1.2	0.9	0.8	1.3	0.9	0.9	0.8	1.0	1.0	0.8	1.1	1.1	1.2	0.9	0.9
FeO	8.8	8.5	8.4	8.7	8.9	5.5	8.4	9.7	9.0	11.8	8.6	8.3	13.0	9.2	8.9	8.3	9.7	9.9	8.3	11.2	10.7	12.4	8.8	8.9
MnO	0.2	0.2	0.2	0.2	0.2	0.1	0.2	0.2	0.2	0.2	0.2	0.2	0.2	0.2	0.2	0.2	0.2	0.2	0.2	0.2	0.2	0.2	0.2	0.2
MgO	27.9	29.8	27.4	25.8	25.3	18.3	25.3	27.1	26.4	37.8	26.6	26.4	40.8	30.1	27.9	30.5	34.1	33.1	29.2	36.7	33.6	39.2	27.6	27.2
CaO	2.4	1.9	2.7	3.2	3.3	7.8	3.6	2.5	2.8	1.1	2.7	2.8	1.2	1.7	2.3	1.9	1.7	1.9	2.2	1.5	2.1	1.0	2.4	2.6
Na2O	0.5	0.3	0.5	0.6	0.6	0.9	0.6	0.4	0.6	0.1	0.6	0.8	0.2	0.2	0.6	0.3	0.3	0.4	0.4	0.3	0.5	0.1	0.5	0.5
K2O	0.0	0.0	0.1	0.0	0.1	0.1	0.0	0.0	0.1	0.0	0.1	0.2	0.0	0.0	0.0	0.0	0.0	0.0	0.0	0.0	0.0	0.1	0.0	0.0
P2O5	0.0	0.0	0.0	0.0	0.0	0.0	0.0	0.0	0.0	0.0	0.0	0.0	0.0	0.0	0.0	0.0	0.0	0.0	0.0	0.0	0.0	0.0	0.0	0.0
Cr2O3	0.5	0.4	0.5	0.9	0.8	0.2	0.5	1.1	0.5	1.2	1.0	0.5	0.4	0.5	0.5	0.6	0.4	0.4	0.5	1.2	0.9	1.3	0.4	0.6
NiO	0.1	0.1	0.1	0.1	0.1	0.0	0.1	0.1	0.1	0.3	0.1	0.1	0.3	0.1	0.1	0.1	0.2	0.2	0.1	0.2	0.2	0.3	0.1	0.1
Total	100.0	100.0	100.0	100.0	100.0	100.0	100.0	100.0	100.0	100.0	100.0	100.0	100.0	100.0	100.0	100.0	100.0	100.0	100.0	100.0	100.0	100.0	100.0	100.0
Mg#	0.8497	0.8615	0.8533	0.8399	0.8350	0.8566	0.8426	0.8321	0.8386	0.8512	0.8460	0.8496	0.8479	0.8534	0.8485	0.8673	0.8617	0.8568	0.8628	0.8541	0.8489	0.8494	0.8491	0.8443
Trace elements																								
ppm																								
Zr	8	8	13	8	7	3	6	7	15	7	15	21	3	5	8	6	5	4	7	4	3	14	12	6
Y	4	3	3	4	5	2	3	5	5	3	4	3	0	3	3	3	2	3	3	0	0	3	4	4
Sr	34	15	44	57	58	190	63	30	46	14	53	69	46	18	39	21	34	37	26	56	51	30	35	43
Rb	2	3	7	3	3	5	3	0	6	4	5	6	4	1	3	1	4	0	2	0	0	5	4	2
Co	93	87	83	88	91	62	93	93	90	140	89	85	162	100	92	85	125	118	88	145	0	138	89	91
Cr	3090	2864	3383	6366	5343	1385	3185	7288	3393	8238	6697	3737	2511	3308	3098	3765	2634	2942	3441	8190	6329	9025	3077	4049
V	111	100	96	125	127	75	118	143	112	81	112	87	31	81	91	112	71	75	85	66	0	97	110	110
Zn	59	59	56	63	60	38	58	74	63	64	66	64	75	66	64	57	62	65	61	73	62	70	59	62
Cu	32	15	22	24	20	14	25	24	26	13	22	22	14	16	20	14	23	29	16	16	32	38	32	34
Ni	609	582	524	711	631	364	593	657	591	2098	692	552	2200	723	648	720	1344	1729	706	1776	1572	2483	680	616
Sc	25	25	24	30	31	21	30	32	29	0	26	26	0	25	26	28	0	0	26	0	0	0	24	24
CIPW-norm																								
wt.%																								
AP	0.05	0.02	0.02	0.02	0.05	0.00	0.00	0.05	0.02	0.05	0.05	0.07	0.00	0.00	0.00	0.00	0.00	0.00	0.05	0.00	0.00	0.07	0.00	0.05
CM	0.66	0.62	0.72	1.37	1.15	0.29	0.69	1.58	0.74	1.77	1.44	0.81	0.54	0.71	0.66	0.81	0.57	0.63	0.74	1.77	1.37	1.94	0.66	0.87
IL	0.26	0.21	0.24	0.21	0.24	0.11	0.23	0.26	0.26	0.19	0.28	0.28	0.08	0.21	0.24	0.23	0.17	0.17	0.21	0.15	0.13	0.19	0.24	0.23
OR	0.06	0.00	0.41	0.06	0.30	0.41	0.00	0.00	0.35	0.00	0.30	0.89	0.24	0.00	0.06	0.00	0.00	0.00	0.00	0.00	0.00	0.59	0.24	0.00
AB	3.98	2.28	4.15	4.65	4.99	7.19	5.25	3.47	4.74	0.51	4.99	7.02	1.35	1.86	4.82	2.62	2.62	3.64	3.72	2.54	4.15	0.68	3.81	4.06
AN	6.37	4.96	8.70	13.14	12.89	36.96	13.67	7.41	8.61	5.18	9.32	6.94	4.87	5.10	6.44	5.32	5.18	5.11	5.04	6.65	8.09	4.91	6.08	7.64
C	0.00	0.00	0.00	0.00	0.00	0.00	0.00	0.00	0.00	0.25	0.00	0.00	0.00	0.00	0.00	0.00	0.00	0.00	0.00	0.00	0.00	0.41	0.00	0.00
MT	1.28	1.23	1.22	1.26	1.29	0.80	1.22	1.41	1.30	1.71	1.25	1.20	1.88	1.33	1.29	1.20	1.41	1.44	1.20	1.62	1.55	1.80	1.28	1.29
DIEN	1.71	1.36	1.38	0.83	0.96	0.49	1.25	1.46	1.56	0.00	1.23	2.09	0.36	1.08	1.52	1.22	1.02	1.33	1.79	0.22	0.74	0.00	1.85	1.64
DIFS	0.38	0.27	0.29	0.19	0.23	0.10	0.29	0.36	0.37	0.00	0.27	0.46	0.08	0.23	0.34	0.23	0.21	0.28	0.36	0.05	0.16	0.00	0.41	0.38
DIWO	2.32	1.82	1.85	1.14	1.31	0.66	1.71	2.01	2.14	0.00	1.67	2.82	0.50	1.46	2.05	1.61	1.36	1.78	2.38	0.29	0.99	0.00	2.50	2.22
HYEN	67.89	71.99	66.55	60.72	60.53	40.10	60.77	65.43	64.11	25.00	64.66	63.15	3.42	68.59	66.49	68.44	45.00	44.46	69.29	22.89	29.99	12.42	66.96	66.10
HYFS	14.99	14.51	14.22	14.10	14.64	8.49	14.17	16.03	15.37	5.41	14.25	13.77	0.79	14.75	14.82	12.99	9.18	9.47	13.78	4.82	6.62	2.73	14.83	15.15
Q	0.06	0.00	0.00	0.00	0.00	0.00	0.00	0.00	0.43	0.00	0.00	0.00	0.00	0.00	0.00	0.00	0.00	0.00	0.00	0.00	0.00	0.00	1.17	0.38
FO	0.00	0.59	0.20	1.82	1.10	3.56	0.60	0.43	0.00	48.39	0.24	0.41	68.48	3.77	1.01	4.40	27.18	25.68	1.20	47.89	37.16	59.79	0.00	0.00
FA	0.00	0.13	0.05	0.47	0.29	0.83	0.15	0.12	0.00	11.54	0.06	0.10	17.45	0.89	0.25	0.92	6.11	6.03	0.26	11.12	9.04	14.46	0.00	0.00
TOTAL	100.01	99.99	100.00	99.98	99.98	100.01	100.00	100.01	100.01	100.00	100.01	100.00	100.04	99.99	100.01	99.99	100.01	100.02	100.01	100.01	99.99	99.99	100.01	100.00

WHOLE-ROCK DATA XRF-ANALYSES: SF-sequence (analysed by Rocklabs cc.)

Sample:	15.92	20.75	30.77	39.97	50.20	60.61	79.06	89.80	100.24	110.60	120.87	129.85	140.47	150.67	166.96	172.56	180.49	192.30	200.53	216.20	222.72	228.85	233.54	243.32	245.49	257.30
wt.%																										
SiO2	49.7	49.6	49.7	49.7	49.7	49.4	49.1	49.7	50.1	50.3	49.8	50.6	50.2	50.0	50.1	50.1	50.2	51.2	50.6	50.2	47.9	49.7	49.3	47.1	49.2	51.2
TiO2	0.1	0.1	0.1	0.1	0.1	0.2	0.1	0.1	0.1	0.1	0.1	0.2	0.1	0.1	0.2	0.2	0.2	0.2	0.2	0.2	0.5	0.1	0.1	0.1	0.1	0.2
Al2O3	22.0	23.1	21.9	21.3	22.4	18.4	28.2	29.2	27.2	28.8	27.5	27.6	28.3	27.4	24.2	23.4	20.8	21.3	19.3	15.2	5.9	18.0	21.2	25.2	28.9	5.9
Fe2O3	0.5	0.4	0.5	0.5	0.5	0.5	0.2	0.2	0.3	0.2	0.3	0.3	0.2	0.3	0.5	0.5	0.6	0.6	0.6	0.9	0.9	0.6	0.5	0.3	0.2	1.2
FeO	4.9	4.4	4.9	5.2	4.9	5.3	1.9	1.7	2.7	2.0	3.0	2.6	2.3	2.6	4.5	4.7	6.2	5.6	6.4	8.8	9.4	5.8	4.8	3.5	1.9	11.9
MnO	0.1	0.1	0.1	0.1	0.1	0.1	0.0	0.0	0.0	0.0	0.1	0.0	0.0	0.1	0.1	0.1	0.2	0.1	0.2	0.2	0.2	0.1	0.1	0.1	0.0	0.3
MgO	9.2	8.2	9.3	9.5	8.7	15.2	3.5	2.3	3.6	2.1	2.8	2.5	2.2	3.2	5.9	6.8	9.2	7.4	10.3	14.5	24.0	14.3	11.5	6.8	3.2	23.6
CaO	11.2	11.8	11.2	11.2	11.2	9.3	14.1	14.2	13.5	13.5	13.7	13.4	13.8	13.8	12.1	11.7	10.4	10.9	10.0	8.0	3.3	9.4	10.5	11.9	14.0	4.2
Na2O	1.8	1.9	1.9	1.8	2.0	1.3	2.4	2.4	2.3	2.5	2.4	2.4	2.4	2.3	2.2	2.1	1.9	2.2	1.9	1.6	0.4	1.4	1.6	1.9	2.2	0.7
K2O	0.3	0.2	0.2	0.2	0.2	0.1	0.2	0.2	0.2	0.3	0.3	0.4	0.3	0.3	0.2	0.3	0.2	0.4	0.3	0.1	0.0	0.2	0.2	0.2	0.3	0.0
P2O5	0.0	0.0	0.0	0.0	0.0	0.0	0.0	0.0	0.1	0.1	0.0	0.1	0.1	0.0	0.1	0.0	0.1	0.1	0.1	0.0	0.0	0.0	0.0	0.0	0.0	0.1
Cr2O3	0.2	0.2	0.2	0.2	0.1	0.2	0.3	0.0	0.0	0.0	0.0	0.0	0.0	0.0	0.1	0.1	0.2	0.1	0.2	0.3	7.5	0.3	0.3	2.7	0.1	0.7
NiO	0.0	0.0	0.0	0.0	0.0	0.0	0.0	0.0	0.0	0.0	0.0	0.0	0.0	0.0	0.0	0.0	0.0	0.0	0.0	0.1	0.1	0.0	0.0	0.0	0.0	0.1
Total	100.0	100.0	100.0	100.0	100.0	100.0	100.0	100.0	100.0	100.0	100.0	100.0	100.0	100.0	100.0	100.0	100.0	100.0	100.0	100.0	100.0	100.0	100.0	100.0	100.0	100.0
Mg#	0.7718	0.7697	0.7723	0.7632	0.7609	0.8373	0.7690	0.7116	0.7046	0.6457	0.6190	0.6277	0.6352	0.6813	0.6984	0.7205	0.7272	0.7016	0.7435	0.7458	0.8202	0.8161	0.8083	0.7763	0.7497	0.7795
Trace elements																										
ppm																										
Zr	36	35	34	35	35	36	28	34	42	47	42	50	39	42	43	38	36	54	40	25	26	24	26	31	34	15
Y	2	2	5	3	4	6	1	4	2	4	3	6	2	1	3	5	5	8	4	3	6	5	0	1	1	10
Sr	337	345	331	318	320	294	433	449	421	427	410	427	429	416	356	343	300	336	295	209	58	258	304	394	450	53
Rb	7	6	4	3	1	3	2	5	5	7	5	8	2	5	4	6	3	10	8	4	4	5	6	6	8	1
Co	32	71	33	60	33	81	11	29	10	33	13	41	9	43	29	61	43	757	45	75	164	50	61	29	37	111
Cr	74	57	56	87	47	64	57	30	22	26	35	21	42	49	46	78	70	95	91	118	458	61	55	145	26	154
V	39	35	44	41	38	44	23	17	27	25	33	28	27	26	37	41	53	53	53	68	171	50	38	55	19	91
Zn	16	18	19	19	20	19	14	20	16	19	22	21	23	15	20	20	18	23	22	21	29	18	10	18	12	26
Cu	192	168	190	199	188	234	32	21	39	27	38	33	34	43	129	146	227	155	230	369	625	308	245	171	27	534
Ni	1169	1029	1081	1058	989	1347	2064	86	164	123	150	126	141	239	579	688	1078	773	1175	1926	51527	2242	1879	18754	620	4844
CIPW-norm																										
wt.%																										
AP	0.00	0.00	0.00	0.00	0.00	0.00	0.00	0.00	0.24	0.24	0.00	0.24	0.24	0.00	0.24	0.00	0.24	0.24	0.24	0.00	0.00	0.00	0.00	0.00	0.00	0.24
CM	0.29	0.29	0.29	0.29	0.15	0.29	0.44	0.00	0.00	0.00	0.00	0.00	0.00	0.00	0.15	0.15	0.29	0.15	0.29	0.44	11.04	0.44	0.44	3.98	0.15	1.03
IL	0.19	0.19	0.19	0.19	0.19	0.38	0.19	0.19	0.19	0.19	0.19	0.38	0.19	0.19	0.38	0.38	0.38	0.38	0.38	0.38	0.94	0.19	0.19	0.19	0.19	0.38
OR	1.77	1.18	1.18	1.18	1.18	0.59	1.18	1.18	1.18	1.77	1.77	2.36	1.77	1.77	1.18	1.77	1.18	2.36	1.77	0.59	0.00	1.18	1.18	1.18	1.77	0.00
AB	15.23	16.08	16.08	15.23	16.92	11.00	20.31	20.31	19.46	21.15	20.31	20.31	20.31	19.46	18.61	17.77	16.08	18.61	16.08	13.54	3.38	11.85	13.54	16.08	18.61	5.92
AN	51.07	53.92	50.64	49.45	51.56	44.08	65.59	68.32	63.31	66.32	63.38	63.36	65.57	63.56	55.57	53.54	47.64	47.07	43.25	34.00	14.30	42.24	50.08	59.04	68.10	12.96
C	0.00	0.00	0.00	0.00	0.00	0.00	0.00	0.00	0.00	0.06	0.00	0.00	0.00	0.00	0.00	0.00	0.00	0.00	0.00	0.00	0.00	0.00	0.00	0.22	0.00	0.00
MT	0.72	0.58	0.72	0.72	0.72	0.72	0.29	0.29	0.43	0.29	0.43	0.43	0.29	0.43	0.72	0.72	0.87	0.87	0.87	1.30	1.30	0.87	0.72	0.43	0.29	1.74
DIEN	1.27	1.30	1.39	1.71	1.11	0.63	1.26	0.56	0.78	0.00	1.05	0.59	0.53	1.23	0.98	1.20	0.88	1.64	1.55	1.55	0.66	1.31	0.60	0.00	0.38	2.06
DIFS	0.47	0.48	0.51	0.65	0.44	0.15	0.42	0.27	0.40	0.00	0.80	0.40	0.37	0.70	0.51	0.56	0.41	0.85	0.67	0.66	0.11	0.36	0.17	0.00	0.15	0.72
DIWO	1.88	1.93	2.06	2.55	1.67	0.86	1.82	0.89	1.26	0.00	1.91	1.03	0.94	2.05	1.59	1.88	1.38	2.65	2.38	2.38	0.86	1.83	0.84	0.00	0.57	3.02
HYEN	15.12	13.42	14.56	15.55	13.66	23.68	3.63	5.17	8.18	5.23	5.38	5.64	4.95	6.74	12.38	12.94	18.29	16.27	19.24	24.42	55.36	22.63	17.89	10.92	5.98	44.55
HYFS	5.57	5.00	5.30	5.91	5.37	5.64	1.21	2.52	4.15	3.35	4.08	3.81	3.52	3.85	6.43	6.11	8.59	8.44	8.35	10.40	9.03	6.30	5.10	2.49	2.31	15.67
Q	0.00	0.00	0.00	0.00	0.00	0.00	0.00	0.30	0.52	1.31	0.00	1.57	1.23	0.12	0.00	0.00	0.00	0.00	0.00	0.00	0.00	0.00	0.00	0.00	0.00	0.00
FO	4.57	3.99	5.05	4.48	4.83	9.49	2.68	0.00	0.00	0.00	0.38	0.00	0.00	0.00	0.93	1.96	2.63	0.36	3.41	7.11	2.63	8.18	7.11	4.21	1.13	8.52
FA	1.86	1.64	2.03	1.88	2.09	2.49	0.98	0.00	0.00	0.00	0.32	0.00	0.00	0.00	0.53	1.02	1.36	0.21	1.63	3.34	0.47	2.51	2.23	1.06	0.48	3.30
TOTAL	100.00	100.00	100.00	99.80	99.90	100.00	100.00	100.00	100.11	99.91	100.00	100.11	99.91	100.10	100.21	100.00	100.21	100.11	100.11	100.10	100.10	99.90	100.10	99.80	100.10	100.11

Sample:	373.00	375.68	442.00	447.00	447.90	449.40	450.20	536.10	546.00	550.05	553.00	557.10	622.48	622.70	626.17	737.00	738.90	754.00	763.45	772.36	773.60	774.00
Depth in																						
NG-sequence in m:	1413.00	1415.68	1482.00	1487.00	1487.90	1489.40	1490.20	1576.10	1586.00	1590.05	1593.00	1597.10	1662.48	1662.70	1666.17	1777.00	1778.90	1794.00	1803.45	1812.36	1813.60	1814.00
wt.%																						
SiO2	52.6	41.6	54.8	55.6	55.1	46.0	51.0	55.5	52.4	42.0	50.2	53.7	53.5	55.1	48.9	55.0	45.5	55.5	50.5	48.6	53.4	51.7
TiO2	0.1	0.1	0.2	0.2	0.2	0.1	0.2	0.1	0.2	0.1	0.1	0.1	0.1	0.2	0.1	0.2	0.2	0.3	0.3	0.3	0.5	0.3
Al2O3	3.6	2.9	3.5	3.5	3.3	3.1	3.4	2.9	2.9	2.8	2.7	3.0	3.3	3.5	2.9	5.1	3.9	7.1	7.0	6.7	10.6	10.6
Fe2O3	0.9	1.2	0.8	0.8	0.8	1.1	0.9	0.8	0.9	1.2	1.0	0.9	0.9	0.8	1.0	0.8	1.1	0.8	0.9	0.9	0.9	1.0
FeO	8.8	12.0	8.1	7.9	7.9	10.9	9.1	8.0	8.8	11.9	10.1	9.0	8.8	8.4	10.3	8.1	11.0	8.5	9.4	9.4	9.1	10.3
MnO	0.2	0.2	0.2	0.2	0.2	0.2	0.2	0.2	0.2	0.2	0.2	0.2	0.2	0.2	0.2	0.2	0.2	0.2	0.2	0.1	0.2	0.2
MgO	29.9	38.9	28.1	27.9	28.7	35.2	31.1	29.0	31.0	39.3	32.5	29.5	29.6	27.5	33.2	24.7	34.1	21.0	25.8	27.5	15.3	17.5
CaO	2.4	1.4	2.7	2.5	2.5	1.9	2.2	2.2	2.2	1.6	1.9	2.2	2.2	2.7	1.9	4.0	2.3	4.5	4.0	4.3	7.2	6.6
Na2O	0.6	0.1	0.6	0.6	0.3	0.5	0.5	0.6	0.7	0.2	0.4	0.6	0.5	0.8	0.5	1.1	0.3	1.2	0.7	1.0	1.8	1.2
K2O	0.0	0.0	0.2	0.1	0.1	0.1	0.1	0.1	0.1	0.2	0.1	0.1	0.1	0.2	0.1	0.3	0.2	0.3	0.5	0.5	0.7	0.2
P2O5	0.0	0.0	0.0	0.0	0.0	0.0	0.0	0.0	0.0	0.0	0.0	0.0	0.0	0.0	0.0	0.0	0.0	0.0	0.0	0.1	0.1	0.1
Cr2O3	0.9	1.5	0.7	0.6	0.8	0.8	1.2	0.5	0.7	0.3	0.6	0.6	0.6	0.5	0.7	0.4	1.1	0.4	0.5	0.5	0.2	0.2
NiO	0.1	0.3	0.1	0.1	0.1	0.2	0.1	0.1	0.1	0.3	0.1	0.1	0.1	0.1	0.2	0.1	0.2	0.1	0.1	0.2	0.1	0.1
Total	100.0	100.0	100.0	100.0	100.0	100.0	100.0	100.0	100.0	100.0	100.0	100.0	100.0	100.0	100.0	100.0	100.0	100.0	100.0	100.0	100.0	100.0
Mg#	0.8581	0.8523	0.8600	0.8625	0.8657	0.8523	0.8591	0.8661	0.8629	0.8547	0.8510	0.8533	0.8577	0.8535	0.8519	0.8439	0.8469	0.8150	0.8305	0.8385	0.7489	0.7513
Trace elements																						
ppm																						
Zr	8	7	21	16	12	12	17	9	10	15	10	18	14	10	12	20	20	33	42	36	25	7
Y	0	2	6	4	3	1	2	2	5	0	0	5	1	4	3	4	4	5	7	7	15	10
Sr	54	45	46	45	43	54	50	42	42	57	40	43	46	70	39	85	59	124	127	114	218	216
Rb	1	1	8	5	1	3	3	4	5	11	6	5	5	5	0	8	8	11	19	18	26	8
Co	101	150	84	85	102	135	101	85	86	158	113	90	101	87	128	78	128	76	103	109	73	71
Cr	5995	10189	5057	4326	5567	5715	8439	3494	4647	1853	4112	4078	4026	3650	4812	3061	7357	2575	3561	3257	1334	1635
V	81	62	94	77	71	58	83	80	88	40	71	77	76	86	69	99	81	127	114	113	159	171
Zn	65	67	61	58	64	64	64	59	63	69	69	69	64	61	71	61	66	66	67	66	70	100
Cu	22	20	41	26	21	29	24	32	66	34	37	29	27	29	32	41	36	45	63	51	39	17
Ni	865	2098	699	673	885	1527	955	688	720	1983	1106	745	982	718	1470	624	1774	449	1006	1392	442	450
Sc	23	12	24	22	19	13	18	24	24	10	20	25	23	26	17	25	15	27	23	20	30	33
CIPW-norm																						
wt.%																						
AP	0.00	0.00	0.00	0.00	0.00	0.02	0.00	0.00	0.02	0.05	0.00	0.00	0.02	0.05	0.05	0.05	0.07	0.12	0.09	0.14	0.19	0.14
CM	1.30	2.19	1.09	0.93	1.19	1.24	1.81	0.75	1.00	0.40	0.88	0.88	0.87	0.78	1.03	0.66	1.59	0.56	0.77	0.71	0.28	0.35
IL	0.21	0.17	0.36	0.30	0.30	0.24	0.28	0.28	0.30	0.23	0.23	0.28	0.28	0.32	0.23	0.45	0.32	0.58	0.62	0.60	0.99	0.51
OR	0.12	0.00	1.24	0.83	0.71	0.47	0.30	0.47	0.47	1.36	0.41	0.53	0.83	1.06	0.65	1.54	1.00	2.07	3.19	2.72	4.02	1.30
AB	4.82	1.18	5.33	5.50	2.54	4.06	4.15	4.65	5.92	2.03	3.81	4.74	4.23	6.68	4.40	9.39	2.28	10.49	5.84	8.80	14.81	9.98
AN	7.18	6.80	6.05	6.27	7.44	6.04	6.85	5.21	4.48	5.80	5.14	5.46	6.40	5.47	5.31	8.08	8.93	12.67	14.33	12.15	18.95	22.84
C	0.00	0.14	0.00	0.00	0.00	0.00	0.00	0.00	0.00	0.00	0.00	0.00	0.00	0.00	0.00	0.00	0.00	0.00	0.00	0.00	0.00	0.00
MT	1.28	1.74	1.17	1.15	1.15	1.58	1.32	1.16	1.28	1.73	1.48	1.30	1.28	1.22	1.49	1.17	1.59	1.23	1.36	1.36	1.32	1.49
DIEN	1.46	0.00	2.35	1.97	1.58	0.97	1.31	1.84	1.92	0.59	1.26	1.65	1.43	2.38	1.19	3.64	0.66	2.83	1.65	2.61	4.55	2.63
DIFS	0.30	0.00	0.46	0.39	0.30	0.21	0.26	0.35	0.37	0.13	0.28	0.35	0.29	0.50	0.26	0.83	0.15	0.78	0.41	0.62	1.84	1.08
DIWO	1.95	0.00	3.13	2.62	2.09	1.30	1.74	2.44	2.56	0.80	1.71	2.21	1.92	3.19	1.60	4.94	0.89	3.96	2.28	3.57	6.89	3.99
HYEN	54.60	12.08	61.60	65.90	69.02	25.26	49.54	67.38	51.34	7.21	44.47	59.05	58.81	61.11	37.77	53.15	26.00	49.47	38.05	24.32	31.01	35.40
HYFS	11.02	2.55	12.17	12.88	13.02	5.42	9.70	12.87	10.00	1.56	9.71	12.54	12.06	12.94	8.17	12.05	5.74	13.70	9.47	5.75	12.55	14.58
Q	0.00	0.00	0.00	0.00	0.00	0.00	0.00	0.00	0.00	0.00	0.00	0.00	0.00	0.00	0.00	0.00	0.00	1.55	0.00	0.00	0.00	0.00
FO	12.91	59.33	4.13	1.06	0.54	43.02	18.71	2.14	16.74	63.05	24.69	8.91	9.44	3.48	30.57	3.24	40.83	0.00	17.22	29.08	1.80	3.93
FA	2.87	13.81	0.90	0.23	0.11	10.18	4.04	0.45	3.59	15.05	5.94	2.09	2.13	0.81	7.29	0.81	9.94	0.00	4.72	7.57	0.80	1.78
TOTAL	100.02	100.00	100.00	100.02	99.99	100.02	99.99	100.00	100.00	99.97	100.01	100.00	100.00	100.00	100.00	100.00	100.00	100.00	100.00	100.00	100.00	100.01

Sample:	261.20	265.66	273.47	285.83	298.96	308.40	316.20	322.10	323.50	337.40	353.30	363.40	375.10	382.80	393.70	403.40	422.20	426.80	434.40	442.70	455.30	461.60	469.60	476.60	481.70
wt.%																									
SiO2	51.9	49.4	50.8	52.0	51.7	52.3	48.8	49.9	50.9	52.1	52.4	48.5	48.7	49.1	49.4	49.1	48.8	50.6	51.0	48.5	48.6	47.1	51.4	52.0	47.5
TiO2	0.3	0.2	0.1	0.2	0.2	0.2	0.1	0.1	0.2	0.2	0.3	0.1	0.1	0.1	0.1	0.1	0.1	0.2	0.2	0.1	0.1	0.1	0.2	0.2	0.1
Al2O3	6.0	6.4	7.5	6.5	7.7	7.3	20.8	7.3	8.2	6.4	4.2	19.9	20.2	14.5	14.5	17.7	20.8	8.3	8.8	20.5	21.7	29.4	8.4	5.6	17.7
Fe2O3	1.1	1.1	1.0	1.0	0.9	0.9	0.4	0.9	0.8	0.9	1.1	0.5	0.5	0.8	0.8	0.7	0.5	1.1	1.1	0.5	0.5	0.2	1.0	0.9	0.6
FeO	11.1	11.0	9.6	9.8	9.3	9.3	4.2	9.1	8.4	9.4	11.5	4.9	5.3	8.0	8.1	6.9	4.9	10.9	11.1	5.5	5.1	1.8	10.3	8.8	5.9
MnO	0.2	0.2	0.2	0.2	0.2	0.2	0.1	0.2	0.2	0.2	0.2	0.1	0.1	0.2	0.2	0.2	0.1	0.3	0.3	0.2	0.1	0.1	0.2	0.2	0.2
MgO	23.5	22.7	25.1	25.1	24.5	24.6	13.3	27.0	24.8	25.1	25.5	13.9	13.1	18.4	18.2	14.5	12.2	22.6	21.7	12.5	11.0	3.4	21.6	27.3	17.5
CaO	3.8	4.8	4.5	3.8	4.0	3.6	10.3	4.2	5.0	3.8	3.0	10.4	10.3	7.3	7.3	9.1	10.8	4.6	4.7	10.7	11.2	13.6	5.3	2.8	8.0
Na2O	0.8	0.6	0.6	0.7	0.9	0.8	1.2	0.6	0.8	0.8	0.6	1.1	1.3	1.0	1.0	1.2	1.2	0.8	0.1	1.3	1.4	1.7	0.8	0.5	1.8
K2O	0.1	0.0	0.1	0.1	0.1	0.2	0.6	0.1	0.1	0.2	0.2	0.2	0.2	0.1	0.1	0.2	0.3	0.1	0.2	0.1	0.1	1.1	0.2	0.3	0.6
P2O5	0.1	0.0	0.0	0.0	0.0	0.0	0.0	0.0	0.0	0.1	0.1	0.0	0.0	0.0	0.1	0.0	0.0	0.0	0.0	0.0	0.0	0.0	0.1	0.1	0.0
Cr2O3	1.1	3.3	0.4	0.5	0.5	0.5	0.2	0.6	0.6	0.6	0.9	0.2	0.2	0.5	0.3	0.2	0.2	0.6	0.8	0.2	0.2	1.6	0.4	1.2	0.2
NiO	0.1	0.1	0.1	0.1	0.1	0.1	0.0	0.1	0.1	0.1	0.1	0.0	0.0	0.1	0.1	0.0	0.0	0.1	0.1	0.0	0.0	0.0	0.1	0.1	0.0
Total	100.0	100.0	100.0	100.0	100.0	100.0	100.0	100.0	100.0	100.0	100.0	100.0	100.0	100.0	100.0	100.0	100.0	100.0	100.0	100.0	100.0	100.0	100.0	100.0	100.0
Mg#	0.7906	0.7866	0.8235	0.8206	0.8246	0.8255	0.8490	0.8414	0.8399	0.8258	0.7987	0.8342	0.8157	0.8029	0.8002	0.7894	0.8148	0.7874	0.7769	0.8032	0.7924	0.7704	0.7894	0.8465	0.8421
Trace elements																									
ppm																									
Zr	25	16	19	15	16	23	22	14	19	25	28	20	23	14	20	21	25	16	24	21	22	28	23	32	20
Y	8	6	3	3	3	5	0	3	2	6	6	4	2	1	3	0	3	5	6	1	0	1	3	5	3
Sr	62	69	106	74	88	77	320	101	104	61	33	280	270	160	202	232	279	77	82	277	287	397	88	69	196
Rb	9	1	5	3	4	9	13	2	3	7	11	4	3	1	2	5	5	2	6	4	3	27	7	13	23
Co	144	103	139	102	134	94	81	92	105	85	138	42	82	75	89	61	62	103	124	44	60	13	124	115	60
Cr	158	289	91	82	87	83	69	97	127	135	149	65	68	49	50	62	40	98	122	54	61	73	102	112	54
V	92	98	76	82	75	80	38	65	71	74	81	43	45	63	65	57	44	78	85	49	47	41	80	69	36
Zn	20	29	25	21	20	18	54	23	13	18	16	14	31	17	47	75	38	16	30	24	13	7	28	19	7
Cu	523	557	498	530	518	559	335	619	450	535	511	239	312	352	366	344	295	474	345	144	140	39	445	930	190
Ni	7645	22715	3014	3285	3209	3317	1351	3773	3775	4118	5871	1617	1314	3239	1898	1490	1646	3830	5307	1177	1144	10825	2845	8270	1534
CIPW-norm																									
wt.%																									
AP	0.24	0.00	0.00	0.00	0.00	0.00	0.00	0.00	0.00	0.24	0.24	0.00	0.00	0.00	0.24	0.00	0.00	0.00	0.00	0.00	0.00	0.00	0.24	0.24	0.00
CM	1.62	4.86	0.59	0.74	0.74	0.74	0.29	0.88	0.88	0.88	1.33	0.29	0.29	0.74	0.44	0.29	0.29	0.88	1.18	0.29	0.29	2.36	0.59	1.77	0.29
IL	0.56	0.38	0.19	0.38	0.38	0.38	0.19	0.19	0.38	0.38	0.56	0.19	0.19	0.19	0.19	0.19	0.19	0.38	0.38	0.19	0.19	0.19	0.38	0.38	0.19
OR	0.59	0.00	0.59	0.59	0.59	1.18	3.55	0.59	0.59	1.18	1.18	1.18	1.18	0.59	0.59	1.18	1.77	0.59	1.18	0.59	0.59	6.50	1.18	1.77	3.55
AB	6.77	5.08	5.08	5.92	7.61	6.77	10.15	5.08	6.77	6.77	5.08	9.31	11.00	8.46	8.46	10.15	10.15	6.77	0.85	11.00	11.85	14.38	6.77	4.23	15.23
AN	12.49	14.77	17.48	14.30	16.68	15.74	49.60	16.93	18.49	13.28	8.18	48.77	48.69	34.78	34.78	42.32	50.49	18.76	22.97	49.81	52.63	67.47	18.74	12.15	38.45
C	0.00	0.00	0.00	0.00	0.00	0.00	0.00	0.00	0.00	0.00	0.00	0.00	0.00	0.00	0.00	0.00	0.00	0.00	0.00	0.00	0.00	0.69	0.00	0.00	0.00
MT	1.59	1.59	1.45	1.45	1.30	1.30	0.58	1.30	1.16	1.30	1.59	0.72	0.72	1.16	1.16	1.01	0.72	1.59	1.59	0.72	0.72	0.29	1.45	1.30	0.87
DIEN	1.66	2.67	1.45	1.36	0.95	0.64	0.46	1.20	1.93	1.48	1.77	0.86	0.71	0.42	0.23	0.81	0.92	1.17	0.10	0.96	0.85	0.00	1.99	0.34	0.38
DIFS	0.53	0.79	0.39	0.37	0.25	0.17	0.10	0.28	0.45	0.38	0.54	0.21	0.20	0.13	0.07	0.27	0.26	0.39	0.03	0.30	0.27	0.00	0.66	0.07	0.09
DIWO	2.39	3.78	2.02	1.90	1.32	0.89	0.63	1.63	2.64	2.05	2.53	1.18	1.00	0.60	0.33	1.18	1.29	1.69	0.14	1.37	1.22	0.00	2.88	0.45	0.52
HYEN	48.11	43.39	42.34	48.00	44.31	48.42	17.35	38.89	39.87	47.31	52.05	19.95	18.47	28.52	29.89	22.87	18.90	39.82	50.19	17.42	16.62	2.65	41.21	53.64	6.57
HYFS	15.28	12.78	11.41	13.02	11.71	12.75	3.79	9.16	9.34	12.28	15.98	4.86	5.19	8.70	9.46	7.68	5.25	13.44	17.83	5.44	5.34	0.56	13.76	11.52	1.56
Q	0.00	0.00	0.00	0.00	0.00	0.00	0.00	0.00	0.00	0.00	0.00	0.00	0.00	0.00	0.00	0.00	0.00	0.00	0.00	0.00	0.00	0.00	0.00	0.00	0.00
FO	6.13	7.34	13.11	9.21	11.04	8.55	10.72	19.03	13.99	9.61	6.79	9.68	9.41	11.83	10.66	8.71	7.40	10.72	2.63	8.94	6.96	4.08	7.43	9.81	25.67
FA	2.15	2.38	3.89	2.76	3.22	2.48	2.58	4.94	3.61	2.75	2.30	2.60	2.92	3.98	3.72	3.22	2.26	3.99	1.03	3.08	2.46	0.94	2.73	2.32	6.74
TOTAL	100.10	99.80	100.00	100.00	100.10	100.00	100.00	100.10	100.10	99.90	100.10	99.80	100.00	100.10	100.20	99.90	99.90	100.20	100.10	100.10	100.00	100.10	100.00	100.00	100.10